The Sixth
International Conference on
Cold Fusion

PROGRESS IN NEW HYDROGEN ENERGY

October 13-18, 1996
JAPAN

New Energy and Industrial Technology Development Organization
The Institute of Applied Energy

Proceedings VOL.1

The Sixth International Conference on Cold Fusion

PROGRESS IN NEW HYDOROGEN ENERGY

Edited by Makoto OKAMOTO

■

October 13-18, 1996
JAPAN

Published by:
New Energy and Industrial Technology Development Organization
The Institute of Applied Energy

Supported by:
The Agency of Natural Resources and Energy of
the Ministry of International Trade and Industry

Proceedings VOL. 1

Preface

The 6th International Conference on Cold Fusion (ICCF6) was held at Lake Toya, Hokkaido, Japan, on October 13th - 18th 1996, with 179 participants registering from 17 countries. 43 oral presentation papers and 77 poster presentation papers were selected out of more than 160 abstracts originally submitted. The Proceedings, ***"PROGRESS IN NEW HYDROGEN ENERGY"***, has been edited as the document of the Conference.

The Local Organizing Committee carried out a series of intensive discussions on the scope of the conference, and decided that it should provide an international forum for discussion of the most recent and academic aspects of the research.

Following the scope, the Technical Program Committee spent many hours reviewing and selecting the papers that were to be presented in the Oral and Poster Sessions. Mainly young researchers performing highly scientific activities were selected, based on their submitted abstracts and the recommendations by related senior scientists, and approximately 30% of the submitted abstracts were rejected. Severe discussions were also made in selecting the presenters that were to be supported financially by the Basic Research Program of the NHE Project, and more than 20 researchers received financial support to attend the Conference. The Local Organizing Committee also planned a technical tour which was a new attempt in the history of ICCF. The tour to the NHE Sapporo Laboratory was realized on October 18th by the generous assistance of Dr. N. Asami (Vice-Chairperson) and his staff.

The topics for papers were arranged into 5 fields : (1) Excess Energy Phenomena in Deuterium/Metal Systems, (2) Correlation Between Excess Energy and Nuclear Products, 3) Nuclear Physics Approaches, (4) Material Science Studies, and (5) Innovative Approaches. All topics covered both experimental studies and theoretical studies. The topics also formed a new base in realizing the scientific and academic conference in the so-called cold fusion research field.

The Conference was formed by two sessions : the Fundamental Session and the Special Session, and both sessions consisted of several sub-sessions. The Fundamental Session had 7 sub-sessions; 1 : Helium and Heat Correlation (5), 2 : NHE (5), 3 : Excess Heat (7), 4 : Material Science Studies (5), 5 : Nuclear Physics Approach (5), 6 : Innovative Approach (2), and 7 : Excess Heat and Nuclear Products (5). The Special Session had 4 sub-sessions; 1 : Russian Activities (1), 2 : Indian Activities (1), 3 : CETI (Paterson Cell) (2), and 4 : Nuclear Transmutation (5). The numbers in parenthesis represent the numbers of oral presentations in each sub-session.

77 abstracts were accepted for poster presentation in the two sessions. The two-minute Poster Previews were successfully carried out before the poster sessions. All poster presentations were displayed on the poster boards for one day to provide adequate time for intensive discussions.

Preface

The Proceedings consist of two parts : the first part for the Fundamental Session and the second part for the Special Session. The volume for each paper was determined in accordance with the academic journals in the science field. Rather than attempting to personally introduce the papers myself, I believe it would be best for each one of you to evaluate and find the significance of each papers yourself. As seen in the Proceedings, recent advances in this extremely wide and intensive research field, from nuclear physics to material science, has made various scientific discussions possible in this attractive but long neglected field of study.

Finally, I would like to express my heartfelt appreciation to all ladies and gentlemen who strongly collaborated in realizing this wonderful scientific conference, especially to the participants, New Energy and Industrial Technology Development Organization, The Institute of Applied Energy, New Hydrogen Energy Laboratory, Technical Program Committee and Convention Linkage, Inc.

Chairperson, Prof. Makoto OKAMOTO,
Local Organizing Committee
The Sixth International Conference on Cold Fusion

Contents

Volume 1

Fundamental Session

Helium and Heat Correlation

NHE Session

Excess Heat

Contents

Material Science Studies

Contents

Nuclear Physics Approach

Contents

Contents

Appendix

Contents

Volume 2

Excess Energy and Nuclear Products

Contents

Innovative Approach

Contents

Special Session

CETI Session

Contents

Transmutation

Russian Activities

Summary

Appendix

Organizing Committees

International Advisory Committee

Prof. Bressani, T.	(University Torino, Italy)
Prof. Fleischmann, M.	(IMRA Europe, U.K.)
Prof. Ikegami, H.	(NIFS, Japan)
Mr. Jaeger, F.	(ENECO, U.S.A.)
Dr. McKubre, K.	(SRI International, U.S.A.)
Prof. Okamoto, M.	(Tokyo Institute of Technology, Japan)
Prof. Pons, S.	(IMRA Europe, France)
Prof. Preparata, G.	(University Milano, Italy)
Prof. Samsonenko, N.	(PFUR, Russia)
Prof. Sánchez, C.	(University Autonoma, Spain)
Dr. Scaramuzzi, F.	(ENEA, Italy)
Dr. Srinivasan, M.	(BARC, India)
Prof. Li, X. Z.	(Tsinghua University, China)

Local Organizing Committee

Prof. Okamoto, M.	(Chairperson)
Dr. Asami, N.	(Vice-chairperson, NHE Sapporo)
Prof. Ikegami, H.	(NIFS)
Director Omura, T.	(NEDO)
Prof. Ota, K.	(Yokohama National University)
Prof. Takahashi, A.	(Osaka University)

Conference Information

Name of Conference

The Sixth International Conference on Cold Fusion

Period

Conference: October 13-17, 1996
Technical Tour: October 18, 1996

Venue

Hotel Apex Toya, Hokkaido
Aza-Shimizu, Abuta-machi, Abuta-gun, Hokkaido 049-57, Japan

Conference Secretariat

c/o NHE-Center, IAE
Shinbashi TS Building, 1-22-5 Nishi-Shinbashi, Minato-ku, Tokyo 105, Japan
Tel: +81-3-3508-8901 Fax: +81-3-3508-8902 E-mail: mac@iae.or.jp

Official Language

English

Fundamental Session

Helium and Heat Correlation
NHE Session
Excess Heat
Material Science Studies
Nuclear Physics Approach

Click here for a more readable copy of this paper.

x-ray, heat excess and ^{4}He in the electrochemical confinement of deuterium in palladium

F. Cellucci[#] P.L. Cignini[#], G. Gigli, D. Gozzi[&], M. Tomellini[*]
Dipartimento di Chimica, Università di Roma La Sapienza, P.le Aldo Moro 5, 00185 Roma, Italy

E. Cisbani[§], S. Frullani, F. Garibaldi, M. Jodice[§], G.M. Urciuoli[§]
Laboratorio di Fisica, Istituto Superiore di Sanità, V.le Regina Margherita 299, 00161 Roma, Italy

Abstract
The energy balance between heat excess and ^{4}He in the gas phase has been found reasonably satisfied even if the low levels of ^{4}He found do not give the necessary confidence to state definitely that we are dealing with the fusion of deuterons to give ^{4}He. In the melted cathode, whose data are reported here, ^{4}He was not found at the achieved sensitivity. X-ray film, positioned at 50 mm from the cell, roughly gave the image of the cathode through spots. The energy of the radiation and the total energy associated to it have been, respectively, evaluated as (89±1) keV and (12.0 ± 0.4) kJ. This value is ≈0.5% of the energy measured by calorimetry in the same interval of time.

1. Introduction

The debate on the anomalous behaviour of the system Pd-D is still open because, in spite of the intense research activity lasted seven years in several laboratories worldwide, a clear-cut picture of all the evidences claimed is still lacking. Since 1989[1], many papers have been published, six international conferences were held on this subject, several patents issued, some promising theory has been proposed but, from an experimental point of view, the crucial initial point, the energy balance, has not yet found a satisfactorily and convincing explanation. All the efforts done to explain the excess heat found as of chemical nature have been so far considered meaningless because no chemical reaction we can imagine in the environment where the experiments of deuterium confinement generally occur is suitable to get comparable amounts of heat. The whole situation, restricted only to the heat excess findings, easily brings to the following consideration: either heat excess measurements are all experimental artifacts or we are dealing with new phenomena. By examining the abundant literature and some critical revisions[2,3] as well as through our direct experience gained in the field[4-6], there are not so strong evidences to believe that we are in the presence of a collective world-wide mistake in measuring the heat excess. Several laboratories, using different techniques and protocols found the same phenomenology and comparable results even if the reproducibility and a full control of the experiments are still lacking.
On the other hand, many experiments show other phenomena associated to the heat excess production the source of which does not seem reasonably to be based on the Chemistry: emission of x-ray[7-9], as it will be shown in this paper, and neutrons[10-13] as well as production of ^{4}He[14-17] and ^{3}H[6,18-21]. Unfortunately, the intensities and the levels of these emissions and productions are so low that their detection is sometimes very critical and difficult to accept as statistically significative

[#] CNR-Centro di Termodinamica Chimica Alle Alte Temperature, c/o Dipartimento di Chimica, Università di Roma *La Sapienza*, P.le Aldo Moro 5, 00185 Roma, Italy
[&] To whom correspondence should be addressed
[*] Dipartimento di Scienze e Tecnologie Chimiche, Università di Roma *Tor Vergata*, Via della Ricerca Scientifica, 00133 Roma, Italy
[§] National Instiute for Nuclear Physics, sez. Sanità, Laboratorio di Fisica, Istituto Superiore di Sanità, V.le Regina Margherita 299, 00161 Roma, Italy

results. Though, for the above reasons, the reliability of such no calorimetric evidences is often poor, the whole picture seems to be very intriguing so that it cannot be shortly ruled out defining it as an *ensemble* of mistakes and artifacts. Can a simple physico-chemical process, like the insertion of deuterium into the Pd lattice, whose energy is ≈ 0.1 eV/cm^3, get x-ray emission or other nuclear products at tenths of keV or some MeV? The answer is not based on the Chemistry we know but the answer seems hard to find also in the current knowledges of Physics. Quite-zero energy of the particles in the solid state, the Coulomb barrier, very low cross-sections of possible nuclear reactions, etc. are very strong arguments to consolidate skepticism and criticism. The scope of this work, based on the electrochemical confinement of deuterium in palladium, is to report and discuss the experimental facts we found in the last experiment which was the most complex and complete among the experiments we did since 1989.

2. Experimental

A detailed description of the entire experimental set-up is given elsewhere[5,6]. Here it will be described the new features added or modified with respect to the past published work.

2.1 Electrochemical & calorimetric cell

It is a Pyrex-stainless steel cell designed to accomplish the following tasks: *i)* to avoid any ^{4}He contamination (^{4}He content in air is 5.24 ppm) of the escaping electrolysis gases in which ^{4}He is to be on line measured. This is obtained by a high-vacuum tested SS holder containing the part of the cell emerging from the thermostatic bath. A stream of ^{4}He free boiling-off LN_2 circulates inside and outside the cell at 35 sccm and 2.25 Bar ; *ii)* to be a flow-calorimeter in which the circulating water can exchange heat only with the electrolytic solution. This is realized by two jackets external to the pyrex tube containing the electrolyte solution. The innermost jacket is used for the circulation of double distillated water at constant flow-rate and the outermost one is sealed under high vacuum and it is mirror-like on the top to minimize the leakage of heat by radiation; *iii)* to maintain constant the level of the electrolyte through an optoelectronic sensor controlling the feed of D_2O which is consumed during the experiment by the electrolysis, according to the Faraday's law, and evaporation; *iv)* to perform *in situ* heat calibrations through an internal resistor. At the stationary state, the energy balance of the cell is given by the equation below as:

$$P_{in} + P_{cal} + P_{exc} = P_w + P_{rad} + P_{sg} \qquad (1)$$

where the subscripts *in*, *cal*, *exc*, *w*, *rad* and *sg* stand, respectively, for the input through the electric power applied to carry out the electrolysis, power through the internal heater for making in situ calibrations, power in excess to be measured, power exchanged by the water stream crossing the innermost jacket, power radiated from the cell toward the bath and the power necessary to saturate with D_2O vapor the gas stream which is composed by the protective gas N_2 and electrolysis gases D_2 and O_2. Its composition, at fixed N_2 flow-rate, q_{N_2}, depends on the electrolysis current I. At t > τ, the time constant of the cell, eqn. 2 below, through eqn. 1, would allow to calculate P_{exc} [6]:

$$P_{exc} + V_h I_h + (V_{in} - V_{th})I = (\rho c_l q)_{H_2O}\Delta\vartheta_{wj,\infty} + \\ + k_{Rad}S_s\left\{\left[\vartheta_{tb} + \Delta\vartheta_{wj,\infty}\right]^4 - \vartheta_{tb}^4\right\} + \qquad (2) \\ + \left(\frac{3I}{4F} + \frac{P}{R\vartheta_r}q_{N_2}\right)\left[\frac{p(\vartheta_s)}{P - p(\vartheta_s)}\right]\left[\left(C_g - C_l\right)_{D_2O}\vartheta_s + \Lambda_{D_2O}\right]$$

Equation 2 can be used provided the temperature difference, $\Delta\vartheta_{wj,\infty}$, at inlet and outlet of water cooled jacket, the temperature of the bath, ϑ_{tb}, the cooling water flow-rate, q, the potential drop, V_{in}(I), at the electrodes, the room temperature, ϑ_r, the temperature of the solution, ϑ_s, and the total pressure P are measured during the experiment. $p(\vartheta_s)$ is the vapor pressure of the solution at temperature ϑ_s. Λ_{D_2O}, C_g and C_l are quantities referred to D_2O, respectively, the heat of evaporation, heat capacity of gas and liquid. V_{th} is the thermoneutral potential (1.5367 V)[22] for the

decomposition of D_2O and the product $V_h I_h$ is the input power applied to the internal resistor when the calibration step is on. S_s is the radiating surface area of the cell and k_{Rad} the Stefan-Boltzmann constant. However, instead of using eqn. 2, it is common practice to perform the calibration of the cell both before starting the electrolysis and in progress by making use of the internal heater in both the cases. Figure 1 shows the typical response of a blank cell (Pt cathode implies that $P_{exc} = 0$) when step-fashion variations of the input power (right scale) are applied to it. In this case, we have superimposition of power generated by the internal heater and a constant thermal power generated by electrolysis. The stationary values of $\Delta\vartheta_{wj,\infty}$ *vs* the input power represent the calibration. The different slopes are connected to the different flow-rates of water in the cooling jacket as reported in Table I. The straight-line behaviour of the calibration curves shows that the 2nd and 3rd term of the right side of eqn. 2 are either negligible or their sum is linear too. This is in fact what one finds by an estimation of the terms P_{rad} and P_{sg} assuming[6]: I= 1A, S_s = 240 cm^2, ϑ_{tb}= 21 °C, ϑ_r = 30 °C, q_{N_2} = 5.8x10^{-7} m^{3}s^{-1} and P=2.25 Bar as typical values. The time constant of the cell is a function of the cooling water flow-rate and, for example, its value in the conditions of Fig. 1 is 270 s. By increasing the flow-rate the time constant decreases but this makes the sensitivity (the slope of the calibration curve) poor.

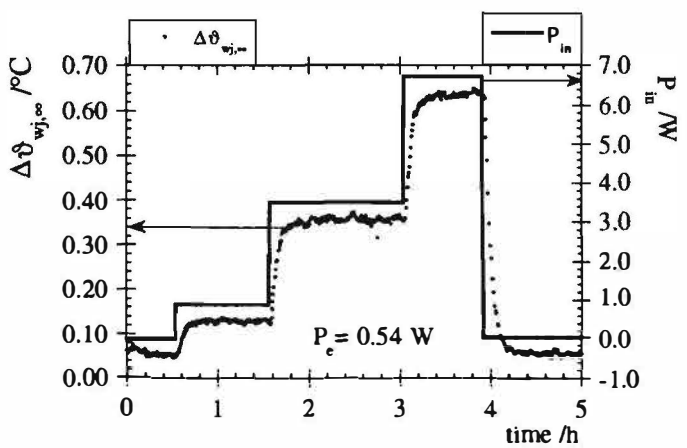

Fig. 1. Response of the cell at step variations of input power generated by the internal heater while electrolysis is running.

Table I.

Calibration curves given by the best fitting equations $\Delta\vartheta_{wj,\infty} = (a \pm \Delta a) + (b \pm \Delta b)\, P_{in}$.

The flow-rates in brackets are the expected values.

Cell #	(a ± Δa)/°C	(b± Δb) /°CW^{-1}	R	flow-rate/cm^{3}s^{-1}
1(blank)	0.02±0.01	0.118±0.001	0.99944	1.9 (2.03)
2	0.00±0.03	0.104±0.002	0.99736	2.1 (2.31)
3	-0.09±0.04	0.144±0.003	0.99738	1.5 (1.67)
4	-0.048±0.009	0.0871±0.0007	0.99965	2.5 (2.75)

Electrodes

All the anodes were made of pure platinum from Engelhard and shaped as gauze cylinders having the skeleton made of 1 mm dia. wires supporting the spot-welded mesh made of 0.35 mm dia. wire. The mesh dimension was 5x4 mm^2 and the anode final size was 48 mm height and 12 mm inner diameter. All the cathodes, except the cathode of the blank cell, were made of pure palladium from Engelhard and shaped as bundle of wires wrapped at the ends by machined cylindrical pieces of 6 mm Pd rods.The overall external dimensions of the cathodes were 6 mm dia. x 55 mm height. The height of the bundle was 40 mm (only 24 mm were out of the wrapping) and its diameter about 4 mm. Two out of three cathodes were constituted by bundles of 150 wires of 250 μm dia. each and the other one by 42 wires of 500 μm. The cathode of the blank cell was shaped similarly but the bundle was realized by 10 Pt wires of 1 mm dia. and wrapped by using SS machined caps. All the cathodes were annealed in high vacuum at 970 °C for 24 hours and cooled at room temperature at a rate of 1 °C/min. This procedure greatly reduces internal stresses and dislocation concentration and it allows the growth of large grains as it was shown by the metallographic analysis which gave a distribution of 2D grain size centered at 35±5 μm (≈ 53 μm in 3D)[23].

2.3 X-ray detection

X-ray films (Kodak, type TM H/RA-1 18x24 cm^2) were used to detect emission from the cells. Before use the film was inserted in a plastic black bag in dark room and put in front of the cell 5 cm distant as reported in figure 2. It is important to point out that the films were not in direct contact neither with any part of the cell nor with chemicals, therefore any damage of the film producing apparent traces or spots was eliminated. The analysis of the film was carried out by microdensitometer by steps of 600 μm along Z-axis making at each step a scan of X-axis by using a 50 μm slit. To convert the optical density data into exposure units (Roentgen), a calibration was done through known expositions of the same type of film (and using the same developing conditions) to the tungsten K_α radiation filtered by 0.5 mm Al.

Fig. 2. Scheme of the X-ray positioning in the experimental set-up. R_t=250 mm is the radius of torus containing the cells (see fig. 8 of ref.6). d=50 mm and f=6.5 mm. The materials in between the cell and film are H2O (45 mm) and perspex (5 mm).

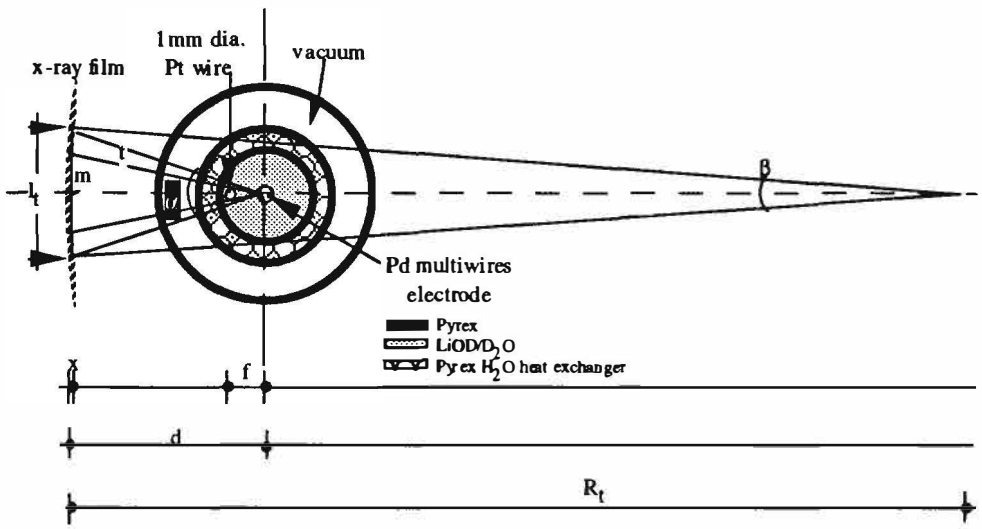

2.4 High Resolution Mass Spectrometry (HRMS)

In the gas stream coming out the electrolytic cells

With respect to the previous procedure reported in literature[14], some important improvements were brought to the ^4He determination in the electrolysis gas phase. In the present case, sampling and measurement are carried out on-line and this allows at least two great advantages: to avoid a potential source of contamination by atmospheric ^4He and to increase considerably the number of measurements. All this has been made possible by implementing the experiment with a high resolution quadrupole mass spectrometer (Balzers QMS 421 gas tight crossbeam ion source and analyzer QMA 410) full PC controlled and equipped with some features which allow to automatize several operations such as the on-line sampling. The nominal mass range of QMS in HR mode is 27 amu. The sampling procedure for ^4He is realized after the deuterium removing system[6] has reduced the deuterium content of the gas mixture coming from the cell. A 150 cm^3 SS cylinder (for each cell line), having at both the ends a three-way electrovalve, is in normal position fluxed with the gas mixture and when both the electrovalves are powered for 10 s, the inlet end becomes closed (the stream of the gas mixture is deviated elsewhere to avoid overpressure on the line) and outlet end is connected to SS charcoal trap kept under vacuum and in LN_2. When the electrovalves are again off the cylinder sucks N_2 from a small tank connected to the LN_2 reservoir. When the pressure inside the cylinder becomes higher than the pressure of the line, the line is again connected to the cylinder ready for an other sampling. The gas mixture trapped in the cylinder is let to be adsorbed in the LN_2 charcoal trap until the pressure becomes lower than a preset threshold (typically $5x10^{-2}$ mbar) then the immission of the gas mixture in the QMS chamber is realised. HRMS measurements were carried out in Multiple Ion Detection (MID) mode and the following ionic currents have been generally monitored for the species: $^4He^+$ (4.0026), valley ^4He-D_2 (4.0111), D_2^+ (4.0282), $^{20}Ne^{++}$ (9.996). The pressures in the QMS chamber, in LN_2 trap and in the sampling cylinder were also monitored during each measurement. The software controls the samplings at a given interval of time (typically every 20 min) as well as each related measurement. The mass corresponding to the

valley between ^4He-D_2 is a key parameter for monitoring the complete separation between the two peaks of ^4He and D_2. This always occurs when the deuterium removing system works properly. The presence of relevant quantities of deuterium with respect to ^4He makes impossible its determination. Reliable ^4He measurements can be obtained if the ratio $D_2/^4He$ is lower than ≈3000. The monitoring of $^{20}Ne^+$ was for the first time used in this kind of measurements by us[14] as marker of a possible air contamination. It was also reported[14] that around 20 amu the mass spectra is complicated by the presence of several species which can compromise the use of such a marker. So, the monitoring of double ionized Ne there proposed[14], it is here preferred because, by making use of a MS with lower resolution, $^{20}Ne^{++}$ appears in a mass range without any relevant interference. Several calibrations made before and during the experiment, according to a well-established procedure[14], were done to have the control of the sensitivity, σ, of the QMS (see below). The equation: $Tat = 2.46 \times 10^{-2} c V_s$ holds between the absolute quantity of ^4He atoms in tera atoms (10^{12} atoms) and their concentration in ppb in the gas mixture contained in the sampling volume V_s, given in cm^3, at stp. This allows to give σ in pA/Tat or in pA/ppb. Specific measurements were performed to establish the transport of a ^4He *parcel* along the line by releasing known amounts of air in the cell.

In the Pd electrodes

A home-made device has been realized to detect helium in the bulk of the Pd cathodes by making use of the Thermal Desorption Spectrometry (TDS). The experimental set-up is constituted by a high vacuum pumping system connected to the heating chamber by a gate valve. The heating chamber is connected to the QMS through a gettering line for removing D_2 before the immission in the QMS. The heating element is a vertical cylinder-shaped tantalum foil 75 μm thick in which a graphite crucible is positioned. The samples, as cut sections of the cathodes, are stored in a multiple sample holder driven by an external manipulator. At fixed displacements of the manipulator, each sample is allowed to fall in the crucible. The standard procedure adopted is first to heat the crucible over the m.p. of Pd (1552 °C) under high vacuum pumping then, after having closed the gate valve, to make the sample to fall into the crucible while increasing temperature above 1650 °C, and maintain this temperature for at least 10 min.; finally a rapid cooling follows. At the same time, the evolved gases are allowed to be gettered and, finally, when the pressure in the system decreases below 2×10^{-5} mbar, the QMS is connected and the measure is carried out in MID mode.

3. Results

Figure 3 shows the time pattern of the excess heat power and the absolute quantity of ^4He measured throughout an entire experiment. ^4He is given in tera atoms. The ^4He measurements before the starting of the electrolysis show that, after 200 hrs, 1.7 Tat., corresponding to 0.5 ppb, were still present though ^4He in boiling-off LN_2 is undetectable when measured directly at outlet of the LN_2 reservoir. Since, each component of the line was carefully tested for leaks and all the connections were proved to be safe (SS Swagelock type), we attribute that value to an incomplete washing of the whole line. This is also supported by several measurements made later on in the experiment which did not give any ^4He. At first glance, there is not a direct time correlation between heat excess and ^4He. However, it is important to remind that the ^4He measurement is not performed in continous mode as the heat power excess, therefore, a significative volume of the electrolysis gas mixture is lost without being analyzed. Just to have the

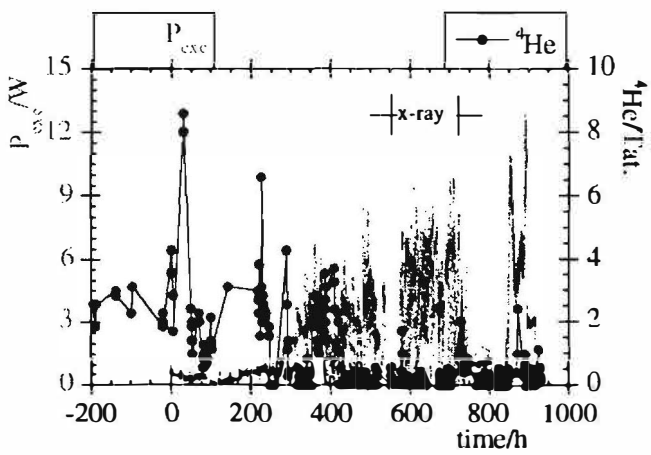

Fig. 3. Excess heat power (left scale) and ^4He (right scale) in an experiment with bundle-type cathode (250 μm dia. wires)

Helium and Heat Correlation

figures, 2.24 m^3 about at stp of gas mixture (mostly N_2, D_2, O_2) passed through the line but only 5.73×10^{-2} m^3 at stp were analyzed in the 382 samplings, the case of fig. 3, 150 cm^3 each. This is less than 2.6 %. Assuming that ^4He is all formed at the surface, it is completely and instantaneously released in the gas phase and the nuclear reaction $d + d = {}^4He + 23.8$ MeV (lattice) holds, we calculated (for space reasons more details will be given elsewhere[24]) the amount of ^4He we have to expect at each sampling of fig. 3 considering the measured heat excess. In figure 4 it is reported this calculation together the excess heat power as in fig. 3. The ratio between the measured and calculated ^4He reported in fig 5 is a parameter to check the energy balance. More specifically, the values of the ratio greater than 1 imply that ^4He detected is of atmospheric nature (in this case, probably, because of incomplete washing). On the other hand, from ~220 hours until to the end of

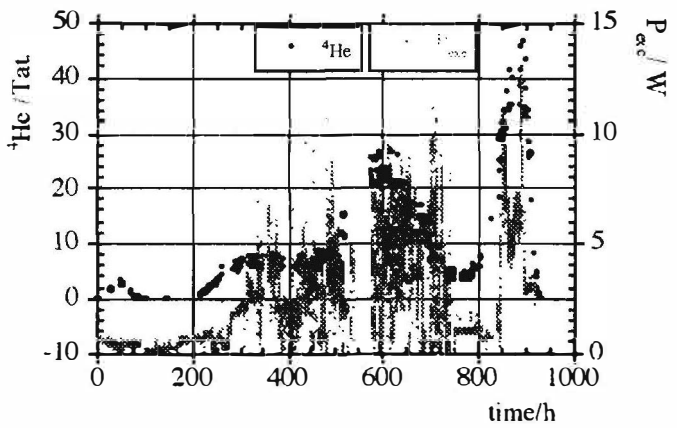

Fig. 4. Calculated ^4He (left scale) and heat power excess (right scale)

the experiment, when the aforementioned ratio is steadily below unity, it is interesting to observe that there are several points definitely greater than zero and fairly close to the energy balance of the process. As for the measurements performed on $^{20}Ne^{++}$ as a marker of contamination these are affected by some uncertainties. Contrarily to the ^4He sensitivity that has been found to be extremely reproducible, 25±3 pA/ppb or 7±1 pA/Tat, during all the experiment, the $^{20}Ne^{++}$ apparent sensitivity was found to be scattered and decreased on time from ~2 to ~0.3 pA/Tat. Moreover the amount of Ne detected has been always at the limit of detectability. The resulting measured ratios He/Ne, in spite of being generally greater than 0.29 (that of the air), are affected by a large error that, conservatively, prevented its use. It must also be kept in mind the findings of our previous experiment where a correlation was found between He and Ne even if the He/Ne ratios were greater than 0.29[14]; in the present experiment the very low range of values observed for the helium makes it difficult to look for the absence of such a correlation. On the other hand, after the experiment, the analysis of ^4He on 9 sections out of 14 of that cathode did not reveal any significative amount of ^4He embedded in the PdD_x lattice over the detection limit of ~2 Tat. Concerning the calorimetric results, they are, respectively, in terms of excess heat and highest ratio P_{exc}/P_{in}, 8.3 MJ and 0.8 as for instance in the case of the cell of fig. 3.

Fig. 5. Ratio between measured and calculated ^4He vs time. The insert is a magnified view in the range from 0 to 1.

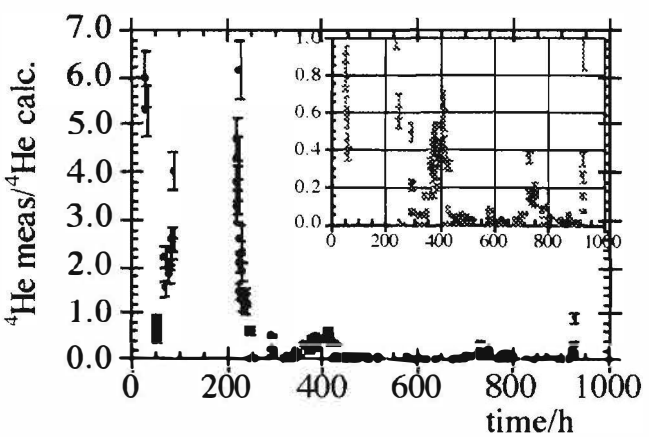

During the experiment, reported in fig. 3, at ≈ 552 hrs since the starting of the electrolysis, a x-ray film was positioned in front to the above cell and an other one in front of the blank cell as reported in fig. 2. After an exposition of a week, the film related to the blank cell did not show any trace whereas the other film showed several spots roughly reproducing the image of the cathode. The intensity, the dimensions and the coordinates of all the spots were measured and reported in figure 6. The spot diameter was found ranging from 0.41 to 2.45 mm. To be sure that an artifact was not occurring, a new film was inserted in the same plastic black bag and exposed to the light of laboratory for some days. The film was not exposed in any point. The plane X,Z is the plane parallel to the film and the vertical axis at X=0 coincides with the Z axis of the cathode, 50 mm far

from the film. In fig. 6 it is clearly visible a quite simmetrical zone, without spots, around the axis at X=0 of the film that could be reasonably attributed to the shadow (m in fig. 2) produced by the 1 mm dia. Pt wire of the anode skeleton (see fig. 2) and parallel to the Z-axis of the cathode. This is supported by the excellent agreement between the shadow width measured (7.00±0.05 mm) and calculated[24] (7.67 mm), assuming the radiation source as point like and localized in the Z-axis of the cathode. If we use the measured value of m to calculate the distance f we obtain f=7.12 mm. There is a deviation of 0.62 mm which is well explained by the deformation of the cathode observed at the end of experiment. The exposition of an x-ray film during an experiment involving energy of a few eV is very difficult to explain in terms of textbook science so that nuclear phenomena have to be necessarily taken into consideration. In the present case, the spot nature further complicates the interpretation of this experimental evidence.

Fig. 6. Microdensitometry of the x-ray film placed parallel to the X,Z plane. Exposure is given in Roentgen (R)

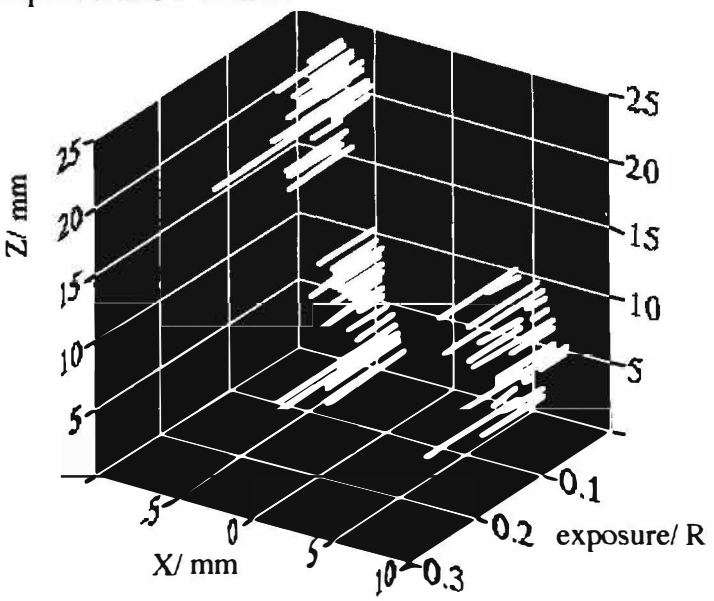

As working hypothesis, consider a whatever primary process which produces directly or indirectly photons sufficiently energetic to cross the cathode and all the materials in between the film. X-ray diffraction can not be reasonably considered because the spot pattern is not a diffraction pattern and, even in the case, the attenuation produced, at the average energy of the K_α lines of Pd (21.61 keV), by all the materials would be total as calculated in figure 7. The question is what is the nature of the source. If the source were coherent, oriented and localized, the pattern found would have its own consistency but we have not enough elements to support this. If the source were a conventional isotropic source some reasonable explanations can be given in terms of physics of radiations. In fact, the first elementary consideration is that the source site is not at the surface of the cathode because a diffuse blakening would be to expected instead of spots. At this point, the shape of the cathode becomes important. In the present case, cathode is bundle shaped and it can be satisfactorily represented by a seven

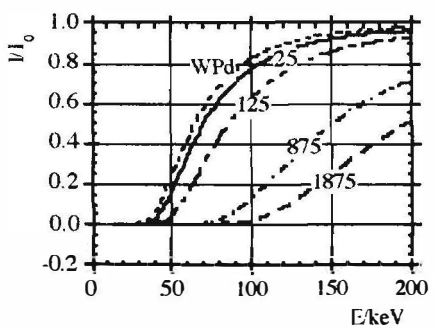

Fig. 7. Attenuation I/I_0 vs photon energy of Pd and materials between cathode and film (WPd=Without Pd) at different thickness (in μm) of Pd crossed.

shells packing as reported below in figure 8. Supposing, for the sake of simplicity, the source in the center of the system, it is easy to verify that the effective path length of the radiation in the cathode depends on the angle of propagation. The minimum and the maximum path lengths, a and b respectively, are expected for a point-like source as in fig. 8. Therefore, the system can be assumed as a system of virtual slits seen as domains in the space where the attenuation, I/I_0, is relatively low according to equation:

$$I/I_0 = \exp[-\sum_i \rho_i(\mu/\rho)_i t_i] = \prod_i \exp[-\rho_i(\mu/\rho)_i t_i] \qquad (3)$$

being ρ, (μ/ρ) and t, respectively, the density, the mass absorption coefficient, which is a function of the photon energy, and the path length of the radiation in a given material i. In the present experimental set-up, the value of eqn. 3 depends only on the photon energy and the position of the source in the cathode, i.e., it depends on the effective path length in Pd. By fig. 7, it is quite evident that at fixed energy the transmission is greatly influenced by that quantity, at least up to 150 keV. As an example, it is shown in fig. 9 the quantity I/I_0 calculated against the angle of propagation of the radiation[24]. The source is supposed to be point-like, localized in the centre of two wires having coordinates (0,0) and

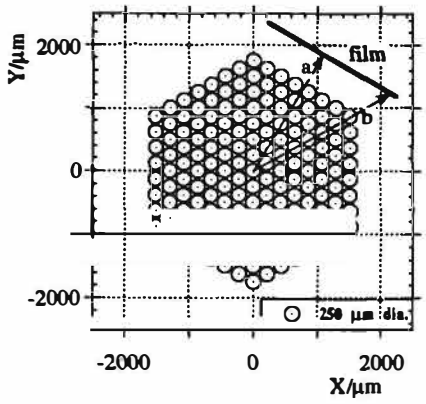

Fig. 8. Representation of the cross-section of an ideal bundle-type cathode with 169 wires of 250 μm dia. The cathodes used were made of 150 wires.

[(433.01,750)-4th shell] and, the emitted radiation, confined, for simplicity, only in a thin slice orthogonal to the z-axis passing in the coordinate origin of fig. 8. It can be shown[24] that more than one peak is found by selecting the source out of the centre of the wire. In principle, the source or sources can be everywhere but we can exclude that they are at the surface of the outermost wires of the bundle because no diffuse blakening of the film was observed. Therefore, sources have to be in the innermost wires. To make an estimation of the energy of the radiation detected the following reasoning can be done:*i.* eqn. 3 is rewritten in the form $I/I_0 = Q\,exp[-\rho_{Pd}(\mu/\rho)_{Pd}t_{Pd}]$ (4) where $Q = \prod_i exp[-\rho_i(\mu/\rho)_i t_i]$ being the Q term independent on the position of source and practically equal for all the sposts in the film; *ii.* each spot is related to the same type of elementary event and the intensity of a spot depends on the path length the radiation makes through the cathode, i.e., I_0 is always the same; *iii.* the more intense spot is associated to a source closer to the film, i.e., the source is in an outermost wire of the bundle but not in the last shell (see above); *iv.* similarly the weakest spot is related to the source more distant from the film. From the ratio between $\frac{I_{min}/I_0}{I_{max}/I_0}$ and by eqn. 4, the value of the mass absorption coefficient, (μ/ρ), of Pd is obtained.

Fig. 9 Calculated transmission at 90 keV with two different positions of the source in the cathode

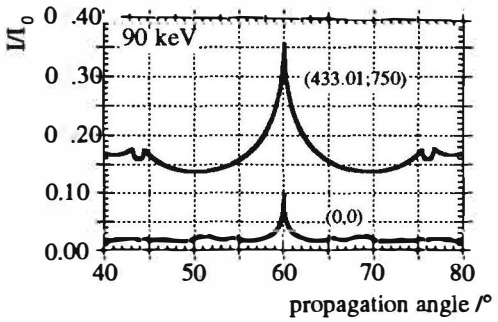

The dependence of (μ/ρ) on photon energy[25] fits very well with the equation $(\mu/\rho)=aE^{-b}$ being a = 310000±5000 and b = 2.676±0.004. Combining the equations, the energy is found by equation: $E = \left[\frac{1}{a\rho_{Pd}\left(t_{min}-t_{max}\right)} ln\frac{I_{max}}{I_{min}}\right]^{-1/b}$ (5). In the above hypotheses, t_{max} and t_{min} have to be selected among the optical paths in Pd which fall in the angle α (fig. 2) correponding to the maximum distance between spots in the film at Z = K (see fig. 6). This angle is 16.32°. The source position has to be selected, respectively, on the surface of any wire in the 6th shell with centre coordinates [0≤X≤1299;750≤Y≤1500] μm and in any wire belonging to the 7th shell with centre coordinates [-1299≤X≤-216.51;-1625≤Y≤-1000] μm. The most appropriate values for t_{max} and t_{min} were found to be, respectively, 250 and 1875 μm. Therefore, E = 89±1 keV was calculated by eqn. 5. The error on E is calculated by taking into account the errors on the fit constant and the experimental error on the intensities which was evaluated less than 2%. At this point, the energy released by this process can be calculated because I_0 can be obtained from eqn. 4. The term Q is represented as function of energy in fig. 7, curve WPd, all the other terms in eqn. 5 are known, I_0 per unity of solid angle is $(4.0\pm0.1)\times10^4$ R. Since the average density of spots in the film is 2750 sterad^{-1}, the total energy on 4π associated to the radiation is 12.0±0.4 kJ (in this calculation, the conversion 1R=87.8 erg has been used). This energy is ≈ 0.5% of the energy measured by calorimetry in the same interval of time during which the film was exposed. Looking at the energy of the K_α lines *vs* the atomic number of the elements, the energy found is close to the energy of the K_α lines of Pb or Bi. Since the chemical analysis did not detect any of them, emission on atomic basis can not be invoked and the nuclear nature of the radiation detected takes place.

Helium and Heat Correlation

Conclusions

The results show a picture with its own internal consistency though the low levels of ^4He do not give the necessary confidence to state definitely that we are dealing with the fusion of deuterons to give ^4He. On the other hand, the contamination is not proved and the energy balance seems quite well satisfied. Moreover, the exposition of the x-ray film is a clear-cut proof (very simple experimental device for which errors of measure and/or of procedure as well as artifacts can not be invoked) that a nuclear phenomenon is at work. We believe that the radiation detected has to be searched among the stable isotopes of Pd or among its impurities having intense nuclear transitions close to the energy found. Work is in progress to check this route.

Acknoweldgements

This work has been supported by the National Research Council (CNR), National Institute of Nuclear Physics (INFN) and University of Rome *La Sapienza.*

References

1. Fleischmann M. and Pons S., *J. Electroanal. Chem.* **1989**, *261*, 301.
2. Noninski V.C. and Noninski C.I., *Fusion Technology* **1993**, *23*, 474.
3. Miles M.H.; Bush B.F. and Stillwell D., *J. Phys. Chem.* **1994**, *98*, 1948.
4. Gozzi D.; Cignini P.L.; Tomellini M.; Frullani S.; Garibaldi F.; Ghio F.; Jodice M. and Urciuoli G. M. , *Fusion Technol.* **1992**, *21*, 60
5. Gozzi D.; Cignini P.L.; Caputo R.; Tomellini M.; Balducci G.; Gigli G.;. Cisbani E.; Frullani S.; Garibaldi F.; Jodice M. and Urciuoli G. M: *Frontiers of Cold Fusion*, Editor H. Ikegami, Frontiers Science Series no.**4**; Universal Academy Press Inc.: Tokyo **1993**, 155
6. Gozzi D.; Cignini P.L.; Caputo R.; Tomellini M.; Balducci G.; Gigli G.;. Cisbani E.; Frullani S.; Garibaldi F.; Jodice M. and Urciuoli G. M, *J. Electroanal. Chem.* **1995**, *380,* 91.
7. Szpak S.; Mosier-Boss P.A. and Smith J.J., *J. Electroanal. Chem.* **1991**, *302,* 255.
8. Karabut A.B.; Kucherov Ya. R. and Savvatimova I.B., *Phys. Lett.A* **1992**, *170*, 265.
9. Iwamura Y.; Gotoh N.; Itoh T. and Toyoda I., Proc.5th International Conference on Cold Fusion, Monte-Carlo, Monaco, April 9-13, 1995, International Conference on Cold Fusion 5, **1995,** Valbonne, France, p. 197
10. Jones S.E.; Palmer E.P.; Czirr J.B.; Decker D.L.; Jensen G.L.; Thorne J.M.; Taylor S.F. and Rafelski J., *Nature* **1989**, *338*, 737.
11. Bressani T.; Calvo D.; Feliciello A.; Lamberti C.; Iazzi F.; Minetti B.; Cherubini R.; Haque A.M.I. and Ricci R.A., *Nuovo Cimento* **1991**, *104A*, 1413.
12. Takahashi A.; Iida T.; Maekawa F.; Sugimoto H. and Yoshida S., *Fusion Technol.* **1991**, *19,* 380.
13. Okamoto M.; Yoshinaga Y.; Aida M.and Kusunoki T., Proc.4th International Conference on Cold Fusion, Lahaina, Hawaii, Dec. 6-9, 1993,Vol. 2, EPRI TR-104188-V2 **1994** , p.3.
14. Gozzi D.; Cignini P.L.; Caputo R.; Tomellini M.; Balducci G.; Gigli G.;. Cisbani E.; Frullani S.; Garibaldi F.; Jodice M. and Urciuoli G. M, *J. Electroanal. Chem.* **1995**, *380,* 108.
15. Bush B.F.; Lagowski J.J.; Miles M.H. and Ostrom G.S.,*J. Electroanal. Chem.* **1991**, *304,* 271.
16. Yamaguchi E. and Nishioka T. : Frontiers of Cold Fusion, Edited by H. Ikegami, Frontiers Science Series no.**4**, Universal Academy Press Inc., Tokyo **1993** p.179.
17. Arata Y. and Zhang Y., *Proc. Japan Acad.* **1995**, *71B*, 304.
18. Chien C.C.; Hodko D.; Minevski Z. and Bockris J.O'M., *J. Electroanal. Chem.* **1992**, *338* , 189.
19. Storms E. and Talcott C.L., *Fusion Technol.* **1990**, *17*, 680.
20. Cedzynska K.; Barrowes S.C.; Borgeson H.E.; Knight L.C. and Will F., *Fusion Technol.* **1991**, *20*, 108; **1992**, *22*, 156.
21. Tuggle D.G.; Claytor T.N. and Taylor S.F., Proc.4th International Conference on Cold Fusion, Lahaina, Hawaii, Dec. 6-9, 1993,Vol. 2, EPRI TR-104188-V1 **1994** , p.7.
22. Balej J. and Divisek J. , J. Electroanal. Chem.**1989** *278* 85.
23. *Quantitative Microscopy,* Edited by R.T. DeHoff and F.N. Rhines, Mc Graw Series in Materials Science and Engineering, Mc Graw-Hill Book Co. New York **1968**
24 D. Gozzi et al., paper in preparation
25 J.H. Habbel, Photocross-sections, attenuation coefficient and energy absorption coefficients from 10 keV to 100 GeV, Natl.Stand. Ref. Data, Ser. 29 (1969)

Helium and Heat Correlation

Mass Spectroscopic Search for Helium in Effluent Gas and Palladium Cathodes of D_2O Electrolysis Cells Involving Excess Power

Shigeru Isagawa and Yukio Kanda

National Laboratory for High Energy Physics (KEK)
1-1 Oho, Tsukuba-shi, Ibaraki-ken, 305 JAPAN

Abstract

A heat burst equivalent to 360W per 1cm^3 of Pd was observed in an open type electrolysis cell using Pd/0.1MLiOD/Pt. It happened, however, only once in all 5 cells ever tested. Although boiling has occurred many times in all cells, no direct correlation has been found between boiling and ^{4}He production. By reducing the gas flow rate and properly adjusting the pressure gradient, the quantitative analysis of ^{4}He could be realized in our Q-mass system with high detection sensitivity (17ppt) in continuous-flow mode and with high resolution in store mode. Two types of closed vacuum furnace were used to degas the Pd samples. An external-heater-type allowed permeation of ^{4}He and H from air when heated above 1000°C. An internal-heater-type, on the other hand, enabled us to heat up the sample at 1200°C without any permeation. No traces of ^{4}He were, however, detected probably due to one of three possible reasons: 1)There have been no ^{4}He in the Pd sample from the beginning. 2)^{4}He was degassed away during the 1st heating at 770°C, but could not be detected due to the then insufficient sensitivity. 3)^{4}He still exists in the Pd lattice, but cannot migrate nor diffuse even at 1200°C, forming many trapped tiny bubbles.

1. Introduction

The low intensity of neutron and the small enrichment of tritium in cold fusion experiments have prompted proposals of nuclear processes that yield only heat and helium as products [1, 2]. Determination of the presence or the absence of ^{4}He as a nuclear product became very essential. Until now we clearly observed a large heat burst equivalent to 110% of the input electric power in an electrolysis cell labeled "VI05(941016)". The cell was an open type using Pd/0.1MLiOD/Pt. The excess heat of 6.3W continued for 13min. It amounts to 360W per 1cm^3 of palladium bulk. Neither increase of neutron emission nor that of tritium content in the cell was observed in this case [3].

The electrochemical cell used was a vacuum-insulated open type dewar that was made of Pyrex® glass and PTFE. Palladium cathode (99.80% pure, Johnson Matthey) was screwed together with 1mmϕ platinum wire and fixed in the center of the cell. Pt anode (1mmϕ x 3m) was symmetrically wound around the cathode. Dimension, mass and surface area of the Pd cathode were 2mmϕ x 7.05mm, 0.227g and 0,435cm^2, respectively. It was annealed *in vacuo* up to about 800°C and charged with D in the furnace just before installed in the cell.

Helium and Heat Correlation

Observation through microscope revealed that Pt as well as Pd, near their interface in particular, had been seriously eroded. The Pyrex® glass was found to be cracked near the end of the cathode due to heat, which probably stopped the reaction. The heat of combustion (232J), the heat of absorption (16J) and any other chemical reaction can never account for the excess enthalpy of 5300J that comes from 6.8W lasting for 13min. If the nuclear reactions were assumed as: 1) $D + D \rightarrow {}^4He + \gamma$ (23.8MeV), 2) $D + D + D \rightarrow D + {}^4He + \gamma$ (23.8MeV), the number of nuclear products should be 2.62×10^{11} s^{-1} per Watt, that is, totally 1.39×10^{15} in case of the heat excess of the VI05(941016) cell. It is very clear that the measurement of ^4He should be accomplished coincidentally with the heat burst as we observed.

2. Mass Spectroscopy System

A mass spectroscopy system was thus built to meet this special demand. Effluent gas during electrolysis as well as electrically charged solid palladium samples can be analyzed with high sensitivity and sufficiently good resolving power [4]. Three difficulties are met with, however, in this case: 1) Mass difference between ^4He (4.0026031 amu) and D_2 (4.0282044 amu) is very small (0.0256013 amu). 2) A large amount of D_2 always exists as a background in both gas and solid phase samples. 3) System is very easy to be contaminated with ^4He from other sources like laboratory air (5.24ppm). Special care should be taken to get reliable data by preparing elaborate gas collecting and analyzing systems. Shown in Figure 1 is the schematic drawing of our mass analyzer system.

The vacuum system is composed of three chambers separated by three manually operated gate valves (GV). The whole system can be evacuated by a main turbomolecular pump (TMP:500l/s) as well as by a modified cryopump (CP) at the top. The Q-mass and the cryopump (CP) chambers are usually separated by a CP-GV, but are bridged with two parallel non-evaporable getter (NEG) pump lines and one bypass line. Two NEG pumps (SAES: GP50-W2F installed with C50-ST101) can be used alternately, while the bypass line is opened only when the D_2 signal is necessary for calibration. Pressures in the Q-mass and the CP chambers are measured with a Bayard-Alpert gauge (BA-G) and a cold cathode gauge (CC-G), respectively.

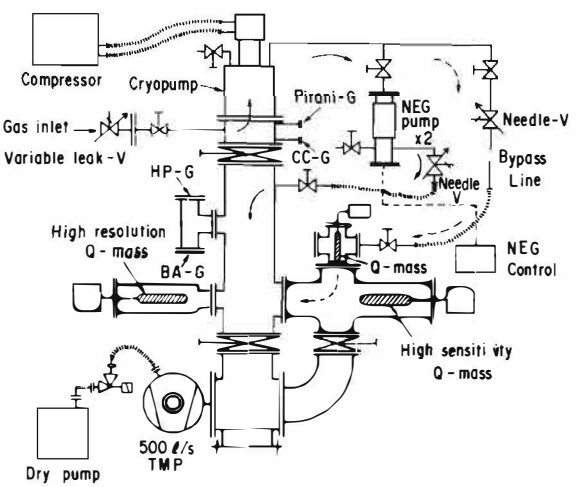

Figure 1. Schematic drawing of the mass analyzer system.

Two types of Q-mass analyzer are used in the Q-mass chamber: a high resolution type (ULVAC: HIRESOM-2SM) and a high sensitivity type (Balzers: QMG112A). Tuning is fixed to mass 4 *M/Z* in the former, while that in the latter is adjusted in the range of 1-22 *M/Z* to monitor the change of gas balance of hydrogen, helium, carbon, water and neon. The differential evacuation is ensured by shutting off the CP-GV and an auxiliary bypass GV. The highest sensitivity can be obtained by putting the main GV in almost close position. As the charcoal absorber is removed from the cryo-panel, our CP has zero pumping speed for noble gases like ^3He, ^4He and Ar. It keeps, however,

a large pumping speed for N_2, O_2 and for water in particular. The NEG pump has, on the other hand, a great pumping effect for hydrogen family. By passing the sample gas through this CP-NEG combined filter we can thus remarkably enrich helium content, if any.

To check the performance, a standard mixture of ^4He (48.6%) and D_2 (51.4%) was prepared. First both signals were obtained by bypassing the NEG filter. Second one NEG pump line was opened with the CP-GV closed, and the same gas was introduced. The peak ratio $I(^4He)/I(D_2)$ was enhanced from $1.45 \times 10^{-9}A/4.55 \times 10^{-9}A = 0.319$ to $3.65 \times 10^{-9}A/1.0 \times 10^{-11}A = 365$ by virtue of a CP-NEG combined filter. An enhancement factor amounts to 1145. On the other hand, according to a factory test [5], the abundance sensitivity of ^4He with respect to D_2 is over 50000, which means in this system we can distinguish 17ppb of ^4He from D_2 [4].

3. Improvement of Sensitivity

QMG112A is about a thousand times more sensitive to mass 4 *M/Z* than HIRESOM-2SM, although a resolution is insufficient to separate ^4He and D_2 signal peaks. As the NEG filter works well to remove the hydrogen gas family (H, D, H_2, HD, T, HT, D_2, DDH, DT and T_2), it can, however, be used to detect a residue of ^3He and ^4He, in continuous-flow mode (See Fig.2(a)).

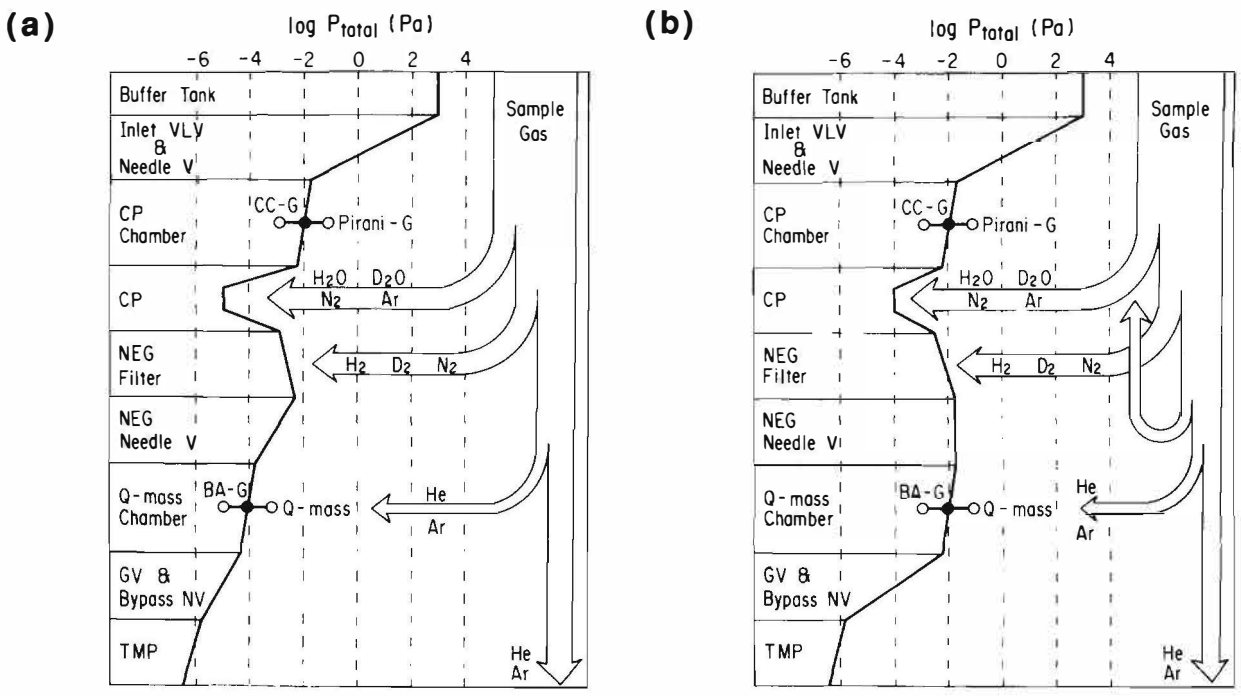

Figure 2. Schematic drawing of flow of sample gas. **(a)** Continuous-flow mode. NEG needle throttled and GV throttled. P_{BA-G} is kept below P_{CC-G}. and **(b)** Store mode. NEG needle throttled and GV almost closed. P_{BA-G} is kept below 10^{-2}Pa. P_{BA-G} can become higher than P_{CC-G}.

As shown in Fig.1, we added needle valves in the NEG filter lines, forming a small but significant modifications to the system originally reported elsewhere [4]. Those needle valves are quantitatively controllable with micrometers. If they are throttled, the flow rate is reduced and the filtering efficiency is very much improved. Escaping probabilities of hydrogen gas family can be, therefore, far more suppressed. Shown in Fig 3 are the signal heights of the high resolution Q-mass versus the entrance pressure measured with CC-G in continuous-flow mode. By using the standard gas, both signals

Helium and Heat Correlation

can be obtained in (a) when the NEG bypass is opened, while D_2 signals are almost completely suppressed in (b) by virtue of the improved NEG filter.

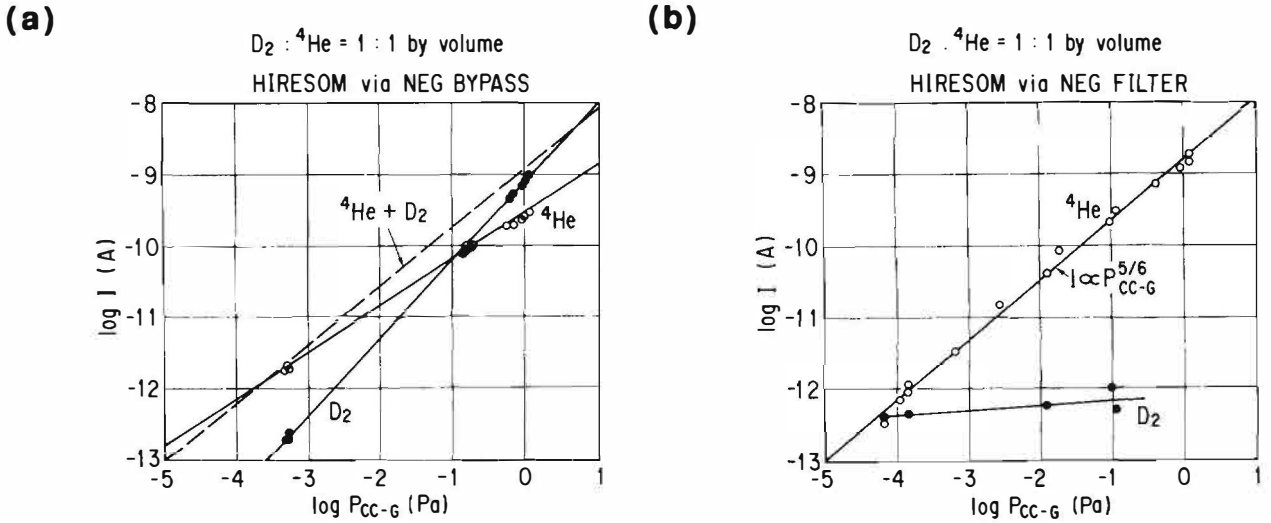

Figure 3. Signal heights of the high resolution Q-mass, HIRESOM-2SM, versus the entrance pressure measured with CC-G.

For comparison, the signal heights of the high sensitivity Q-mass under the same conditions are illustrated in Fig.4 with respect to CC-G pressure. As for M/Z 4, a similar straight line can be obtained over current range extending on three orders of magnitude higher level than that for the high resolution Q-mass. As shown in Fig.3(b) it is now clear that these M/Z 4 signals can be entirely attributed to ^{4}He. This means that, in combination with the NEG and NEG needle valves, the high sensitivity Q-mass provides a detection sensitivity for ^{4}He a thousand times as high as that for the high resolution type. We can expect to distinguish a much smaller amount, only about 17ppb x 10^{-3} = 17ppt, of ^{4}He from D_2. When high mass resolution is required as in case of calibration, the high resolution type can of course be used in store mode, almost closing the main GV, as shown in Fig.2(b).

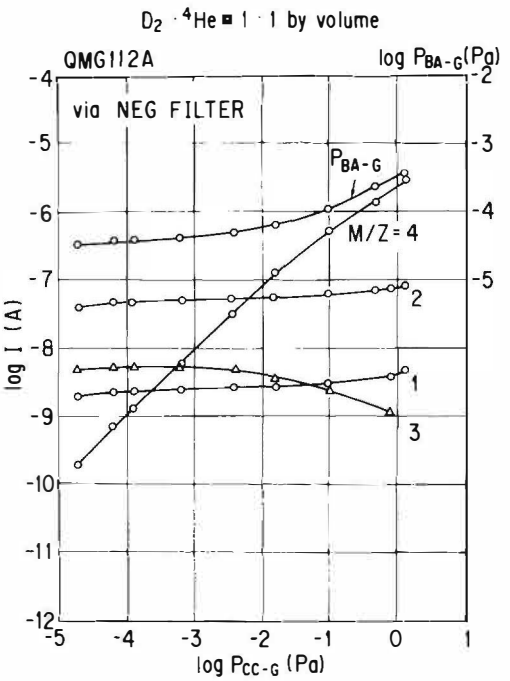

Figure 4. Signal heights of the high sensitivity Q-mass, QMG112A, versus the entrance pressure measured with CC-G in continuous-flow mode.

4. Helium in Effluent Gas?

Preliminarily ^{4}He was observed in the effluent gas collected after the heat burst phenomenon. The detection was, however, not 100% sure due to the possible contamination through PTFE from air [3]. To make it clearer, improvements were made in the gas sampling system as shown in Fig.5 and a new series of electrolysis was started. All PTFE tubing, cocks and glass bottles with plastic caps were replaced by stainless steel flexible hoses, bellow valves, and all-metal or glass-metal combined vessels with Kovar-glass seals. Before use every component was helium leak tested and connected with VCR® joints using nickel gaskets. PTFE and Viton® O rings were only left in a

tee piece, a cock in D_2O feeding line and a double flange of the dewar. On the downstream of the 2nd bubbler, two parallel branches were prepared, consisting of several metal valves, one metal vessel about 130ml in volume and a 3rd bubbler. Before use air in each branch was purged with ›99.9999% pure nitrogen. Each line can be used alternately to ensure successive batch sampling of the effluent gas.

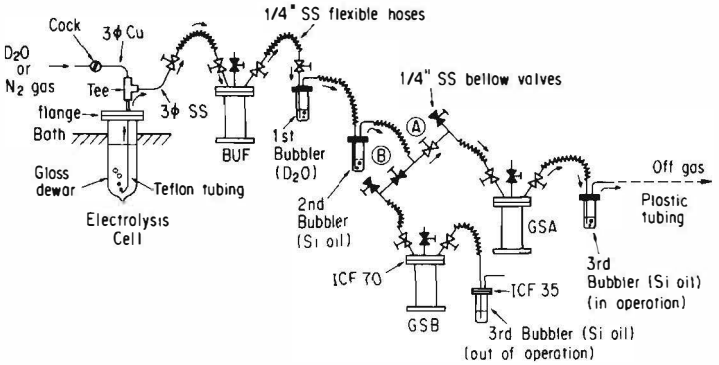

Figure 5. Newly improved gas sampling system.

A very small residue of ^4He can still be detected with our high sensitivity Q-mass system probably due to the contamination from air caused by limited use of PTFE and Viton® as well as by prolonged electrolysis period. Our target is, however, to detect a large amount of ^4He coincidentally. No direct correlation between boiling and ^4He has been found so far. Another heat burst phenomenon is now being expected to make decisive conclusions.

5. Helium in Palladium Cathode Samples?

Soon after the excess heat burst, the Pd cathode sample of the VI05(941016) cell was degassed up to 770°C in a closed vacuum furnace. Then the extruded gas was analyzed in the Q-mass system. No trace of ^4He could be, however, detected in that sample as reported before [3], partly due to the insufficient sensitivity of the old system and the old way of Q-mass analysis. Whether ^4He would be extruded from this Pd sample or not, if it were heated up at much higher temperature, aroused our great interest recently [6].

Experiment was first performed, using an external-heater-type furnace, on another Pd sample that showed boiling several times. The sample was pinched off in a small SUS316 vessel with pure nitrogen gas of 1atm. The vessel was then set in a furnace and connected to a pre-evacuated buffer tank. Furnace temperature was increased up to 1180°C. Results of heat processing with this furnace are summarized in Table I.

The difference of starting pressure is due to volume difference of vessels as well as of buffer tanks used. Pressure minimum observed during heat processing in one of the blank experiments was probably caused by nitriding of inner surface of SUS316. Formation of ammonium radicals might promote this reaction that must be very sensitive to temperature and gas pressure of N_2 and H_2. Above 1000°C pressure began to increase and large amount of ^4He was surely observed in the extruded gas.

Table I. Summary of heat processing with external-heater-type furnaces

Sample	Pd/Pt VI06(950609)	BLANK (Ceramic tube)	BLANK (Ceramic tube)
Type of Furnace	ARF-30M Horizontal hot wall (SUS316)	KM-600 Vertical hot wall (SUS316)	ARF-30M Horizontal hot wall (SUS316)
Carrier Gas	Pure N_2 (B) >99.9995%	Pure N_2 (B) >99.9995%	Pure N_2 (S) >99.9999%
Temperature x Time	1185°C max x 24h	1100°C max x 14h	1190°C max x 24h
Before heat processing	1.11Torr	5.55Torr	1.39Torr
Pressure during h.p. (After 12h of h.p.)	Monotonously increasing (1.9Torr)	Passing through a minimum (5.13Torr)	Monotonously increasing (1.9Torr)
After heat processing	2.62Torr	6.11Torr	2.70Torr

Helium and Heat Correlation

The pressure increase, however, could be mostly attributed to permeation of hydrogen from moisture in air through furnace body made of stainless steel (SUS316). ^{4}He itself could also be attributed to this permeation.

According to a literature [7], activation energy for helium migration is estimated to be very large, (2.06 ± 0.08) eV, for the AISI316 steel (SUS316). Due to the high temperature, however, the SUS316 steel became unstable and changed its structure and properties. Presence of He in it can also induce helium embrittlement. ^{4}He and H could thus penetrate the wall (See Fig.6(a)). Palladium treated in this furnace showed an interesting facetting structure. Ablation of Pd could be observed, too (See Fig.9(a)).

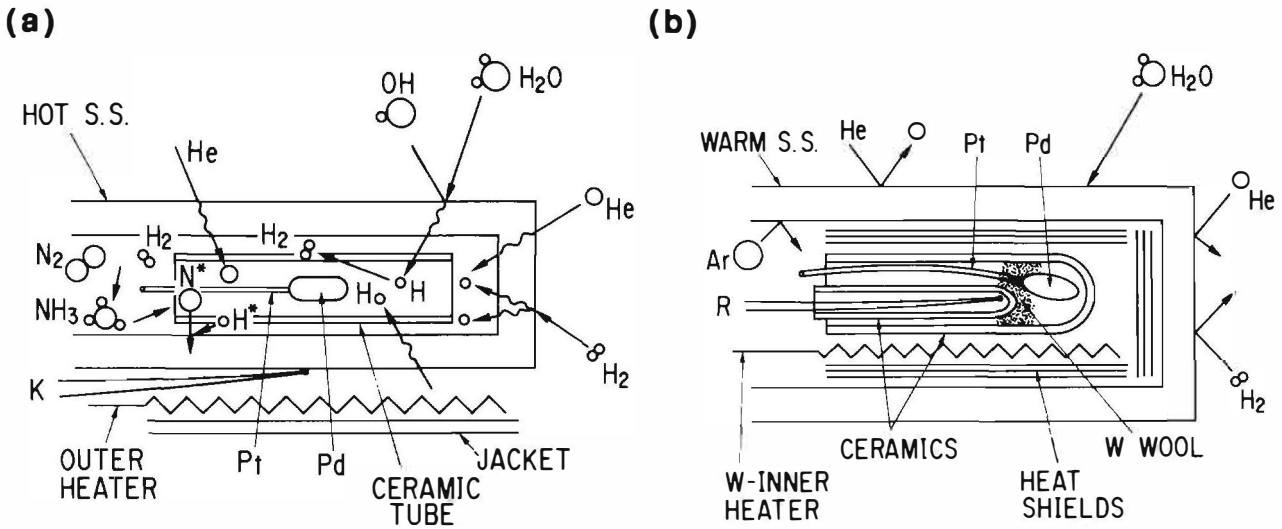

Figure 6. Improvements in heat processing. **(a)** External-heater-type furnace with N_2 as a carrier gas. Although H_2 content in air is one order of magnitude smaller than He, H can be made by dissociation of H_2O from moisture in air. Nitriding of SUS can be realized by ammonium radicals formed by N and H at high temperatures. **(b)** Internal-heater-type furnace with Ar as a carrier gas. Wall temperature of SUS can be kept low by several layers of heat shields.

To prevent contamination by ^{4}He and H from air, improvements have been made in heat processing apparatus. External heater was changed to internal heater made of tungsten that was surrounded by several layers of heat shields. The sample was contained in a ceramic crucible placed in a spiral-shaped W heater. As a carrier gas, ›99.9999% pure Ar was used instead of pure N_2. Nitriding of tungsten heater can be thus avoided even during heat process lasting for about 24h. Before use every component in hot area including crucible was degassed *in vacuo* by using another conventional vacuum furnace.

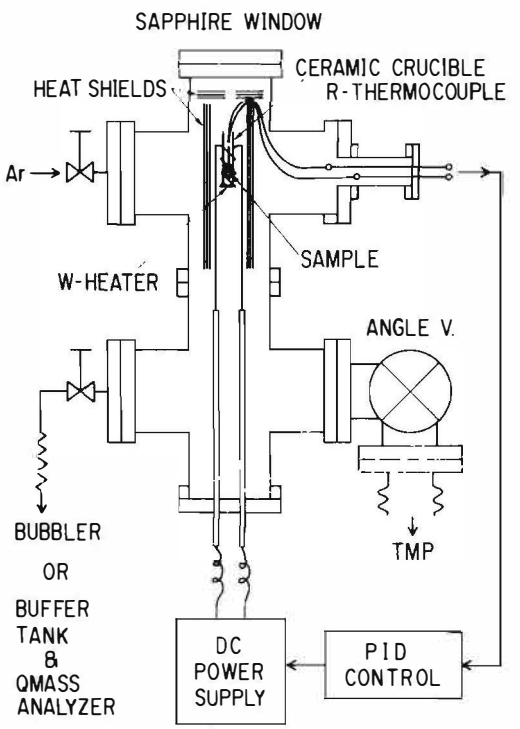

Figure 7. Internal-heater-type furnace.

6. Experimental Results and Discussions

Signal heights of the high sensitivity Q-mass, QMG112A, versus CC-G pressure are illustrated in Fig.8 semi-logarithmically. First a blank experiment was

performed by heating up the furnace, installed with a vacant crucible, up to 1200°C for 24h (①). Second the Pd/Pt cathode sample of VI05(941016) cell was loaded in and heated up under the same conditions. Q-mass analysis has been done twice consecutively (② and ③). Lastly the carrier Ar gas itself was analyzed after being prepared in the same manner but without heat processed (④). Repeated run in ③ presents smaller signal heights only due to the gas consumption. No significant difference is seen in the data except ③. We can thus conclude that no ^{4}He could be detected in the gas sample extruded from the cathode of VI05(941016) cell.

In a non-defective lattice, if helium is trapped at an interstitial site, transport will be controlled by the activation energy for migration between interstitial sites. Although we could not find the very data just on He in Pd, the barrier for this process is generally very high. For example, in case of Ni (fcc), W (bcc) and Mo (bcc), the activation energy for migration of interstitial He and the activation energy for dissociation of He out of a vacancy are 0.1, 2.2 eV; 0.3, 4.2 eV; and 0.2, 3.0 eV, respectively [8]. The significance of such a high value is that migration of He in this manner will be slow even at elevated temperatures.

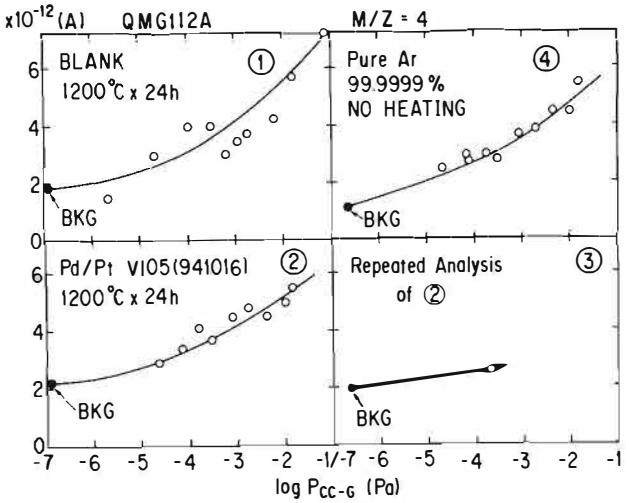

Figure 8. Signal heights of the high sensitivity Q-mass, QMG112A, versus CC-G pressure. The Internal-heater-type furnace was used for heat processing.

According to literature [8, 9], helium in metals precipitates into bubbles due to its insolubility. It means that there is a possibility that 1200°C for 24h is still insufficient for degassing He out of our Pd cathode samples. Microscopic view of the sample that was heat-processed in the internal-heater-type furnace shows clearly a 120° grain growth of Pd and something like tiny bubbles in each grain (See Fig. 9(b)).

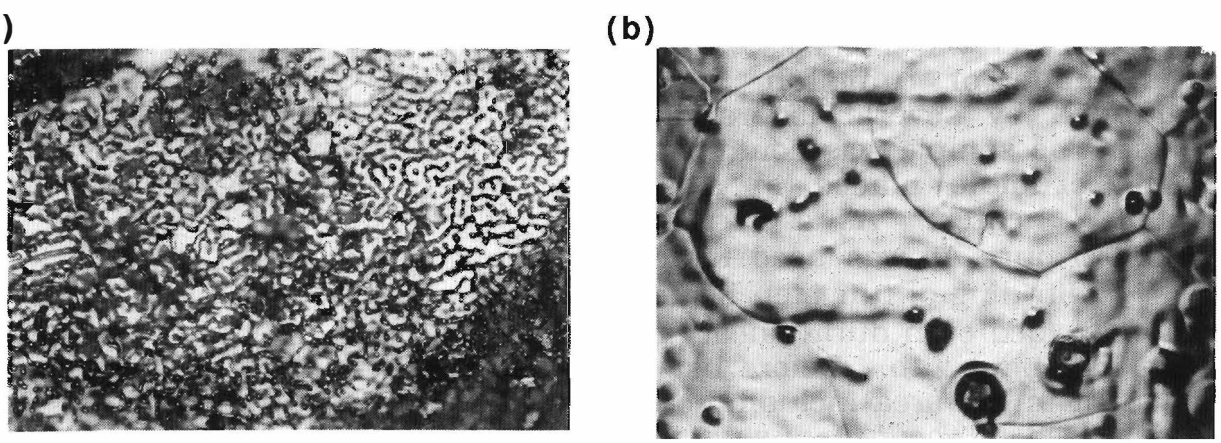

Figure 9. Pd heat processed (a) in N_2 by external-heater-type furnace and (b) in Ar by internal-heater-type furnace.

7. Conclusion

A heat burst equivalent to 110% of the input was observed in an open type electrolysis cell using Pd/0.1M LiOD/Pt. It happened, however, only once in all 5 cells ever tested and seems very difficult to be reproduced. Although boiling has occurred many times in all cells, mainly caused by build-up of cell

voltage in constant current mode, no direct correlation has been found so far between boiling and ^{4}He production.

By reducing the gas flow rate through the NEG filter, the detection sensitivity for ^{4}He could be a thousand times increased. By properly adjusting the pressure gradient, the quantitative analysis of ^{4}He could be realized with high detection sensitivity (17ppt) in continuous-flow mode and with high resolution in store mode.

Two types of closed vacuum furnace were used to degas the Pd samples. In case of an external-heater-type using SUS316 body, analysis proved to be difficult owing to permeation of ^{4}He and H, as well as material instability of SUS316 when the furnace was heated above 1000°C up to 1180°C.

In case of an internal-heater-type, heat processing at 1200°C proved to be possible. No traces of ^{4}He were found in Pd cathode samples showing several times of boiling or involving the heat burst. As the latter sample was once degassed up to 770°C and analyzed with less sensitivity before, three possibilities can be conjectured: 1) There have been no ^{4}He in the Pd sample from the beginning, 2) ^{4}He was degassed away during the 1st heating at 770°C, but could not be detected due to the then insufficient sensitivity, 3) ^{4}He exists in the Pd sample, but cannot move nor diffuse even at 1200°C by forming trapped tiny bubbles in the Pd lattice.

To make it clearer a parallel study of ^{4}He in Pd is now being prepared by ion implantation technique. Another option is of course to process the Pd sample again at much higher temperatures above 1200°C. Anyway to determine the presence or absence of ^{4}He as a nuclear product in effluent gas and/or palladium cathode, it becomes far more essential to reproduce the another excess heat burst as clearly observed before [3].

Acknowledgements

Continuing encouragement of Professors H. Sugawara, Y. Kimura and K. Takata are gratefully acknowledged. Thanks are also due to E. Komoda of Hakuto Co. Ltd. for kindly lending a high-sensitivity Q-mass analyzer for this experiment. This work is partially supported by the Thermal & Electric Energy Technology Foundation.

References

[1] Takahashi, A., J. Nucl. Sci. and Tech., **26** (1989) pp558-560.
[2] Becker, E. W., Naturwissenschaften, **76** (1989) 214.
[3] Isagawa, S., Kanda,Y. and Suzuki, T., Proc. of 5th International Conf. on Cold Fusion, Monte-Carlo, Monaco, April 9-13, 1995, pp124-131.
[4] Isagawa, S., Proc. 13th International Vacuum Conf. 9th International Conf. on Solid Surfaces, Yokohama, Japan, September 25-29, 1995, Vacuum **47** (1996) pp497-499.
[5] Yanagishita, K., private communication.
[6] Arata, Y. and Zhang, Yue-Chang, Koh-on gakkaishi **21** (1995) pp303-306 [in Japanese].
[7] Sekiguchi, H. et al., "Diffusion of He in Austenitic stainless steels studied by TDPAC", J. Nucl. Mater. **133/134** (1985) 468.
[8] Scilling, W., "Diffusion of Helium in Metals", In *Point Defects and Defect Interactions in Metals,* Yamada Science Foundation, University of Tokyo Press, 1982, pp303-308.
[9] Donnelly, S. E. and Evans, J. H., *Fundamental Aspects of Inert Gases in Solids,* NATO ASI Series Vol **279**, 1991, Plenum Press.

Helium and Heat Correlation

Heat and Helium Measurements Using Palladium and Palladium Alloys in Heavy Water

Melvin H. Miles and Kendall B. Johnson

Chemistry & Materials Branch, Research & Technology Division
Naval Air Warfare Center Weapons Division
China Lake, CA 93555-6100, USA

and

M. Ashraf Imam

Physical Metallurgy Branch, Materials Science & Technology Division
Naval Research Laboratory
Washington, DC 20375-5320, USA

Abstract
Excess power was measured in 28 out of 94 electrochemical experiments conducted using palladium or palladium-alloy cathodes in heavy water. Reproducibility continues to be the major problem in this controversial research area. Based on our experiments, this lack of reproducibility stems from unknown variables in the palladium metal. The best reproducibility for excess power was obtained using palladium-boron alloy materials supplied by the Naval Research Laboratory (NRL), Washington, DC. A high success ratio was also obtained using Johnson-Matthey materials. Calorimeters that are capable of detecting excess power levels of 1 watt per cubic centimeter of palladium are essential for research in this field. Results from our laboratory indicate that helium-4 is the missing nuclear product accompanying the excess heat. Thirty out of 33 experiments showed a correlation between either excess power and helium production or no excess power and no excess helium. The only valid experiments that showed significant excess power but no excess helium involved a Pd-Ce cathode. The collection and analysis of the electrolysis gases place the helium-4 production rate at 10^{11} to 10^{12} atoms per second per watt of excess power. This is the correct magnitude for typical deuteron fusion reactions that yield helium-4 as a product.

1. Introduction

The objective of our program was to investigate anomalous effects in deuterated systems and answer two basic questions: (1) Is the apparent excess power real? and (2) If so, can it be reproduced regularly? The answer to the first question, based on our research is yes, but the answer to the second question is no. The lack of reproducibility has made this research exceedingly difficult. This report examines the possible production of excess power and helium-4 during the electrolysis of heavy water (D_2O) using palladium (Pd), palladium-cerium (Pd-Ce), and palladium-boron (Pd-B) alloys as cathodes.

2. Experimental

Excess power measurements involved the electrolysis of D_2O + LiOD in open isoperibolic calorimeters. A detailed discussion of this calorimetry has been published.[1] In June of 1995, Roger M. Hart, founder of Hart R and D Inc., Mapleton, Utah, and an expert in the design, construction, and testing of calorimeters visited our laboratory. After carefully examing our calorimetric design and techniques, he agreed with our stated error range of ±20 mW or ±1% of the input power, whichever is larger. This is especially true over our normal operating temperature

Approved for public release; distribution is unlimited.

range of 40 to 60°C for the cell temperature. At higher temperatures, nonlinear effects such as heat transport by radiation and by the evaporation of D_2O become larger. At low cell temperatures, the fraction of heat lost through the top of the cell becomes larger.

Three compositions of Pd-B alloy were prepared and characterized at NRL. The three alloy compositions had nominal boron concentrations of 0.75, 0.50, and 0.25 weight % boron. The glow-discharge mass spectroscopic analyses showed the three alloy compositions actually contained 0.62, 0.38, and 0.18 weight percent boron. X-ray diffraction studies showed two distinct phases of the same cubic structure in all three compositions of the alloy.[2] The palladium-cerium alloy tested was obtained from M. Fleischmann of IMRA Europe.

Experimental procedures for the collection of electrolysis gas samples and subsequent analysis for helium-4 have been previously reported.[3]

3. Results

The best reproducibility of the excess power effect was obtained using Pd-B alloys supplied by NRL. Seven out of eight experiments that used Pd-B cathodes produced excess power. The excess power measurements for our first experiment using a Pd-B cathode is shown in Figure 1. The excess power averaged about 100 mW during the second half of this experiment. This cathode was prepared as 0.75 weight % boron and had a 6-mm diameter and a 2.0 cm length with rounded ends. This Pd-B experiment was turned off and then restarted 8 days later. Excess power was again observed similar to the first experiment.[4] This demonstrates that excess power can be obtained in repeated experiments using the same cathode.

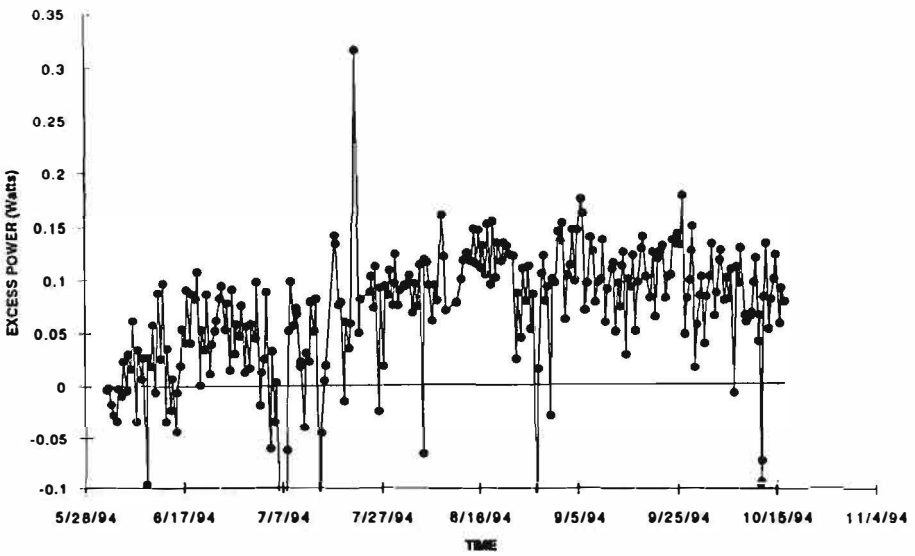

Figure 1. Excess Power Measurements for an NRL Palladium-Boron Rod (6.0 mm x 2.0 cm, 0.75 weight % boron), Cell B.

The next two studies of NRL Pd-B alloys showed excess power in one experiment, but no significant effect in the other experiment. These measurements are shown in Figures 2 and 3. The excess power for cell C showed a gradual increase with time and reached levels exceeding 300 mW (Figure 2). The second cell run in series (cell D) showed fluctuations mainly within ±50 mW and no significant production of excess power (Figure 3). There was clearly no gradual increase of excess power as shown in Figure 2. It was noted at the beginning of this experiment that the cathode in cell D was poorly aligned. This leads to an uneven current distribution and low loading of deuterium into the cathode. After this experiment, examination of the Pd-B cathode that did not produce excess power (cell D) showed an obvious flaw. Swaging of this rod had produced a large, folded-over metal region that would act as a long crack. In contrast, the heat-producing Pd-B cathode had no obvious flaws or cracks. Both cathodes consisted of 0.75 weight % B, with a rod

Helium and Heat Correlation

diameter of 2.5 mm and a length of 2.5 cm (V = 0.12 cm^3). The end of the heat-producing electrode was left straight, while the end of the other cathode was rounded using a file. No helium measurements were performed for these experiments or for any later experiments, because we were directed to focus only on the excess-heat effect during the last year of this program.

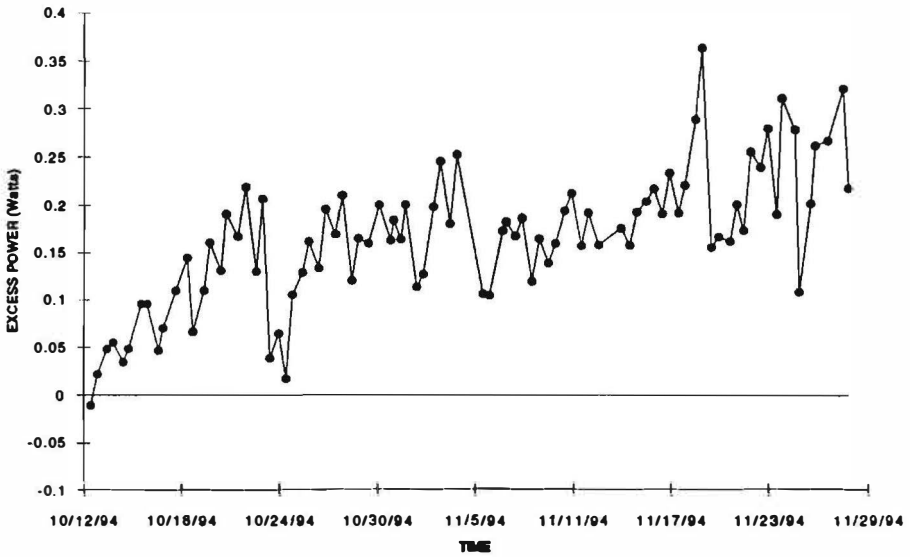

Figure 2. Excess Power Measurements for an NRL Palladium-Boron Rod (2.5 mm x 2.5 cm, 0.75 weight % boron), Cell C. A gradual increase in the excess power was observed. No flaws were visible for this cathode.

The next series of Pd-B alloy studies explored the effect of lower boron concentrations. Two studies of the 0.5 weight % boron alloy gave a fairly steady excess power effect after 11 days of electrolysis with typical levels of 50 to 100 mW.[4] Results for the 0.25 weight % boron alloys yielded excess power averages of about 100 mW for one cell with peaks of 150 to 200 mW.[4] In contrast, the other cell showed only a 5-day period of excess power early in the experiment and then no other episodes of significant excess power.[4] There was no clear relationship between the production of excess power and the boron concentration of the alloy. Results for deuterium loading into Pd-B alloys are presented elsewhere.[4,5]

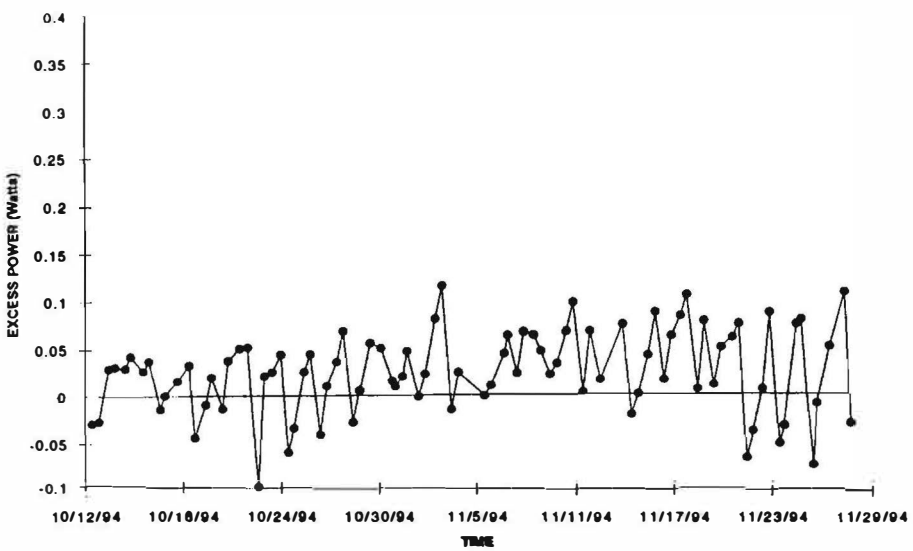

Figure 3. Experiment Showing No Significant Excess Power for an NRL Palladium-Boron Rod (2.5 mm x 2.5 cm, 0.75 weight % boron), Cell D. This rod contained a folded-over metal region that would act as a long crack.

Helium and Heat Correlation

The 0.5 and 0.25 weight % boron alloys all had dimensions of 4 mm x 2 cm (V = 0.25 cm^3). Microscopic examinations of these four Pd-B cathodes following the experiments did not reveal any significant cracks, folded-over metal regions, or other flaws for these NRL materials. The high-success rate for excess-power production for Pd-B alloys suggests that this would be a fruitful area for further research. Perhaps the presence of B initially as an impurity in the palladium or the incorporation of B from the glass into the palladium during the experiment is a factor in the reproducibility problem for excess-heat production. It is also possible that the increased hardness of the palladium due to the added B allows it to better withstand the high stresses induced by the experiments.

A Pd-Ce alloy material was provided to us by Martin Fleischmann. The experiment using this cathode began on 15 February 1994 and the onset of excess power production was observed on 4 March 1994. The excess power versus time for the Pd-Ce cathode is displayed in Figure 4. The excess power levels for this cell reached values as high as 350 mW or 1.1 W/cm^3. The excess power production for Pd-Ce remained for over 100 days of electrolysis. A repeated run with the same Pd-Ce cathode again showed excess power levels up to 150 mW.

A puzzling helium result was obtained for the Pd-Ce cathode that produced the large excess power effect shown in Figure 4. Despite excess power measurements as large as 300 mW, no excess helium could be detected. These results are presented in Table 1. The companion cell employing a NRL Pd rod gave no excess power and almost the same amount of helium-4 (4.6 ±1.4 ppb) as found for the Pd-Ce experiment. This represents our only studies where valid excess power was measured but no excess helium was detected. An earlier experiment using a palladium cathode yielded 11% excess power (290 mW) but no detectable helium.[6] This 1990 experiment, however, was flawed due to a very low D_2O level in the cell.[6] Later experiments showed that this low D_2O level could produce a calorimetric error that would account for most of the reported excess power. There were no other palladium cathodes in 33 studies that did not show a correlation between excess power and helium production or no excess power and no excess helium.

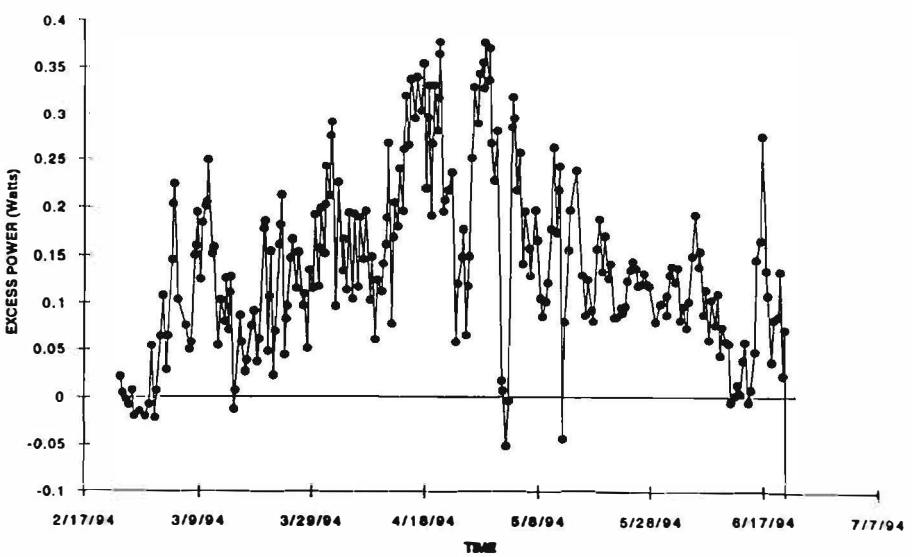

Figure 4. Excess Power Measurements for a Palladium-Cerium Alloy Rod (4.1 mm x 1.9 cm) Obtained From Martin Fleischmann, Cell C. Excess power peaks of 350 mW were observed.

Helium and Heat Correlation

TABLE 1. Excess Power and Helium Measurements in Experiments Using a Palladium-Cerium Cathode.

Electrode	Flask/cell, date	$^4He^a$, ppb	Px, W	$^4He/s \cdot W^b$
Pd-Ce Rod[c] (4.1 mm x 1.9 cm)	1/C (3/30/94)	4.6 ±1.4	0.17	0
Pd-Ce Rod[c] (4.1 mm x 1.9 cm)	4/C (4/19/94)	4.7 ±1.3	0.30	0
NRL Pd Rod[c] (4.1 mm x 1.9 cm)	3/D (3/30/94)	4.6 ±1.4	0	...
NRL Pd Rod[c] (4.1 mm x 1.9 cm)	2/D (4/19/94)	>1000[d]	0	...

[a] Metal collection flasks, analysis by U.S. Bureau of Mines, Amarillo, Texas.
[b] Corrected for background helium level of 4.5 ±0.5 ppb.
[c] D_2O + LiOD (I = 600 mA).
[d] Broken solder joint on metal flask.

One Johnson-Matthey palladium sample (1-mm wire) had previously given both excess heat and helium production at China Lake. There was an ample supply of this wire, hence the final experiments outlined for our laboratory by our sponsor were to use this wire. Four experiments using this palladium wire with our standard calorimeters were completed at China lake as the final segment of our program.[4] Excess power was obtained in one of these experiments. As shown in Figure 5, the excess power effect for this cell peaked at about 250 to 300 mW or 10% above the input power. There was a consistent excess power effect for this cell over most of the experiment. Turning the cell off for 3 days and then back on showed normal behavior, hence the excess power was not due to any calibration changes in the cell. A second calibration check was performed about 2 weeks later as shown in Figure 5. The experimental protocol used in the four Pd-wire experiments was to run at 100 mA/cm^2 for a day and then at 200 mA/cm^2 for 10 days. Calorimetric measurements were made at the normal cell operating current of 400 to 600 mA (1000 to 1500 mA/cm^2). The higher current density used for these small cathodes (A = 0.32 cm^2, V = 0.016 cm^3) is consistent with the higher power density of 15 W/cm^3 that was obtained. Most of our experiments yield about 1 watt of excess power per cubic centimeter of palladium at 100 to 200 mA/cm^2.

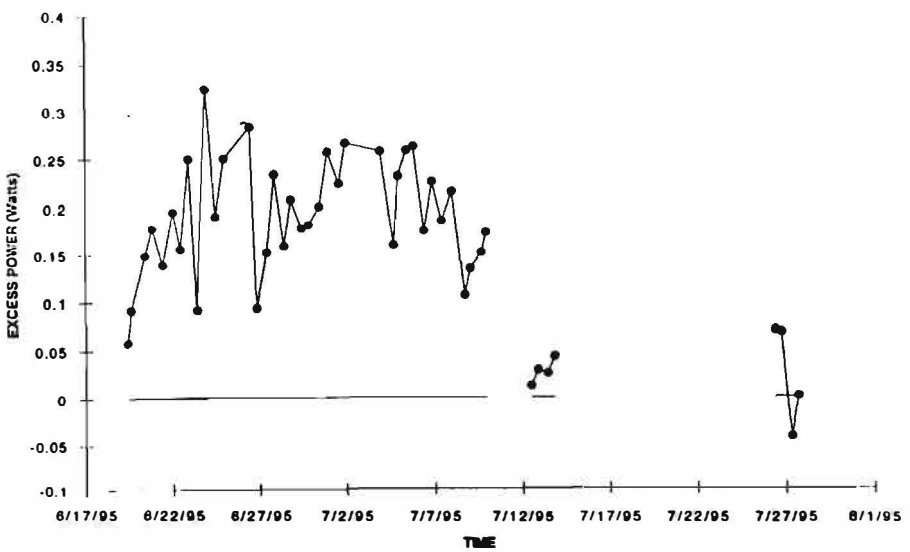

Figure 5. Excess Power Measurements for a Johnson-Matthey Palladium Wire (1 mm x 2.0 cm), Cell C. Significant excess power exceeding 200 mW was consistently observed. Calibrations checks following this experiment verify the excess power observations.

Helium and Heat Correlation

4. Discussion

Fifteen experiments were completed where metal flasks were used in place of glass flasks to collect electrolysis gas samples for helium analysis. The use of metal flasks prevents the diffusion of atmospheric helium into the flasks after they are sealed. The valves used in these flasks were modified to effect a metal seal with a nickel gasket.

Six experiments using metal flasks where no excess power was measured are shown in Table 2. These samples were all from experiments that never produced any evidence for excess heat. The mean value of 4.5 ±0.5 ppb ^{4}He show that our experimental procedures are very consistent. The two Pd-Ce experiments shown in Table 1 fit in well with this mean value, hence no excess helium was produced.

In experiments producing excess power, seven helium measurements using these same four metal flasks were completed. Results for these experiments are given in Table 3. These results are all for experiments where steady, consistent excess power effects were measured. For example, the Pd-B rod results in Table 3 are for the experiment shown in Figure 1. Unlike the Pd-Ce alloy (Table 1), excess helium was measured for the Pd-B alloy. This was the only helium measurement conducted for the Pd-B alloy studies. After correcting for the background level of helium measured in Table 2 (4.5 ppb or 5.1 x 10^{13} atoms/500 mL), each experiment in Table 3 yields a helium-4 production rate close to 1 x 10^{11} ^{4}He/s•W. These results using metal flasks are consistent with our previous helium results using glass flasks.[6]

TABLE 2. Helium Measurements in Control Experiments Using Metal Flasks. No excess power was measured.

Electrode	Flask/cell, date	^{4}He[a], ppb	^{4}He, atoms/ 500 mL
Pd Rod[b] (4 mm x 1.6 cm)	1/C (2/24/93)	4.8 ±1.1	5.5 x 10^{13}
Pd-Ag Rod[b] (4 mm x 1.6 cm)	2/D (2/24/93	4.6 ±1.1	5.2 x 10^{13}
Pd Rod[b] (4 mm x 1.6 cm)	3/C (2/28/93)	4.9 ±1.1	5.6 x 10^{13}
Pd-Ag Rod[b] (4 mm x 1.6 cm)	4/D (2/28/93)	3.4 ±1.1	3.9 x 10^{13}
Pd Rod[c] (1 mm x 1.5 cm)	3/C (7/7/93)	4.5 ±1.5	5.1 x 10^{13}
Pd Rod[d] (4.1 mm x 1.9 cm)	3/D (3/30/94)	4.6 ±1.4	5.2 x 10^{13}
(Mean)		4.5 ±0.5	(5.1 ±0.6 x 10^{13})

[a] Helium analysis by U.S. Bureau of Mines, Amarillo, Texas.
[b] D_2O + LiOD (I = 500 mA).
[c] H_2O + LiOH (I = 500 mA).
[d] D_2O + LiOD (I = 600 mA).

Helium and Heat Correlation

TABLE 3. Helium Measurements Using Metal Flasks.
Experiments producing excess power.

Electrode	Flask/cell, date	$^4He^a$, ppb	Px, W	$^4He/s \cdot W^b$
Pd Sheet[c] (1.0 mm x 3.2 cm x 1.6 cm)	3/A (5/21/93)	9.0 ±1.1	0.055	1.6×10^{11}
Pd Rod[c] (1 mm x 2.0 cm)	4/B (5/21/93)	9.7 ±1.1	0.040	2.5×10^{11}
Pd Rod[c] (1 mm x 1.5 cm)	1/C (5/30/93)	7.4 ±1.1	0.040	1.4×10^{11}
Pd Rod[c] (2 mm x 1.2 cm)	2/D (5/30/93)	6.7 ±1.1	0.060	7.0×10^{10}
Pd Rod[d] (4 mm x 2.3 cm)	1/A (7/7/93)	5.4 ±1.5	0.030	7.5×10^{10}
Pd Rod[d] (6.35 mm x 2.1 cm)	2/A (9/13/94)	7.9 ±1.7	0.070	1.2×10^{11}
Pd-B Rod[d] (6 mm x 2.0 cm)	3/B (9/13/94)	9.4 ±1.8	0.120	1.0×10^{11}

[a] Helium analysis by U.S. Bureau of Mines, Amarillo, Texas.
[b] Corrected for background helium level of 5.1×10^{13} ^4He/500 mL.
[c] D_2O + LiOD (I = 400 mA).
[d] D_2O + LiOD (I = 500 mA).

For our 33 experiments involving heat and helium measurements, excess heat was measured in 21 cases and excess helium was observed in 18 studies. Thus 12 experiments yielded no excess heat and 15 measurements gave no excess helium. If one uses these experimental results as random probabilities of $P_h = 21/33$ for excess heat and $P_{He} = 18/33$ for excess helium, then the probability of random agreement (P_a) for our heat and helium measurements would be

$$P_a = P_h \bullet P_{He} + (1 - P_h)(1 - P_{He}) = 0.512 \quad (1)$$

and the probability of random disagreement (P_d) would be $P_d = 1 - P_a = 0.488$. The presence or absence of excess heat was always recorded prior to the helium measurement and was not communicated to the helium laboratory. Based on our experimental results, the random probability of the helium measurement correlating with the calorimetric measurement is not exactly one-half. This is analogous to flipping a weighted coin where heads are more probable than tails. The probability of exactly three mismatches in 33 experiments, therefore, would be

$$P_3 = \frac{33!}{30!3!}(0.512)^{30}(0.488)^3 = 1.203 \times 10^{-6} \quad (2)$$

Similar terms can be calculated for two ($P_2 = 1.221 \times 10^{-7}$), one ($P_1 = 8.009 \times 10^{-9}$), or zero ($P_0 = 2.546 \times 10^{-10}$) mismatches in 33 experiments. The total probability of three or less mismatches in 33 studies would be

$$P = P_3 + P_2 + P_1 + P_0 = 1.333 \times 10^{-6} = \frac{1}{750{,}000} \quad (3)$$

This statistical treatment shows that the odds are approximately one in 750,000 that our complete set of heat and helium results could be this well correlated due to random experimental errors in our calorimetry and helium measurements. Furthermore, it is very unlikely that random errors would consistently yield helium-4 production rates in the appropriate range of 10^{11} - 10^{12} atoms/s per watt of excess power as given in Table 3.

Helium and Heat Correlation

Finally, the three mismatches are the two Pd-Ce experiments given in Table 1, and the flawed 1990 calorimetric measurement where the D_2O level was much too low. Critics should carefully consider the probabilities presented in Equations 2 and 3 before dismissing this new science of anomalous effects in deuterated materials.[4,7]

TABLE 4. Summary of Palladium Materials Tested for Excess Power.

Source	d, cm	V, cm^3	Px/V, W/cm^3	Success ratio	
NRL Pd-B (0.75%)	0.6	0.57	0.6	2/2	
NRL Pd-B (0.75%)	0.25	0.12	2.1	1/2	(7/8)
NRL Pd-B (0.50%)	0.40	0.25	0.4	2/2	
NRL Pd-B (0.25%)	0.40	0.25	0.8	2/2	
JM Pd	0.63	0.36	1.4	9/14	
JM Pd	0.63	0.67	0.3	1/1	
JM Pd	0.40	0.20	0	0/2	(17/28)
JM (F/P) Pd	0.20	0.038	3.1	1/1	
JM (F/P) Pd	0.10	0.012	14.0	1/1	
JM Pd	0.10	0.02	15.0	3/7	
JM Pd-Ce (F/P)	0.41	0.25	1.1	2/2	
NRL Pd	0.40	0.25	0.4	1/2	(2/5)
Tanaka Pd sheet	...	0.05	1.2	1/3	
NRL Pd	0.40	0.25	0	0/4	
NRL Pd-Ag	0.42	0.21	0	0/3	
IMRA Pd-Ag	0.40	0.20	0	0/2	(0/19)
WESGO Pd (1989)	0.14	0.09	0	0/6	
Pd/Cu	(0.63)	0.02	0	0/2	
John Dash Pd sheet	...	0.04	0	0/2	
Co-deposition (1992)	(0.63)	0.002	75	2/34	

Most of the palladium materials investigated at China Lake are summarized in Table 4. Distinct groupings of the success ratio are readily apparent based on the source of the palladium material. A high-success ratio is found for Johnson-Matthey materials where 17 out of 28 studies gave excess heat. The highest success ratio is for NRL Pd-B materials that showed excess power in seven out of eight experiments. Other NRL materials, however, gave poor results, such as NRL Pd-Ag (0/3) and NRL Pd (1/6). The single excess-heat result for NRL Pd involved a second run of the same cathode. Several other Pd and Pd-Ag sources failed to yield any excess heat-producing

experiments. This polarization of successful experiments according to the palladium source would be very difficult to explain by random calorimetric errors. These results indicate that the metallurgical preparation of palladium is a major factor for observation of the excess enthalpy effect. A similar conclusion concerning reproducibility of the excess-power production has been reported by McKubre et al.[8] Our results suggest that the presence of boron within the palladium may be a critical variable.

5. Summary

This field of anomalous effects in a deuterated system, which has come to be called "cold fusion," is a far more difficult research area than we might have thought 7 years ago. Progress at various laboratories around the world has not been as rapid as one might have hoped. Two technically challenging problems restrict progress: (1) irreproducibility and (2) scarcity of energetic (nuclear) products.

Although we have not succeeded in solving the irreproducibility problem, our results indicate that helium-4 is the missing nuclear product. This ^{4}He is the most likely nuclear product that could have remained so well hidden during the past 7 years.

The remarkable correlation of excess power with the source of palladium in Table 4 cannot be easily explained by any calorimetric errors. Furthermore, 30 experiments at our laboratory have shown a striking correlation between either excess power and helium production or no excess power and no excess helium. It is highly unlikely that our heat and helium correlations could be due to random errors. Finally, our calorimetric results, conclusions, and problems are practically identical to those reported by the SRI laboratory. In our opinion, these factors provide compelling evidence that the anomalous effects measured in deuterated systems are real.

This research area has the potential to provide the human race with a nearly unlimited new source of energy. Although our program is no longer funded, we hope that other scientists will continue to investigate this difficult research area until the challenging problems impeding progress are solved. It is still possible that anomalous effects in deuterated systems will prove to be one of the most important scientific discoveries of this century.

6. Acknowledgments

The authors thank D. Miles of the Naval Air Warfare Center Weapons Division for many helpful computer calculations and data analyses, R. Hart from Hart R and D Inc., H. Bergeson and S. Barrowes from the University of Utah, and W. Hansen from Utah State University for many helpful discussions. We also thank M. Fleischmann and S. Pons of IMRA Europe for the loan of electrode materials as well as helpful discussions. Appreciation is extended to the Office of Naval Research for support of this work.

7. References

1. M. H. Miles, B. F. Bush, and D. E. Stilwell, *J. Phys. Chem.*, **98**, 1948 (1994).
2. D. D. Dominguez, P. L. Hagans, and M. A. Imam, "A Summary of NRL Research on Anomalous Effects in Deuterated Palladium Electrochemical Systems," Report Number NRL/MR/6170-96-7803, January 9, 1996.
3. M. H. Miles and B. F. Bush, *Trans. Fusion Tech.*, **26**, 156 (1994).
4. M. H. Miles, B. F. Bush, and K. B. Johnson, "Anomalous Effects in Deuterated Systems," NAWCWPNS TP 8302 (September 1996).
5. K. B. Johnson and M. H. Miles in Proceedings of the Sixth International Conference on Cold Fusion, Hokkaido, Japan, 13-18 October 1996 (submitted).
6. M. H. Miles, B. F. Bush, and J. J. Lagowski, *Fusion Technol.*, **25**, 478 (1994).
7. M. H. Miles, J. Phys. Chem. (submitted).
8. M. C. H. McKubre, S. Crouch-Baker, A. K. Hauser, S. I. Smedley, F. L. Tanzella, M. S. Williams, and S. S. Wing in Proceedings of the Fifth International Conference on Cold Fusion, Monte Carlo, Monaco, 9-13 April 1995, pp. 17-33.

Helium and Heat Correlation

Click here for a more readable copy of this paper.

Measurements of ^4He Production from D_2 gas-loaded Pd Sample

E. Botta[1], T. Bressani[1,2], D. Calvo[1], C. Fanara[1,3], F. Iazzi[1,4]

[1] INFN, Sezione di Torino, I-10125, Torino, Italy
[2] Dipartimento di Fisica Sperimentale, Università di Torino, I-10125, Torino Italy
[3] Fiat Avio, I-10129, Torino, Italy
[4] Dipartimento di Fisica del Politecnico di Torino, I-10129, Torino Italy

Abstract
A Pd sheet gold plated at both ends was loaded with D_2 in a Cold Fusion cell operating on the basis of the Coehn effect. The procedure was the same followed in a previous experiment. The gas has been analyzed by means of a high resolution mass spectrometer before the absorption into Pd and after desorption: a significant presence of ^4He after desorption has been measured, in agreement with the previous results.

1.Introduction

In the frame of the Cold Fusion research, the aim of the Torino group was always to search for signatures of nuclear reactions occurring inside D-Metal systems.
Following this line, after a set of experiments devoted to the detection of 2.45 MeV neutrons [1, 2] with a suitably designed detector [3, 4, 5], the efforts were directed to the measurement of the ^4He content in the D_2 gas after absorption and desorption from a Pd metal lattice.
Since in the scientific debate about Cold Fusion it is generally accepted that the atomic ratio α = [D]/[Pd] plays a quite crucial role for the positive measurement of neutron production, ^4He content and heat excess, a particular care has been devoted to the technique of loading the Pd lattice with D over the thermodynamical value $\alpha = 0.67$. The Torino group has chosen a technique based on the Coehn effect that allows the d^+ ions to move along a Pd conductor toward the cathode.
A cell has been designed and constructed to take advantage of this effect in order to accumulate the Deuterium in a volume near the cathode, up to values of α greater than 0.67. The complete apparatus has been already described [6] and results of a first set of measurements (dedicated mainly to explore the best operating parameters) were shown during the ICCF5 (1995) Conference. The following main conclusions were reached in those measurements: a) the electromigration of d^+ ions (Coehn effect) could be applied to gas loaded Pd sheets and seemed to be effective to speed up the loading of D_2 into Pd up to $\alpha \approx 0.7$; b) higher gas pressure and accurate polishing of the Pd surface helped the absorption; c) the temperature of the Pd sample should not exceed 70 °C in order to avoid thermomechanical troubles.
The D_2 gas desorbed from two different Pd samples was analyzed by means of a high resolution mass spectrometer and in one case an amount of $7.5 \cdot 10^{16}$ ^4He atoms was observed, roughly corresponding to a specific power of ≈ 25 W/cm^3.
In the experiment we are presenting here, the experimental set-up was the same (a part for some small modifications in the vacuum circuit) and the Pd sheet used was shaped and gold plated following the indications obtained in the previous experiment. Four values of the

electric field were applied to the Pd sample for different time intervals and after the last two absorption-desorption runs, the gas was analyzed and the ^4He content was measured by the high resolution mass spectrometer.

2.Experimental apparatus and calibrations

The experimental apparatus has been completely described in a previous paper [6]; only the main features are reported here. The cell (166±1 cm^3 volume), containing a Pd sheet clamped by two copper electrodes (see fig.1), is connected to a vacuum circuit (3900±5 cm^3) equipped with two Turbomolecular pumps and a mass spectrometer (ULVAC HI-RESOM 2SM) with resolution M/ΔM=200 (see fig.2).

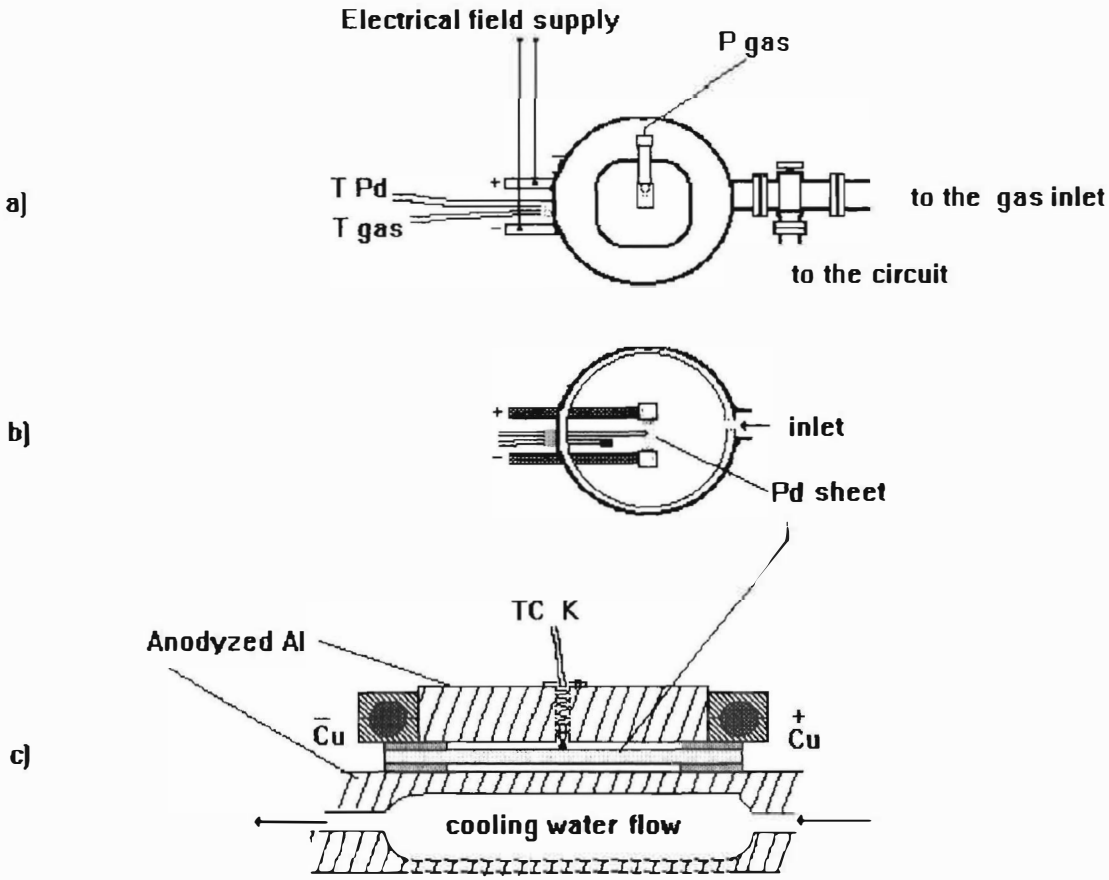

Fig. 1 Cell layout (not in scale); a) External top view, b) Internal top view (upper cover removed), c) lateral view.

To ensure a good quality of the measurements, a particular care has been taken in the vacuum control of the circuit and in the calibration of the instrument. Several days of degassing led to an overall residual pressure of $2 \cdot 10^{-6}$ mbar. The switching-off of the pumps brougth to $2 \cdot 10^{-5}$ mbar in two hours, a value that remained quite constant over two days, proving then the tightness of the circuit. The calibration of the spectrometer was performed introducing at subsequent times a known amount of ^4He into the analyzing tube and recording the peak heights (i.e. the ionic currents) and the pressure in the region M/e=3.9÷4.1.

Helium and Heat Correlation

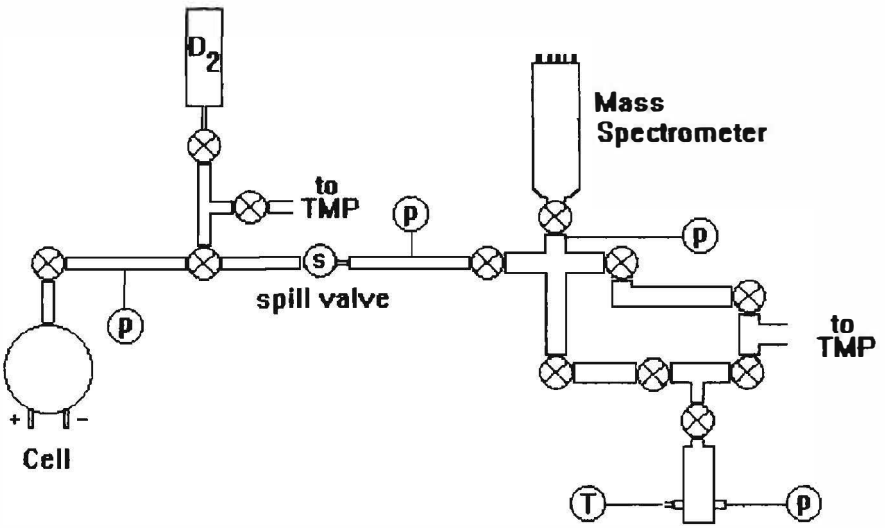

Fig.2 Experimental apparatus: vacuum circuit, Coehn Cell and mass spectrometer. (TMP = Turbomolecular pump, T = Thermocouple, P=pressure gauges).

The sensitivity, defined as the ratio between current and partial pressure value, calculated from repeated measurements, gave a mean value of $\varepsilon = (2.20\pm0.17)\cdot10^{-4}$ A/mbar, showing a quite good stability of the instrument. The pressure range variation of these measurements, between $2\cdot10^{-5}$ and $1\cdot10^{-4}$ mbar, was the same during the experiment.

3.Results and Discussion

A Pd sheet ($8\times1\times1\cdot10^{-2}$ cm^3), gold plated at both ends for a length of 1.5 cm (gold thickness

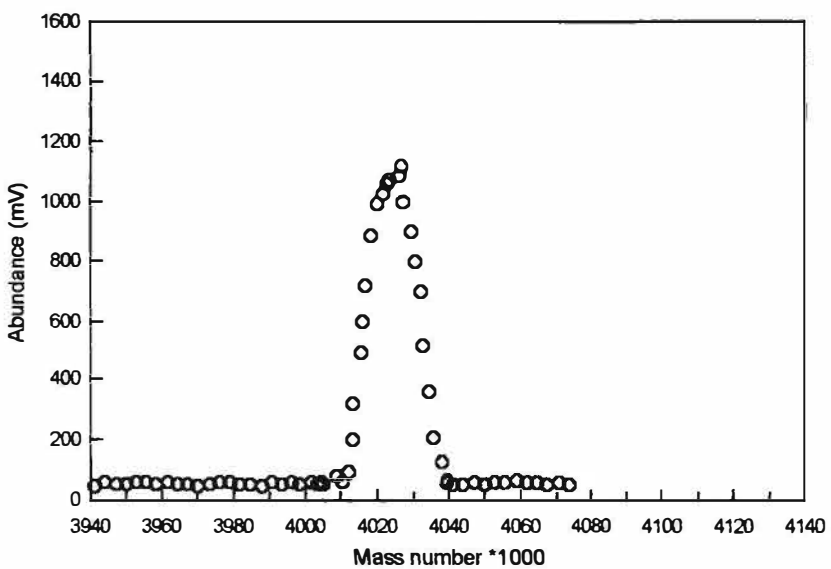

Fig.3 Mass analysis of the gas immitted in cell in the M/e 3.9÷4.1 range (blank measurement). Only the D_2^+ peak (M/e=4.028) is visible.

≈15 μm), has been clamped by the two Cu electrodes inside the cell.
During degassing the cell has been continuously in contact with the vacuum circuit. After an immission of D_2 gas, reaching a final pressure of 2.7 bar, the valve separating the cell from the rest of the circuit was closed and the gas herein was analyzed by the spectrometer. This analysis is considered the blank measurement (see fig.3).
After 18 hours from gas immission, the loading of the Pd sample reached a value of $\alpha \approx 0.5$ due to thermodynamical absorption (without electric stimulation). At the beginning (first 5 hours) of this time interval, the α ratio increased rapidly, while later on, it rised much slower, as shown in fig.4.

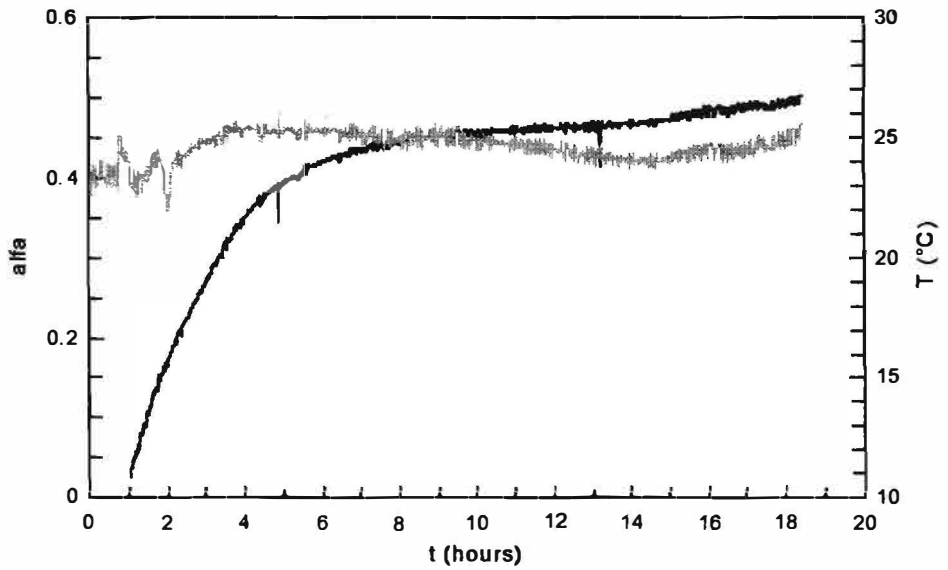

Fig.4 Variation of the loading ratio α measured by means of the thermodynamic parameters (black) and sample mean temperature (grey), during the first 18 hours.

The sheet temperature was continuously monitored and looks quite constant (after an initial transient) at the equilibrium (around 25°C) between the exotermic absorption and the external cooling water temperature .
Table 1 summarizes the sequence of the operations performed on the sample. The first column shows the start time of the operation from gas immission; in the second column the mean value of the loading ratio (averaged on the whole sheet volume) before the operation is reported; the mean and maximum values of the applied current appear in the third column, while its duration is listed in the fourth column. The fifth column indicates whether a gas analysis has been performed at the end of the operation involved, and the last one reports whether a ^{4}He production above background level has been observed.

Table 1 - Operations performed on Pd sheet

Time (hours)	<α>	I (A)	duration (hours)	Gas analysis	^{4}He
18	0.48±0.02	150 max 125 mean	0.3	No	No
65	0.66±0.02	225 max 100 mean	2	No	No
95	0.83±0.02	300 max 175 mean	1	Yes	No
117	0.80±0.02	440 max 330 mean	0.4	Yes	Yes

Helium and Heat Correlation

During the operation with electric field, the thermocouples measuring the sheet temperature were disconnected due to some noise caused by the very high circulating currents.
Fig.5 shows the behaviours of the current and of α during the application of the electric fields corresponding to the last row of the Table 1.

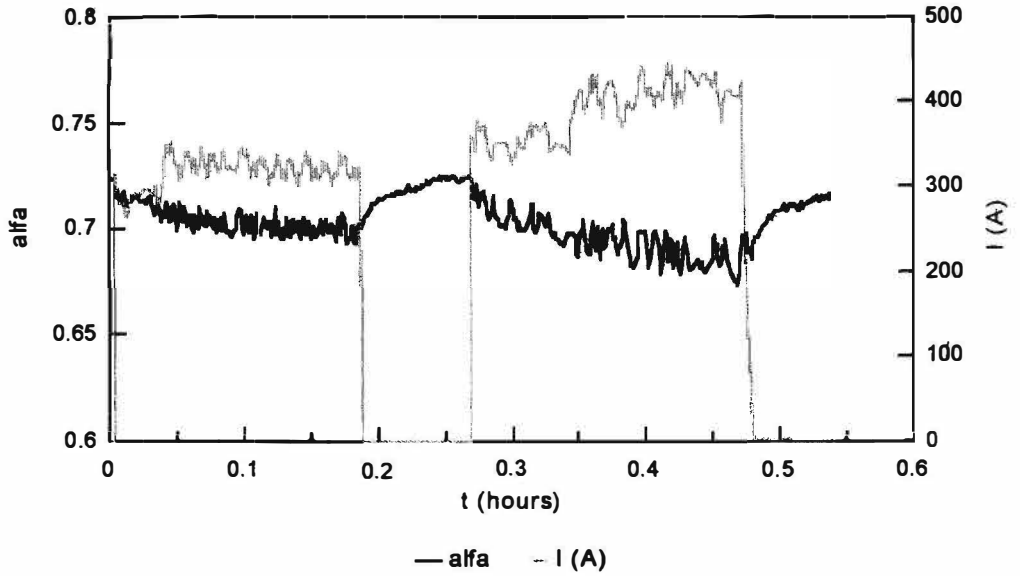

Fig.5 Behaviour of loading ratio α, measured by means of the thermodynamic parameters (black), during application of electrical current (grey).

The decrease of α when the electric field is applied and the increase when the field is switched off, have been interpreted in the following way: the electric field favours electromigration of the d^+ ions toward the cathode raising the concentration in the gold coated zone, but also favours desorption of D from the Pd uncoated region (this last phenomenon increases the pressure of the external D_2 gas); as the current is switched off, probably α is higher near the cathode, while the uncoated central region is deeply depleted; in this region, without electric field, the Joule effect stops and D_2 is strongly adsorbed, producing an increase of the average α.
The desorbed gas was analysed by the mass spectrometer (see rows 3 and 4 of table 1); the results of the last analysis are shown in fig.6, where a peak around the atomic mass of ^4He is evident.
The analysis of the gas was repeated several times, always giving the same clear evidence of ^4He presence.
From the peak height a partial pressure, and thus a percentage of ^4He in the analyzed gas, was obtained; in this way, a total value of $(5.3\pm0.7)\cdot10^{18}$ atoms produced in the cell has been inferred.
Since the ^4He presence in the background measurement (fig.3) is not detectable, the production inside the gas loaded Pd sheet is at least equal to this value: in fact, an amount of produced ^4He could have been trapped inside the Pd sheet.

Helium and Heat Correlation

Some comments can be made about the very high value reported above, corresponding to the same number of nuclear reactions

$$d + d \rightarrow {}^4He + 23.8\ MeV \qquad (1).$$

The heat excess (in the simplified hypothesis that all the energy in (1) is converted into heat), of the order of $(2.0\pm0.3)\cdot10^7$ J, is compatible with the values (heat or ^4He production) reported by other experiments. Considering nuclear reactions, their occurrence seems quite well estabilished by so huge numbers.

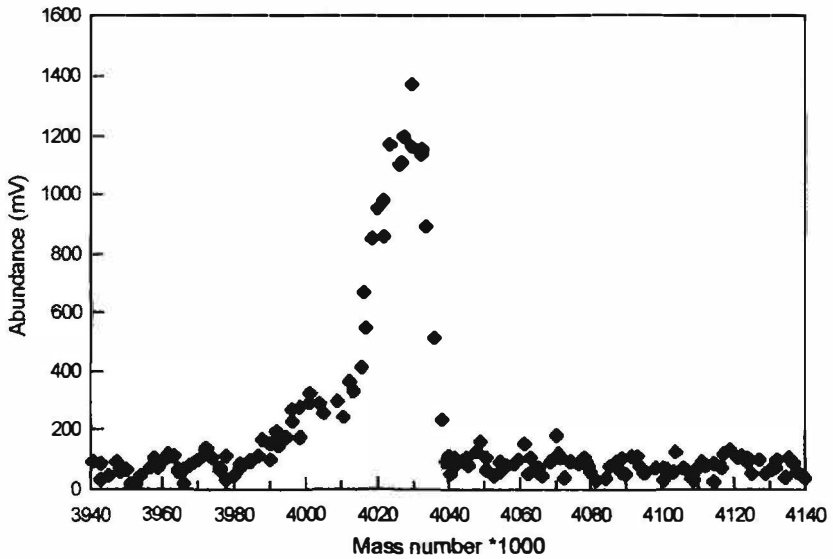

Fig. 6 Mass analysis of the gas desorbed from the Pd sheet after the fourth application of electrical field (see table 1). A ^4He peak (M/e=4.0026) is appreciable near the D_2 one (M/e=4.028).

Looking at the generated power, this experiment cannot determine the time interval during which the nuclear reactions occurred inside the Palladium. In fact, the total time of the experiment overcome 5 days and the sheet was considerably loaded nearly from the beginning. As extreme hypothesis, the ^4He production could start quite soon; in this case the average production rate should be of $(1.2\pm0.2)\cdot10^{13}$ $^4He/s$ (corresponding to a generated power of 46±7 W). But, if we believe that every application of the electric field is sufficient to empty the sheet from the adsorbed gas, the production should be considered as starting from the first field application; in this case, the total time should be $7.56\cdot10^4$ s, with a production rate of $(7.0\pm0.1)\cdot10^{14}$ $^4He/s$ and a generated power of the order of $(2.6\pm0.4)\cdot10^2$ W. So, the corresponding excess heat, is fully compatible with the tens of Watts generally reported by other experiments.

As a final remark, the total Pd sample volume in which the nuclear reactions occurred was of $8\cdot10^{-2}$ cm^3: the ^4He production density should then be $(6.6\pm0.9)\cdot10^{19}$ $^4He/cm^3$ and the rate per unit volume, in the shorter production time hypothesis, is $(8.8\pm0.1)\cdot10^{15}$ $^4He/(s\cdot cm^3)$, corresponding to a power production of $(3.3\pm0.5)\cdot10^3$ W/cm^3.

4.Conclusions and Perspectives

A new technique, based on the Coehn effect applied to Pd sheets, has been used in order to overload Pd with D over the thermodynamical limit α=0.67. A sequence of four values of electric fields with increasing maximum current intensities, was applied, each separated by periods of field off. In this period a loading value exceeding α= 0.8 has been reached. The mass spectroscopic analysis of the gas desorbed from the Pd sheet shows a clear peak at the atomic mass corresponding to ^{4}He, while a similar measurement performed on the gas before the absorption shows a background consistent with zero.

The ^{4}He production is of the order of $5 \cdot 10^{18}$ atoms, a strong evidence for the occurrence of nuclear reactions.

Concerning the rates, the sequence of operations in the present experiment, didn't allow the determination of the time interval in which the ^{4}He was produced, as well as no precise indication of local overloading values (perhaps greater than 0.8÷0.9) could be inferred from the data.

Future efforts will be directed to explore a sequence of adsorption-desorption cycles with more frequent spectroscopic analysis of the gas (still remaining successful in the ^{4}He production); a second goal will be to reach a better control of the temperature and voltages along the Pd sheet, in order to deduce more information about the electromigration and local concentration of the deuterium in the metallic lattice.

Acknowledgments

We wish to thank technical staff of INFN - Sez. Torino, and particularly O. Brunasso and G. Dughera for their disponibility, even outside their usual duties.We feel also indebted to Mr. U. Ferracin for some useful suggestions.

References

[1] T. Bressani et al., Il Nuovo Cimento 104 A (1991) 1413.
[2] T. Bressani et al., Il Nuovo Cimento 105 A (1992) 1663.
[3] G.C. Bonazzola et al. NIM A299 (1990) 25
[4] F. Benotto et al. IEEE Trans. Nucl. Sci. 39 (1992) 838
[5] M. Agnello et al. IEEE Trans. Nucl. Sci. 39 (1992) 1270
[6] E. Botta et al. "Search for ^{4}He production from Pd/D_2 systems in gas phase", Proc. of the 5th Int. Conf. on Cold Fusion (ICCF5), Montecarlo (1995), p. 233.

Helium and Heat Correlation

STUDY OF EXCESS HEAT AND NUCLEAR PRODUCTS WITH CLOSED D_2O ELECTROLYSIS SYSTEM

K. Yasuda , Y. Nitta† and A. Takahashi

Department of Nuclear Engineering , Osaka University , 2-1 Yamadaoka , Suita , Osaka , Japan.

† Present address , Matsushita Electric Industrial Co.,Ltd.

Abstract

Using a closed type heavy water electrolysis system , deuterium loading ratio D/Pd , output power (by using mass flow calorimetry method) and neutrons were measured in-situ simultaneously . Mass spectrum analysis of upper-cell gas and palladium cathode by a quadrupole mass spectrometer and tritium measurement in a sampled electrolyte were done by off-line techniques .

Excess heats up to approximately 4 to 5W were produced with the cold worked and copper layered (0.95 μ m) cathode . However , during excess heat , nuclear products (neutrons) were not observed over the 3 σ limit line of background level . In a few mass spectrum analyses , slight increases of helium-4 peaks were observed . However , helium-4 might not absolutely increase , because it was difficult to calibrate the mass spectrometer to deduce total amount of helium-4 from samples.

1.Introduction

The aim of this work is to study the correlation between excess heat by heavy water electrolysis with Pd cathode and deuteron-related nuclear products , i.e. , neutron , helium-4 and tritium .

The attainability of high loading of deuterium into various batches of Pd is reported to be one of the key parameters which govern generation of excess heat and nuclear products . Only SRI International[1] and IMRA-Japan[2] have ever given phenomenological relations between loading ratio (D/Pd) of deuterium and excess heat rates by in-situ measurements . However , their experiments lacked the measurements of nuclear products to see the correlation with excess heat . Miles et al.[3] have reported the correlation between excess heat and helium-4 and showed that the quantity of observed helium-4 could correspond to the assumed reaction of D + D $\rightarrow$ ^{4}He +23.8MeV as the heat generating nuclear reaction . Therefore , "cold fusion" may not be the normal D-D reaction which should produce neutron and tritium , but would be a new class of fusion in solid . Therefore , in order to prove the existence of the new class of nuclear reaction in metal / deuterium system essentially and find a solution to the mechanism of possible reaction , the simultaneous in-situ measurement of loading ratio (D/Pd) , excess heat and nuclear products with their correlations must provide us key evidences .

In the present work , D/Pd ratios , excess heats and nuclear products were tried to measure simultaneously in-situ in a closed heavy water electrolysis system . To carry out accurate calorimetry , a newly designed closed electrolysis cell which enabled heat measurement by using the

mass flow calorimetry method was manufactured.

With this system , seven experiments have been done by different cathode materials , i.e. , using several pre-conditioned palladium plates (cold worked , annealed , with or without copper surface layer) .

2.Experimental

Closed electrolysis cell

Fig.1 shows a cross sectional view of a newly designed cell . This cell has relatively large volume (738.4±4.1cc) , so that the electrolysis can be carried out with relatively high input power , i.e. , several-tens watts . The cell vessel is made of stainless steel coated with Teflon and a spiral copper cooling pipe is brazed around it . Temperatures at the inlet and the outlet point of cooling water were measured with CA thermocouples . A catalyst made of 0.5% Pd alumina pellets recombines dissociated deuterium by electrolysis with oxygen to form D_2O being fed back to electrolyte . The jointing part of plumbing was equipped with the lid , and a space between the lid and the vessel was sealed with copper gaskets . Loading ratio of deuterium could be determined by measuring the change of D_2 gas pressure of upper cell volume where air at the beginning of mounting was evacuated and replaced with D_2 gas (about 3atoms) . Even small quantity of helium-4 generated continuously or intermittently during electrolysis can be stored without loosing for many hours . By sampling the upper cell gas after the electrolysis run and analyzing it by the quadrupole mass spectrometer , the production of helium-4 can be detected .

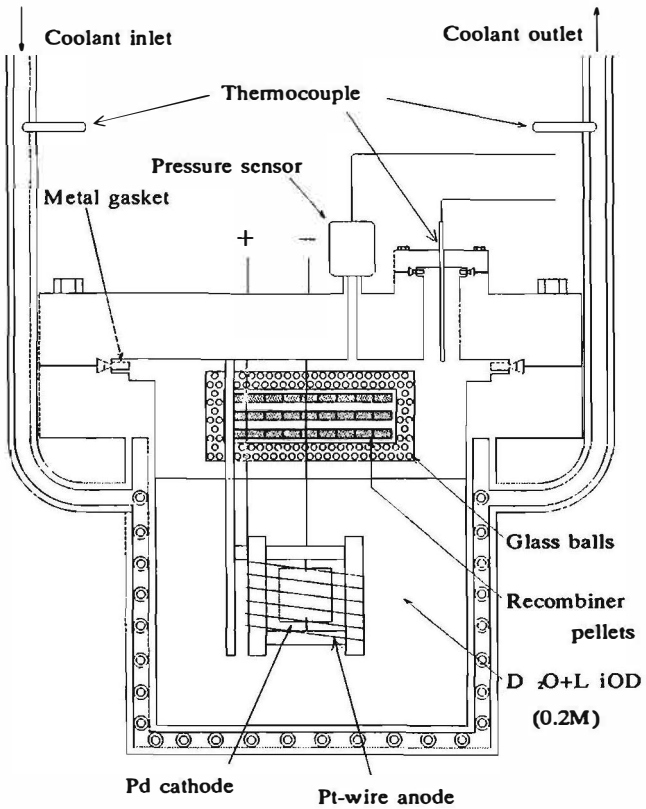

Fig.1 Closed electrolysis cell

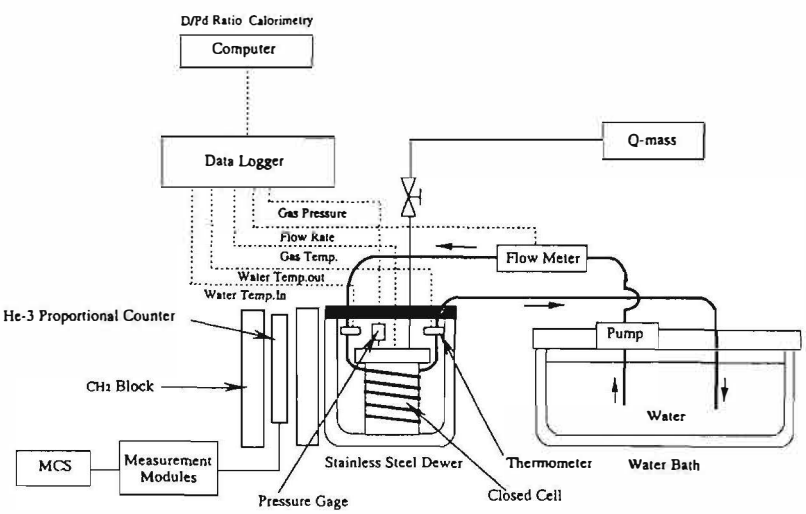

Fig.2 Experimental System

Helium and Heat Correlation

Neutron measurement

Fig.2 shows the measuring system of the experiment , where is a heilum-3 proportional counter (LND-2531) set up inside polyethylene blocks . The counter has 8 inch (about 20.3cm) effective length and 1.93 inch (about 4.1cm) effective diameter . LLD and ULD of the single channel analyzer (SCA) were adjusted to count the signals within the ROI area (MCA-7800 , SEIKO EG&G) of ^{3}He(n,p) reaction thermal peak in pulse height spectrum to detect only neutrons . Discriminated neutron signals were counted every four minutes with multi-channel scaler (MCS) . Fig.3 shows the flow chart of neutron measurement system .

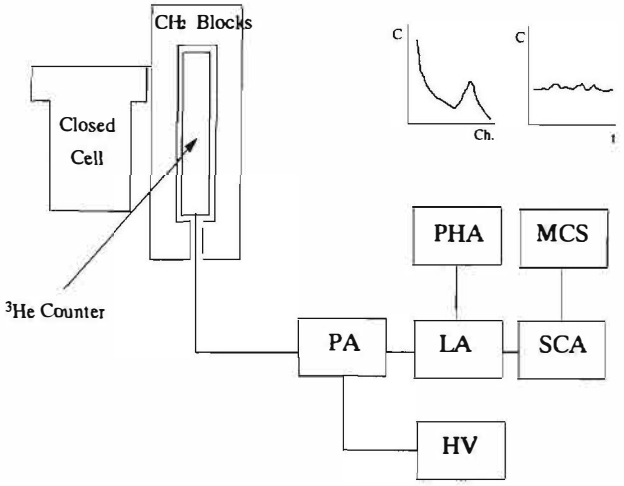

Fig.3 Block Diagram of Neutron Measurement

High resolution quadrupole mass spectrometer

High resolution quadrupole mass spectrometer (HIRESO-2SM , Vacuum Science and Engineering Co.Ltd.) was used to analyze mass spectrum (mainly mass four) of samples of upper cell gas and palladium cathodes . Minimum detectable partial pressure was about 10^{-11} Torr for helium-4 by this analyzer which corresponded to a number of atoms about 10^{14} . This analyzer has high resolution , i.e. , Δ M/M=0.02 (M : mass number) . Therefore helium-4 (mass number 4.0026) and deuterium (mass number 4.0282) can be measured as clearly separated two peaks .

On some of experiments , a hydrogen-getter-pump (SORB-AC100G , ULVAC Co.Ltd.) was used to remove deuterium from analyzed gas to increase the sensitivity for helium-4 detection .

Tritium analysis

Tritium was analyzed with the liquid scintillation counter . A 15cc liquid scintillator cocktail (AQUASOL-2) was mixed with 1cc electrolyte sampled before (and after) an experimental run for about a week or more and luminescence by β-decay was counted by the LSC method .

Experimental condition

Table 1 shows a summary of experimental conditions .

Seven experiments have been done using a 0.2M LiOD electrolyte and plate palladium cathodes (25 $\times$25$\times$1mm) . Several pre-conditioned palladium (cold worked , annealed , with or without copper surface layer[0.95 μ m]) were used for the cathodes . The Pd cathode used in Exp.3 was annealed for 10 hours at 900℃ with a heat furnace and was cooled down by the rate 10℃/minute . Pd cathodes in Exp.5 and Exp.6 had been already annealed before experiments .

No.	Pd cathode condition	Batch	Enclosed Gas	Electrolyte	Electrical current
Exp.1	Annealed	Nilaco#2	D_2(Sample1)	0.2MLiOD(350ml)	80～160(mA/cm^2)
Exp.2	Coldworked	Nilaco#2	D_2(Sample1)	0.2MLiOD(350ml)	160～320(mA/cm^2)
Exp.3	Coldworked	Nilaco#2	D_2(Sample2)	0.2MLiOD(350ml)	80～320(mA/cm^2)
Exp.4	Coldworked , Cu layer	NHE	D_2(Sample2)	0.2MLiOD(350ml)	80～320(mA/cm^2)
Exp.5	Annealed , Cu layer	NHE	D_2(Sample2)	0.2MLiOD(350ml)	80～320(mA/cm^2)
Exp.6	Annealed	Nilaco	D_2(Sample2)	0.2MLiOD(350ml)	80～320(mA/cm^2)
Exp.7	Coldworked	TNK	D_2(Sample2)	0.2MLiOD(350ml)	80～320(mA/cm^2)

Table1 Experimental Condition

3.Results and Discussions

Table 2 shows the summary of results for measurements of loading ratio (maximum values) , excess heat , neutrons , helium-4 and tritium .

No.	D/Pd ratio (Max)	Excess heat	Neutron	^{4}He(Upper-cell gas)	^{4}He(Ref. Sample)	Tritium
Exp.1	0.74	No	No	—	—	—
Exp.2	0.85	No	No	No	—	No
Exp.3	0.87	Yes (?)	No	Yes (?)	—	No
Exp.4	0.83	Yes	No	Yes (?)	Yes (?)	No
Exp.5	0.86	No	No	No	No	No
Exp.6	0.87	No	No	No	—	—
Exp.7	0.90	Yes	No	Yes (?)	—	—

(?): marginal level

Table2 Summary of Experimental Results

Figs.4 and Fig.5 show variations of excess heat and loading ratio (D/Pd) as a function of time .

In the run of Exp.3 , between 120 hours and 140 hours after the start of electrolysis , excess heat looked coming up . However , it was within the 3 σ (=3.9W) level of 99% confidence . Whenever anomalous excess heat was not produced , heat balance was at zero-line as looked like Fig.4 except the 120-140 hours interval.

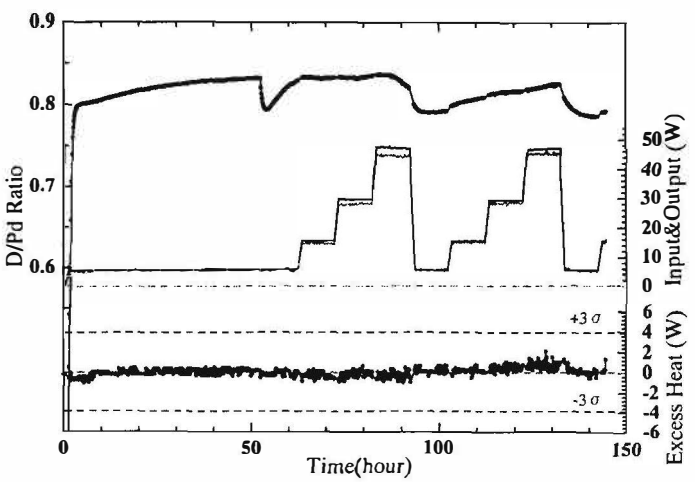

Fig.4 Variation of Loading Ratio , Excess Heat , Input and Output Powers with time (Exp.3)

Helium and Heat Correlation

In the run of Exp.4 , excess heats were produced from the time when input current mode was changed to the stepping up mode . Maximum excess heat exceeded 3.5 σ level of the standard deviation and therefore very confident . Then D/Pd ratios were observed here to be almost constant ($\sim$ 0.83 with small variation) in spite of the drastic change of currents by the stepping up .

In the run of Exp.7 , electrolysis by the stepping up mode continued for about 200 hours , for about a day we stopped electrolysis and changed to the L (1A) / H (4A) mode with 6 hours duration per each of L or H mode which continued for about 240 hours . The L / H mode electrolysis technique was fully used by the open system study group of our laboratory[4] . Fig.6-1 shows variations of excess heat and loading ratio in Exp.7 .

Excess heat was observed but not over the 3 σ level . And loading ratios were higher than those of Exp.4 as a whole but changed periodically in average , from 0.82 to 0.87 corresponding to the current changes of the L / H mode as shown with the upper most graph of Fig.6-1 . In the step-up made run of Exp.7 , excess heats with 5W max. were observed with maximum D/Pd = 0.90 (see Fig.6-2) .

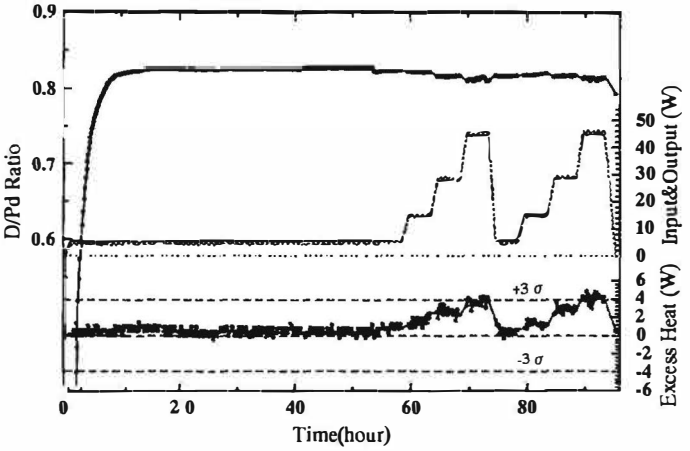

Fig.5 Variation of Loading Ratio , Excess Heat , Input and Output with time (Exp.4)

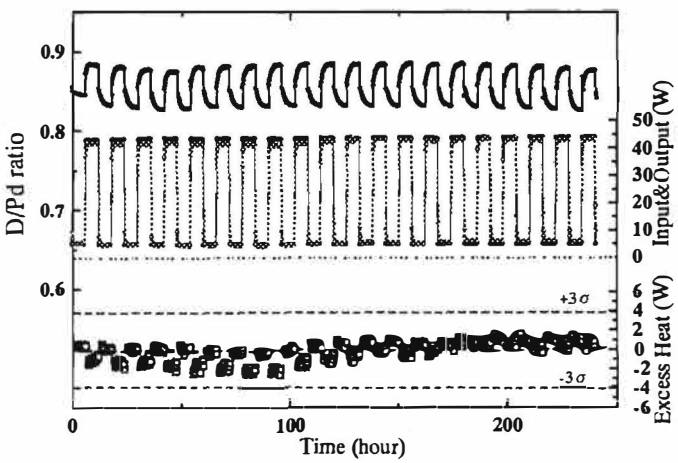

Fig.6-1 Variation of Loading ratio , Excess Heat , Input and Output with Time (Exp.7)

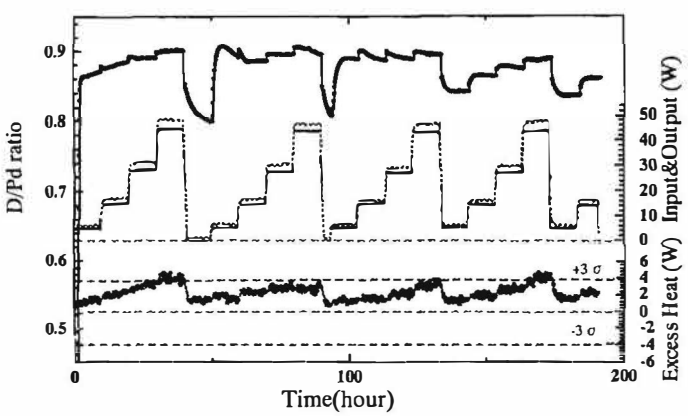

Fig.6-2 Variation of Loading Ratio ,Excess Heat Input and Output Powers with Time (Exp.7)

Helium and Heat Correlation

Fig.7 and Fig.8 show results of mass four spectra for cylinder gas samples (reference BG runs) in Exp.3 and Exp.4 . Judging from these diagrams , used original deuterium gas was regarded to be contaminated very slightly with helium-4 . However , in Exp.7 , helium-4 peak was not observed with the same deuterium gas sample of used D_2 gas cylinder , probably because the sensitivity of quadrupole mass spectrometer was getting worse than before .

Fig.9 through Fig.11 show results of mass four spectra for gas samples from the upper cell in Exp.3 ,

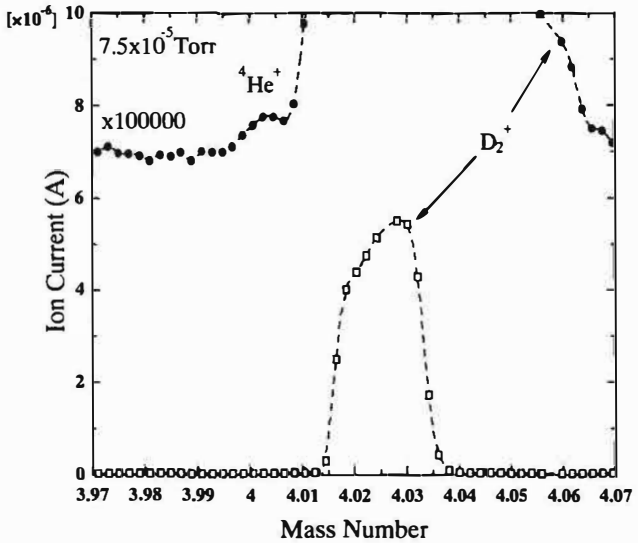

Fig.7 Mass Spectrum
(Exp.3 Gas Sample without Getter Pump)

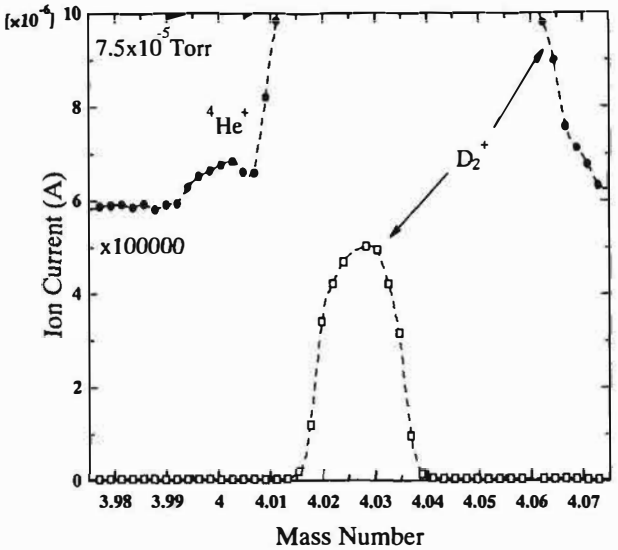

Fig.8 Mass Spectrum
(Exp.4 Gas Sample without Getter Pump)

Exp.4 and Exp.7 . In these analysis , ion currents of herium-4 peaks were observed with meaningful increases compared with ones of the original sample gas . Content of helium-4 in the sample gas from the upper cell was regarded as concentrated to be about twice through three times of the beginning D_2 gas after about 1 through 2atm D_2 gas was absorbed to Pd plate . So , amount of helium-4 peak-increases in Exp.3 , 4 and 7 should be regarded as marginal levels though Exp.4 showed the largest ^{4}He peak . It is necessary to calibrate quantitatively the mass spectrometer and fix the total quantity of helium-4 from the sample .

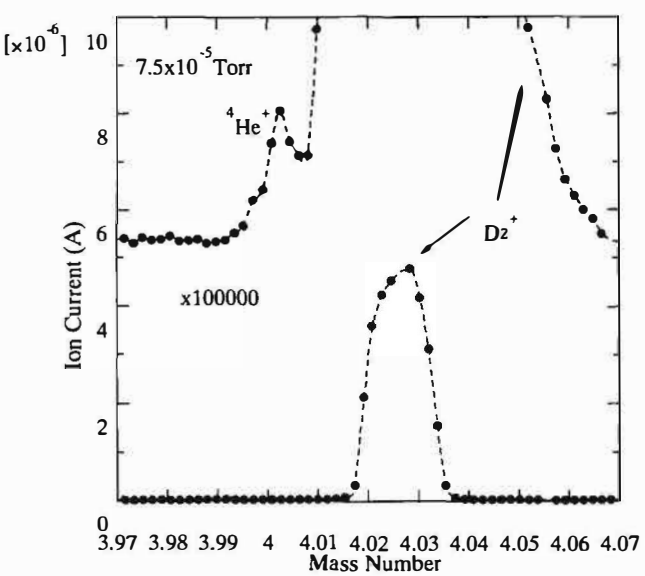

Fig.9 Mass Spectrum
(Exp.3 without Getter Pump)

Helium and Heat Correlation

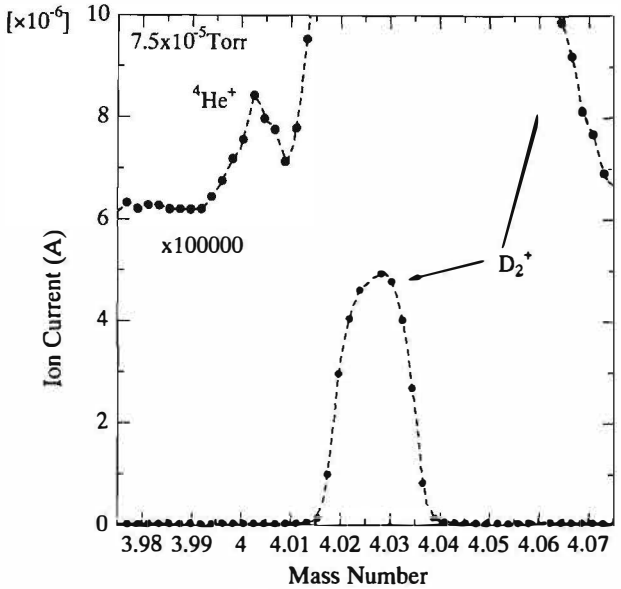

Fig.10 Mass Spectrum
(Exp.4 without Getter Pump)

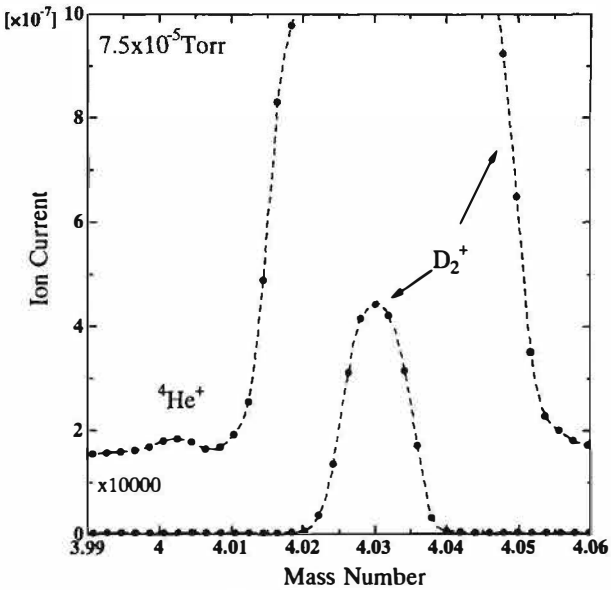

Fig.11 Mass Spectrum
(Exp.7 with Getter Pump)

In all the experiments , neutrons were not observed over the 3 σ limit line of the background level and clear increases of tritium in electrolyte were not observed either .

Fig.12 shows the MCS data of neutron in the run of Exp.4 . At four hours after electrolysis start , a count rate was observed over +3 σ level. However , since the neutron source facility "OKTAVIAN" near our experimental place was eventually running at the same time and skyshine neutrons were thought to shower , increase of neutrons might not be due to generation of neutrons from the palladium cathode .

Fig.13 shows results of tritium analysis in Exp.2 through Exp.5 . Tritium activity of electrolyte before electrolysis was defined as background and one after it as foreground . There was difference in tritium level between that of Exp.2 and those from Exp.3 to Exp.5 because electrolyte was exchanged to new one after Exp.2 ; tritium concentration (selective absorption of lighter isotope , i.e. , H and D to palladium plate) during the long electrolysis would be suggested .

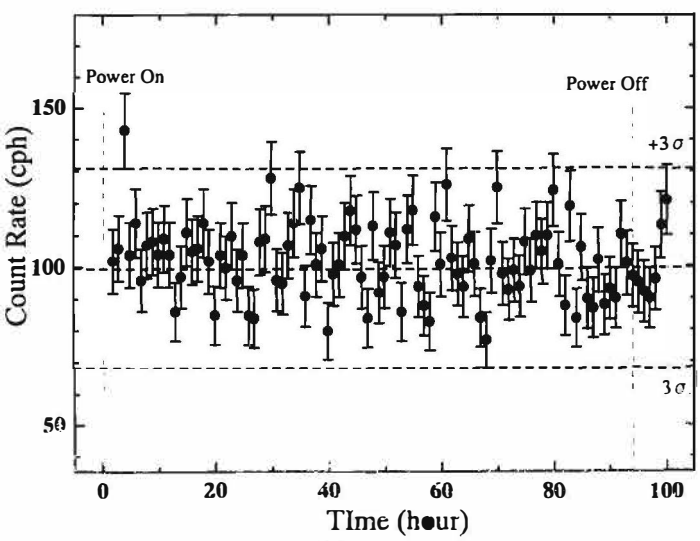

Fig.12 MCS data of Neutron (Exp.4)

Helium and Heat Correlation

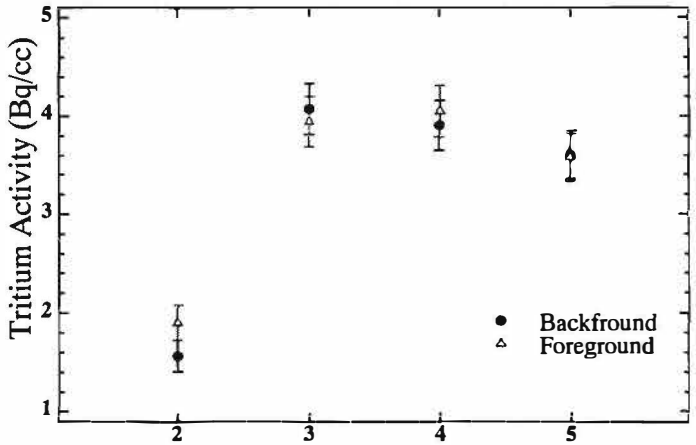

Comparison of Background and Foreground for Tritium Activity (Exp.2-Exp.5)

4.Conclusions

In the run of Exp.4 and Exp.7 , excess heats up to approximately 4 to 5W were observed with very confident level. And D/Pd ratios there were observed to be almost constant in spite of drastic change of current . However , during the excess heats , nuclear products (neutrons) were not observed , and clear increases of helium-4 and any increase of *tritium* were not observed either . As regards to mass spectrum analysis , because it was necessary to calibrate correctly mass spectrometer and fix quantity of helium-4 , the generation of helium-4 could not be definitely concluded although visible increases of helium-4 peaks were observed for three cases of upper-cell gas . Because of limited number of experiments the correlation or non-correlation between the generation of excess heat and nuclear products could not be confirmed . Now the two cells in series connection are running simultaneously in order to establish the more confident measurement system , to study the correlation of excess heat with the degree of loading ratio D/Pd using different pre-conditioned cathodes ,and hopefully to identify the correlation of excess heat and helium-4 generation .

References :

1)M.C.H.Mckubre, et al. : Proc. ICCF-5, Monte Carlo, (1995) P.17

2)J.Minato, et al. : Proc. ICCF-5, Monte Carlo, (1995) P.383

3)Miles and Bush, : Fusion Technology, 26, P156 (1994)

4)H.Fukuoka : This Conf. , Hokkaido

NHE Session

Excess Heat in Fuel Cell Type Cells from Pure Pd Cathodes Annealed at High Temperatures

Hiroshi Kamimura, Toshio Senjuh, Sigeru Miyashita, and Naoto Asami

R&D Center for New Hydrogen Energy
The Institute of Applied Energy
Atsubetsu-ku, Sapporo 004, JAPAN

Abstract

An excess heat measured as a rise of cell temperature from a calibration curve has been observed in fuel-cell type cells using pure palladium cathodes and apparently depended on their thermal treatments. All the Pd cathodes tested were at least 99.99 ("four nines") pure, but the treatment conditions of the cathodes appear to have affected the loading ratios and presence of excess heat. The Pd cathodes exhibiting excess heat were annealed for ten hours at a high temperature (850 or 1000 °C) in a high vacuum environment. The excess heat from the samples ranged from 7-18 % of the electric input power. However, these results should be confirmed with a flow calorimetry system.

1. Introduction

A research and development project, "New Hydrogen Energy" project, was started in November 1993 under New Energy and Industrial Technology Development Organization (NEDO) in Japan. In the project, several experimental systems in which an excess heat had been detected were set up in our laboratory[1]. One of the systems, a fuel cell type electrolysis system[2] has pressurized cells with a reversible hydrogen anode based on fuel cell technology. In a few cases excess heat had been detected using the system by Apr. 1995 in our laboratory. Reproducibility of the excess heat was poor, probably because of the use of many kinds of Pd. However, useful information about Pd rod processing has been obtained[3] improving the ability to acquire higher loading ratio (D/Pd) than 0.85, which appears to be indispensable for excess heat generation. The main conclusions are that (1) Pd electrodes with higher purity and stable grains reach high D/Pd, (2) Grain size and/or grain boundaries may be significant for high D/Pd, and (3) Cracks on the Pd surface very likely inhibit high loading.

In this study, Pd rods were fabricated of high purity "four nines" Pd, melted in vacuum, processed at room temperature, and surface machined, in keeping with protocols which have previously achieved positive results. In addition, samples with various pre-electrolysis treatments have been tested with the fuel cell type electrolysis system. The effects of pre-electrolysis treatments on the D/Pd and excess heat measured are discussed in this paper.

2. Experimental

2.1 Pd cathode

A "standard" process to prepare Pd rods for electrolysis experiment was determined[4] based on the past experimental results[3]. The results indicate that high D/Pd loading can be achieved under

the following conditions: (1) Pd electrodes with higher purity and stable grains reach high D/Pd, (2) Grain size and/or grain boundaries may be significant for high D/Pd, and (3) Cracks on the Pd surface very likely inhibit high loading. Therefore, the Pd cathodes, which were 4 mm in diameter and 20 mm in length, were made of "four nines" Pd, melted in vacuum, processed in room temperature, and the surfaces were machined away to a depth of 0.2 mm by Tanaka Kikinzoku Kogyou (TKK).

In addition, we attempted various pre-electrolysis treatments[4] to the samples by the "standard" process described above to increase the D/Pd. The results of the attempt using a resistance measurement system, which could estimate D/Pd from a change in resistance of Pd during electrolysis, were presented by us in other paper[5]. The major treatments were (1) a surface etching in aqua regia to remove surface defects and to clean the surface, and (2) a vacuum annealing to release the stress, to re-crystallize the grains, and to clean the surface by thermal etching. The etching

Table 1 The Pd samples prepared to experiments

Sample No.	Exp. No.	Etching time (min)	Heat treatment (°C x h)
0	EX11C1	-	200 x 3(degassing only)
1	EX11C3	-	850 x 1
2	EX11C4	10	850 x 1
3	EX11C5	10	850 x 10
4	EX11C6	-	850 x 10
5	EX14C5	-	1000 x 1
6	EX13C3	10	1000 x 1
7	EX13C5	10	1000 x 10
8	EX13C6	-	1000 x 10

in aqua regia was done before the vacuum annealing. Both the samples etched and not were prepared to examine the effect of the etching. The samples were etched for ten minutes in aqua regia. The annealing was performed for 1 or 10 hours at 850 or 1000 °C at a vacuum environment of 1 mPa. One untreated sample and eight variously treated samples described in Table 1 were used in the experiments. Sample #0, the untreated sample, had grains ranging in size from 100 to 300 μm varied by the rod processing. On the other hand, the heat-treated samples had non-stressed grains whose sizes were 50 to 100 μm in diameter. However, there was no difference in grain size resulting from the treatment temperature or the treatment time, as determined by observing the surface structure of the samples with an optical microscope.

2.2 Measurement apparatus and method

The fuel cell type electrolysis system is shown in Fig. 1. The system, developed by IMRA-Japan, had six pressurized cells with a reversible hydrogen anode based on fuel cell technology. The Pd sample was set at the center of a pressure vessel as a cathode electrode, and surrounded by a gas diffusion electrode, "fuel cell anode". The pressure vessel was filled with 1 M LiOD electrolyte of 50 cm^3 and D_2 gas up to 9 kg/cm^2. Three Type K thermocouples were used to measure the temperatures of the Pd rod, the electrolyte, and the gas. The D_2 gas pressure was measured by a pressure gauge (VALCOM VPRNP17KA). The cells were set in a thermostatic water bath (ADVANTEC LF680) at 10°C constant temperature.

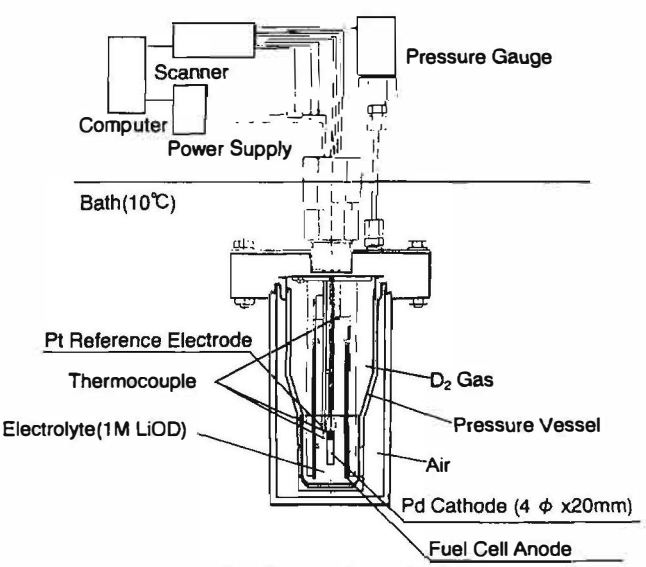

Fig. 1 Fuel cell type electrolysis system

A computer (NEC PC9801) controlled a power supply (KIKUSUI PAD16-10LP) to provide a constant electrolysis current and measured the cell pressure, the temperature at the three points, the cell voltage, and the electrolysis current through a scanner (ADVANTEST R7430), recording data at one minute intervals.

Both the D/Pd and excess heat are estimated by monitoring the temperatures and D_2 gas pressure during electrolysis. D/Pd was estimated by the following expression:

$$\frac{D}{Pd} = \frac{2(n_0 - n_1)}{Pd_{mol}}, \quad (1)$$

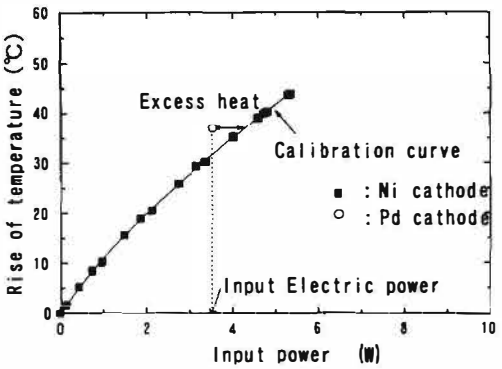

Fig.2 An example of calibration curve determined with Ni cathode and excess heat from calibration curve

where n_0 is the molarity of D_2 gas before electrolysis; n_1 is the molarity of D_2 gas at the time of estimation; Pd_{mol}, the molarity of Pd rod. Thus, n_0 can be calculated from the gas pressure and gas temperature measured before electrolysis. Then n_1 can be also be calculated during electrolysis.

The excess heat was estimated by a rise of the cell temperature based on a calibration curve between input power and the cell temperature previously determined using a Ni cathode. Fig. 2 shows an example of calibration curve and excess heat (energy) estimated from the curve. The accuracy of excess heat estimation depends mainly on the accuracy of assembling the cell. We evaluated the deviation of the calibration curve using data of five experiment cases performed at a certain period, and concluded that the deviation from the calibration curve was within ±2%. Therefore, we assume that only a measurement larger than 5% could be attributed to excess heat generation.

2.3 Electrolysis condition

The electrolysis was performed under constant current control. A typical applied current profile is shown in Fig. 3. The current was maintained at 125 mA corresponding to 50 mA/cm^2 surface current density on Pd samples for 6 days after the start of electrolysis, and then the current was changed step by step after stable equilibrium was reached. The temperature of the cathode became stable within three hours after a current change according to results of the calibration experiments. Therefore, the time constant of the system was about three hours, so the excess heat was estimated on the basis of the cathode temperature measured three hours after a step change in supply current.

The current profile for 17 days after start was fixed as the same loading condition. Following that time, the profiles were varied. In all, the samples were electrolyzed in the system for more than one and a half months.

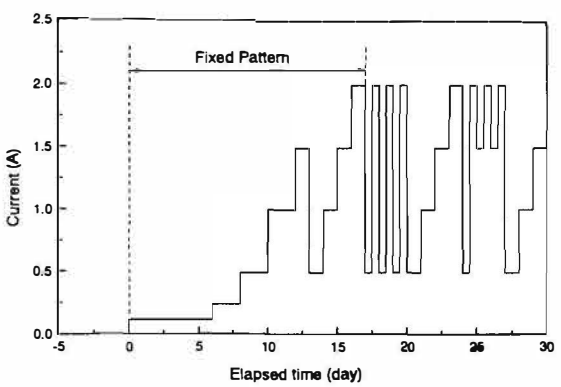

Fig.3 An example of electrolysis current pattern

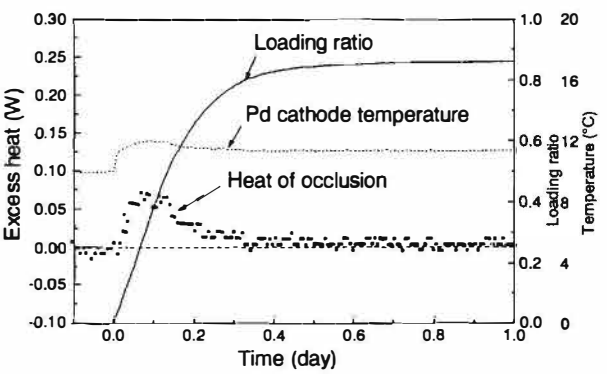

Fig.4 Heat of occlusion, loading ratio, and Pd cathode temperature at the state of beginning of electrolysis.

Fig. 4 shows the heat of occlusion measured at the state of beginning of electrolysis. The excess heat estimated from the cathode temperature was not exact under transient conditions, as described above, but it showed that the system had sensitivity to detect the heat of occlusion. The heat of occlusion estimated as integration of the excess heat was of about 780 J. The calculated value was about 350 J. This difference in these values was probably caused by the lack of correction for the system response function.

3. Results and discussion

The experimental results on excess heat and D/Pd are shown in Table 2. The excess heat is the maximum during electrolysis. The percentage is the ratio of the measured excess heat to the input electric power. From the results, it seemed that (1) excess heat of 0.35-0.75 W (7-18 %) was

Table 2 Experimental results on excess heat and D/Pd

Sample No.	Etching	Heat treatment (°C x h)	Excess heat*(W(%))	D/Pd**
0	no	200 x 3	-	0.80
1	no	850 x 1	-	0.81
2	yes	850 x 1	-	0.80
3	yes	850 x 10	0.7 (11)	0.87
4	no	850 x 10	0.35 (7)	0.87
5	no	1000 x 1	-	0.88
6	yes	1000 x 1	-	0.88
7	yes	1000 x 10	0.7 (16)	0.89
8	no	1000 x 10	0.75 (18)	0.85

* Maximum excess heat (normally, electrolysis current = 2 A)

** Maximum D/Pd during experiment

measured in only four samples annealed for 10 h at the temperature both of 850 and 1000 °C, (2) the loading ratio of the samples with excess heat was 0.85-0.89, significantly higher than the 0.80

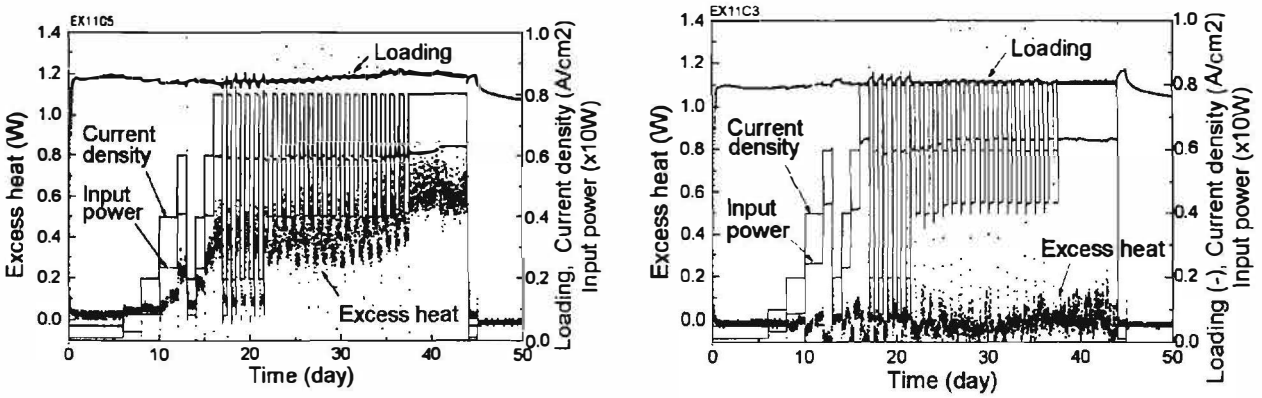

(a) Sample #3 observed excess heat (850°Cx10h)

(b) Sample #1 observed no excess heat (850°Cx1h)

Fig.5 Two experimental results with and without excess heat

attained by the untreated sample (#0), and (3) the aqua regia etching before annealing was not effective in achieving D/Pd and excess heat in these experiments.

Two experimental results (sample #3 and #1) with and without excess heat are shown in Figs. 5 (a) and (b), respectively. The same current pattern was applied in both the experiments, but different results were measured. Sample #3 achieved D/Pd of 0.85 and generated 0.7 W of excess heat. On the other hand, #1 had lower D/Pd and no excess heat. The excess heat in Fig. 5(a) was continuously detected after 2 weeks from the electrolysis start. The excess heat observed in other samples also showed the same trend.

The etching conditions of #1 and #3 were different from each other. Sample #3 was etched, but #1 was not etched. However the etching was not effective for the generation of excess heat and an increase of D/Pd, because the etched sample of #2, which had the same heat treatment as #1, also had no excess heat and the same low D/Pd as #1. In other experimental pairs with etching or not (#3 & #4, #5 & 6, #7 & #8), their results on excess heat were also unrelated to the etching treatment.

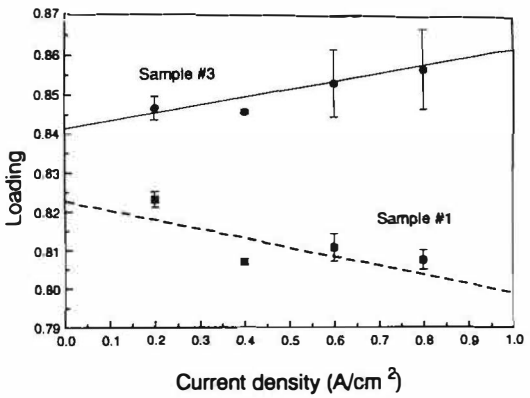

Fig.6 Loading ratio as a function of current density supplied, comparing the two samples; #1 without excess heat and #3 with excess heat.

The loading ratio as a function of current density supplied is shown in Fig. 6. To calculate this relationship, the data from 2 weeks after the start of electrolysis and in stable equilibrium (i.e., more than three hours following a step change in current) were used. The D/Pd ratio of sample #1 with no excess heat became lower at higher current density. The D/Pd of sample #3 with excess heat increased or did not declined at high current density supplied.

Relationships between the loading ratio and the current density in all the experiments with or without excess heat are shown in Figs. 7(a) and (b), respectively. The electrolysis patterns in the

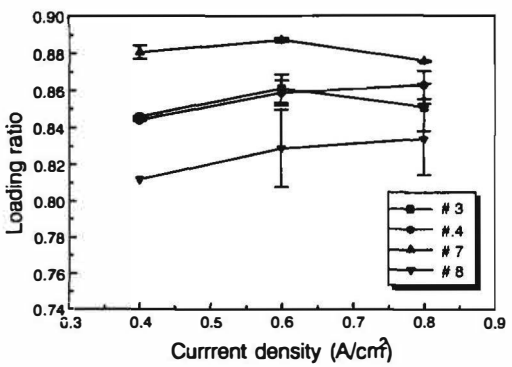

(a) Cases of samples with excess heat

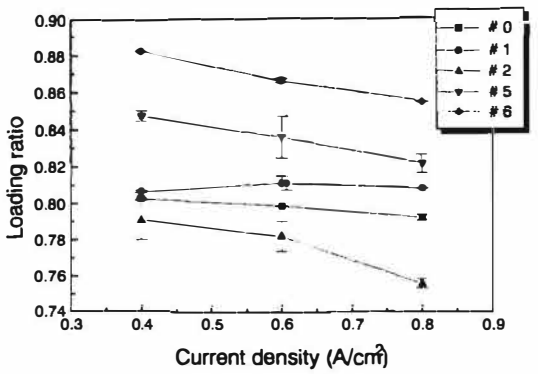

(b) Cases of samples with no excess heat

Fig. 7 Experimental results of loading ratio as a function of current density supplied.

experiments were not entirely identical to each other, but were the same for 17 days from the start, as previously described. D/Pd for cases in which excess heat was observed tended to increase or remain constant at higher current. On the other hand samples exhibiting no excess heat tended to decrease the loading at higher current.

The relation between excess heat and loading ratio on the samples #1 and #3 are shown in Fig. 8. The measured data used were the same data for Fig. 5. In sample #1 the excess heat was within ±2%, so we judged it to be no excess heat. However, sample #3 attained a higher D/Pd (up to 0.87) than #1, and generated over 5 % of

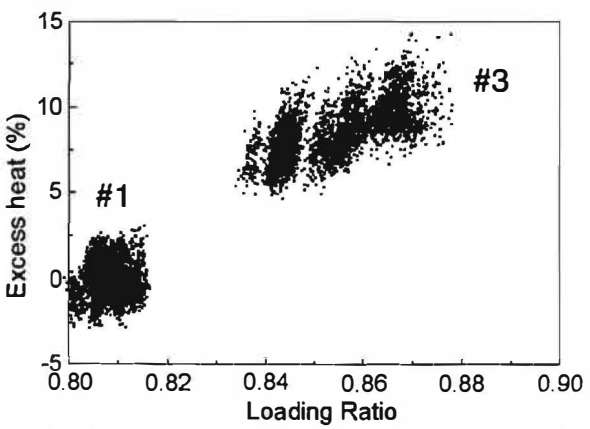

Fig.8 Excess heat vs. loading ratio on the sample #1 annealed at 850 °C x 1h and #3 annealed at 850 °C x 10h.

excess heat.

Similar results were obtained for samples annealed at 1000 °C. Excess heat was only measured for sample annealed for ten hours. According to these results, the time of 10 hours for annealing was sufficient to re-crystallize the grain, and/or to clean the surface by thermal etching, but 1 hour was insufficient.

Typical relationships between input power and excess heat in the experiments are shown in Fig. 9. The solid line is a quadratic fit using the least squares method. The excess heat increased quadratically as the input power corresponding to the surface current density increased. However, these results alone are not sufficient to prove the existence of an anomalous source of excess thermal energy in this system. Although previously it had been estimated that the deviation of the calibration curve, which might cause a false positive excess heat, was less than 5%, it is not possible to rule out the possibility that some other unknown factor might increase the deviation from the calibration curve for the system.

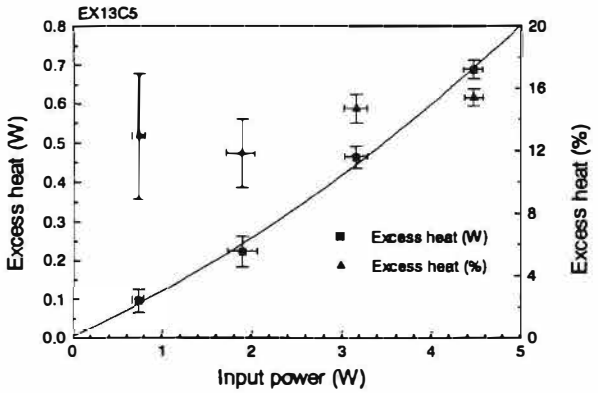

Fig.9 An example of excess heat vs. Input power on the sample #7 annealed at 1000 °C x 10h.

A problem of the fuel cell type system is that it does not measure net excess heat directly. Therefore, the existence of the excess heat from Pd is not considered proven in these experiments. To measure the excess heat exactly, a flow calorimetry system[4] has been manufactured which is compatible with the fuel cell type cell and which can directly measure the excess heat from the cell by measuring the input/output temperature and mass flow of coolant. It remains to confirm the existence of excess heat with the flow calorimetry system.

4. Conclusions

Experimental results on excess heat and D/Pd using a fuel cell type electrolysis system have been presented. Pd rods were made of high purity "four nines" Pd, melted in vacuum, processed in room temperature, and surface-ground. Samples with various pre-electrolysis treatments were tested to examine the effect of the treatments on the excess heat and the D/Pd.

The pre-electrolysis treatments were (1) a surface etching in aqua regia to remove surface defects and to clean the surface, and (2) a vacuum annealing to release stress, to re-crystallize the grains, and to clean the surface by thermal etching. The annealing temperature have ranged from 850 to 1000 °C, and the annealing time varied from 1 to 10 hours.

Excess heat has been observed in our experiments. Apparently, thermal treatment conditions of the cathodes affected loading ratios and excess heat. Excess heat has been only observed from the Pd samples which were annealed for 10 hours at a high temperature (850 or 1000 °C) in a high vacuum environment (1 mPa). Excess heat from the samples has been 7-18 % of the electric input power. However, the system was not able to measure the net excess heat directly. Therefore, it is recommended that excess heat from Pd be confirmed using a flow calorimetry system before concluding that the system does in fact produce excess energy.

Acknowledgment

This study has been conducted under the auspices of the New Energy and Industrial Technology Development Organization (NEDO). The authors acknowledge Professor Okamoto, Professor Ikegami, and Dr. Kunimatsu for useful discussions.

NHE Session

References

[1] N. Asami, et al.: Proceedings of ICCF5, p.87 (1995).
[2] K. Kunimatsu, et al.: Proceedings of the ICCF3, p.31 (1993).
[3] N. Hasegawa, et al.: Proceedings of ICCF5, p.449 (1995).
[4] N. Asami, et al.: to be presented in ICCF6.
[5] T. Senjuh, et al.: to be presented in ICCF6.
[6] A. Kubota, et al.: to be presented in ICCF6.

NHE Session

Development and Experiments on a Flow Calorimetry System

Akihiko KUBOTA, Shinichi TAKAMA, Toshiya SAITO,
[1]Norifumi HASEGAWA, [2]Satoru SUKENOBU, Masao SUMI, Naoto ASAMI

R&D Center of New Hydrogen Energy, The Institute of Applied Energy
3-5, Techno Park 2-Chome, Shimonopporo, Atsubetsu-ku, Sapporo 004, JAPAN

[1]IMRA JAPAN Co., Ltd.
3-6, Techno Park 2-Chome, Shimonopporo, Atsubetsu-ku, Sapporo 004, JAPAN

[2]Research & Development Center, Toshiba Co., Ltd.
4-1, Ukishima-cho, Kawasaki-ku, Kawasaki 210, JAPAN

Abstract

Demonstration experiments of excess heat generation have been conducted using the Fuel Cell Type Electrolysis System at NHE Laboratory since January 1994. In April 1995, a mass flow calorimetry system (FCS) was developed at the NHE Laboratory. A new series of experiments, referred to as NHE-FCS, combines the Fuel Cell Type Electrolysis System with mass flow calorimetry. The system is comprised of fuel cell type electrolysis cells, power supplies, vacuum insulators, water coolant, temperature measurement equipment, and a personal computer which controls the power supplies and digital multimeters. A data acquisition occurs every 60 seconds. Total input power is typically 10W. As a result of careful modification of the components, a heat recovery efficiency of ~98% has been attained. It has been confirmed that an excess heat of 0.2W is measurable in calibration tests.

Excess heat has been observed in the "Fuel Cell Type Electrolysis System". Observations of 7-18% excess heat have been reproduced in 11 cases. However, the reproducibility issue still remains. NHE-FCS experiments have been performed used identical protocol. Excess heat has not been observed yet in spite of the fact that we have attempted to duplicate the electrode materials that produced excess heat. One reason may be that other experimental conditions have differed in detail in cases in which excess heat has been observed.

1. Introduction

In previous experiments using the "Fuel Cell Type Electrolysis System", excess heat is calculated by comparing the measured temperature of the electrode and the electrolyte with a calibration curve. The calibration curve is provided from the measured temperature of a Ni electrode and the electrolyte. Thus this method is not a direct calorimetric measurement. If the measurement points are somehow moved during cell assembly after the calibration, the accuracy of calibration would be lost. Therefore it is necessary to improve the measurements and confirm the measured excess heat by other methods.

A flow calorimetry system, such as which has been developed by Stanford Research Institute,

provides a direct measurement capability. Thus, a flow calorimetry system for NHE was designed and developed to confirm the observed excess heat at NHE Laboratory.

2. Experimental

2-1 Measurement System.

Fig.1 shows the overall system of NHE-FCS. As a matter of fact, 2 experimental cells are able to be measured at the same time for one system. Water in bath A as coolant is kept at the same temperature of bath B (23°C const.), and send to bath B using a constant-flow-rate (0.7g/s) pump through a degasser. Coolant water is continuously purified by an ion exchange resin bed. To damp the flow rate fluctuation, an accumulator is inserted between the pump and electrolysis cell. The temperature of water is close to that of bath B as it flows through the tube section in bath B before entering in the cell. The flow rate of water after exchanging heat at the cell is measured by the flow meter as it returns to bath A.

The temperature of the coolant water at inlet and outlet are sensed by Pt thermal resistors. Input voltage and current of electrolysis and heater, output of flow meter and vacuum meter, and the resistance of Pt thermal resistors are measured by digital multimeters. The power supplies and multimeters are controlled by a personal computer (PC).

The data acquisition typically occurs every 60 seconds. Constant total input power is assured by regulating the power supplies every 10 seconds. The PC can output the data files to magneto optical (MO) disk while the measurement program is running, so it is possible to analyze the results of experiments later.

2-2 Electrolysis Cell.

At first, two kinds of cells that have the different position of the heat exchange tubes were designed and made at April 1995, they are called "Type A" and "Type B" respectively. The "Type A" cell was showed at figure 6 of our ICCF5 report[5]. After that, they have modified to improve the variations of heat measurement. It is called "Type C". All experiments have been performed using "Type C" cells since January 1996.

Fig.2 shows the electrolysis cell "Type C" in the vacuum insulator for NHE-FCS. It is the fuel cell type electrolysis cell composed of a cathode, the gas diffusion electrode, electric heater, and the pressure vessel. The electric heater is made from coiled Ni-Cr wire and sealed PTFE tubes. This cell has the heat exchange tube in its side, bottom, and cover wall. The coolant water enters into and goes out the cell through the cover of the vacuum vessel. The temperatures of the inlet and outlet coolant water are measured in the tubes under the cover by Pt thermal resistors.

The ceramic hermetic seals are used for the connectors between the inside and outside of the pressure vessel, and at the cover of the vacuum vessel for electrolysis and heater input lines. Their voltages are sensed at the connectors.

To prevent the gas leakage, a metal O-ring is used for the pressure vessel's seal.

2-3 Protocol.

Experiments are performed in two steps.

The first step is to measure the cell's heat recovery, using a Pt cathode and an electric heater, in order to determine cell performance. The estimated heat recovery is used for the calculation of excess heat during electrolysis with a Pd cathode.

The second step is the Pd electrolysis experiment, carried out according to the following protocol:

1. The Pd electrode is prepared according to the appropriate protocol.
   The cell components are cleaned and the cell is assembled and leak-checked.

2. The electrolyte is added, cell volume is measured, D_2 gas is pressurized at 9 kgf/cm^2.
3. The cell is installed in bath B, and left until the pressure and temperature reach steady-state conditions.
4. The heater is turned on (kept at 10W const. typically).
5. Electrolysis begins after the pressure and temperature reach constant values.
6. Output heat is measured as the electrolysis current changes.

The current profile was initially the same as that of the reference conditions. Afterwards, open circuit, Hi-Lo current exchanging, and anodic treatment are tried.

2-4 Calculations.

The method of calculation of D/Pd is same as previously used for the "Fuel Cell Type Electrolysis System". However, the cell volume, PTFE fixers and the electrolyte volume are relatively larger than for previous cases. Thus, the volume of gas effluent from the PTFE fixers and electrolyte outgasing must be accounted for when calculating D/Pd. Likewise, the averaged temperature of the gas is estimated from the calibration experiments.

Excess heat, W_{ex}, is calculated with the following equation.

$$W_{ex} = m \times c_p \times \Delta T / \xi - W_t$$

where m is the flow rate, c_p is the specific heat of water, ΔT is the difference between inlet and outlet fluid temperature, ξ is the heat recovery efficiency as determined from calibration experiments, and W_t is the total input power.

In this equation, the recovery power is $m \times c_p \times \Delta T$. Changes in the flow rate influences the heat recovery, therefore the flow rate setting at the pump is not changed for other experiments.

3. Results and Discussion

3-1 Calibration.

In calibration experiments using a Pt cathode and electric heater input, the heat recovery of each cells is 0.983 ± 0.010. Fig.3 shows the results of the calibration experiments using one of Type C cell. In this case, the heat recovery, ξ, was 0.977. The heat recovery is determined by averaging the last 60 minutes of all constant current terms during the total input power kept at 10W.

Another heater was assembled in this cell as the dummy excess heat generator, and supplies 0.2W for 2 hours (designated with *1 in Fig.3 and Fig.4). Fig.4 shows that the calorimeter is capable of observing such small values of thermal energy.

In addition, the figure shows that the calculated results of excess heat was almost 0 ± 0.1W except during the periods when the test heater was on. The 3-sigma uncertainty for this cell was 0.09W with the input power regulated at 10W. The 3-sigma value for other cells was estimated at 0.09 to 0.16W. Accordingly, it can be concluded that NHE-FCS has enough sensitivity to detect excess heat of 0.2W at total 10W constant input condition.

3-2 Pd Electrolysis.

All experiments of Pd cathodes have been performed used identical protocol which showed excess heat in prior "Fuel Cell Type Electrolysis System" experiments. Fig.5 shows typical results at Pd electrolysis using NHE-FCS. The material and treatment of Pd cathode and experimental procedure were identical.

Total input power was kept at 10W with heater before starting Pd electrolysis. In the first of measurement, the changing of the results of excess heat is presumed that the recovering of heat is

unsteady because of the complexity of the heat exchanging tubes. D/Pd reached a maximum of 0.82, but slightly decreased at high current density. Excess heat was almost 0 ± 0.1W during all over the experiment. Therefore it was decided that excess heat was not observed in this experiment.

In some experiments, D/Pd reached a maximum of 0.84, and 0.89 in one experiment. In the results from all experiments in this series, excess heat has not been observed. This may be insufficient for excess heat generation. Past experience indicates that D/Pd in the range of 0.85~0.90 are necessary for excess heat generation.

3-3 Discussion.

One possible reason that net excess heat has not been observed is that the experimental conditions have necessarily differed in slight details from those of prior experiments. Specifically, on account of the cooling method, the temperature of the cathode is different in the "Fuel Cell Type Electrolysis System" than in the NHE-FCS. Fig.6 shows the electrolyte temperatures versus input power for several experimental systems. In the "Fuel Cell Type Electrolysis System", the temperature rises at 10°C/W from 10°C. However, the NHE-FCS cathode is exactly 38°C when total input power is kept at 10W. It is presumed that the temperature influences the D/Pd.

4. Summary

A mass flow calorimetry system (NHE-FCS) has been developed to confirm the observed excess heat at "Fuel Cell Type Electrolysis System" experiments. The heat recovery of NHE-FCS cells has been measured at 0.983 ± 0.010 during calibration experiments with a Pt cathode and electrical heater. NHE-FCS is capable to detect excess heat of 0.2W at total 10W constant input condition.

All experiments using Pd cathode have been performed used identical protocol which showed excess heat at the "Fuel Cell Type Electrolysis System". Max D/Pd has been 0.84 in some experiments cells, and 0.89 in one experiment. Excess heat has not been observed at all experiments.

One possible reason is that D/Pd may be insufficient for excess heat generation, for the temperature is deferred by the cell designs and influences the D/Pd.

5. Acknowledgment

This work is one part of the New Hydrogen Energy Project supported by the Ministry of International Trade and Industry (MITI), and by the New Energy and Industrial Technology Development Organization (NEDO). The authors would like to acknowledge those contracting parties and the persons concerned for their continuous support.

The authors appreciate the valuable advice of Professor Ohta and Dr. Kunimatsu for NHE-FCS development. The authors would also like to thank Mr. Matsui, Director of NHE, and other members of NHE-Center and Laboratories for their collaboration.

6. References

1) *Proc ICCF-1*, Mar. 28-31, 1990.
2) T. Bressani, E. Del Giudice, G. Preparata, ed., *The Science of Cold Fusion (Proc. ICCF-2)*, Jun. 29--Jul. 4, 1991, Società Italiana di Fisica (1991)
3) H. Ikegami, ed., *Frontiers of Cold Fusion (Proc. ICCF-3)*, Oct. 21-25, 1992, Frontiers Science Series No.4, Universal Academy Press, Inc. (1993)
4) *Proc. ICCF-4*, Dec. 6-9, 1993
5) *Proc. ICCF-5*, April 9-13, 1995

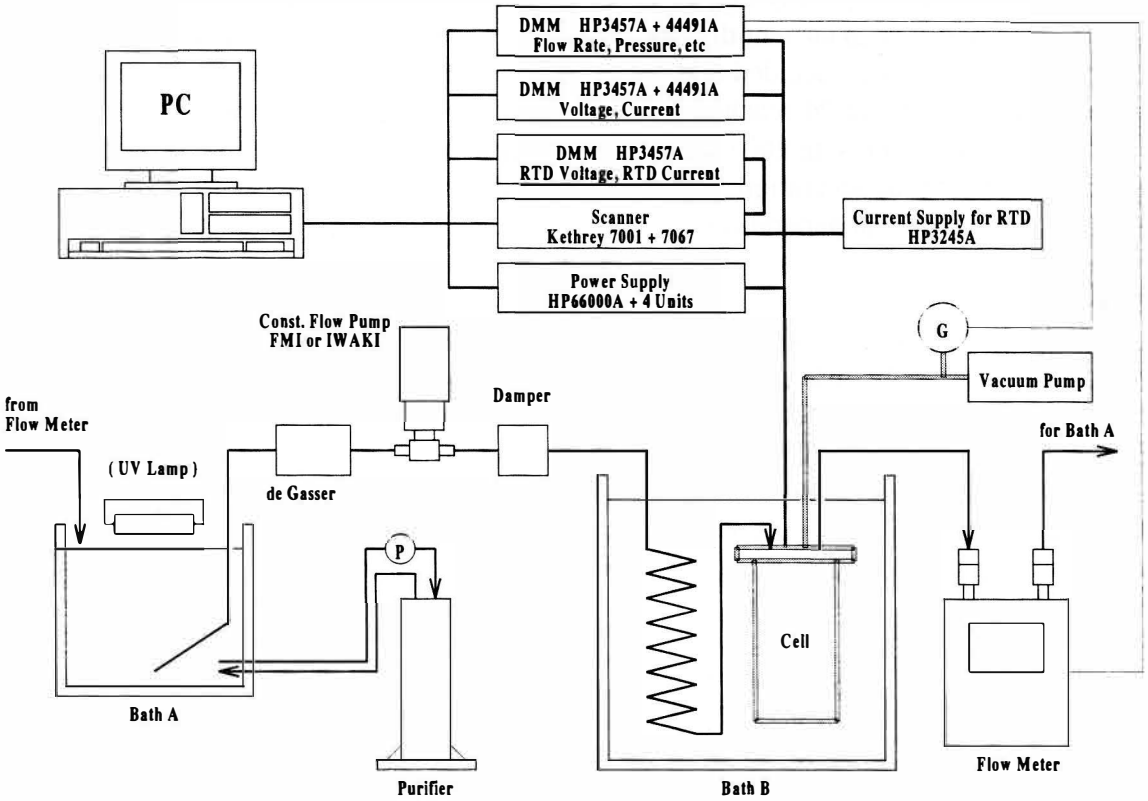

Fig. 1 The Overall System of NHE-FCS

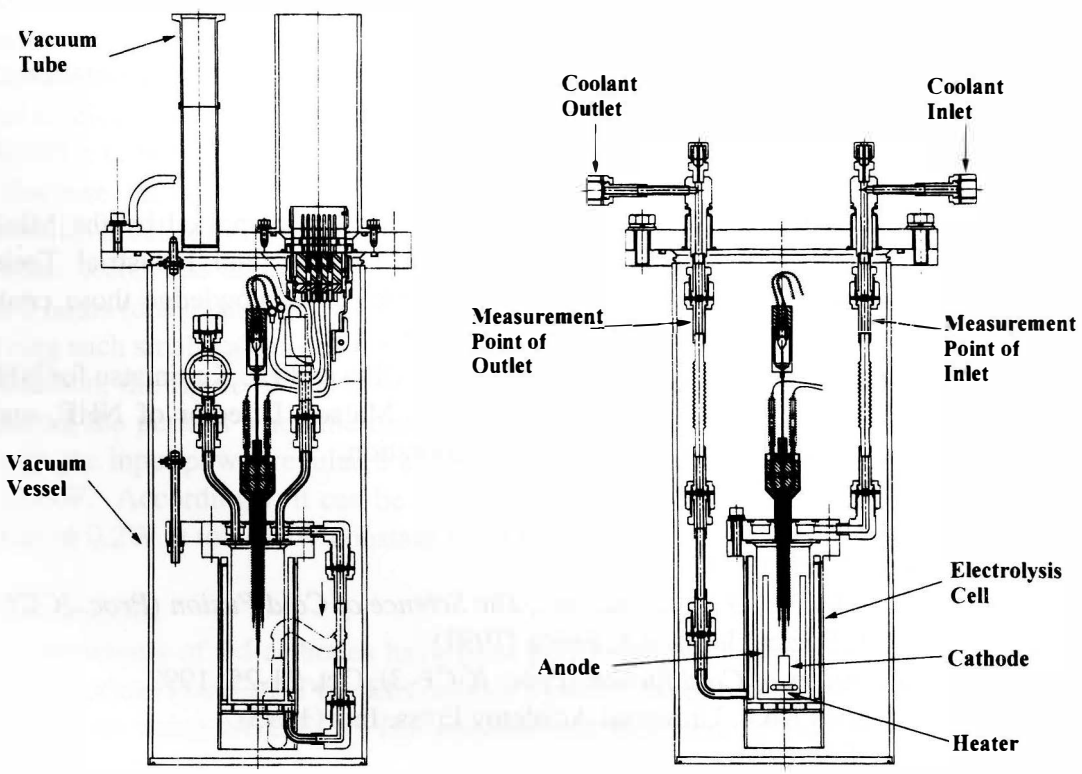

Fig. 2 The Cell Structure of Type C for NHE-FCS

NHE Session

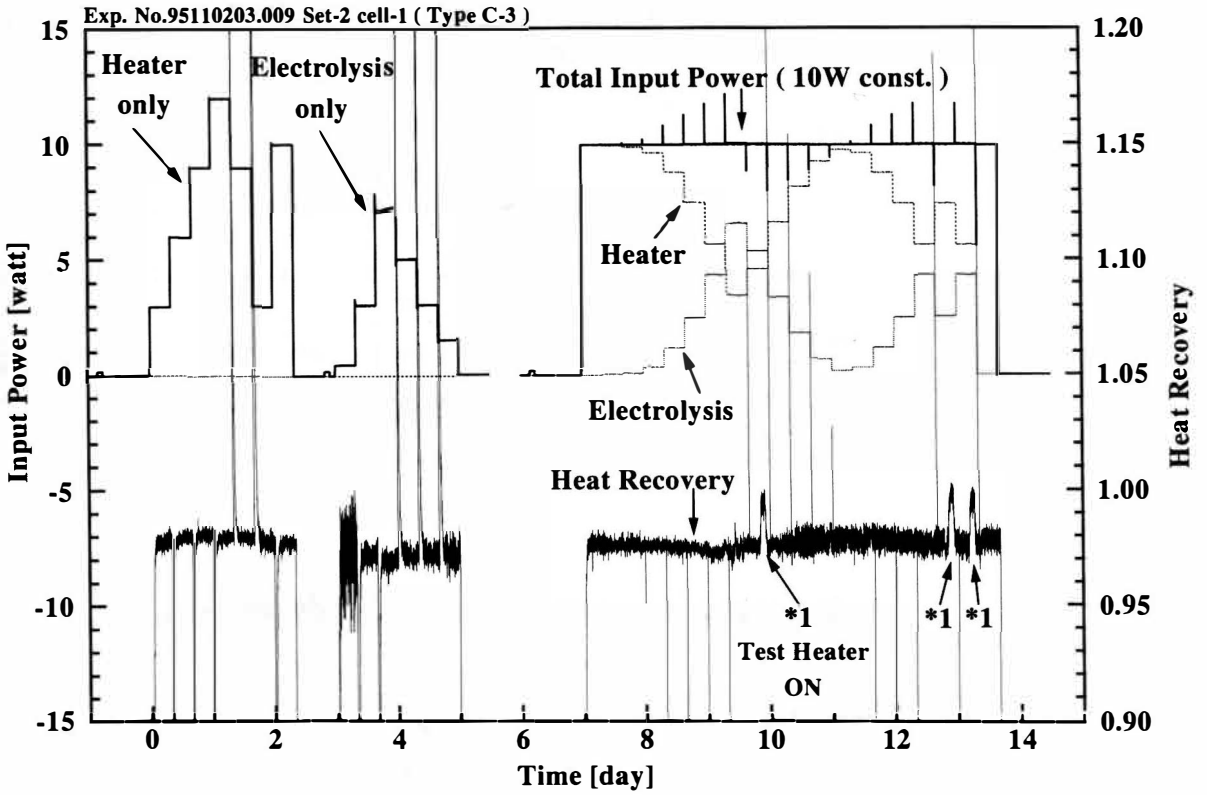

Fig. 3 Input Power, Heat Recovery v.s. Measurement Time

Pt(ϕ4 X 15), 1M LiOD, Inlet Fluid Temp 23deg.C

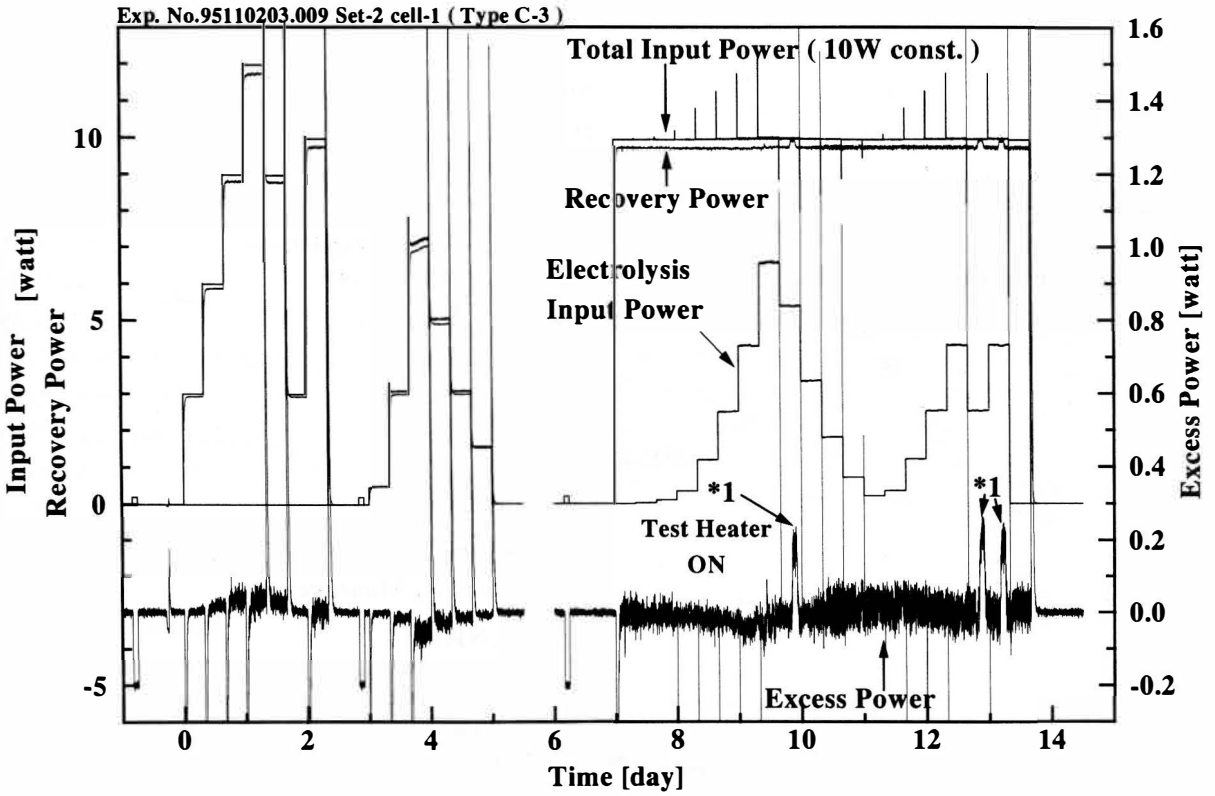

Fig. 4 Input Power, Recovery Power, Excess power v.s. Measurement Time

Pt(ϕ4 X 15), 1M LiOD, Inlet Fluid Temp 23deg.C

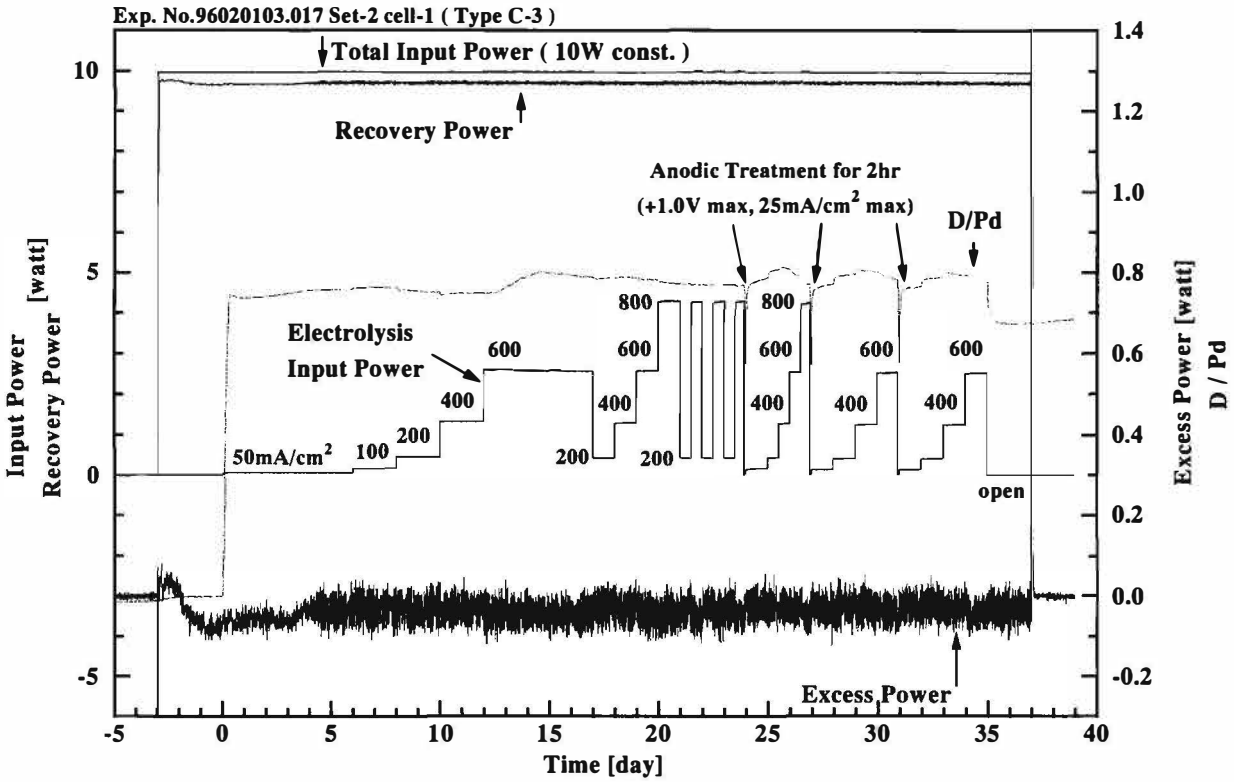

Fig. 5 Input Power, Recovery Power, Excess Power, D/Pd v.s. Electrolysis Time

Pd(4N Hyojunzai ϕ4 X 15, 10min etching in Aqua regia, 1000deg.C 10hr annealed)
1M LiOD, Inlet Fluid Temp. 23deg.C

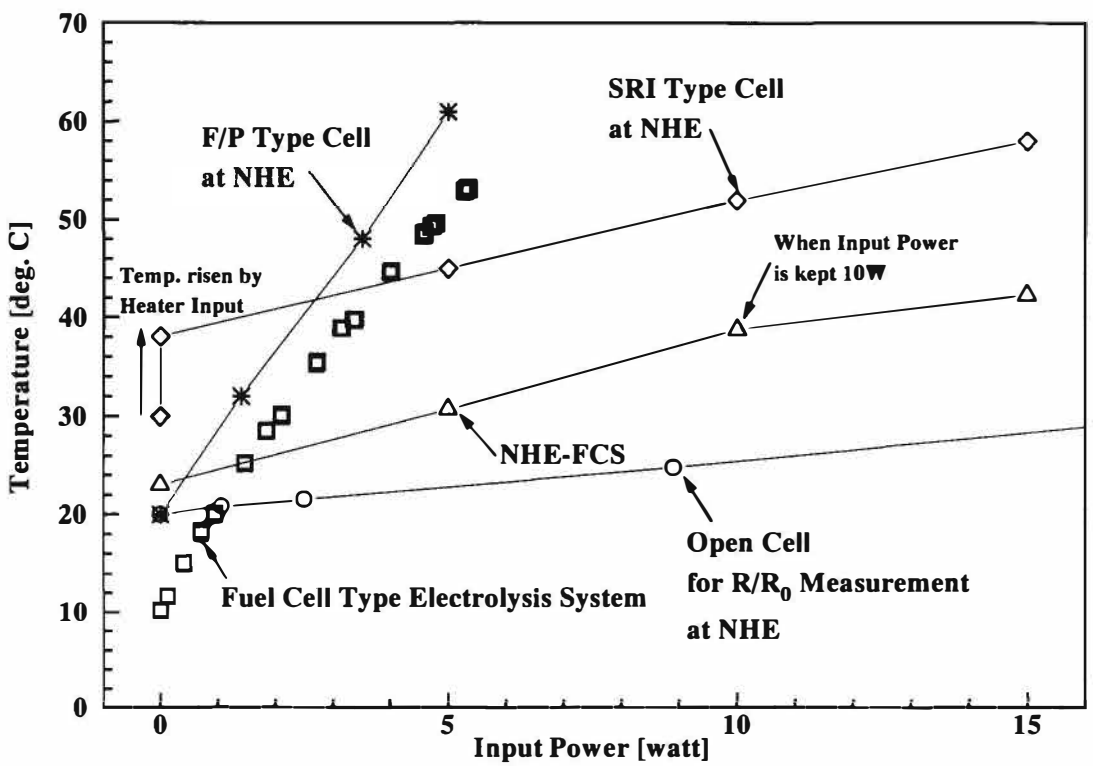

Fig. 6 Electrolyte Temp. of each System v.s. Input Power

NHE Session

STUDY OF MATERIAL PROCESSING AND TREATMENT FOR HIGH DEUTERIUM-LOADING

T. Senjuh, H. Kamimura, T. Uehara, N. Asami, * K. Mori, and ** T. Sigemitsu

R&D Center for New Hydrogen Energy, The Institute of Applied Energy
3-5, Techno Park 2-chome, Shimonopporo, Atsubetsu-ku, Sapporo 004, Japan
*Tanaka Kikinzoku Kogyo K. K.
2-73 Shinmachi, Hiratsuka-city, Kanagawa 254, Japan
**Nuclear Fuel Industries, Ltd.
950,Noda,Kumatori-Cho,Sennan-Gun,Osaka 590-04,Japan.

ABSTRACT

The electrochemical deuterium loading behavior of Pd cathodes in $LiOD/D_2O$ system has been studied experimentally using a resistance measurement method. The material conditions of Pd cathodes significantly affect the attainable D/Pd loading ratio. In addition, the D/Pd is affected by the applied current density profile, pattern of increasing current and anodic treatments.

As a result of the experiments, it was concluded that higher annealing temperatures (~1000 °C) result in higher D/Pd. In addition, etching in aqua regia proved to be a better surface treatment than polishing. It was confirmed that using the pre-electrolysis treatments resulted in higher D/Pd. The electrolysis current pattern and anodic treatment cycles likewise affected the D/Pd.

On the other hand the electrochemical hydrogen loading behavior of Pd cathode in $LiOH/H_2O$ system has been studied by a volume/weight measurement method. This shows analogous effects due to annealing as loading experiments with deuterium.

1. Introduction

Many results have been reported regarding the D/Pd reached during electrolysis, but the maximum D/Pd is dependent upon on the manufacturing history of the electrodes and the conditions of electrolysis. It has been pointed out by several observers that attaining a deuterium loading ratio greater than 0.85 is a prerequisite for observing excess heat generation phenomena [1].

A resistance measurement method was used in order to establish a procedure for selecting electrodes which can be expected to give a high D/Pd. In this study relationships were found for the D/Pd and the following parameters: heat treatment of the electrodes, current pattern, cycle of electrolysis, and surface treatment of electrodes.

On the other hand, the H/Pd was studied by a volume/weight measurement system in order to compare the H/Pd of several kinds of Pd.

2. Experimental

2-1. D/Pd by resistance measurement

All samples for cathode were made of Pd (2 mm in diameter and 50 mm in length) with a purity of more than 99.99%. The standard protocol for these Pd samples includes melting and casting in

vacuum and cold working at room temperature. These samples were used to study the effect of heat treatment (see section 3-1.a below), current density effect (3-1.b.) and the effect of multiple repetition of current cycles (3-1.c.). The Pd cathodes were subjected to various pre-electrolysis treatments, such as (1) a vacuum annealing to release the stress, to recrystallise and to clean the surface by thermal etching, and (2) a surface treatment to remove surface defects and to clean the surface. The D/Pd loading ratio is affected by the current density profile, current increasing pattern and anodic treatments.

Figure 1 shows the schematic figure of electrolysis cell and system for a resistance measurement method. D/Pd values were estimated from the resistance of the Pd measured by 4-point probe measurements with an AC signal (1mA, 1kHz) during electrolysis, using a milli-ohmmeter made by NF Electronic Instruments. D/Pd was calculated as a function of R/R_0 using an empirical method by McKubre [1] (see Fig. 2). Five Pt wires (2 current leads, 2 potential leads and one electrolysis lead) were spot welded on a Pd electrode. This electrode was positioned at the center of a spiral Pt anode in an open electrolysis cell filled with 1M LiOD. The cell is made by Teflon, is cold in water bath at 20 °C. Electrolysis was performed with stepwise current density patterns and repetition of cycles. A reverse potential of 0.75V was applied after each cycle of electrolysis.

2-2. H/Pd by volume/weight measurement

Fig. 3 shows the cells for the volume/weight measurement system. The cell was made entirely of Pt. Pd electrodes were immersed in 0.1M LiOH solution. Electrolysis was performed with a current density of 100 mA/cm^2. After electrolysis the gaseous volume of hydrogen discharged from Pd electrode was measured using a measuring cylinder and then the weight of the Pd electrode was weighed in order to measure the increased weight due to the absorption of hydrogen. The H/Pd of the Pd electrode was calculated using the gas volume and the weight increase.

Table 1 and 2 describe the experimental results and conditions of each experiment. Table 1 shows the comparative effects of purity, heat treatment and the presence or lack of an upper electrode. Table 2 describes the effects of etching, heat treatment (temperature, time and environment),exposure times of sample in air after heat treatment and degassing (deoxygenating) in a 0.1M LiOH solution through which a reducing or inert gas was bubbled. The effects of various heat treatments is likewise extracted from there results.

3. Results and discussion

3-1. D/Pd by resistance measurement

a. *Heat treatment of electrodes.* Figure 4 shows the resulting D/Pd for electrodes with different heat treatments. There were a vacuum annealing to release the stress, to recrystallise and to clean the surface by thermal etching. Pd electrodes heat treated at 200 °C for 3 hours (dehydrogenation treatment), 850 °C for 3 hours, and 1000 °C for 3 hours after manufacturing were used in this study. The results show that electrodes heat treated at higher temperatures yielded a higher D/Pd.

b. *Current density of electrolysis.* Figure 5 shows the resulting D/Pd obtained from four electrolysis current density patterns during two cycles. A current pattern which starts from a lower current density (20 mA/cm^2) gives a higher D/Pd (D/Pd =0.90) and a current pattern with a higher starting current density (200mA/cm^2) gives a lower D/Pd (D/Pd = 0.83). This tendency can be observed more clearly in the second cycle. A tentative hypothesis has been formed to explain this behavior. Deuterium entering at 20 mA/cm^2 due to its slow loading, may be able to diffuse inward. However, deuterium at 200 mA/cm^2 is more rapidly absorbed near the surface, possibly creating PdD near the surface and straining the lattice. This may have interfered with the ability to absorb deuterium later on.

c. *Repetition of current cycles.* Figure 6 shows how the D/Pd changed as the cycle was repeated. This result shows that the maximum D/Pd reached in the first cycle (D/Pd = 0.86) was lower than those reached in the second (D/Pd ≈ 0.90) and the third cycle (D/Pd ≈ 0.95). With each repetition of electrolytic cycles, the maximum D/Pd was larger than the D/Pd reached in the previous cycle. This likewise resulted in improved D/Pd. By this reverse potential, deuterium absorbed on the surface layer was desorbed. Thus density of deuterium was decreased in the surface layer. As a result in the next cycle more deuterium was easily absorbed. However, there is still a limiting value of the D/Pd value for reasons which are not entirely clear.

d. *Surface treatment of electrodes.* We also studied the effect of surface treatments of Pd electrodes. Heat treatment of NHE standard material results in changing the grain size difference between the inner and near surface regions. Figure 7 illustrates the manufacturing process of Pd electrodes which we used in this study. Special treatments include forging, homogenizing and modification of grain size. The resultant grain size is 50 μ to 100 μ, which is referred to as small grain. Figure 8 shows the D/Pd for electrodes with different surface treatments; i.e. polishing with diamond grit and etching with aqua regia. Electrodes etched with aqua regia showed higher D/Pd (D/Pd = 0.95) than electrodes polished with diamond grit (D/Pd = 0.92). For example, etching the cathode in aqua regia resulted in higher loading than polishing with diamond grit. Also, short etching time appears to be better than etching for longer time.

3-2. H/Pd by volume/weight measurement

a. *Heat treatment.* The 850 °C treatment samples achieved a higher loading ratio than the untreated samples and the 200 °C samples as shown in Table 1. It appears that the H/Pd was slightly higher when samples were annealed at 1000 °C than at 850 °C ones as show in Table 2. Heat treatment times of 1000 C are affected to H/Pd.

b. *Other effects.* Aqua regia etching also affected H/Pd. In addition, there may be small effects due to other variable which have not yet been clearly identified. At any rate there is considerable variability in the process, as shown in Tables 1 and 2.

4. Conclusions

The electrochemical deuterium loading behavior of Pd cathodes in $LiOD/D_2O$ system has been studied experimentally using a resistance measurement method. The material conditions of Pd cathodes significantly affect the attainable D/Pd loading ratio. In addition, the D/Pd is affected by the applied current density profile, pattern of increasing current and anodic treatments.

On the other hand the electrochemical hydrogen loading behavior of Pd cathode in $LiOH/H_2O$ system has been studied by a volume/weight measurement method.

The following conclusions follow from the experimental results.

(1) Pd electrodes heat treated at higher temperatures yield a higher D/Pd. The same results for H/Pd were obtained by a volume/weight measurement system. A heat treatment of 1000 C was more effective than 850 C, which in turn was more effective than 200 C.

(2) The D/Pd attained higher values for an initial current density of $20mA/cm^2$ than for an initial current density of $200mA/cm^2$

(3) The repetition of electrolytic cycles resulted in a larger D/Pd than in the previous cycle.

(4) Etching by aqua regia was more effective than polishing for D/Pd.

5. Acknowledgment

NHE Session

The New Hydrogen Energy Project has been supported by the Ministry of International Trade and Industries (MITI), and by the New Energy and Industrial Technology Development Organization (NEDO). In addition, the authors would like to acknowledge members of NHE Center and Laboratories for their collaboration.

Reference:

[1] M. C. H. McKubre et al., *First Annual Conf. on Cold Fusion Proceedings*, p.20 (1990).

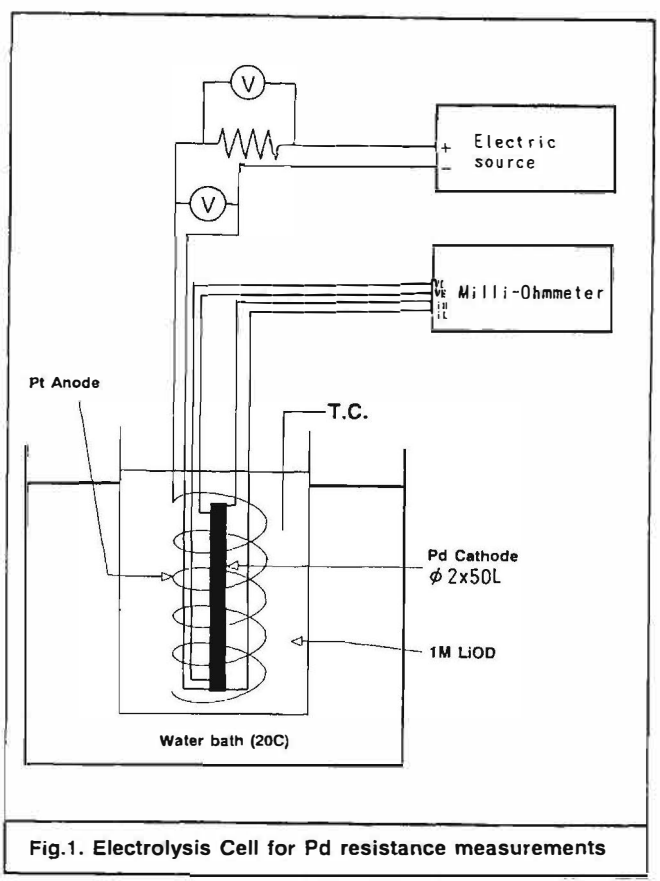

Fig.1. Electrolysis Cell for Pd resistance measurements

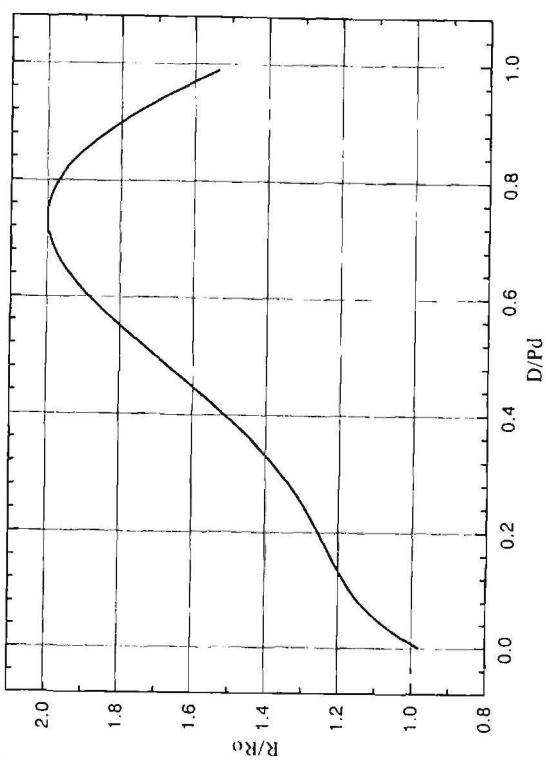

Fig. 2. Correlation Between D/Pd and R/Ro.[1]

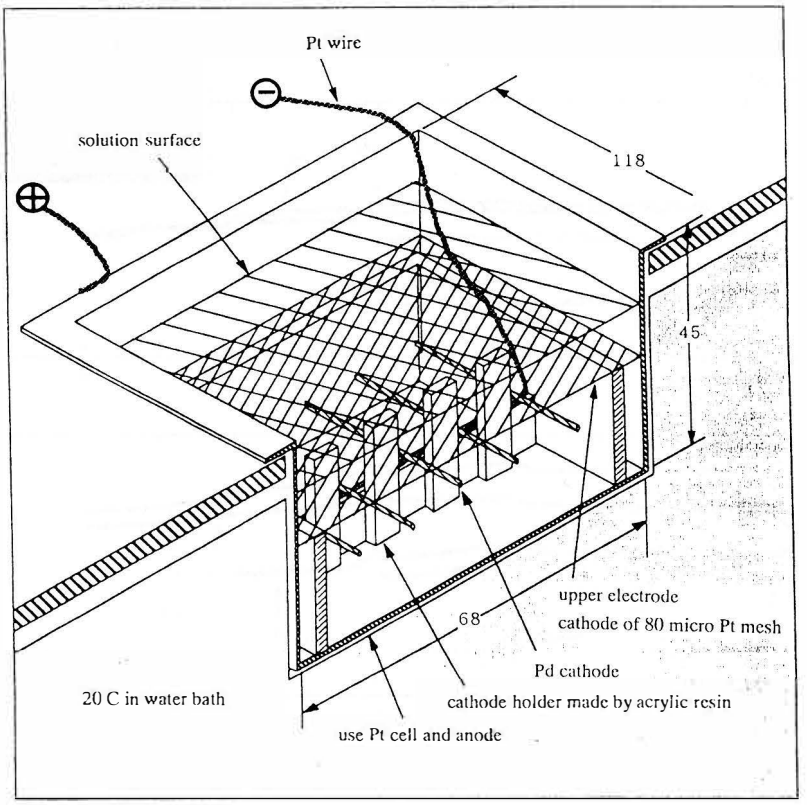

Fig 3. The schematic figure of "volume-weight method" electrolysis cell

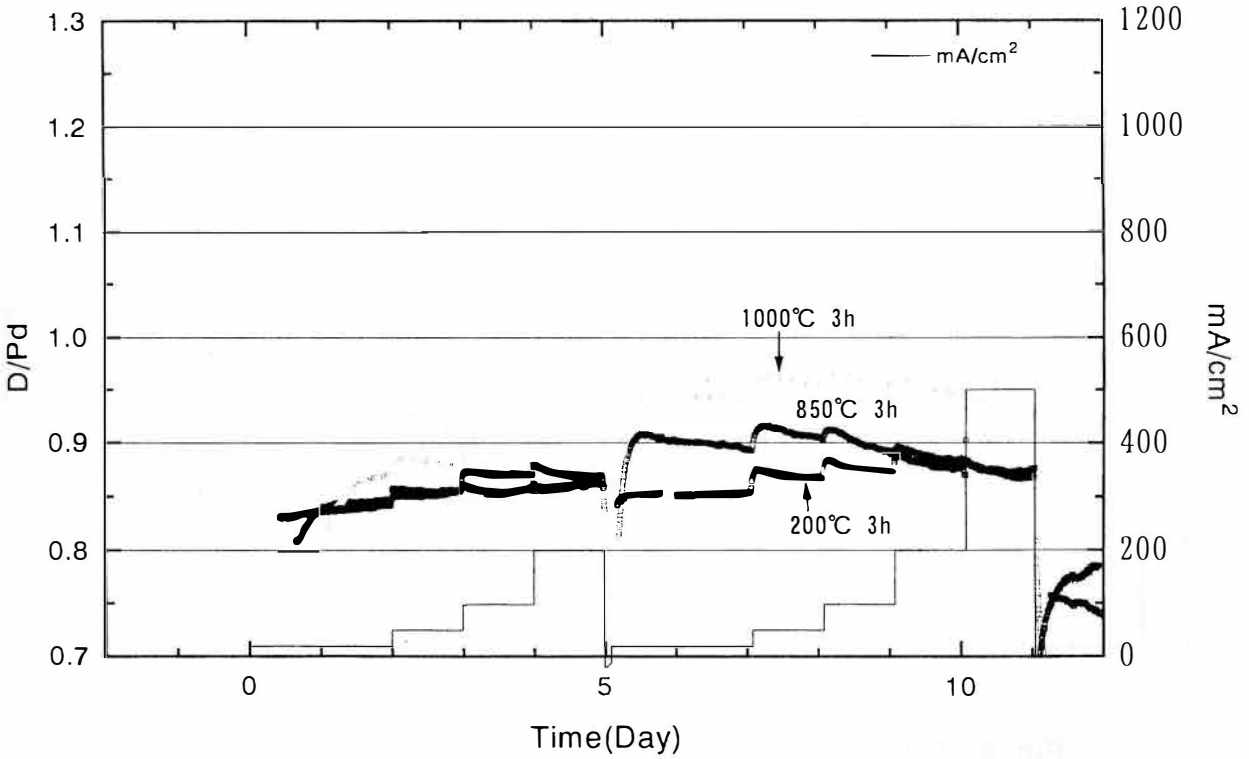

Fig. 4. Effect of Heat Treatment on D/Pd

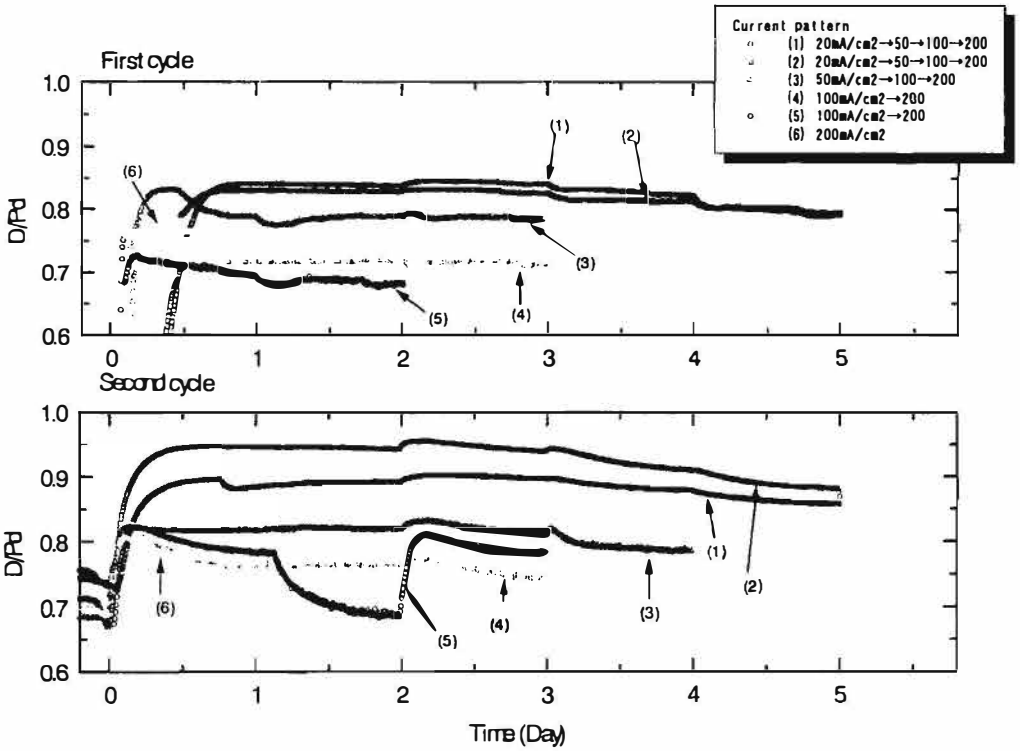

Fig. 5. Effect of Initial Current Density on D/Pd

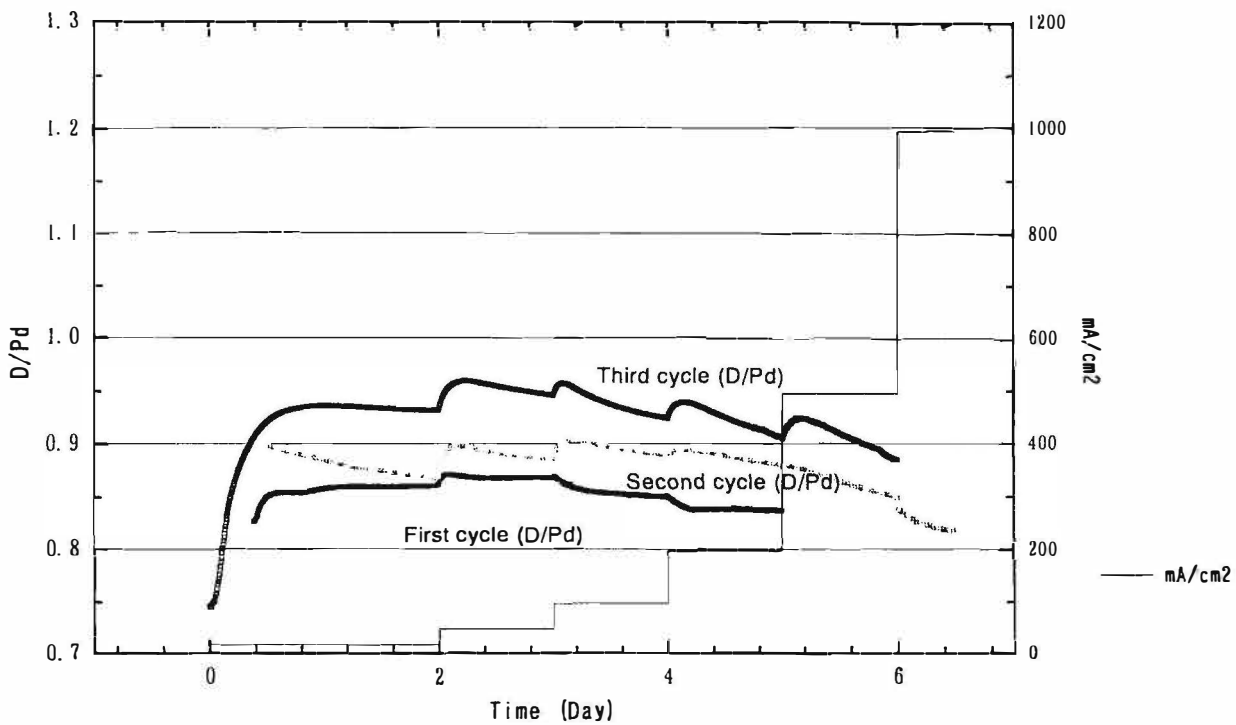

Fig. 6. Effect of current cycle repetitions on D/Pd

Treatment : 850 C 10 Hr Etched 10min

Modification of Grain size

	Process	Form
1	Raw material	Purity of Pd:99.99%up
2	Casting and melting in vacuum	30 □ mm
3	Machining	30 □ mm → 27 □ mm
4	Forging 900 ℃ × 1h in air	27 □ mm → 23 □ mm
5	Working	23 □ mm → 15 ϕ mm
6	Homogenizing	Annealed in N2 at 850 ℃ for 30 min
7	Working	15 ϕ mm → 2.0 ϕ mm
8	Cutting	Size 50mm length
9	Modification of grain size	Annealed in Ar at 850 ℃ for 30 min

Figure 7. Manufacturing procedure of Pd Electrode

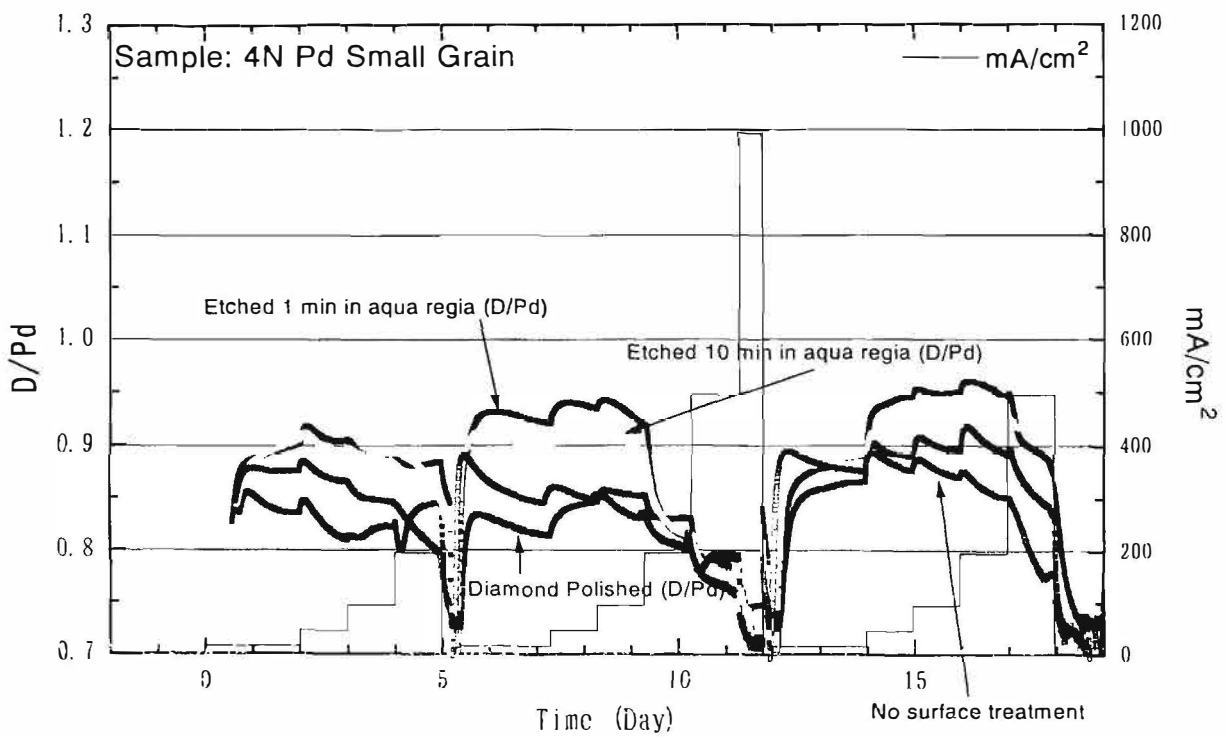

Fig. 8. Effect of Surface Treatment on D/Pd

Table. 1. Hydrogen Experimental Results -1

No	Purity	Homogeneous treatment	Heat treatment	H/Pd	Average
1	3N	—	—	0.809	X=0.811
8	4N	○	—	0.813	
2	3N	○	200 C (3hr)	0.821	X=0.816
7	4N	—	200 C (3hr)	0.810	
5	3N	—	850 C (3hr)	0.915	
6	3N	○	850 C (3hr)	0.925	X=0.914
4	4N	○	850 C (3hr)	0.904	
3	4N	—	850 C (3hr)	0.913	

Table. 2. Hydrogen Experimental Results -2

No.	Etched	Heat Treatment	Exposure	Degas	H/Pd	Average 1	Average 2
1	—	850 C (1hr)	1 min	—	0.925		
7	—	850 C (1hr)	2 days	Ar	0.920	X=0.926	
11	—	850 C (4hr)	2 days	H2	0.927		
13	—	850 C (4hr)	1 min	Vac.	0.930		X=0.926
2	○	850 C (4hr)	1 min	—	0.935		
8	○	850 C (4hr)	2 days	Ar	0.917	X=0.927	
12	○	850 C (4hr)	2 days	H2	0.927		
14	○	850 C (1hr)	1 min	Vac.	0.930		
3	—	1000 C (4hr)	2 days	—	0.934		
5	—	1000 C (4hr)	1 min	Ar	0.938	X=0.928	
9	—	1000 C (1hr)	1 min	H2	0.920		
15	—	1000 C (1hr)	2 days	Vac.	0.921		X=0.932
4	○	1000 C (1hr)	2 days	—	0.935		
6	○	1000 C (1hr)	1 min	Ar	0.939	X=0.936	
10	○	1000 C (4hr)	1 min	H2	0.937		
16	○	1000 C (4hr)	2 days	Vac.	0.932		

>99.99%Pd

Etched: Used aqua regia before heat treatment
Exposure: Exposure times of sample in air after heat treatment
Degas: deoxygenate in solution

NHE Session

MATERIAL BEHAVIOUR OF HIGHLY DEUTERIUM LOADED PALLADIUM BY ELECTROLYSIS

Naoto Asami, Toshio Senjuh, Hiroshi Kamimura, Masao Sumi, Elliot Kennel,
Takeshi Sakai*, Kenya Mori**, Hisashi Watanabe***, and Kazuaki Matsui

R&D Centre for New Hydrogen Energy
The Institute of Applied Energy
Sapporo,Hokkaido 004,Japan
*Nuclear Fuel Industries,Ltd.,**Tanaka Kikinzoku Kougyou Ltd.,***NEDO

Abstract

Studies on several kinds of palladium cathodes have been conducted using electrochemical cells using LiOD/D2O electrolyte to necessary and sufficient conditions for attaining high deuterium loading. Comparative observations of microstructure and analysis of surface impurities have been carried out on palladium specimens with various pre-electrolysis treatments. Single crystal samples of Pd absorbed deuterium rather slowly, but nevertheless reached comparatively high 0.89 D/Pd loading ratio. Many fine slip band structures were observed on the surface, and several micro-cracks existed in the crystal of post electrolysis specimens. High purity (>99.99%) polycrystalline Pd samples with surface purification treatment such as annealing at 850-1000 C in ultrahigh vacuum, also showed high (0.91 in max.) loading characteristics. Thermal etching effects were observed on the surface of annealed specimens at higher temperatures and high vacuum conditions. Surface micro-cracks along the grain boundaries as well as blistering of the electrode surface were observed in some cases. Surface impurities analysis showed that
Li atoms penetrate into the Pd cathode to a depth of several hundred to a thousand Angstroms from the surface. From these observations and analysis of various processed and treated Pd specimens, the material characteristics of Pd cathode achieving high loading ratio are discussed.

1. Introduction

A research and development project, referred to as the "New Hydrogen Energy" project [1], was started in Japan in November 1993, with the main goal of reproducing and verifying the existence of excess heat generation during electrolysis in Pd-LiOD systems.

It has been supposed that the reproducibility of these phenomena is mainly dependent upon achieving control of cathode material properties as well as the electrolysis environment. It has been pointed out by several observers that attaining a deuterium loading ratio (that is, the ratio of deuterium to palladium atoms) greater than 0.85 is a prerequisite for observing excess heat generation phenomena [2][3]. Thus, achieving high reproducibility of anomalous effects depends upon achieving reproducible high deuterium loading ratios.

Material development has proceeded according to this concept. Therefore, material observation and analysis using various techniques has been emphasised in this R&D project.

2. Experimental Procedure

a. Electrolysis Cell and System. Deuterium loading experiments are carried out to verify the excess heat generation during the electrolysis of heavy water with Pd electrode using fuel cell type electrolysis cells [4]. A schematic diagram of the electrolysis cell is shown in Fig. 1. The inner wall of the cell body containing 1 M $LiOD/D_2O$ electrolyte is coated with a Silicon based ceramic film. The Pd cathode, fuel cell anode, reversible hydrogen electrode and thermocouple are fixed in the cell body. Electrolysis is performed with a constant direct current and the current value is changed after equilibrium conditions have been well established for the temperature of electrode, electrolyte and gas phase and deuterium over-voltage at the cathode. The deuterium loading ratio, D/Pd, is determined from the following equation:

$$\frac{D}{Pd} = -2V\left(\frac{P_o}{T_o} - \frac{P}{T}\right)nR \quad ,$$

where V is the internal gas phase volume of the cell, n is the total number of mols of metal atoms in the Pd cathode, R is the universal gas constant, P is the deuterium gas pressure T is the deuterium gas temperature, and P_o and T_o refer to the initial values of P and T prior to electrolysis.

b. Material Preparation. Various Pd cathode materials are prepared and examined to determine their suitability for achieving high deuterium loading. Pd materials and electrolyte used in the series of experiments are tabulated in Table 1. A commercially available rod (TK-A) is cast in a radio frequency induction-heated furnace in air with an oxidation resistant material. It is then worked by a swaging machine at ambient temperature. Single crystal (TK-AS) was prepared using the floating zone melting method in an argon atmosphere using a TK-A rod as the source material. High purity (>99.995) rods (TK-VA) are cast in vacuum and worked at room temperature. The higher defect density surface zone is removed by machining the outer 200 microns. Other high purity (>99.99) rods (JM-Z) were cast in a hydrogen-nitrogen atmosphere, and worked and annealed before final 20% reduction. After electrodes are machined to final dimensions (4.0 mm x 20 mm length), the surface is polished using diamond paste or diamond spray, and the surface is cleaned with acetone, ethanol, and purified water in an ultra-sonic cleaner. Several finish treatments are examined to remove surface impurities and to make a clean activated surface. Both acid etching for ten minutes in concentrated aqua regia and high temperature vacuum annealing (~850-1000 C for 10 h in a $<5 \times 10^{-6}$ vacuum) have been used. Heat treatment under high vacuum and high temperature have both effects of recrystallisation and surface cleaning by thermal etching.

For cold-worked specimens, a 200 C vacuum process is used to remove hydrogen from the Pd cathode.

c. Observation methods and impurity analysis. Pre-electrolysis and post-electrolysis observations of the microstructure of the specimens are performed using OM, SEM, and FE-SEM, and the impurity analysis are carried out with AES, SIMS and EPMA. The measurement of lattice parameter and phase change are observed by X-ray diffraction. An *in situ* video observation method of surface microstructure has been developed to investigate microstructural change during electrolysis process and to observe deuterium bubble formation and release process.

3. Results of the deuterium loading

A typical history of current density, D/Pd ratio, input power and excess heat are shown in Fig. 2 for the case of TK-VA-3. At the beginning of electrolysis the current density was set at 50 mA/cm^2 for 6 days, and then the current density was changed step by step to 100, 200, 400, and 600 mA/cm2 for two days at each level. After this current cycle, the current density was decreased abruptly to 200 mA/cm^2 and again stepped up to 800 mA/cm^2, and followed by additional high current pulse or

ramps. These changes of electrolysis condition were performed to investigate the dependence of D/Pd ratio and excess heat generation upon current density. In this case, the maximum D/Pd reached 0.91 at 200 mA/cm2 and 0.89 at 800 mA/cm^2, 28 and 24 days after the start of electrolysis respectively. Excess heat generation phenomena has been reproducibly observed with suitable material preparation and treatment in the fuel cell type electrolysis cells .[3]

Loading ratios attained by similar electrolysis condition described as above, are tabulated also in Table 1 for several Pd materials.

4. Results of material observations and analysis.

a. *Microstructural change during loading and deloading.* Single crystal Pd samples (TK-AS) absorbed deuterium slowly. However the maximum loading ratio reached the rather high value of 0.89. Many regular slip band bands about 2 μ in breadth, along the (111) plane were observed on the surface as shown in Fig. 3. The x-ray diffraction pattern of the post electrolysis specimen shows the sample no longer has a purely single crystal structure. Several internal crack like defects are observed in the post electrolysis single crystal specimen as shown in Fig. 4. These might be caused by the deformation of the crystal due to deuterium absorption and transitions between the α and β phases.

The surface structure of high purity polycrystalline Pd (TK-VA) after high temperature vacuum annealing is shown in Fig. 5a. Grain boundaries and fine surface structures are observed in the grains as shown in Fig. 5b, which were probably formed by thermal etching in high vacuum. Fig. 5c shows the surface structure of TK-VA-2 after electrolysis. Several cracks along the grain boundary are observed and fine slip band bands are also observed in the crystal grains. The basic mechanism of the formation of slip bands is presumed to be the same as for the case of single crystal samples.

The microstructure of EH-L1 specimens before electrolysis and after are shown in Fig. 6a-c. The average grain size is about 200 μ. Sub-grain-like fine structures are observed at the inside of initial grains on the etched surface. Fine granulation seems to be proceeded by the transition between α and β phases.

Figs. 7a-b show the cross sectional views of a relatively low loading state (D/Pd=0.20). The α + β phase region progresses radially toward the centre and fine granulation is also observed in the initial grains. Diffusion enhancement at grain boundaries, which is normally expected, seems to be have less effect in this system.

Fig. 8a-b show that blistering due to deuterium gas occurred on the surface of electrode during electrolysis in some annealed specimens. Clear cracks along the grain boundaries were formed on the top of the blistering. This phenomena may be explained by assuming existence of some kind of defect such as closed pore, inclusion, or plane shape defects near the surface before electrolysis. Deuterium gas may accumulate in the defect, and as a result the gas pressure increases several hundredfold. The annealed surface is then deformed by blistering.

b. Surface impurity analysis. Fig. 9a shows the AES surface impurity analysis after electrolysis. Impurities such as S, Cl, C, and O are detected in most post electrolysis specimens. However it is confirmed by an ion-sputtering method that the impurity layer is less than 20 Angstroms thick. The existence of C and O are confirmed by EPMA analysis. Fig. 9b shows the depth profile of the near surface region of the palladium cathode by AES. The penetration of Li atoms from LiOD into the Pd cathode is confirmed by SIMS. The penetration depth ranges from several hundred to a thousand Angstroms, according to the depth profile analysis.

5. Discussion

Absorbed deuterium into the Pd crystal will be expected to occupy the octahedral sites of fcc Pd lattice for D/Pd ratios up to unity, and tetrahedral sites for over unity. It is believed that the

tetrahedral site of Pd acts as a transient site for the diffusion process. As an analogical model of deuterium loading, it could be considered that the Pd lattice forms a volume for the deuterium atoms (ions). The D/Pd ratio can be calculated as the integral difference of inlet flow and outlet flow of deuterium atoms in this specific volume element. To first order, during steady-state electrolysis, inlet flow and outlet flow will be mainly dependent on the surface conditions, the concentration of deuterium atom density and the electronic potential field on the Pd electrode surface, and surface microscopic and macroscopic structures. The inlet flow and outlet flow are considered to be controlled by absorption, desorption and diffusion through several kinds of paths in the Pd material. The effect of the value of the diffusion rate on the maximum loading ratio would be somewhat complicated; however the diffusion rate is generally small. Diffusion is enhanced by introducing lattice defects such as point defect, dislocation and grain boundary defects. The migration rate of deuterons is increased and saturation of loading ratio is prompted by the introduction of lattice defects. However, the final saturation value of loading ratio will be decreased because the outlet flow responds more sensitively to the state change of flow channels on the surface especially at high loading ratios (D/Pd > 0.8).

From these simplified considerations, the basic requirements for Pd material capable of achieving a high loading ratio are as follows:

1) to have large numbers of vacant absorption sites (O-sites).
2) to have a large absorption area during electrolysis;
3) to minimise dissociation area and prevent the incremental loss of deuterium;
4) to minimise the quantity of dissociated deuterium during the electrolysis process.

Table 2 shows the favourable state mentioned above and the corresponding material treatments. From these considerations, the specification of Pd material and the treatment having high loading ratio have been selected as follows:

A) Specification: (1) Initial purity > 99.99%, (2) vacuum melt, (3) forging and annealing to homogenise, (4) machining the outer 0.2 mm to remove surface defects.

B) Treatment: (1) Surface cleaning and etching by aqua-regia to remove surface impurities,
(2) Ultrahigh vacuum (oil free) high temperature annealing to recrystallise and to form an activated surface.

The TK-VA material series of Table 1 is made on the this concept, and achieved the highest loading ratio of 0.91. Further modifications are necessary to prevent blistering, crack formation at grain boundaries, and loading reduction at higher current density. The material must maintain good ductility and resistance against the deformation due to the stress release which accompanies deuterium loading and transformation. The effects of deposition of surface impurity and Li penetration have to be clarified.

Acknowledgement.

The New Hydrogen Energy Project has been supported under the direction of New Energy and Industrial Technology Development Organisation (NEDO). The authors are indebted to Porf. Okamoto, Prof. Ikegami, Dr. Kunimatsu and all of the NHE-committee members for their guidance and valuable advice in promoting the NHE-Project. We would like to thank all members of NHE-Centre and Laboratory for their collaboration.

Reference

[1] N. Asami, K. Matsui, F. Hasegawa, Proceedings of the 5th international conference on cold fusion. April 9-13, (1995) Hotel Loews, Monte-Carlo, Monaco. P87

[2] M.C.H. McKubre, et al., Frontiers of Cold Fusion (H. Ikegami, ed.), p5, Univ. Acad. Press, Tokyo, 1992 (Proc. of the 3rd in ternational conference on cold fusion, Oct. 21-25, Nagoya, Japan).

[3] H. Kamimura, T. Senjuh, S. Miyashita, N. Asami, To be presented in ICCF-6 Oct. 13-18, Hotel APEX Toya, Japan. To be published in the Proceedings.

[4] K. Kunimatsu, et al., Frontiers of Cold Fusion (H. Ikegami, ed.), p5, Univ. Acad. Press, Tokyo, 1992 (Proc. of the 3rd international conference on cold fusion, Oct. 21-25, Nagoya, Japan).

Table 1 Material list of Pd samples used in experimental series.

lot No	purity (major impurities)	cast	working	grinding	polishing	spec. processing	etching	heat treatment	Hv hard.	loading ratio max. D/Pd(H/Pd)		D/Pd range
TK-A	>99. 95 Pt. Ag. Al. B. Ca	RF in air	RT. swaging	none	Al ₂O ₃	–	-	as cold worked 200℃ evacuate	141	0. 83	(0. 87)	0. 80-0. 83
TK-AS	>99. 97 Pt. Ag. Al. Fe	RF in air	RT. swaging	-	–	single crystallize by floating zone	-	200℃ evacuate	-	0. 89		0. 87-0. 89
TK-VA-1	>99. 995 Fe. Sn. Au	RF in vac.	RT. swaging	0. 2mm dia.	spray	-	-	as cold worked 200℃ evacuate	106	0. 82		0. 80-0. 88
TK-VA-2	>99. 995 same as above	RF in vac.	RT. swaging	0. 2mm dia.	spray	-	-	1000℃ x10hr. in Vac<5-10-6torr	59	0. 90		0. 85-0. 90
TK-VA-3	>99. 995 same as above	RF in vac.	RT. swaging	0. 2mm dia.	spray	-	aqua-regia.	1000℃ x10hr. 10 min. Vac<5-10-6		0. 91	(0. 94)	0. 85-0. 91
TK-VA-4	>99. 995 same as above	RF in vac.	RT. swaging	0. 2mm dia.	spray	-		850℃ x10hr. in Vac<5-10-6torr		0. 88		0. 83-0. 88
JM-Z-1	>99. 99	RF in H ₂-N ₂		none	dia. paste	-		as 20% worked 200℃ evacuate	-	0. 85		0. 83-0. 85
EH-LI-1	>99. 8 Ca. Si. Pt. B. Al	RF in air		0. 2mm		received fromSRI		850℃ x3hrinVac		-		
IM-VB-1	>99. 95	RF in Vac.	RT. swaging			-	aqua-regia	200℃ evacuate		0. 88		0. 87-0. 88

Note ; Manifacturer = TK : Tanaka Kikinnzoku Kougyou. JM:Jhonson Mathey. EH:Engelhart. IM:IMRA Material. Sample size = final size 4mm Φ x 20mm.
Electrolyte = 1M LiOD/D2O. Purity of D2O:>99. 9% (<0. 1%H2O) RF:radio-frequency induction furnace. RT:cold work at room temp. . Hv:Vicker's hardness.

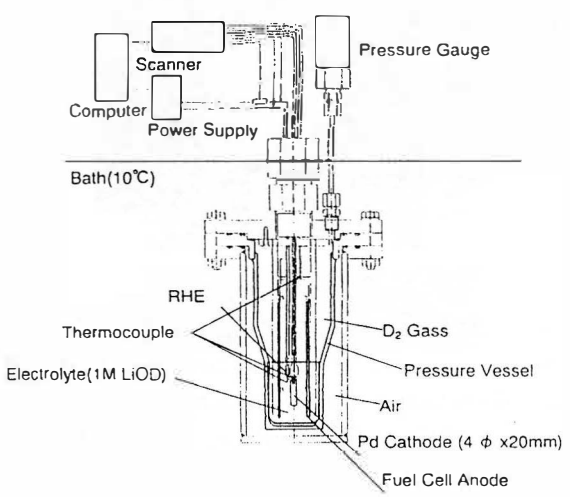

Fig. 1 Schematic diagram of the electrolysis cell

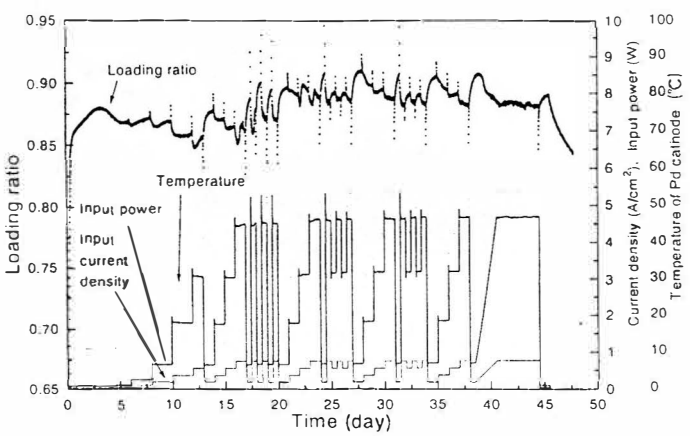

Fig. 2 Typical history of loading ratio D/Pd, input current, input power, and temperature of Pd cathode (TK-VA-3)

Fig. 3 Many regular slip bands were observed (by FE-SEM) on the surface of post electrolysis single crystal (TK-AS)

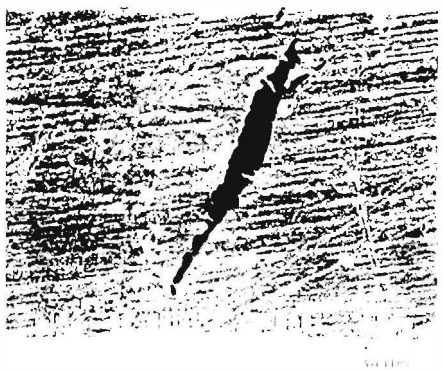

Fig. 4 Internal crack-like defect in the post electrolysis single crystal (TK-AS) observed by SEM

Fig. 5a-c Surface structure of TK-VA annealed at 1000 C x 10 hr in high vacuum (< 5 x !0 -6 torr). Grain boundary and fine surface structures are observed in the grain, probably formed by thermal etching in high vacuum (Fig. 5b). Several cracks along the grain boundary and fine slip bands are observed in the crystal grains of the sample after electrolysis (Fig. 5c).

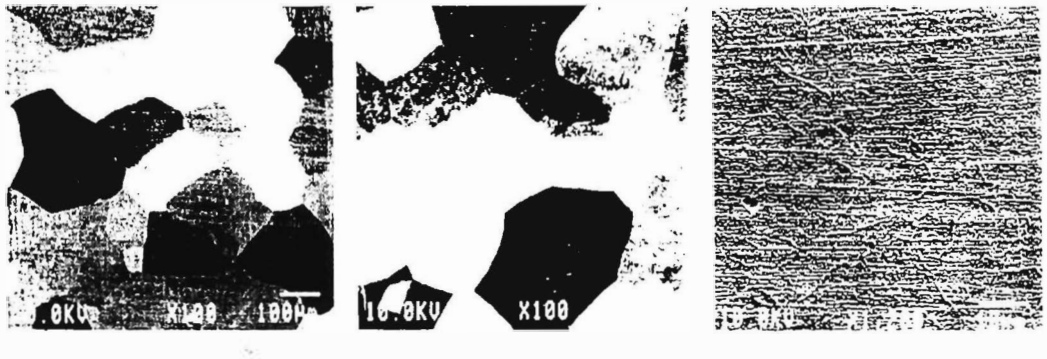

Fig. 6a-c Polished and etched surface structure of cross section of EH-L1 before (6a), and after (6b and 6c) electrolysis. Sub-grain-like fine structures are observed at the inside of initial grains as shown in Fig. 6c

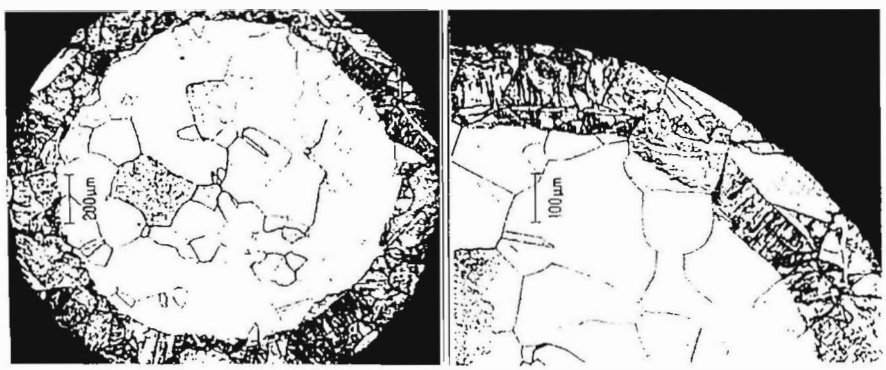

Fig. 7a-b Cross sectional view of relatively low loading state of TK-VA. The $\alpha + \beta$ region progresses radially toward centre and fine granulation is advanced.

Fig. 8a-b Blistering due to deuterium gas occurred on the surface of electrode during electrolysis in some annealed specimens (TK-VA). Fig. 8b shows the top structure of blistering and several cracks are formed along to the grain boundary.

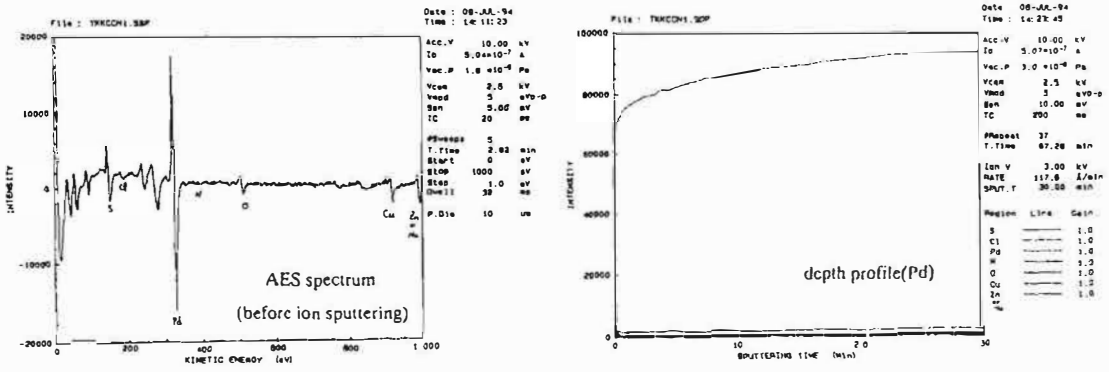

Fig. 9a-b AES surface impurity analysis after electrolysis (TK-A). Impurities of S, Cl, C, and O are detected in most post electrolysis specimens (Fig. 9a). Depth profile of palladium atoms on the near surface region after electrolysis is shown in Fig. 9b. The penetration of Li atoms from LiOD into the Pd cathode is confirmed by SIMS analysis.

Table 2 Basic characteristics of high loading material and corresponding treatments.

Favorable Material State	Corresponding Treatments
(1) Make Vacant state of Absorption Site(O-Site)	
Remove impurity atoms on O-site	High purity material, Vacuum melt, and
Reduce inclusion / precipitates / closed pore	Evacuate at high temp. . ultrahigh vacuum
(2) Maximize Absorption Area & Not Reduce	
Remove surface bad impurities	Ultra-sonic cleaning, Etching by aqua-regia
	High vacuum & high temp. treatment
Prevent adsorption of bad impurities	Purification of electrolyte
(3) Minimize Dissociation Area & Prevent Increment	
Remove surface macroscopic crack	Surface machining, Annealing stress
Reduce open pore, surface inclusion	Vacuum melt, Clean working processing
Reduce closed pore, defect in near surface	Vacuum melt, Homogenized treatment
Reduce surface scratch, roughness	Fine surface polishing
Minimize Dissociation channel	Suitable grain size, Homogenization
(4) Suppress Dissociation Quantity During Electrolysis	
Keep ductility/toughness against deformation	Suitable grain size, Additional cold working
Keep high loading ratio at high current density	Optimize electrolysis condition,

NHE Session

NEW HYDROGEN ENERGY RESEARCH AT SRI

M. C. H. McKubre, S. Crouch-Baker and F. L. Tanzella, M. Williams and S. Wing
SRI International, Menlo Park, CA USA

Abstract

With financial support from the Institute for Applied Energy (IAE), SRI International has undertaken a research and development program in the field of New Hydrogen Energy production. The long-term goals of this program are: (i) to understand the phenomenology and identify the mechanism(s) of new hydrogen energy production, and (ii) to increase the rate of energy production to useful levels. To these ends, in addition to research at SRI International, collaborative research with IAE has been undertaken at SRI and IAE's facility in Sapporo.

Research has been performed in a number of areas: Firstly, calorimetric studies of the palladium/heavy water system have been carried out using electrochemical cells housed in well-qualified mass flow calorimeters, one design of which is capable of accurate measurement of the helium content of the cell. Although most results have been obtained for electrolyte temperatures in the range 25-40°C, some experiments have been undertaken in the vicinity of the boiling point of heavy water. In addition to these calorimetric experiments, extensive studies have been made of the electrochemical loading of deuterium into palladium obtained from a variety of sources.

While the results obtained are consistent with those obtained previously, by various researchers, it is clear that attainment of the necessary conditions for excess heat production is greatly impeded by a materials-induced variability of a critical parameter which is not presently under our control.

1. Introduction

For the past two years, SRI International has participated in the New Hydrogen Energy (NHE) program, run under the auspices of NEDO, Japan. The underlying goal of this program is to understand the origin of the various calorimetric and nuclear anomalies which have been reported recently in connection mostly with the electrochemical insertion of deuterium into palladium.

An important aspect of any experimental program is the need to achieve consistency and replicability of results. The studies carried out under the NHE program have necessarily been tightly focused on the achievement of the immediate project goals: the reproducible attainment of excess heat, or, failing this, to obtain an explanation for the apparent absence of replicability.

In previous experiments we have established empirically a hypothesis or phenomenological model for the occurrence of "excess heat" in the D/Pd system. This model predicts that, for 1 and 3 mm diameter, pure palladium wires, loaded electrochemically with deuterium in 1 M LiOD electrolytes, we expect[1] to observe anomalous "excess" heat if we meet the following four criteria:

i) we need to achieve and maintain a D/Pd loading at or above some critical value (0.85-0.90)

ii) for periods of time (several hundred hours) substantially longer than the diffusional time constant of D in the Pd lattice

iii) at currents (or current densities) above some threshold value (several hundred mA or mA cm^{-2})

iv) in the presence of some flux of D passing through the interface.

This model has been quantified[1] in the form of the following equation;

This model has been quantified[1] in the form of the following equation;

$$P_{xs} \propto (I - I^{\circ})\,(x - x^{\circ})^2 \frac{\delta x}{\delta t} \qquad [1]$$

There is no fundamental basis for equation [1], although the terms are consistent with some theoretical descriptions of heat production via lattice-induced nuclear processes.[2] Equation [1] is almost certainly overly simple, and suffers from the added difficulty that its terms are not orthogonal: the current affects the flux, the flux affects the loading, and the current affects the loading. It is the character of this last interrelationship, which is both surprising and unfortunate, that is the subject of this paper.

2. Experimental

A feature of our D/Pd experiments is that, despite nominally and apparently identical metal source, metal preparation and electrolytes, different cathodes exhibit different loading and overvoltage responses to the same electrochemical treatments.[3] Until we can control this variability, we have adopted what we call a "farmed" approach to our calorimetric experiments. Typically, six experiments are started together in "farms" which are intended to perform two functions: (i) explore in a statistical way,[3] the role of various variables affecting loading; (ii) identify two candidate cells, adventitiously well loaded, to be studied in two stations of our L-series mass flow calorimeters.[1]

Table 1 summarizes the results of calorimetry performed in this way, since ICCF5. This table is broken horizontally into three data blocks: cathode source and size; important characteristics of the behavior of the cathode in the degree of loading (DoL) farm; some features of the behavior in the calorimeter. Where cells do not have an entry in the DoL columns, they were started directly in the calorimeters.

Table 1 reveals several important details in the context of the hypothesis regarding excess heat production, that we are attempting to test. In all cases the maximum current experienced by the cathode exceeded the maximum threshold current previously observed for excess heat production. In almost all cases, the experiment duration exceeded the minimum initiation period. In many cases, the maximum loading inferred from the measured resistance- ratio/loading functionality,[4] was certainly at the level where excess heat might be expected. Despite the separate attainment in many experiments of most of the criteria that we have identified as being important, none of the 13 experiments listed in Table 1 displayed excess power outside the range of measurement uncertainty, during steady state operation.

One possible explanation for this failure can be found in footnote 2 in Table 1. In general, the current density of maximum loading was ~100 mA cm^{-2}. As the current was raised significantly above this level in the attempt to generate excess power, the cathodes de-loaded; in some cases, this de-loading was precipitous.

Such rapid de-loading has not always been observed. Figure 1 shows results from two experiments published previously.[5] Experiments P15 and P16 were prepared identically and operated simultaneously. Both employed Engelhard Lot #l palladium (1/8" machined to 3 mm diameter and 3 cm long) in 1 M LiOD containing 200 ppm Al. The surface of the cathode P16 was modified by implantation of ^{3}He, although this detail is not regarded as salient in the following discussion.

Table 1. L-Series Calorimetry - Summary of Results

Batch	Cathode dia. (mm)	length (mm)	Degree Start	of Loading Farm Cell	Duration (days)	Max D/Pd	Calorimeter Duration[1] (days)	Maximum[2] D/Pd	I(A)
LL5 Eng.#3	3	30	Apr-95	S3	20	0.92	22	>0.96	3
LL6 Eng.#3	3	30	Apr-95	S4	20	0.93	22	0.91	3
LL7[3] Eng.#5	3	30	Jun-95				7	<.85	1.15
LL8[3] Eng.#5	3	30	Jun-95				7	<.85	1.15
LL9 Engelhard	1	30	Jun-95				60	0.92	2
LL10 Engelhard	1	30	Jun-95				60	0.92	2
LL11 IMRA	1	30	Jul-95	U4	76	>.97	65	0.94	1.5
LL12 IMRA	2	30	Jul-95	U1	76	>.97	64	0.93	3
LL13 IMRA	1	30	Sep-95	V4	40	>.95	39	0.92	1.5
LL14 JM(Z)	1	30	Sep-95	V2	40	0.95	39	0.95	1.5
LL15 IMRA	1	30	Oct-95	W3	36	>.95	84	0.97	1.5
LL16 IMRA	1	30	Oct-95	W4	36	0.94	84	0.94	1.5
LL17 Pt	1	30	Mar-96				14		2.5
LL18 IMRA	1	30	Apr-96	X3	75	0.96	36	0.9	3
LL19 Pt	1	30	Apr-96				36		2.5
LL20 Pd sheet	1 x 10	20	Jun-96				43		2
LL21 Pd sheet	1 x 10	20	Jun-96				43		2
LL22 JM(Z)	2	30	Aug-96	Z2	21	0.94	38	0.9	2
LL23 JM(Z)	2	30	Aug-96	Z5	21	0.92	38	0/9	2
					461		801		

[1] Duration addition to any time spent in DoL Farm.
[2] In general, cathodes begin to deload at current densities above approximately 100 mA $cm^{2;}$ *i.e.* maximum current and maximum loading do not occur simultaneously
[3] LL7 and LL8 terminated early due to mechanical problems.

Figure 1 shows time series data in a 100 hour interval during which the cathodes were subjected to their third current ramp (the first with any evidence of excess power). The current is the thick line referenced to the right axis. The left axis show the resistance ratio together with values of the average loading inferred from previous calibrations.[4]

In response to the current ramp, cathode P16, initially well loaded, accepts further loading until the current reaches its plateau value of 1.5A (~500 mA cm^{-2}). During the current plateau, the resistance of cathode P16 starts slowly to increase. There is a period of lost data indicated by the dashed line, and when the cathode is observed again at ~780 hours the resistance ratio has risen to ~1.7, a loading of ~0.925. During this period, P16 gave no indication of excess power within the measurement uncertainty (±50 mW).

A similar, but rather more satisfactory response to the current ramp is observed for cathode P15. Initially slightly better loaded than P16, this advantage persists through the current ramp. More significantly, during the plateau at 1.5A, cathode P15 shows no indication of de-loading, and even loads further to a value of nearly 0.97. A small amount of de-loading occurs when the current is raised from 1.5 to 1.65 A, but for almost the entire interval the loading remains above 0.95. The excess power for P15, referenced to the right axis, is clearly significant compared with the measurement uncertainty, (±50 mW).

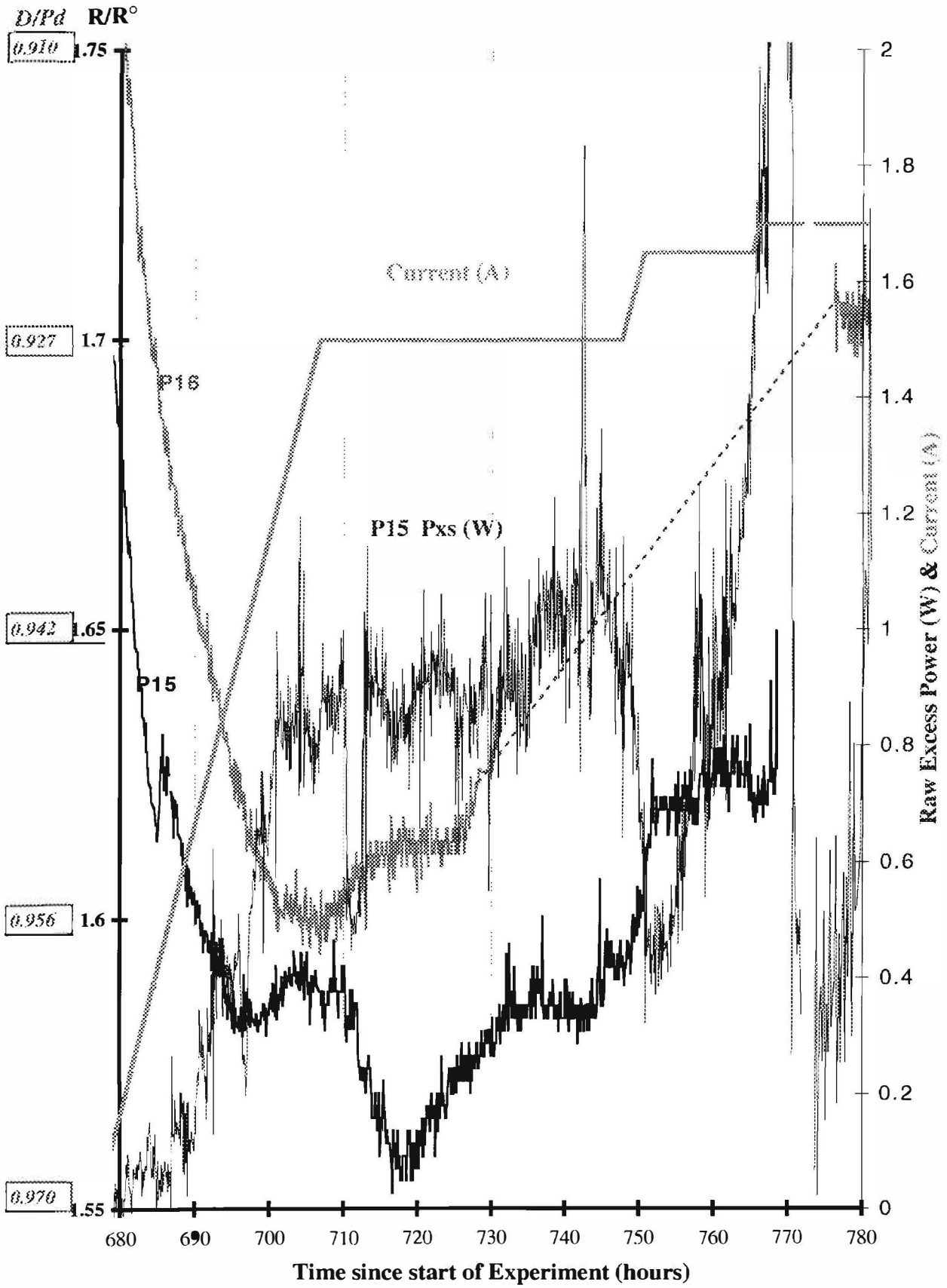

Figure 1 Experiments P15 and P16 Current, Resistance Ratio and Excess Power.

NHE Session

Figure 2 shows the loading and excess power response of LL5, the best performing cathode in Table 1. This cathode also was 3 mm in diameter and 3 cm long pure Engelhard palladium, in this case Lot #3. When transferred from the DoL farm after 20 days of observation, the resistance ratio initially was at the maximum ($R/R^\circ = 2.0$, see Figure 2). During ~12 hours at open circuit, cathode LL5 de-loaded to the left side of the resistance maximum ($D/Pd < 0.725$). The response to small current steps to 50, 100 and 150 mA (17, 33 and 50 mA cm^{-2}) was encouraging, with the cathode exhibiting a rapid uptake followed by an asymptotic approach to some limit at each new current value.

Figure 2b shows a 100 hour data interval for cathode LL5 to allow more direct comparison with Figure 1. With the onset of the current ramp the cathode LL5 initially starts to load, and obtains a value almost identical to the maximum obtained by P15. A significant difference is that, for P15, this maximum loading was attained at 1.5A (~500 mA cm^{-2}), while for LL5 this maximum was held only for currents between 0.3 and 0.6 A (~100-200 mA cm^{-2}). A more glaring difference is apparent in Figure 2b, and one of more urgent concern. When the current is ramped above 0.6A, cathode LL5 de-loads, first abruptly, and then steadily as the current ramp proceeds.

Measured excess power is referenced to the right axis in Figures 2a and 2b. The small, flat endotherm from 90 to 190 hours in Figure 2a, coinciding with the current ramp, is due to the departure of the calorimeter from its steady and initial state, as the calorimeter and its contents are heated by the input electrochemical power. This energy is yielded during the exothermic "spikes" at ~200 and ~230 hours as the electrochemical and heater currents are turned off, and the calorimeter returns to its initial state. In Figure 2b a simple correction has been made to the excess power for this departure from the steady state, by adding a term:

$$P_{Non\text{-}SS} = \overline{m\ C_p}\ \ \delta T_e/\delta t$$

where $\overline{m\ C_p}$ is the heat capacity of the cell and its contents, and $\delta T_e/\delta t$ is the (measured) rate of change of the electrolyte temperature during the current ramp. Figures 2a and 2b indicate no evidence of anomalous excess power in cathode LL5, a situation clearly different from that manifest by cathode P15 in Figure 1.

The de-loading observed for cathode LL5, beginning at ~103 hours (Figure 2) is both rapid and undesired. From the time series data it is possible to extract further information that may allow us at least to understand, and potentially to prevent, such precipitous de-loading.

Figure 2c shows on an expanded scale the current density and measured resistance ratio for 6 hours, covering the period of the most abrupt de-load during the initial stages of the current ramp. The resistance ratio increases from ~1.55 ($D/Pd \approx 0.97$) to ~1.75 ($D/Pd \approx 0.90$) in a period of about 3 hours. Since the maximum possible resistance ratio is ~2.0, a natural question is; how can such a rapid change in resistance occur?

In an electrode devoid of pores and cracks, all de-loading occurs by diffusion of atoms in the solid phase to, and evolution of molecules from, the surface. We have developed a simple model to account for the observed resistance gain and deuterium loss from the cathode based on the following conditions and assumptions:

i) Before the period of rapid de-loading the composition in the cathode is approximately uniform, with $R/R^\circ = 1.55$ and $D/Pd = 0.97$.

ii) During this time the activity of deuterium adsorbed on the surface of the cathode (controlled by the electrochemical process) is everywhere equal; the chemical potentials of adsorbed and absorbed D are equal; there is no net absorption or desorption.

iii) At the onset of de-loading, the activity of adsorbed deuterium is reduced to a value capable of supporting a much lower D/Pd loading; this change occurs instantly, and everywhere on the cathode surface.

NHE Session

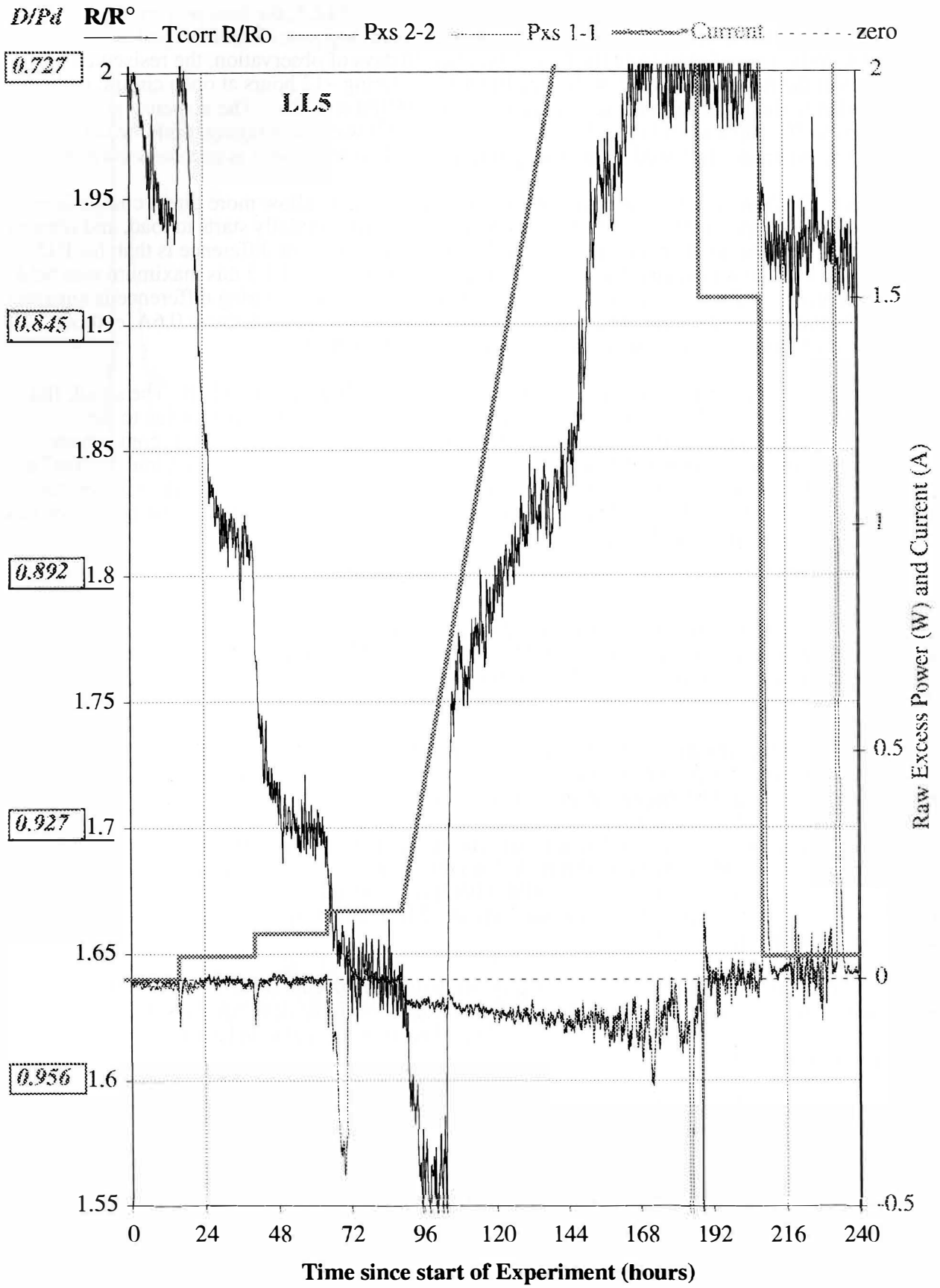

Figure 2a Experiment LL5; Current Density, Resistance Ratio and Excess Power.

NHE Session

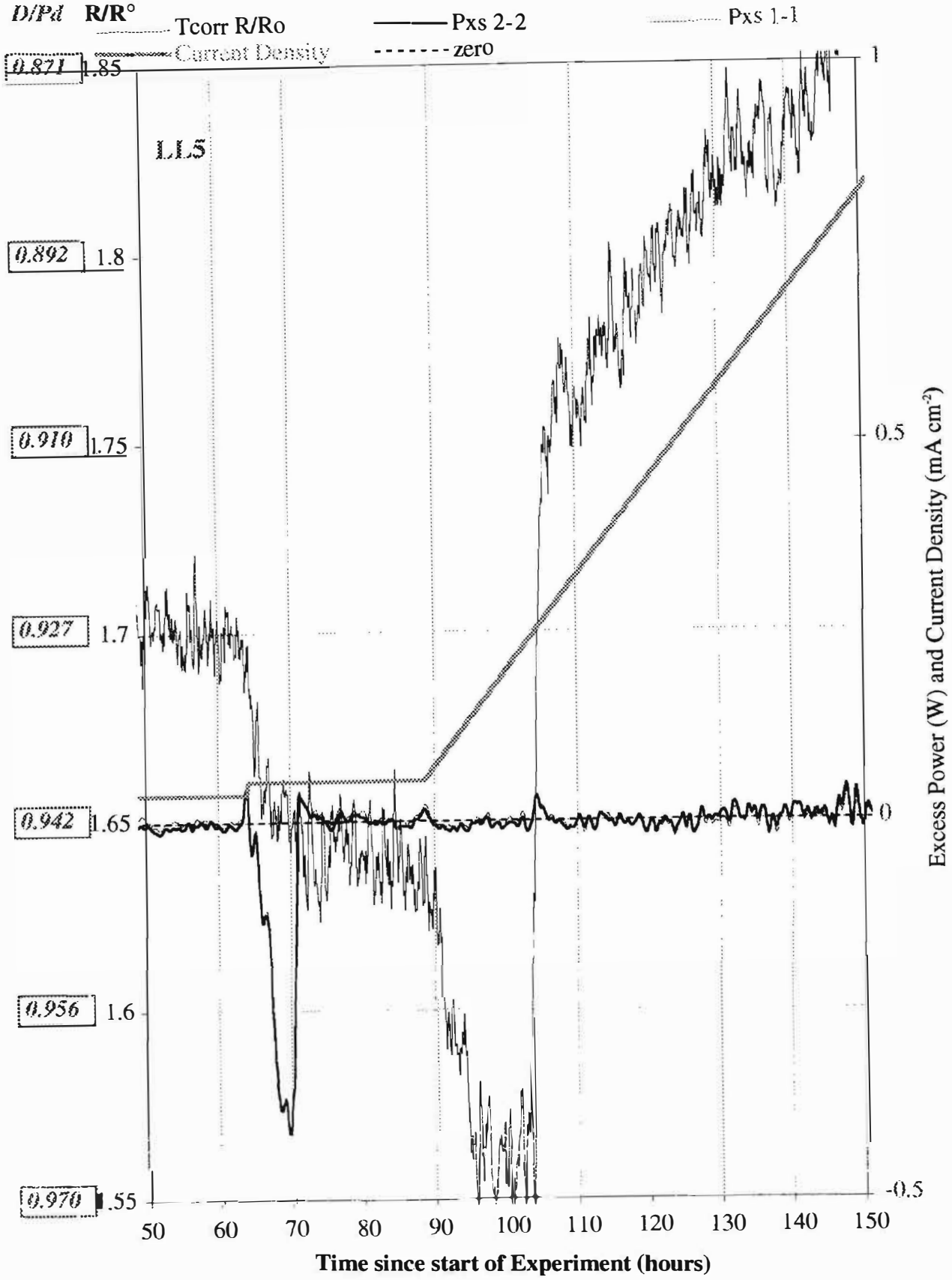

Figure 2b Experiment LL5: Current, Resistance Ratio and Excess Power.

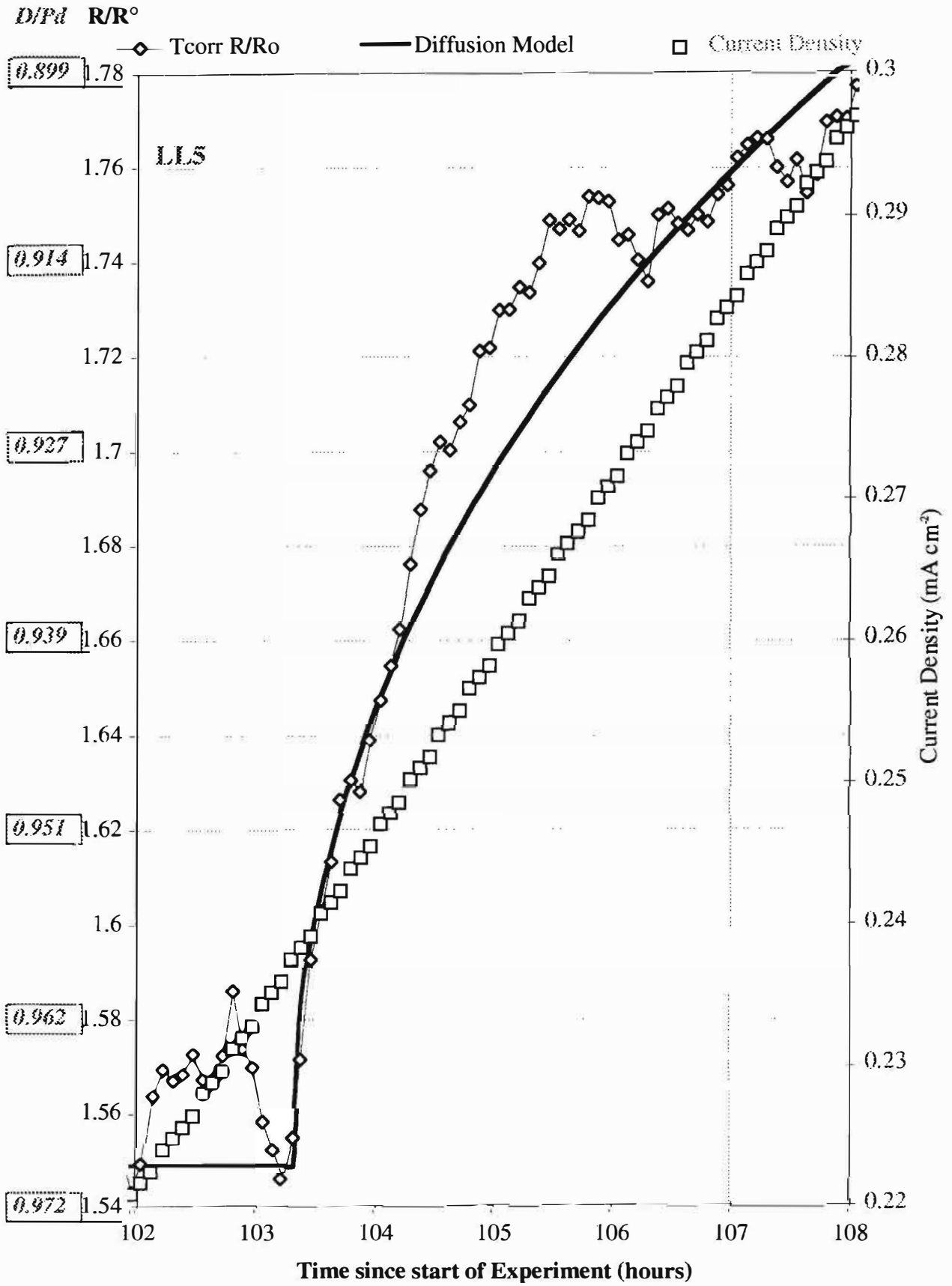

Figure 2c Experiment LL5; Current Density and Resistance Ratio: Measured and Predicted.

iv) Diffusion of deuterium occurs in response to the established gradient of chemical potential; the de-loading rate is controlled by the mass transport of deuterium atoms to the cathode surface.

The solid line in Figure 2c shows the results of a model calculation for the radial symmetry of the (3 mm diameter) cathode, with the two additional constraints:

v) The diffusion coefficient for D in PdD_x is taken to be 1.7×10^{-7} cm^2 s^{-1}.

vi) At t = 103.4 hours, the boundary concentration steps from D/Pd = 0.97 to D/Pd = 0.725.

Selection of the value of 0.725 for the final surface D/Pd loading requires some further comment. A difficulty in the modeling is explaining how the resistance can rise so quickly. The de-loading process cannot occur faster than diffusion brings species to the surface, so our assumption is that mass transport is rate limiting. The de-loading rate is proportional to the participating area, so the assumption is made that all of the surface is involved. The resistance ratio cannot rise higher than its value at the maximum (R/R°=2.0 at D/Pd=0.725), so our assumption is that 0.725 is the final value attained. There are several other reasons, however, which justify this last choice: (i) R/R° = 2.0 is the value finally obtained for the average loading in the bulk (see Figure 2a); (ii) this is the value "normally" obtained by "poor" loading cathodes; (iii) the roughly parabolic shape of the R/R° versus D/Pd functionality makes it relatively insensitive to composition in the vicinity of the resistance maximum.

For the reasons given in the preceding paragraph, it is hard to imagine a model that would or could give a faster rate of de-loading, than the one which we have employed. While not exact, there is a close conformity in Figure 2c between the diamonds (measured) and the solid line (predicted) values of R/R. This agreement suggests that the model described by conditions and assumptions (i) - (vi), above, closely reflects the situation of this cathode, in the time period shown. That is, abruptly and apparently spontaneously, the activity of deuterium in the surface layer drops from one previously held high value, over all the surface of the cathode, to a second much lower value, which is maintained even in the presence of an increasing electrochemical current density.

3. Discussion

Four years separate experiments P15 and LL5. Experiment P15, while slightly better performing than its replicate, P16, exhibits a loading behavior which is by no means atypical of the set in which it was performed. Similarly, cathode LL5 performed better than average but the response of loading to current was reproduced, qualitatively, in every experiment in Table 1, involving a Pd wire cathode. It is clear that something has changed. An important, perhaps critical, component of our experiments is not under our control. Contributing complexity to the resolution of this problem is the probability that elements of irreproducibility exist in the electrolyte (impurities and additives), in the surface preparation, and in the metallurgy of our palladium samples. Very significant effort has been expended in understanding the electrochemical factors which affect loading; some of our findings are discussed in a companion paper.[3] Despite this effort and the time that has been spent in attaining understanding and attempting to obtain control of the electrochemical insertion of deuterium into palladium, one of the clear imperatives in the field latterly called "New Hydrogen Energy", is the need to achieve replicability in our experiments, or understand its absence.

One manifestation of the observed irreproducibility, is the ability of cathodes to maintain high states of D/Pd loading, at high electrochemical current densities. A model has been developed which describes, adequately, the circumstance of the rapid de-loading of cathode LL5. A sudden, and apparently spontaneous change occurred on the cathode surface during the course of a very slow current "staircase". In a period of less than 4 minutes, and with a current density difference of less than 1 mA cm^{-2}, a catastrophic change occurred all over the cathode surface from a state capable of sustaining a very high loading and an extraordinary chemical activity, to one where the loading is uninteresting, and the activity close to unity. A sudden drop in the activity of surface-adsorbed H

atoms is most easily explained in terms of a change in electrochemical mechanism from that of "fast discharge-slow desorption" to that of "slow-discharge-fast desorption". The former is capable of sustaining high activities; the latter not. ("Desorption" in this context refers to either the Tafel or Heyrovsky steps[6]).

Unfortunately, such an explanation only begs the question of what causes the mechanism to change suddenly or, more precisely, what causes the relative rate constants for the various mechanistic steps to change. That the transition occurs catastrophically and over all the cathode surface suggests the critical involvement of an easily disturbed, fragile structure, other than the electrolyte and solid phases. Here, we shall refer to this structure as a "film", formed adventitiously from impurity species initially present in the electrolyte or leached from the solid surfaces within the cell, including the Pd. We speculate that attainment of the high loading state is possible (perhaps only) in the presence of this film. Failure of the film, mechanically, electrically or electrochemically, at least one part of the cathode surface results in a change in electrochemical mechanism to that which is more appropriate to a "clean" surface. The result is sudden de-loading, the rapid formation of gas bubbles at the metal/film interface, and mechanical disruption of the film over a wider area. Evidence for the presence and critical role of a surface film is provided by studies of well-loaded cathodes under ultrasonic irradiation.[7] Such electrodes, even while maintained cathodically polarized, deload on irradiation, presumably due to the removal of a critical surface structure or agent.

An auto-catalytic process such as that postulated in the previous paragraph obviously is capable of explaining a catastrophic loss of loading. This loss is precisely what we wish to avoid. If our model is correct, then it behooves us to examine more closely the surface structure, its constitution and character, and seek methods of controlling its properties so that we can assert reproducible control over loading.

4. Acknowledgments

The financial contribution and collaborative research support provided by the New Energy and Industrial Technology Development Organization, the Institute of Applied Energy, and the New Hydrogen Energy Laboratory (Sapporo) are gratefully acknowledged.

5. References

1. M. McKubre, S. Crouch-Baker, A. Hauser, S. Smedley, F. Tanzella, M. Williams and S. Wing; "Concerning Reproducibility of Excess Power Production," Proceedings of the Fifth International Conference on Cold Fusion (ICCF5), Monte Carlo, Monaco (1995).

2. F. Tanzella, S. Crouch-Baker, A. McKeown, and M.C.H. McKubre, M. Williams and S. Wing; "Parameters Affecting the Loading of Hydrogen Isotopes into Palladium Cathodes," Proceedings of the Six International Conference on Cold Fusion (ICCF6), Sapporo, Japan (1996).

3. P. Hagelstein, "Update on Neutron Transfer Reactions" Proceedings of the Fifth International Conference on Cold Fusion (ICCF5), Monte Carlo, Monaco (1995).

4. M. McKubre, R. Rocha-Filho, S. Smedley, F. Tanzella, J. Chao, B. Chexal, T. Passell and J. Santucci; "Calorimetry and Electrochemistry in the D/Pd System" Proceedings of the First International Conference on Cold Fusion (ICCF1), National Cold Fusion Institute, Salt Lake City, UT, 1990, p. 20.

5. M. McKubre, S. Crouch-Baker, R. Rocha-Filho, S. Smedley, F. Tanzella, T. Passell, and J. Santucci "Isothermal Flow Calorimetric Investigations of the D/Pd System" J. Electroanal. Chem., **368** (1994) p. 55.

6. J. O'M. Bockris and P. K. Subramanyan, Electrochim. Acta, 16, 2169 (1971).

7. A. Wark, S. Crouch-Baker, M. McKubre, F. Tanzella; J. Electroanal. Chem., accepted for publication

Click here for a more readable copy of this paper.

RESULTS OF ICARUS 9 EXPERIMENTS RUN AT IMRA EUROPE

T. Roulette, J, Roulette, and S. Pons

IMRA Europe, S.A., Centre Scientifique
Sophia Antipolis, 06560 Valbonne , FRANCE

INTRODUCTION

We describe herein the construction, testing, calibration and use of a high power dissipation calorimeter suitable for the measurements of excess enthalpy generation in Pd / Pd alloy cathodes during the electrolysis of heavy water electrolytes at temperatures up to and including the boiling point of the electrolyte. With the present design, power dissipation up to about 400W is possible. Excess power levels of up to ~250% of the input power have been observed with these calorimeters in some experiments. Extensions of the design to include recombination catalysts on open and pressurized cells will be the subject of a future report.

DESIGN AND EXPERIMENTAL CONSIDERATIONS

A schematic diagram of the basic construction of the calorimeter is shown in Figure 1. These

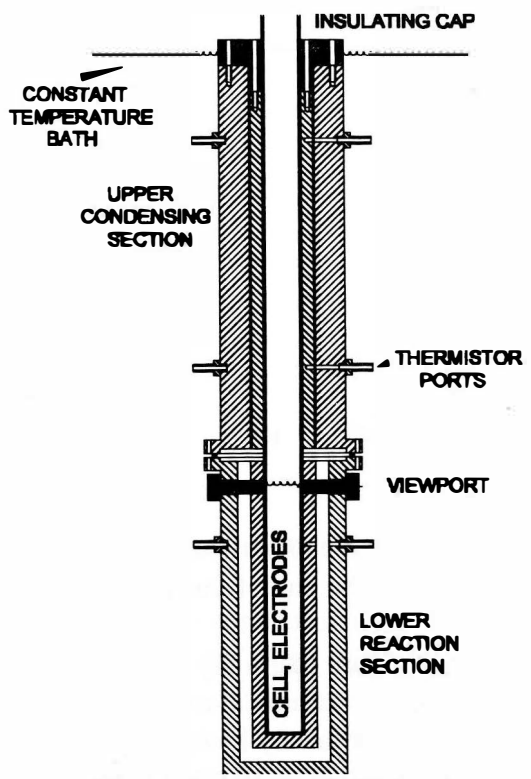

Figure 1 The ICARUS 9 calorimeter

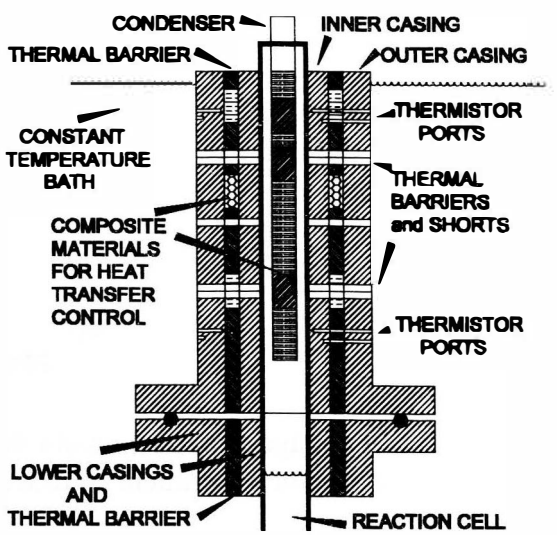

Figure 2 Top section expanded details

calorimeters are much improved in thermal dissipation, sensitivity, precision, and accuracy compared to the original calorimeters used in these laboratories from 1992 to 1995. The present design

incorporates better seals at all liquid / casing interfaces, and at the thermistor inlet ports. The viewing ports are also more robust and clear. The heat transfer characteristics can now be easily be modified at various vertical positions in the inner casing, the inner insulator, and the internal condenser to give more controllable overlap between the various sensitivity zones, Figure 2. The resulting heat transfer characteristics are now more linear in the radial direction than in previous designs. Foam rise in the calorimeter at the boiling temperature has been minimized.

In the basic configuration, there are three sets of differential temperature measuring thermistors at key vertical locations in the inner and outer casings so that the radial temperature distribution throughout the calorimeter can be characterized conveniently and accurately. The cell potential, cell current, and cell temperature are measured independently, Figures 3-5.

The principle of operation of these calorimeters is straightforward. Power dissipation in the cell is determined by measuring the differences in temperature between the thermistor sets as a function of input power. Excess enthalpy generation is calculated by comparing the data to those obtained by calibration as described below. It is pointed out that these calorimeters have been used thus far primarily for measurements in the steady state, i.e. when the input power levels, bath temperature, and the rates of electrochemical and ohmic enthalpy generation in the cell are constant. Under these conditions, thermal equilibrium is attained in all sections of the calorimeter. Extensions to measurements in the non-steady state are necessary for larger devices, and are certainly possible (these are beyond the scope of the present report).

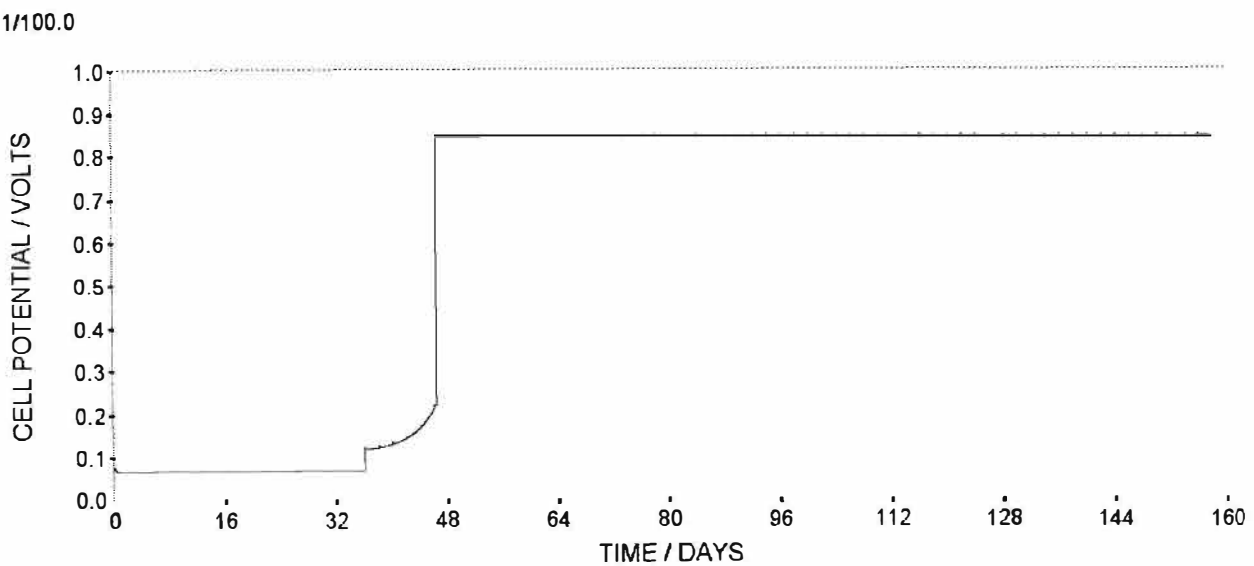

Figure 3 Measured cell voltage as a function of time for the duration of the experiment. All data presented in this report are for experiment #4 described in the Table at the end of this report.

The casings in the top section (measuring / condensing section) are thermally isolated from the lower section (reaction section). As the temperature due to an electrochemical reaction in the cell in the bottom section rises, heat is transferred to the upper section primarily by (a) heat contained in the vapor of the solvent rising from the lower section, and (b) by conduction through the walls of the glass reaction cell. We consider that the overall effects of (b) is small compared to effect (a), especially when the contents of the reaction cell are at or near the boiling point. The calorimeter was initially designed primarily for measurements when the cell contents are boiling, but the calorimeter is indeed suited for measurements at all temperatures below the boiling point. In the basic configuration (simple solid casings and insulation) the lower set of thermistors are the most accurate at lower temperatures since they are located closer to the top surface of the solvent. The middle and upper sets of thermistors are located in the upper section, and these are more sensitive as the temperature

rises towards boiling.

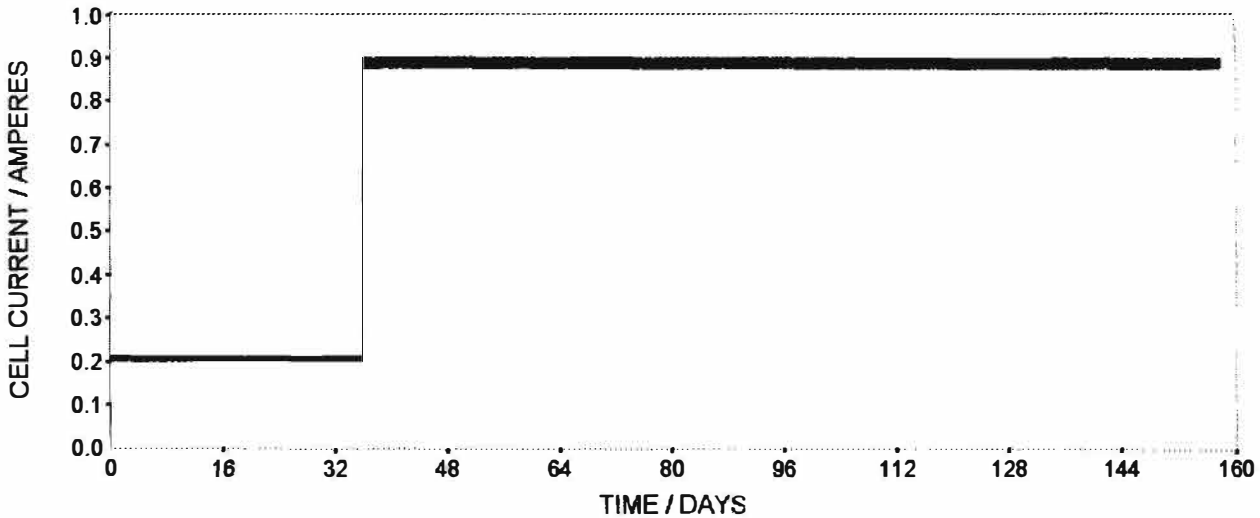

Figure 4 Cell current as a function of time.

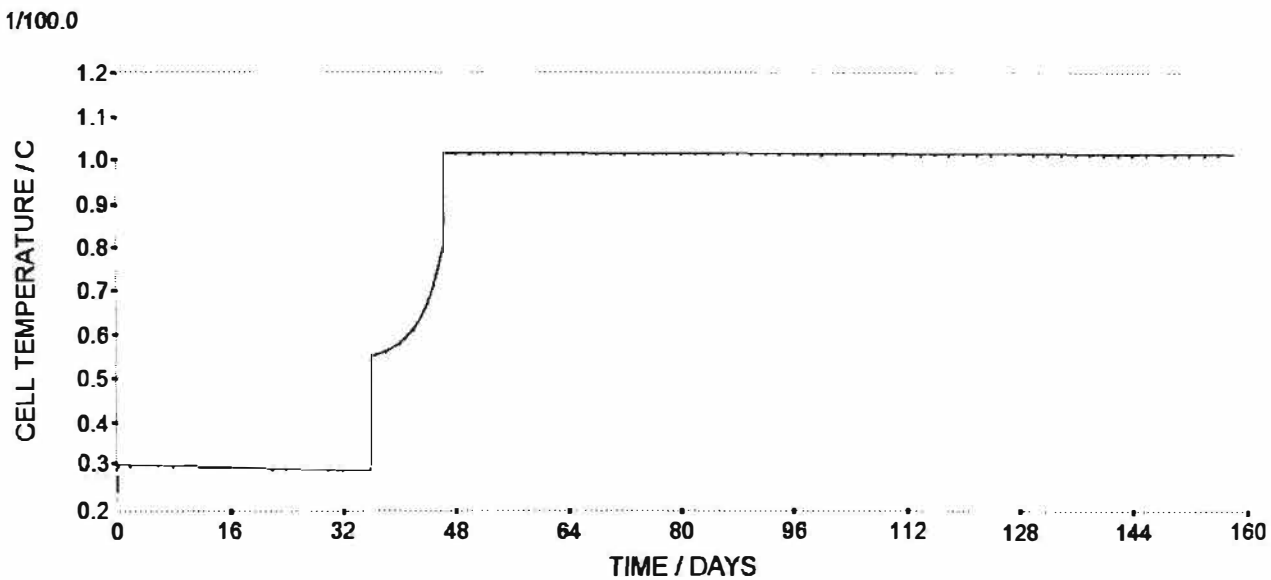

Figure 5 Internal cell temperature as a function of time.

As the temperature of the solvent rises, the vapor pressure of the fluid also rises and the temperature of the vapor increases progressively in the upper portions of the calorimeter. At boiling, the temperature of the vapor just above the liquid is at the boiling point of the solvent. If the rate of boiling is increased, due either to increased external power input or to excess heat generation, the rate of boiling increases and the height of the hot vapor head rises to increasingly higher levels in the calorimeter. Since the temperature of the vapor cannot exceed the temperature of the boiling liquid at a given atmospheric pressure, the temperature measured at any inner casing thermistor can not exceed the boiling point of the solvent. Therefore, if the bath temperature remains constant, then the temperature difference measured between the inner and outer thermistor of each set will rise to a maximum value, which is independent of the power input level. When this maximum is reached, any increases in the power in the bottom of the cell will have no further effect on the measured temperature difference. For this reason, in the basic configuration, the lower thermistor set is

sensitive only at low temperatures (up to about 30 watts of power dissipation in the reaction cell). At higher powers, there is no further changes in the temperature difference at this lower set of thermistors. The middle set of thermistors then become more sensitive, and at very high power dissipation rates, the upper set of thermistors become more sensitive. In other configurations, it is possible to modify the sensitivity of each thermistor set by changing the materials and construction of the internal condenser plug and/or the inner casing, as well as placing annular ring insulators at various heights of the inner casing, and/or thermal shorting devices between the inner and outer section casings. Finally, similar enhancements are obtained by changing the materials in, and the geometry of the insulating barrier between the inner and outer casings, Figure 2.

Due to these operating characteristics, it will be noticed in some of the figures that there are high or low calculated rates of excess enthalpy generation at very low power inputs, especially at the middle and upper thermistor sets. These data must be ignored since they are due to the systematic errors described further below.

The calorimeters are calibrated by several methods, including (a) the electrolysis of (i) light water or (ii) heavy water using Pt cathodes, and (b) encapsulated and open platinum resistor heaters. At thermal equilibrium, the input power and the temperature differences at each set of thermistors is measured over a long time period. The procedure for calibration calls for the application of fixed input powers to the cell for approximately 12 hours. The time constant of the calorimeter is considerably less than this time period, so one obtains a large number of steady state calibration points from which a good statistical average value can be obtained. Gaussian statistics are used to determine histograms and probability functions on each set of input power and temperature difference data sets for each point and for each thermistor set. Non-steady state values at short times after the input power is changed are rejected on the basis of their contribution to the known determinate error (the non-steady state). Rejection of data is continued (up to about 10% of the entire data set) until a zero slope linear fit is found for the temperature difference as a function of input power. The intercept of this line then gives the "best" temperature difference value. Confidence limits and prediction limits are then determined for each set of data. Inflection points for the confidence and prediction curves are then determined, which gives a "best" value of the input power. Gaussian histograms and cumulative curves are additionally determined, from which the "best" mean value of both the temperature difference values and the input power values. If these are in agreement with the values determined by the previous method, then they are accepted. If not, they are rejected and the measurements are repeated. Generally, calibrations are always very reliable at power inputs above about 3W. When the calorimeter is serviced after each experiment, the calibration curves are carefully checked by re-calibration at several input powers to assure that the calibrations have not changed during the prior operating or servicing period.

Following this procedure, calibrations curves are constructed over the entire input power range of the calorimeter for each of the thermistor sets. For simplicity in on-line data monitoring, best fit curves are calculated by linear and non-linear regression analysis over various sections of the calibration data. We use a variety of basis trial models such as Boltzman, multiple exponential, sigmoidal Gompertz, sigmoidal logistical, Weibull, Richards, and Hill functions. The calibration curves shown in this report were obtained from such composite best fit curves through all of the experimental calibration power / temperature data, and then plotted at integer values of the input power. Segments to these curves are almost always added to these curves for very low values (<2-3W) of input power since the error between the actual values and fitted curves were about 5%.

During an experiment, measurements identical to those used in the calibration method are made, and the temperature differences between the three sets of thermistors are compared with those of the blanks, at the same input power level, see, for example, Figure 6 . If there are any excess enthalpy effects, then the data points will fall above the input power - thermistor difference temperature calibration lines. The horizontal distance from a high data point to the calibration line to the right gives the value of the excess enthalpy generation rate. Excess enthalpy effects cannot be

observed at high temperatures at the bottom thermistor set. Figures 7-9 reflect these calculated rates of excess power generation at each of the three thermistor sets. Derived analyses may then be calculated from these data: for example the excess power percentage of input power, the excess energy, and the accumulated excess energy as a function of time; see Figures 10 and 11.

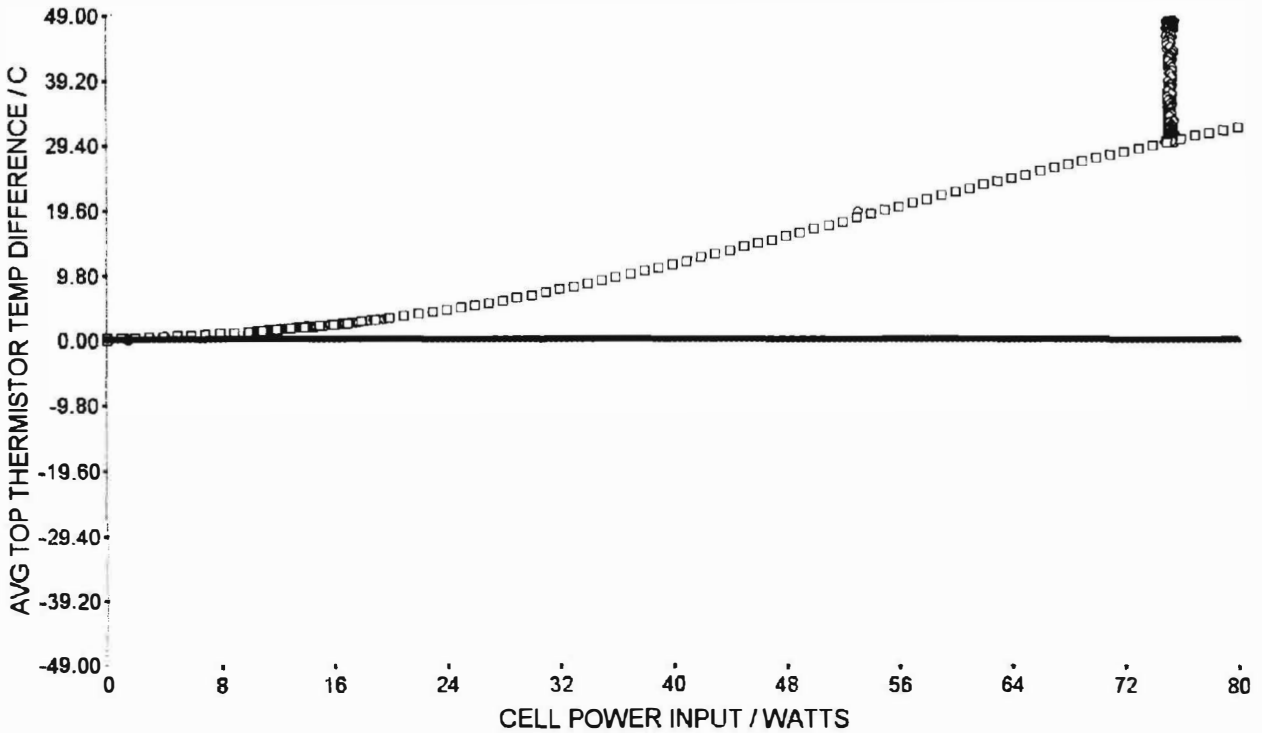

Figure 6 Average values of consecutive sets of 25 points of temperature differences at the top set of thermistors as a function of the average cell input power. Calibration: squares; Data: circles.

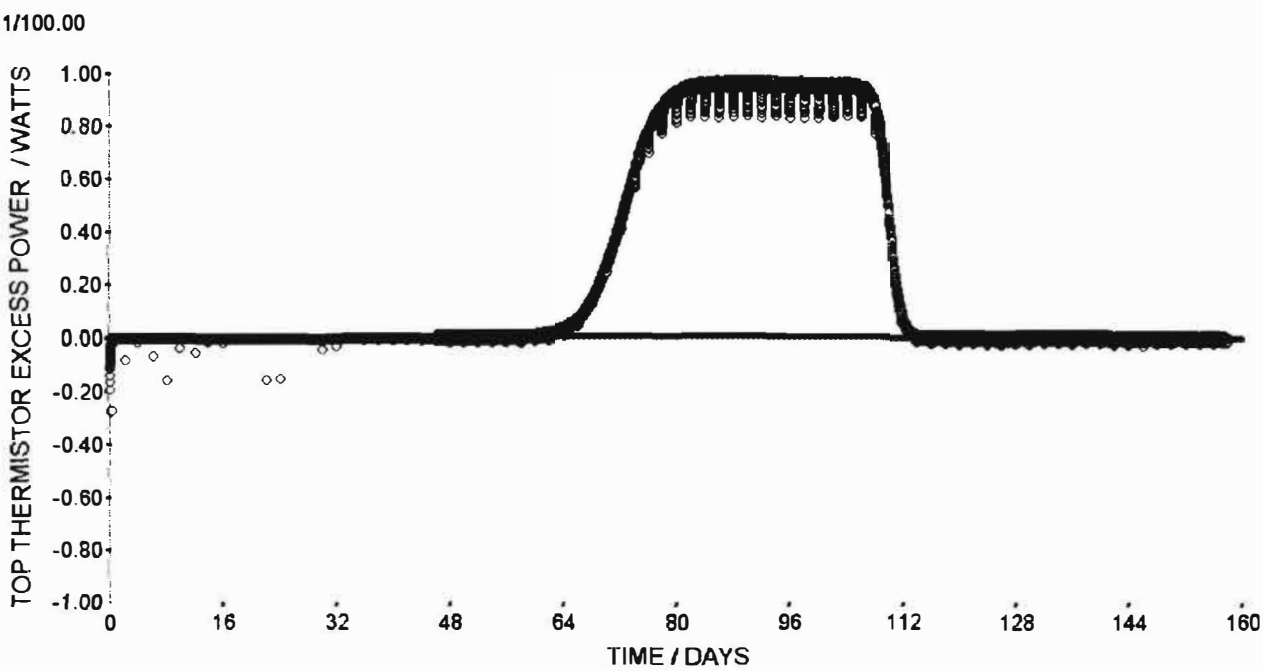

Figure 7 Excess power as a function of time measured at the top thermistor set.

Excess Heat

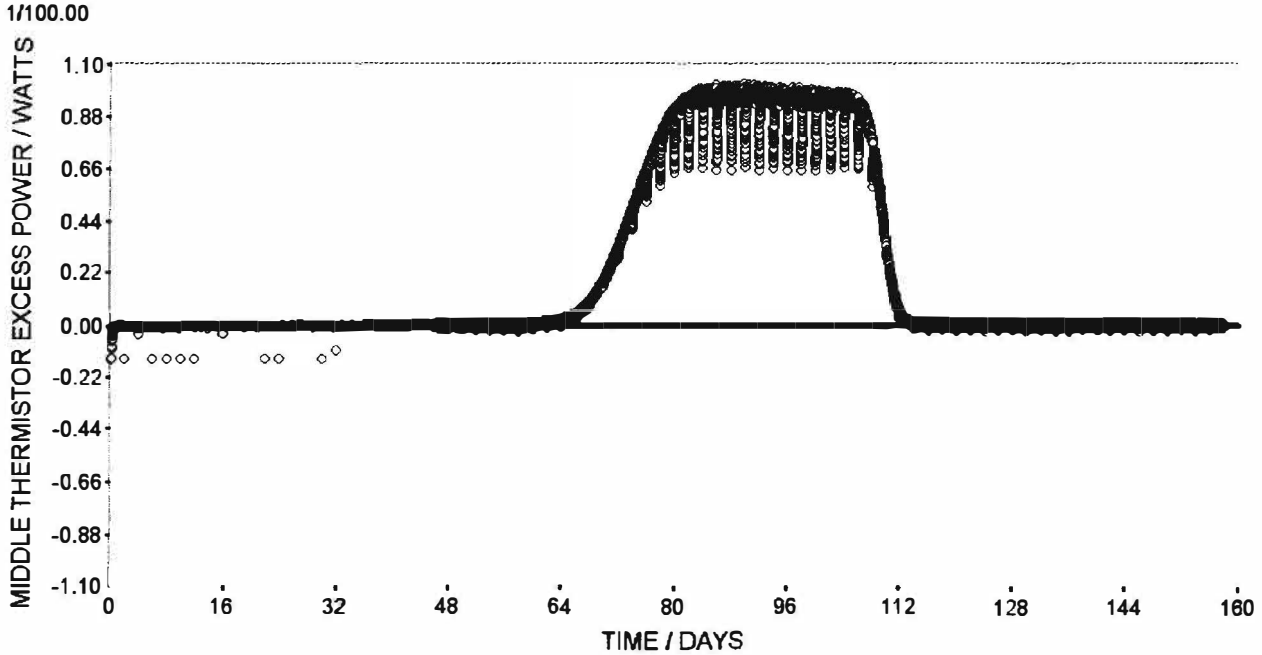

Figure 8 Excess power as a function of time measured at the middle thermistor set.

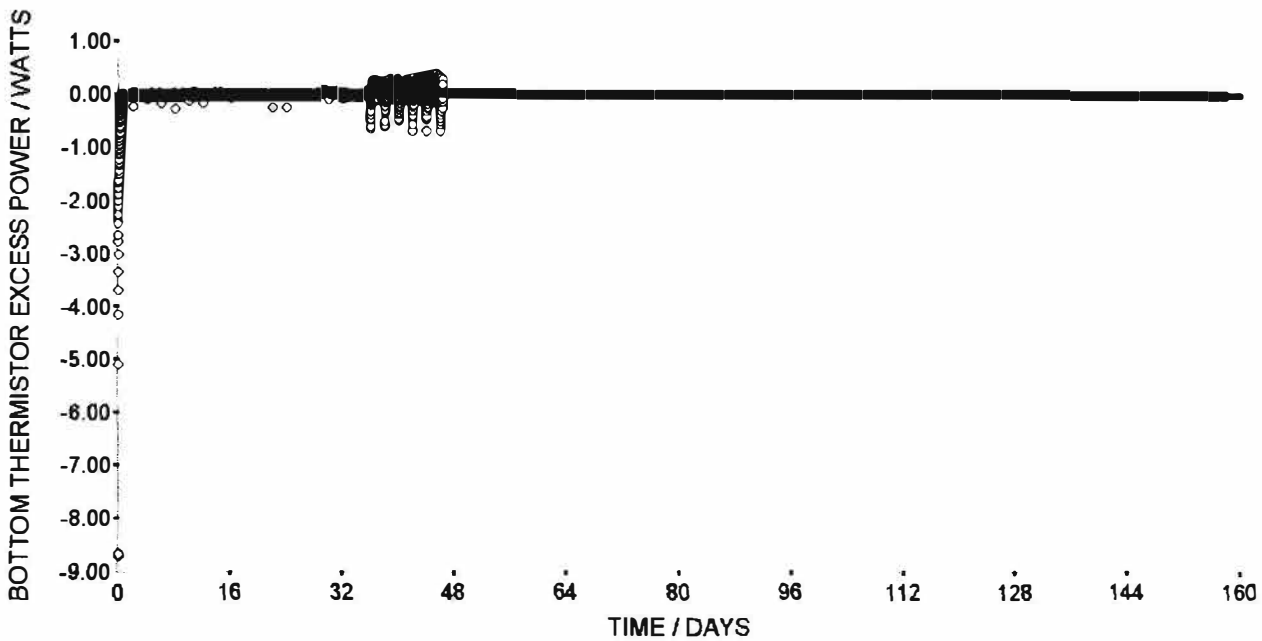

Figure 9 Excess power as a function of time measured at the bottom thermistor set.

It has been pointed out previously that there can be anomalous values of excess heat or cooling observed in these experiments. Such anomalies are seen in the experimental response curves for each of the top, middle, and bottom thermistor pairs. These anomalies must always occur during periods of the non-steady state which may be imposed externally or internally on the experiment. Low anomalous values of heat generation (i.e. cooling) must appear during (a) the period immediately following the addition to the cell of solvent which is colder than the cell contents, (b) the period immediately following an increase in the input power, (c) the period immediately following an increase in the bath temperature, and in general, (d) the period immediately following any event in which the interior casing of the calorimeter becomes cooler with respect to the exterior casing and which does not result in an exactly compensating decrease in the input power

Anomalous high values of excess heat must be observed during (a) the period immediately

following the addition to the cell of solvent which is warmer than the cell contents, (b) the period immediately following an decrease of the power input to the cell, (c) the period immediately

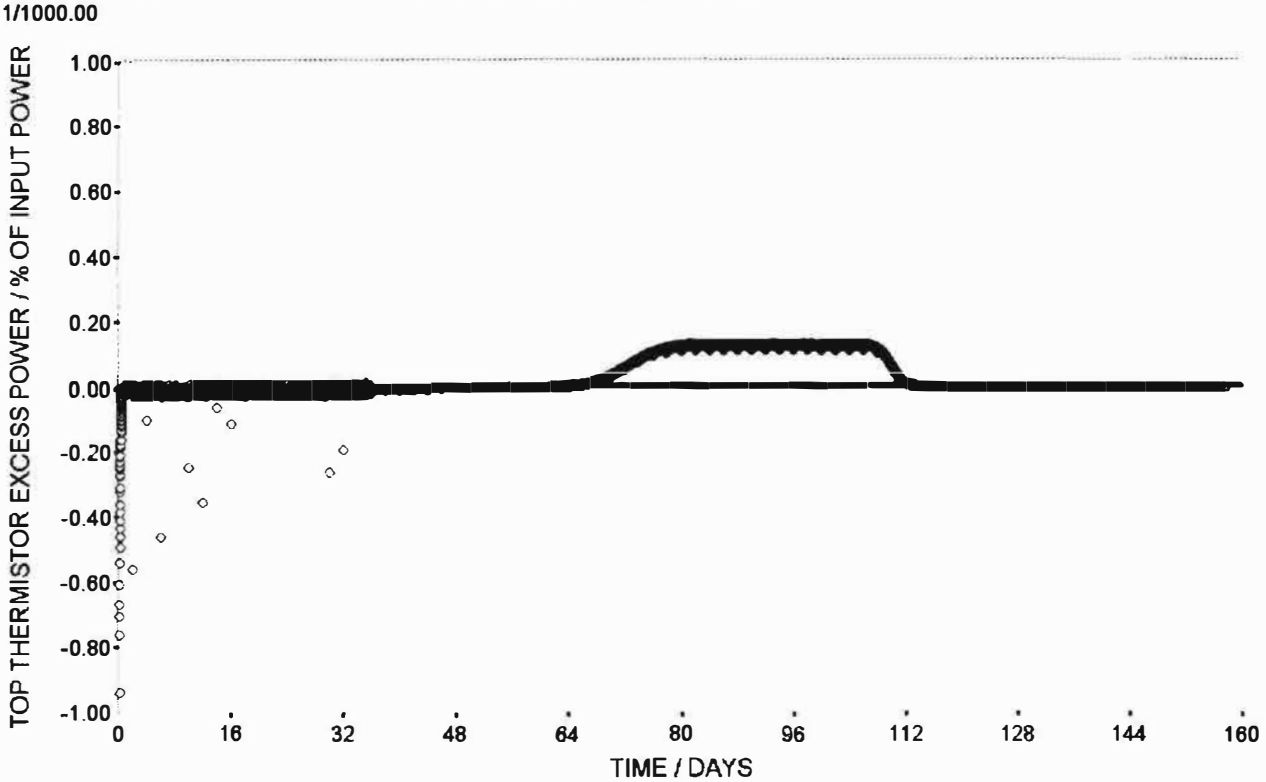

Figure 10 Excess power percentage of input power as a function of time: top thermistor set.

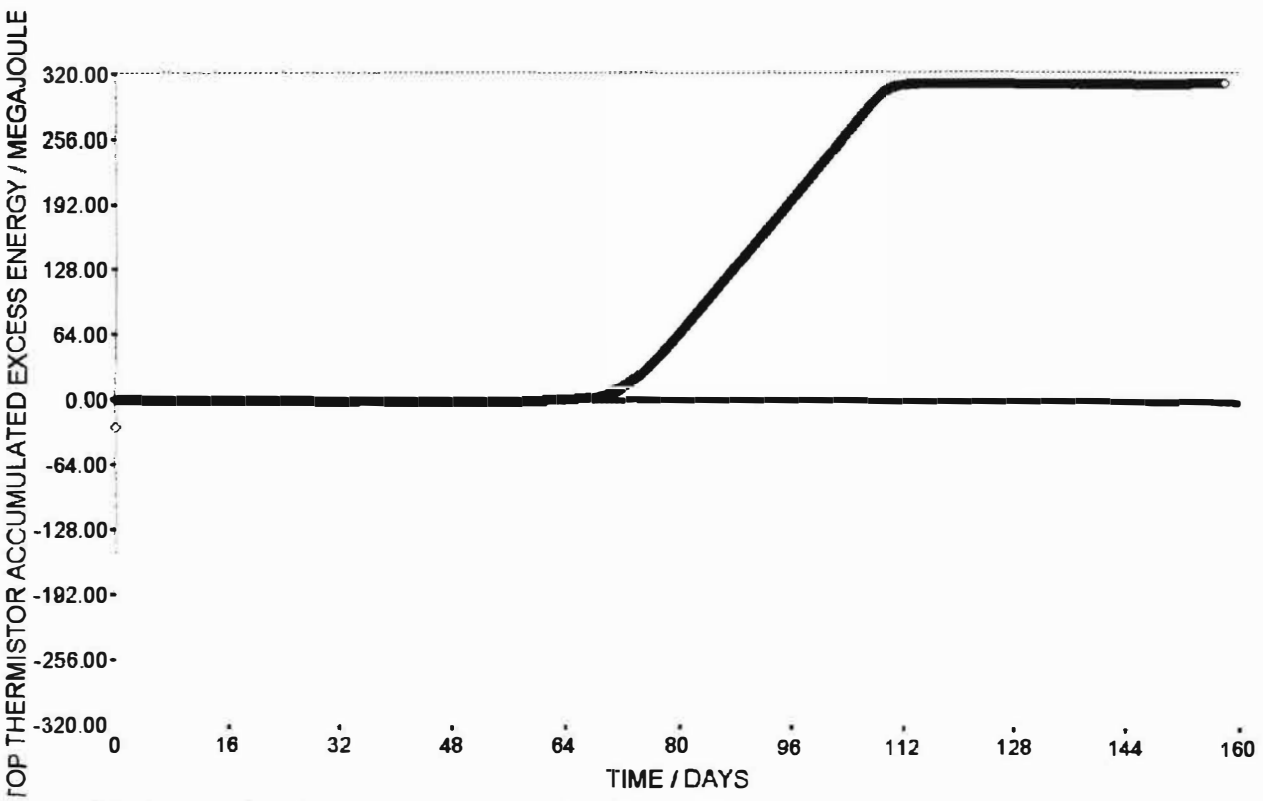

Figure 11 Accumulated excess energy as a function of time: top thermistor set.

following a decrease in the bath temperature, (d) the period immediately following the onset of any excess enthalpy generation in the cell, and in general, (e) the period immediately following any event

in which the interior casing of the calorimeter becomes warmer with respect to the exterior casing and which does not result in an exactly compensating increase in the input power.

Each of the perturbations listed in the last paragraph are non-equilibrium effects. Attention therefore is normally focused only to those data which are recorded when the cell is known to be at thermal equilibrium, i.e. at the majority of the data points in the experiments reported here.

One is also cognizant of the fact that non-equilibrium effects may also be imposed by ambient conditions of the laboratory environment on the components of the cell which pass from the calorimeter into the ambient air, such as cables and leads, the glass lead tubes, the plastic plugs, and the plastic condenser. Conduction effects can certainly affect the stability of the measurements. For this reason, the fluctuation of the air temperature in the laboratory is always maintained to +/- 0.15°C, and within +/- 0.5°C of the bath temperature. The fluctuations are therefore reduced to negligible values, and there are observable fluctuations of +/- 0.05°C only at very low power inputs and at the top thermistor only.

The table below summarizes the last set of 7 experiments undertaken with the new calorimeter system at IMRA Europe. As can be seen, the experiments fall into two clear categories of success or failure. Long charging times at low current densities, and careful experimental protocols are always utilized in the experiments, and tend to increase the success rate of excess enthalpy generation. However, the necessary condition for excess enthalpy generation remains the quality and preparation of the cathode materials and electrolyte. A more careful investigation of the materials properties and preparation continues, and these studies have certainly led to increased excess enthalpy generation rates for longer periods of time. These studies will be detailed in our future reports.

Experiment	1	2	3	4	5	6	7
Cathode	Pd	Pd	Pd	Pd	Pd	Pd	Pd
Rod size, mm	100x2	100x2	100x2	100x2	100x2	12.5x2	12.5x2
Anode	Pt coil	Pt coil	Pt coil	Pt coil	Pt coil	Pt mesh	Pt mesh
Electrolyte:0.1M	LiOD	LiOD	LiOD	LiOD	LiOD	LiOD	LiOD
Electrolyte, mL:	90.7	90.0	90.6	97.0	97.0	90.4	90.9
Expt time, days	94	134	158	123	123	47	60
Pwr_{excess}/W/4.2hr	-0.1	-0.6	101	17.3	13.8	74.5	39.4
Total energy, MJ	-0.0	-5.5	294	102	0.3	30.5	-7.6
% excess power	0	0	150 (30d)	250 (70d)	0	Variable	~0

Excess Heat

NEW KINDS OF ELECTROLYTIC REGIMES AND GEOMETRICAL CONFIGURATIONS TO OBTAIN ANOMALOUS RESULTS IN Pd(M)-D SYSTEMS

F. Celani[1], A. Spallone[1], P. Tripodi[1,4], D. Di Gioacchino[1],
P. Marini[2], V. Di Stefano[2], A. Mancini[3], S. Pace[4]

1- INFN-LNF Via E. Fermi 40, 00044 Frascati, Italy
2- EURESYS Via Lero 40, 00144 Roma, Italy
3- ORIM, Via Concordia 65, 62100 Macerata, Italy
4- INFM c/o LNF, Via E. Fermi 40, 00044 Frascati, Italy

1. Abstract

Electrolyses of long and thin Pd (and PdY alloy) wires, in dilute solutions of LiOD-D_2O and LiOH-H_2O at large operating voltages, were made. An innovative kind of geometrical set-up to improve the efficiency of electromigration effect in proton conductors was developed: the usual "single-ended" geometry at the most cathodic point of the wire changed to the "central wire" geometry. The detected excess heat seems to be related to: (H/D) isotopic effect, lattice characteristics, geometrical set-up, dynamic variation of concentration inside Pd wire, anode-cathode and inter-cathodic voltages.

2. Motivation

The rationale of the experiments were:

A) development of new experimental procedures in order to determine the *origin* of any anomalous effects (excess heat and/or nuclear ashes) during and after the electrolysis of Pd(M)-Pt in LiOD-D_2O solution. Because these reasons, we selected 3 control parameters:

A1) on-line resistance ratio R/Ro (loading);

A2) excess heat (by *isoperybolic* and *flow* calorimetry);

A3) off-line detection of "new" elements at the cathode surface (by SEM analysis);

B) making large efforts in order to improve the *reproducibility* of the anomalous effects, even though at *low intensity*.

3. Experimental set-up and procedure

In respect to our previous experiments [1], we developed a new geometry of the system named "*wires, twisted pair* "[fig.1]. The Pd wires were very long (160cm) and thin (100μm), faced (1cm distance) to Pt wire (1mm diameter). The Pd geometrical dimensions and physical parameters were: 78 $10^{-6}cm^2$ of cross-section, $5cm^2$ of total surface area, 12.5 $10^{-3}cm^3$ of volume, 150mg of weigth and 20Ω of initial electrical resistance. In case of PdY alloy, see later, the initial resistance was 50Ω at NTP.

Excess Heat

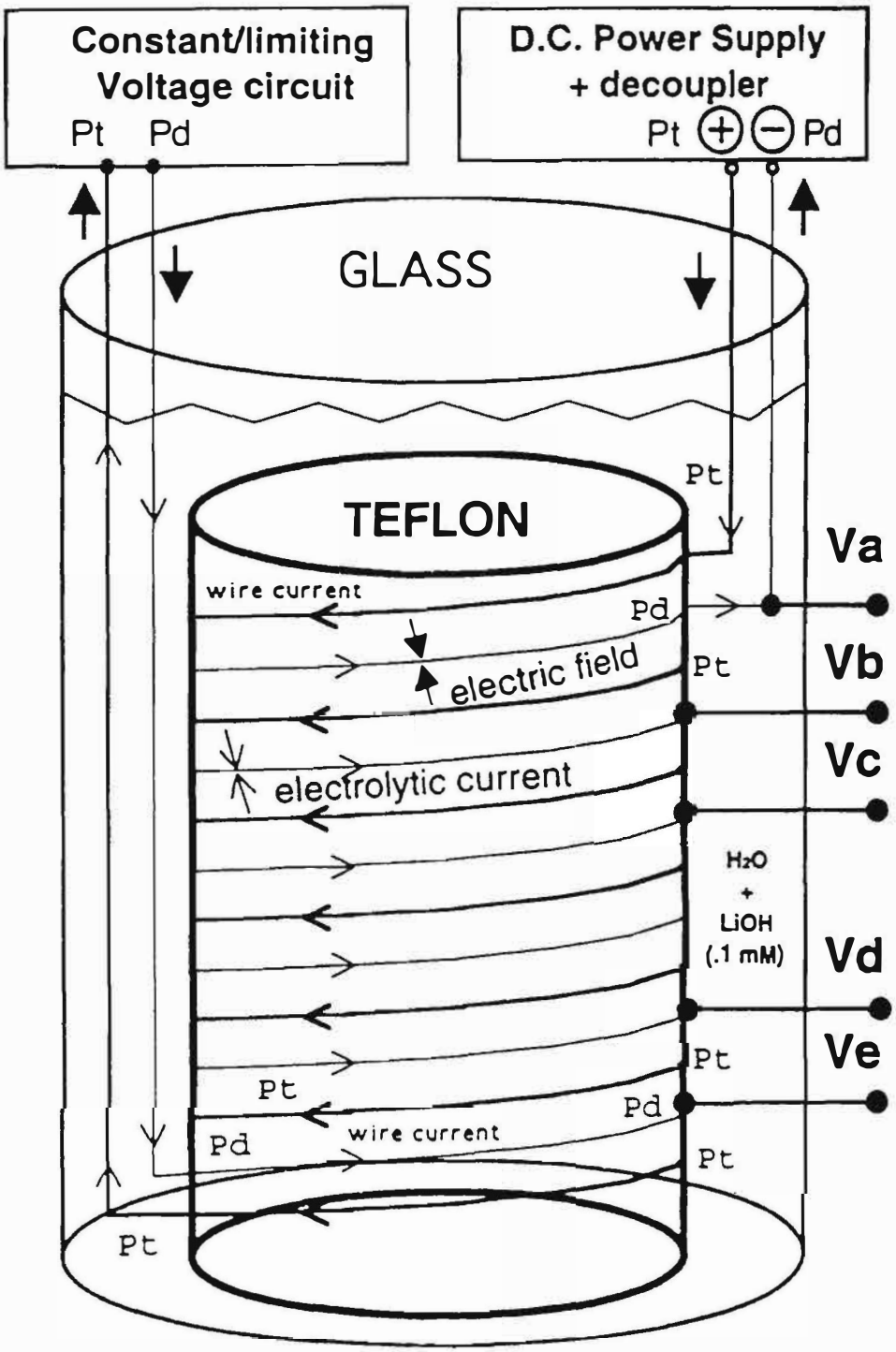

Fig. 1: Electrolytic cell. Pd/Pt double twisted wires on teflon cylinder sample-holder.

The main drawback of this kind of geometry is the electrolyte resistivity. Usually, this parameter is enough low (few Ωcm), at the LiOD concentration tipically used in Cold Fusion experiments (0.1-1N), and changes over time because temperature and several aging effects. It can strongly affect the measurements of wire resistance because of inpredictable paralleling effects.

In our experimental conditions we used an electrolyte concentration in the range 0.1-1 mN. Overall, a quite innovative electronic circuitry and experimental set-up [fig.2] was developed: in principle, it *eliminates* all the problems related to electrolyte variations because the anode is almost not connected to reference ground for AC signals (used for measurement of chatode resistance) and the effective AC current flowing at the wire end is also measured. Moreover, this circuitry is able to detect sources of errors, in the computing of Pd wire resistance, arising from: instabilities and/or leakages of "voltage to constant current converter" [fig.3] and "high impedance booster" [fig.4].

4.1 Innovative approach on electromigration effect

We have performed further studies about the electromigration effect from the point of view of loading and *dynamic storage*. We have developed an innovative geometrical configuration of the Pd wire set-up, called "*collider*" [fig.5], that can improve H-D loading and, mainly, the *dynamic storage* in respect to the usual unidirectional one.

The electromigration effect, studied since 1929 [2], is a powerful tool, at least in principle, in order to increase largely the H-D-T concentration in host materials where these elements behave as *proton conductors*. Recently, this kind of effect was used, from several authors, in order to increase the deuterium concentration in Pd (and/or Pd alloys) over the thermodynamic equilibrium condition in the framework of the Cold Fusion studies.

The basic equation related to electromigration effect is:

$$C(x) = C_o \, e^{-[\, eZ^* V(x) / K_B T \,]} \qquad (1)$$

where:

- C_o is the initial concentration of H-D-T in host material;
- Z^* is the effective charge number of H -D-T in Pd [the value is 1 at low concentrations (H/Pd < 0.6), is about 0.1 at high concentrations (H/Pd > 0.8) and/or at high temperature (T > 30 °C)];
- $V(x)$ is the voltage drop along the host material in the limit of its homogeneity (no large dislocations or fracture);
- K_B is the Boltzmann constant;
- T is the temperature, in Kelvin.

From equation (1) it follows that an increase in the concentration gradient results from a large voltage gradient in the cathode wire, once it is provided that some proper concentration Co of H-D-T is continuosly fed to the Pd (by gas loading or proper electrolytic technique). We will remark that the

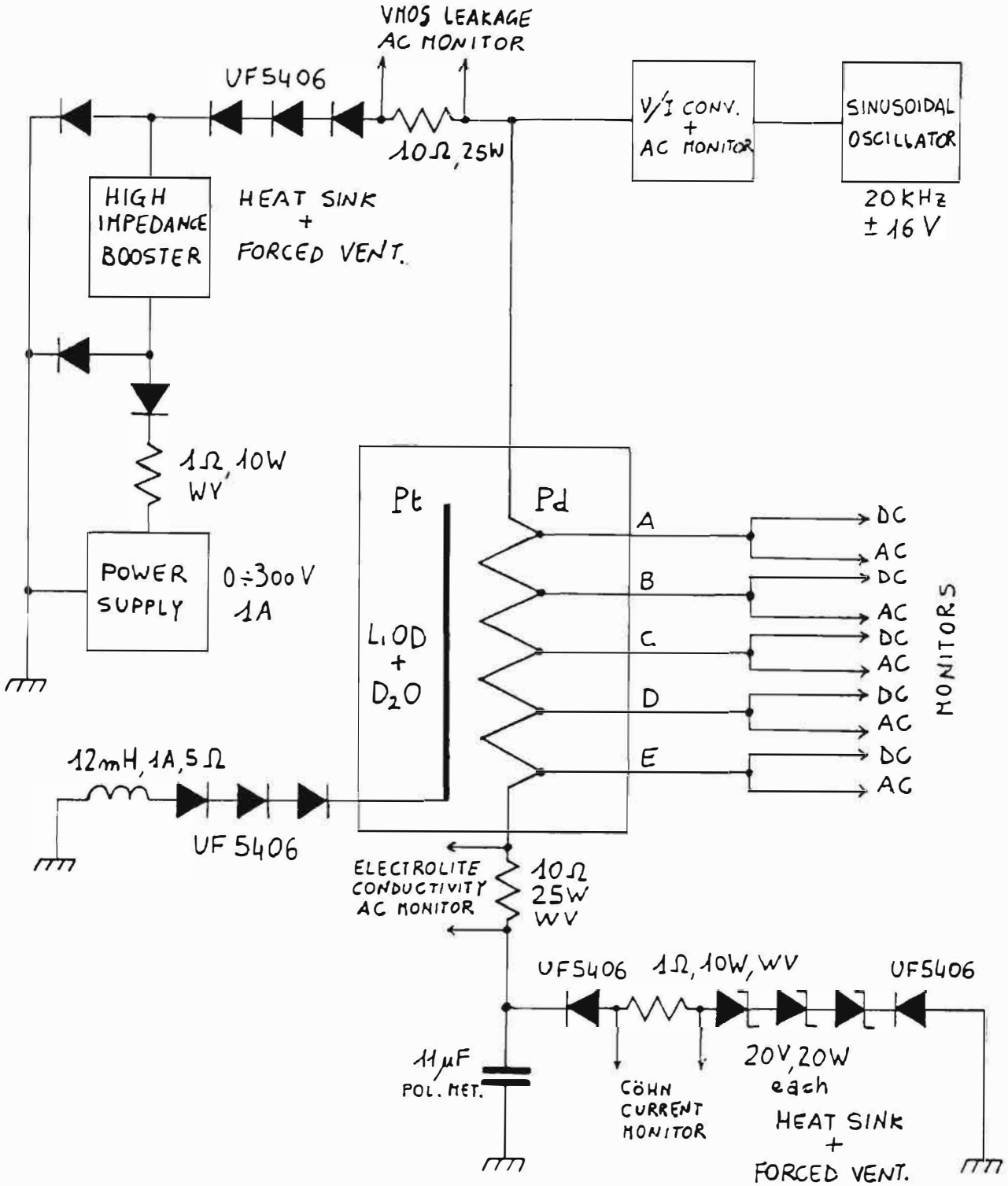

Fig.2: Electronic circuitry and innovative experimental set-up devoted to avoid errors in Pd wire resistance measurement due to electrolyte paralleling effects.

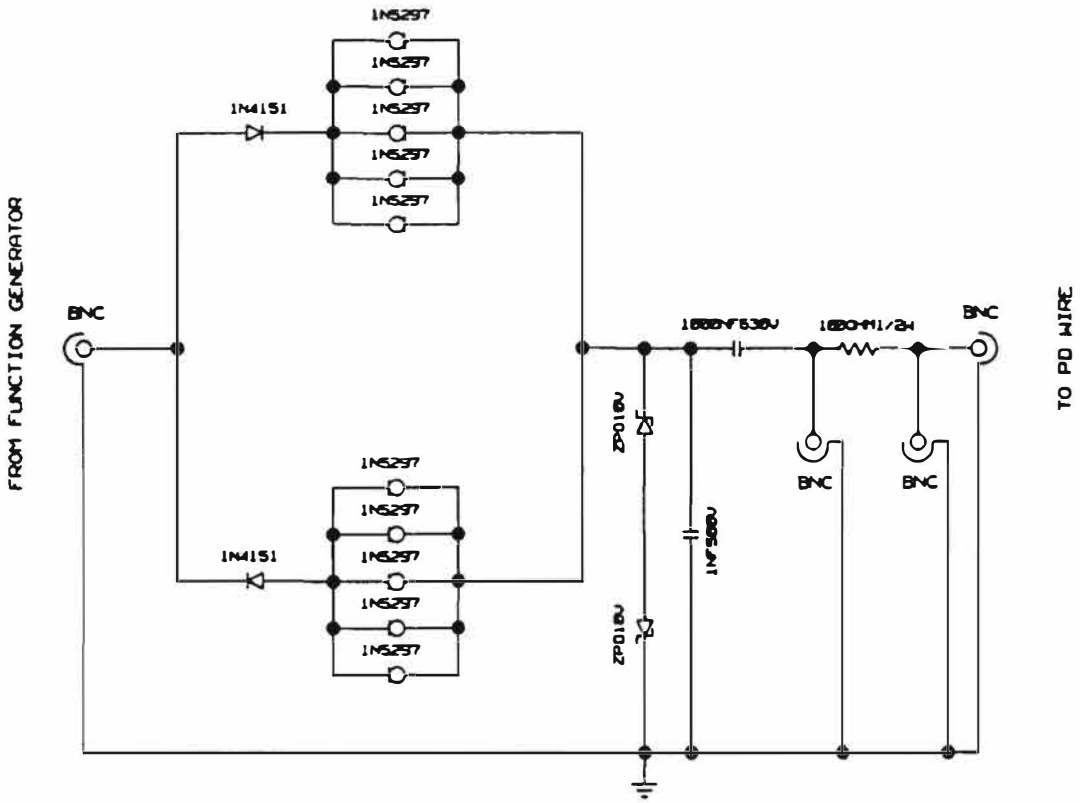

Fig.3: Details of "voltage to current converter" electronic circuit.

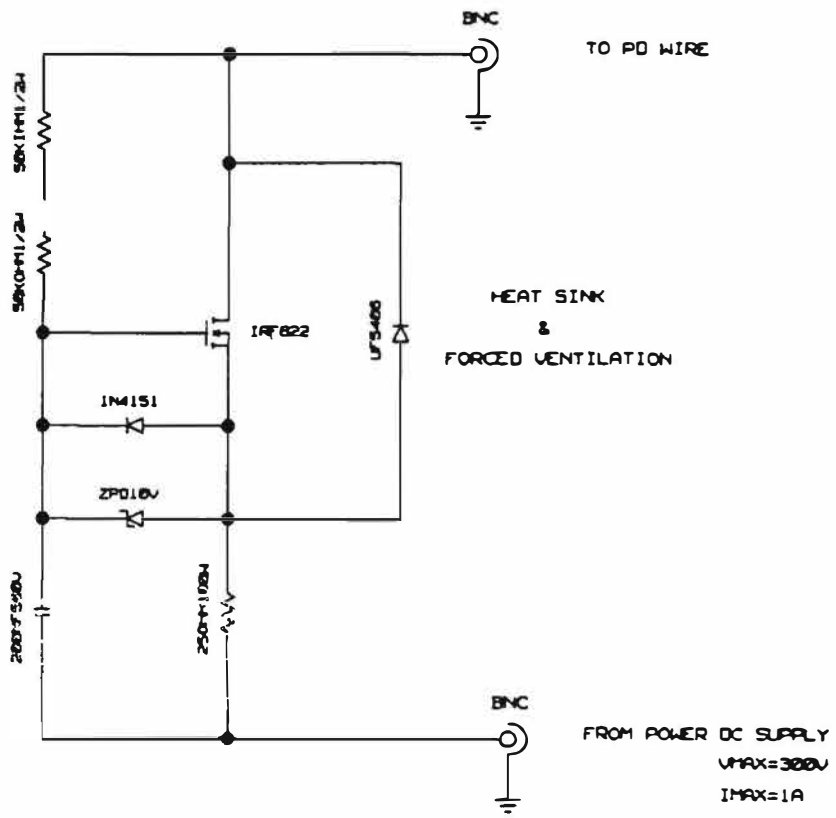

Fig.4: Details of "high impedance booster" electronic circuit.

proper feeding of deuterium to Pd wire (Co) is an intrinsically difficult task because the diffusion speed of incoming deuterium is only 10^{-7}-10^{-8} cm s^{-1} (β phase) while the moving-crossing-escaping has a diffusion speed 100-1000 times larger (γ phase).

The easiest way to *maximize* the voltage drop and to *minimize* the power dissipated by Joule effect is to use *long* and *thin* cathode wire [3]:

$$V = I R = I \rho l / S \tag{2}$$

$$W = V^2 / R \tag{3}$$

Equation (2) represents the voltage drop along the cathode wire and equation (3) represents the dissipated Joule power: ρ is the intrinsic resistivity, l is the wire length and S is the cathode wire cross-section area.

4.2. Limits to electromigration effect

Regarding the electromigration effect, there exists an intrinsic limitation.

The deuterium concentration increases at the end of the cathode wire, where the voltage drop is at the most negative value, but it can escape from this side if there is no physical barrier at the end. These barrier can be mechanical (metal covered with gold, copper or nickel) or electrical (deuterium chemical potential on the palladium surface larger than deuterium chemical potential inside palladium). Sometimes this barrier is made just by soldering the Pd (by Sn-Pb alloy) with copper wire, feeding the necessary current to the system [4,6]. This kind of procedure can be likely because the wire for the connection is copper. This element, in proper conditions, can penetrate onto the Pd surface and has the peculiarity (together with nickel) of decreasing the Pd lattice parameter [5]. This alloy, at the skin of the wire, reduces the speed of deuterium deloading, just because it acts as a mechanical barrier. The trick of copper barrier has some physical limitations and the effectiveness is largely procedure-dependent. One of the main drawbacks arises when it is necessary to reverse the polarity of the electrolysis and the copper can dissolve into the solution, worsening the low conductivity behaviour of the solution (LiOD 250 μN). Low conductivity is necessary to keep large anode-cathode voltage at enough low current (e.g. 100V, 500mA, 160cm wire length, 1cm anode-cathode distance, 30°C temperature) in order to get large Deuterium-H-T loading [4].

In DC conditions it is quite difficult to get an effective *adhesive strength* able to withstand hundred of thousand (or even milion) of atmosphere of pressure necessary, speculatively, to get Cold Fusion just by pressure.

The pulsed condition helps to reduce the necessity of using strong barriers at the end of the cathode wire because, in proper conditions, it is concievable that the *highly concentrated deuterium inside the wire is itself like a dynamic barrier.*

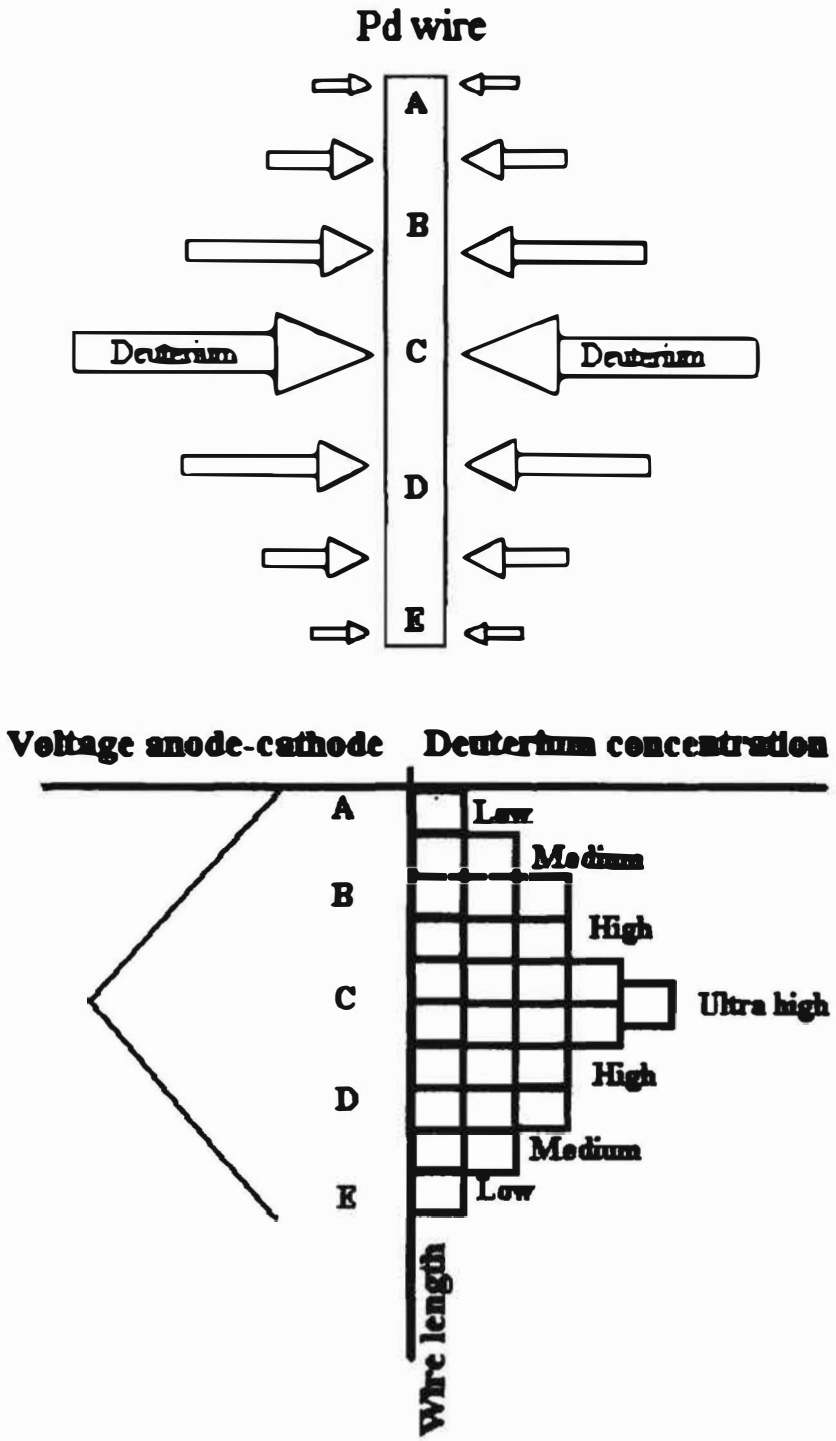

Fig.5: Skech of enhanced electromigration by "central wire geometry" (collider). The point C is the most negative input voltage, the points A and E are electrically connected.
$|V_A| = |V_E|$; $|V_C| > |V_{B,D}| > |V_{A=E}|$

According to the new set-up, at least in principle, it is not necessary at all to have a barrier against the escape of deuterium because the barriers are two, dynamics: they are just the highly concentrated deuterons themself coming from opposite and symmetric directions, with the (nominal) same intensity.

This kind of geometry can be further improved using *pulsed current* because it is possible to reach larger gradient of concentrations, due to larger voltage drops (upto 100+100 V along the length of 80+80cm of 100μm Pd wire diameter in our experiment, peak current of about 23A) during pulsing, in respect to the few volts (typically about 9+9 V) achievable in DC conditions with 1A total current.

Thanks to this geometry, through loading experiments using the Pd resistance measurement, will be possible to clarify whether the *anomalous excess heat* arises from *static* or *dynamic* conditions of deuterium inside palladium. Dynamic condition is equivalent to high speed of D concentration variation.

5. Pd-Y alloy wire

We studied, since 1994, the effect of elements that contract or enlarge the Pd lattice with endothermic or exothermic behaviour [1]. Now, we experimentally studied the Pd-Y alloy (Y=3.9% in weigth), an exothermic enlarged lattice, from the point of view of isotopic effect (H,D) using both normal wire geometry (*usual electromigration*) and central wire geometry (*collider*): four kinds of different experiments in total.

The PdY alloy was selected for two main reasons. The first reason was that the Y itself is an element that can absorb H-D-T in large amounts (up to 2.8:1) and the hydride is stable even at high temperature (1100K; 10,000ns). The second reason was that the intrinsic resistance of this alloy is, noticeably, 2.5 times larger of pure Pd: it is possible to experimentally test, also, the new theory developed from G.Preparata [3] about the "electrical confinement" of H-D-T in Pd due to larger voltage drop along the wire.

6. Pulsing procedure

We further verified the effect of high power pulsing (peak current in the range as high as 20,000-200,000 A/cm^2; pulse width of 500ns; peak voltage between anode and cathode up to 300V) about rise time(80-300ns) and repetition rate (100-50000 Hz) with respect to loading and excess heat.

In our experience, the excess heat detected by proper pulsing, given an experimental set-up and kind of Pd wire used, is about twice in respect to the most effective DC operation conditions that we can adopt.

The main drawback of pulsing operation is that, up to now, we are not able to measure R/Ro with enough high resolution because large noise intrinsically emitted from the pulse: it affects adversly the low level (5-10mA, 20KHz) sinusoidal signal used for resistance measurement. One of the main advantages (and extra benefit) of pulse procedure is that it can be very effective for *conditioning* the Pd cathode wire to subsequent loadings, with anomalous effects, in high voltage DC conditions.

7. Main results

We summarize the main results obtained using Pd 99.92% (from ORIM, isoperibolic calorimetry, 5 months of experiments) and Pd-Y (from Tanaka K.K., flow calorimetry, 3 months of experiments) wires (both 160cm length and 100μm diameter):

- **a)** loading (by R/Ro absolue value measurements and behaviour observations) show that R/Ro loading with D is larger than R/Ro loading with H, as expected;
- **b)** the maximum loading is achieved with central wire geometry, in comparison to normal wire geometry;
- **c)** excess heat using LiOD-D_2O solution is larger than LiOH-H_2O solution (fig.6, PdY alloy, normal-wire geometry, D_2O and H_2O experiments);
- **d)** excess heat measured using central wire geometry is larger than using normal wire geometry.

In fig.7 are shown the results using pure Pd, central wire geometry.

The input power was about 50W and in this specific experiment, lasted about 20 hours, after the procedure of FLOATING (2 minutes) and subsequent restart (at the same electrical parameter, constant current), it was detected a very large amount (up to a maximum of 200 W) of excess heat. The amount of excess heat seems related to the *speed of loading* , as shown in fig.7 (time 4,000-6,000 seconds), and not to the absolue value of loading (time 48,000-52,000 seconds): although the R/Ro value (at time 50,000) is lower then at the beginning of the experiment, the excess heat begins to vanish because the speed of variation of loading is very low.

In our opinion, this specific experimental result is quite significative to understand (and hopefully to control in the future) the phenomenology of Cold Fusion, at least from the point of view of excess heat generation.

The behaviour of loading of PdY (fig.8,9) seems to have 2 components: the first seems related to pure Pd (R/Ro increases and after, in proper condition, can decrease), the second seems to related to Y (R/Ro increases linearly with the time, up to some limiting value).

The detection of excess heat even with this lattice expanded material (with normal wire geometry) can support the idea that large cathode-anode voltage (because large resistivity of this alloy) is quite effective to *confine* the H/D inside lattice [3].

8. Some general conclusions and further developings.

The PdY alloy has the peculiarity of very large resistivity and good mechanical properties (not britle even after several cycles of loading-deloading). In proper experimental conditions, it seems that this material always gives anomalous excess heat, althoug at limited value (15-25%) in comparison with pure Pd. As main advantage, the generation of excess heat does not need of any kind of *special* pre-treatment of the wire (used, as received, from Tanaka K.K., just cleaned by organic solvents), as generally necessary for pure Pd (at our experience) like conditioning by high current or pulsing.

Excess Heat

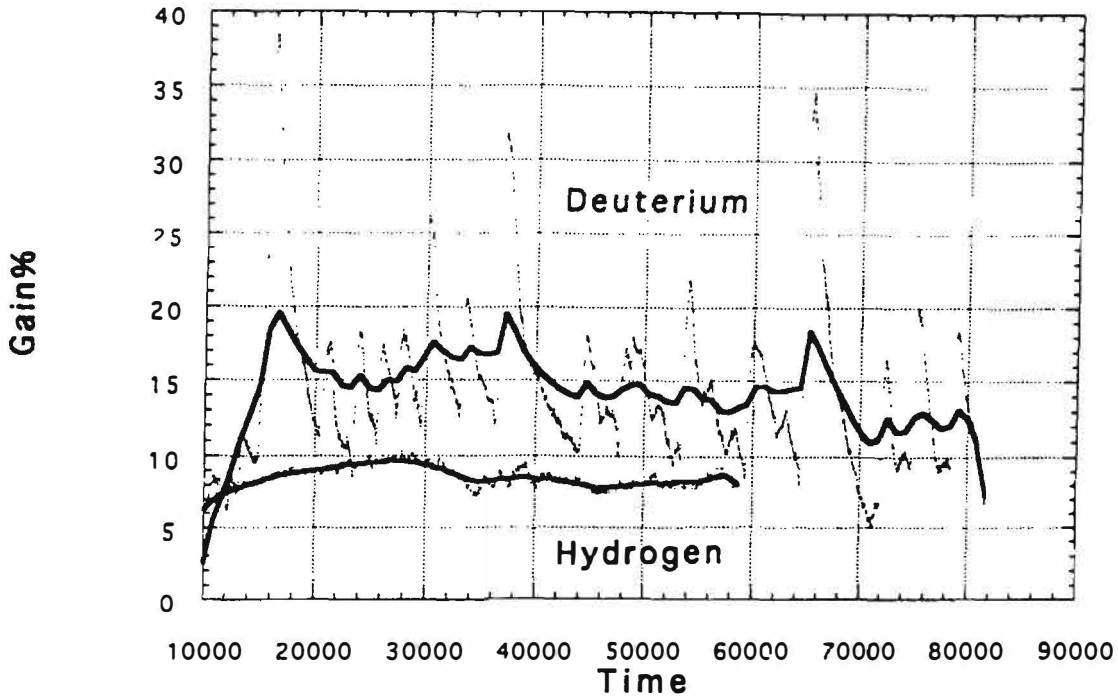

Fig.6: Isotopic behaviour of normal wire geometry set-up using flow-calorimetry (1% accuracy). We used the same wire, before loaded by D and later by H. We notify that after six loading/deloading procedure (washing) the excess heat of Pd/Pt/H system decreased to about 3%.

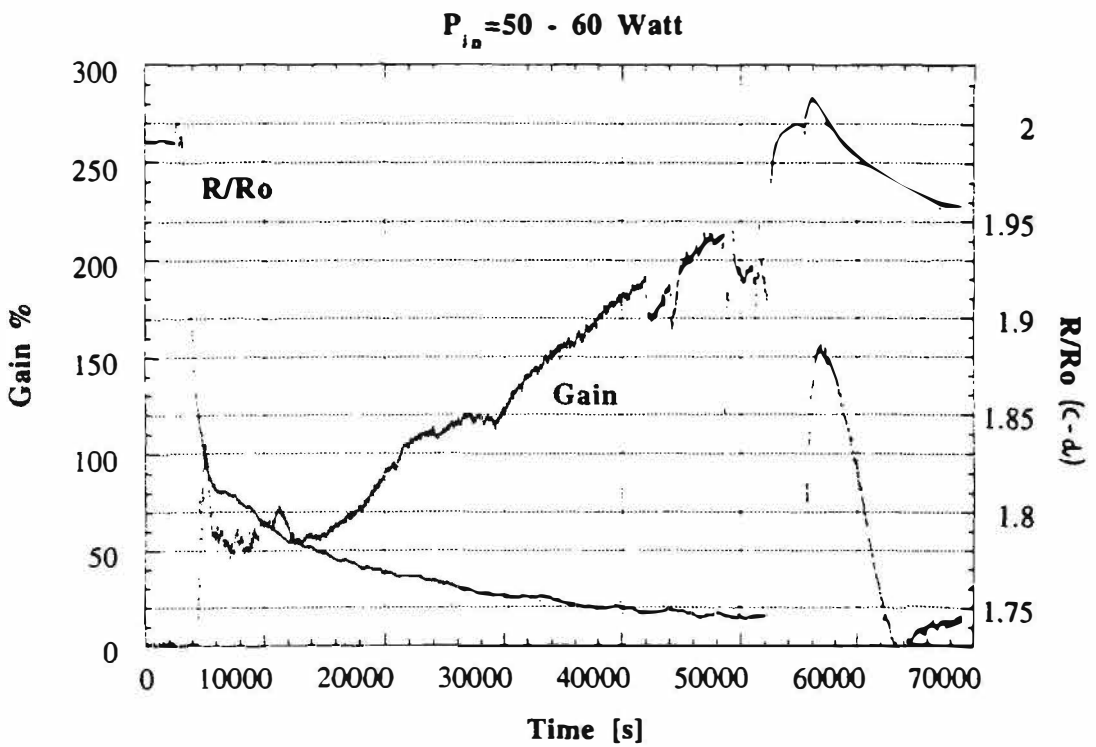

Fig.7: Pure Pd "central wire geometry" results. Isoperibolic calorimetry (15% accuracy).

Excess Heat

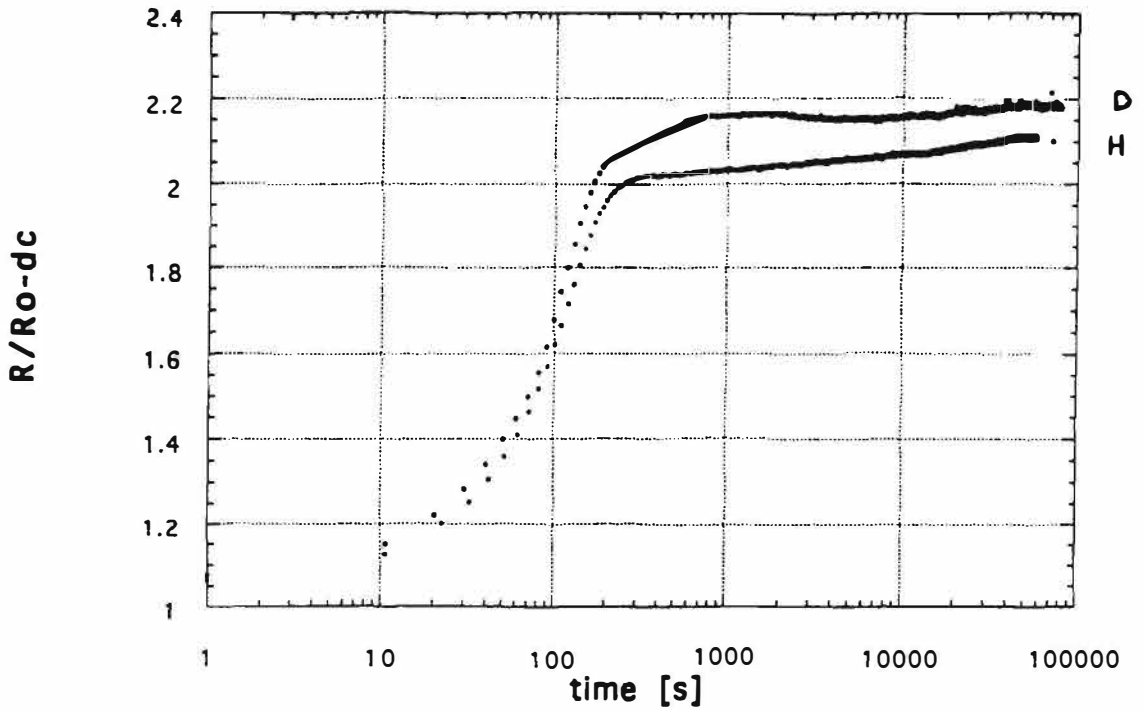

Fig.8: Normal wire geometry resistance behaviour of PdY. Isotopic effect clearly detected.

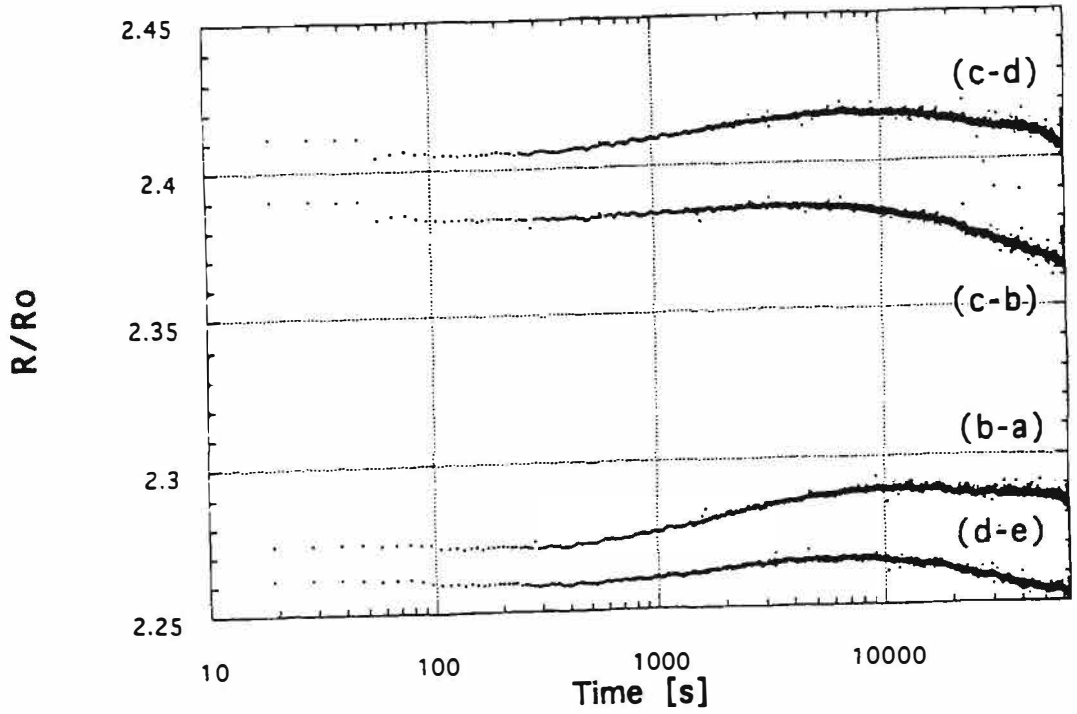

Fig.9: Central wire geometry resistance behaviour of PdY-D: details of the wire 4 different sections.

Excess Heat

The beneficial effect of central wire geometry (developed at INFN-LNF since February 1995 and extensively studied from October 1995), from the point of view of both larger loading and excess heat generation, also in this lattice expanded material, seems confirmed.
Comparison of experimental results between *normal* and *central* wire geometry suggest that the origin of anomalous excess heat can be related to the *movement* of D (H?) in Pd. It can remember the original idea of A. Takahashi [7] with Low-High current electrolysis, in order to get some moving of D in Pd plates. The pulsing obviously is effective for this purpose, at least in order to increase the overall efficency of excess heat generation.

Aknoledgments

Work supported from: INFN (Italy); NEDO-NHE (Japan), ORIM s.r.l. (Italy).
Palladium (99.92%) wires kindly provided from ORIM. Palladium Yttrium alloy provided from TANAKA K.K. (Japan) in a joint collaboration between NEDO-NHE, IAE and INFN, under the supervising of NHE Director Dr. Kazuaki Matsui.
We are indebted to Prof. Makoto Okamoto (Tokyo Institute of Technology) for deep suggestions about isotopic effect in our experimental set-up: his comments and criticism were for us unvailable.
Prof. Akito Takahashi (Osaka University) gave us very useful warnings and suggestions about behaviours of isoperibolic and flow calorimetry in our unusual electrolytic cell geometry.
Obviously, we never can forget the illuminating idea about the thin wire geometry and its peculiarity that Prof. Giuliano Preparata (Milano University) gave us continuosly.

Reference

[1] F. Celani et al. Physics Letters A 214, pg.1-13 (1996).
[2] Alfred Coehn, Z. Elektrochem. 35, 676 (1929).
[3] Giuliano Preparata, private communications(1995) and patent pending (1996).
[4] F. Celani et al.: Int. Workshop "On the loading of Hydrogen/Deuterium in metals: characterization of materials and related phenomena", Asti, Italy--- Oct.11-13, 1995.
[5] Y. Sakamoto et al, Ber. Buns. Phys. Chem. 99, 807, Vol.6 (1995).
[6] F.Celani et al.: Int. Workshop "Material behaviours for large deuterium loadings" Kawaguchi-ko, Japan--- Sept 5-7,1994.
[7] A. Takahashi et al.: Proc.ICCF3: Frontieres of Cold Fusion, H.Ikegami ed., Universal Academy Press (1993), pp.79-92.

Click here for a more readable copy of this paper.

Some Thoughts on the Nature of the Nuclear-Active Regions in Palladium

Edmund Storms

ENECO
270 Hyde Park Estates
Santa Fe, NM 87501, USA

ABSTRACT

A large collection of palladium samples, supplied by IMRA Materials (Japan), were studied to determine the relationship between energy production and various properties including the amount of excess volume, the open-circuit-voltage, and the maximum D/Pd ratio. The following conclusions result from the work:

1. Palladium, no matter how well prepared, is very inhomogeneous with respect to the properties relevant to cold fusion. Therefore, most general conclusions can not be based on the behavior of one or a few samples.

2. The bulk properties do not represent the properties of the nuclear-active-regions. Theoreticians need to take special note of this observation.

3. Energy active palladium will continue to produce excess energy even after being subjected to acid treatment or physical removal of the surface. Therefore, "good" palladium is difficult to ruin.

4. A pretest method has been developed to identify "good" palladium.

1. INTRODUCTION

The ability to provide a large amount of nuclear-active-palladium to researchers is essential to the eventual acceptance and commercialization of the Pons-Fleischmann Effect. At the present time, active palladium is discovered largely by accident when energy generation is observed using a calorimeter. This process is slow. A better method involves rapid measurement of properties that influence energy production. In this manner, large batches of palladium can be rapidly sorted into active and inactive material for use in a variety of studies.

Three properties were chosen to be examined: the tendency to produce cracks during loading with deuterium, the maximum average D/Pd ratio that can be achieved, and the chemical activity of deuterium at the surface. A few samples were also studied to determine the deloading rate in air and to locate those regions on the surface from which deuterium loss was occurring. The relationship of these properties to heat production was determined in a few cases.

Additional experimental results are described in several papers published in Infinite Energy[1; 2]. Future results will be published in the same journal.

2. METHODS

2.1 Composition

The composition was measured in two ways; by weighing the cathode and by determining the amount of oxygen released when deuterium dissolved in the cathode. Because loading was done in a sealed cell, containing a recombiner, the amount of oxygen could be measured by displacing oil onto a balance. The oil-constant was approximately 7300 g of oil per 1 mol of dis-

solved deuterium. At the end of the loading process, the cathode was weighed (±0.00005 g) and the value used to determine the oil constant for the study. The steady composition achieved after 24 hours was used as the limiting composition. The effects of temperature and current were studied. Typical behavior is shown in Fig. 1. Bubbles on the cathode become visible when the D/Pd deviates from the ideal value.

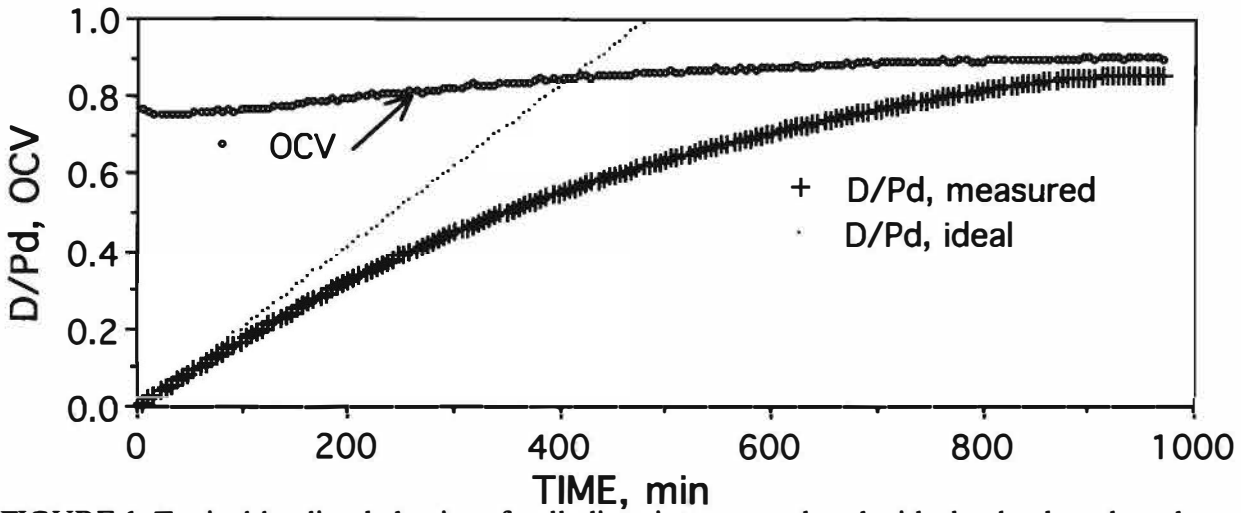

FIGURE 1. Typical loading behavior of palladium is compared to the ideal value based on the applied current. The open circuit voltage is also shown using the same scale.

2.2. Crack Formation

Palladium expands by more than 12% when it is loaded with hydrogen. However, the amount of expansion is frequently greater than that predicted from the published relationship between X-ray lattice parameter and composition. This excess volume is found to fall between 1 and 25% of the initial volume. The excess volume is proposed to result from the formation of cracks, blisters, and dislocations. When these features penetrate the surface, they accelerate loss of deuterium and prevent regions near these structures from achieving a high deuterium content. Because the average crack volume is a mixture of structures that do not contact the surface and those that exit at the surface, the overall effect is highly variable and permits only general conclusions.

The physical volume was measured using a micrometer (±20 μm for early samples, ± 2 μm later) before and after loading. The following formula was used to calculate the excess volume:

Excess Volume (EV) = [(Final Volume)-(Initial Volume)]/(Initial Volume) - (0.0172+0.14125*D/Pd)

2.3. Chemical Activity of the Surface

The voltage generated between the surface and a reference electrode is proportional to the chemical activity of deuterium in the surface. A Luggin capillary was used to provide a conducting bridge between the cathode and a piece of platinum gauze located outside of the cell. The applied voltage to the cell was interrupted for a short time (5-10 sec.) while the voltage (±0.001 V) was measured between the cathode and the gauze. Pure palladium produced a voltage of 0.02±0.05 V relative to platinum before loading started. Samples returned to this value after all deuterium had been removed.

2.4 General Deloading

The weight loss was monitored as a function of time after the sample was removed from the cell. When the D/Pd ratio is plotted as a function of $\sqrt{}$time, a straight line results which can be extrap-

olated back to zero time. In this manner, a determination is made of the composition existing in the cell immediately before the current was stopped. The slope of the resulting line was recorded for many samples. Values between $1x10^{-3}$ and $22x10^{-3}$ (D/Pd)/√min were observed. This property was very sensitive to how the sample had been treated.

2.5 Localized Deloading

Some samples were examined while deloading under methanol or acetone. The bubble pattern revealed those regions experiencing rapid loss of deuterium. A variety of structures were seen by this technique. The concentration of deloading sites was very nonuniform.

2.6. Power Production

A glass, isoperibolic calorimeter was used. The cell was sealed, contained an internal recombiner, and was stirred at a constant rate. The internal temperature was measured at two positions within the electrolyte and at the cathode. A water-cooled jacket provided a constant reference temperature. Power production was measured relative to the electrolyte power applied during the first few hours of electrolysis, before excess power production started. Figure 2 shows a typical calibration. The standard deviation in excess power of a typical data set was ±0.15 watt. A drawing of the calorimeter can be found in reference[1].

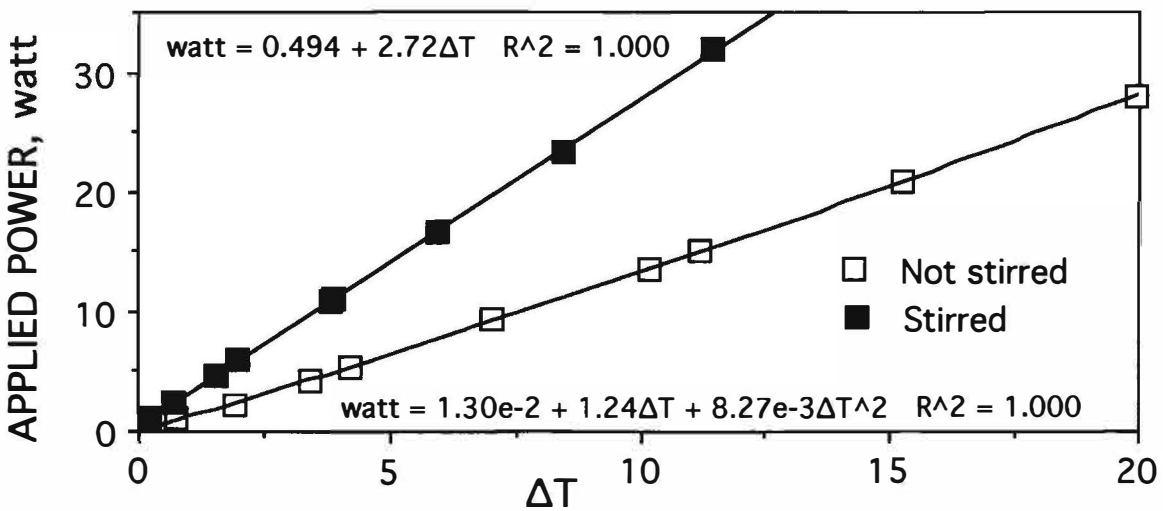

FIGURE 2. Typical relationship between applied electrolytic power and the temperature across the cell wall. Stirring produces a more linear relationship and a steeper slope.

3. RESULTS

Eighty samples which fell into eight sets were examined. One half of the sets contained 500 ppm boron while the remainder were nominally pure palladium. The samples had been subjected to various annealing and surface treatments by IMRA. Each sample was approximately 10 mm wide, 20 mm long and 1 mm thick.

All properties showed a wide distribution around a mean value. It is, therefore, impossible to arrive at a general conclusion based on the behavior of a single or a few samples. Unfortunately, some of the sets contained an insufficient number of samples to make statistical analysis meaningful. Consequently, only a few general conclusions will be presented. These will address the effect of adding boron and the effect of etching the surface with Aqua Regia.

Excess Heat

3.1 Composition

Figure 3 shows a histogram that compares samples with and without added boron. The presence of 500 ppm boron both improves the limiting composition as well as making it worse. Clearly some pure samples are better in this regard than are some samples containing boron. The reverse is also true. In addition, samples containing boron lost about 0.00015 g as a result of the electrolytic process. This loss indicates that the surface region is depleted of boron during the loading process.

An Aqua Regia treatment tends to make the property more uniform but does not lead to especially high values.

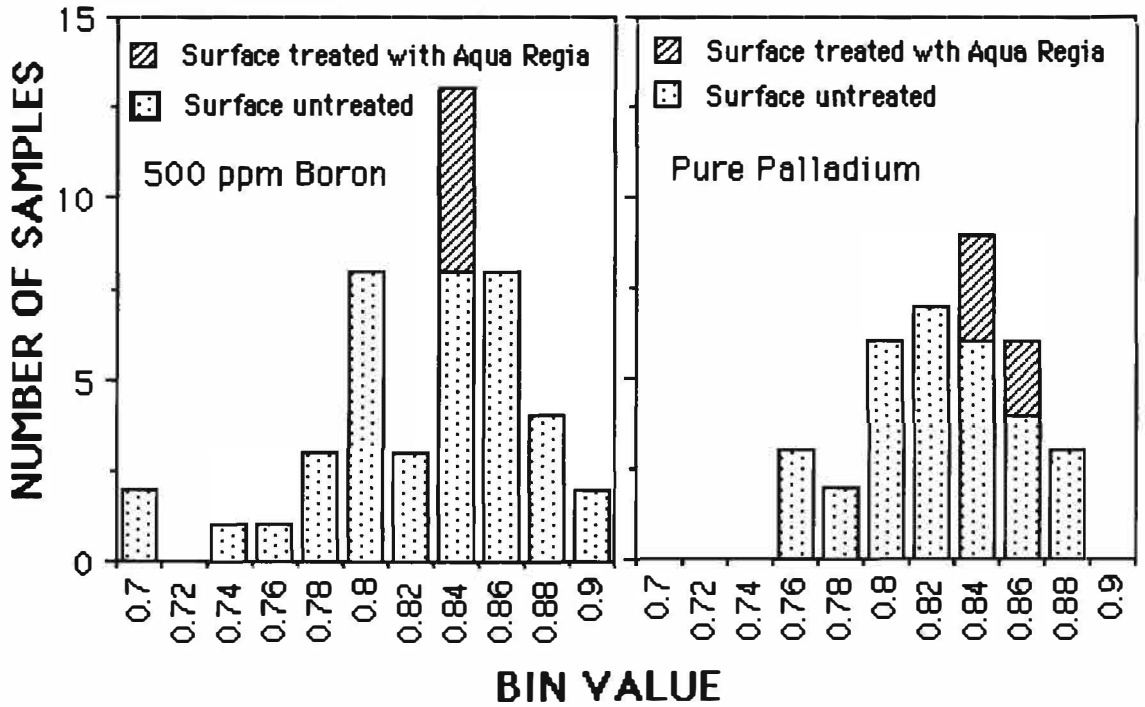

FIGURE 3. The histograms compare the limiting composition of samples containing 500 ppm boron with those that are untreated. The effect of Aqua Regia treatment using 5 samples from each set is superimposed. The bin value for 0.90, for example, shows the number samples having a value between 0.88 and 0.90. Because of edge effects, the values have only a relative meaning.

3.2 Crack Concentration

Shown in Fig. 4 is the excess volume (EV) for "pure" palladium and for samples containing 500 ppm boron. The values are corrected to D/Pd=0.85 because the amount of excess volume tends to increase as the composition within the β-phase is increased. The presence of boron increases the average excess volume from 4.3% for pure palladium to 5.6%. In addition, the boron produces a significant number of values over 10%. An Aqua Regia surface treatment appears to have no significant effect on this property.

Samples having a EV near 1% do not form additional EV even after they are deloaded and reloaded. However, the presence of a larger initial EV produces additional EV each time the sample is reloaded. The amount of additional EV is variable between samples.

3.3 Chemical Activity of the Surface

The open-circuit-voltage (OCV), measured during loading, is compared to the average D/Pd in Fig. 1. The initial rapid increased was always followed by slight drop. Those samples that

eventually produced excess power usually continued to increase to values above 1.0 V.

Figures 5 and 6 compare the OCV of two samples during deloading. The sample shown in Fig. 5 is a piece of palladium foil that did not make excess power. Thicker samples show the same behavior but naturally take much longer to return to the α-phase. The sample shown in Fig. 6 made excess power immediately before the current was interrupted. Indications of a new phase having a OCV above that of β–PdD were occasionally seen in other active samples. However, this sample (#42) gave the highest OCV measured thus far.

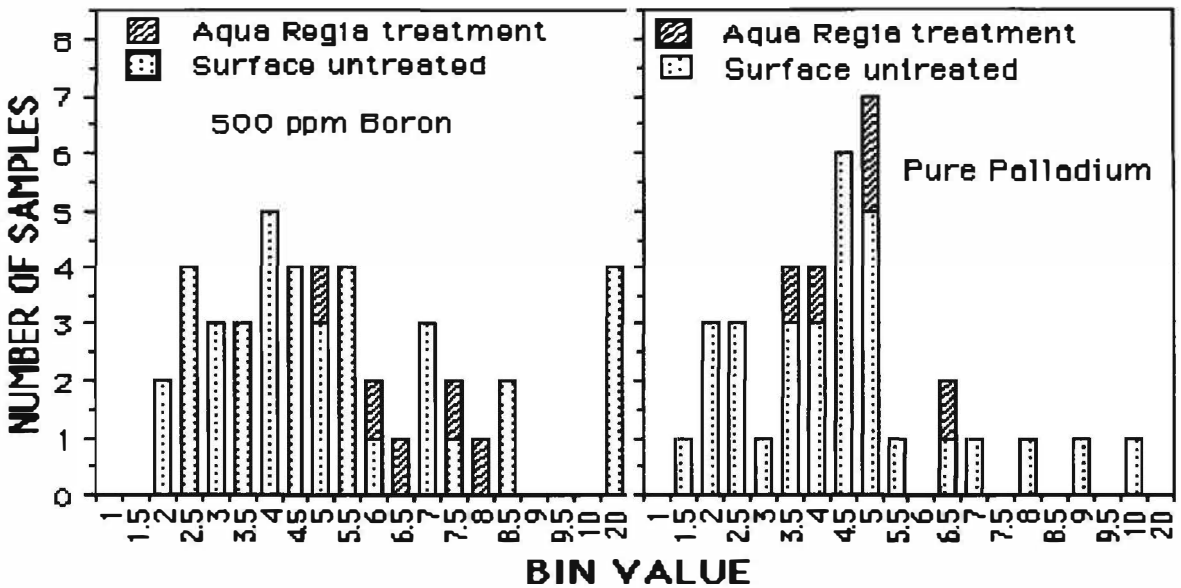

FIGURE 4. The histograms compare the percent excess volume of samples containing boron with those to which boron was not added. The effect of Aqua Regia treatment using 5 samples from each set is superimposed. The bin value for 8.0, for example, shows the number samples having a value between 7.5 and 8.0 percent. Values are extrapolated to D/Pd=0.85.

3.4 Excess Energy

Excess power (EP) production is compared to the measured properties in Table 1. The listed properties were measured after the power measurements. Only general conclusions can be drawn from these few examples because other important variables were not measured and because each sample was very nonuniform with respect to those variables that were studied.

After sample #42 made excess power, a study was undertaken to determine how much abuse to the sample would be required to stop energy production. After the sample had been fully loaded to D/Pd=0.86, EP was sought by increasing the applied current in steps to 3 A. Each current was held for 10 min. while the calorimeter came to equilibrium. Figure 7A shows the EP at 3A. Brief current interruptions had little effect on EP production even when the sample was removed from the cell for a short time. Longer interruptions reduced EP production and required additional time before the previous EP was restored. Between figures 7A and 7B, the sample was washed with Aqua Regia, the surface was polished with 400-600 mesh SiC paper, and all deuterium was removed at 110°C. The OCV was 0.01±0.01V before loading was started. After being fully loaded, the sample produced the behavior shown in 7B. Regular bursts of EP every 2 hr were seen while the current was constant at 2A. These bursts were sensitive to applied current and cell temperature. EP continued to increase after 5 g of Li_2SO_4 was added to 40 ml of electrolyte.

Before the data shown in Fig. 8 was taken, the calorimeter was enlarged and improved. The Pt mesh anode was replaced by a spiral of palladium wire and fresh 0.4 M LiOD electrolyte was used. In addition, ≈40 μm was removed from the sample surfaces by diamond polishing followed by an Aqua Regia etch and heating in air at 325°C. After reloading, the composition was D/Pd=0.816 with 2.8% EV. Calibration was done on day 0. Thereafter, EP at 3A increased as

shown in Fig 8. A current reverse at day 8 produced a minor reduction on day 9. An attempt to determine the composition on day 9 caused the sample to self-heat in air resulting in loss of most contained deuterium. Upon being returned to the cell, energy production resumed after 1 day and continued to increase until the sample was removed and sent for measurement of γ-emission. No γ-emission was detected.

TABLE 1
Comparison between measured properties and excess power production

Sample Number	Designation	Excess Volume, %	Composition D/Pd	OVC	Excess Power, W (at 3 A)
Tanaka 1*		1.7	0.82		7.5
IMRA #38	A1-B3	2.0	0.875	1.25	2-4
Tanaka 4*		2	0.84		2
IMRA #42	A1-B4	1 to 2	0.891	1.35	4.6
IMRA #84**	A2-B2	6.9	0.83	1.00	1.6
IMRA #39	A1-B3	4.1	0.87	1.08	1.1
IMRA #57	A2-B1	6.0	0.83	1.05	0.0
IMRA #10	A1-B1	6.6	0.82	1.00	0.0
IMRA #27	A1-B1	1.0	0.85	0.96	0.0
IMRA #58	A2-B1	4.1	0.79	0.70	0.0
IMRA #62	A2-B1	2.3	0.83	0.66	0.0
IMRA #44	A1-B4	16.1	0.78	0.60	0.0
Tanaka 2*		13.5	0.75		0.0

* Tanaka samples from Refs. [3; 4]
**Surface layer containing O and Si of sufficient thickness to partially flake off during loading.
A1-B3 = pure Pd+ basic process + annealed in vacuum at 750°
A1-B4 = + treatment with Aqua Regia
A2-B1 = 500 ppm B added + basic process
A2-B2 = + annealed in air at 750°

4. CONCLUSION

The properties of palladium relevant to "cold fusion" are very nonuniform even when samples are treated in an apparently identical manner. To achieve excess energy production, material should have a low excess volume, be able to acquire a D/Pd ratio above 0.85 and have an open-circuit-voltage in excess of 1.0 V referenced to platinum. Because of edge effects, the limiting composition applies only to the sample shape used in this study. Occasionally, a sample will fail to meet one or more of these requirements and still make excess power. Apparently, additional variables are important beyond the ones reported here.

Samples that are found to produce excess power can be reactivated even after being completely deloaded and after the surface is removed. Apparently, the required surface can be reestablished if the properties of the base material are suitable. This discovery means that active samples can be identified and used in other studies without losing the ability to produce heat during transfer.

The bubble pattern seen when a sample is allowed to deload in acetone is an effective method to study the concentration of microcracks and other imperfections that cause local reduction in composition at the surface. Three types of sites are seen; isolated bubbles, lines of bubbles associated with scratches and cracks, and active loss from blisters. Some samples have

large regions from which no bubbles are seen to leave.

The behavior of the OCV suggest the presence of a phase having a much larger deuterium activity than pure β-PdD when excess energy is produced. Very large OCV values obtained for samples having a bulk composition consistent with β-PdD, in the absence of EP, suggest that the surface activity is being modified by the presence of deposited impurities.

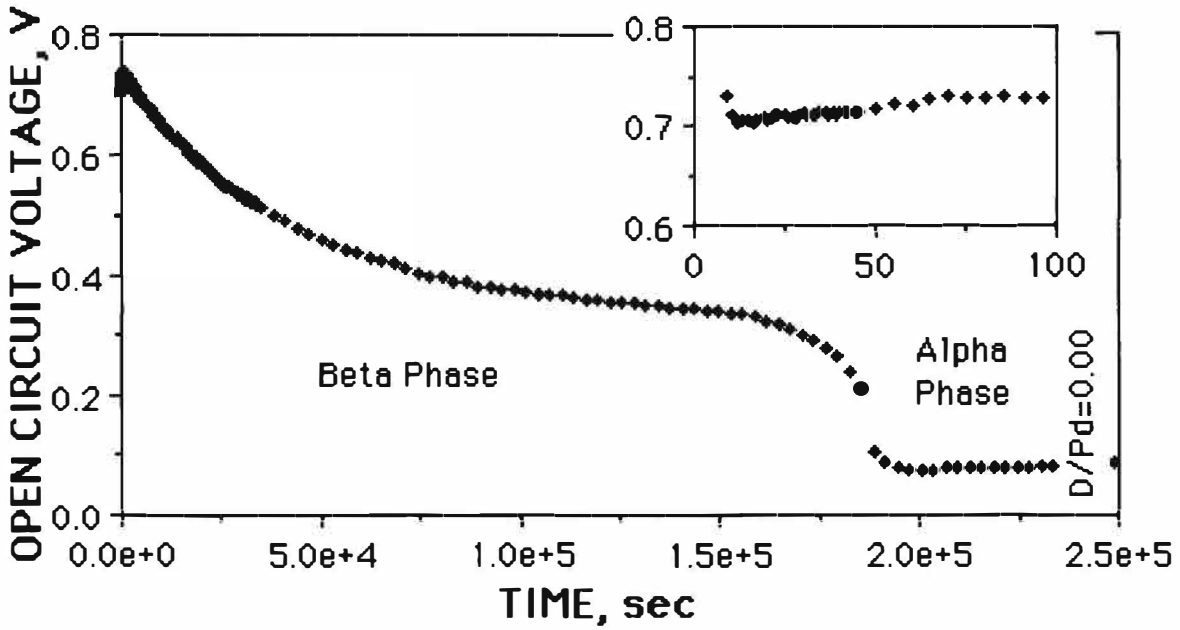

FIGURE 5. Open-Circuit-Voltage of a 50 μm thick Pd foil during deloading in the cell at 30°C. This material did not produce excess power before deloading. The insert shows a characteristic initial increase.

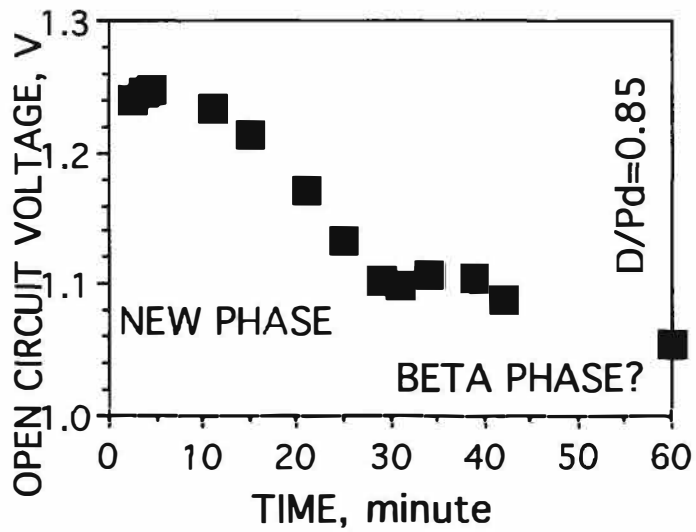

FIGURE 6. OCV of Sample #42 deloaded in a cell at 9°C. This sample produced excess power before deloading

ACKNOWLEDGEMENTS

The author wishes to thank Mr. Yoshihisa Kamiya and Toshihisa Terazawa of the IMRA Materials Laboratory, and Dr. Keiji Kunimatsu of IMRA Japan for providing the samples. Prof. Hideo Ikegami was very helpful in making the arrangements. Mr. Fred Jaeger (ENECO) provided some of the financial support needed to carry out these studies. Prof. Steve Jones (BYU) was very kind to provide some equipment that was used during the early phase of the work. Future

studies will benefit from the help provided by Dr. David Nagel (NRL).

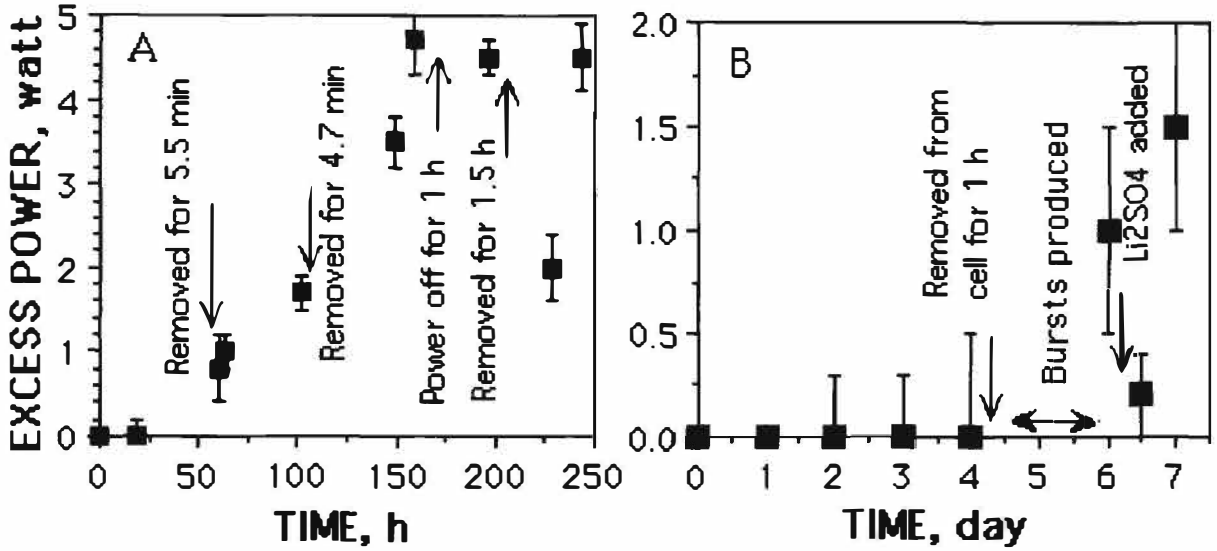

FIGURE 7A. Initial onset of power production.

FIGURE 7B. Onset of power production after surface was removed.

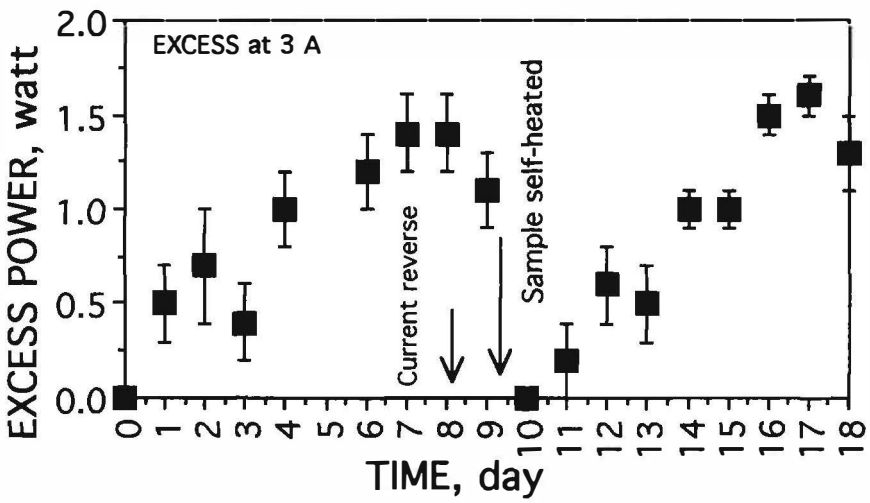

FIGURE 8. Onset of power production after at least 0.080 mm was removed and the sample was washed with Aqua Regia. Self heating occurred when the sample was exposed to air because of a rapid D_2+O_2 reaction.

References

[1] Storms, E., "A Study of Those Properties of Palladium that Influence Excess Energy Production by the "Pons-Fleischmann" Effect", Infinite Energy **2**, #8, 50 (1996).

[2] Storms, E., "The Nature of the Energy-Active State in Pd-D", Infinite Energy, **1**, 77 (1996).

[3] Storms, E., Measurements of Excess Heat From a Pons-Fleischmann-Type Electrolytic Cell Using Palladium Sheet, Fusion Technol. **23** (1993) 230.

[4] Storms, E., Some Characteristics of Heat Production Using the "Cold Fusion" Effect, Proc. Fourth International Conference on Cold Fusion, , Lahaina, Maui, Dec. 6-9, 1993, EPRI TR-104188-V2 (1994), p. 4. Electric Power Research Institute, Palo Alto ; Ibid , Trans. Fusion Technol. **26** (1994) 96.

Excess Heat

Click here for a more readable copy of this paper.

Reproduction of Fleischmann and Pons experiments

G. Lonchampt, L. Bonnetain ,CEA - Centre d'Etudes Nucléaires de Grenoble 17, rue des Martyrs - 38054 Grenoble cedex 9, (France)

P.Hicter, Ecole Nationale Supérieure d'Electrochimie et d'Electrométallurgie de Grenoble, BP 75, 38402 Saint Martin d'Hères, (France)

Abstract

The objective of this work is to check the reliability of the initial Fleischmann and Pons calorimeter for studying cold fusion from ambient to boiling temperature. After describing our experimental set up, the assessment of excess heat from the enthalpy balance is discussed. On the electrodes after electrolysis, we have observed deposits which, in our opinion, have a determining rôle for the excess heat generation. We show raw data of three runs. It is concluded that this calorimeter is well adapted for such cold fusion investigation.

1- Introduction

Since the announcement of the cold fusion phenomenon by Fleischmann and Pons [1] in 1989, various techniques have been utilized to produce excess heat. Numerous results have been obtained that are dispersed, and even sometimes contradictory with each other.

Being aware of that, we have decided to "simply" reproduce the exact experiments of M.Fleischmann and S. Pons as described in their 1993 article [2]. The purpose of our work is to ascertain the various phenomena involved and the conditions of their apparition in order to master the experiments.

2- Experimental

2.1 Description of the experiment

The cell we use is identical to the one used by M. Fleischmann and S. Pons [2]. It is described in figure 1. It is a pyrex Dewar which upper part is silver coated to prevent heat radiation losses in this area, and to make the heat losses by radiation insensitive to the water level. The various parameters are as follows:

- the electrolyte: LiOD, 0.1 M l^{-1},
- the cathode: palladium cylinder (platinum for blanks), diameter 2 mm, length 12.5 mm is spot welded on a platinum wire,
- the anode: platinum wire, diameter 0.2 mm,
- a thermistor for temperature measurement of the electrolyte, with a precision of ± 0.01°C at 20°C and of ± 0.1°C at 100°C,
- a resistor for heat pulses generation,
- a kel'f plug for electrical connections, and a duct for replacing the water eliminated by electrolysis and by water vapor carried away in the electrolysis gases.

The cell is immersed in a constant temperature bath (20°C), as shown in figure 2. Electrolysis is performed at constant current, with a high accuracy power supply, having a maximum voltage of 150 Volts. Current, voltage, temperature and atmospheric pressure are recorded by computer, with an AOIP interface box. Water is added automatically everytime 1 cm^3 is consumed. Data are collected every 6 seconds, and averaged every minute.

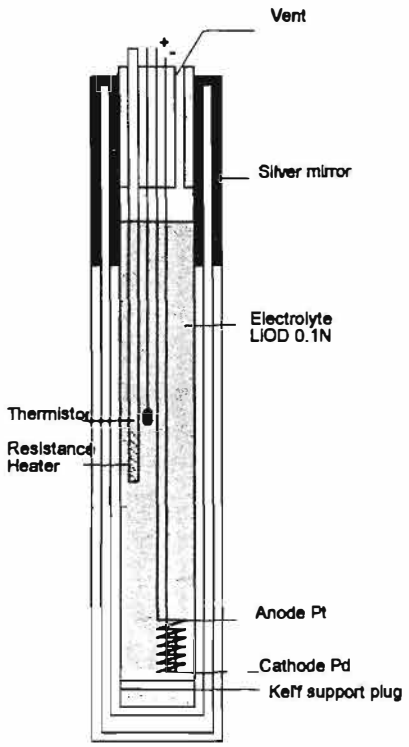

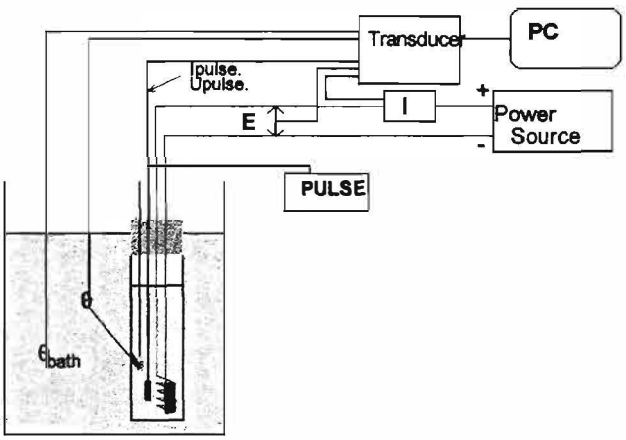

figure 1. Fleischmann and Pons type cell

figure 2. Experimental stand

2.2 Experimental procedure

The Dewar is cleaned with acetone, and dried in air. Heavy water (85 cm^3) is filled in the cell in an argon atmosphere to avoid contamination by CO_2 and H_2O from the air. Experiments are performed in a constant temperature room ± 0.1°C at 20°C. A typical experiment starts at low current: 0.2A (0.26A cm^{-2}) until temperature reaches 40 °C. This period lasts typically one to two weeks. This "loading" period does not show any excess heat production. Current is then raised at 0.5 A ($0.66Acm^{-2}$) until boiling temperature.

3- Assessment of excess heat

Excess heat is evaluated two ways. At temperatures below boiling we calculate excess heat on a continuous mode, while the experiment is being performed. At boiling the excess heat is calculated once all the water of the cell has been evaporated without addition of water.

3.1 Excess heat calculation below boiling temperature

In this regime, the excess heat is calculated from the energy balance[2] as detailed below.

$$\textbf{Excess heat} = A + B + C - D \qquad (1)$$

Excess Heat

Enthalpy flux	**Evaluation formulae**	
"A" is the enthalpy losses (by radiation) to the water bath	$K_R(\theta^4 - \theta^4_{bath})$	(2)
"B" is the enthalpy content of the gas stream[2]	$\frac{3I}{4F}\frac{P}{P^* - P}L$	(3)

"I" is the electrolysis current, "F" is the Faraday constant, "P", the water pressure at the temperature of the bath, and "P^*", the atmospheric pressure. "L" is the enthalpy of vaporization of the water (41,000 J.mol^{-1}).

"C" is the variation in the enthalpy content of the calorimeter	$C_{pD_2O,l}M_0\frac{d\theta}{dt}$	(4)

$C_{pD2O,l}$, is the heat capacity of D_2O, M_0 is the heavy water equivalent of the calorimeter

"D" is the input electrical enthalpy	$(E - E_{th})I$	(5)

Relation (1) is valid when there is no calibration pulses, and not at boiling, where the analysis using this approach becomes difficult because the denominator of (3) is close to zero as the temperature approaches boiling and water vapor pressure is close to the atmospheric pressure. At boiling, a different analysis is made which is described below. The only unknown parameter that needs to be calibrated is K_R. All other variables can be measured independently. K_R is determined by calibration with a platinum cathode.

3.2 Excess heat calculation at boiling temperature

When temperature reaches a value close to boiling, i.e. typically 99 to 101°C, we stop adding water to the cell, and we measure the total enthalpy necessary to evaporate the contents of the cell. The excess enthalpy is therefore given by the formula:

$$\text{Excess heat} = A + L - D \qquad (6)$$

Where "A","D" and "L" have the same definition as above. It is difficult to follow accurately the level of water during this period because of the formation of foam, so it is only at the end of the experiment, when the cell is dry that the excess heat can be calculated with precision.

3.3 The various experimental regimes

a) Low temperature regime: $\theta < 70°C$

In this region relation, (1) becomes:

$$\text{Excess heat} = A - D \qquad (7)$$

Since temperature is low, the water vapor pressure is negligible, therefore "B" can be ignored. In this region, temperature varies slowly with time, hence "C" can be neglected.

This domain is the one used during calibration to determine K_R, since during blanks runs, there is, by definition, no excess heat produced, K_R is therefore given by:

$$K_R = \frac{(E - E_{th})I}{(\theta^4 - \theta^4_{bath})} \qquad (8)$$

b) Intermediate temperature regime: 70°C < θ < 99°C

In this region all terms of relation (1) must be taken into account. Since the water pressure becomes high, "B" becomes important and since the temperatures varies rapidly, "C" cannot be neglected.

c) Boiling regime: θ > 99°C

The boiling temperature is only progressively reached as the bubbles, here initiated by electolysis incorporate more and more water vapor. In this region, the full calculation using equation (1) gives wrong positive excess heat measurements, and therefore cannot be applied. This is probably due to a erroneous estimation of "B" which is very sensitive to pressure and temperature measurements. Up until now we have not been able to get a good blank experiment with platinum in this region using the full equation. Therefore, instead, we use the measurement of the enthalpy produced to evaporate the total amount of water contained in the cell, as described in section 3.2.

4- Basic phenomena occuring during electrolysis

The main effect of electrolysis is generation of deuterium and oxygen gas at the electrodes. However in this type of cell, other side reactions occur which possibly have major importance in the production of excess heat. The basic phenomenon discussed here is the formation of an overvoltage on the electrodes. Table 1 shows a synthetic view of what we believe is happening:

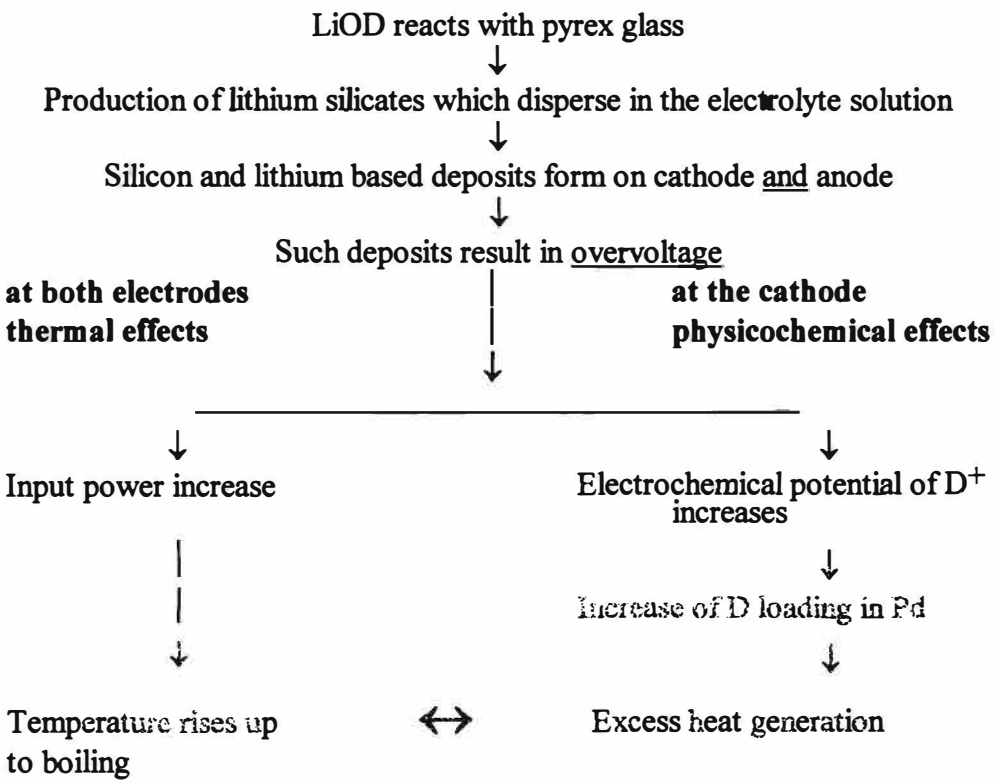

Table 1

5- Calorimetric results

Excess Heat

5.1- Calibration experiments

As mentioned above, the two unknown parameters, M_0 and K_R, must be deduced from calibration since they cannot be calculated accurately.

K_R is deduced from blanks with platinum cathodes of same size and positioned exactly as the palladium cathode. By definition, we assume that platinum does not produce excess heat. In the low temperature regime, below 70°C, relation (1) simplifies, and we use (8) to calculate K_R.

Figures 3a and 3b show a small apparent excess heat when temperature rises. This is most likely due to the heat losses by conduction, not taken into account in our formulas that assume all heat transfer is radiative. In any case, this apparent excess heat is low, at most 50 mw, or 1.25% of to the energy input. We have made attempts to change K_R with temperature, but without any significative change in the final result. Therefore, in our analysis, we have kept K_R constant with temperature.

M_0, the heavy water equivalent of the calorimeter is evaluated in runs without electrolysis by adding controlled heat pulses and measuring the rate of temperature change.

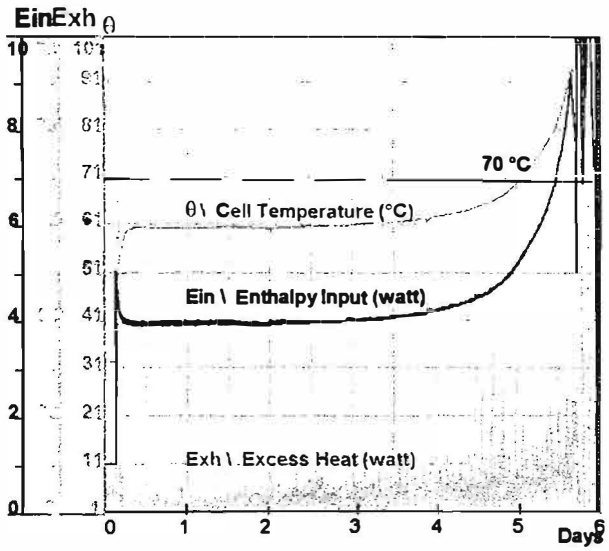

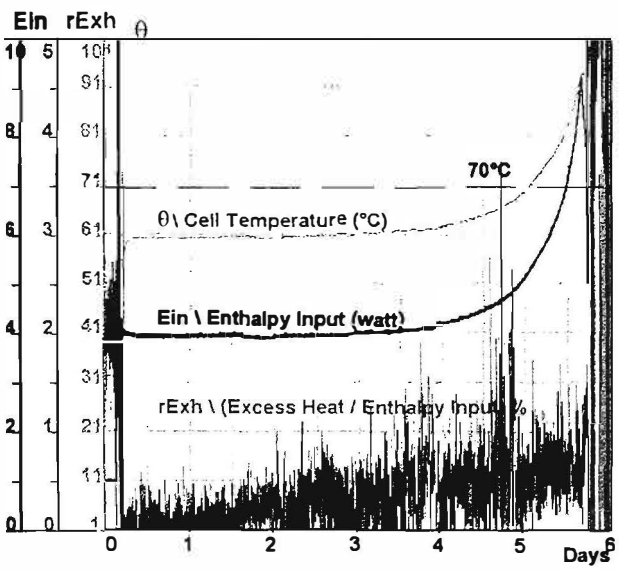

Raw data June the 10th, 1996 Cell P3 $K_R = 0.078$

fig. 3a **fig. 3b**

Calibration experiment (platinum cathode)

5.2- Palladium cathodes experiments

Since the beginning of our experiments, in 1993, 18 runs have been carried out. Only five of them have produced excess heat, with high purity palladium cathodes. Figures 4a and 4b show a run with a pure palladium cathode, etched in aqua regia for five minutes. The sample has been loaded for ten days at low current (0.2A), then the current is raised to 0.5A. Excess heat increases from 70 mW to 170 mW at 70°C. At that point, contrary to our standard procedure, current is decreased to 0.25 A (voltage decreases simultaneously) and the input power decreases. However, the excess heat does not decrease, and has even a tendency to increase.

Excess Heat

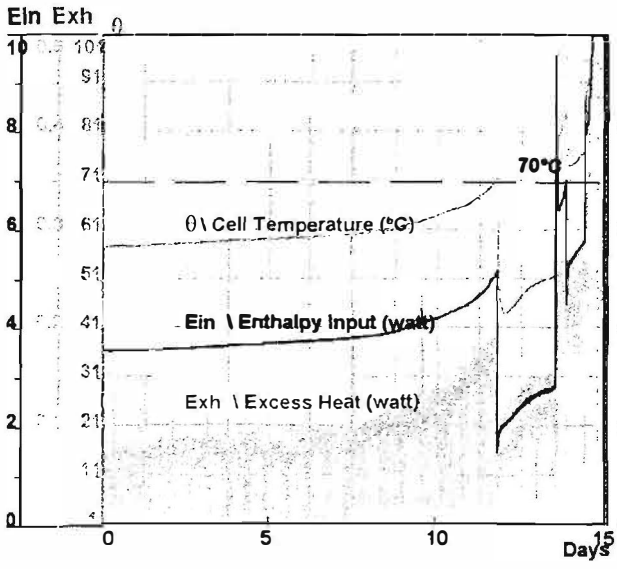

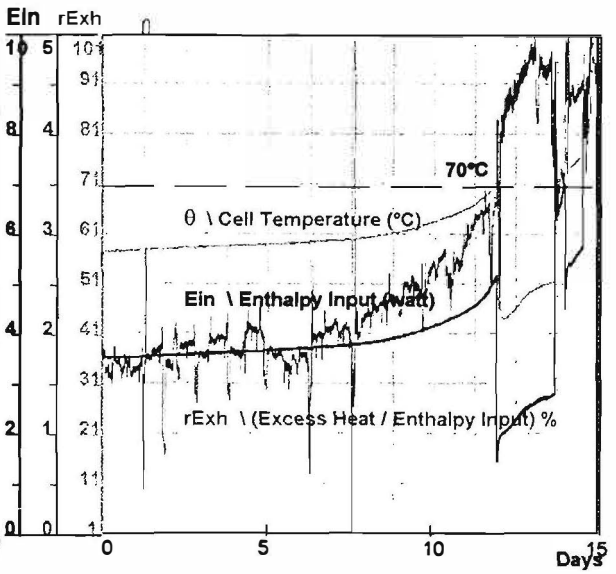

Raw data January the 30th, 1996 Cell P1 $K_R = 0.075$

fig. 4a **fig. 4b**

High purity palladium cathode (preliminary treatment in aqua regia)

Figures 5a and 5b show another run, were during the first three days, voltages have been switched, and therefore the palladium was anodic. This has the effect of oxidizing the palladium surface, and then after making the palladium cathodic, to reduce the surface and to create a rough surface similar to palladium black. Also in this run heat pulses have been applied every 24 hours for a duration of 12 hours. At the beginning, the excess heat is 40 mW, then raises to 100 mW when temperature reaches 60°C, and sharply rises to 300 mW above 75°C.

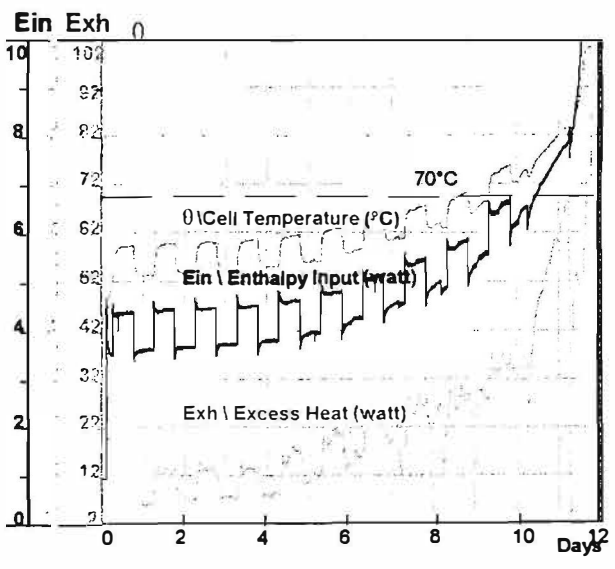

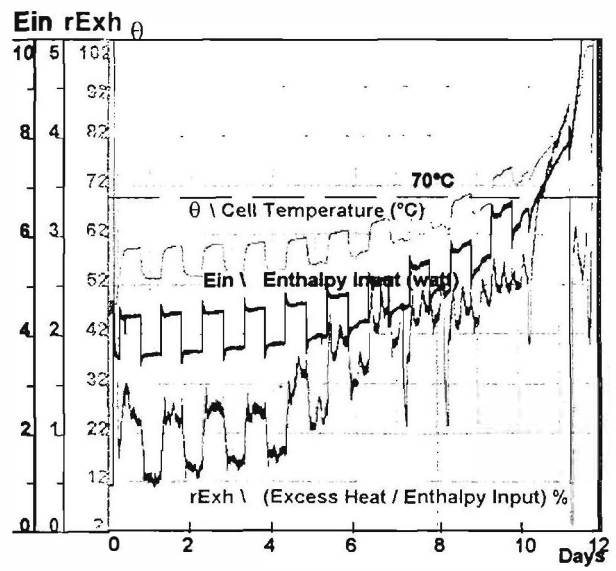

Raw data September the 30th,1996 Cell P2 $K_R = 0.0905$

fig. 5a **fig. 5b**

High purity palladium cathode (initially inversed current).

Excess Heat

At boiling, the electric current is maintained constant, (0.5A), and as the overvoltage increases, the input energy grows up to the maximum of the power supply, in our case 75 Watts (maximum voltage 150 Volts). In all of our experiments showing excess heat at boiling, we have observed a sudden jump in power input towards the end of the experiment indicating a sudden change in the overvoltage. This might be due to the formation of a water gas film at the surface of the cathode when large quantities of heat is produced, either by electrical heating or possibly by the excess enthalpy itself. As described in section 3.2, the exact evaluation of the excess heat can be made only at the end of the experiment, since it is difficult to follow accurately the water level during the experiment. However it is very likely that most of the excess heat occurs at the end of the experiment after the voltage burst. We call this last period the "grand finale".
Table 2 shows five experiments that have brought to boiling, along a platinum experiment. The final column relative to the last phase is calculated assuming no excess heat before the voltage jump.

Experiment	Date	Electrolyte Volume (cm^3)	Enthalpy Input (electrolysis) (joules)	Enthalpy losses (to bath water) (joules)	Available Enthalpy (joules)	Enthalpy used for total vaporisation (joules)	Excess Heat (joules)	Mean relative Excess Heat %	Relative Excess Heat during "grand finale" %
P1 Pd 1st sample	january 30th,1996	84	419,100	254,700	156,876	181,499	24,623	**16**	153
P1 Pt	CALIBRATION march 18th, 1996	85.5	425,700	240,600	185,100	184,740	360	0.2	no burst
P3 Pd 1st sample	september 3th, 1996	80	318,700	151,000	167,700	172,856	5,156	**3**	18
P3 Pd 1st sample	september 14th, 1996	74	221,200	72,190	149,010	159,892	10,882	**7**	36
P2 Pd 2nd sample	september 30th, 1996	72	308,600	178,700	129,900	155,570	25,670	**20**	97
P3 Pd 2nd sample	october 2nd, 1996	78	290,700	132,800	157,900	168,535	10,635	**7**	29

Table 2 Boiling regime: enthalpy balance

6- Discussion

Several questions raised during our work have been answered, but many more are still open. In this section we will try to give indications of what we believe is correct and what still needs more work.

One of the criticism of the Fleischmann and Pons work has been the temperature uniformity inside the cell. If temperature varies, the radiation law is not valid, and all radiation losses calculations should be wrong. We have looked carefully at this point, and by raising the thermistor, from its standard location in the middle of the cell all the way to the surface of the water, we have seen no significant temperature variation, indicating that mixing by the gases of the electrolysis is sufficient.

On the assumption that all heat losses are due to radiation, our platinum blank experiments indicate that this is a good approximation, and that the maximum error might be in the higher temperature range, and should not exceed 1%.

Concerning condensation on the inner surface of the plug, again our platinum runs indicate that it is negligible.

Excess Heat

The main point that needs to be addressed is the importance of the various parameters that make these experiments irreproductible. Many known and many more unknown parameters are important and deserve discussion.

We have shown that overvoltage is very important. Probably it helps increase the deuterium loading in the near surface region of the cathode, especially in the final phase.

Many groups have emphasized deuterium loading as the important factor. In our case we have not measured it, but we are not sure that this is an important information, since all electrical or weight measurements are average values that are not valid in this type of experiments where most likely reactions occur near the surface.

It is our experience that the palladium history is of prime importance. However we have been enable of deciding if a simple treatment like aqua regia is good or bad. Impurities might play a rôle, but we do not know which ones are necessary. What is the rôle of lithium, not as the electrolyte, but as part of reaction?

Another important aspect is the quality of the heavy water. We have used D_2O with a purity of 99.5%. It is also possible that in the loading phase the electrolyte gets purified slowly by differential electrolysis of the light water that escapes first. The long loading period might then be necessary to eliminate hydrogen.

This last assumption is one of the reasons why loading might be long,up to several weeks.

We have never observed any heat after death as mentioned by Fleischmann and Pons[2].

7- Conclusions

Our experience during this last three years, leads us to conclude that the Fleischmann and Pons calorimeter is very accurate and well adaptated to study cold fusion phenomenon. It is simple and precise. However precautionary measures must be taken:

- the Dewar must be of excellent quality, i.e. good vacuum, in order to eliminate heat losses by conduction, and operate with radiation losses only,
- temperature calibration of the thermistors must be done very precisely,
- all electrical feedthroughs must be sealed off in order to eliminate spilling off of electrolyte by capillarity.

Our results concerning the relative excess heat (percentage of excess heat to enthalpy input) can be summarized as follows:

- below 70°C, between 0 and 5%
- between 70°C and 99°C, about 10%
- at boiling, up to 150% especially in the final phase which appears as the best condition to get a large amount of excess heat.

As already done by S.Pons, with ICARUS 9, it is necessary to operate at boiling on a permanent basis to obtain the most signignificant results.

Acknowledgments: we would like to thank M. Fleischmann and S. Pons for all their technical information. We thank J.P. Bibérian for his contribution for presentation of this work.

References

(1) M. Fleischmann and S. Pons, J.Electroanal. Chem, 261, 301 (1989)
(2) M. Fleischmann and S. Pons, Phys.Letters. A 176, 118 (1993)118 - 129

Excess Heat

EXCESS HEAT MEASUREMENT AT HIGH CATHODE LOADING BY DEUTERIUM DURING ELECTROLYSIS OF HEAVY WATER USING Pd CATHODE

Toshihide NAKATA, Masafumi KOBAYASHI, Masatoshi NAGAHAMA,
Hidemi AKITA, Norifumi HASEGAWA and Keiji KUNIMATSU
IMRA JAPAN CO., LTD.
2-3-6 Techno-Park Shimonopporo, Atsubetsu-ku, Sapporo 004, JAPAN

INTRODUCTION

We reported excess heat data as a function of cathode loading by deuterium, D/Pd, using various kinds of Pd materials as a cathode in fuel cell type closed cells developed in our laboratory [1]. Since then we have tried to reproduce the excess heat data by employing a different kind of calorimetry, mass flow calorimetry, at better cathode loadings because the previous data was restricted to the cathode loading lower than 0.86. The issue of electrolytic loading of deuterium into a Pd cathode was investigated in terms of the bulk and surface properties of the cathode, and it was concluded that the surface and the bulk properties plays an essential role respectively for a given bulk and a surface properties [2].

We have employed three major approaches to improve the cathode loading based on these studies: (1)pretreatment of the Pd samples by either annealing at high temperature or by chemical etching in aqua regia, (2)application of the partial deload-reload cycles, (3)alloying with rhodium.

We report a summary of the 26 excess heat measurements by mass flow calorimetry under the improved cathode loadings.

EXPERIMENTALS

Electrolysis was conducted either in fuel cell type closed cells or electrolytic type closed cells with an internal recombiner which is a gas diffusion electrode placed in the gas phase, which is 1atm Ar when electrolysis was started. Figure 1 shows structure of the cells used in the excess heat measurement. The cathode loading D/Pd for Pd cathodes or D/M for Pd-Rh alloy cathodes, were determined in-situ during the excess heat measurement from the pressure decrease of deuterium gas in the fuel cell type closed cells and from the resistance measurement using AC four-terminal method in the electrolytic type cells. The resistance measurement was conducted by an Milliohm meter using probe current of 1mA and 1KHz. The relation between the resistance

an Milliohm meter using probe current of 1mA and 1KHz. The relation between the resistance ratio R/Ro and D/Pd reported by our laboratory at ICCF5 was employed for the determination of D/Pd from the resistance measurement [2].

Figure 2 shows the overview of the mass flow calorimetry system developed in our laboratory. Flow rate of the heat exchanging fluid, water, was monitored by an auto siphon which is a 1 liter triangular flask with a goose-neck shaped glass tube to discard the water, the typical flow rate being 0.5g/sec. Temperature of the flowing fluid at the inlet to the cell, Tin, was ca. 20°C which was monitored continuously together with its temperature at the outlet of the cell, Tout, by platinum resistance thermometer at the resolution of 0.01°C. The heat output from the cell was calculated by

$$Wout = C_{H2O} \times g \times (Tout-Tin)/k$$

where C_{H2O} is specific heat capacity of water and g is the flow rate in g/sec. The heat recovery efficiency k was determined by applying a known calibration power to the system which was generated either by an internal heater or by conducting electrolysis using a platinum cathode. The k value was typically ca. 0.98, and it was not significantly influenced by the nature of the calibration power. In many experiments electrolysis cells had an internal heater and the total input power to the cell was kept constant, typically 10 W, by adjusting the heater power and electrolysis power.

Cathode materials used are Pd (IMRA Materials, 3N), Pd (Johnson Matthey, 3N, 4N), Pd (Tanaka, 3N) and Pd-Rh (5, 10at%, J/M). The size of the cathodes was either 4mmϕ×25mm in fuel cell type cells or 2mmϕ×40mm in electrolytic type cells. The cathodes were annealed either at 200°C for 2 hours or 1000°C for 24 hours in vacuum. Chemical etching in aqua regia was also applied to some of the cathodes before they were set in the electrolysis cell.

The electrolyte solution, 1M LiOD, was made up by dissolving metallic lithium(99.9%) into D_2O (ISOTEC 99.8 D%) and its pre-electrolysis was conducted by using a Pd cathode and a Pt anode for isotopic purification as well as for eliminating the organic and the inorganic impurities.

RESULTS AND DISCUSSION

Table 1 shows a list of the 26 experiments named EFC series with cell type, cathode material and its size and source, pretreatment, maximum D/Pd and current density and electrolyte temperature at the loading, duration of experiment, and the result of excess heat measurement. We can see that although in many experiments using a Pd cathode the maximum loading ratio exceeded 0.86 for current density higher than 0.2 A/cm^2, no significant excess heat was observed, while we reported excess heat at ICCF4 under these conditions.

Figure 3 shows the raw data for EFC50 for which maximum loading of 0.92 was attained at 0.11A/cm^2 by using a Pd cathode (IMRA Materials) annealed at 1000°C in vacuum for 24 hours. The figure contains change of resistance ratio and current density for over forty days and the time when the maximum loading was attained is marked. Electrolysis was started by applying a slow

step up current mode, and the resistance ratio went through a peak of about 2.0 and came down to the minimum corresponding to D/Pd=0.91 between 0.1 and 0.2 A/cm^2. After applying deload /reload cycle the loading ratio increased to 0.92. The heat balance observed under a constant total power mode at ca. 10 W is shown in Fig. 4 with so-called $\pm 3\sigma$, ca. ± 0.2 W, of the heat measurement determined from the calibration data, and the histogram of all the data points in Fig. 4 is shown in Fig. 5. The results presented in Fig. 4 and Fig. 5 suggests that no statistically meaningful excess heat was observed in this experiment.

Figure 6 shows the data for EFC46 which was conducted by using a Pd cathode (J/M) annealed at 1000°C in vacuum for 24 hours and the highest maximum loading of 0.94 (0.96 if the resistance ratio is converted to D/Pd by applying the SRI curve [2]) of all the EFC series experiments using a Pd cathode was attained during the step up current mode around 0.2 A/cm^2 after applying the deload/reload cycle. The excess heat measurement was conducted under a constant total power mode around 10 W, however the heat balance observed during the experimental period shown in Fig. 6 shows little sign of excess heat as shown in Fig. 7. The larger noise amplitude which appeared after 55 days is due to increase in the power noise from the heater.

After the step up current mode shown in Fig. 6, we tried ramp mode electrolysis up to 1 A/cm^2 as shown in Fig. 8. The total input power was increased to ca. 25 W around 110 days in order to ramp the current up to 1 A/cm^2. Although the cathode loading tends to decrease at the higher current densities, D/Pd maintained a value around 0.88/0.89 at 1 A/cm^2. The heat balance during the ramp mode, however, did not give sign of excess heat as shown in Fig. 9. The average level of the heat balance is shifted to around -0.25 W for the period of 25 W total input, which is caused most likely by mismatch of the heat recovery efficiency determined by the heater power only.

Absence of excess heat at high cathode loadings and high current densities is most highlighted in EFC40 and EFC41 conducted by using a Pd-Rh (10at%) cathode, for which the maximum D/M(=Pd+Rh) of 0.96 and 0.99 were attained respectively at 0.53 A/cm^2 with no observable excess heat. Figure 10 shows change of D/M and current density for EFC41 with a Pd-Rh (10at%) cathode conducted in a fuel cell type cell. The loading ratio increased with stepping up of the current density and reached the maximum value of 0.99 at 0.53A/cm^2. However, no excess heat was observed as shown in Fig. 11 which shows the heat balance during the experiment. The large spikes are seen upon stepping up and down of current density as the electrolysis was not conducted under a constant power mode for this experiment. The heat balance is sifted to about +50mW during the period of the highest current density and D/M but this is within the typical 3σ level of ca. 0.2 W shown in Fig. 4 and cannot be interpreted as significant. It would be necessary to improve the accuracy of our heat measurement to say something more definite on the nature of the positive shift presented in Fig. 11.

Finally we have tried to interpret our present results using Pd cathodes and the former data of excess heat in terms of the cathode loading and current density. In Fig. 12 we plot the maximum

Excess Heat

D/Pd for a given current density for all the experiments. It is clear that the cathode loading has been greatly improved for any current densities between 0.1 and 1 A/cm^2 compared with the previous studies, while no significant excess heat was observed under the improved conditions. This may be interpreted:

1. Some unknown factors in addition to the cathode loading and current density may be operating for the excess heat generation.
2. Sensitivity of our mass flow calorimetry system may not be high enough to detect anticipated excess heat for the cathode volume.
3. Accuracy of our former excess heat data needs to be reinvestigated.

Currently we are organizing a new series of experiments based on the above interpretation.

REFERENCES

1. N. Hasegawa, N. Hayakawa, Y. Tsuchida, Y. Yamamoto, and K. Kunimatsu, ICCF4 Proceedings Vol. 1 page 3-1～3-30, EPRI, 1994.
2. J. Minato, T. Nakata, S. Denzumi, Y. Yamamoto, A. Takahashi, H. Aida, Y. Tsuchida, H. Akita, and K. Kunimatsu, ICCF5 Proceedings page 383-406, International Conference on Cold Fusion 5, 1995.

Table 1. Summary of the 26 experiments called EFC series using Pd and Pd alloy cathodes

No.	Cell Type	Cathode				Electrolyte	D/M	R/Ro	I	Temp.	Period	Excess
		material	size	source	remarks		max.	min.	[Acm-2]	[°C]	[day]	Heat
EFC01	Fuel Cell	Pd	ϕ4×25	J/M		1M LiOD	0.88	-	0.50	30	333	no
EFC02	Fuel Cell	Pd	ϕ4×30	J/M		1M LiOD	0.89	-	0.50	30	329	no
EFC05	Fuel Cell	Pd-5%Rh	ϕ4×25	J/M		1M LiOD	0.91	-	0.30	26	110	no
EFC06	Fuel Cell	Pd	ϕ4×20	TANAKA	C type	1M LiOD	0.85	-	0.10	22	110	no
EFC07	Fuel Cell	Pd	ϕ4×20	IMRA		1M LiOD	0.82	-	0.50	32	97	no
EFC09	Fuel Cell	Pd	ϕ4×25	J/M 4N		1M LiOD	0.93	-	0.50	30	154	no
EFC10	Fuel Cell	Pd	ϕ4×25	J/M 4N		1M LiOD	0.89	-	0.50	32	174	no
EFC22	Electrolytic	Pd	ϕ2×40	J/M 4N		1M LiOD	0.92	1.72	0.30	22	12	no
EFC23	Electrolytic	Pd	ϕ2×40	J/M 4N		1M LiOD	0.92	1.72	0.30	22	12	no
EFC24	Electrolytic	Pd	ϕ2×40	J/M 4N		1M LiOD	0.92	1.72	0.17	21	41	no
EFC25	Electrolytic	Pd	ϕ2×40	J/M 4N		1M LiOD	0.91	1.77	0.24	21	41	no
EFC31	Electrolytic	Pd	ϕ2×40	IMRA	AR etching	1M LiOD	0.89	1.83	0.20	21	15	no
EFC32	Electrolytic	Pd	ϕ2×40	IMRA	AR etching	1M LiOD	0.93	1.67	0.15	21	46	no
EFC33	Electrolytic	Pd	ϕ2×40	IMRA	AR etching	1M LiOD	0.91	1.77	0.04	20	38	no
EFC36	Electrolytic	Pd	ϕ2×40	J/M 4N		1M LiOD	0.92	1.73	0.23	22	27	no
EFC37	Electrolytic	Pd	ϕ2×40	J/M 4N		1M LiOD	0.93	1.70	0.43	23	27	no
EFC38	Electrolytic	Pd	ϕ2×40	IMRA	AR etching	1M LiOD	0.94	1.65	0.30	22	185	no
EFC39	Electrolytic	Pd	ϕ2×40	IMRA	AR etching	1M LiOD	0.93	1.67	0.23	21	176	no
EFC40	Fuel Cell	Pd-10%Rh	ϕ4×20	J/M		1M LiOD	0.96	-	0.60	26	52	no
EFC41	Fuel Cell	Pd-10%Rh	ϕ2×40	J/M		1M LiOD	0.99	-	0.60	27	52	no
EFC42	Electrolytic	Pd	ϕ2×40	IMRA	AR etching	1M LiOD	0.90	1.81	0.02	21	21	no
EFC46	Electrolytic	Pd	ϕ2×40	J/M 4N	1000°C-24hr.	1M LiOD	0.94	1.65	0.10	26	130	no
EFC47	Electrolytic	Pd	ϕ2×40	J/M 4N	1000°C-24hr.	1M LiOD	0.90	1.80	0.04	23	5	no
EFC48	Electrolytic	Pd	ϕ2×40	J/M 4N	1000°C-24hr.	1M LiOD	0.91	1.76	0.15	24	90	no
EFC49	Electrolytic	Pd	ϕ2×40	IMRA	1000°C-24hr.	1M LiOD	0.88	1.87	0.15	22	90	no
EFC50	Electrolytic	Pd	ϕ2×40	IMRA	1000°C-24hr.	1M LiOD	0.92	1.73	0.11	25	90	no

Excess Heat

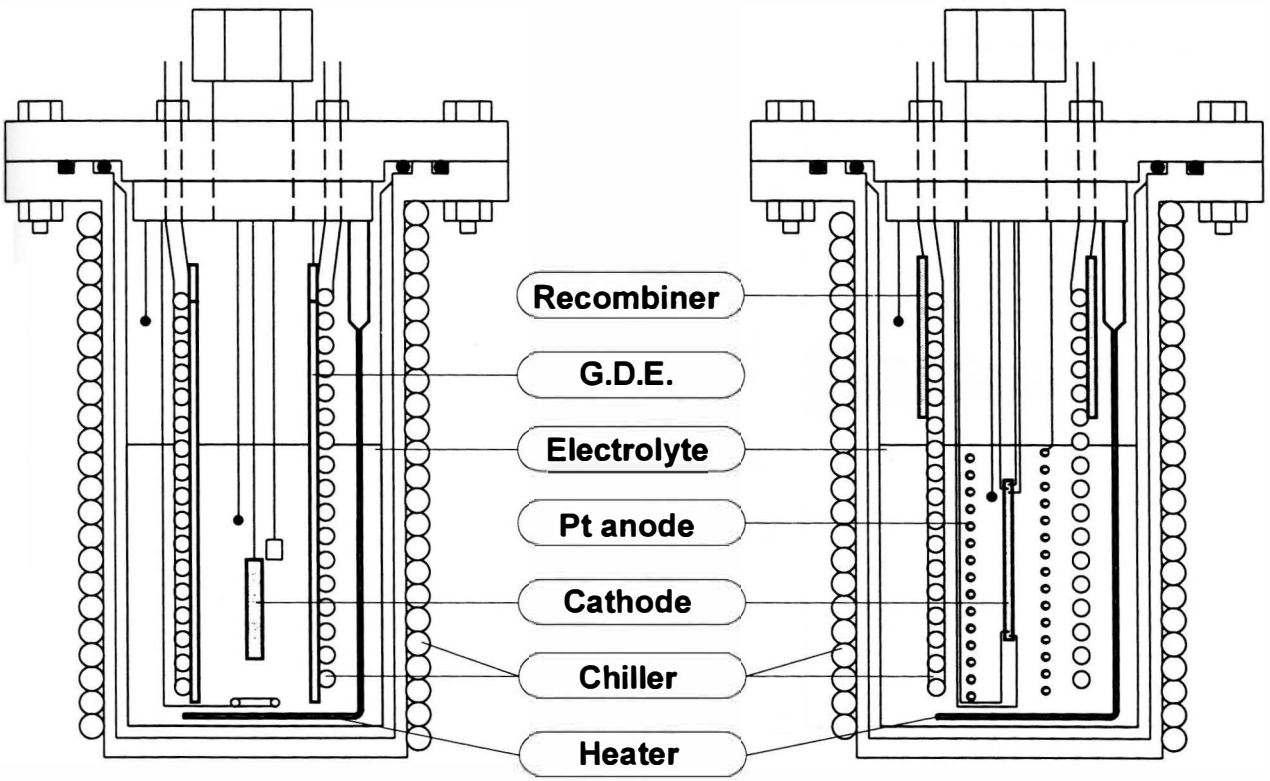

Fig. 1 Structure of the electrolysis cells

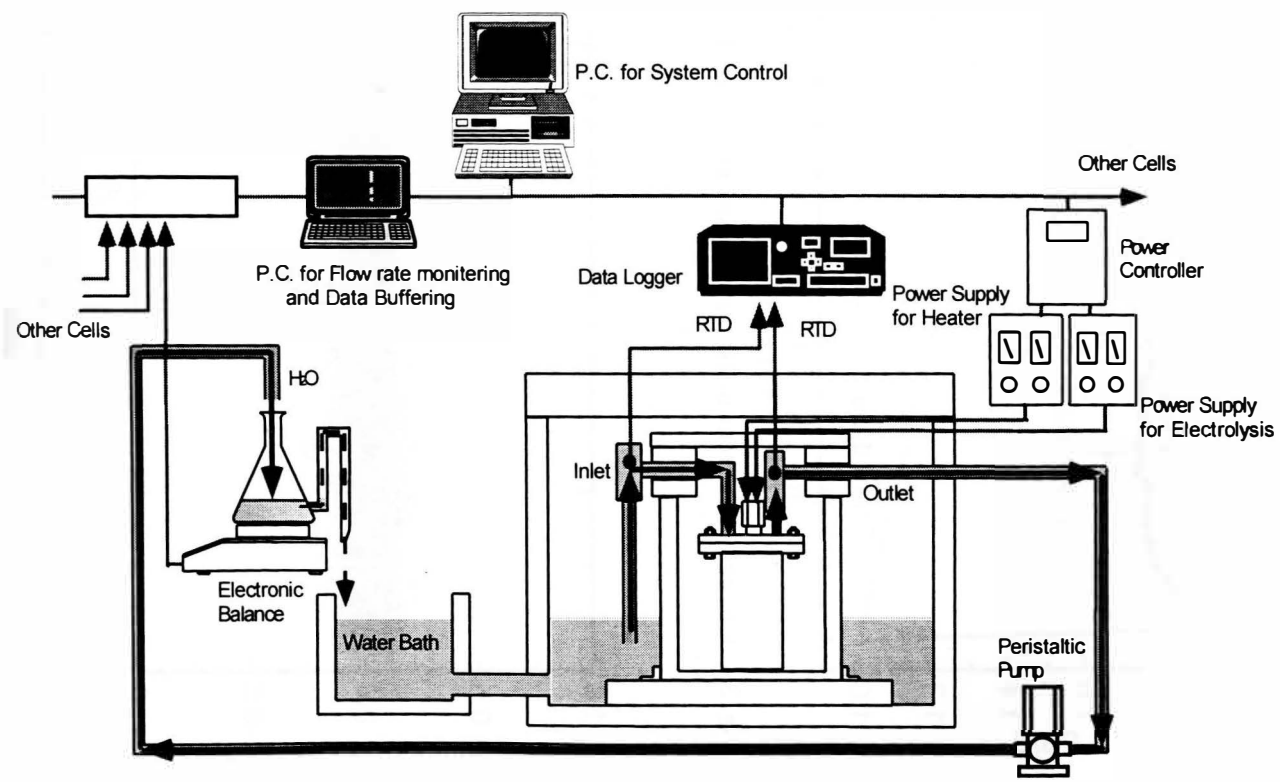

Fig. 2 Overview of the mass flow calorimetry system

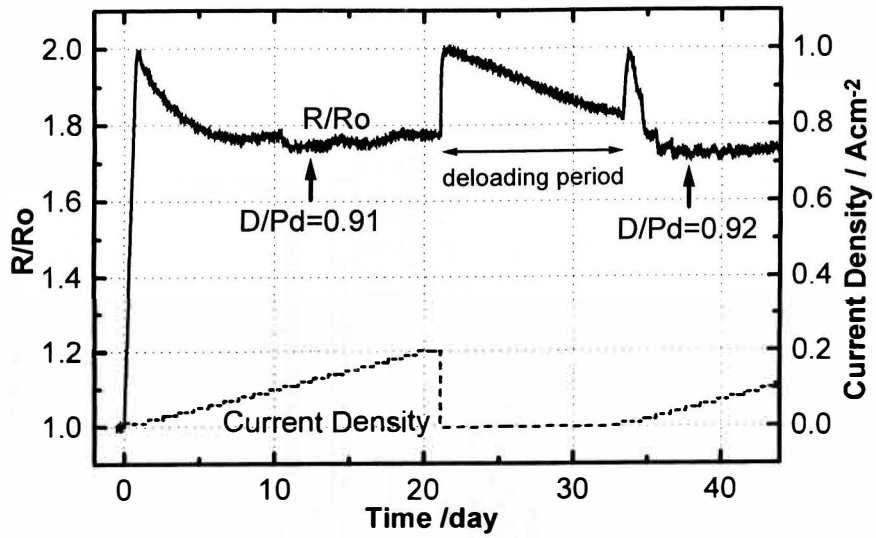

Fig. 3 Change of current density and resisitance ratio for EFC50

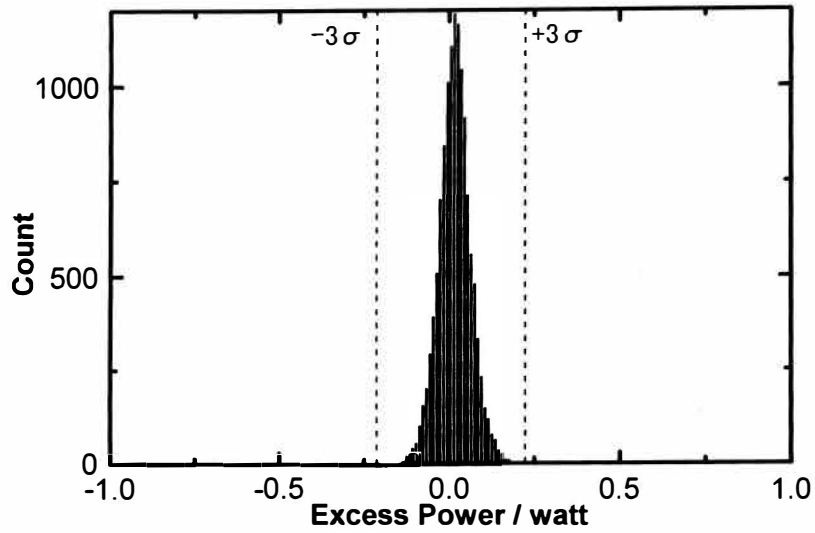

Fig. 5 The histogram of excess power for EFC50

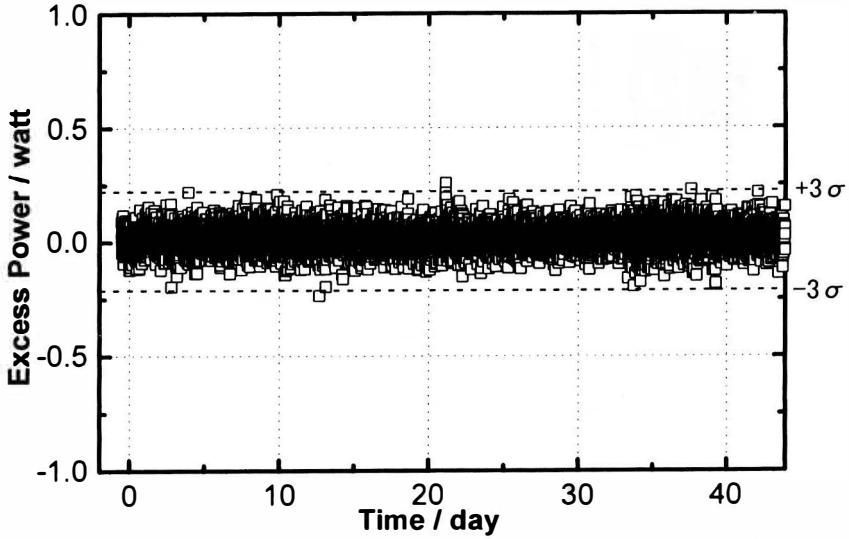

Fig. 4 Observed heat balance with ± 3σ lines for EFC50

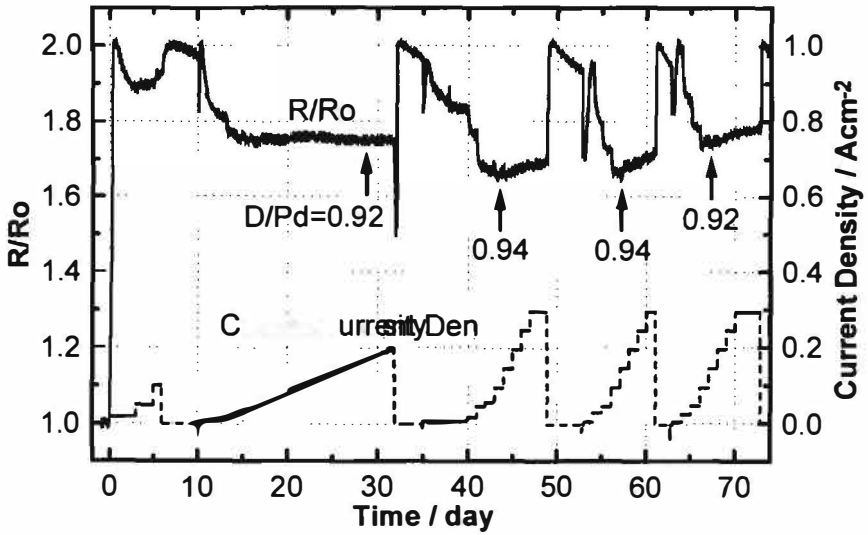

Fig. 6 Change of current density and resistance ratio for EFC46 during the step up current mode electrolysis

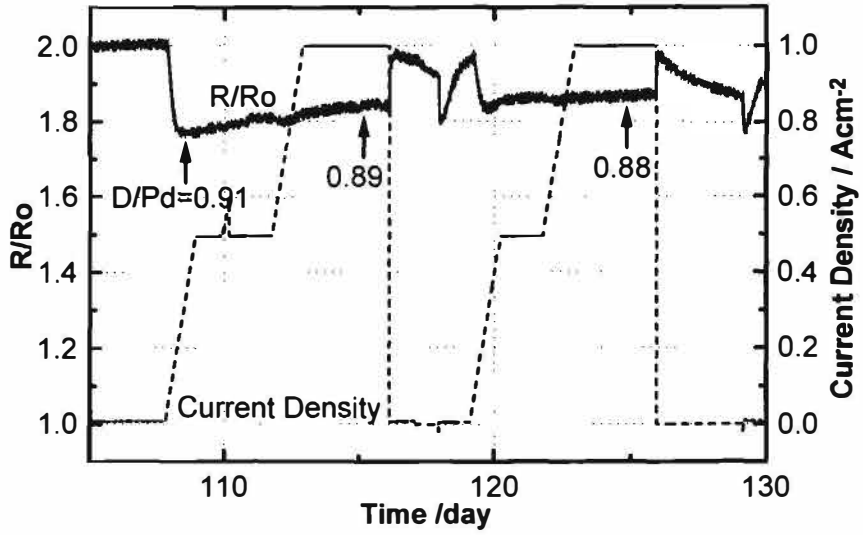

Fig. 8 Change of current density and resistance ratio for EFC46 during the ramp mode electrolysis

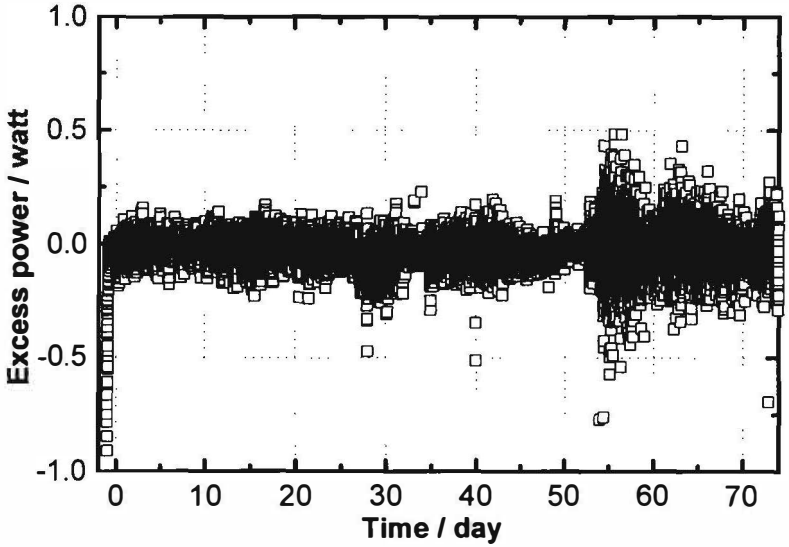

Fig. 7 Heat balance for EFC46 during the step up current mode

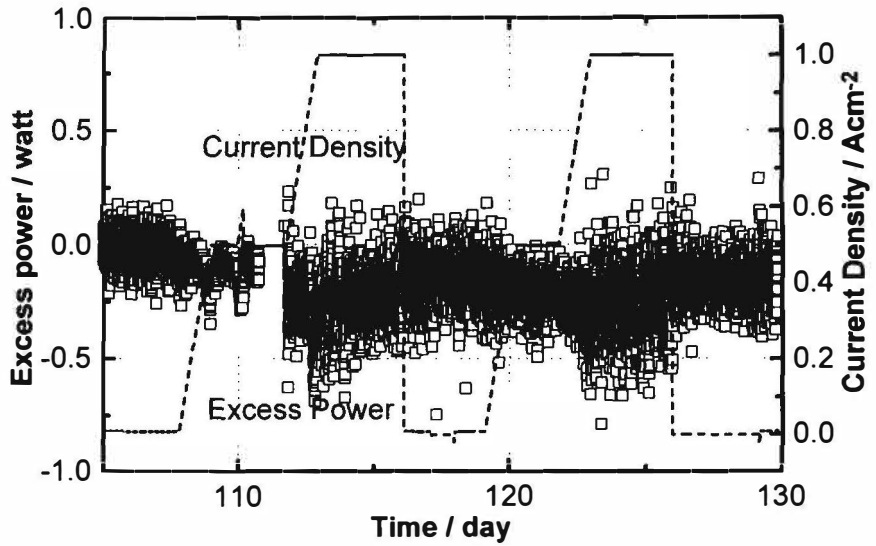

Fig. 9 Heat balance for EFC46 during the current ramp mode

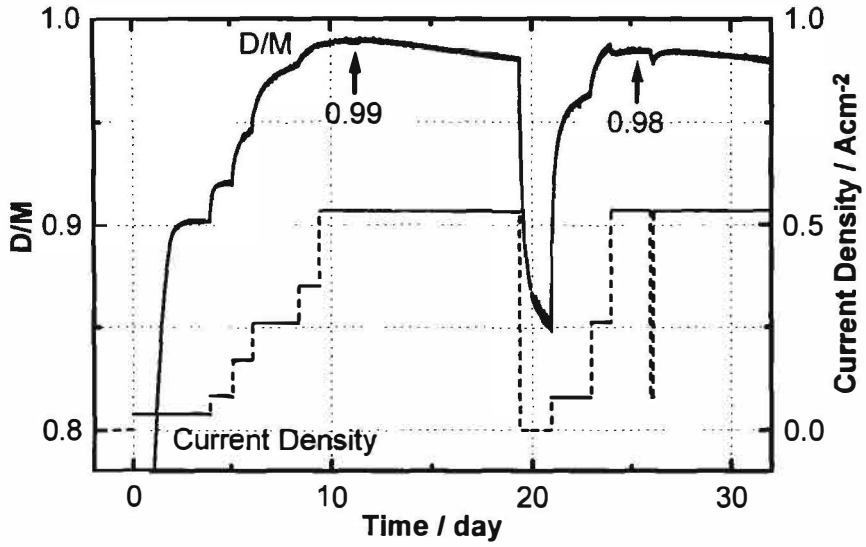

Fig. 10 Change of current density and D/M for EFC41 with a Pd-Rh (10at%) alloy cathode

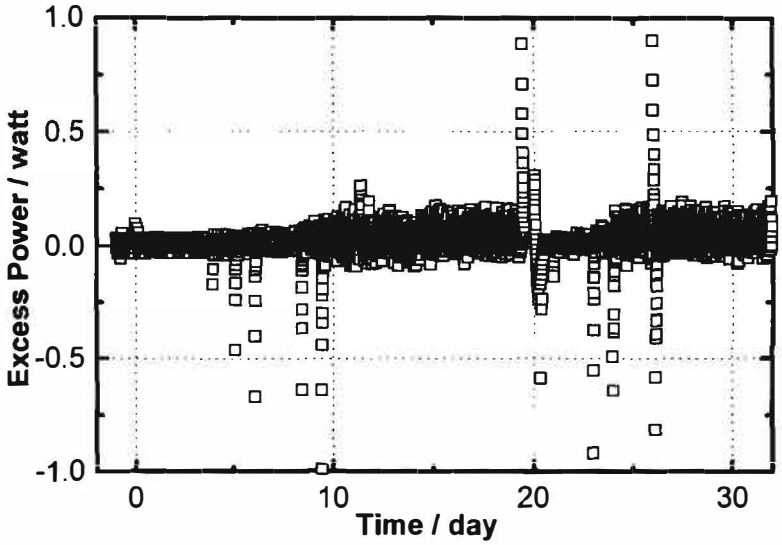

Fig. 11 Observed heat balance for EFC41

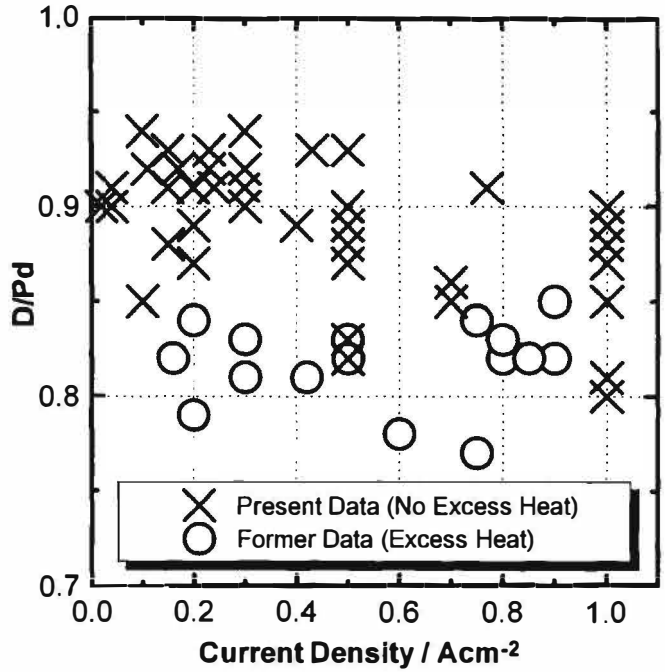

Fig. 12 Plot of the maximum D/Pd for a given current density for the present and the former series of excess heat measurements using Pd cathodes

Excess Heat

Achievement of Solid-State Plasma Fusion ("Cold Fusion")

YOSHIAKI ARATA and YUE-CHANG ZHANG
Osaka University, 11-1 Mihogaoka Ibaraki, Osaka 567, Japan

Abstract : In a series of studies, a significantly large amount of helium ($^4_2He/D_2 \simeq (1\sim0.2)\times10^{-2}$, D_2: "fuel" ^4_2He: "ash") was clearly detected with a quadrupole mass spectrometer (QMS) as the deuterium nuclear reaction product ("ash") released from the highly deuterated palladium host-solid (Pd-black $\approx$ 0.04 [μ]: distributed 0.02 ~ 0.06 [μ]) that had produced large amounts of anomalous excess energy (200 ~ 500 [MJ/cm^3]) through long period such as 5000 [hrs], when it was heated in a high vacuum ($\simeq10^{-8}$ [torr]), high temperature ($\geq$1000 [°C]).

On the other hand, a simultaneous measurement by an another QMS detected no signal of the existence of ^3_2He and ^3_1T (including its compounds). In comparable measurements from non-deuterated samples, any helium and deuterium were not detected. This means that there exist no the well-known Rutherford type of the deuterium nuclear reaction within Pd host-solid, and an inherent feature of solid-state with much valency electron cloud such as Pd presents a circumstance for a new type of deuterium nuclear fusion reaction which directly produces ^4_2He as main reaction product.

Because the ^4_2He was observed only after each sample had been heated in a vacuum, in each case, the laws of physics require that this helium could not have diffused from any outside source other than the Pd metal sample. Also because helium was observed only after the sample was heated to a relatvicly high temperafure, in each case, it must have been trapped within an interior location of the sample. Because there is no known process that can account for the diffusion of the large amounts of ^4_2He into the interior locations of the various samples at the levels that were measured, the only possible explanation for the ^4_2He being trapped in this fashion is that it was trapped within each sample after it was first produced as the nuclear ash from an electrolytically induced (Cold Fusion) deuterium nuclear reaction.

To understand these results, the authors have constructed a theory, based upon a coherent process that is believed to be induced in highly deuterated Pd black crystals. In this theory, it is postulated that Cold Fusion is initiated through the formation of a Strongly Coupled Plasma ("SC-Plasma"), reminiscient of the SC-plasma's that are found within stellar interiors. This postulate is consistent with the assumption that a deuterium nuclear reaction is initiated in a localized zone within a host solid, and it is indispensable that the deuterium be transformed coherently for at least a few picoseconds into a SC-plasma, which the authors refer to as a deuterium "coherent plasma" within the solid-state. It is also postulated that this "coherent solid-state plasma fusion" is initiated through a violent, localized vibration of the lattice, which the authors refer to as a "Latticequake". This "Latticequake" is essentially accompanied with both of an intense electromagnetic turbulence and violently shaking electron cloud under a many body effect in coherent-state.

I) Indroduction: Proof for a deuterium nuclear fusion reaction inside a solid must clear the two criteria as shown in Fig. 1. First is that the host solid must have continuously generated a large amount of excess energy. Second is that there must be "residual products" ("ash") within the host solid corresponding to the amount of excess energy generated. It is well known that many past studies were not taken seriously up to now and did not still satisfy these two critical criteria.

In general, the most essential reaction product of the deuterium fusion reaction is considered to be helium, irrespective of the "well-known (Rutherford reaction) and/or unknown reactions"[1,2]. In other words, when deuterium nuclear reaction take place inside solid-state, this helium should be abundantly stored as main "residual product" within the solid.

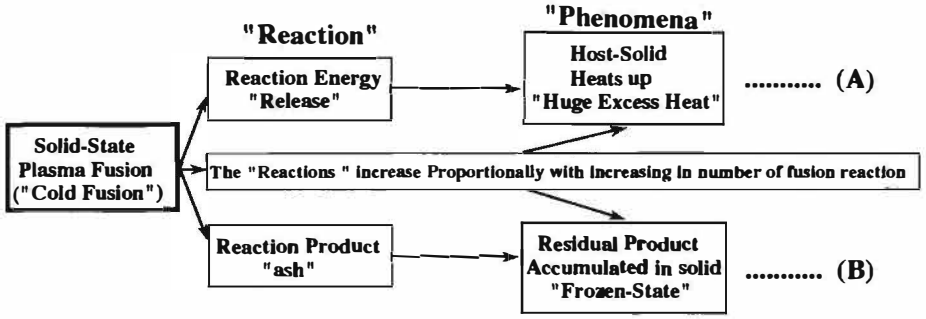

Fig. 1 Two criteria to prove a deuterium nuclear reaction inside solid.
Note: The first criterion for determining the existence of a nuclear fusion reaction inside solid is that a large amount of energy must be released from highly deuterated solid, and the solid should be heated proportionally to the number of fusion reactions that take place as shown in Fig. 1 (A). The second criterion, there must also be large amounts of nuclear fusion products as a "ash" inside the solid corresponding to the amount of energy generated as stated in the formula in Fig. 1 (B).

It is well known that it is extremely difficult to dissolve helium in metals[3,4,5]. If helium does exist in solid metal, it must be the result of shooting helium that has been accelerated into a solid metal, as the results of β decay ($^{3}_{2}$He from $^{3}_{1}$T in PdT_x over long period) or as the result of a nuclear fusion reaction inside the metal. There is no naturally known case where helium exists inside solid metals. On the other hand, when helium exists inside solid metal, it is hardly ever released to the surroundings[4,5]. Helium trapped inside solid metal should be in a "frozen state" and tremendously accumulated within the solid proportionally with the increased number of fusion reactions, and it is released only when the host metal is heated to high temperatures[5]. It is simple to understand this helium plays a vital role in determining the existence of a nuclear fusion reaction within a solid.

When the well-known Rutherford type deuterium nuclear fusion takes place continuously in a solid, the reaction product will be both spontaneously emitted as "out-going products" of high energy light elements such as $^{1}_{0}$n, $^{1}_{1}$p, γ and confined in a "frozen state" as "residual products" such as $^{3}_{2}$He, $^{3}_{1}$T and also $^{4}_{2}$He as their end product, and moreover a large amount of energy released will drastically heat the solid. As a result, when Rutherford reaction takes place within a solid, $^{3}_{2}$He and $^{3}_{1}$T as "residual product" of primary reaction must be abundantly detected much more than secondary product $^{4}_{2}$He.

On the other hand, when a large amount of $^{4}_{2}$He is detected as a main "residual product" within a solid, it is clear that a new type of deuterium nuclear fusion reaction which directly produces $^{4}_{2}$He take place inside the solid-state.

II) Proof of Huge Exess Energy within DS-cathode: As first criterion for proof of "Cold Fusion", highly deuterated solid must have continuously generated a large amount of excess energy as follows.

Using closed cell system and DS-cathode in detail as showm in Fig. 2 over the past 4 years from 1992, all of the DS-cathodes created the large amounts of excess heat. Fig. 3 shows the most important basic characteristic of this cell-system with Pt-anode and Pt-cathode, that is cell power $Q_{\odot} \simeq 0$ in lower input power and $Q_{\odot} < 0$ (negative in cell power) in higher input power over 100 [watt] (usual case in authors' experiment), and all of the excess energy data were obtained by only changing the Pt-cathode to DS-cathode. This shows principle of DS-cathode[6].

Fig. 4 (a) and (b) show the data for the two cathodes currently in use. The data for cathode (a) shows that several hundred [MJ/cm^3] of excess energy has been created over several thousand hours using Pd-black 3 [gr], while cathode (b) has generated approximately 50 [MJ] over 800 hours with 5[gr] of Pd-black, The rate at which the excess energy is being generated is roughly equal for the two, and other samples were also at a similar level (200 ~ 500 [MJ/cm^3]).

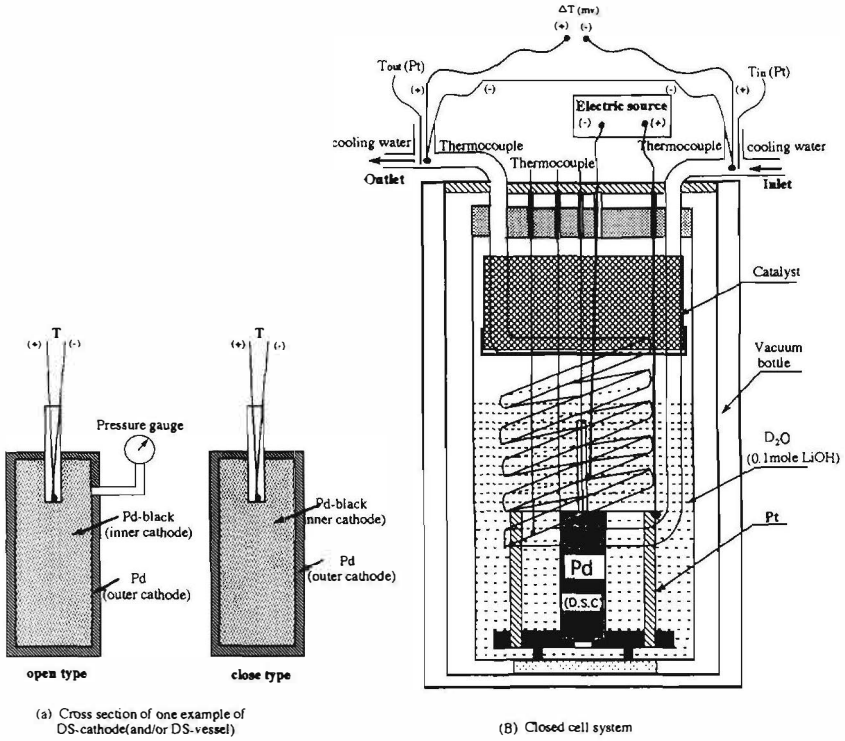

Fig. 2 Closed cell system with DS-cathode

Note: This diagram is authors "Closed Cell" system. Left side shows DS-cathode; open type and closed type. This open-cathode can detect inner pressure; up to about 900 atomsphere which is limited by only pressure gage.

On the contrary, closed-cathode will be rising up some thousand atmosphere [atm]. Rightside diagram is authors "closed-cell"; inlet and outlet water temperature are measured by both of reversely-connected thermocouple and Pt-Resister at the same time.

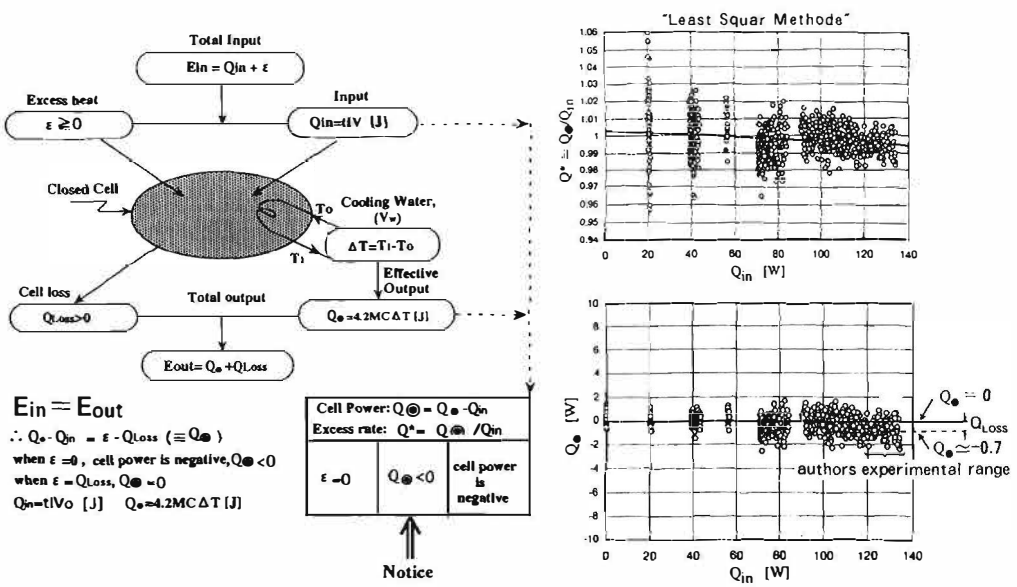

Fig. 3 Priciple and basic characteristic of authors closed cell.

Note: Leftside diagram shows principle of our measurement system in which it is emphasized that the most important parameter is "Cell Power" Q_e which includes "Excess Energy" ε and "Cell Loss" Q_{Loss} as defined in this diagram. This "Cell Power" is negative in essence, when no excess energy. This feature must be noticed. Rightside diagram is inherent feature of our "closed-cell" and indicates the most important basic data using Pt anode and Pt cathode. Our usual experimental range is around 120-150 watts and "cell-power" is clearly negative with about minus one watt as shown in this diagram. Our all data were obtained by only changing the Pt-cathode to DS-cathode.

Excess Heat

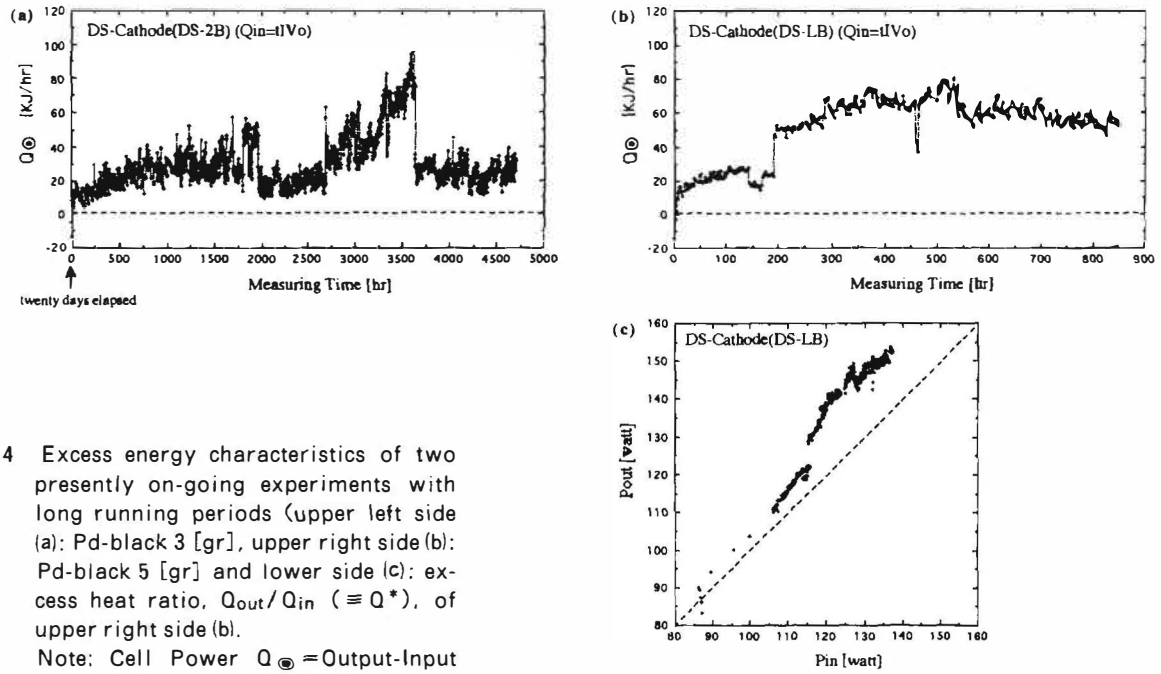

Fig. 4 Excess energy characteristics of two presently on-going experiments with long running periods (upper left side (a): Pd-black 3 [gr], upper right side (b): Pd-black 5 [gr] and lower side (c): excess heat ratio, Q_{out}/Q_{in} ($\equiv Q^*$), of upper right side (b).
Note: Cell Power $Q_{◉}$ =Output-Input [KJ/hr] (10 watt: 36 [KJ/hr]).
Note: Generating pattern of each sample displays significant difference with chronological change, however, each total amount of excess energy included the eight samples used from 1992 to now was almost same.

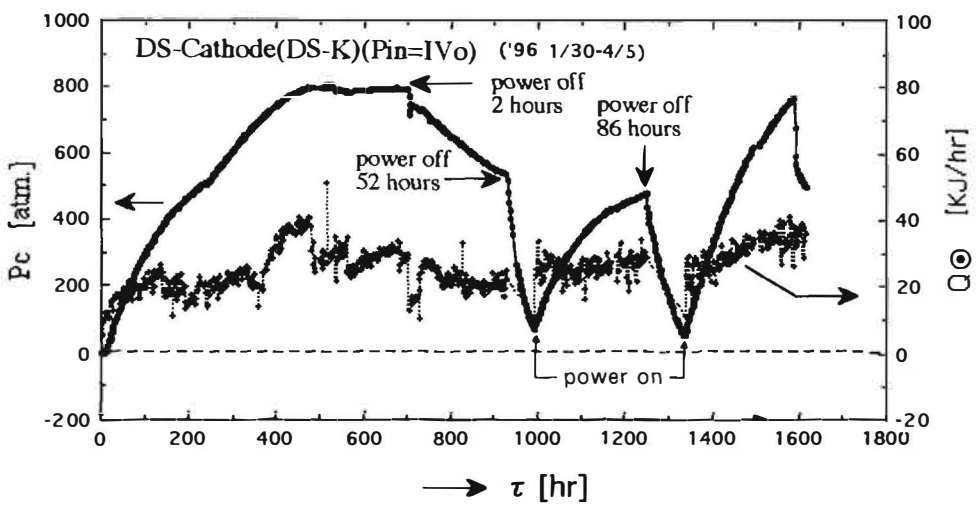

Fig. 5 Relation between pressure Pc [atm] inside "Particles-Gap", and cell power (excess energy) $Q_{◉}$ [kJ/hr].
Note: Pc-inner pressure inside DS-cathode which includes only both pure Pd-black and pure deuterium ("spillover deuterium"), can be rising up several thousands atmosphere [atm] by the phenomenon of the "spillover-effect". It serves as a one of the most important factor for generation of nuclear reaction. It is very important phenomenon that the relation between Pc and $Q_{◉}$ seems that the generation of excess energy was corresponding to Pc increased.

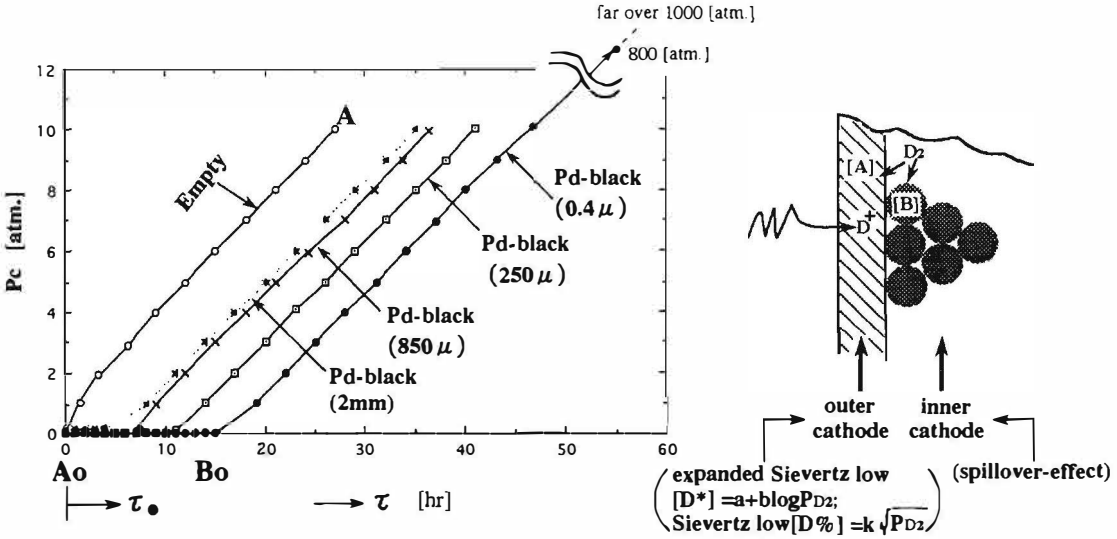

A) Relationship between Pc-τ ($\tau_{◉}$: incubation-period) in DS-cathode

B) Relation between concentration of [A] an [B] under same pressure P_{D2}

Fig. 6 Inferent feature of "Spillover deuterium" insid DS-cathode. (Principle of DS-cathode)
Note: This diagram is typical example of characteristic of open type DS-cathode which was used in order to study the dynamic behavior of the inner cathode.
In rithtside diagram, deuterium concentration inside outer cathode, [A], and inner cathode, Pd-black, [B], are significantly difference. [A] is controlled by expanded "Sievertz law" and [B] is by "spillover effect" which brakes "Sievertz law". This reason is that when [A] is 90%, deuterium pressure inside the cathode is required over one hundred thousand atmosphere by "Sievertz law", on the contrary, [B] becomes almost 100% instantaneously, if within 100Å in size, such as so called "Atom Cluster". By the way, deuterium pressure inside our DS-cathode can easily achieve some thousand atmosphere.
Left side diagram demonstrates long incubation period, Ao-Bo range, which is explained by only "spillover effect", and it is called "spillover deuterium" when deuterium behaves under "spillover effect". Consequently, during this incubation period deuterium comes only to Pd-black rather than vacuum space such as "Particle Gaps". There are a principle of DS-cathode.

Two kinds of DS-cathods were used, that is the closed type and open type as shown in Fig. 2 (a). Open type is used to measure an inner pressure P_C [atm] of the DS-cathode. Inner pressure is one of the most important characteristic of DS-cathode as shown in Fig. 5. It seems that cell power Q◉ increases proportionally with Pc increased. Fig. 6 shows the "Spillover effect"; the most importaut characteristic of Pd-black. This effect overcomes against "Sievertz law" and serves to give high concentration deuterium for Pd-black, and especially first stage deuterium accumulates, does not in space of "particle-gap", on the powder surface and the interior over incubation period. This is a key action of Pd-black, especially when it becomes activated "atom cluster" with isolated and/or embedded-state, it displays violent action to mix instantaneously with almost same concentration of both atoms of host-solid and deuterium in "atom-cluster" zone within 10^3~10^5 atoms.

III) Proof of Large Amount of "Residual Helium" within a Solid: Before moving on to the second criterion, the measurement method and accuracy of the quadrupole mass spectrometer ("QMS") were devated first, in short, by setting the observed target mass in the region 3.95-4.05, repeated measurements enabled chronological description of the elements of this mass. There are two elements $^4_2$He (4.00260) and $^2_1D_2$ (4.02820) in this range. Deuterium always exists as the fuel, but if there is $^4_2$He, a "coupled spectrum" with $^2_1D_2$ will appear.

There are many difficulties, however, which need to be overcome in order to detect the "residual helium" being released from its "frozen state" within a host solid when the host solid is heated in a vacuum due to the nature of

the process by which this helium is released. That is the problem of the "accuracy" and "reliability" of "QMS" system for "released helium".

There are two kinds of "pollutant gases" contaminating "QMS" detection zone, and it is "substantial pallutant" and "pollutant helium". Using "QMS" system, therfore, it must be extremely noticed that there exist certainly many "substantial pollutants" and especially "pollutant helium" inside "QMS" system, It is certain that "pollutant helium" will always exist in lubricant of molecular pump and/or non-metal materials, and if any body, hitherto, would did not take care this vital problem, such "pollutant helium" have been certainly mis-detected as hilium released from the cathode.

In order to study to accurate behaviors of "released helium", authors developed a new type "closed QMS" system which is entirely isolated from all other system including all exhaust system and constructed by only sample vessel, Getter pump and QMS vessel made by all stainless steel and metal packing, as shown in Fig. 7. When highly deuterated sample includes "residual helium" is heated up high temperature, the "closed QMS" precisely detects the "released helium", and especially helium can remains in just the state inside the "closed QMS" any number of days.

As a result, "closed QMS" can measusre not only helium but even any elements released from the sample during heating up to melt from room temperature.

Fig. 8 and 9 demonstrate chronological change of "Coupled Spectrum" ($^4_2$He: D2) that the "closed QMS" detected "residual products" which is released from highly deuterated sample during heated up to 1300 [°C] from room temperature, and it was obtained the ratio $^4_2He/D_2 \simeq [10^{-2}]$ in this situation.

Many samples were measured by "closed QMS" and similar results to Fig. 8 and 9 were obtained with fully reproducible.

In "closed QMS" experiments, mass M_3 and M_4 were simultaneously detected in detail within "closed QMS". Fig. 10 shows existence of almost same quantity of M_3 and M_4, and at the same time, M_4 is almost $^4_2$He and neglisible D_2. Even if M_3 contains "DH" and $^3_2$He, it can be estimated that "DH" (in other words, $^4_2$He as shown at $_3M_4$ in Fig. 10 [A]) exists in the absolute majority and $^3_2$He is considerably less than "DH" as can he understand from Fig. 10 (B). If M_3 is reaction product in Rutherford reaction, $^3_2$He should be significantly larger than $^4_2$He inside "closed QMS".

As a result, it is demonstrated crucially as the first experimentally clear proof that new type deuterium nuclear reaction which directly produce $^4_2$He as a main reaction product, take place inside solid.

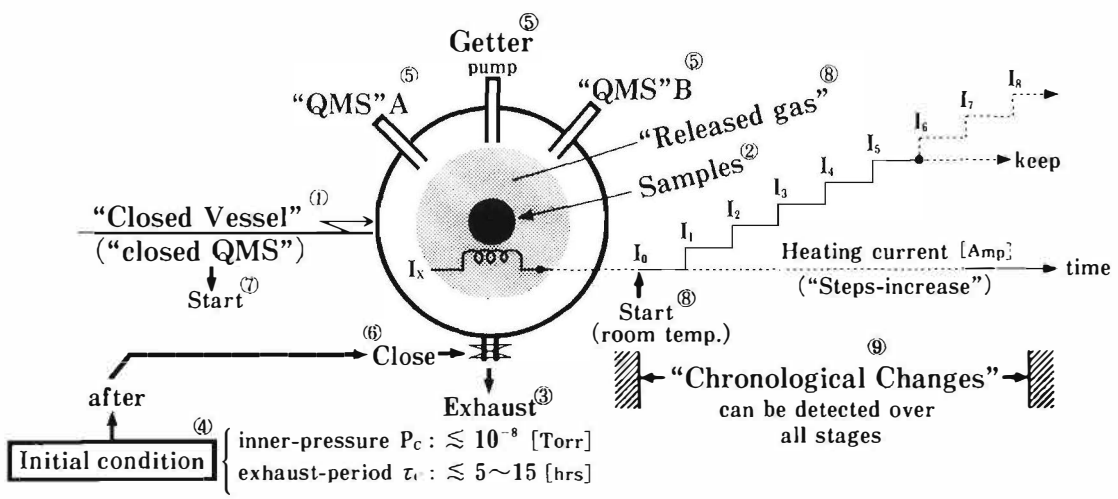

Fig. 7 Principle of "closed QMS".
Note: 1) "Released Gas" remains in just the state of any number of days; especially "Helium". 2) Repeatedly can detect to reconfirm, any time. 3) Chronological change with increased temp. can be perfectly detected. 4) "Getter action": no works for Helium, but strongly affects pollutants such as "D_2" (against $^4_2$He), "DH" (against $^3_2$He), pollutants decreases and disappears in the end, therefore; the ratio, $^4_2$He/$^3_2$He (if exist), $^4_2$He/D_2 are cortainly obtained. Numbers of ①~⑨ indicate the order of "closed QMS" operation.

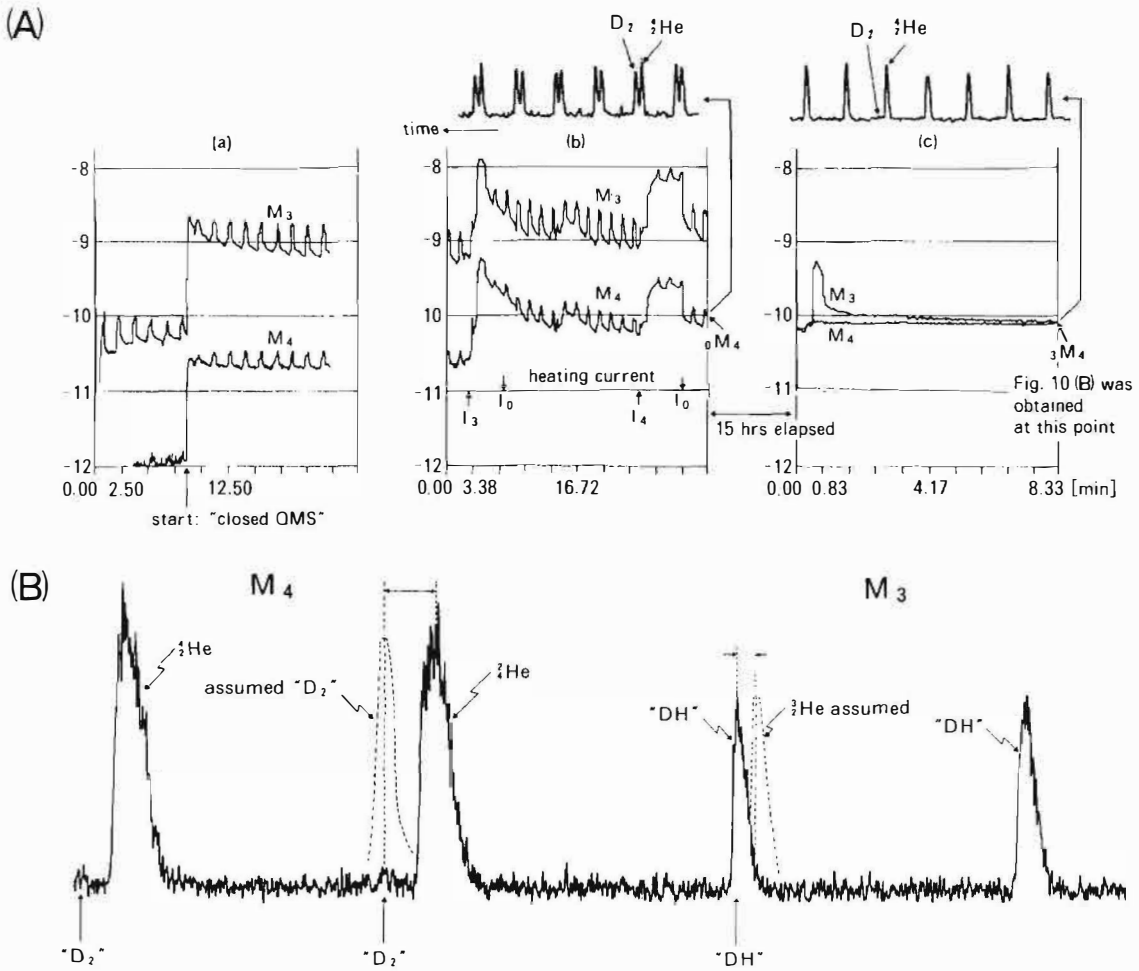

Fig. 10 Chronological change of characteristics of mass M_3 and M_4.
Note (1): (A) shows their intensity change using normal mode and (B) shows their spectrums using high resolution mode at point of ${}_3M_4$ in Fig. 10 ((A), and M_4 is almost ${}^4_2He$, M_2 is "DH" (${}^3_2He$ could not detect, even if exist at least less than $\frac{1}{10}$ ${}^4_2He$). As a result, main reaction product is ${}^4_2He$ and this means a new type deuterium nuclear reaction take place inside solid due to its inherent feature.
Note (2): Resolution (Re≃M/ΔM), Sensitivity (Se=[A]/[Torr]. For ${}^4_2He$: "closed QMS" {Re≃39.1M (12% PH). (limit of "QMS" (Re≃37M (10% PH)}. For ${}^4_2He$ "closed QMS" {Re≃169M (35% PH). (limit of "QMS" (Re ≃107M (10% PH)}.
For sensitivity of "closed QMS"; high resolution (Se≈0.3 ppt); normal (Se≈0.003 ppt).

REFERENCES AND NOTES

1. Y. Arata and Y. C. Zhang, J. High Temp. Soc. **22**, 29 (1996).
2. A. Takahashi, J. Nucl. Sci. Technol., **26**, 558 (1989); T. Matsumoto, Fusion Tech., **16**, 532 (1989); E.W. Becker. Naturwissenschaften. **76**, 214 (1989); J. Kasagi, et al., JPS (JPN), **64**, 77 (1995); T. A. Chubb and S.R. Chubb. Bulletin of APS, **41**, #1, 332 (1996): Fusion Tech. **24**, 403 (1993); Ibid, **20**, 93 (1991).
3. G. J. Thomas, Radiat, Eff. **78**, 37 (1983); W. G. Wolfer, Philos. Mag. A **58**, 285 (1989); **59**, **87** (1989); T. Schober, Fusion Technol. **14**, 637 (1988).
4. R. C. Bowman. Jr., R. S. Carlson, and R. J. DcSando, Trans. Am. Nucl. Soc. **24**, 496 (1976).
5. G. C. Abell, et al., Phy. Rev. B, **41**, 1220 (1990).
6. Y. Arata and Y. C. Zhang, Proc. Japan Acad., **70 (B)**, 106, (1994); Ibid, **71 (B)**, 98, (1995); Ibid, **71 (B)**, 304, (1995); J. High Temp. Soc. **21**, 130, (1995).

EVERYTHING YOU ALWAYS WANTED TO KNOW ABOUT COLD FUSION CALORIMETRY*

Giuliano Preparata

Dipartimento di Fisica - Università di Milano

INFN - Sezione di Milano

via Celoria 16 Milano Italy

Abstract
The long standing problem of calorimetry in Cold Fusion (CF) experiments is analysed on the basis of the findings of two recent campaigns of CF experiments, where a surprising difference in the behaviour of blank and "black" cells was observed. We also present evidence for large excess power production in modified Fleischmann-Pons electrolytic cells.

1. Introduction

Seven years have already passed since that day of the spring of 1989 which marks the beginning of what we may call the Cold Fusion (CF) Era: an important event of which we are presently celebrating. And yet the problems that have plagued the difficult and painful journey of us, the "true believers", are in a sense (at least to a superficial look) still with us: an elusive calorimetry, and an even more elusive nuclear physics. The aim of this talk , as suggested by its title (derived from a bestseller of the Sixties dealing with a much more popular and appreciated subject !) , is to contribute to the solution of the former problem, while for the latter I cannot see any other way than a massive experimental program, possibly enlightened by the ideas that appear in Chapt. 8 and 11 of a recent book of mine [1].

And with regard to theory I would like to emphasize once more [2] (and for the last time in this talk, which deals mostly with experimental CF) that one of the serious obstacles in the road towards CF has been the insufficient effort made by the CF community to understand, on the basis of the most advanced tools of Quantum Field Theory (which are dealt with in the book of Ref [1]), the relevant new aspects of the interactions that allow deuterons to fuse through exotic nuclear reactions in a **cold** Pd-metal matrix.

But let's get back to the subject proper of this talk: in Sect. 2 I will present the case for the calorimetric strategy chosen originally by Martin Fleischmann, i.e. isoperibolic calorimetry. In Sect. 3 I will make the case for the existence of a basic difference between blank and "black" cells, a particularly nasty way employed by Nature to hide itself. In Sect.4 the (preliminary) response of a

* But were afraid to ask.

more conventional flux-calorimetry will be presented and compared with the isoperibolic one.The conclusions will appear in the final Sect. 5.

2. The case for isoperibolic calorimetry

As we know well, the strategy chosen by Martin Fleischmann to demonstrate the production of excess enthalpy in electrolytic cells, electrolysing heavy water with a Pd-cathode, consisted in using the D_2O of the cell as a calorimetric fluid, whose temperature was constantly monitored with respect to that of a constant temperature bath, in which the cell was immersed.

Assuming full mixing of the fluid,* i.e. a constant temperature $T = T_{cell} - T_{bath}$ throughout the cell, the calorimetric equation reads (M is the equivalent water mass of the calorimeter and C_P its constant pressure specific heat)

$$MC_P \frac{dT}{dt} = W(t) - f(T,t), \tag{1}$$

where $W(t)$ is the power produced inside the cell:

$$W(t) = W_{in}(t) + W_x(t), \tag{2}$$

$W_{in}(t)$ being the power supplied to the cell minus the power spent to electrolyse D_2O, and $W_x(t)$ the sought excess power.

As for the "dissipation function" $f(T,t)$, which for convenience we write:

$$f(T,t) = \alpha(T,t)T(t)\ ,^{\dagger} \tag{3}$$

it gives a global description of the physical processes that dissipate to the bath the energy produced inside the cell. From (1) it follows that in order to determine the power $W(t)$ produced in the cell, one must know the dissipation function $f(T,t)$. How can this be achieved ? The usual (I would say "conventional") answer is to determine $f(T,t)$ by "calibration", i.e. to assume that $f(T,t) = f(T)$ is independent of the dynamical evolution of the system, and substitute to the electrolytic any other known source of power W, thus constructing the $f(T)$ profile to be injected in the calorimetric equation (1).

The basic flaw of such "conventional" calorimetry is that it stands on the "obvious" assumption that the thermodynamics of the cell is independent of the physical processes through which energy gets generated: a particularly dangerous assumption when such processes are poorly known, such as those of CF.

In order to circumvent this difficulty Fleischmann's brilliant idea was to "observe" the "dissipation coefficient" $\alpha(T,t)$ in his calorimetric system continually, by subjecting it periodically (isoperibolically) to a known calibration heat pulse $W_H(t)$, with the aim of determining it in its possible evolution with the state of the Pd-cathode, and of the CF-phenomena occurring inside it. The definite advantage of this procedure is to avoid making "a priori" assumptions on the behaviour

*A detailed account of this approach can be found in Ref [3]

† This decomposition of $f(T,t)$ is suggested by the fact that for conductive dissipation, that is dominant in our experiments (see Sect. 3), α is constant, and that it is in general a slowly varying function of temperature and time.

of the calorimetric fluid in presence of possible odd new physical processes, and to exploit a small power perturbation $W_H(t)$ of a basically discontinuous character.

Suppose in fact that the system is in a steady state at the time t_0, when we apply a constant heat pulse of power W_H. Calling $\Delta T(t) = T(t) - T(t_0)$ the calorimetric equation for ΔT reads

$$MC_P \frac{d}{dt} \Delta T = W_H + W'(t) - \left[a(T,t)T(t) - a(T_0)T(t_0)\right], \tag{4}$$

where $W'(t)$ (with $W'(t_0)=0$) is the additional power, positive or negative, that stems from the perturbative thermodynamic changes that occur in the system as a consequence of $W_H(t)$. By making use of the smallness of the perturbation we can set with a good approximation*

$$a(T,t)T(t) - a(T_0,t_0)T(t_0) \cong a(T_0)\Delta T(t)\,. \tag{5}$$

The next and final step needed to obtain $a(T_0)$ is to fit (in several different manners, see [3]) the observed temperature profile for $t - t_0 < 3\tau$ $\left(\tau = \frac{MC_P}{a(T_0)}\right)$ by approximating the additional power as $W'(t) \approx W(t - t_0)$. In this case the predicted temperature profile is given by $(a = a(T_0))$

$$\Delta T(t) \cong \frac{W_H}{a}\left(1 - e^{-\frac{t}{\tau}}\right) + \frac{W\tau}{a}\left(\frac{t}{\tau} - 1 + e^{-\frac{t}{\tau}}\right), \tag{6}$$

and it depends on two unknowns $a(T_0)$ and W, which may thus be easily determined.

3. Blank cells, "black" cells

The isoperibolic calorimetric strategy, as I have just remarked, has the obvious advantage of following the thermodynamic changes of the calorimeter, whose fluid is the D_2O of the electrolytic cell. One may wonder whether this is really necessary, for it clashes with the expectation that the cell thermodynamics only depends on the thermodynamic variables, i.e. T_{cell} and T_{bath}, and much of the calorimetry in CF studies has just proceeded from this "self-evident" Ansatz. Incidentally, one of the more frequent criticisms to Fleischmann's calorimetry is that a single temperature measurement of the D_2O is rather risky, due to important gradients within the cell. And it is for this reason that in a first campaign of experiments, that shall be reported in this Section, we decided to measure temperature (with very sensitive Pt100 devices) in three different places (see Fig.1), thus obtaining a clear picture of the temperature distribution in the cell, allowing us (see Ref. [3], and in particular Appendix A) to make the necessary corrections to the simple calorimetric model of the previous Section.

The campaign of measurements, alluded to above, began with blank cells, mounting a Pt-anode 250 μm in diameter and a cathode of Pt-wire long about 250 cm and 50 μm in diameter, wound solenoidally, in a number of electric configurations, ($V_{A/C}$, $V_{C/C}$).

*Please note that the extra small terms that have been neglected in (5) can be absorbed in $W'(t)$.

Excess Heat

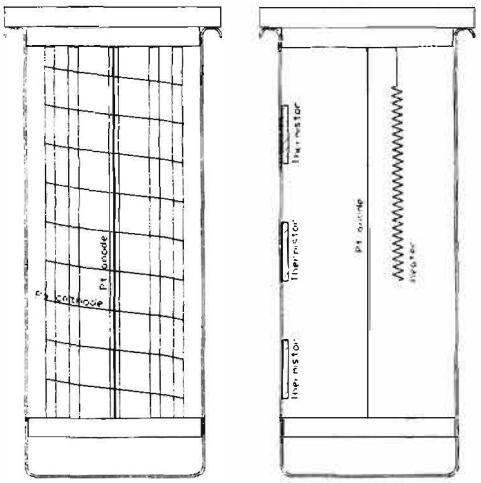

Fig.1 A schematic drawing of the cell (diameter approximately 28 cm). On the left the elicoidal Pd (Pt for the blank run) cathode (diameter 50 μm, length 250 cm) and the Pt anode (diameter 250 μm) are shown, together with their quartz supports. On the right the spatial configuration of the Pt100 thermistors array and the resistance heater used to calibrate the cell are shown.

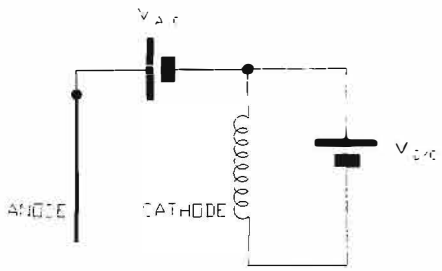

Fig. 2 The electric arrangement of the electrolytic cell.

A typical determination of a appears in Fig. 3, where the isoperibolic period lasts six hours. Use of the calorimetric equation with such "dissipative coefficient" yields the typical result of Fig. 4, where the efficiency $\varepsilon = \frac{W_x}{W_{in}}$ is plotted. The "blankness" of the cell is particularly noteworthy. Also noteworthy is the fact that Figs. 3 and 4 are representative of dozens of experiments, that yielded within the experimental errors the same null results.

We then turned to "black" ("black" here is used as the opposite of "blank", which stems from the French *blanc*, white), i.e. the perfect copies of the "blank" cells, but for the cathode, where the Pt-wire is replaced by a Pd-wire, of equal length and diameter. The big surprise came from plots of the type reported in Fig. 5 where, after an initial determination of the dissipative coefficient close to that of the typical "blank" cell, we note an almost sudden substantial increase of a, and with it of the excess power (see Fig. 6).

Again the same fact was observed in the about fifty similar experiments that we have conducted. Figs. 3-6 are to my mind a dramatic asseveration of Martin Fleischmann's insight and wisdom. Had he followed the obvious choices, he would have completely missed the new wonderful physics of the "black" cells.

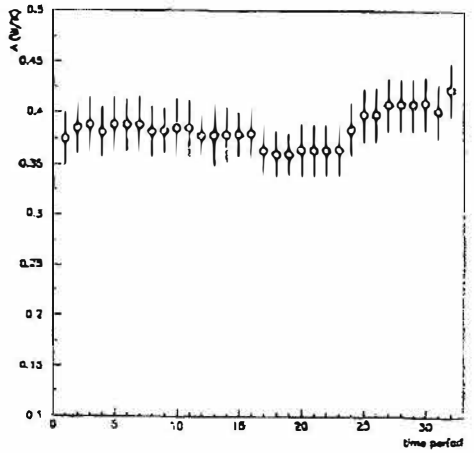

Fig.3 The calculated dissipation coefficient $a(t)$ for the blank cell. Every point corresponds to a period of 6 hours and during this period a is assumed constant.

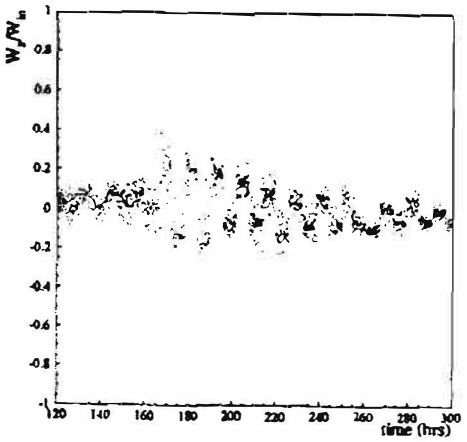

Fig.4 The efficiency ε vs. time for the blank cell. The typical error for this run is about 0.7 W.

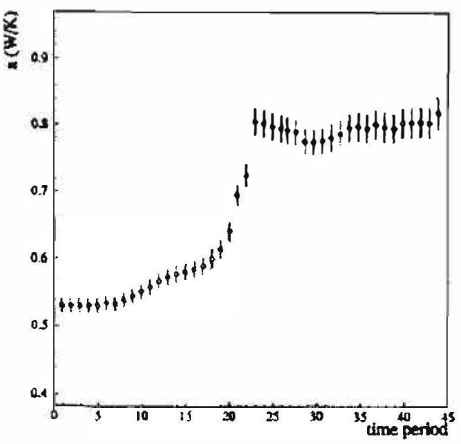

Fig.5 The same as Fig.3 for the black cell.

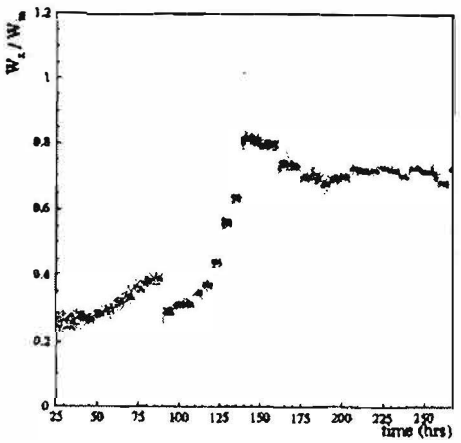

Fig.6 The same as Fig.4 for the black cell.

But what is then such new physics ? As far as theory is concerned I have already argued (see in particular Chapt. 8 of Ref . [1] and Ref . [2]) what are the new aspects that must be at play in CF phenomena, QED coherence of the deuteron plasmas foremost among them. And it is precisely the incredibly subtle coherent motion of the fusing deuterons that should make us expect mechanisms of energy release that are also highly coherent, very different from the disorderly interaction that heats, for instance, a conductor when an electric current flows through it. Among such mechanisms (leaving aside the nuclear ones that may well be responsible for the appalling alchemy that seems to be associated with CF [4]) most important is the coherent production of a rich spectrum of X-rays, mainly soft (of a few tens of eV), that get absorbed only partly in the calorimeter, and may produce transient states in the D_2O (high temperature steam) that could leave the system through the escape routes of the gases of the electrolysis.

If that is the case, we have now a satisfactory way to understand the difference between the situations depicted in Figs. 3-4 and Figs. 5-6, and the disheartering elusiveness of the CF excess heat. Furthermore we have now also good reasons to believe that what we measure by isoperibolic calorimetry is but a lower bound of the energy that gets produced through CF, the isoperibolic heat

pulse is in fact a very conventional energy source whose mixing through heavy water to the exotic CF energy source is rather unlikely to be complete.

A second campaign of measurements has been conducted with somewhat different cells (see Fig. 7) and considerably higher W_{in} and ($V_{A/C}$, $V_{C/C}$). Figs. 8 and 9 show a typical experiment with a blank cell, while Figs. 10 and 11 refer to a typical "black" cell output: a full confirmation of the strange observations of the first campaign [5].

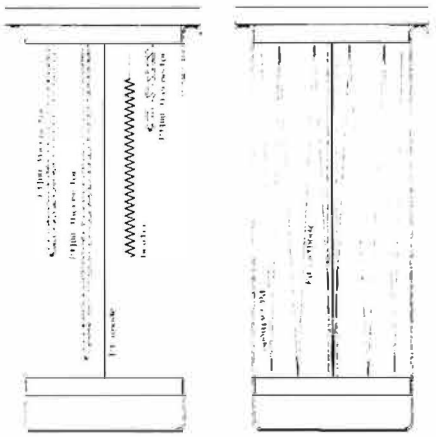

Fig. 7 The cell of the "second campaign".

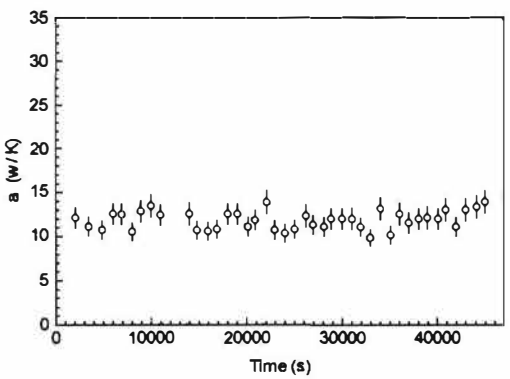

Fig. 8 The calculated dissipation coefficient $a(t)$ for the blank cell.

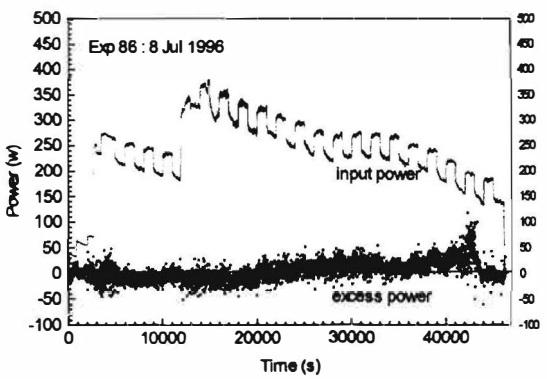

Fig. 9 The input power and the excess power vs. time for the blank cell. Note in the input power the calibration pulses that allows the determination of the coefficient a.

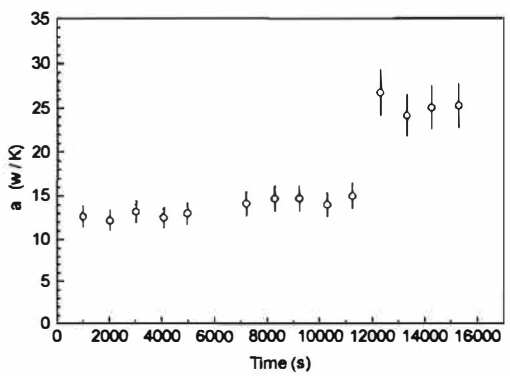

Fig. 10 The same as Fig.8 for the black cell.

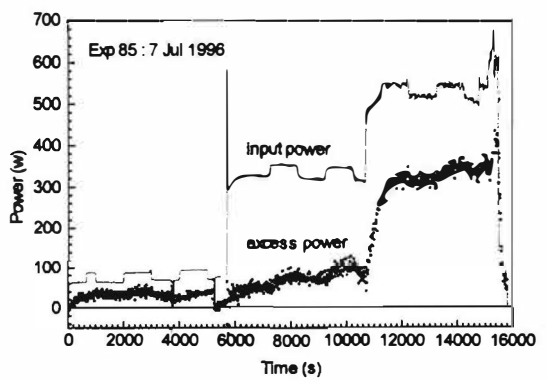

Fig. 11 The same as Fig.9 for the black cell.

4. The (preliminary) response of a more traditional calorimetry

In order to give a more direct proof of the surprising deductions of the previous Section, we decided to embed our cells in a flux calorimeter, according to the scheme appearing in Fig. 12.

The experimentation began on Oct. 1, 1996: it is thus a very preliminary stage. However, in Fig. 13 let me show to you what we saw when we turned our experiment on. When the electrolysis started (at time t=29000 s) we injected into the cell about 80 W, the reading of the flux calorimeter rose with its typical time constant of about 200 s, but it stopped short of break-even and it began to decrease in coincidence with a reading of the resistance of the Pd-wire indicating the reaching of high loading (x>1). At this point it was realized that the flux calorimeter might be not fully hermetic and some glass-wool was added at its top (see Fig. 13), hindering the energy flow through the gas escape route. As a result the reading began to steeply rise until, in the attempt to check the hermeticity of the calorimeter, the glass-wool isolation was removed. The ensuing sudden drop of the reading stopped when the isolation was reinstated: at that point the reading continued to rise until it reached a level more than twice the input power. An unfortunate power failure occurred then at t=34000 s, stopping both the electrolysis and the acquisition. When the system was on again, one had certainly lost the high loading (as a measurement of the resistance indicated) and with that CF, and the calorimeter reading just confirmed this latter fact.

As one can see from the steps in the input power, the isoperibolic heat pulse that we applied was 14 w, allowing us to measure at the same time the output power isoperibolically. Our analysis shows that when the flux calorimeter reading is W_{out}=170 w, the isoperibolic estimate is W_{out} =135 ± 5 w, still in excess of W_{in} = 87 w, but substantially lower than the one indicated by the flux calorimeter.

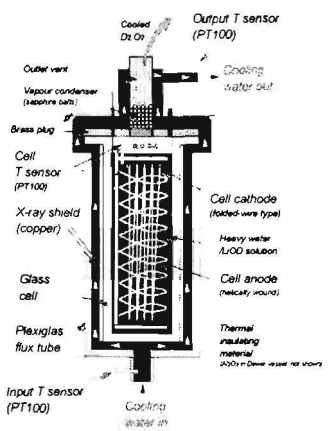

Fig. 12 The flux calorimeter and the electrolytic cell.

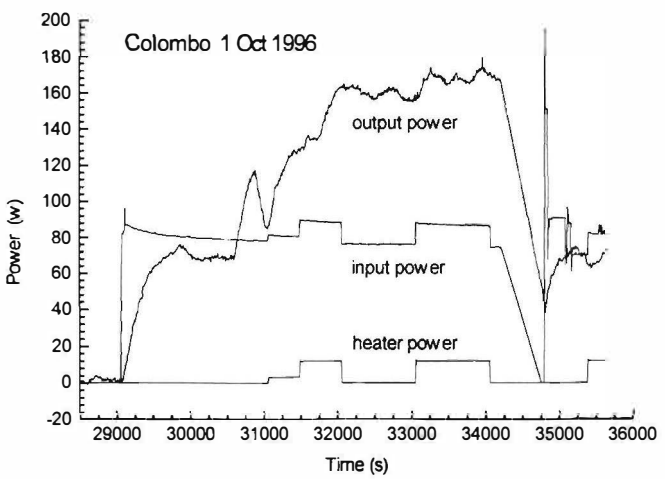

Fig. 13 The first observations with flux calorimetry.

The sequence of events just described leads us to conclude that:

(i) the gas escape route is a very important dissipation channel for "black" cells;

(ii) the isoperibolic calorimetry yields a lower bound for W_{out} ;

(iii) when the "black" cell becomes blank, the flux calorimeter as well as the isoperibolic method show unmistakably such happening.

5. Conclusion

The new campaign of measurements fully confirms the previous one, reported in Ref . [3]. On the basis of this finding we may confidently state that:

(a) electrolytic cells with Pd-cathodes in the new electric configuration produce large quantities of excess heat;

(b) the efficiencies $\varepsilon = \frac{W_x}{W_{in}} \cong 1 \div 2$;

(c) the W_x's that can be obtained are several hundred watts;

(d) the CF power densities can reach the incredible values $w_{CF} \cong 50 \div 100$ kw/cm^3.

Based on the above points the commercial production of low-grade heat producing devices (boilers, domestic heaters etc.) before the end of the millennium does not seem to belong anymore to the realm of beautiful dreams.

REFERENCES

[1] G. Preparata, QED Coherence in Matter, World Scientific, (Singapore, May 1995);

[2] G. Preparata, Cold Fusion 93: Some Theoretical Ideas, Proc. ICCF4, Maui, Usa 6-9 December 1993;

[3] G. Preparata, M. Scorletti and M. Verpelli, Isoperibolic Calorimetry on Modified Fleischmann-Pons Cells, Journ. Electroanal. Chem. **411**, 9-18 (1996);

[4] G. Miley and J.A. Patterson, Nuclear Transmutations in thin film Ni coatings undergoing Electrolysis, II Int. Conf. on Low Energy Nuclear Reactions, Texas A&M, College Station, September 1996.

[5] R. Barni, E. Del Giudice, R. Pagliarani, G. Preparata and D. Uglietti, in preparation.

Material Science Studies

PROGRESS REPORT ON THE RESEARCH ACTIVITIES ON COLD FUSION AT ENEA FRASCATI

F. De Marco, A. De Ninno, A. Frattolillo, A. La Barbera, F. Scaramuzzi, V. Violante
ENEA - Dipartimento Energia - Divisione Fusione, Centro Ricerche di Frascati
C.P. 65 - 00044 Frascati, Rome, Italy

ABSTRACT

Since 1992 the ENEA Frascati Group has performed successful experiments aimed to measuring the excess heat produced in electrolytic cells with heavy water and a Palladium cathode. These experiments were characterized by a substantial lack of reproducibility. On the other side, it has become more and more clear that reaching, and possibly exceeding, a threshold in the amount of Deuterium absorbed in the lattice (usually called the D/Pd ratio) is a necessary condition in order to produce excess heat (D/Pd $\geq$ 0.9 atomic). These considerations pushed the Group to concentrate its activity in the study of the connection between the Palladium characteristic parameters and the maximum reachable D/Pd ratio, by analysing and interpreting the relative absorption mechanisms. Mastering this aspect of the experiment should allow obtaining reproducibly high charging ratios, well above the quoted threshold, and thus hopefully reproducible production of heat excess.

This has been done in the last year, with quite promising results, that will be reported in this paper.

1. INTRODUCTION

Starting in 1992, the ENEA Group of Frascati has concentrated its attention on the phenomenon of heat excess production in electrolytic cells working with a Palladium cathode in heavy water, with LiOD as the electrolyte. Due to the substantial lack of reproducibility in the results reported up to then, a feature common to all laboratories, and to the consequent skepticism of the traditional scientific community, it was clear that the accuracy of the calorimetry was paramount, and this has been the aspect to which the Group has dedicated most of its attention in the first years. A flow calorimeter was developed, reaching a very high degree of reliability, with a high sensitivity, which permitted to keep the experimental errors in the measurement of excess power well within 100 mW for time durations up to the order of months. Since then a series of experiments has been performed, some of which with relevant figures as far as heat excess is concerned, with the addition of some very stimulating side features: all of them have been presented at the International Conferences on Cold Fusion and published in their Proceedings and in other journals (1-4). In Table 1 the most relevant events of heat excess production measured by the Group are listed, in order of time, with the indication of the most meaningful parameters. Note that at least in two of the quoted experiments it was possible to exclude, by an accurate energy balance of the whole run, the hypothesis, claimed by many skeptics, that the excess heat could be attributed to the accumulation in the system, by an unknown mechanism, of chemical energy, the successive libera-

Material Science Studies

Table 1. The most relevant events of heat excess production obtained by the ENEA Frascati Group from 1992 to 1995.

Cathode	Anode	Excess of Heat Life (h)	Time to have the excess (days)	ΔE (MJ)	Power excess (W) (max)	ΔP/P max (%)	Current density (A/cm^2)
Pd foil	Pd	50	15	0.25	3	1000	0.2-0.8
Pd foil	Pd	50	10 (h)	0.3	3	800	0.1-0.4
Pd foil	Pd	8	40	0.08	4	9	1
Pd wire	Pd	60	30	0.6	11	137	2
Pd wire	Pt	720	20	0.35	0.2	25	0.1-0.2

tion of which could justify the production of heat. Thus, the conviction was reached in the Group that the heat excess production in deuterated Palladium was a reality and could not be attributed to known chemical processes.

A feature that has been increasingly clear, since the 2nd International Conference on Cold Fusion, in Como in1991, is the correlation between the heat excess production and the amount of Deuterium absorbed within the Palladium lattice, usually measured as the D/Pd ratio (atomic). It has been demonstrated that a threshold in the D/Pd ratio has to be exceeded, in order to obtain the production of heat excess: the value of this threshold is of about 0.9, at least at the normal operation temperatures (around 300 K). Whether this condition is also sufficient has still to be proved. However, reaching such high ratios is not at all straightforward, and can depend on many parameters of the experiment, first among which the characteristics of the Palladium used. [We experienced very neatly this feature. After the first two positive results reported in Table 1, obtained with Palladium foils already present in the laboratory, we had to get more Palladium, and we did so, buying it from the same firm, with the same nominal characteristics; with it we made more experiments, but did not succeed in obtaining heat production. An analysis *a posteriori* of samples of the two stocks showed a different "texture" in the metal, a different hydrogen solubility and a different surface morphology.] This feature has had the effect of shifting the search for reproducibility from the whole experiment to the ability to obtain high D/Pd ratios. In the last two Conferences of this series we have witnessed the strong effort performed by many groups to face this problem.

The ENEA Frascati Group has dedicated most of its resources in the last year to the study and to the solution of this problem. The first step was to master the measurement of the D/Pd ratio, through the measurement of the electrical resistance of the cathode. Then a fundamental approach was chosen, which consisted in the attempt to analyse rationally the mechanisms responsible for the absorption of Hydrogen (or Deuterium) in Palladium, trying to single out features that could be responsible for the difficulty in absorption above D/Pd $\cong$ 0.7. The stress field created by the concentration gradients during absorption has been investigated, with the aim of finding ways to overcome its negative effects. This will be described in next chapter.

Other two activities of the Group are worth mentioning, but will not be considered any more in the following:

- the development of a quantum mechanical approach, with a model aimed to explain possible mechanisms that justify cold fusion (5);
- the development of a circuit for the detection of ^4He as a nuclear ash of the process, which is in progress.

2. STRESS FIELD EFFECTS ON THE LOADING OF HYDROGEN ISOTOPES IN PALLADIUM CATHODES

The dissolution of hydrogen isotopes into a metal lattice is not only a problem of thermodynamic equilibrium between the hydrogen inside the lattice and the hydrogen in the external phase, but is also a problem of non- equilibrium in the metal, because of the occurrence of a transport process. Both aspects of the phenomenon are correlated, since the equilibrium concentration of the solute is achieved when the chemical potentials of the hydrogen in both phases are equal and the transport process inside the metal lattice is driven by the gradient of the chemical potential. On the other side, the chemical potential of the hydrogen in solid solution in a metal lattice is strongly influenced by all field forces, such as the stress field, which modify the free energy of the system. The hydrogen isotopes dissolving into a metal (e.g. palladium) occupy interstitial positions and expand the lattice. This process generates a stress field when remarkable concentration differences (strong gradients or coexistence of different phases) are created. This stress field can inhibit the diffusion process. In the presence of a stress field the chemical potential of the hydrogen in the palladium is modified:

$$\mu = \mu^0 - \overline{V}\sigma_h \tag{1}$$

where μ^0 is the chemical potential in the system without stress, $\overline{V}$ is the molar volume of the solute and σ_h the trace of the stress tensor. In the presence of a stress field the flux equation becomes:

$$J = -D(\nabla C - \frac{C\overline{V}}{RT}\nabla\sigma) \tag{2}$$

where C is the hydrogen concentration, R the gas constant, T the temperature, and σ the local stress. The diffusive flux becomes zero if:

$$\frac{\Delta\sigma}{\Delta C} = \frac{RT}{C\overline{V}} \tag{3}$$

It is easy to evaluate that, for Pd, $\Delta\sigma$ is less than σ around a dislocation (6). From the previous consideration it is clear that, during the loading process, the stress field can strongly affect the equilibrium concentration of the hydrogen in the lattice.

In Palladium, during the loading procedure, regions of higher lattice parameter (β phase) grow within regions of lower lattice parameter (α phase). In the region of coexistence (α + β phases), see fig.1a, the lattice parameter mismatch at the border between the two phases generates a very strong localised stress field, which is unfavourable for diffusion (coherent stress). If internal stresses can be removed, either by plastic deformation or by dislocation slipping, such stress-free strained crystals become "incoherent": see fig.1b. We have suggested that the negative effects due to the coexistence of α and β phases can be avoided during the loading process, by selecting an appropriate path on the pressure-concentration phase diagram: a detailed explanation of such a procedure is exposed in another paper presented at this Conference, together with the encouraging results obtained (7).

The loading process can be inhibited also by a stress gradient behind the external surface. The stress field effect behind the metal surface is similar, in terms of stress production, to the effect of a strong temperature gradient. The zone at higher temperature (concentration) is forced to expand, but is bound to a zone at lower temperature (concentration) that doesn't expand or expands

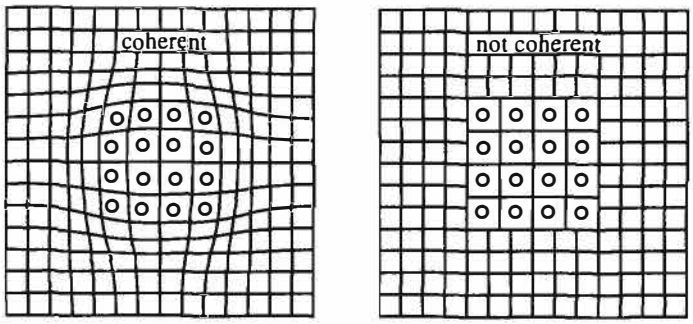

a) b)

Figure 1. Coherent (a) and incoherent (b) stress in a crystal.

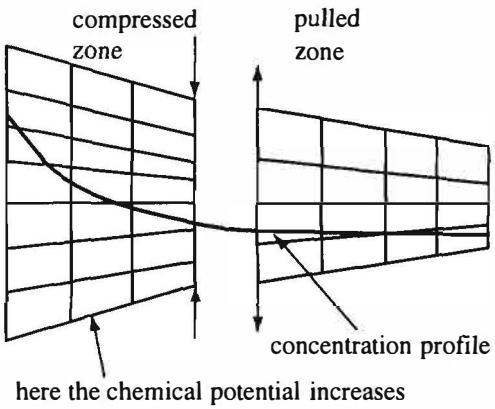

Figure 2. The effect of the Hydrogen concentration profile on the stress field.

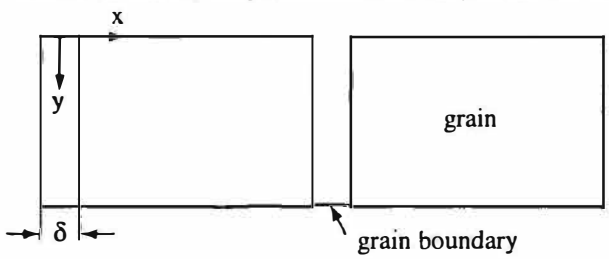

Figure 3. Sketch of the grain/grain boundary system.

much less. Thus, in the zone at high concentration, compressed by the zone at low concentration, the chemical potential of the solute increases and the loading can be inhibited: see fig.2. This condition can be modified by creating a metallurgical structure in the sample able to minimize the gradients of concentration. Now we can study, in the case of an ideal system, the effect of some metallurgical parameters, like the boundary grain size and the diffusivity, on the mass transport process taking place during the loading (8). The grain/grain-boundary system is sketched in fig.3; a simple diffusive mass balance across the grain-boundary and across the grain gives the following system of differential equations (9):

$$\frac{\partial C_b}{\partial t} = D_b \frac{\partial^2 C_b}{\partial y^2} + \frac{2D_g}{\delta}\left(\frac{\partial C_g}{\partial x}\right)_{x=\delta/2}$$

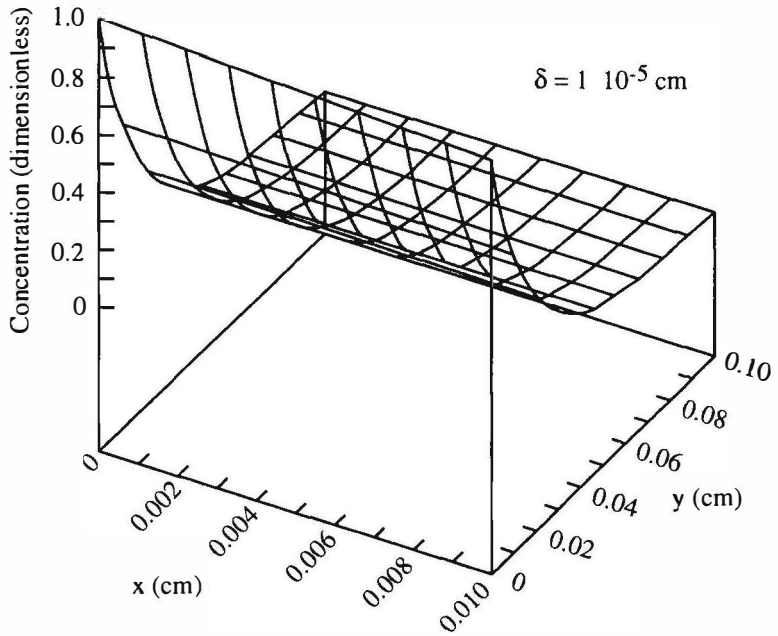

Figure 4. Concentration profile within a grain with a boundary grain size of 0.1 μm.

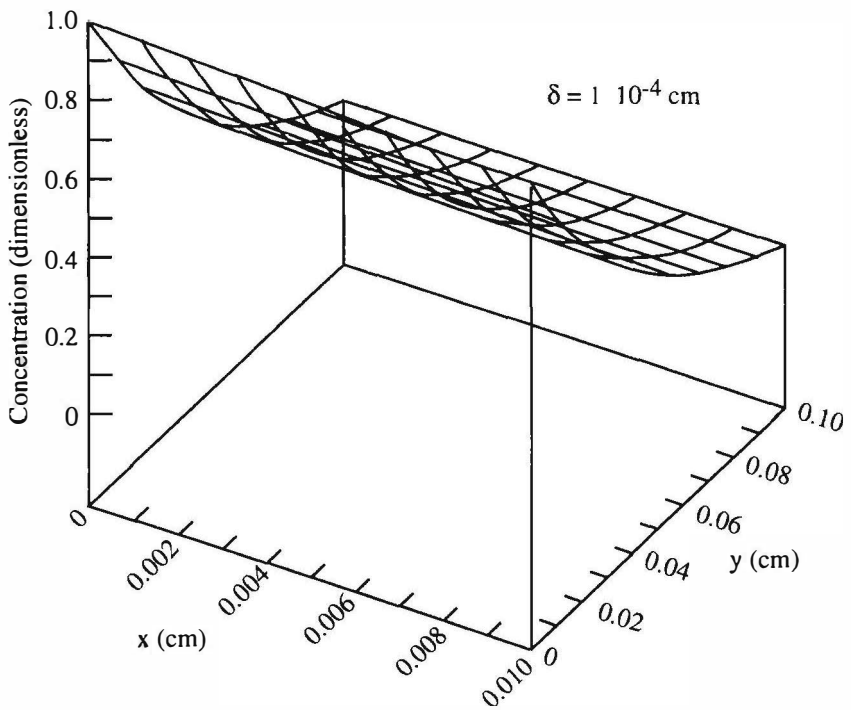

Figure 5. Concentration profile within a grain with a boundary grain size of 1 μm.

$$\frac{\partial C}{\partial t} = D_g \nabla^2 C_g$$

with boundary conditions: y=0, t=0, $C=C_0$; y>0, t=0, C=0; x=0, $C_g=C_b$,, where the indexes g and b refer to the grain and the grain-boundary respectively; δ is the grain-boundary size, D the diffusion coefficient and C the solute concentration.

Material Science Studies

In fig. 4 and 5 the surface plots of the concentration profile in a grain are reported for two different cases, after the same loading time. In fig. 4 the size of the grain boundary is 0.1μm while in fig.5 it is 1 μm. In the former the resulting concentration gradient in the grain is larger than in the latter. This result has been obtained under the hypothesis of an ideal system, without impurity at the grain boundary. When impurities are present at the grain-boundary, the grain-boundary diffusion coefficient generally is smaller. If, in our simulation, we consider two different situations, with the same grain boundary size, but with a different grain-boundary diffusion coefficient, the outcome is that the concentration gradient in the grain is larger in the system where the diffusion coefficient at grain-boundary is lower: in other words, the presence of impurities can increase the concentration gradient.

Let us now consider the effect of the stress-field produced by the concentration gradient during loading, in terms of equilibrium loading. By using the well known stress (σ) vs strain (ε) relationship, $\sigma=E\varepsilon$ (where E is the Young module), and the relationship between strain and concentration for the Pd beta phase (10):

$$\varepsilon(C) = [1 + 0.044(C - C_{\beta\,min})]$$

the following transport equation is carried out:

$$\frac{\partial C}{\partial t} = D\frac{\partial^2 C}{\partial x^2} - (1-\eta)\frac{\bar{V}}{RT}0.044E\left(\frac{\partial C}{\partial x}\right)^2 - (1-\eta)\frac{\bar{V}}{RT}0.044EC\frac{\partial^2 C}{\partial x^2}$$

where η is the percentage of relaxed stresses.

Figure 6 shows the result of the calculations: when the percentage of the relaxed stresses is sufficiently high (η≥0.85), the behaviour is substantially Fickian and the asymptotic loading value is H(D)/Pd=1; but, if the system is not able to relax more than 70% of the stresses produced by the loading, the asymptotic evolution changes. A further reduction of η produces a spontaneous deloading and the equilibrium concentration can be modified. The sample considered here is supposed to have been gas pre-loaded according to the technique described in (7).

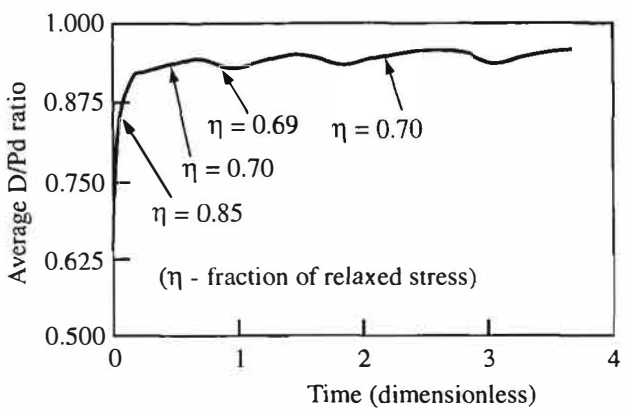

Figure 6. Effect of the unrelaxed stresses, produced by the diffusing Hydrogen, on the H/Pd value.

Thus, a further increase of the loading can be obtained if the stresses are allowed to relax. The value of the yield stress gives us useful information on the ability of the material to relax stresses, on the basis of its initial metallurgical properties. Hence, the initial state of the sample is very important in reducing the blocking force arising from the stress field. We measured the yield stress for Pd-H samples submitted to gas pre-loading. Samples where the coexistence of the α and β phases was avoided show a yield stress 50% lower. Higher values were obtained for cold worked samples, see Table 2.

Table 2. The correlation between the yield stress values and the different treatments of Palladium.

	Loading ratio	Yield stress MPa
Cold worked	0.6-0.7	275
Heated (1000°C)	0.6-0.7	148
Heated (1000°C) pre-loaded in gas	0.7	102

3. EXPERIMENTAL RESULTS IN ELECTROLYSIS

On the basis of these considerations, we decided to perform some metallurgical treatments on the Pd samples, then submitting them to electrolytic charging of Hydrogen or Deuterium, looking for maximum loading. The description of the tests performed with this purpose, including cold working and annealing at different temperatures for different times, is exposed in detail in the paper already mentioned, presented at this Conference (7). This allowed us to select the structure that better fits the afore mentioned characteristics. In particular, by varying the thermal treatment temperature from 700 to 1100°C, we found that the grain dimension and the dislocation slipping form a kind of percolative network for samples conditioned at 900°C for one hour. A possible interpretation of such a result is that in this sample the concentration profiles are quite flat, since the hydrogen diffusion is enhanced by the dislocation cores and/or by the ability of such a material to relax the stresses. Charging ratios of 1 for Hydrogen and 0.96 for Deuterium were obtained with a satisfactory reproducibility.

Another interesting effect found in the experiments is the correlation between the loading dynamics and the loading ratio. We observed that after loading at constant current density for a certain time, the concentration of the solute in the metal doesn't increase any more and sometimes a de-loading takes place. On the basis of the concepts exposed in the previous section we assumed that such a behaviour was promoted by the creation of a stress field very close to the surface of the sample under cathodic loading. Then we tried to remove the stresses by inverting the current for a few seconds (anodic polarization of the sample) and/or applying a low-high current mode, just to avoid the creation of a new stress field. The effect of this technique is well described in fig.7. A change in the period of the low-high current mode and an increase of the current also produce a positive effect on the loading ratio.

The material showing the best hydrogen (deuterium) solubility has been used for calorimetric measurements under electrochemical loading in heavy water. The calorimetric system was the same described in previous papers (1-4). The cathode was a palladium foil 150 μm thick and with a surface of 2 cm^2 for each side. The loading ratio achieved a value of 0.96 with a current

density of 50 mA/cm^2, and an excess heat could be measured as a function of the current density, in good agreement with the well known Storm's curve, reaching a maximum of 150 mW for 100 mA/cm^2. In Fig. 8 three successive runs are shown, the last of which, performed after a refilling of the solution, "killed" the effect. This effect seems to confirm that the region close to the surface plays a fundamental role in the process.

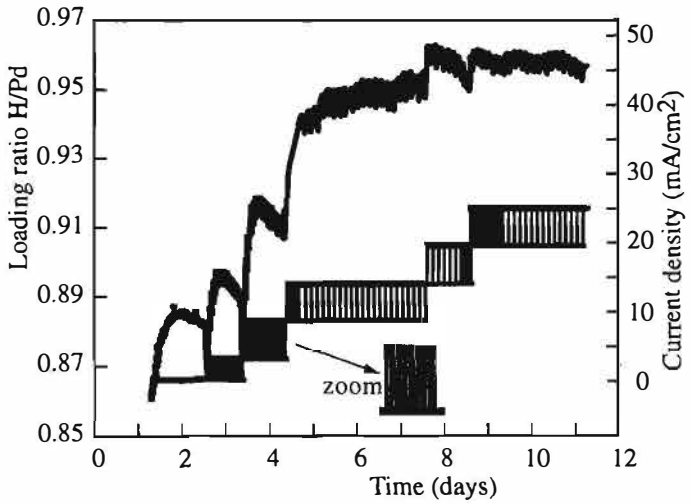

Figure 7. Influence of the loading dynamics on the equilibrium value of H/Pd.

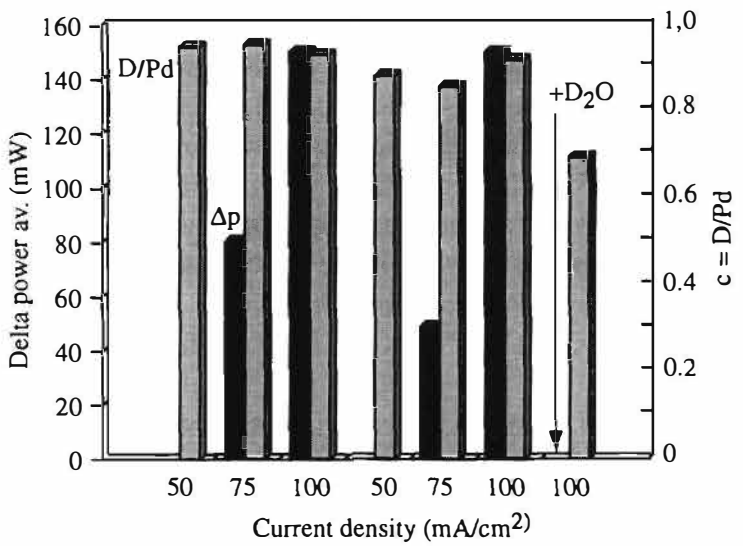

Figure 8. D/Pd ratio (light) and heat excess (dark) in three successive tests, for which the value of the current density is reported. For the last the D/Pd ratio was lower then the threshold: thus, no heat excess was measured. Total time ≈ 1 month.

4. CONCLUSIONS

The main activity of the ENEA Frascati Group in the last year has been concentrated on the achievement of high Hydrogen or Deuterium loadings in Palladium cathodes in a reproducible way. A rational approach has been chosen, by analysing the absorption mechanisms in terms of the stress fields created in the sample, and the consequent concentration gradients, which can be responsible of inhibiting the loading.

In practice, three roads have been followed, in order to overcome this problem, in the light of the quoted analysis:

- a particular charging procedure has been settled, consisting in a pre-loading in gas of the sample with a path (on the phase diagram) aimed to avoid the coexistence ($\alpha+\beta$) phase;
- an optimized pre-treatment of the sample (annealing at 900°C for 1 hour) has been chosen;
- the dynamics of charging, i.e., short anodic polarization and high-low mode of the current, has helped as well.

All three procedures have contributed to the achievement of reproducible high charging ratios in Palladium samples (up to 1 for Hydrogen and to 0.96 for Deuterium). The first tests with heavy water in a calorimeter seem to indicate that heat excess is produced when the well known threshold for D/Pd (0.9) is exceeded.

AKNOWLEDGMENTS

The authors express their high appreciation for the skilled participation to the activity described here of Mess.rs Domenico Lecci, Giuseppe Lollobattista and Fabrizio Marini. A particular thank is due to Mr. Livio Bettinali for his contribution to the yield stress measurements.

BIBLIOGRAPHY

(1) L. Bertalot, F. De Marco, A. De Ninno, A. La Barbera, F. Scaramuzzi, V. Violante , P. Zeppa, "Study of Deuterium charging in Palladium by the electrolysis of heavy water: heat excess production" in Il Nuovo Cimento vol.**15 D**, N 11, Nov.1993, 1435

(2) L. Bertalot, F. De Marco, A. De Ninno, A. La Barbera, F. Scaramuzzi, V. Violante , P. Zeppa, "Study of Deuterium charging in Palladium by the electrolysis of heavy water: search for heat excess and nuclear ashes", "Fronteers of Cold Fusion", Proceedings of the 3th International Conference on Cold fusion (ICCF3), ED. by H. Ikegami, Universal Academy Press Inc. Tokyo, 365 (1993)

(3) L. Bertalot, F. De Marco, A. De Ninno, A. La Barbera, R. Felici, F. Scaramuzzi, V. Violante, "Behaviour of a Pd Membrane During Deuterium Electrochemical Loading:Excess heat Production", Proc. of IV Int. Conf.on Cold Fusion (ICCF4) ", Maui, Hawaii, USA, 6-9 Dec. 1993, vol.1, 4-1, ed by Electric Research Power Institute, Palo Alto, Ca

(4) L. Bertalot, F. De Marco, A. De Ninno, A. La Barbera, F. Scaramuzzi, V. Violante , "Power excess production in electrolysis experiments at ENEA Frascati"
Proc. of V Int. Conf.on Cold Fusion (ICCF5) ", Monte-Carlo, Monaco 9-13 Apr. 1995, publ. by Int. Conf. on Cold Fusion V, Valbonne, France, 34

(5) V. Violante, A. De Ninno, "Collision between two deuterons in condensed matter: ion trap mechanism", Proc. of V Int. Conf.on Cold Fusion (ICCF5) ", Monte-Carlo, Monaco 9-13 Apr. 1995, publ. by Int. Conf. on Cold Fusion V, Valbonne, France,355

(6) R.A. Oriani, Transaction of Fusion Technology 26 (1994) 235-266

(7) A. De Ninno, A. La Barbera, V. Violante, "Selection of Palladium metallurgical parameters to achieve very high loading ratios", presented to ICCF 6, (1996)

(8) J.D. Fast, " Gases in Metals", The Gresham Press, (1976) 148.

(9) P.G. Shewmon, Diffusion in Solids" Mc Graw Hill (1967) 166

(10) A. De Ninno, A. La Barbera, V. Violante, "Consequence of Lattice Expansive Strain Gradient in Loading Hydrogen in Palladium", submitted to Phys Rev B

Material Science Studies

Search for neutron emissions induced by electric currents and phase transitions in titanium deuteride films

F. Cuevas, J.F. Fernández and C. Sánchez.

Dpto. Física de Materiales C-IV. Universidad Autónoma de Madrid. Cantoblanco 28049. Madrid. Spain.

Abstract

A complete set of NRS (Nuclear Reactions in Solids) experiments has been performed on the Ti-D system checking as triggering mechanisms of these phenomena the imposition of electric fields and the crossing of the δ–ε and β–δ phase boundaries. The experiments were accomplished using a high pure iodide-titanium film as the initial metal matrix. Neutron measurements were monitored while doing these experiments and no clear evidence of the nuclear fusion reaction $D+D \rightarrow {}^{3}He+n$ has been detected, the upper detection limit for this reaction being $\Lambda=3x10^{-21}$ f/pds.

1. Introduction

The intensive study followed during last years on NRS indicates that the achievement of these phenomena is usually associated to certain experimental conditions. This conditions can be summarized as follows: firstly, the employment of a metal matrix with suitable chemical and physical properties[1] secondly, the achievement of a high deuterium loading in the matrix[2] and finally the imposition of non-equilibrium perturbations in the deuterium-metal system[3].

Considering the three main conditions mentioned above, we present in this paper a complete set of NRS experiments that were performed using an iodide-titanium sample as the initial metal matrix. This sample was produced in our lab by a modified technique of the iodide process[4] which has as its main goal the possibility of preparing very pure titanium metal. Afterwards the iodide-titanium film is highly deuterated from the gas phase and is subjected to a wide test of different non-equilibrium conditions in order to trigger deuterium fusion reactions in the Ti-D system. A more detailed report has been submitted for publication elsewhere.

2. Methods

2.1 Experimental procedures

An iodide-titanium sample of 55mg mass was deposited uniformly over an electrically selfheated tungsten filament (dimensions 40x2x0.025 mm^3) that was supported in the middle of a glass reaction chamber by two thick tungsten electrodes. The typical composition of the sample was checked for a twin sample by EDX and AES analyses. The content of gaseous impurities is as follows: C<1.5at%, N<2at% and O=2at%, while no metallic impurities where detected in the outer part of the film at a typical detection sensitivity of 0.2at%. It should be remarked that there is some diffusion of the tungsten substrate into the titanium film which reaches at most half of the deposited film[5]. Same analyses were carried out in a commercial sample of 99.6% nominal

purity yielding a content of gaseous impurities ten times higher than that of our film. It is well known that the presence of gaseous interstitial impurities in titanium reduces its maximum deuterium uptake, since these impurities also occupy similar sites in the metal matrix. Therefore, a higher deuterium loading of the metal can be performed in iodide-titanium samples in comparison with that of the commercial ones that are commonly used in NRS experiments.

The titanium film was deuterated in the same chamber that was used for its deposition, so it is never exposed to air in order to avoid any superficial oxidation effects. The experimental system for the deuteration of the sample and the performance of NRS experiments is shown in Fig.1. It essentially comprises of two different equipments: one dealing with the thermodynamical and electrical control of the iodide-titanium film (upper part of the figure) and the other with the neutron detection system (lower). Both parts are time interconnected and the first one will be now described to explain how the deuterium loading of the metal and the performance of NRS experiments were accomplished.

The iodide-titanium sample is supported by two tungsten electrodes that allow passing an electric current through the film which is generated by a dc power supply (Kenwood PD35-20D) and is controlled by a function synthesizer (Keithley 3910). In addition, two thin tungsten wires are connected to the edges of the sample, so that the well known four probe method can be used for resistance measurements. A thermocouple (NiCr-NiAl) is located in the outer part of the reaction chamber to get an idea about gas temperature at the environment of the sample and for safety precautions. The reaction chamber, which is kept in vacuum after the titanium deposition, is made of glass and is connected through a very thin glass separator to a deuteration reservoir. The

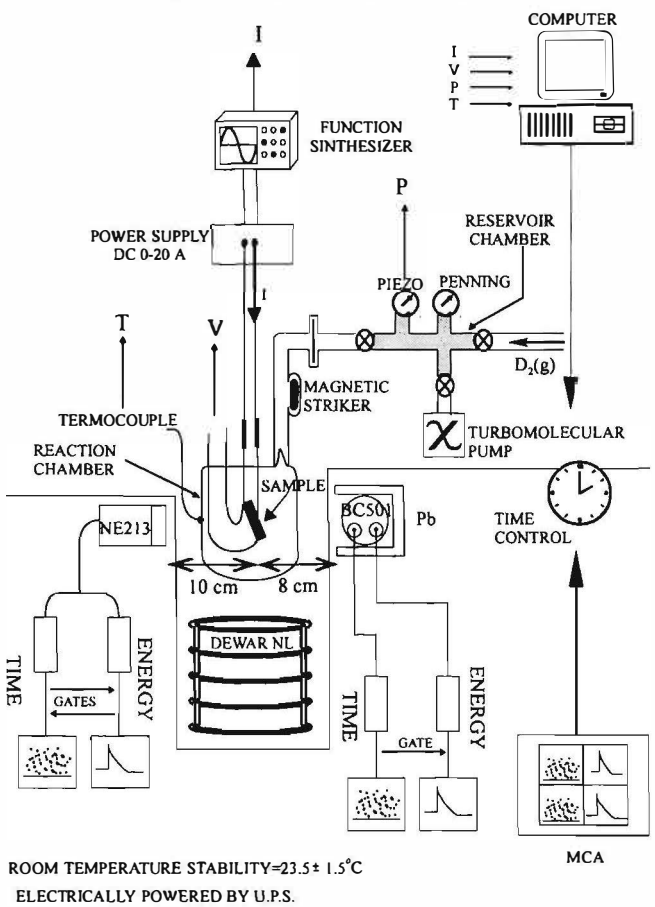

Figure 1: Sketch of the experimental system used for the sample deuteration and the performance of NRS experiments.

whole set constitutes a Sieverts type apparatus composed of two volumes: the reservoir chamber (V=77.5±1.5ml) and the reaction chamber (V=374±10ml). The reservoir chamber is attached to a deuterium inlet (purity 99.999%) and also to a turbomolecular pump, and is equipped with a piezoresistive transducer (Kistler 4043A) and a penning gauge. All thermodynamic and electrical parameters are monitored by a PC with an acquisition time of 10 seconds.

To perform the titanium film deuteration, the reservoir chamber is first evacuated down to 10^{-5}torr and then deuterium gas is admitted into this chamber after crashing the glass separator with a magnetic striker. Afterwards, the deuterium pressure is fixed to 300mbar and connections to vacuum and deuterium inlets are closed so that both chambers form a closed system. Under these circumstances the sample is heated up to glowing temperature (1200K) by passing a high dc current (13A) through it. Finally, a decreasing electric ramp is programmed through the sample to cool it slowly down to room temperature, leading to the deuterium absorption into the film as dictated by the characteristics of the P-X-T phase diagram of Ti-D[6]. The deuterium concentration in the pure titanium film after this treatment was evaluated, from the overall pressure drop in the system to be in the high concentrated δ-phase (x atomic ratio D/Ti≥1.6).

Once a high deuterium concentration is achieved in the sample, it is necessary to provoke non equilibrium conditions in the system for triggering the NRS phenomena. To this aim, we performed two different sets of experiments. In the first set, we applied different electric fields in the sample by passing different electric current patterns through it. The second set of experiments deals with the possible influence of phase transitions on the achievement of NRS.

The imposition of electric fields in a solid deuteride system induces important perturbations such as the presence of electromigration processes[7] and Ampere forces[8] in the system. Considering this scope, there were three experiments performed -denoted as Exp1, Exp2, and Exp3- corresponding to different electric current patterns, as show in Fig.2. In Exp1 two constant electric currents of ≅1A and ≅4A were passed through the sample. In Exp2, the electric current was changed abruptly between 0.2A and 3A at a frequency of 0.8mHz. Finally, in Exp3, a triangular current pattern between 0A to 7A at a frequency of 0.4mHz was programmed.

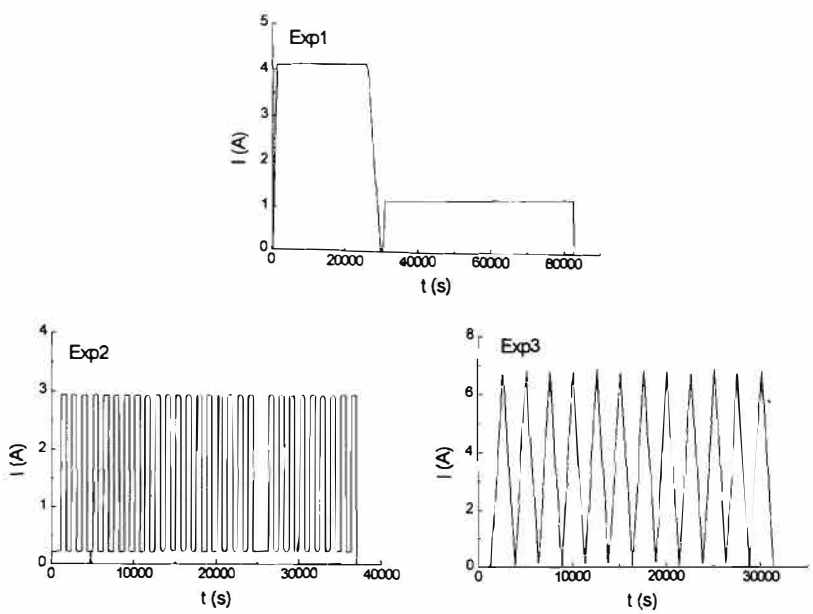

Figure 2: Time-evolution of the electric current patterns imposed through the sample in Exp1, Exp2 and Exp3.

In relation with phase transition experiments, there are some publications that report the detection of NRS in titanium deuteride when this system is thermally cycled around room temperature[9,10]-which can be related to the δ–ε phase transition- or around the β–δ phase transition itself[11,12]. To check these triggering conditions we performed two experiments, Exp4 and Exp5, in which the sample was forced to undergo the above mentioned transitions. In order to provoke the δ–ε phase transition (Exp4) the reaction chamber was surrounded by a liquid nitrogen dewar, meanwhile triangular electric current cycles up to 9.5A were passed through the sample. This procedure induces thermal cycling of the sample from nearly liquid nitrogen temperature to some value above room temperature, as checked by sample resistivity measurements. Twelve of these cycles were programmed at a frequency of 0.4mHz. Finally, the β–δ transition was provoked in Exp5 by cycling a high electric current pattern between 6A and 13A through the sample with an initial deuterium pressure of 300mbar in the closed reactor. Sixteen triangular-shaped cycles were conducted at a frequency of 0.8 mHz and sixteen more at a double speed. To verify the accomplishment of this transition both electric resistance of the sample and deuterium pressure in the closed reactor were monitored simultaneously, reflecting without doubt the mentioned transition as is discussed in another publication[13].

2.2 Neutron count analysis

Neutron detection measurements were carried out, while doing all the described experiments, by two liquid scintillation counters (NE213, from Nuclear Enterprise and BC501, from Bicron Corporation). The γ–n discrimination of the scintillation counters was accomplished by two electronic systems using a pulse shape discrimination technique. Both energy spectra and counting time-evolution are finally recorded in different Multichannel Analyzers. In the case of the counting time-evolution, the detected neutrons (namely counts) are collected up every 20 seconds, while in the energy spectra the counts are integrated during the duration time of every experiment (typically 9 hours). The absolute efficiency of the detectors, taking also into account the geometrical configuration of the set-up, are 6.6×10^{-4} for NE213 and 5.7×10^{-3} for BC501 at the interesting energy of 2.45MeV corresponding to the $D+D \rightarrow {}^{3}He+n$ reaction. The background counting rate the detection systems are 5.3×10^{-3}c/s and 0.26c/s, respectively. Further information about calibration of the equipment and other technical characteristics can be found elsewhere[14].

In order to examine the possible existence of the NRS phenomena in the described experiments it is indispensable to compare the neutron measurements that are monitored during the experiments with those corresponding to the natural background. To this end, we recorded the background signals for eleven days after the completion of the NRS experiments. Due to the fact that the time pattern of the emitted neutrons is unknown in advance (e.g. bursts or time-continuous emissions), it is convenient to analyze the neutron counting rate for different integration times. Selected integration times (t_i) for these analyses are 20s, corresponding to the minimum acquisition time in the experiments; 1200s, corresponding to the typical time of electric current cycling frequency and 9h, corresponding to the typical elapsed time of the experiments.

The frequency distribution of neutron counts must obey a Poisson distribution if they are originated by random phenomena, as is essentially expected for the natural background. This behaviour is shown in Fig.3a, where the absolute frequency distribution of the natural background at t_i = 20s for the BC501 is compared to the Poisson distribution that corresponds to the average value of the neutron counts (λ) during t_i. To discern neutron emissions during the experiments from the Poisson background it should be establish a confidence level that dictates the neutron detection limit of the system. Taking 99.9% as the confidence level, the detection limit for BC501

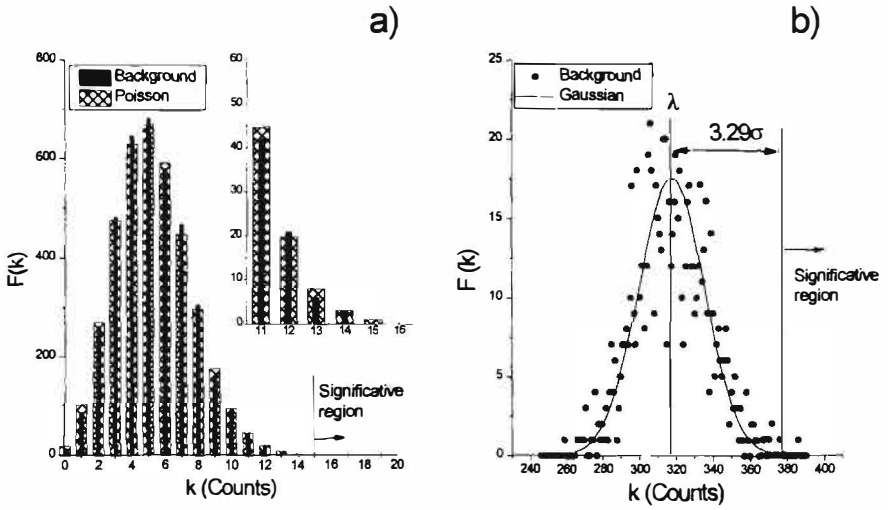

Figure 3: Absolute frequency of the neutron background detected by the BC501 system and statistical approximations at integration times of 20s (a) and 1200s (b). In both graphics the significant region corresponding to a confidence level ≥99.9% is expressly pointed out.

is 15 counts at t_i = 20s, corresponding to a neutron emission rate of 85 n/s. This detection limit implies that if 15 or more counts per 20s are detected by the BC501 system, they can be considered as NRS significant signals at a 99.9% of confidence level.

A similar analysis has been performed for the other t_i values. At t_i = 1200s the Poisson distribution approaches to Gaussian, as the value of λ considerably increases (Fig.3b). The confidence level of 99.9% corresponds now to a deviation value of 3.29σ from λ, the detection limit in the BC501 is 377 counts per 1200s and the neutron emission rate is 9n/s. Finally, at t_i=9h the registered background time is insufficient to get good approximations to a statistical function. Nevertheless, it can be considered that we are still dealing with a Gaussian distribution and to take the deviation value of the neutron counting for significant signals as 3.29σ. However, the Tchebychev theorem states that the confidence level for this assumption is only of 90%. The minimum neutron emission that can be detected in the BC501 is in this case of 3n/s. This detection limit implies, considering the sample titanium mass (55 mg) and its deuterium content (X=1.5) a neutron detection rate limit of $\Lambda=3\times10^{-21}$ f/pds. In Table I, the neutron detection limits for both detection systems at the different integration times are summarized.

Table I: Neutron detection limits in the NE213 and BC501 systems at different integration times (t_i). The detection limit is given as neutrons per second emitted from the sample and counts per t_i detected by the equipment.

	NE213		BC501	
Integration time	Neutron detection limit (n/s)	Significant counting level (Counts)	Neutron detection limit (n/s)	Significant counting level (Counts)
20s	220	3	85	15
1200s	11	15	9	377
9h	2	λ+3.29σ	3	λ+3.29σ

3. Results and Discussion

The neutron measurements were analyzed for every integration time and compared with the neutron background. It should be remarked that the electronic system associated with the NE213 detector suffered a misfunction during Exp4, so that no neutron data will be offered for this detector in Exp4. All other neutron data are now presented and discussed.

The highest values of counting rate registered at t_i=20s for every experiment are summarized in Table II. For this value of t_i, the significant events respond to a counting rate equal or higher than 3 counts in NE213 and 15 in BC501. The most anomalous result has been found in Exp1, in which 3 counts were detected once in NE213 and 16 counts were detected twice in BC501. Nevertheless, the absolute frequency of these events for the background Poisson distribution is still important: 0.76 for NE213 and 0.37 for BC501. Besides, there is no time correlation between the significant signals in both detectors. Therefore, in spite of the detection of these anomalous events, we can not assert the presence of the NRS phenomena at short integration times (t_i=20s) with a detection limit of ≈100n/s.

Table II: Significant events monitored by the neutron detection systems at t_i=20s. k-F(k) indicates the highest counting value in the experiments and its absolute frequency (in parenthesis). F(k) background stands for the absolute frequency in the background of the monitored significant events in experiments. The absolute frequency is only given in significant events.

		Exp1	Exp2	Exp3	Exp4	Exp5
NE213	k-F(k)	3(1)	2	3(1)	-	2
	F(k) background	0.76	-	0.29	-	-
BC501	k-F(k)	16(2)	15(1)	16(1)	16(1)	14
	F(k) background	0.37	0.51	0.14	0.15	-

The significant events at t_i=1200s -corresponding to the typical cycling time- are those with a counting rate equal or higher than 15 counts in NE213 and 377 counts in BC501. While no significant events have been detected in NE213, some significant ones were observed in BC501. The most anomalous outstanding events present a deviation from the background average of 5.0σ (Exp3) and 4.3σ (Exp5). It should be noticed that both experiments were done with similar electric current patterns: triangular-shaped waves reaching high electric current values. The neutron counting in BC501 and the electric current time evolution for both experiments are shown in Fig.4. It can be observed that the significant events were detected in both cases after the imposition of many electric current cycles and also that the detected counts in every interval have often a higher value than the background average level. All these observations could indicate a slight neutron emission from the titanium deuteride film, however other facts contradict this possibility. Firstly, as was previously pointed out, no significant events were detected by NE213, being the detection limit for both scintillation counters practically the same: 11n/s in NE213 and 9n/s in BC501. Secondly, there was found no correlation in every experiment itself between the significant events and similar electrodynamic states, as is denoted in Fig.8 by the vertical lines. In other words, while imposing the same electrical conditions to the sample not always significant events were detected. From this point of view, the significant events detected by BC501 could possibly be related to a shift in the natural background or to a small drift in the electronic system associated with this detector. In conclusion, it is not possible to claim for sure the presence of NRS phenomena in the conducted experiments with a time pattern similar to the electric current cycling frequencies. Nevertheless, future experiments would be desirable to be done for checking

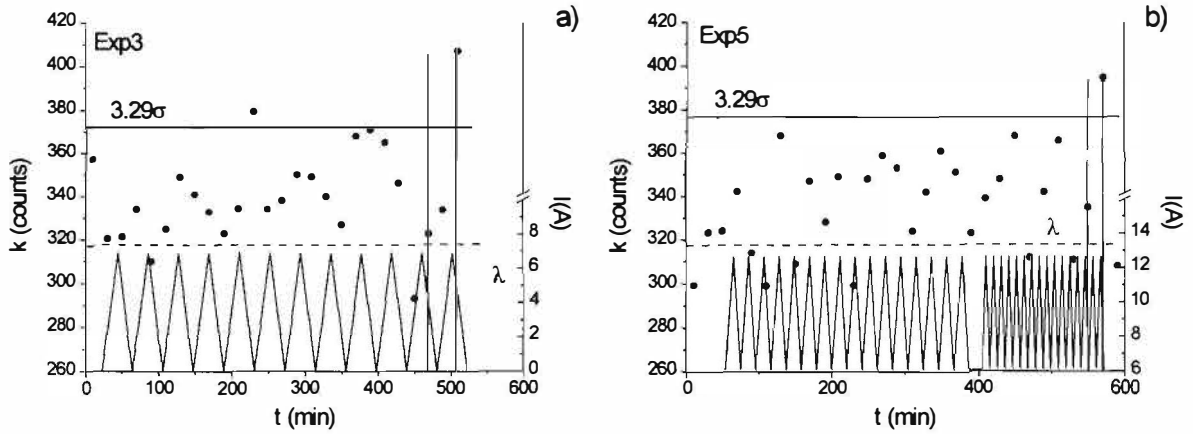

Figure 4. Counting time evolution detected by the BC501 system at t_i=1200s in Exp3(a) and Exp5 (b). The electric current time-evolution in these experiments is also depicted. The horizontal dotted lines indicate the average counting value of the background (λ). The horizontal continuous lines stand for a deviation value of +3.29σ from λ. The different counting rate between two events monitored at identical electrodynamical conditions is indicated by vertical continuos lines

if long electric cycling at high currents could induce the presence of NRS phenomena in titanium deuteride.

Finally, the whole neutron counting for every experiment was analyzed and the results are presented in Fig.5. The results match well with the background measurements, except in the case of the detected counts by BC501 in Exp3, where a deviation of 3.6σ from the background average was monitored. In any case this possible neutron emission was not corroborated by NE213. It should also be realized that the collected counts are in most of the cases higher than the background average recorded after completion of the NRS experiments, indicating a possible shift of the registered background level. To conclude, there was no detection of any continuous NRS phenomena in these experiments at a detection limit of 2n/s, corresponding to a fusion nuclear reaction rate in the sample of $\Lambda=3x10^{-21}$f/pds.

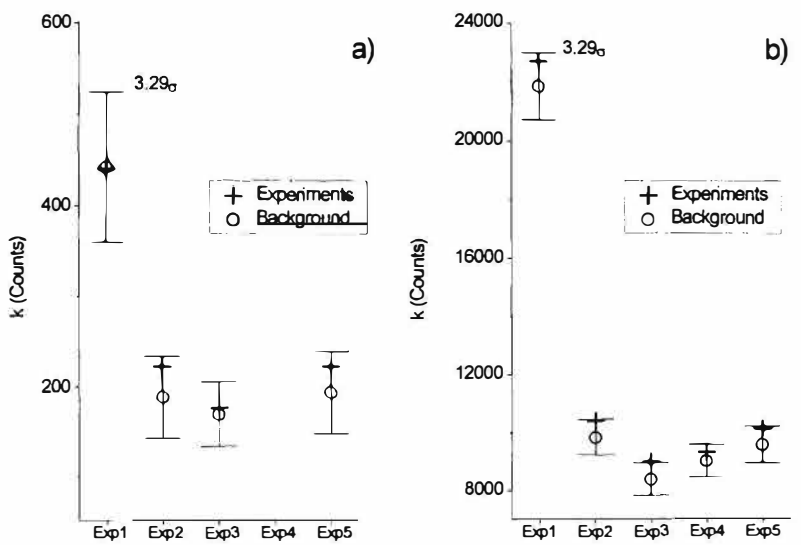

Figure 5: Neutrons detected by the NE213 system (a) and BC501 system (b) during the whole elapsed time of every experiment. The experimental data is represented by cross symbols, the background signal average (λ) by circular symbols and the deviation of ±3.29σ form λ by error bars.

4. Conclusions

There has been a complete set of NRS experiments performed after deuteration of a high pure iodide-titanium film. This sample has been subjected to different electric fields and has been forced to undergo the δ–ε and β–δ phase transitions in order to trigger deuterium fusion reactions in the Ti-D system. Neutron measurements monitored during these experiments have been analyzed considering distinct time patterns and have been compared with the natural background. No clear evidence of the presence of NRS phenomena during experiments have been found, being the upper limit for the rate of the $D+D \rightarrow {}^{3}He+n$ reaction of $\Lambda=3x10^{-21}$ f/pds. Nevertheless, some anomalous events were monitored in one of the neutron detectors when multiple electric current cycles up to high values were performed in the samples, which makes desirable a further investigation on this aspect.

Acknowledgements

Financial support from the Spanish DGICYT (PB93-0266) is gratefully acknowledged. Technical assistance from F. Moreno, A. Bergas and SEGAINVEX is also recognized. Special thanks are given to Dr. J. A. Rubio (C.E.R.N.) for providing us the D_2 gas and M. Fernández (Inst. T. Quevedo, C.S.I.C.) for the AES measurements.

References

1. D. Gozzi, P.L. Cignini, R. Caputo, M. Tomellini, G. Balducci, G. Gigli, E. Cisbani, S. Frullani, F. Garibaldi, M. Jodice and G.M. Urciuoli, in Frontiers of Cold Fusion, p. 155, H. Ikegami Ed., Universal Academy Press, Tokyo, 1993.
2. M.C.H. Mckubre, S. Crouch-Baker, A.M. Riley, S.I. Smedley and F.L. Tanzella, in Frontiers of Cold Fusion, p. 5, H. Ikegami Ed., Universal Academy Press, Tokyo, 1993.
3. A. Legget and G. Baym, Phys. Rev. Lett. 63 (1989) 191.
4. R.F. Rolsten "Iodide Metals and Metal Iodides", Wiley, New York, 1961.
5. F. Cuevas, Doctoral Thesis, Universidad Autónoma de Madrid, 1996. In Spanish.
6. A. San Martin and F.D. Manchester, Bull. Alloy Phase Diagram, 8 (1987) 30.
7. K.G. Rajan, U.K. Mudali, R.K. Dayal and P. Rodríguez, Fusion Technol., 20 (1991) 100.
8. 8 M. Rambaut, Phys. Lett., A, 163 (1992) 335
9. A. de Ninno, A. Frattolillo, G. Lollobattista, L. Martinis, M.Martone, L. Mori, S. Podda and F. Scaramuzzi, Europhysics Letters, 9 (1989) 221.
10. H.O. Menlove, M.A. Paciotli, T.N. Claytor, H.R. Maltrod, O.M. Rivera, D.G. Tuggle and S. E. Jones, in Anomalous Nuclear Effects in Deuterium-Solid Systems, p. 287, A.I.P. Conf. Proc. 228, New York (1991).
11. V.F. Zelenskij, V.F. Rybalko, A.N. Mozorov, G.D. Tolstolutskaya, V.G. Kulish, S.V. Pistyak and I.S. Martynov, Preprint KNFTI, TsNIIatominform, Moscow, (1989) p.61.
12. I.L. Beltyukov, N.B. Bondarenko, A.A. Janelizde, M. Gapanov, K.G. Gribanov, S. Kondratov, G. Maltsev, P. Novikov, S. Tsvetkov and V. Zakharov, Fusion Technol., 20 (1991) 234-238.
13. F. Cuevas, J.F. Fernández and C. Sánchez, to be published in J. Alloys and Compounds.
14. J.F. Fernández, F. Cuevas, M. Algueró and C. Sánchez, to be published in Fusion Technol.

Material Science Studies

Calorimetric Enthalpies in the β-phase regions of Pd black-H(D) Systems

Y.Sakamoto, M.Imoto, K.Takai and T.Yanaru

Department of Materials Science and Engineering, Nagasaki University,
Nagasaki 852, Japan

Abstract

The enthalpies for the reaction of gaseous hydrogen and deuterium with palladium black in β-phase region have been measured in the temperature range 323 K to 194.5 K and pressures up to about 7.6 MPa of $H_2(D_2)$ using a differential heat flow low temperature calorimeter. The calorimetrically determined enthalpies, $\Delta H_{H(D)}$, for solution in the β-phase regions of $0.7<H/Pd<0.9$ and $0.65<D/Pd<0.83$ for Pd black-H(D) systems become less exothermic almost in a linear fashion with increasing H(D) content, independently of temperature. The variation in $\Delta H_{H(D)}$ values with H(D) content are in agreement with that calculated from van't Hoff plots of the relative chemical potentials of hydrogen and deuterium. Enthalpies of almost the same magnitude are obtained from the desorption data. At the same H(D) content, the ΔH_H values for Pd black-H system are a slightly more exothermic than the ΔH_D values for the Pd black-D systems. The corresponding entropy, $\Delta S_{H(D)}$, on absorption calculated from the calorimetrically determined $\Delta H_{H(D)}$ and the relative chemical potentials have a tendency to decrease gradually with increase of H(D) content independently of temperature, however there is no marked difference in the magnitude of the $\Delta S_{H(D)}$ values between the two systems.

1. Introduction

The excess heat generation in "cold fusion" reactions [1-3] during electrolysis of D_2O/LiOD solution at room temperature by Pd cathode, although observed with poor reproducibility, seems to be closely related to highly deuterated Pd, $D/Pd>0.83$ [4-7], where the electrical resistance of the deuterated Pd electrodes should still be high, even though the resistance passes through the maximum near $D/Pd=0.75$ [8,9]. Many experimentally unknown factors exist, for instance the electrical quantities introduced into the electrolysis up to the onset of the heat generation, the action of the Li ions contained in the electrolyte on the electrode surface, and the variations in electrolysis current density and electrode overpotential etc. during the electrolysis.

Material Science Studies

If the key factor for the excess heat generation is a "high deuterium content" in Pd, the observation of any heat generations by a gas phase method is rather free from unnecessary complications compared to the electrochemical method mentioned above. Calorimetric enthalpies obtained by gas phase method, together with p-c isotherm measurements, should also reflect the dynamic conditions as the electrolysis method, because the dynamic conditions are related to the hydriding or dehydriding processes.

In previous measurements [10] of the calorimetric enthalpies for the reaction of gaseous hydrogen and deuterium with bulk Pd as a function of H/Pd and D/Pd contents up to about 0.865 and 0.85, respectively, in the temperature range 298 K to 194.5 K using a differential heat flow low temperature calorimeter, it has been found that the calorimetrically determined enthalpies, $\Delta H_{H(D)}$, for solution in the β-phase regions of both systems becomes less exothermic almost in a linear fashion with increasing H(D) content, independently of temperature. The $\Delta H_{H(D)}$ values are in agreement with the values determined from van't Hoff plots of the chemical potential of dissolved hydrogen and deuterium in Pd measured by Wicke and Nernst [11]. At the same H(D) content, the ΔH_H values for Pd-H system are a slightly more exothermic than the ΔH_D values for the Pd-D system. Enthalpies of almost the same magnitude are obtained from the desorption data. These results are also in agreement with the previously reported values by Flanagan et al. [12], although the enthalpies for absorption of hydrogen determined by Tkacz and Baranowski [13] using a high pressure device in the range of H/Pd=0.87 to 0.995 show a large exothermicity with increase of hydrogen content.

The present study was to obtain calorimeteric information about the enthalpies of reaction of gaseous hydrogen and deuterium with Pd black at high H(D) contents at temperatures between 323 K and 194.5 K by a combination of twin-cell, differential heat flow calorimetry and p-c isotherm measurements.

Frieske and Wicke [14] have shown that the assumption that p-c isotherm, p(r), and magnetic susceptibility, χ(r), measured on Pd black are valid for bulk Pd generally leads to misinterpretations. The characteristic differences between bulk Pd and Pd black are as follows : Pd black has 1) reduced hysteresis loops, ans 2) displacements of the p(r) and the χ(r) isotherms towards higher r values, and 3) smaller susceptibility at $r \rightarrow 0$ compared with bulk Pd. These differences can be attributed to the special features of the dispersed state of Pd black with high surface area and strong lattice distortions. However, the values obtained for the critical temperature, Tc=290±3 °C and pressure, p_c=19.5±0.2 atm agree with the results for bulk Pd within the experimental errors [14]. Therefore, it is also interesting to examine whether there is a difference in calorimetric enthalpies or not between Pd black-H(D) and bulk Pd-H(D) systems.

Arata and Zhang [15,16] have reported that in their cold fusion experiments using a double structure cathode vessel filled with Pd black (0.1 mol), an excess energy higher

than 200 MJ was obtained with an average rate of 50-100 $kJhr^{-1}$, although in this case the chemical reaction energy between Pd and deuterium is only 4 kJ.

2. Experimental details

The Pd black used in this study was powder less than about 45 μm of Wako Pure Chemical Industries Ltd. The purity is > 98.1 %, the remainder is moisture. The twin-cell differential heat flow calorimeter used in this study is the Setaram low-tempretaure calorimeter (model BT 2.15 II). The two identical hydriding cells, i.e., the reaction (sample) vessel and reference vessels of the calorimeter are connenected to a Sieverts p-c isotherm measurement apparatus, where a filter gasket was inserted between the connecting tube and both the vessels in order to avoid suction effect disturbaces of powder samples on evacuating.

About 6 gr. of Pd black was used as a sample in the reaction vessel by mixing Cu foils with about 50-60 μm thickness and about 2 mm x 2 mm. An amount of Cu, whose volume was the same as that of the (Pd black + Cu foils) in the reaction vessel, was placed in the reference vessel in order to improve the heat conduction. In order to obtain an highly active state for the p-c isotherm measurements and calorimetry, the vessels were completely outgassed at about 4×10^{-6} Pa and at 573 K, and then the samples were exposed to hydrogen gas of about p_{H2}=0.1 to 3 MPa for 10 min. Subsequently, the vessels were slowly cooled down to ice water, and dehydriding was then accomplished by re-heating at the same temperature. This hydriding-dehydriding treatment was repeated more than ten times.

In addition to the calorimetry at 298 and 323 K, low temperature calorimetry at 273 K, 237 K (Pd black-H), 233K (Pd black-D) and 194.5 K was carried out, respectively by controlling temperatures with a Setaram CS-32 controller under cooling with a liquid nitrogen flow. The variation in the temperature was ±0.01 to ± 0.02 K at all the measurement temperatures.

For the high pressure experiments, it is in general difficult to obtain precise p-c isotherm data even for Pd-H(D) systems, because of the small variations in the high pressures due to the gas valve-handling operations and small variations in temperature of the measuring system, leading to significant errors in hydrogen moles absorbed or desorbed. In this study in order to avoid the difficulty of obtaining H(D)/Pd values at higher pressures, it was assumed that high pressure solubilities coincide with the values obtained by extrapolating from low to high pressure isotherms using a relation of log $f_{H2(D2)}$=-A(T) + B(T)·H(D)/Pd [10,11], where $f_{H2(D2)}$ is the fugacity of gases, A(T) and B(T) are temperature-dependent constants ; by measuring the initial and final equilibrium pressures during the absorption and desorption processes, the H(D)/Pd values were calculated according to the relations. Furthermore, the low temperature calorimetric

measurements with higher $p_{H2(D2)}$ pressures at low temperature are generally difficult [1], because when the reaction valve for $H_2(D_2)$ absorption (introduction) was opened, an instantaneous heat flux was produced from the reference vessel towards the sample vessel before the occurrence of heat flux due to the heat of solution. Conversely, on opening the valve for $H_2(D_2)$ gas desorption (removal), an heat flux in the opposite direction is instantly produced. The origin of the instantaneous heat flux generation on opening the reaction valve for absorption or desorption is unknown, however, it may be associated with the differences in heat conductivity and/or in specific heat between the sample vessel containing Pd and Cu foil samples and the reference vessel containing only Cu foils, i.e., with the difference in heat transfer effects between both the vessels from the gas reservior which is not at the calorimeter temperature. Therefore, these phenomena lead more or less to the errors in enthalpy values derived from the integration of the heat flux vs. time curves.

3. Results and discussion

Figures 1 and 2 show the calorimetrically determined enthalpies for hydride and deuteride formations at different temperatures for Pd-H and Pd-D systems, respectively, together with calculated enthalpies from van't Hoff plots of relative chemical potentials shown in upper part of the same figures.

It can be seen that the calorimetrically determined enthalpies for hydrogen and deuterium absorptions in the β-phase region become less exothermic almost linearly with increasing H and D contents, independently of temperature, and that the linearly decreasing tendencies for both systems are in agreement with the calculated values from van't Hoff plots. The dependence of the present calorimetric enthalpies on H and D concentrations in the range $0.70<H/Pd<0.90$ and $0.60<D/Pd<0.83$ is expressed as :

$$|\Delta H_H| \ (kJ(molH)^{-1}) = 48.06 - 42.39 \cdot H/Pd$$

and

$$|\Delta H_D| \ (kJ(molD)^{-1}) = 44.99 - 41.89 \cdot D/Pd$$

At the same H(D) content, the enthalpies for Pd-H system are a little more exothermic, about 3 $kJ(molH)^{-1}$ than that for Pd-D system. Enthalpies of almost the same magnitude are obtained from desorption data. Compared to the previously determined enthalpies for bulk Pd-H(D) systems [10], there is no marked difference in the magnitude of $\Delta H_{H(D)}$ values within the experimental errors between the bulk Pd and Pd black samples.

Figures 3 and 4 show the corresponding entropies calculated from the relation of $\Delta S_{H(D)} = \Delta H_{H(D)}/T - R\ln p_{H2(D2)}^{1/2}$ for Pd-H and Pd-D systems, respectively, together with values determined from van't Hoff plots. There are scatter in the entropy values, however, it can be seen that the entropies for H and D absorptions have a tendency to decrease gradually with H(D) content independently of temperature. At the same H(D)

content, the entropies for absorption in Pd-H system are a little larger than that for Pd-D system.

References

1. M.Fleishman and S.Pons, J.Electroanal.Chem., 261 (1989) 301. Erratum, 263 (1989) 187.
2. M.Fleishman, S.Pons, M.W.Anderson, L.J.Li and M.Hawkins, J.Electroanal.Chem., 287 (1990) 293.
3. "Frontiers of Cold Fusion, Proc. of ICCF 3, Nagoya 1992", Frontiers Science Series No. 4, ed. H.Ikegami, Universal Academy Press Inc., Tokyo (1993).
4. M.C.H.Mckubre, S.Crouch-Baker, A.M.Riley, S.I.Smedley and F.L.Tanzella, ref.[3], p. 5.
5. E.Storms, ref.[3], p. 21.
6. K.Kunimatsu, N.Hasegawa, A.Kubota, N.Imai, M.Ishikawa, H.Akita and Y.Tsuchida, ref.[3], p. 31.
7. N.Hasegawa, K.Kunimatsu, T.Ohi and T.Terasawa, ref.[3], p. 377.
8. B.Baranowski and R.Wisniewski, Phys.stat.sol., 35 (1969) 593.
9. J.C.Barton, F.A.Lewis and I.Woodward, Trans.Faraday Soc., 59 (1963) 1201.
10. Y.Sakamoto, M.Imoto, K.Takai, T.Yanaru and K.Ohshima, J.Phys : Condensed Matter, 8 (1996) 3229.
11. E.Wicke and G.H.Nernst, Ber.Bunsenges.Phys.Chem., 68 (1964) 224.
12. T.B.Flanagan, W.Luo and J.D.Clewley, J.Less-Common Met., 172-174(1991)42.
13. M.Tkacz and B.Baranowski, Roczniki Chemii Ann.Soc.Chim.Polonorum, 50 (1976) 2159.
14. H.Frieske and E.Wicke, Ber.Bunsenges.Phys.Chem., 77 (1973) 48.
15. Y.Arata and Y.C.Zhang, Proc. Japan Acad., 70B (1994) 106.
16. Y.Arata and Y.C.Zhang, Proc. Japan Acad., 71B (1995) 98.

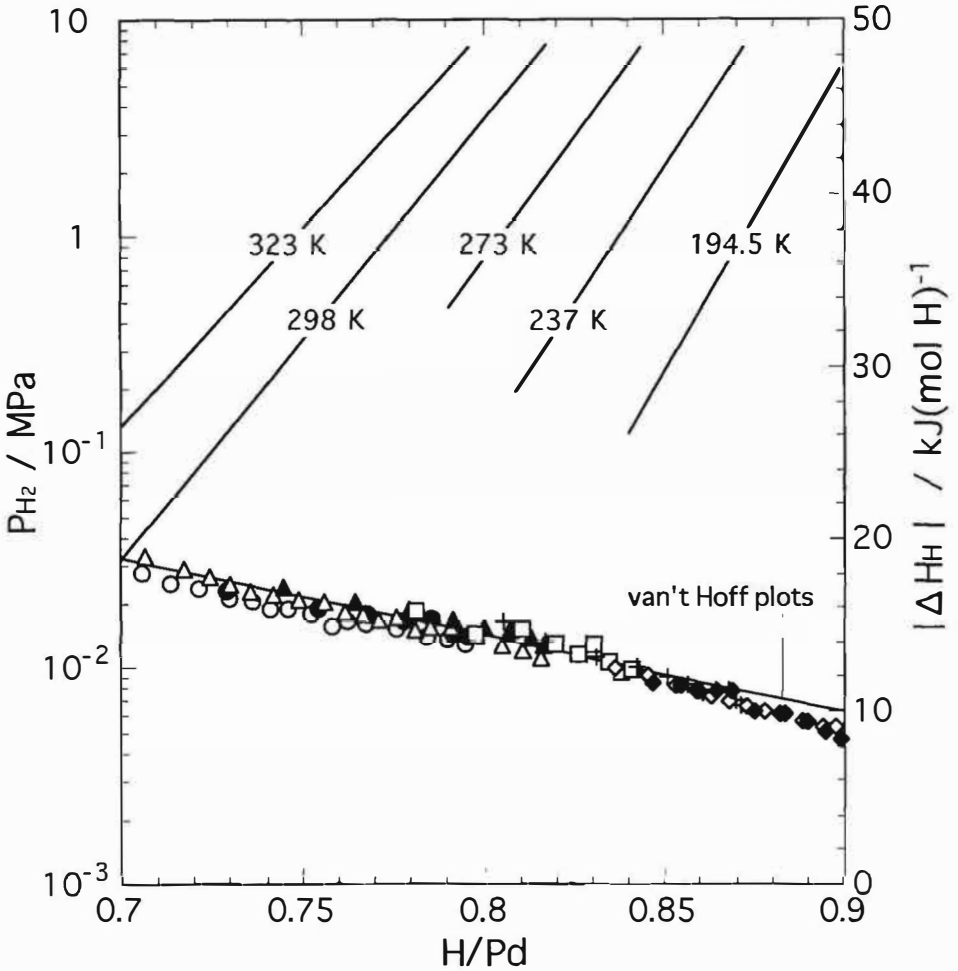

Fig. 1 Calorimetrically determined enthalpies for hydride formation at different temperatures in Pd-H system,together with calculated enthalpies from van't Hoff plots.○,●,323 K,△,▲,298 K,□,273 K,+,237 K,◇,◆,194.5 K (open symbols =absorption,closed symbols=desorption). The p_{H2}-H/Pd isotherms at each temperature[10,11] are shown in the upper part.

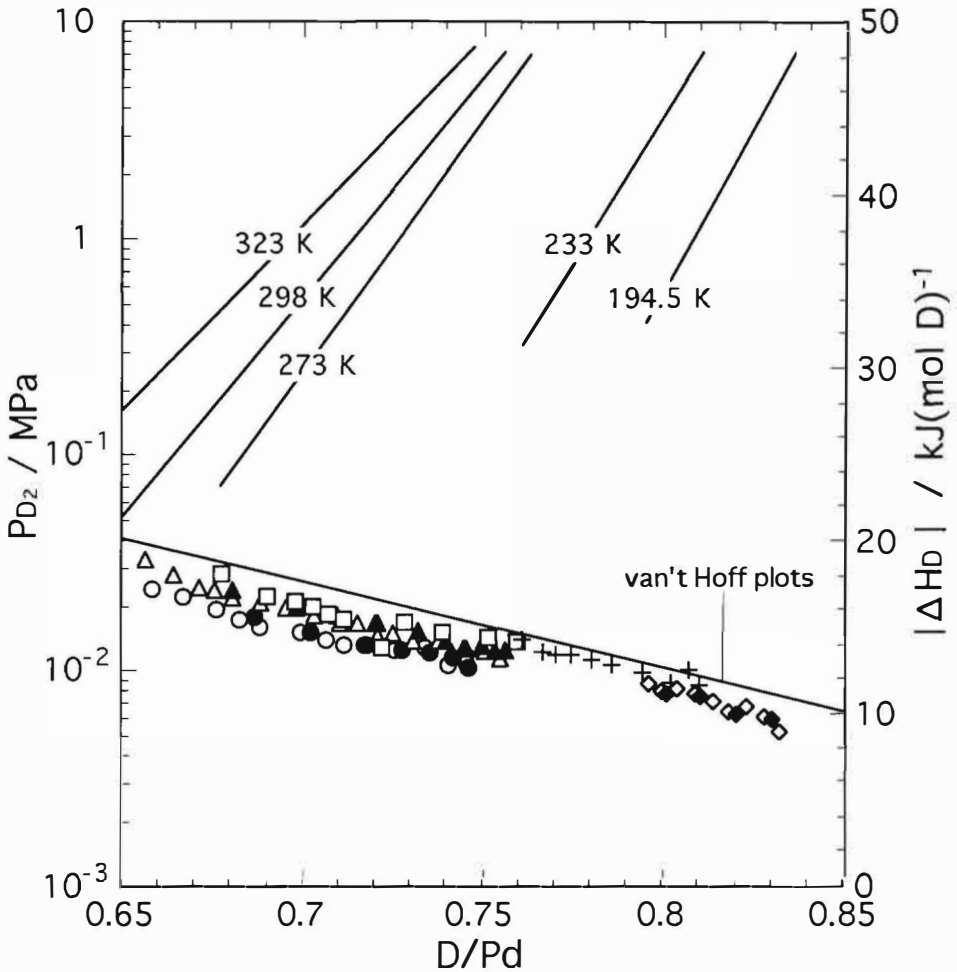

Fig. 2 Calorimetrically determined enthalpies for deuteride formation at different temperatures in Pd-D system,together with calculated enthalpies from van't Hoff plots.○,●,323 K,△,▲,298 K,□,273 K,+,237 K,◇,◆,194.5 K(open symbols =absorption,closed symbols=desorption). The p_{D2}-D/Pd isotherms at each temperature[10,11] are shown in the upper part.

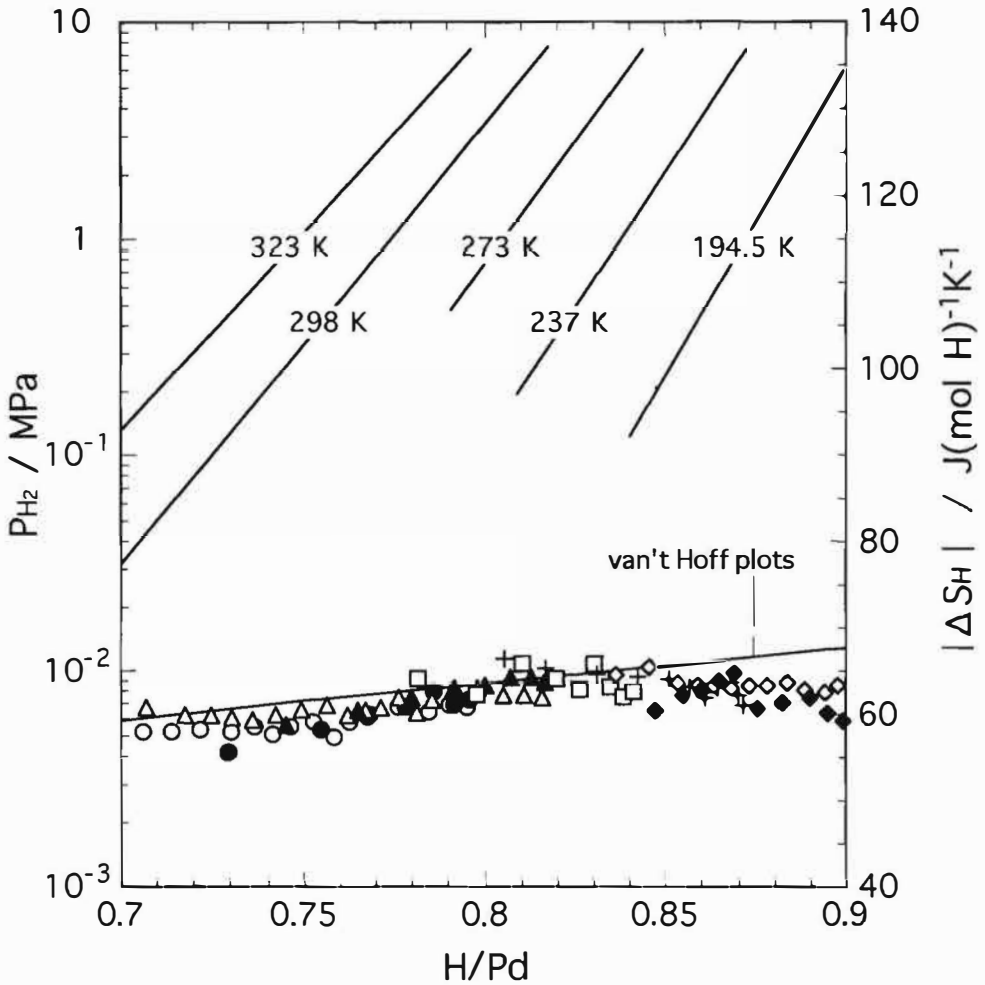

Fig. 3 Relative partial molar entropies for hydride formation at different temperatures in Pd-H system,together with calculated entropies from van't Hoff plots. ○,●, 323 K, △, ▲, 298 K,□,273 K,+,237 K,◇,◆,194.5 K (open symbols=absorption, closed symbols=desorption).The p_{H2}-H/Pd isotherms at each temperature[10,11] are shown in the upper part.

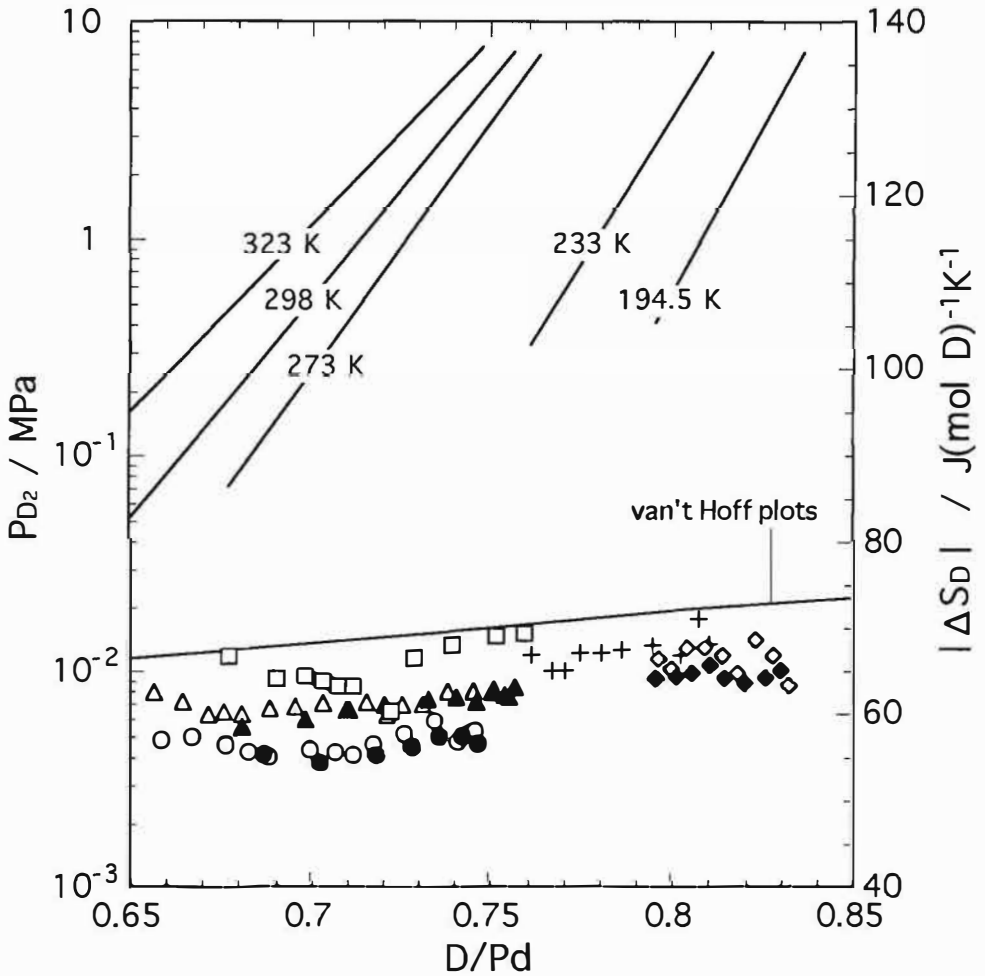

Fig. 4 Relative partial molar entropies for deuteride formation at different temperatures in Pd-D system,together with calculated entropies from van't Hoff plots. ○,●, 323 K, △, ▲, 298 K,□,273 K,+,233 K,◇,◆,194.5 K (open symbols=absorption,closed symbols=desorption).The p_{D2}-D/Pd isotherms at each temperature[10,11] are shown in the upper part.

Click here for a more readable copy of this paper.

PARAMETERS AFFECTING THE LOADING OF HYDROGEN ISOTOPES INTO PALLADIUM CATHODES

F. L. Tanzella, S. Crouch-Baker, A. McKeown*, and M.C.H. McKubre,
M. Williams and S. Wing
SRI International, Menlo Park, CA USA,

*Present Address: University of Strathclyde, Glasgow, Scotland

Abstract

We have tested our new Degree of Loading (DoL) cell design which can be directly transferred to the SRI mass flow calorimeter. We have shown that appropriately prepared Pd cathodes can reach high loadings in this new design and that the cells can be transferred to the calorimeter without degrading the cathode's or cell's performance. In all of the experiments the cathode deloaded at higher current densities, and ostensibly identical cathodes yield significantly different D:Pd loading/current density profiles.

In the new cell design high purity Pd from IMRA Materials and Johnson Matthey have generally loaded better than recent lots of 99.9% Engelhard Pd. Pd that IMRA Materials cast in air with added CaB_6 held its loading best at higher current densities. Electrolyte additives Al, Si, Nd and Sm had no perceptible effect on loading behavior. The regular addition of Cl^- ion, similar to what might happen when topping up open cells, can increase or maintain loading. The presence of Cu is detrimental to good loading.

Electrochemical surface potential (E_{surf}) measurements made in H_2SO_4 yield potentials similar to those predicted by high pressure H_2 loading experiments. LiOH (LiOD) significantly affects E_{surf} but that effect may be deconvolved to allow an estimate of the surface loading in alkaline electrolytes.

1. Introduction

Our laboratory has been studying[1-6] the electrochemical deuterium loading characteristics of palladium for over 7 years. This is in conjunction with our program to measure for anomalous heat effects reported to occur in such experiments. We have measured[1-3] these anomalous effects, excess power, several times in our mass flow calorimeters. We have found certain D:Pd loading levels and current protocol parameters necessary, but not sufficient, to yield excess power. We use a pre-calorimeter trial, which we refer to as a degree-of-loading (DoL) "farm", to ascertain which cathodes can achieve these loading/current criteria. We observe a lack of reproducibility among replicates which we ascribe to metallurgical, chemical, or physical differences presently beyond our control.

The near-surface loading of hydrogen isotopes into Pd will affect the bulk crystalline loading, $H(D):Pd_{bulk}$, as well as the Pd surface potential. Fleischmann[7] and Storms[8] have separately reported using Pd potentials as a predictor of oncoming excess power in these experiments. We report here our efforts to measure Pd surface potentials (E_{surf}) and correlate those potential with $H(D):Pd_{bulk}$.

As shown in our earlier reports we have found three necessary, but not sufficient, simultaneous conditions for production of excess power in the D/Pd electrolysis system:

- High D:Pd loading (>0.89)
- High current densities (> 300 mA-cm^2)
- Long times at loading

Most of our early successful experiments used a single lot of Pd obtained from Engelhard designated as E#1. We found our original preparation protocol yielded more reproducible, better loading, when compared to using Pd as received. These early cells also used a relatively small electrode chamber with rather uniform current distribution. The original calorimeter cell design was modified to accommodate larger cathodes, larger inventory of electrolyte, more efficient heat transfer,

and special safety procedures. Loading results in this modified design were poor. We also attempted to transfer already-loaded cathodes from small DoL cells into the larger calorimeter cells, with disappointing results. New calorimeter cells were redesigned with an electrode chamber similar to that used in earlier experiments. These cells were operated thermodynamically closed with internal recombiner catalysts and capable of withstanding 5 atm. pressure for calorimetric reasons.

Based on reports[7,8] of using cell potential measurements to predict excess power production, we devised experiments to correlate cell voltage, surface potential, and bulk loading measurements. We used results of Baranowski[9] to correlate surface potential (E_{surf}) with surface loading ($H(D):Pd_{surf}$).

2. Experimental

Figure 1 shows a schematic diagram of the DoL cell used in this program. The electrode chamber and experimental protocol are similar to those described earlier.[1-3]

Electrolyte is added to the cell only after potential is applied to prevent oxidation of the pure Pd. The initial current density is chosen such that $17 \leq \bar{i} \leq 35$ mA-cm^{-2}. The cell is then flushed with 5 volumes of $H_2(D_2)$ or N_2. To ascertain steady-state loading measurements, the current is stepped to high values of $\bar{i}$ in regular intervals. The length of time at each current is chosen to minimize de-loading at higher current densities. After $H(D):Pd_{max}$ is achieved in the first loading cycle the cell current is reduced to the minimum current density and an automated current step protocol is initiated. This protocol has a repeat period of 48-96 hours. Table 1 shows a typical current step protocol for a 1 mm x 30 mm cathode, where positive currents are cathodic and negative currents anodic.

Table 1
Current Step Protocol

Time (hr)	0	0.5	24	32	40	48	56	64	72	80	88	96 = 0
$\bar{i}$ (mA/cm^2)	-35	35	50	100	200	300	400	500	750	1000	35	-35

Sometimes the length of time at higher current densities is reduced to minimize deloading.

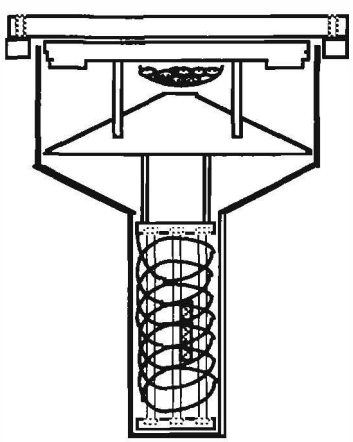

Figure 1. Degree of Loading Cell

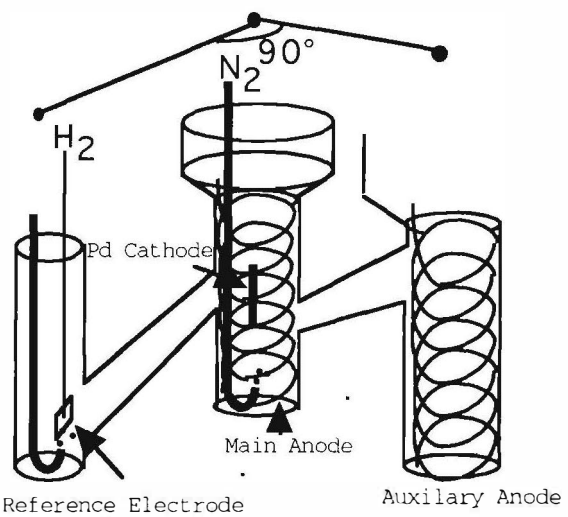

Figure 2. Electrochemical Surface Potential Measurement Cell

The Pd cathode rods, either 1, 2, or 3 mm diameter, were 30 mm long. Engelhard 99.9% Pd was machined from either 3.2 mm diameter to 3.0 mm or from 3.0 mm dia. to 2.8 mm diameter. No surface machining was applied to the Pd from other sources. Cathodes larger than 2 mm dia. usually had notches machined near each end to accept Pt wire contacts. The experimental data acquisition system has been described elsewhere. Cathodes were prepared from Pd supplied by Engelhard (E#n, where n is our lot number), IMRA Materials (I/M) or Johnson Matthey (J/M). DoL cells were operated in an air-cooled safety enclosure containing a quartz double-bubbler filled with D_2O

connected to the cell's gas outlet tube to minimize contamination from moist air. The gas inlet tube was stoppered with a rubber septum and used to make gas or liquid additions.

Figure 2 shows the three-compartment cell used for electrochemical surface potential measurements. Two quartz cylindrical cells, 25 mm dia. x 70 mm tall were connected together with a quartz tube. The reference electrode compartment is a quartz tube, 10 mm dia. x 70 mm tall attached at right angle to the central electrolysis chamber. The connecting tubes have vertical slopes as shown in the figure to minimize O_2 contamination in the reference compartment and the main electrolysis chamber during the surface potential measurement. The cell was sealed with two H_2O-filled double bubblers. H_2 was continually bubbled over the Pt reference electrode (5 x 5 x 0.1 mm), which had been platinized for 20 seconds at 50 mA in a 2% H_2PtCl_6 solution. N_2 continually flushed O_2 out of the central electrolysis chamber. This cell design was chosen as analogous to the method for reference potential measurement used in the DoL cells which cannot accommodate a Luggin capillary.

Johnson Matthey (J/M) special lot "Z" (low Pt-group metal) 1 mm wire was cut to 10 mm long and solvent cleaned for this experiment. The cathode was annealed, Pt lead wires attached and acid etched as described in earlier reports.[1-3] A 24-hour repeating automatic current protocol similar to that described for the DoL cell was employed. Every hour the cell was set to open circuit for 2 seconds and the potential between the hydrogen electrode and the Pd cathode was recorded at ~ 25 ms intervals. Fifteen minutes before each open circuit decay the power supply anode connection was moved from the central anode to the auxiliary anode using a computer controlled 40 A mechanical relay. This was done to allow the N_2 to purge the O_2 from the main electrolysis chamber. The data acquisition system was similar to that used for the DoL cells.

A DoL cell used for empirical E_{surf} measurements had D_2 bubbled over a platinized Pt hydrogen reference placed directly below the Pd cathode. The potential was measured without the use of an auxiliary anode.

3. Results

Since we are unable to design experiments which are guaranteed to yield high loading we perform replicates of those experiments which we feel are most likely to do so. From these replicates we choose the cells which best meet our three criteria and transfer them to the calorimeter. This requires us to load Pd cathodes in the DoL farm using the identical cell used in the calorimeter. We therefore tested different Pd sources for cathodes that can load well in a closed cell, with a recombiner catalyst at room temperature.

There are three criteria which must be met to assure the viability of the DoL farm concept: (1) The cathode must survive extended periods, up to 120 minutes, of open-circuit without degrading subsequent loading performance. (2) Cathodes must load well at room temperature in a closed cell with a recombiner catalyst. (3) The cell must survive the physical transfer from the DoL farm into the calorimeter without degrading its performance.

Testing the first criterion, Figure 3 shows a typical loading curve (R/R_O vs time) for a 3 mm diameter cathode under three different current protocols designed to test a cathode's sensitivity to open-circuit. The three current protocols used are (1) a 5 hour open circuit step; (2) a 4.5 hour open circuit step immediately before a 0.5 hour anodic strip; and (3) a 0.5 hour anodic strip. The open-circuit step does not degrade and probably enhances the cathode's subsequent loading, at least for the next few cycles.

Although this experiment used E#5 Pd, 3 mm diameter x 30 mm long annealed before use, we have found this result to hold true for all of the Pd that we have tested. This protocol may allow surface impurities to desorb slowly without disturbing the Pd near-surface structure. Alternatively, absorbed D may relax slowly until $D:Pd_{bulk}$ and $D:Pd_{surf}$ are equal, minimizing stress on the Pd grain structure. We are not yet able to distinguish the effects of these and any other possible mechanism initiated by an open-circuit step.

Figure 4 shows the results of our attempts to load a cathode of I/M#1 Pd (cast in air with CaB_6 added), 1 mm diameter x 30 mm long, with D to D:Pd > 0.95 ($R/R_O < 1.6$). This experiment verifies

that we can load a Pd cathode to high loading in the new DoL cell for transfer into the calorimeter. However, the cathode deloads at extended times and at higher current densities. It is encouraging that the loading of ~ 0.95 is maintained at ~ 400 mA-cm^{-2}, which implies that other cathodes from this lot should be able to sustain high loading at moderate current densities for extended periods.

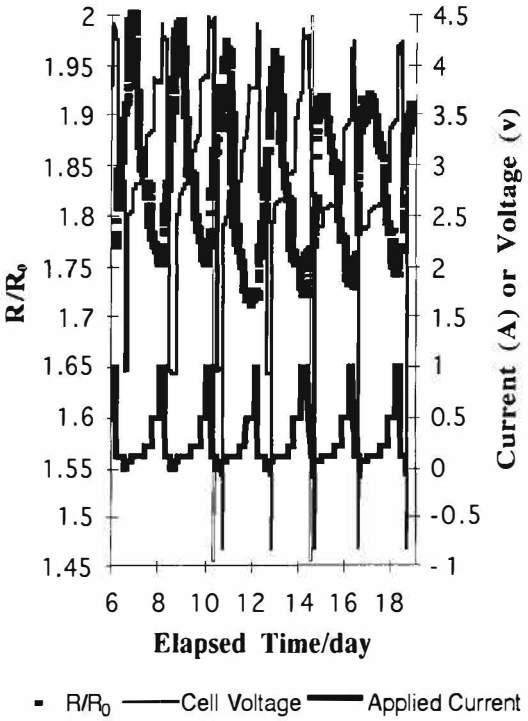

Figure 3. Effect of open-circuit and anodic strip protocols on loading

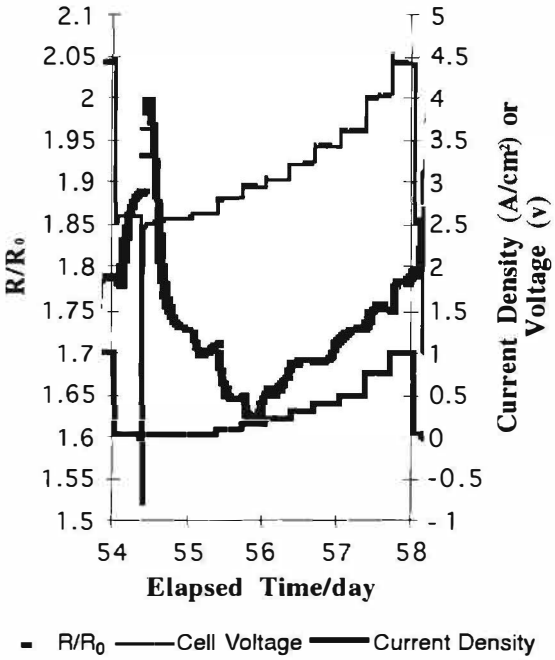

Figure 4. Typical loading curve for a well loaded Pd cathode

In another experiment, cathodes identical to those used for the experiment shown in Figure 4 with a 1 M LiOD electrolyte with no additives, yielded significantly different D:Pd$_{max}$ results. Occasionally the loading for the poorly-loaded Pd increases with current such that cathodes which had significantly different loading at lower current densities have the same mediocre, but stable loading, at some higher current. Loading performance is quite reproducible over several cycles within the same experiment. The good individual reproducibility allows us to draw conclusions about different parameters by comparing the best loading performance from each set of replicates or about different additives by making additions during experiments.

Next, we studied Pd cathodes of a different source and treatment, all performed in 1M LiOD without electrolyte additives. The results are shown in Table 2. Obviously in this cell design, I/M #1, I/M #2 and J/M "Z" are better than E#5 for initial loading. However I/M #1 holds its loading best at higher current densities. Also we found earlier that annealing and etching the Engelhard Pd cathodes in our laboratory was necessary for good loading but similar processing by IMRA Materials at the time of manufacture made further processing at SRI unnecessary and, in some cases undesirable.

Having established the baseline performance of different cathodes in pure LiOD we compared this to the performance found using electrolytes containing 200 ppm Al, shown in Table 3. This Al in LiOD electrolytes shows no beneficial effect on any of the cathodes tested in the new cell design when compared with LiOD. Also shown is a comparison of loading results in the old cell designs using Engelhard cathodes with LiOD and Al, where the E#3 cathode loaded very well. Dissolved Al usually improved and never diminished the loading in the old cell design.

Table 2
Different Pd Sources, No Additives

Sample	Pd	D:$Pd_{max}/\bar{i}$ (mA-cm^{-2})	D:Pd @ 300 mA-cm^{-2}
AA5	E#5, 3 x 30 m, anneal, etch.	0.93/300	0.93
V4	I/M#1*, 1 x 30 mm, etch	> 0.95/100	0.93
X3	I/M#2*, 1 x 30 mm	> 0.95/200	0.9
Y6	J/M ("Z") 1 x 30 mm, etch	0.95/150	0.94

* Annealed and etched by manufacturer

Table 3
Effect of Al in Electrolyte

Sample	Pd Source	Additive	D:$Pd_{max}/\bar{i}$ mA cm^{-2}	D:Pd @ 300 mA cm^{-2}
AA5	Eng. #5	--	0.93/300	0.93
U5	Eng. #5	Al	0.92/100	0.88
V4	I/M #1	--	> 0.95/100	0.93
U3	I/M #1	Al	0.95/100	< 0.88
V2	J/M "Z"	--	0.95/150	0.93
V3	J/M "Z"	Al	0.92/100	0.8
S2†	Eng. #3	Al	0.97/160	0.93
S4	Eng. #5	Al	0.93/80	0.91

Old Cell Design

Table 4 summarizes the effect of some dissolved species and some *in-situ* additions on cathode loading. The Rare Earth elements Sm and Nd were added at the suggestion of Professor Hagelstein of MIT in hopes of depositing them onto the Pd to yield anomalous radiation or thermal effects. The presence of these metals, attached to the Pt anode, had no significant effect on loading performance. Experiments U3 and U2 had ~ 200 ppm Al dissolved in the electrolyte at the outset and both cathodes had loaded to D:Pd_{max} = 0.95. On day 21 of the experiment ~ 1000 ppm Si and ~ 2000 ppm Cu were added to cells U3 and U2, respectively. The Si addition had no significant effect on the loading performance of the U3 experiment while the Cu addition reduced D:Pd_{max} = 0.91.

Open cells may yield higher loading than those in closed cells due to Cl^- and other ion additions during the D_2O top-up which may contain impurities leached from the storage bottle. Experiment X1 had run with no electrolyte additives until day 50 when 1 ppm LiCl was added, whereafter the maximum loading increased from D:Pd = 0.9 to ~ 0.93 after the Cl^- addition, but diminished back to 0.9 after 3 current-step cycles.

Table 4
Effect of Various Additives

Sample	Pd	Additive	D:$Pd_{max}/\bar{i}$ mA cm^{-2}	D:Pd @ 500 mA cm^{-2}
Z2	J/M "Z", anneal, etch	--	0.91/500	0.91
Z4	J/M "Z", anneal, etch	Sm	0.9/500	0.9
Z5	J/M "Z", anneal, etch	Nd	0.9/500	0.9
U3	I/M #1*	Al, Si†	0.95/100	< 0.88
U2	I/M #1*	Al, Cu†	0.91/100	< 0.85
X3	I/M #2*	--	> 0.95/200	0.9
X1	I/M #2*	Cl^-†	0.93/200	0.88

*Annealed and etched by manufacturer

†Added during experiment

Material Science Studies

Thermodynamically relevant electrochemical surface potentials (E_{surf}) can be used to estimate surface loading ($H:Pd_{surf}$) in this system. A good estimate of $H:Pd_{surf}$ can be used to estimate $H:Pd_{bulk}$ at steady state cathode loading without intrusive axial resistance measurement. We designed a cell (see Figure 2) to simultaneously measure E_{surf} and $H:Pd_{bulk}$. The overpotentials affecting the measurement have been mathematically eliminated using the current interruption method. We used H_2SO_4 electrolyte, with no dissolved cations or metals, to minimize interfering reactions on the Pd surface that could change E_{surf} and to assure the attainment of high loading in H_2O.

The electrochemical surface potential of the Pd cathode, E_{surf}, is reported relative to the standard hydrogen electrode (SHE). E_{surf} is positive when $H:Pd < 0.7$ and negative when $H:Pd > 0.8$ as shown by Lewis.[10] For ease of presentation $-E_{surf}$ is plotted since only the region where $H:Pd > 0.8$ is shown. Figure 5 shows $-E_{surf}$, $D:Pd_{bulk}$, and i measured on a J/M "Z" 1 mm diameter x 10 mm long, cathode in 0.1 M H_2SO_4. The relatively reproducible $H:Pd_{bulk}$ reaches a maximum of ~ 0.93 at ~ 0.9 A cm^{-2}. The most negative potential obtained at $H:Pd_{max}$ (0.93) was E_{surf} = -0.12V vs. standard hydrogen electrode (SHE). After 5 cm^3 of electrolyte was removed and replaced with 5 cm^3 of 0.1 M Li_2SO_4, no effect attributed to the Li^+ ion, including simple Li adsorption, was seen during the 36 hour remainder of this experiment. However, the addition caused the cathode to load more poorly during the remaining two current step cycles. Figure 5 shows $-E_{surf}$ tracking $H:Pd_{bulk}$ at this lower value.

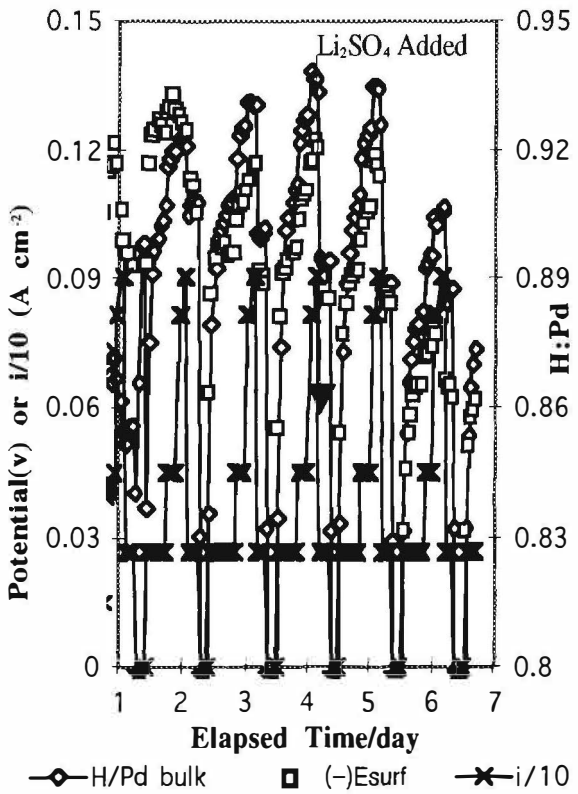

Figure 5. Correlation of surface potential with H:Pd in 0.1 M H_2SO_4

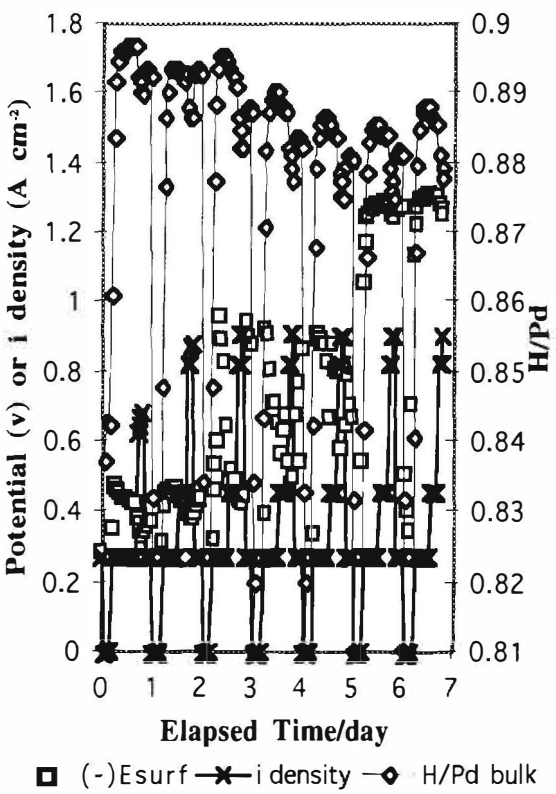

Figure 6. Correlation of surface potential with H:Pd in 0.2 M LiOH

At the experiment's termination the electrolyte was replaced with 0.2 M LiOH. The results of this new experiment are shown in Figure 6. Using the same current-step cycles the maximum cathode loading is ~ 0.9. The largest negative value of E_{surf} obtained was -0.4V for the first two current cycles then alternated between -0.4V and -0.9V, and reached a stable value of -1.3 V when $H:Pd_{bulk}$ = 0.89. E_{surf} varied from -1.15 V to -1.3V tracking $H:Pd_{bulk}$ as it varied from ~0.85 to ~ 0.89 after cycle 4. These results suggest a surface film formed during the electrolyte replacement when the cathode was exposed to air, probably oxide and/or hydroxides of surface lithium. Another surface

film formed gradually, or replaced the first, starting with the third current cycle. This latter "film" may be Li absorption into the Pd cathode.

A technically simpler experiment was performed in a modified cell, where *in-situ* E_{surf} measurements were made in 1 M LiOD. Measuring the potential at the end of each current step to assure the attainment of the $D:Pd_{bulk}$ steady state, the maximum loading obtained was ~ 0.91 and most negative $E_{surf} \approx -1.02$ V. These raw values of E_{surf} can be empirically modified to approximate the potentials predicted for E_{surf} versus D:Pd (see below).

4. Conclusions

We have designed, constructed, and run on the bench several cells to measure D:Pd loading and have successfully transferred these cells to our mass-flow calorimeter system. We have met the criteria necessary to assure the viability of the DoL farm concept. While testing the effect of open-circuit we have shown that a combination of open-circuit and anodic strip steps generally yields improved cathode loading.

We have verified that different types of Pd have different loading characteristics in our new cell design and that Pd from specific sources load differently in the new cell design when compared to performance in the original cell design. I/M #1, which was cast in air with CaB_6 added to the melt, held its loading to higher current densities than did I/M #2, which was cast in *vacuo* with no additives although both were processed from the same high-purity Pd powder. Although vacuum processing may introduce deleterious impurities, it is more likely that air processing was beneficial. High temperature air processing may form volatile oxides of deleterious impurities which volatilize. A more subtle explanation may involve CaB_6 particles acting as inter-granular or intra-granular stress-relief facilitators at high D flux (large $\bar{i}$).

We have also shown that high purity Pd (I/M #1, I/M #2 and J/M "Z") loads better than 99.9% pure Pd from Engelhard. Loading performance for the high purity Pd is not enhanced by further annealing immediately before use. Poor replicability among ostensibly identical experiments remains an important problem. This may be due to irreproducible metallurgy and/or random surface contamination along the length of Pd rods or imperceptible differences in cell preparation procedures.

In the series of experiments described here, loading performance in 1 M LiOD electrolyte with 200 ppm (molar) Al was no better and sometimes worse when compared to those performed in pure LiOD. Of the electrolyte additives tested, either present at the experiment's commencement or added *in situ*, only Cl^- ion was found to be beneficial, yielding a temporary loading increase. This Cl^- ion addition may unintentionally take place during top-up of open cells. The addition of Cu ions was detrimental to loading while Nd, Sm, and Si had no observed effect on performance.

We have measured the electrochemical surface potential (E_{surf}) and $H:Pd_{bulk}$ (using axial resistance measurement) of a Pd cathode electrolyzed in H_2SO_4 and LiOH. At loadings of H:Pd < 0.8 the potential versus loading curve reproduces that reported by Lewis.[10] Using recent data from Baranowski[9] for H:Pd vs $[H_2]$, hydrogen fugacity (f(H)) versus H:Pd curves have been generated. Using the Nernst equation the $H:Pd/E_{surf}$ relationship can be estimated and fit to a third order equation:

$$H:Pd_{surf} = 0.727 - 1.78 * E_{surf} - 0.29 (E_{surf})^2 + 9.814 (E_{surf})^3$$

We found $H:Pd_{surf} > H:Pd_{bulk}$ during increasing loading and at high loading, but at steady state loadings of D:Pd < 0.94 the bulk and surface loadings were found to be sensibly the same in the absence of reducible cations.

The addition of Li^+ ions to an acid electrolyte yielded poorer cathode hydrogen loading, possibly due to disruption of a beneficial film already formed on the Pd surface, but did not otherwise affect E_{surf}. Exposing the cathode to air during electrolyte transfer caused a significant change (-300 mV) to the Pd surface potential, possibly due to the formation of a stable oxide or hydroxide of lithium. Continued cathodic electrolysis yields the slow (72-hour) formation of a new surface state which changed the potential by -1.2V relative to that measured in acid. Assuming that Li has diffused in the Pd cathode this new potential may be due to a Pd Lix/H surface reaction or a mixed potential of

the Pd/H and Li/H reactions in OH^-. We hope to identify the species and/or surface states which correspond to this measured E_{surf} in future studies.

We have also measured E_{surf} in 1 M LiOD in a modified version of our DoL cell. The stable measured potential E_{meas} (- 1V @ D:Pd = 0.91) after several loading cycles was 900 mV more negative than the E_{surf} predicted in the absence of reducing cations. Also, since at high current densities the D_2 bubbling does not completely flush the O_2 from the cathodes electrolyte environment, E_{meas} contains a reproducible current-dependent voltage offset. The equation

$$E_{surf} = E_{meas} + 0.89 + 0.05\ (i)\ (D{:}Pd_{bulk} > 0.88)$$

where i is the positive cathodic current in A, yields values of E_{surf} comparable to those measured in H_2SO_4. These can be used to compare $D{:}Pd_{surf}$ to $D{:}Pd_{bulk}$ in order to predict which Pd cathodes are capable of achieving high bulk loading with a chemically clean surface. We hope to also identify the reactions and/or surface states from which these surface potential arise. In sum, we have been able to correlate measured electrochemical surface potentials with bulk loading in the Pd electrolysis system in H_2SO_4, LiOH and LiOD electrolytes.

Acknowledgments

We gratefully acknowledge the financial support and collaborative research support provided by the New Energy and Industrial Technology Development Organization, the Institute of Applied Energy, and the New Hydrogen Energy Laboratory (Sapporo). We are also grateful to the IMRA Materials Laboratory and the IMRA Japan Laboratory for supplying much of the Pd used in these studies.

References

1. Proceedings of the First International Conference on Cold Fusion (ICCF1), National Cold Fusion Institute, Salt Lake City, UT, 1990, p. 20.
2. Proceedings of the Second International Conference on Cold Fusion (ICCF2),"The Science of Cold Fusion," Eds. T. Bressani, E. Del Giudice, and G. Preparata, Conference Proceedings Vol. 33, Italian Physical Society, Bologna, 1992, p. 419.
3. Proceedings of the Third International Conference on Cold Fusion (ICCF3), "Frontiers of Cold Fusion", ed. H. Ikegami, Universal Academy Press, Inc., Tokyo. p. 5 (1993).
4. Proceedings of the Fourth International Conference on Cold Fusion (ICCF4), EPRI TR-104188, Maui, Hawaii (1993).
5. Proceedings of the Fifth International Conference on Cold Fusion (ICCF5), Monte Carlo, Monaco (1995).
6. M. McKubre, S. Crouch-Baker, R. Rocha-Filho, S. Smedley, F. Tanzella, T. Passell, and J. Santucci "Isothermal Flow Calorimetric Investigations of the D/Pd System" J. Electroanal. Chem., 368 (1994) p. 55.
7. Personal Communication
8. Personnel Communication
9. B. Baranowski, "Metal-Hydrogen Systems at High Hydrogen Pressures", Hydrogen in Metals II, ed. Alefeld and Volkl, Topics in Applied Physics, vol. 29, p. 157, Springer-Verlag, Berlin (1978).
10. F. Lewis "The Palladium Hydrogen System", Academic Press, London (1967).

Material Science Studies

Sustentation of Higher Deuterium Loading Ratio in Palladium

Toshihisa TERAZAWA, Toshiyuki SANO, Yoshihisa KAMIYA,
Yosuke OYABE and Tamio OHI

IMRA MATERIAL R&D CO., LTD.
5-50 Hachiken-cho, Kariya, Aichi 448, JAPAN

Abstract

Higher deuterium loading and its sustentation are considered to be a key issue for generating excess heat on "cold fusion". In our previous works, several conditions to achieve a high deuterium loading ratio of palladium were found. It is, however, often observed that the deuterium loading ratio starts decreasing after reaching a maximum value under a same electrolytic condition, and the maximum loading ratio could not be sustained for a necessary period of time to come up to observe any excess heat.

To maintain such achieved high loading ratio, we have devised and confirmed a new technique based on a finding that a cell voltage during the electrolysis is one of the most important key factors to control such deloading.

As the result of our new method, when the cell voltage is kept constant, accordingly electrolytic currents increase at a certain rate, the maximum deuterium loading can be maintained for more than 200 hours. It is found that the decrease in cell voltages is mostly due to the decrease in the deuterium overpotential, by measuring the deuterium overpotential on a palladium cathode.

1. Introduction

M. McKubre and coworkers of SRI [1] reported necessary conditions for the reproducibility of excess heat with their empirical formula. In our previous works [2], two kinds of palladium surface treatments were found to be effective to increase the deuterium loading ratio. One is by etching a palladium rod with aqua regia, and the other is by annealing it under a vacuum. After either/both of these conditionings, a loading ratio as high as D/Pd = 0.95 was achieved by our "step-up current" electrolysis method.

It is, however, often observed that the loaded deuterium start deloading after

reaching a maximum loading ratio if the same current density is kept. Figure 1 shows a typical example. Therefore, the higher loading ratio could not be sustained for a necessary period of time to come up to observe any excess heat generation.

The present paper reports on studies on new techniques that make it possible to maintain the achieved high loading ratio and on the primary factors of which lead to such deloading.

2. Experimental

2.1 Method to Suppress Deloading

Figure 2 shows changes of a cell voltage (the voltage between the anode and the cathode), and the electric resistance ratio of the palladium rod cathode during the electrolysis. As already mentioned, the cell voltage is observed to decrease, after reaching a maximum cell voltage with each current density which is kept constant. And the deuterium loading ratio is observed to decrease in accordance with the cell voltage. It is consider that the cell voltage during the electrolysis is one of the key factors to control the deloading, and two kinds of new technique to hold the cell voltage constant have been devised. The schematic figures to explain our new methods are shown in Fig.3.

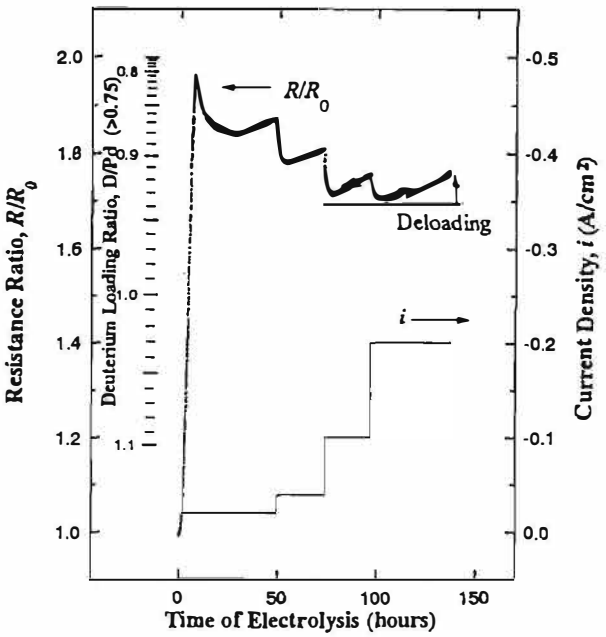

Fig. 1. Changes of the resistance ratio of a palladium cathode and the step-up current density during the electrolysis of 1M-LiOD at 298 K.

Pd cathode: 2 mm dia. and 50 mm length

Etched in HCl/HNO_3 (4:1)

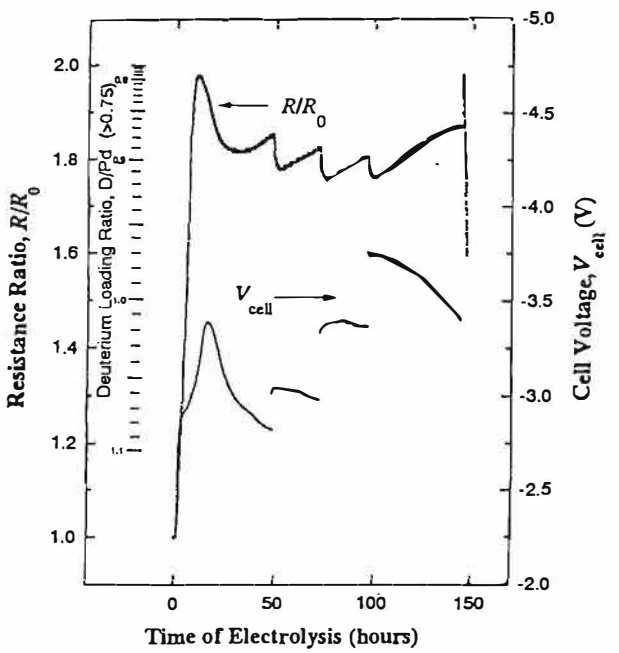

Fig. 2. Changes of a cell voltage during the electrolysis of 1M-LiOD.

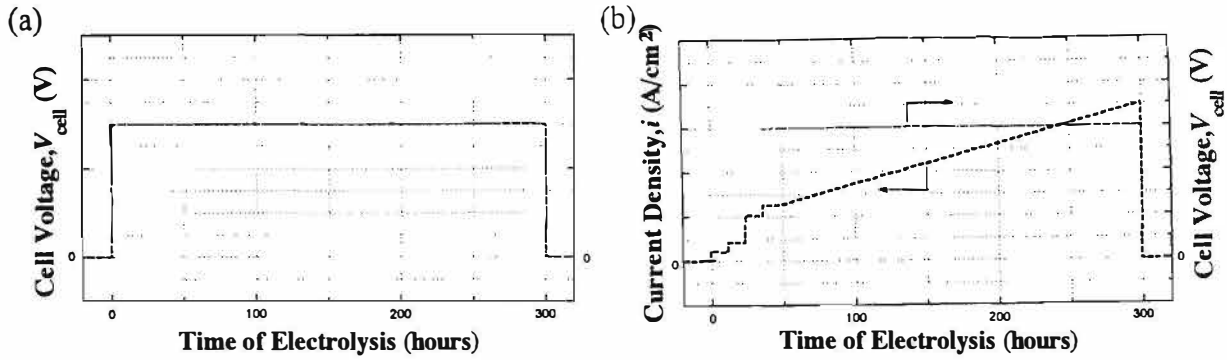

Fig. 3. Schematic figures to explain our new methods:
(a) *Full constant cell voltage electrolysis* and (b) *Step-up and ramp current electrolysis*

Method 1: *Full constant cell voltage electrolysis*

The predesigned cell voltage is applied at the start of the electrolysis and is kept constant.

Method 2: *Step-up and ramp current electrolysis*

After the maximum loading ratio is attained by the "step-up" current electrolysis, the cell voltage is kept constant, and accordingly the electrolytic currents increase at a certain rate under the constant cell voltage.

2.2 Experimental Confirmation

Deuterium loading into a palladium rod was performed by electrolysis in an open cell. Figures 4 and 5 show the electrolytic cell and the detailed configuration of electrodes used in the loading experiments detail, respectively.

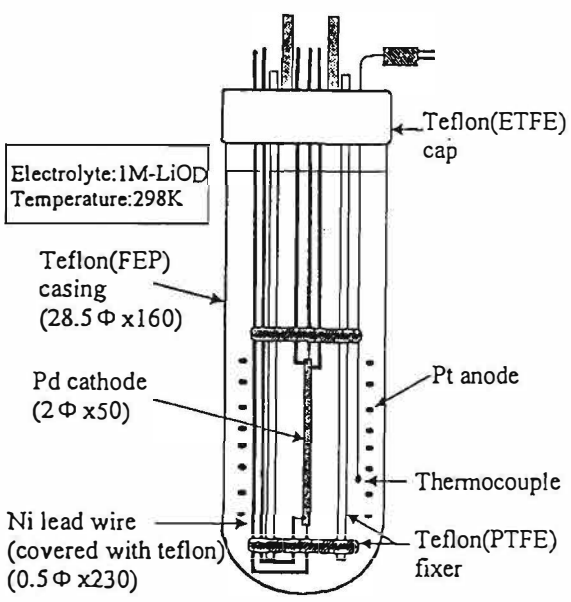

Fig. 4. Electrolytic cell for the palladium resistance measurement.

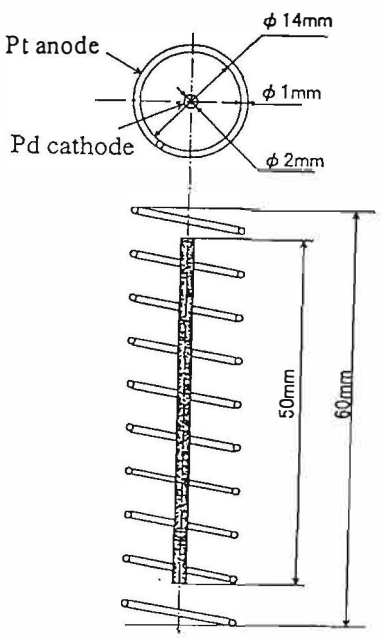

Fig. 5. Detailed configuration of the electrodes.

Raw material	Purity of palladium: 99.95% up
Casting	Melted under vacuum to form a rod of 16mm in dia.
↓ Homogenizing	Annealed under vacuum at 750℃ for 1 hour
↓ Swaging	Cold-worked to 10mm in dia.
↓ Annealing	Annealed under vacuum at 750 ℃ for 1 hour
↓ Swaging	Cold-worked to 2mm in dia.
↓ Cutting	Size: 2mm in dia. and 50mm in length
↓ Annealing	Annealed under vacuum at 850℃ for 4 hour
↓ Polishing	Polished with diamond slurry for 30 min.
↓ Etching	Etched in HCl/HNO_3 (4:1) for 10 min. at 20℃
↓ Degassing	Degassed in furnace for 24 hours at 200℃

Fig. 6. Working processes of palladium cathodes.

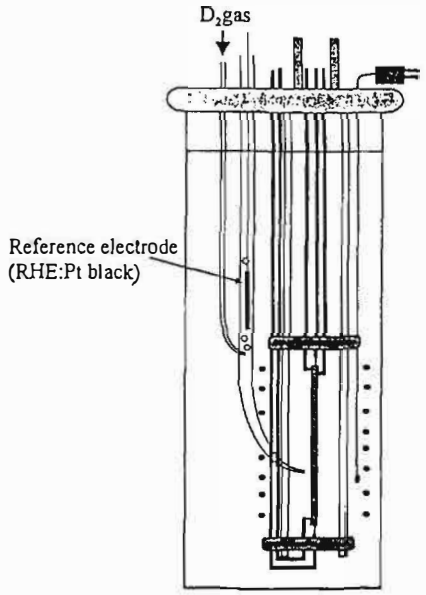

Fig. 7. Schematic electrolytic cell for measuring the electrode potential on the palladium.

Working processes of palladium cathodes are shown in Fig. 6. The experiments were carried out with palladium rods etched with aqua regia for 10 min. at 293K under a cathodic condition, because the rods could reach higher loading ratios above 0.90. The rods were 2 mm in diameter and 50 mm in length. The deuterium loading ratios were determined by the resistance method, whose details were given in reference [2].

The full constant cell voltage electrolysis was accomplished by employing a potentiostat/galvanostat (Hokuto Denko Co., Ltd. , HA-301). For the step-up and ramp current electrolysis a function generator (Hokuto Denko Co., Ltd. , HB-105) was employed. The ramp rate was determined in reference to the constant cell voltage during the electrolysis.

2.3 Measuring Ohmic Drop and Deuterium Overpotential

The ohmic drop between the anode and the cathode was measured by the current interruption method. To measure the electrode potential, RD(H)E was installed as a reference electrode in the cell without any structural change as shown in Fig. 7. A platinum black electrode with bubbling D_2 gas in a Luggin capillary as an RDE located near by the palladium cathode. The deuterium overpotential on the palladium cathode was approximately determined by subtracting the ohmic drop from the electrode potential.

3. Results and Discussion

3.1 Full Constant Cell Voltage Electrolysis

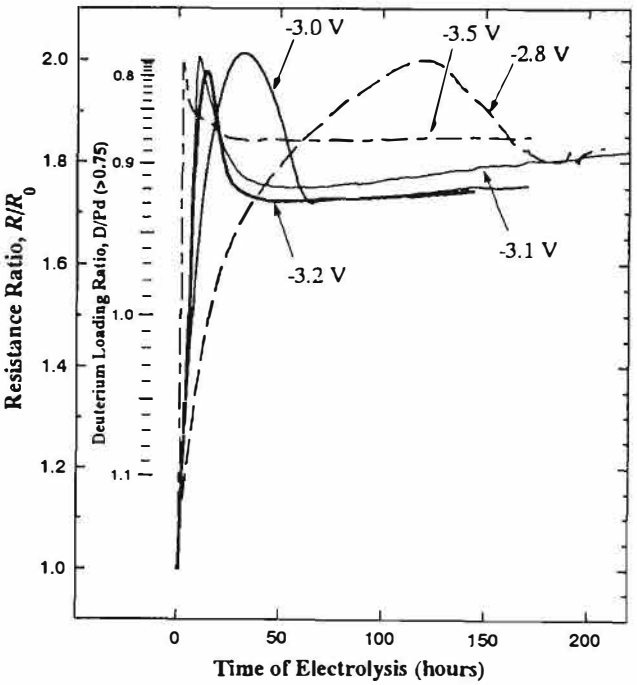

Fig. 8. Changes of the resistance ratios (R/R_0) with various fixed cell voltages.

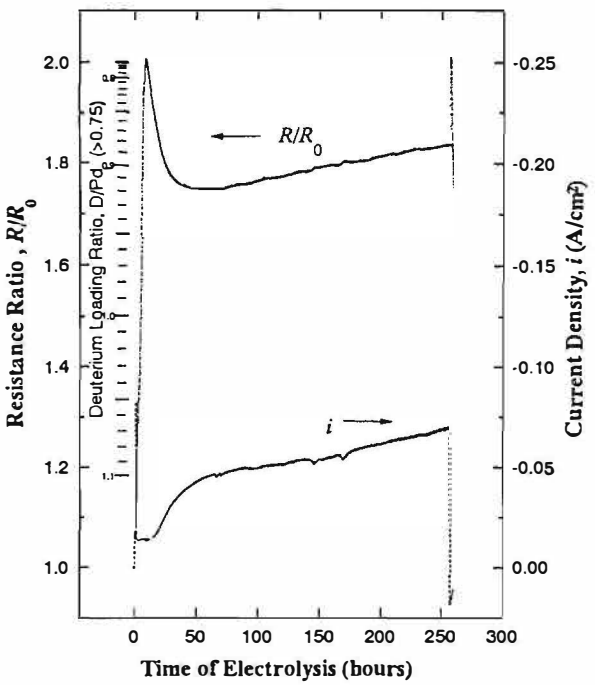

Fig. 9. Changes of the resistance ratio of a palladium cathode with the full constant cell voltage (3.1V).

Changes of the resistance ratios (R/R_0) with various fixed cell voltage are shown in Fig. 8. From these results, the deuterium loading rate was observed to increase, as the cell voltage increased. With the cell voltage above 3.5 V, the maximum loading ratios over 0.90 could not be obtained. With the cell voltage less than 2.8 V, the time to reach the maximum loading ratios was too long and the value of the maximum loading ratios was lower than those obtained with the cell voltage between 3.0 V and 3.2 V. Therefore, the optimal constant cell voltage is estimated to locate between 3.0 V and 3.2 V in our cell.

One of the results with our full constant cell voltage electrolysis is shown Fig. 9. The constant cell voltage is chosen at 3.1 V. The maximum loading ratio exceeding 0.92 is attained, but the loaded deuterium is observed to decrease gradually. The decrease rate, however, was smaller than some of those constant current electrolysises followed by a step-up current electrolysis. Therefore *full constant cell voltage electrolysis* is effective in a loading enhancement, but not perfect with regard to the deloading.

Observation of the electrolytic current revealed, current spikes were generated at the start of electrolysis. Then, until the resistance ratio went up to (R/R_0) = 2.0, the small electrolytic current flew. Subsequently, the electrolytic current rapidly increased with the decrease of the resistance ratio. And then the electrolytic current increased gradually with the decrease of the loading ratio after the loading ratio reached the maximum value.

3.2 Step-up and Ramp Current Electrolysis

Material Science Studies

Figure 10 shows the variation in time of the resistance ratio of a palladium cathode rod with a step-up and ramp current electrolysis, as compared with that with a step-up and constant current electrolysis. The rump rate was chosen as 0.625 $A \cdot cm^{-2} \cdot hr^{-1}$.

At the conventional step-up and constant current electrolysis, after the maximum loading ratio, D/Pd = 0.92 was obtained at the maximum cell voltage during the 0.125 A/cm^2 constant current electrolysis, deuterium loading ratios were observed to decrease in association with a decreasing cell voltage with the constant current still maintained.

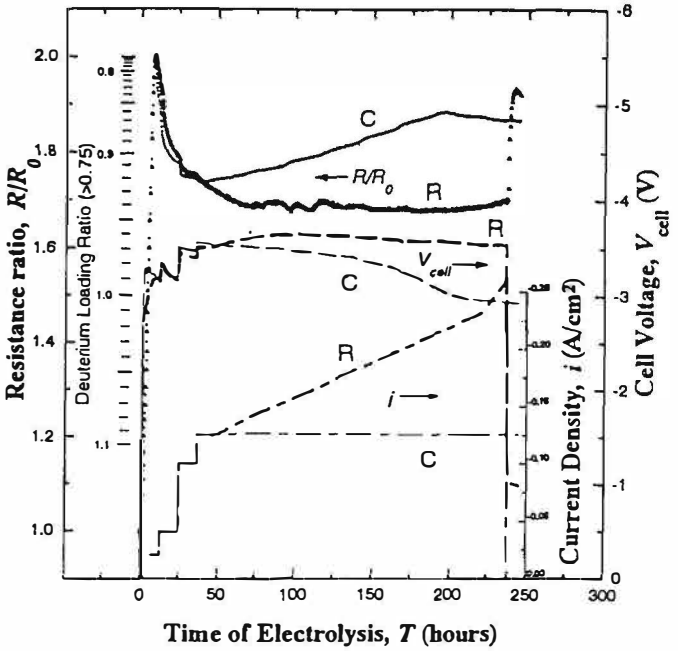

Fig. 10. Variation in time of the resistance ratio of a palladium cathode rod with a step-up and ramp current electrolysis (R), as compared with that with a step-up an constant current electrolysis (C).

On the other hand, at the step-up and ramp current electrolysis, the cell voltage was kept constant at about 3.6 V by slowly increasing the current, and, as expected, the maximum loading ratio as high as 0.93 could be maintained for more than 200 hours. This satisfactory result can be obtained only by the step-up and ramp-up current electrolysis.

Concerning the difference between these two methods, the sustentation of higher loading ratios were considered to be affected by electrolytic procedures before attaining to the maximum loading.

3.3 Cause of Cell Voltage Decrease

A possible mechanism to cause the cell voltage decrease under a constant current electrolysis was considered. In general, the cell voltage, V_{cell}, can be expressed by Eq. (1).

$$V_{cell} = V_d + \eta_D + \eta_O + IR, \qquad (1)$$

where V_d, η_D, η_O and IR are thoretical decomposition voltage, deuterium overpotential, oxygen overpotential, and ohmic drop, respectively. The decomposition voltage, V_d, is an invariant under a constant condition, and it is specifically 1.26 V at 293 K under 0.1 MPa.

Material Science Studies

Our deuterium loading was carried out in a open cell, where the electrolysis always concentrates the electrolyte. Consequently, the ohmic drop between the anode and the cathode lowers due to a decrease in the electrolyte resistance, and the deuterium and oxygen overpotentials will change also as the concentration changes.

It is conceivable that the deuterium and oxygen overpotentials should change as well, since the electrode surface will be modified with the electrolysis.

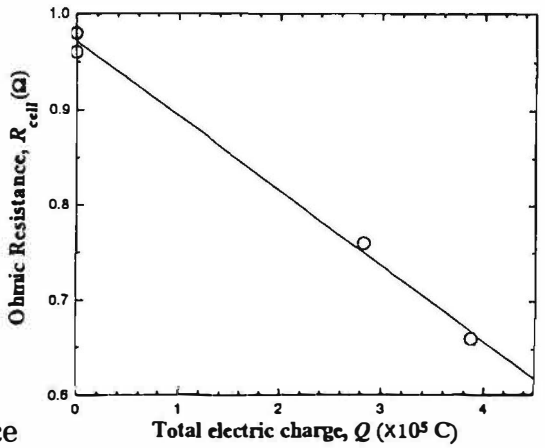

Fig. 11. Changes of the ohmic resistance between the anode and the cathode in our electrolytic cell against the total electric charge.

The changes of ohmic drop and overpotentials are considered as follows:

a) Ohmic Drop

Changes of the ohmic resistance between the anode and the cathode in our electrolytic cell against the total electric charge is shown in Fig. 11. The cell ohmic resistance is observed to decrease linearly with the total electric charge. The decrease of the ohmic drop was estimated to be approximately 0.1 V for the electrolysis with 0.125 A/cm^2 (electrolytic current 0.4 A) for 200 hours (the total electric charge $Q = 2.9 \times 10^{-5}$ C). Therefore, the cell voltage decrease in excess of 0.6 V cannot be accounted for only by the ohmic drop.

b) Deuterium and Oxygen Overpotential

Changes of the deuterium overpotential with electrolysis time at the constant current density 0.125 A/cm^2 followed by step-up current electrolysis are shown in Fig. 12. The deuterium overpotential is observed rapidly to decrease with the electrolysis, despite with the constant current. Furthermore, relationship between

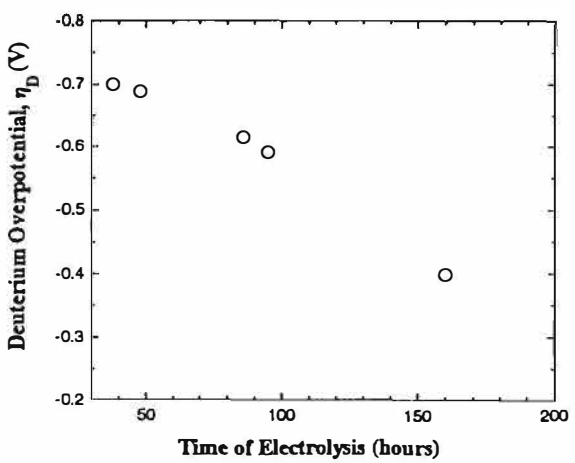

Fig. 12. Change of the deuterium overpotential on the palladium cathode with electrolysis time at the constant current density 0.125 A/cm^2.

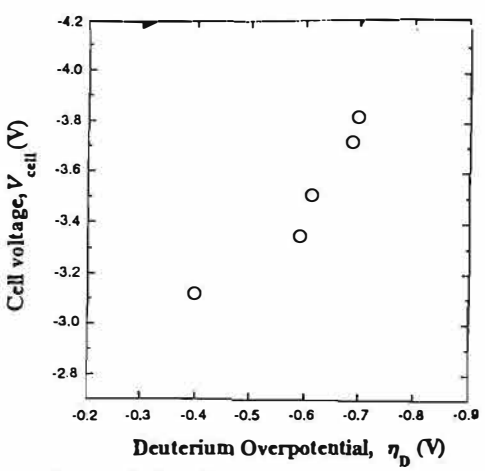

Fig. 13. Relationship between the cell voltage and the deuterium overpotential during electrolysis at the constant current density 0.125 A/cm^2.

the cell voltage and the deuterium overpotential is shown in Fig. 13, which indicates an approximately linear relation between the cell voltage and the deuterium overpotential. The rate of decrease in the deuterium overpotential, $\Delta\eta_D$, can be estimated to be approximately 0.3 V for the corresponding cell voltage decrease of 0.7 V.

In Eq. (1), the decrease of the oxygen overpotential, $\Delta\eta_O$, will be considered almost equal to the one of the deuterium overpotential, $\Delta\eta_D$.

Concerning the deuterium overpotential, K. Ota et al. claim that it is higher with a higher concentration of LiOD electrolyte, which leads to the conclusion that the decrease of the deuterium overpotential cannot be ascribed to the concentration change of LiOD. Consequently, it is clear that the decrease of the cell voltage is mostly due to the decrease in the deuterium and oxygen overpotentials.

Judging from these, it is concluded that those changes in deuterium loading ratios are attributed mainly to the changes in the deuterium overpotential, and that it is necessary to control the deuterium overpotential to suppress the deloading.

4. Conclusions

(1) The maximum deuterium laoding ratio of the palladium cathode can be maintained for more than a week by using the palladium cathode etched by aqua regia and by electrolytic loading with the increasing electrolytic currents.
(2) During a long term electrolysis, the deuterium overpotential on a palladium cathode is observed to decrease, which will cause the deloading.
(3) It is confirmed that when the deuterium overpotential is controlled not to decrease by our method of increased current electrolysis, the deloading can be suppressed.
(4) Higher deuterium loading ratios can be maintained by our method for a substantially long period of time.

References

1. M. C. H.McKubre, S. Crouch-Baker, A. K. Hauser, S. I. Smedley, F. L. Tanzella, M. S. Williams and S. S. Wing, "Concerning Reproducibility of Excess Power Production", in *Proceedings of the 5th International Conference on Cold Fusion*, Monte-Carlo, Monaco, p.17-33 (1995).
2. H. Okamoto, T. Sano, Y. Oyabe, T.Terazawa and T. Ohi "Approach to Obtain Higher Deuterium Loading Ratios of Palladium Cathodes", in *Proceedings of the 5th International Conference on Cold Fusion*, Monte-Carlo, Monaco, p.419-429(1995).
3. K. Ohta, T. Karikomi, H. Yoshitake and N. Kamiya, *Denki Kagaku*, 62, p146-151 (1994)

Material Science Studies

Loading Ratio Study in a Gas-loading System

Feng Shan Bu, Xing Zhong Li*, Lan Gao*, Hang Shi*, Gui Song Huang**

Beijing General Research Institute for Non-Ferrous Metals, Beijing 100088, CHINA
*Department of Physics, Tsinghua University, Beijing 100084, CHINA
**Department of Physics, Beijing University, Beijing 100871, CHINA

Abstract
Using the tungsten wire, the deuterium gas is loaded into a palladium wire with the loading ratio higher than 0.75 under the pressure less than 1 atm. at the room temperature. The metallography shows that its grain size is greater than 100 micra. This study facilitates the combination of a gas-loading system with a calorimetric system.

1. Introduction

The " heat after death"[1] phenomena revealed an important point that the " excess heat" might appear in a gas-loading system as well. This is important for both the practical and academic purposes. As a practical energy source, the " excess heat" should be released under a higher temperature in order to enhance the heat efficiency; thus, the electrolyte in an electrolytic cell is an undesirable factor which may limit the temperature to a value less than its boiling point. On the other hand, we would like to study the loading process in a simple environment. The electrolytic cell might contaminate the palladium sample with various impurities from both the electrolyte and the electrodes. The gas-loading system is a desirable system for this academic purpose also. Particularly, Oates and Flanagan [2] showed that the gas-loading system was able to load hydrogen into the palladium to a high loading ratio with the highest reproducibility than that in any other experiments. This attracts us to study the gas-loading system in combination with a calorimetric system. A such system has been constructed to show that the high loading ratio is feasible, and the grain size in palladium wire may be greater than 100 micra. Hence, it is possible to study the " excess heat" in this gas-loading system[3].

2. High Loading Ratio under the Normal Pressure and Temperature

The early study on the hydrogen-palladium system showed that the high pressure or low temperature is necessary to reach a high loading ratio (i.e. the atomic ratio of hydrogen to palladium, H/Pd or D/Pd.) For example, at the room temperature (20 ~ 25 °C), in order to reach the

loading ratio of D/Pd=0.70, the deuterium gas pressure is supposed to be higher than 100 atm.[4], or 70 ~ 150 psia[5]. In order to use the thin wall stainless steel vacuum dewar system for gas-loading, it is desirable to operate under the pressure less than 1 atm.. Hence, the first step is to check whether a piece of incandescent tungsten filament will load the deuterium gas into the palladium wire under the pressure less than 1 atm.. Fig. 1 is a schematic of the apparatus. A piece of tungsten filament (ϕ 0.1mm) is set at the center of a quartz frame, upon which the palladium wire (ϕ 0.34mm×250cm) is wound. The Pt thermometer and the manometer are used for monitoring the temperature and the pressure. The loading ratio can be measured by the gas pressure, P_2, and temperature, T_2. If the volume of the gas-loading system is V_o , which is filled to pressure, P_1, at the temperature, T_1, initially; then, the loading ratio is

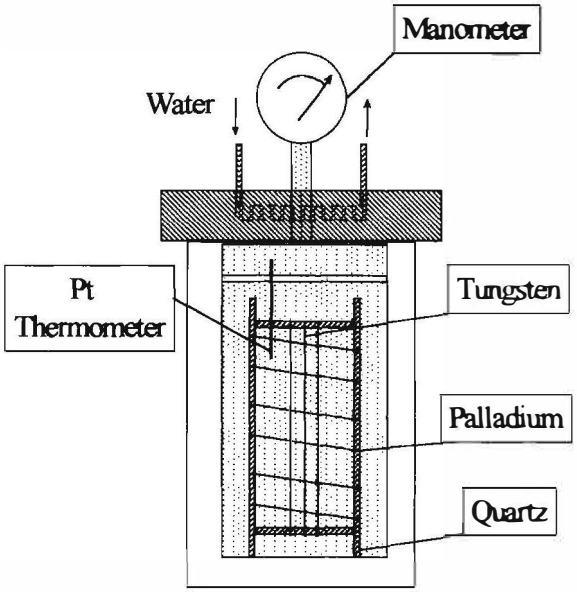

Fig.1 A Schematic of Gas-loading System

$$x = \frac{2M_{Pd}V_o}{W_{Pd}N_o k}\left[\frac{P_1}{T_1} - \frac{P_2}{T_2}\right] \qquad (1)$$

Here, W_{Pd} and M_{Pd} are the weight of the palladium wire, and atomic weight of the palladium, respectively, $(N_o k)$ is the universal gas constant (8.31×10^7 erg/(K-mole)). The absorption of deuterium in the stainless steel wall is assumed to be negligible. On the other hand, Mckubre[6] and Kunimatsu[7] have shown that the resistance of the palladium wire, R, is a function of this loading ratio, which might be described by a fifth order polynomial as

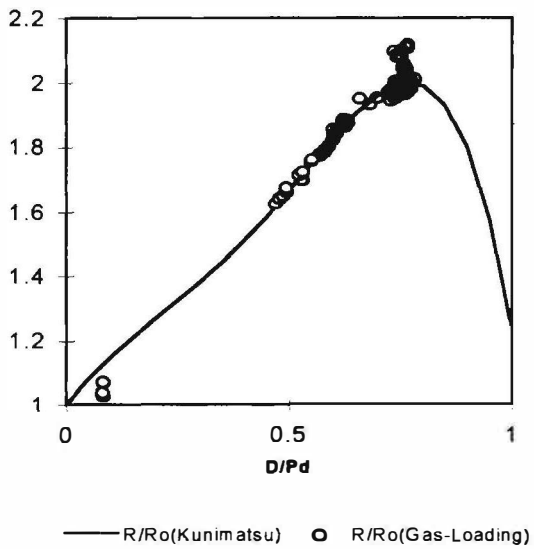

Fig.2 Gas-Loading Feature of a D/Pd System

$$\frac{R}{R_0} = -5.0216x^5 + 1.4416x^4 + 5.3328x^3 - 3.3145x^2 + 1.7948x + 0.9993 \qquad (2)$$

Here, R_0 is the resistance of the palladium wire before loading at the same temperature. This polynomial is valid in the range of $0<x<1$ for deuterium with the correlation coefficient higher than 0.998. In comparison with the experimental observation this resistance ratio is expressed as a function of loading ratio in Fig.2 (solid line). The open circles are the experimental results in our gas-loading experiments.[8] The good agreement between the expectation and the experimental observation confirms that the loading ratio, D/Pd, has reached the value of 0.78 under the pressure

less than 660 Torr (P_1) at the room temperature (T_2=14 °C ~ 34 °C). This high loading ratio has been kept for more than one month.[8]

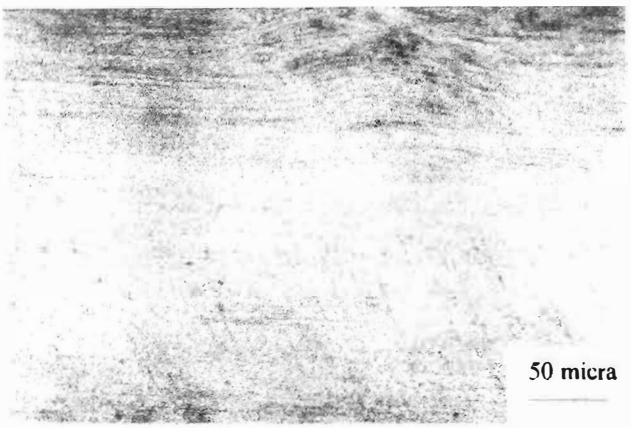

Fig3. Palladium Metallographic Photo before Annealing

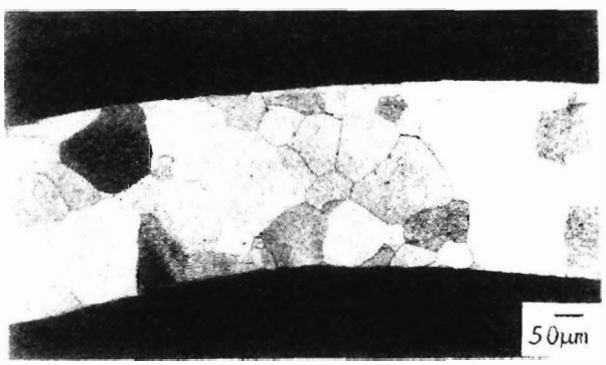

Fig.4 Palladium Metallographic Photo after Annealing

3. Metallographic Examination

The theory [9] of " resonance penetration of the coulomb barrier via lattice confined ions" anticipates that the grain size in the palladium crystal should be greater than 50 ~ 100μ in order to have enough density of state in the lattice energy band. The experimental observation [10] also tells us that annealing process is important to get the high reproducibility in the electrolytic cell. We would like to check the importance of annealing process in the gas-loading system also. Two annealing procedures have been tried. The first is to anneal palladium wire in a big oven; then, shift the palladium wire into the dewar system. The second is to anneal palladium wire *in situ* using an electrical current in the palladium wire. The second annealing procedure is particularly useful for the thin wire and is desirable in a combination of the calorimetric system with the gas-loading system. Fig.3 and Fig.4 show the metallographic photos for the palladium wire before and after the annealing, respectively. The palladium wire (ϕ 340μ) was wound on a quartz frame, and was put into an electrical oven to be heated to 900 °C for 3 hours in 10^{-5} Torr; then, it was cooling down in the oven for more than 5 hours. The photos are taken across the longitudinal cross-section. The largest grain size is greater than 100μ , which is suitable for the " excess heat" experiment.

In order to try the second annealing procedure, a long thin palladium wire (ϕ 80μ × 300 cm) is wound on a quartz frame. A piece of tungsten filament (ϕ 80μ × 40cm) is fixed at the center of the quartz

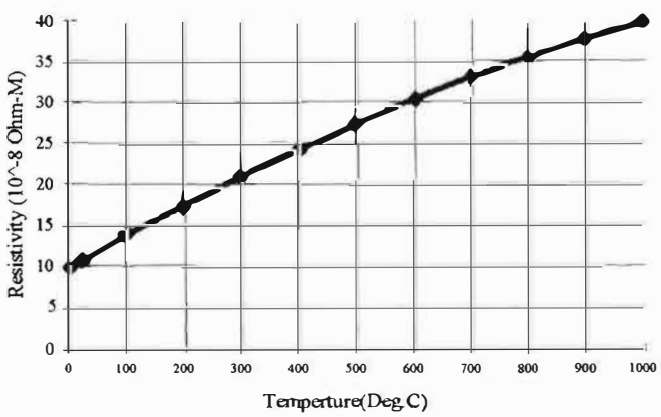

Fig.5 Resistivity of Palladium versus Temperature

frame. Using the electrical current through the palladium wire, it was heated to 800 °C, in the vacuum (~ 4 Pa) and kept at this temperature for 3 hours. Then, the electrical current was reduced gradually as follows: 800 °C–700 °C (53min.), 700 °C–600 °C (47 min.), 600 °C–500 °C (30 min.), 500 °C–400 °C (40 min.), 400 °C–300 °C (30 min.), 300 °C–200 °C (60 min.); then, the current was shut off. The palladium wire reached the room temperature after 10 hour cooling in the dewar. The temperature of the palladium wire was determined by its resistance according to Fig.5[11]. After this annealing procedure, the tungsten filament is heated to 1800K in vacuum (4 Pa). Its temperature was determined by its resistance according to Fig.6[12]. The hydrogen is then introduced into the dewar at low pressure (~ 0.8 atm.). The temperature of tungsten filament drops quickly to 750K due to the high heat conductivity of hydrogen gas. Meanwhile the dewar temperature increases gradually. After 2.5 hours, the dewar temperature reaches 156 °C. Then, the heating current in tungsten wire is reduced gradually. At the same time the resistance of the palladium wire increases gradually as shown in the Fig.7. The highest resistance ratio, R/R_o, reaches 1.79±0.02. This corresponds to a loading ratio of H/Pd=0.69 ~ 0.78.

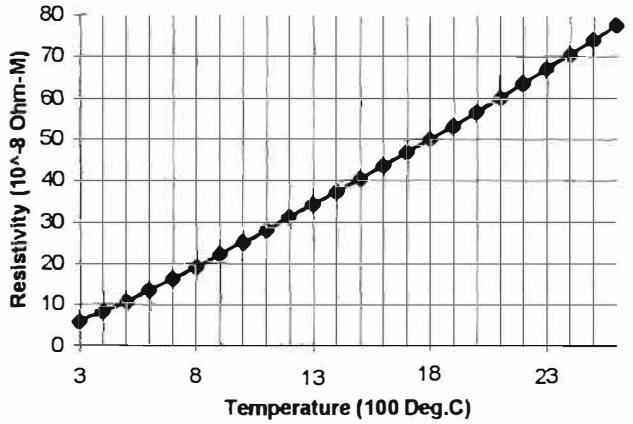

Fig.6 Resistivity of Tungsten versus Temperature

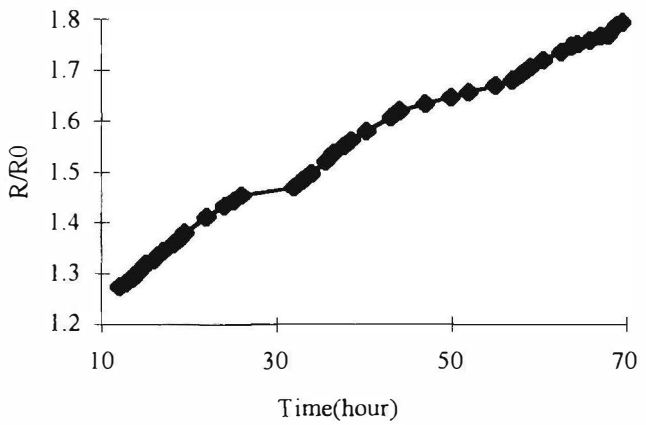

Fig.7 Tungsten Wire Effect on the Gas-loading in a D/Pd System

Fig.8 and Fig.9 are the metallographic photos for the wire before and after the loading process. In order to obtain the clear image of the grain boundary, careful etching is necessary after polishing the samples which were embedded in an epoxy substrate. Nitric acid or the mixture of nitric acid and chlorhydric acid is used for chemical etching

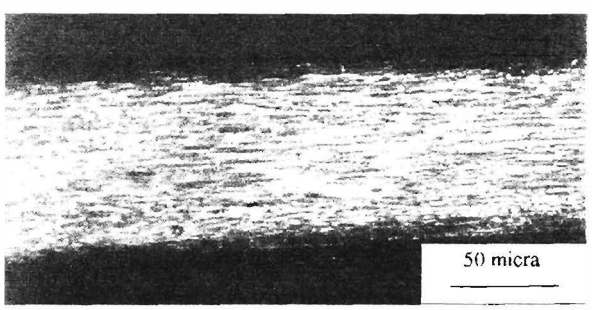

Fig.8 Metallographic Photo of Palladium Wire (80 micra in diameter) before Annealing

(1 ~ 5 minutes). It is evident that the largest grain size is almost as the diameter of the palladium wire (ϕ 80μ).

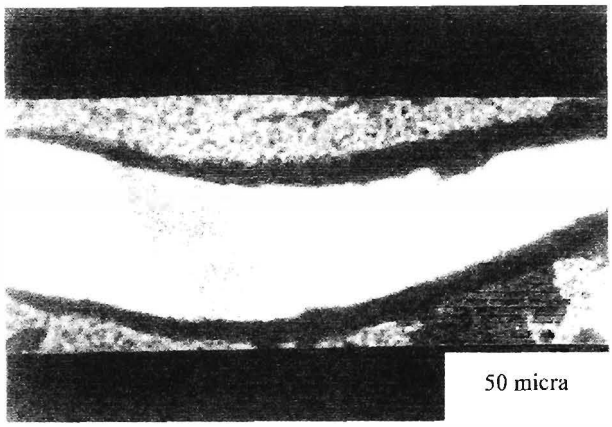

Fig.9 Metallographic Photo of Palladium Wire (80 micra in diameter) after Annealing *in situ*

4. Conclusion

Gas loading system can be realized in a low pressure (<1 atm.) dewar vessel. The annealing process ***in situ*** is feasible in such a system. The highest loading ratio observed is 0.78. It seems that even higher loading ratio is attainable as well (see Fig.7). The grain size can be of the order of 50 ~100μ. Therefore, the " excess heat " measurement in such a gas-loading system is very desirable[3], [13].

References

1. S. Pons and M. Fleischmann, "Heat after Death," Transactions of Fusion Technology, 26, 87 (1994).
2. W. A. Oates and T. B. Flanagan, "Formation of Nearly Stoichiometric Palladium-Hydrogen Systems," Nature Physical Science, 231, 19 (1971).
3. X. Z. Li et al., "Excess Heat Measurement in Gas-loading D/Pd System," Proceedings of ICCF-6 (1996, October 13-18, Toya, Japan).
4. Y. Fukai, "The Metal-Hydrogen System", Springer-Verlag, Berlin, Heidelberg (1993), p.4.
5. T. Claytor, Private Communication (1994).
6. M. C. H. Mckubre, et al. "Calorimetry and Electrochemistry in the D/Pd System," The Proceedings of the First Annual Conference on Cold Fusion (1990, March 28-31, Salt Lake City, USA) p.20.
7. J. Minato, K. Kunimatsu, et al., "Materials /Surface Aspects of Hydrogen/Deuterium Loading into Pd Cathode," Proceedings of ICCF-5 (1995, April 9-13, Monte Carlo, Monaco), p.383.
8. G.S.Huang, X.Z.Li, et al., "A Possible Phase Transition in a Gas-loading D/Pd System," Proceedings of ICCF-6 (1996, October 13-18, Toya, Japan).
9. X. Z. Li, "Solving the Puzzle of Excess Heat without Strong Nuclear Radiation," Proceedings of ICCF-5 (1995, April 9-13, Monte Carlo, Monaco), p.285.
10. M.C.H.Mckubre et al., "Concerning Reproducibility of Excess Heat Production," Ibid., p.17.
11. CRC Handbook of Chemistry and Physics (1992), 12-33, 10-285.
12. Handbook for Manufacture of Noble Metallic Materials, Metallurgical Industry Press, (1978), p.149 (in Chinese).
13. X. Z. Li, et al., " 'Fine Tuning' Mechanism for Resonance Tunneling in D/Pd Systems, " Proceedings of ICCF-6, (1996, October 13-18, Toya, Japan).

Material Science Studies

Selection of Palladium metallurgical parameters to achieve very high loading ratios

Antonella De Ninno [(a)], Aurelio La Barbera [(b)], and Vittorio Violante [(a)]

[(a)] Associazione EURATOM-ENEA sulla Fusione, Centro Ricerche Frascati
C.P. 65 - 00044 Frascati, Rome, Italy
[(b)] ENEA/INN/NUMA, Centro Ricerche Energia Casaccia

Abstract

It has been extensively proved that a threshold in D/Pd concentration must be overcome to observe the heat excess production phenomenon. However, it is very difficult to obtain Pd samples with an high loading ratio in a reproducible way, then the actual reproducibility of the cold fusion experiments is critical.

We will show that strong concentration gradients arise in the material during the loading procedure so that permanent deformation can be produced. Loading dynamic and metallurgical parameters will both affect strongly the ultimate loading ratio achievable.

Thus a loading procedure has been selected such as to avoid the anaelastic strains of the α-β phase, and its consequence in terms of elastic parameters has been evaluated. We studied, both experimentally and theoretically, the influence of Pd microstructure and dislocations on the loading ratio in order to select the material that better matches the cold fusion experiments requirements.

1. Introduction

In presence of a force F the Hydrogen flux in the lattice (as a continuum) is well described by the law:

$$J = -nDgradc + ncMF \tag{1}$$

where c is the H atomic concentration, D is the diffusion coefficient, M is the H mobility and n is the number of lattice atoms per unit volume.

Stress gradients within a sample cause an additional force on the Hydrogen interstitials:

$$F = Pgrad(s_{ijkl}\sigma_{kl}) \tag{2}$$

where P is the trace of the dipole-moment tensor and s_{ijkl} and σ_{kl} are tensor components of the elastic coefficient and of the stresses respectively.

The stress induced by Hydrogen diffusive flux will cause an inhomogeneous distribution of the solute. The eq. (1) will be in this case:

$$J = -D(\nabla c - \frac{c\bar{V}}{RT}\nabla\sigma) \tag{3}$$

where $\bar{V}$ is the molar volume of Hydrogen into the metal. Kandasamy [1] showed that a suitable strain can stop the diffusion of Hydrogen driven by the concentration gradient.
If internal stresses can be removed either by plastic deformation or by dislocation slipping, such stress-free strained crystal can be defined "incoherent". In the opposite case a deformation field will be associated to the strain and the crystal can be defined "coherent". The "real" crystal will be a mixture of the two cases depending on the initial metallurgical state.
From (3) it follows that the diffusive flux can be blocked if

$$\nabla\sigma = \frac{RT}{c\bar{V}}\nabla c \tag{4}$$

assuming $\nabla c = c - 0$, σ =140 MPa (V = 1.68 cm^3/mol, c= 0.7) that is a typical value of yield strees for Palladium [2]. This means that the stress produced by loading Hydrogen (and its isotopes) in Palladium can induce plastic deformations into the lattice.
Thus the loading dynamic it is very important in order to avoid the dislocation growth related to a strong concentration gradient.

2. Dynamic influence on loading process

Starting a diffusive process can produce very high strain field just under the surface thus making the further Hydrogen uptake very difficult.
We can overcome the problem essentially in two ways. Firstly avoiding the growth of strong concentration gradient either with a very slow loading or with a suitable loading procedure. The second approach is to relieve the stresses generated in the metal through dislocation slipping.
The adsorption isotherms for Hydrogen in Palladium show that, at room temperature and for a concentration above c=0.008 H/Pd atoms, an α phase with low Hydrogen content and an expanded, Hydrogen-rich, β phase coexist in the solid solution up to a concentration of c=0.607. It is well known that during the loading expanded β areas grow near the α areas, so that, during the coexistence phase, very strong deformation fields are generated at the border of the two phases, due to the different lattice parameters.
Coexistence of α+β phases can be avoided during the loading process by selecting an appropriate path on the p-c(D)-T diagram (see fig.1). Increasing the isothermal temperature over the critical point (T=310°C, p=34 atm) it is possible to reduce the percentage of non-relaxed stresses by skipping the coexistance phase.

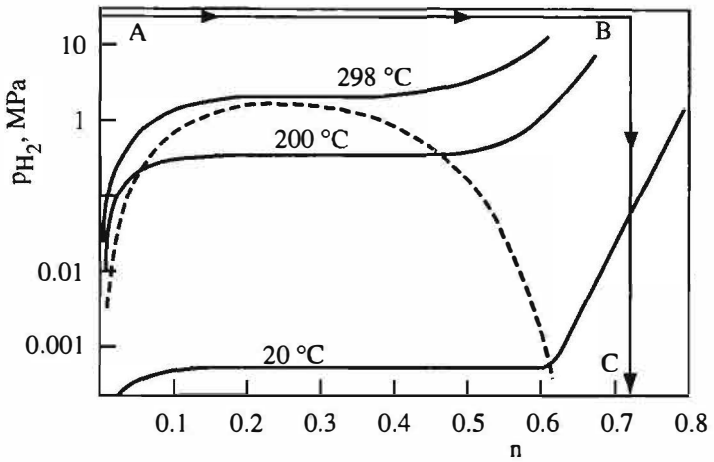

Figure 1 - Hydrogen-Palladium phase diagram. The gas loading experimental path is the line ABC. A thermodinamic quasi-reversible process must be obtained with a slow loading. At the end of the loading sequence the loading ratio is evaluated by weighting the sample.

3. Experimental details

Palladium 14 by 10 mm sheets 150 μm thick were submitted to cathodic discharge in LiOH solution. The Hydrogen concentration was monitored, measuring the variation of electrical resistance with a lock-in amplifier based system. The ratio R(c)/R(c=0), defined in the following as R/R_0, is related to the concentration c so that it is possible to follow the concentration in real time during the electrolysis. Samples were temperature treated in vacuum for 0.5 hour at 900 °C.

We compare the maximum loading reached with two different procedures:

- a) sheet was charged in electrolysis ;
- b) sheet was pre-charged in H_2 gas.

The loading procedure for the pre-charged samples is the following:
the Palladium sheets were heated to 400 °C under vacuum and then Hydrogen pressure of 40 atm was set up. A very slow cooling to room temperature keeping the pressure constant was performed and, after a suitable time, the vessel was evacuated. This path allows to skip the coexistence phase avoiding the growth of high stress field at the border of α-β phases (see fig. 2): the curve (a) refers to sample loaded only in electrolysis without any particular care, the current density being $I=2.5$ mA/cm^2 ; the curve (b) refers to a sample pre-loaded in gas and then electrolyzed as the previous one.
It is very clear the effect of the different loading procedure.
A further concentration increase is obtained allowing both the stress relieve through the anodic stripping (a short anodization of Pd) of the surface and the reduction of the concentration gradient changing the current density periodically (see fig.3).

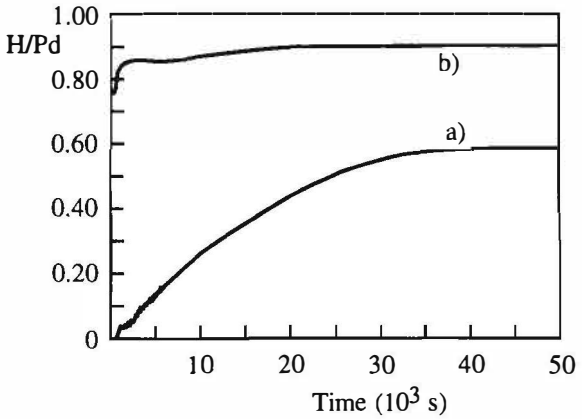

Figure 2 - Comparison of loading curves.
a) sample loaded only by electrolysis. I = 10 mA (2.5 mA/cm^2)
b) sample pre-loaded in gas phase and then electrolyzed.

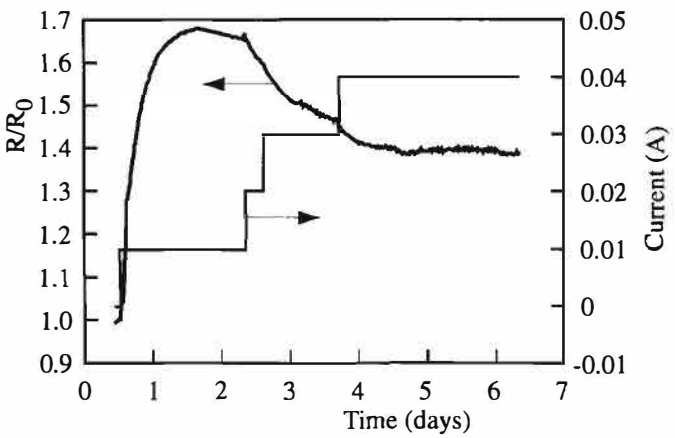

Figure 3 - Anodic stripping effect. Here the anodic stripping (current sign change) accelerated the loading process. A further current increase stabilized the concentration. In this experiment the maximum value of concentration is close to 1.

4. The influence of the microstructure

The metallurgical character of Pd could strongly affect the final loading ratio.
Assuming that the main problem is to avoid high stress field inside the lattice we must choose the best metallurgical structure for such a goal.

- the grain influence both the diffusion times and the elastic energy storage
- the defects density affects the possibility to relieve stresses through the dislocation slipping
- the recristallization determines the grain boundary size

We investigated on the above mentioned parameters on samples cold worked and heat conditioned and found a clear effect of the heat treatment temperature on the final loading ratio (see. Fig.4).
Fig.5 shows three different samples:
•Fig. 5a) the lattice is strongly deformed because of the cold working with a very high dislocation density

Material Science Studies

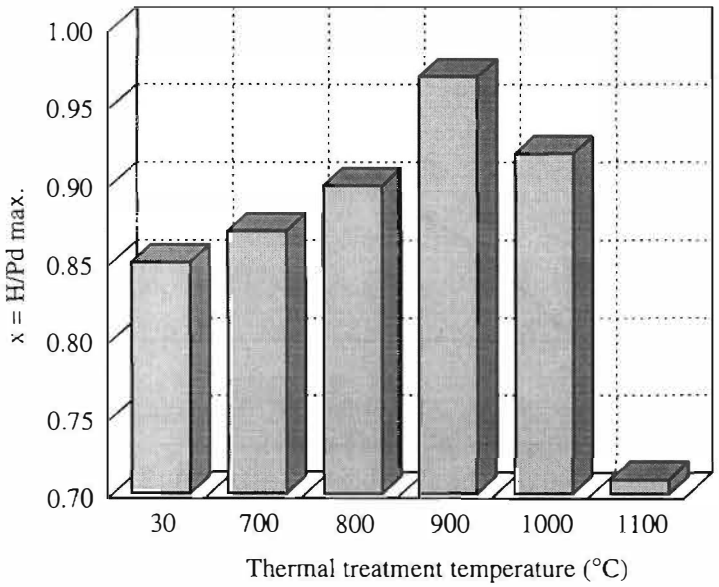

Figure 4 - Influence of thermal treatment on the maximum loading achievable.

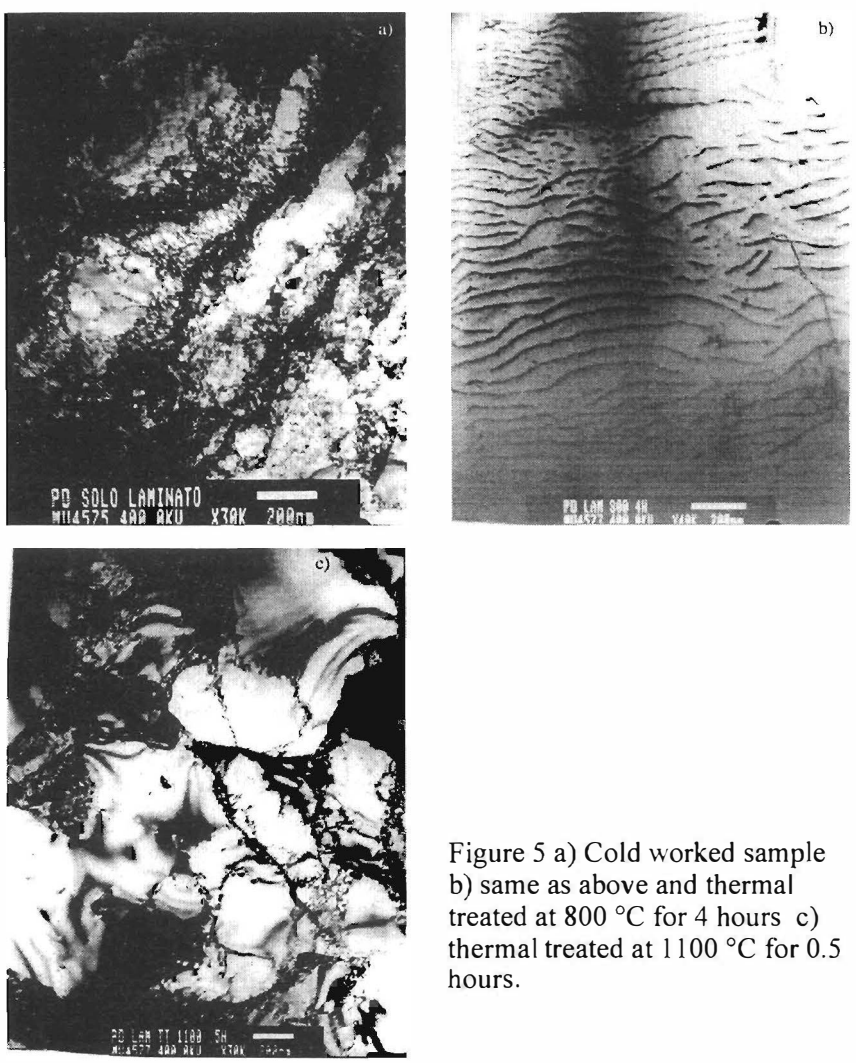

Figure 5 a) Cold worked sample b) same as above and thermal treated at 800 °C for 4 hours c) thermal treated at 1100 °C for 0.5 hours.

•Fig. 5b) thermal treatment induces the slipping of the dislocation that arranges in percolative paths.
•Fig. 5c) a too high temperature causes a too big grain growth and destroys the network formed before.

5. Conclusions

On the basis of both the ideas examined in the introduction and the experimental activity we found that:

- the self-stress due to Hydrogen loading into the lattice is mostly responsible for the difficulty in obtaining high loading ratios.
- the maximum loading ratio achievable for each sample is strongly conditioned by the loading dynamic
- the initial metallurgical state of the sample can be chosen in order to minimize the growth of an high strain field growth.

Studying both the experimental procedures and the initial metallurgical state of the sample we improved the reproducibility in obtaining high concentration of Hydrogen in Palladium, increasing the maximum loading ratio achievable in electrolysis (c≅1 H/Pd) at room temperature and using very low current density (of about 10 mA/cm^2).
We obtained same results for Deuterium-Palladium system too [3].
These results look very promising to improve the reproducibility of the cold fusion experiment and to prove that the concentration threshold to overcame is a necessary and sufficient condition to obtain the heat excess.

Bibliography

[1] K.Kandasamy, J. Hydrogen Energy **20**, (1995), 455-463
[2] R.A. Oriani, Trans. Fusion Technol. **26** (1994), 235
[3] A. De Ninno, A. La Barbera, V. Violante, submitted to 'MH96' Internat. Symp. on Metal-Hydrogen Systems, Les Diablerets, Aug. 1996

Material Science Studies

A Possible Phase Transition in a Gas-loading D/Pd System

Gui Song Huang, Xing Zhong Li*
Department of Physics, Beijing University, Beijing, 100871, CHINA
*Department of Physics, Tsinghua University, Beijing 100084, CHINA

Abstract
A resistance jump is identified at the loading ratio, D/Pd, approaching 0.58 in a gas-loading D/Pd system. This jump may be related with the transition between the α phase and the β phase of the deuteride. Its implication for measuring the loading ratio is discussed.

1. Introduction

After analyzing the gas-loading data for 6 months in a gas-loading D/Pd system, a resistance jump is identified when the loading ratio of palladium wire is in the range of 0.50 ~ 0.60. Based mainly on the experimental data in an electrolytic cell (Mckubre[1] and Kunimatsu [2]), the resistance of the palladium wire was used to determine its loading ratio (the atomic number ratio of deuterium to palladium, D/Pd). This sudden change of the resistance was interpreted as a sudden change of the loading ratio; however, it contradicted with the pressure and the temperature measurement, which provided the information of gas-loading also. The another interpretation is the possible jump between the two hysteresis branches. This later interpretation is consistent with the pressure and temperature data; however, it implies that the loading ratio of our gas-loading system is mostly less than 0.74, i.e. on the left hand side of the resistance peak.

2. The Sudden Jump of the Resistance during the Degassing Process

The electrical resistance, R, of a long thin palladium wire (ϕ 340μ × 250cm) is monitored during the deuterium gas-loading process (Li [3]). The resistance has been used as one of the parameters for determining the loading ratio, D/Pd. Since the resistance of a palladium wire reaches its maximum value at the loading ratio of (D/Pd) ~ 0.74, and the "excess heat" is supposed to happen on the right hand side of the peak (Fig.1), we are interested in monitoring whether the loading process reaches the right hand side of peak. Usually, one may monitor the pressure and temperature in the vessel to judge if the palladium wire is absorbing or desorbing. If the resistance of a palladium wire is increasing while it is desorbing the deuterium gas; then, one might expect that the loading process has reached the right hand side of the resistance peak. Fig.2 shows the resistance of the palladium wire as a function of time (triangle shape marks). A sudden jump of resistance was found at ~ 63,000 seconds while the pressure in the vessel was increasing (diamond shape marks) which meant

that the palladium wire was desorbing the deuterium gas (temperature changed very little in that period). It was believed that this was an evidence showing the loading process had reached the right hand side of the resistance peak. Particularly, the resistance had a peak 18 hours before this jump (Fig.2), and this was used as an additional evidence saying that the loading process had reached the right side of the peak. However, there are arguments against this interpretation as well. Using the temperature, T_2 , (square shape marks) and the pressure, P_2 (dotted line), we may calculate and draw the loading ratio, $x \equiv D/Pd$, as a function of time (open circles)[3]:

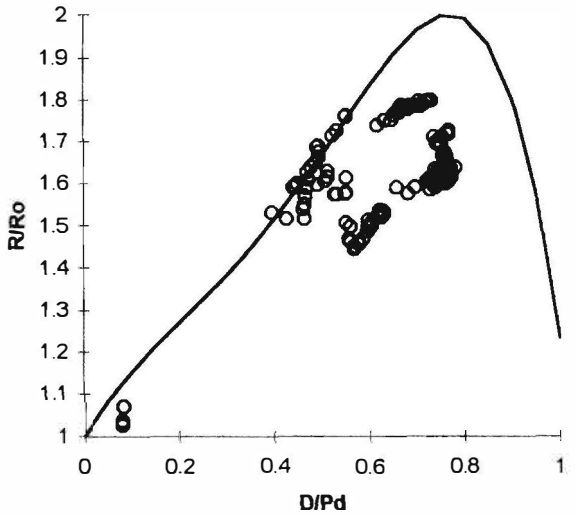

Fig.1 R/R_o[Kunimatsu] Curve and Experimental Data Points(open circles). R_o=2.7 Ohm

$$x = 1.2 \times 10^{-3} \cdot V_0 \cdot \left[\frac{P_1}{T_1} - \frac{P_2}{T_2} \right] \qquad (1)$$

Here, P_1 and T_1 are the initial pressure and temperature in this vessel before loading (in unit of Torr and Kelven, respectively). V_0 is the volume of the vessel (in cm^3). In the present experiment, P_1=660 Torr, T_1=287.4 K, and the weight of the palladium wire is 2.845 g.. The calculation shows that the palladium wire starts desorbing deuterium gas from the beginning. If we took the resistance peak at ~5000 seconds as a peak corresponding to that in Fig.1; then, the loading ratio at this peak should be 0.74. However, the calculated number according to equation (1) is 0.7. Moreover, the loading ratio is supposed to be increasing before and after this peak at ~ 5000 seconds if it were the peak in the Fig.1. Indeed, the loading ratio, x, is decreasing from the beginning in the experiment.

The discrepancy becomes more serious at the sudden jump point (~ 63,000 seconds). The loading ratio there is only ~ 0.58. However, if it were at the right hand side of the resistance peak, the loading ratio should have been greater than 0.74 at least. Now the question is how to explain this sudden jump in resistance if it was not at the right hand side of the resistance peak in Fig.1.

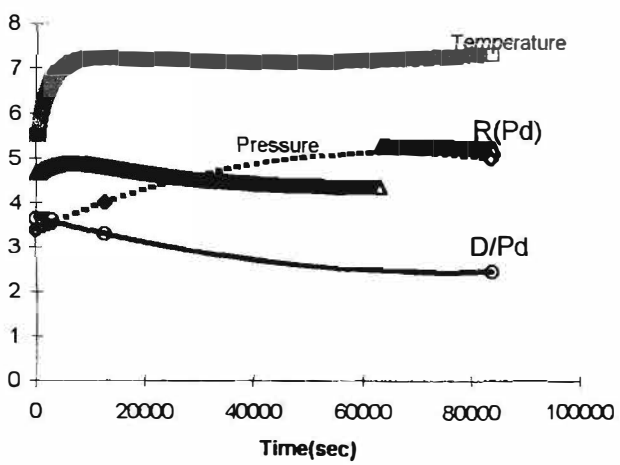

Fig.2 Loading History Showing a Resistance Jump of the Palladium Wire and a Resistance Peak 18 hours before the Jump(unit: Temperature: 10 Deg.C; Pressure: 100 Torr; R(Pd): Ohm; D/Pd: 0.2)

3. A Possible Phase Transition near x=0.58

The pressure-composition isotherms of the D/Pd system is very similar to the P-c-T curves of a van der Waals gas (Fukai [4]). The transition from α phase to the β phase for the deuterized palladium is similar to the transition from the gas phase to liquid phase. Particularly, the hysteresis behavior appears both in the D/Pd system and in the van der Waals gas. In the coexisting region, both the α phase and β phase can exist just like the coexistence of the gas phase and the liquid phase of the van der Waals gas. Moreover, similar to the over-cooling vapor or the overheating liquid there are "over-cooling α phase" or "overheating β phase" of D/Pd system also. The overheating liquid may change suddenly into the vapor coexisting with the liquid, while keeping the total volume unchanged. Similarly, The "overheating β phase" D/Pd system may change suddenly into the α phase coexisting with the β phase, while keeping the loading ratio unchanged. Kunimatsu[2] showed that near the point of loading ratio, x=0.58, the D/Pd system will complete its transition to the pure β phase. If we heat this pure β phase slowly as shown in the Fig.2, the "overheating β phase" may suddenly change into the α phase coexisting with β phase while keeping loading ratio unchanged as that shown in Fig.2 also.

Apparently, the curve of the resistance versus loading ratio in Kunimatsu's study[2] did not include the effect of "overheating β phase", because in their studies, the electrolytic cell was kept at a constant temperature (20 °C).

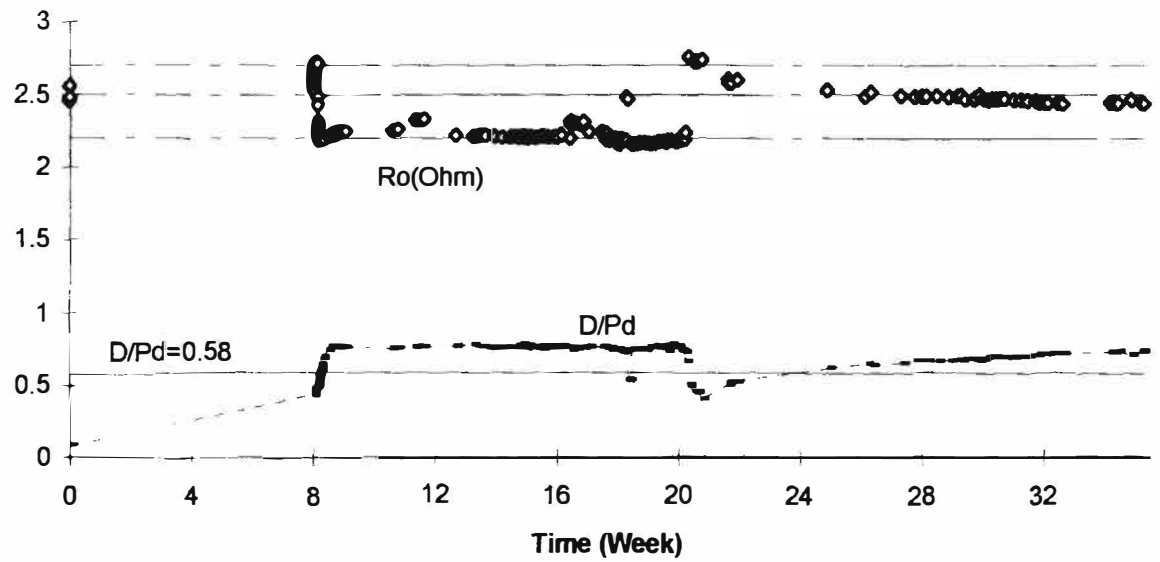

Fig.3 Loading History of D/Pd and R_o (Feb.24—Nov.1,1996)

Fig.3 shows the loading history of the D/Pd gas-loading system in the present studies. The lower part shows the loading ratio, D/Pd , which are calculated from the pressure and the temperature data based on equation(1). The upper part shows the resistance of the palladium wire with no

deuterium in it at initial temperature, R_o , which are calculated from the electrical resistance of the palladium wire, R, measured at different temperature with different loading ratio (see later). In more than 6 month studies, there were three cycles with five chances in which the D/Pd system passed the point of $x \sim 0.58$ as shown in the lower part of the plot. The resistance of the palladium wire changed step-wise every time when the loading ratio, D/Pd, passed the value of 0.58. The resistance stepped up when loading ratio was going downwards, and the resistance stepped down when loading ratio was going upwards. Possibly, the resistance of the palladium wire is a function of the ratio of the α phase to β phase of the deuteride also. In the equation (1), which is based on Kunimatsu's experimental data, the resistance is a single value function of one variable---loading ratio. In the gas-loading experiment, this is no longer true. For a single value of loading ratio, x. There are more than one value of resistance corresponding to this single x. It depends on the hysteresis branch on which the loading process is going. To show this, in Fig.3 the resistance of the palladium wire with no deuterium, R_o , is calculated using the Kunimatsu's value of R/R_o (equation (1)). The value of R_o is clearly divided into three groups.

(1) $R_o \approx 2.7$ when loading ratio $x<0.58$(in the first cycle, near the 8-th week, and in the second cycle, near the 20-th week);

(2) $R_o \approx 2.5$ when loading ratio $x<0.58$ (in the first cycle , during the 1-st week ; in the second cycle, during the 18-th week); and $x>0.58$ (in the third cycle, after 24-th week) .

(3) $R_o \approx 2.2$ when loading ratio $x>0.58$ (in the first cycle , during the 8—18-th week; and in the second cycle, during the 18—20-th week).

Possibly, they correspond to three different fractions of "overheating β phase" in the deuteride.

In order to obtain the ratio R_o in Fig.3, we have to consider the dependence of resistance on temperature also. Unfortunately, the temperature coefficient of resistance is only available for palladium hydride[1], not for palladium deuteride . We just make an assumption that the temperature coefficient of resistance for deuteride is similar to that for hydride, and extrapolate its behavior to the range of $0<x<1$. Based on the Fig.2 in Ref.[1], an analytical fit is obtained as

$$\alpha(x) = 0.0438x^5 - 0.1202x^4 + 0.1187x^3 - 0.0493x^3 + 0.0037x + 0.0042 \qquad (2)$$

Here $\alpha(x)$ is the temperature coefficient of resistance(in unit of K^{-1}) as a function of loading ratio. As a result, we can calculate

$$R_o = \frac{R}{S(x)\cdot[1+\alpha(x)(T_2 - T_1)]} \qquad (3)$$

Here, R is the resistance of the palladium wire at temperature T_2; $S(x)$ is an analytical fit of the Kunimatsu's data [3]

$$S(x) \equiv \frac{R(T_1,x)}{R(T_1,0)} = -5.0216x^5 + 1.4416x^4 + 5.3328x^3 - 3.3145x^2 + 1.7948x + 0.9993 \quad (4)$$

The x value is obtained through equation (1) in terms of pressure and temperature measurements. Both analytical fits (equation (2) and (4)) are valid in the range of $0<x<1$.

Fig.4 gives the final comparison between the experimental observation and the theoretical expectation with the concept of "overheating β phase " modification. That is: for each different period the different R_o is applied to calculate the ratio R/R_o. The agreement is fairly well.

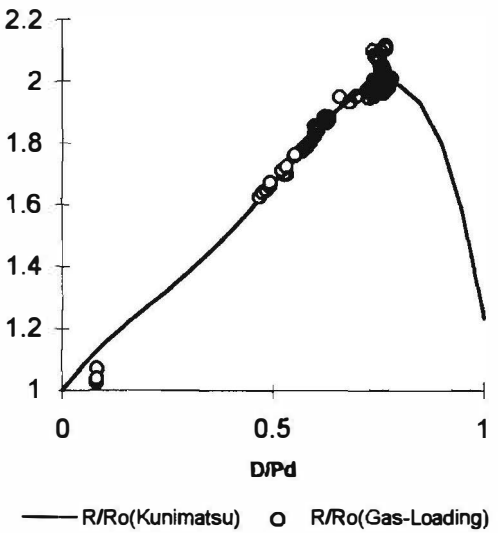

Fig.4 Comparison with Kunimatsu Formula after the Modification of R_o

4. Conclusion

The sudden change of electrical resistance of the palladium wire is likely due to the transition between the " overheating β phase" and the α+β coexisting phase. This phenomenon was missed in the electrolytic cell loading experiments where the cell temperature was kept as a constant. This explanation is consistent with the pressure and the temperature measurements. On the other hand, it means that in our present gas-loading experiment the loading ratio is mostly on the left hand side of the resistance peak. In order to enhance the " excess heat", it seems necessary to follow the Oates and Flanagan's recipe, i.e. to load the deuterium at even lower pressure with an incandescent tungsten wire.

Acknowledgments

This work is supported by the State Commission of the Science and Technology, the Natural Science Foundation of China, the Basic Research Fund of Tsinghua University. Many thanks to Mr. Karl Chang, the co-founder of the VeriFone Inc., for his generous support.

References

1. Mckubre et al., "Calorimetry and Electrochemistry in the D/Pd System," The Proceedings of the First Annual Conference on Cold Fusion (1990, March 28-31, Salt Lake City, USA), p.20.
2. J. Minato, K. Kunimatsu, et al., "Materials/Surface Aspects of Hydrogen/Deuterium Loading into Pd Cathode," Proceedings of ICCF-5 (1995, April 9-13, Monte Carlo, Monaco), p.383.
3. F.S. Bu, X. Z. Li, et al., "Loading Ratio Study in a Gas-loading System," Proceedings of ICCF-6 (1996, Oct. 13-18, Toya, Japan).
4. Y. Fukai, " The Metal-Hydrogen System," Springer-Verlag, Berlin, Heidelberg (1993), p.4.

Material Science Studies

Effect of Cold Work of Palladium on Electrolytic Hydrogen Absorption

Nobuyuki Kamiya, Yuzuru Sakai, Yasuyuki Watanabe, Osamu Yamazaki,
Naobumi Motohira, Ken-ichiro Ota and Kenya Mori *

Yokohama National University
79-5 Tokiwadai, Hodogaya-ku, Yokohama 240 JAPAN
* Tanaka Kikinzoku Kogyo
2-73 Shinmachi, Hiratuka 254 JAPAN

Abstract

The effect of cold work of Pd has been studied to find out the mechanism of hydrogen absorption in the Pd crystal. The H/Pd decreased with extending the cold working. With the 30% cold working specimen, the H/Pd was 0.924. On the contrary, only 0.842 was obtained for the 90% cold working specimen. The stagnant potential obtained by the current interruption method well corresponded with the H/Pd. Absorbed hydrogen was found to diffuse mainly into bulk.

1. INTRODUCTION

The Pd cathode absorbs hydrogen in aqueous solution very easily and it is often pointed out that the amount of absorbed hydrogen in Pd depends on many factors such as the electrolysis conditions and the material properties. In this study, the effect of cold works of Pd on the amount of absorbed hydrogen has been studied quantitatively.

2. EXPERIMENTAL

Pd rods of 1 mm diameter (Tanaka Kikinzoku Kogyo) having different cold working ratio, i.e., 30, 60 and 90% (called thereafter as R30%, R60% and R90%, respectively) were used for electrode specimens. In order to investigate the anealing effect, these Pd rods were heated at the appropriate temperatures under a high vacuum of 10^{-4}～10^{-5} torr for 2 h, unless otherwise indicated. The specimens treated by cold working-annealing were represented like; e.g., R30%-T900 for 30% cold working and then annealing at 900℃. R30-none means 30% cold working and no annealing.

One tenth M (M=moldm^{-3}) sulfuric acid light water solution prepared with ultra pure water was used for the electrolyte. Pt anode of which surface area is large enough to the Pd cathode was placed surrounding the Pd in an equal distance as shown in the right side drawing in Fig. 1. Electrolysis was carried out at the constant current density of 100 mAcm^{-2} and 296±2K in an acrylic cell.

The absorbed hydrogen was measured directly by combining two methods, i.e., volumetry and gravimetry methods[1]. By means of a buret, the volume of gas evolved from the Pd cathode was measured for 4 h after stopping the electrolysis. The left side drawing of Fig. 1 shows the apparatus for the measurement. At the end of the measurement, no more gas evolution was observed. This is the volmetriy method. On the other hand, Pd still contained hydrogen in the bulk. The weight of hydrogen remaining in the Pd cathode after the volumetry measurment was determined by the gravimetry method. i.e., by a semi-micro balance. By these measurements, the molar ratio of

hydrogen to palladium. i.e., H/Pd was determined.

3. RESULTS AND DISCUSSION

The cross and parallel section of Pd cathode before and after the electrolysis were observed by a metallograph. Figure 2 (a) through (c) shows the photographs of the cold worked Pd surfaces before electrolysis. The grain size of 30% cold working specimen was 30～200 μm. On the other hand, the size of 90% cold working was 5～30 μm and was distributed with the elongation toward the cold working direction. After the electrolysis, the surface of the electrode was slightly reformed maybe by the thermal exapnsion

The specimens of 90% cold working specimens were annealed for 2 h at 900, 600 and 300℃. As shown in Fig. 2 (d) through (f), the recrystalization takes place more easily at the higher temperature. At 300, almost no annealing effect was observed and only the small grains as seen in the nontreated specimen were observed with elongation toward the cold working direction.

Figure 3 shows the dependence of H/Pd on electrolysis time for cold working Pd electrodes in H_2SO_4 under the constant current electrolysis of 100mAcm^{-2}. Small points in the middle of the figure represent the H/Pd of gravimetry. The difference between the large points in the upper part and the small points indicates the H/Pd of volumetry. The total H/Pd values with R90% and R60% specimens increased with time and got to the steady value in about 70 h. However, the value with R30% looked to decrease after reaching the maximum at about 70 h. The gravimetric H/Pd value of all the specimens also related to the total H/Pd. The stagnant potential (Eoff,s) obtained by the current interuption method[2] also corresponded well to the above relations. It was reported that the stagnant potential well corresponded to the H/Pd[1] for a thin Pd film. This relation fits also the cold working specimens.

Figure 4 shows the dependence of H/Pd with 90% cold working specimens on annealing condition. The low H/Pd with the high cold working specimen recovered extensively especially when annealed at high temperature. As indicated in Fig. 2, annealing at the high temperature induces the formation of the large grain and the absorption of hydrogen would preferentially takes place through the grain boundary. As for R90%-T300 specimen, no difference of the H/Pd was observed. Temperature at least higher than 600℃ may be required.

Figure 5 shows the average value of H/Pd after 72 h of electrolysis in 0.1M H_2SO_4 for the specimens treated under various conditions. The time of 72 h may be the maximum point of H/Pd and therefore it would be best to compare each other. Considering the bottom three cases, the H/Pd does not depend on the extent of the cold working if the specimens are annealed at the high temperature like 900℃.

Figure 6 shows the photograph of Pd bulk after electrolysis and indicates the absorbed hydrogen did not diffuse along the grain boundary but diffuse mainly into the bulk.

4. Conclusion

The H/Pd ratio depended on the degree of cold working. At 30% cold working Pd, the H/Pd ratio got the maximum 0.92 at 70 h and decreased to 0.89 after 290 h. For 90% cold working Pd, the maximum H/Pd was 0.85 at 70 h. Since the grain boundary diffusion of hydrogen in Pd was not observed and the cut off potential of Pd cathode well coincided with the H/Pd ratio, the H/Pd ratio might be affected by the hydrogen desorption overvoltage of Pd cathode.

References

1) O. Yamazaki et al; J. Electroanal. Chem., 390 127 (1995).
2) T. Maoka, M. Enyo; Electrochim. Acta, 26 607 (1981).

Material Science Studies

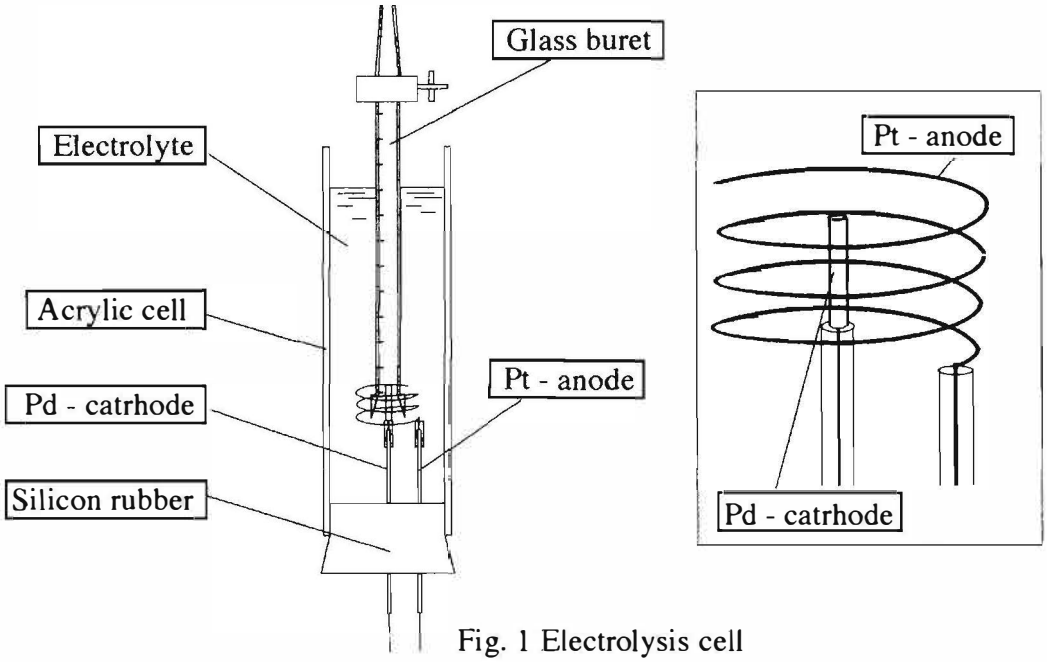

Fig. 1 Electrolysis cell

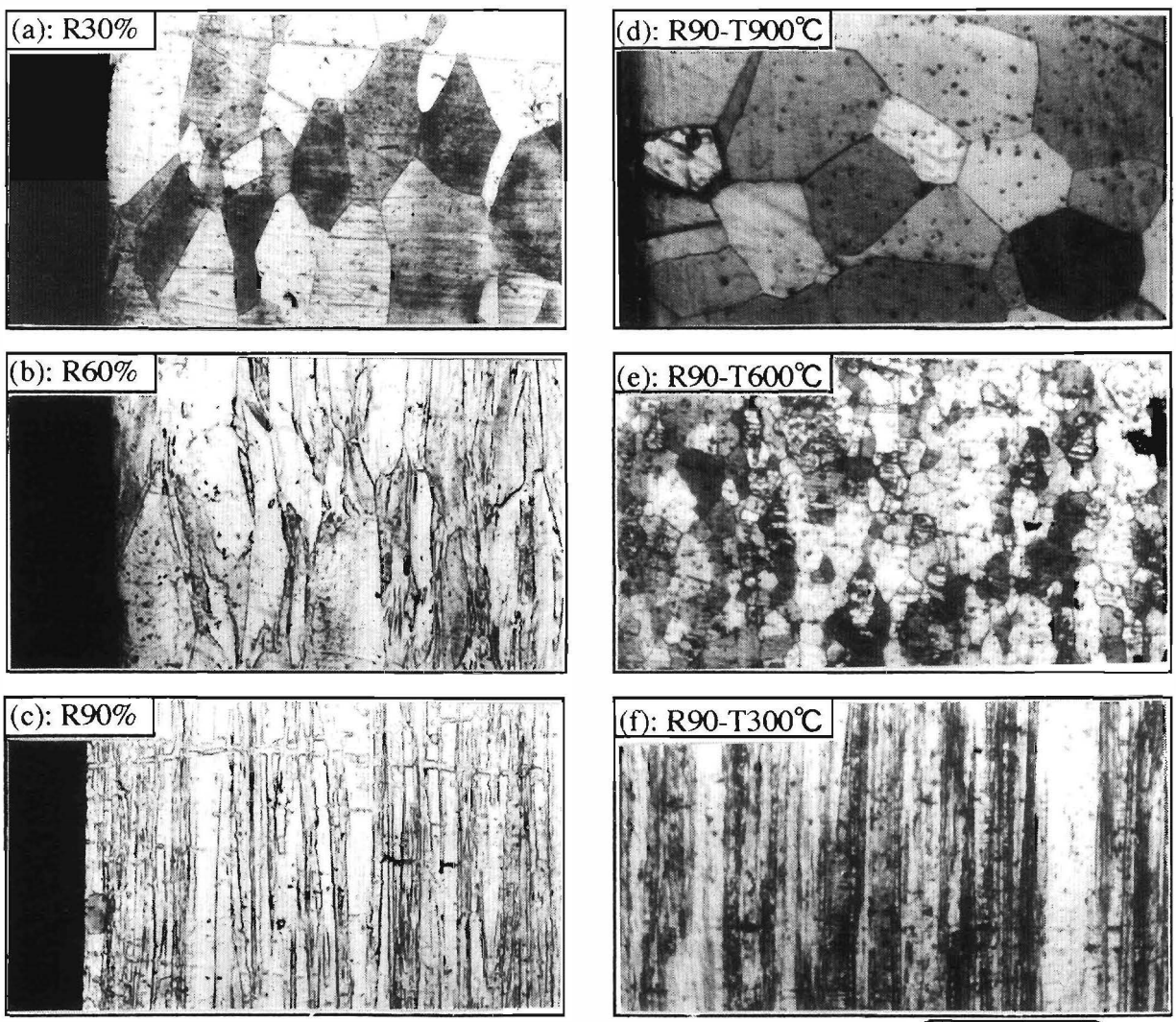

Fig. 2 Photographs of Pd bulk before electrolysis.
(a): R30%, (b): R60%, (c): R90%
(d): R90-T900℃, (e): R90-T600℃, (f): R90-T300℃.

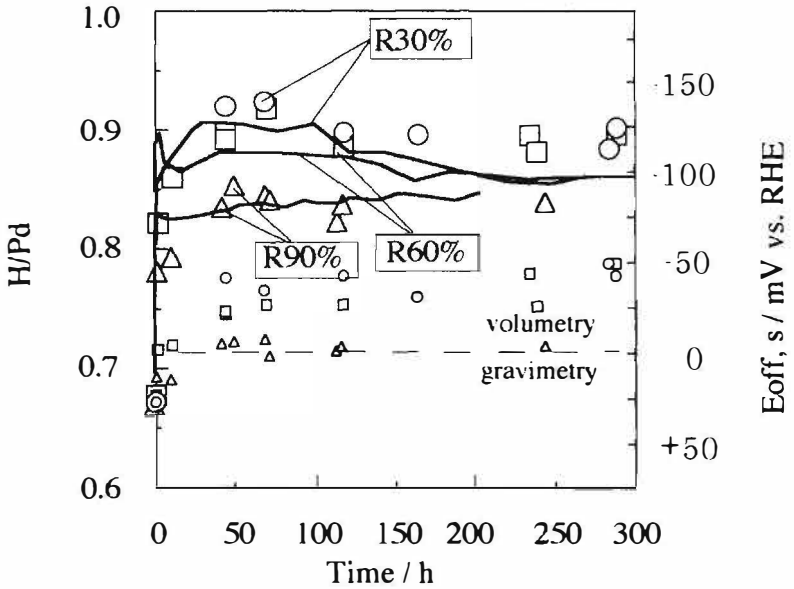

Fig. 3 Dependence of H/Pd on Electrolysis time for cold working electrode in H_2SO_4.
C.D.; 100mAcm^{-2}.
(○) : 30% cold working, (□) : 60% cold working,
(△) : 90% cold working.
(——): R30, (——): R60, (——): R90.

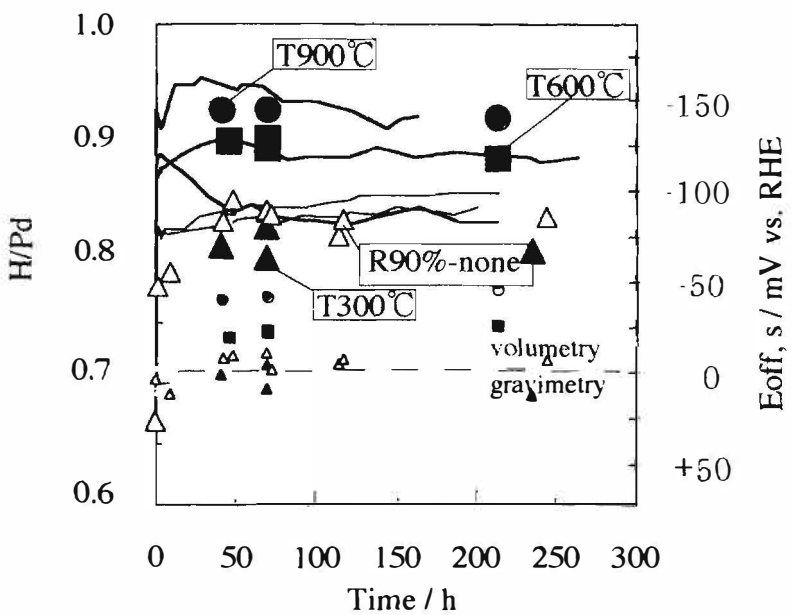

Fig. 4 Dependence of H/Pd on Electrolysis time for annealed electrode in H_2SO_4.
C.D.; 100mAcm^{-2}.
(●), (——) : annealed for 2h at 900℃,
(■), (——) : annealed for 2h at 600℃,
(▲), (——) : annealed for 2h at 300℃,
(△), (——) : none annealed (R90%).

Material Science Studies

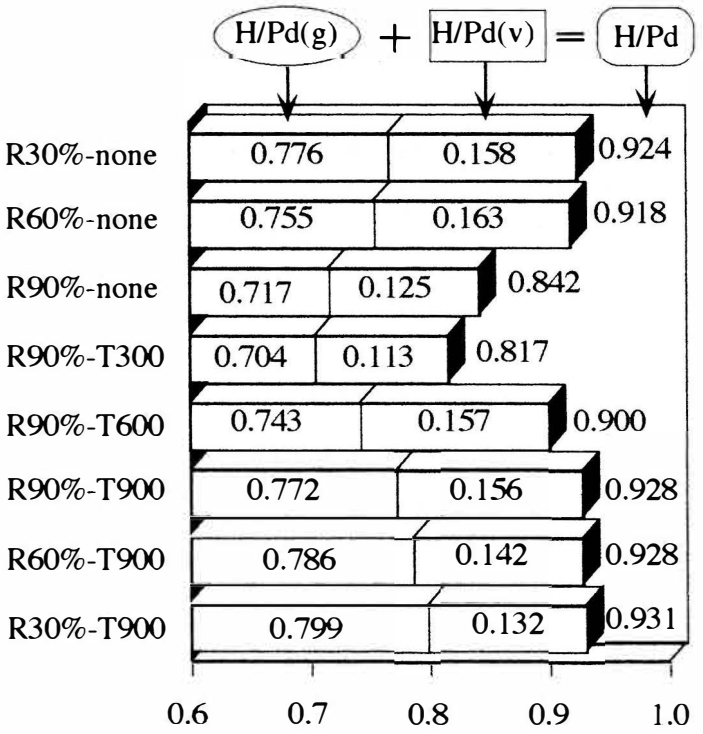

Fig. 5 The value of average for H/Pd after 72h electrolysis in 0.1M H_2SO_4 at 23℃.
C.D.; 100mAcm^{-2}.

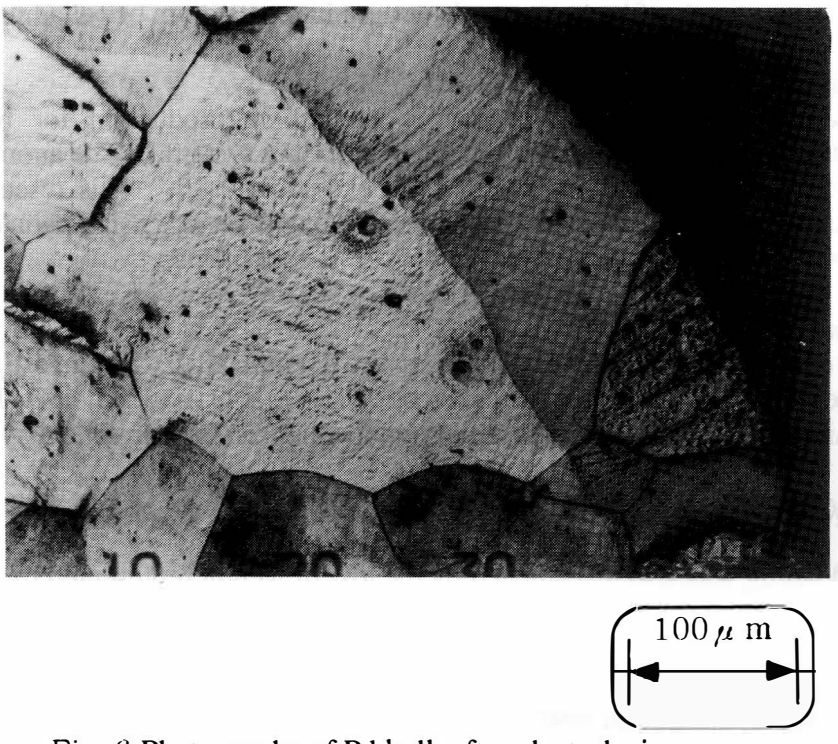

Fig. 6 Photographs of Pd bulk after electrolysis for 10min. C.D.: 100mAcm^{-2}.

Material Science Studies

Click here for a more readable copy of this paper.

Electrochemical Loading of Hydrogen and Deuterium Into Palladium and Palladium-Boron Alloys

Melvin H. Miles and Kendall B. Johnson

Chemistry & Materials Branch, Research & Technology Division
Naval Air Warfare Center Weapons Division
China Lake, CA 93555-6100, USA

and

M. Ashraf Imam

Physical Metallurgy Branch, Materials Science & Technology Division
Naval Research Laboratory
Washington, DC 20375-5320, USA

Abstract
Excess power production and other anomalous effects have been observed during the electrolysis of heavy water using palladium and palladium-boron alloys as the cathode materials. This study focused on hydrogen and deuterium loading into palladium and palladium-boron alloys. Improved calorimetry provided for the detection of the exothermic heat of absorption of deuterium into palladium and palladium-alloy cathodes. The addition of boron to palladium does not significantly affect the initial loading rate but slows further loading to higher levels. The presence of boron in the palladium significantly slows the rate of the deloading process. Cracks or other surface defects prevent high loading levels of hydrogen or deuterium into palladium or palladium-boron alloys.

1. Introduction

We have observed anomalous excess power and helium production for both the palladium-deuterium system and the palladium-boron alloy-deuterium system.[1,2] The anomalous excess power effect apparently requires a loading ratio of D/Pd exceeding 0.85.[3] This research investigates the extent of loading and the rate of the loading and deloading processes using palladium and palladium-boron alloys as cathodes in electrochemical electrolysis experiments.

2. Experimental

The hydrogen or deuterium loading of palladium or palladium alloys was investigated by the weight gain of the electrode during constant current electrolysis in H_2O + LiOH or D_2O + LiOD solutions. The weight gain of the metal (M) due to deuterium loading can be represented by

$$M + x\ D_2O + xe^- \rightarrow MD_x + x\ OD^- \qquad (1)$$

The rate of deloading was also investigated by the loss of weight represented by

---

Approved for public release; distribution is unlimited.

Material Science Studies

$$MD_x \rightarrow M + \frac{x}{2} D_2 \qquad (2)$$

The weighing method involved interrupting the electrolysis and removing the electrode from the solution. In addition, the use of a sensitive calorimeter determined the rate of the loading process by measuring the power produced during the initial exothermic loading process.[1,4] For example, ΔH = -35,100 J per mole of D_2 for the formation of PdD_x for $x \leq 0.6$.[5]

3. Results

Initial studies were conducted on palladium rods (1-mm diameter) and palladium sheet electrodes in H_2O + 0.1 M LiOH solutions to test the reliability of the weighing method. Upon interrupting the constant current electrolysis and removing the palladium electrode from the cell, it was found that the loss of weight could be readily measured and that the weight change was linear with time. For five or more weighings over a 10-minute period, the plot of the H/Pd ratios versus time was extrapolated back to zero minutes to yield the initial H/Pd loading when the electrolysis was interrupted.

Loading levels of H/Pd $\geq$ 0.7 were readily obtained in all experiments. Both a 1-mm diameter palladium rod (Johnson-Matthey) cathode and a palladium sheet cathode (Tanaka Metals, Japan) were used in these investigations. The highest loading level for the palladium rod was H/Pd = 0.923 while the highest value for the palladium sheet was H/Pd = 0.821. No obvious correlation between the loading level and the current density could be established. The type of anode used in the cell apparently affected the loading level. Higher loading levels were obtained using a platinum anode than when a nickel anode was employed. The H_2O + LiOH solution eventually became dark due to corrosion products when the nickel anode was used.

Although a loading level of H/Pd = 0.7 was readily obtained in all experiments using palladium cathodes, only a few experiments yielded H/Pd ratios approaching 0.9. The highest loading occurred following the heating of the loaded palladium rod with a heat gun that caused it to glow red due to a run-away exothermic reaction of the hydrogen exiting the surface with oxygen from the air.

The study of the H/Pd ratio over a 21 day period for a palladium rod cathode showed several peaks and valleys in the loading ratio versus time. The H/Pd ratio varied from 0.79 after 3 days to a low of 0.72 at 6 days and a maximum of 0.92 at 16 days. There was no obvious correlation between the loading ratio and any experimental variable. For most experiments, the change in H/Pd after interrupting the electrolysis was generally about -0.01 per minute.

A new calorimeter designed and built at China Lake[1,4] was used to measure the heat of absorption of deuterium into the palladium rod cathode. This result is shown in Figure 1. A power output of approximately 6.5 mW is observed for 2 hours. This yields 47 Joules that compares very favorably to the expected 44 Joules based on the cathode size (1 mm x 4.3 cm), a loading level of $PdD_{0.6}$, and using the reported value of ΔH = -35,100 J per mole of D_2.[5] Figure 1 shows that most of the loading up to D/Pd = 0.6 is completed within 2 hours of the start of the electrolysis. Further loading beyond the D/Pd = 0.6 ratio yields a discontinuity in the enthalpy value.[5]

Energy storage due to endothermic processes early in the experiments has been proposed as an explanation for the excess heat effect.[6] Figure 1 shows that there is no endothermic or energy storage behavior during D_2O electrolysis, hence this argument by S. E. Jones et al.[6] is invalid. Excess power was observed for this electrode later in the experiment.[4]

Loading studies for two palladium-boron alloys, both containing 0.75 weight % boron, are shown in Table 1. The loading process is much slower with the boron present than observed with pure palladium. While loading levels of D/Pd = 0.6 could be attained within a few hours for palladium

cathodes, nearly 12 days of electrolysis is required to reach this loading level for the palladium-boron alloy (Table 1). Judging from Table 1, the Pd-B alloy in cell C slowly loaded to higher levels. After 100 days, the D/Pd ratio was 0.85 for the alloy in cell C but only 0.63 for the alloy in cell D. A surface flaw caused this difference. The Pd-B alloy used in cell D had a long folded-over metal region produced by the swaging of this very hard material. This acted as a long crack in the surface. Cracks or similar surface defects are a major factor in preventing high hydrogen or deuterium loading levels. Significant levels of excess power were observed for the Pd-B alloy used in cell C.[2] No excess power was measured for the flawed Pd-B alloy used in cell D.[1,2]

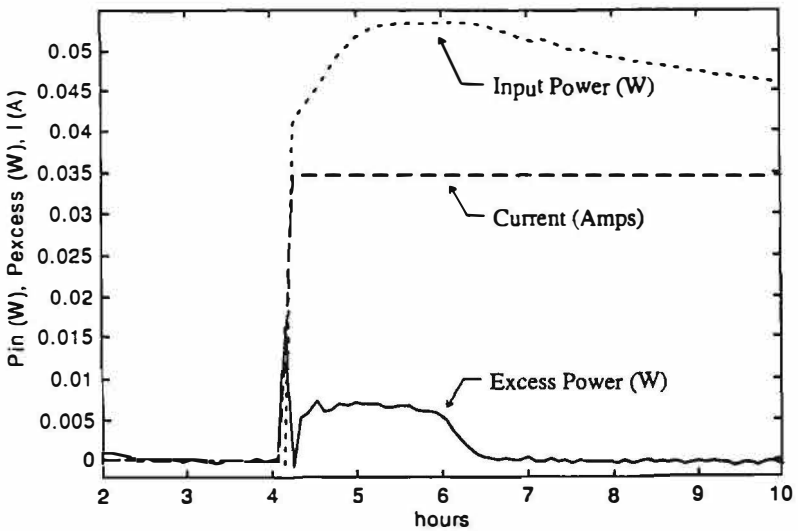

Figure 1. Measurement of the Exothermic Heat of Absorption of Deuterium Into a Palladium Wire Cathode (1 mm x 4.3 cm) Using the New Calorimeter Developed at China Lake.

TABLE 1. Loading Studies by the Weighing Method.

Time (days)	Pd-0.75% B (Cell C)	Pd-0.75% B (Cell D)
7	0.580	0.550
12	0.614	0.594
100	0.85	0.63

Further experiments investigated the effect of the boron concentration on the D/Pd loading level. Table 2 presents loading studies by the weighing method for Pd-0.50 weight % B and Pd-0.25 weight % B cathodes. Loading to the D/Pd = 0.6 level becomes considerably faster as the amount of boron is decreased as shown in Tables 1 and 2. Higher D/Pd ratios are obtained initially for the alloys containing the smaller amount of boron. Excess power was measured in all four experiments listed in Table 2.[1,2]

Calorimetric studies at China Lake showed that the initial exothermic loading of deuterium into the Pd-B alloys is nearly as fast as observed with pure palladium cathodes. This was a surprising result. Further loading to higher levels, however, appears to become very slow for the Pd-B alloys compared to the palladium cathodes (Tables 1 and 2).

TABLE 2. Loading Studies by the Weighing Method Following 5 Days and 10 Days of Electrolysis.

Electrode	Xo (5 days)[a]	Xo (10 days)[b]
Cell A—Pd-0.5% B	0.643	0.640
Cell B—Pd-0.5% B	0.604	0.652
Cell C—Pd-0.25% B	0.692	0.716
Cell D—Pd-0.25% B	0.647	0.695

[a] I = 50 mA for 5 days.
[b] I = 100 mA for the second 5-day period.
NOTE: Microscopic examinations showed surface nicks and scratches but no major flaws on electrodes.

Coulometric measurements of the loading were attempted for the palladium-0.75 weight % B alloy. The currents obtained by potentiostatically controlling the cell voltage were only 2-4 mA, hence less than 10% of the deuterium could be reacted electrochemically (Equation 3) even after 28 hours of electrolysis. Measurements by the weighing method also showed very slow deloading rates for the Pd-0.75 weight % B alloys, i.e., the D/Pd ratio change was less than -0.001/minute. This is more than ten times slower than observed for palladium electrodes. It took 2 weeks to reach an equilibrium weight for these alloys.

Deloading studies by the weighing method for the Pd-0.50 weight % B and Pd-0.25 weight % B alloys are shown in Table 3. The deloading rate again is much slower than for palladium cathodes. About 10 days was required to reach an equilibrium weight.

Tables 1-3 show that small amounts of boron added to the palladium can produce major changes in the deuterium deloading rates. The initial rates of loading, based on calorimetry, are similar for palladium and palladium-boron alloys. Perhaps boron accumulates in the grain boundaries during the initial loading and then hinders both the further ingress and egress of hydrogen or deuterium into and out of the metal lattice.

TABLE 3. De-loading Studies by the Weighing Method.

Time (hours)	Pd-0.5% B (Cell A)	Pd-0.5% B (Cell B)	Pd-0.25% B (Cell C)	Pd-0.25% B (Cell D)
0	0.617	0.643	0.687	0.687
12	0.490	0.497	0.518	0.512
36	0.350	0.368	0.446	0.367
67	0.228	0.261	0.215	0.190
112	0.152	0.161	0.108	0.069
181	0.100	0.051	0.034	0.010
282	0.065	0.003	0.010	0.003

4. Summary

Loading and deloading of hydrogen and deuterium in palladium and palladium-boron alloys can be readily studied by the weighing method. Cracks or other surface flaws affect the degree of loading that can be obtained. Small amounts of boron alloyed with palladium can slow the deloading rate by a factor of ten or more. Excess power was observed for all Pd-B alloys used in these loading experiments except for one that had a surface flaw.[1,2]

5. Acknowledgments

Appreciation is extended to the Office of Naval Research for support of this work.

6. References

1. M. H. Miles, B. F. Bush and K. B. Johnson, "Anomalous Effects in Deuterated Systems," NAWCWPNS TP 8302 (September 1996)
2. M. H. Miles, K. B. Johnson and M. A. Imam, "Heat and Helium Measurements Using Palladium and Palladium Alloys in Heavy Water" in Proceedings of the Sixth International Conference on Cold Fusion, Hokkaido, Japan, 13-18 October 1996 (submitted).
3. M. C. H. McKubre, S. Crouch-Baker, A. M. Riley, S. I. Smedley, and F. L. Tanzella in Frontiers of Cold Fusion, H. Ikegami, Editor, Universal Academy Press, Tokyo, pp. 5-19, 1993.
4. K. B. Johnson and M. H. Miles, "Improved, Open Cell, Heat Conduction, Isoperibolic Calorimetry" in Proceedings of the Sixth International Conference on Cold Fusion, Hokkaido, Japan, 13-18 October 1996 (submitted).
5. J. Balej and J. Divisak, *J. Electroanal. Chem.*, **278**, 85 (1989).
6. S. E. Jones and L. D. Hansen, *J. Phys. Chem.*, **99**, 6966 (1995).

Material Science Studies

In situ Potentio, Resisto and Dilatometric Measurement of Repeated Hydrogen Absorption in Pd Electrode by Electrochemical Cathodic Loading Method

Hiroo NUMATA and Izumi OHNO

Faculty of Engineering , Tokyo Institute of Technology
O-okayama, Meguro-ku, Tokyo Japan 152

ABSTRACT

The physico-chemical properties of hydrogen in Pd have been studied by *in situ* potentio, resisto and dilatometric measurement. A set of potential, resistance ratio and increase of dilation($\Delta l/lo$) was recorded simultaneously after the establishment of an equilibrium of hydrogen with Pd lattice. The hydrogen electrode potential is converted to 'equivalent hydrogen pressure', which might signify gaseous pressure in a void or on a surface. The structural phase transition ($\alpha \rightarrow \beta$) occurred during the cathodic discharging of hydrogen and the characteristic values of this phase change are well consistent with those predicted from Pd-H diagram. Hydrogen infusion causes lattice expansion, which resulted in the dilation of Pd electrode. Repeated absorption and desorption cycle deteriorates the mechanical properties, where the hysteresis of R/Ro vs. hydrogen pressure diagram was appeared depending on the mode of electrolysis(the extent of H/Pd ratio).

INTRODUCTION

Palladium readily absorbs large amounts of hydrogen gas where hydrogen atom exists in interstitial sites. Recently, deuterium loading more than $x \simeq 0.9(PdD_x)$ results in cold fusion involving D atoms. So far hydrogen infusion into the steels causes hydrogen embrittlement.

A common aspect to these hydrogen-metal related phenomena is the sporadic nature of neutron emission or heat bursts and that of microscopic change of solid, i.e., dislocation generation and motion accompanying crack formation in certain condition. For Pd, the dissolved hydrogen into interstitial sites at first expands the α phase lattice and creates elastic strain fields resulting some deviation from an ideal hydrogen behavior, designated as, electrode potential deviation from Nernst equation. Further insertion of hydrogen occurs an α-β phase transition, where the α and β phases have different partial molar volume. It is apparent that during the α-β phase transition anisotropic each crystal expands independently generating structural defects, i.e. dislocation, slip bands, fault and rifts, which are similar to the characteristics of the heavily cold worked Pd.

In our experiments, where an annealed Pd cathode(9mmϕ, 10cm long) was used during a long-term deuterium evolution, neutron count rate was observed. In the second experiment (21mmϕ, 32mm long), initial term electrolysis had no significant count rate of neutron, while high count rate of neutron was appeared for several days after raising current density step by step and after raising temperature[1]. Metallographic observation results in two faults, blisters, cross slips and holes on Pd surface. *In situ* measurements of physico-chemical properties of metal-hydrogen system

remained open.

It is noted that the materials are encountered by *critical conditions* through the prolonged and high current electrolysis, immediately before sporadic microstructural changes. Since repeated hydrogen absorption and desorption cycles are useful for simulating heavily worked Pd, mechanical and physical properties of Pd under hydrogen absorption and desorption cycles have been *in situ* measured to evaluate the critical conditions in terms of the repetition of the α-β phase transition.

In this study, the electrochemical behavior, dilation and resistance of Pd electrode have been *in situ* measured using a computer controlled potentiostat, dilatometer and miliohm meter under electrochemical cathodic discharging of hydrogen in glycerin and phosphoric acid solution.

EXPERIMENTAL

A set of potential, dilation and resistance of Pd electrode was measured after the establishment of an equilibrium of hydrogen with Pd(2 and 0.8mmϕ 50mm long). The measurement system was constructed by a computer controlled potentiostat, miliohm meter and dilatometer. The electrolytic cell was the modified three-electrode cell. An electrolyte is the mixture of glycerin and phosphoric acid(2:1 volume ratio). The electrolyte acts as the permeability barrier to hydrogen once introduced into Pd lattice[2]. The details of experimental procedure are described elsewhere[3].

The electrolysis was performed using three types of galvanostatic pulsed current as shown in Fig.1. A mode electrolysis reveals that a set of pulsed currents(absorption) is applied immediately after accomplishing the preceding set of one(absorption). Thus, repeated hydrogen absorption and possible desorption(during off pulse) is continued until the saturation of hydrogen content takes place. The saturation of hydrogen is easily detected by attaining time independent resistance. In B and C mode electrolysis desorption by pulsed current reversal technique is intervened between one set of pulsed current(absorption) and next one(absorption). The difference of these two modes is in the form of current supply, i.e., galvanostatic pulsed current and potentiostatically controlled constant current. During both mode electrolysis the decision of supplying next pulsed current has been done by diagnosis of complete recovery of resistance.

RESULTS AND DISCUSSION

The formation of microscopic holes and faults on Pd surface was previously explained by the geothermal phenomenon on the earth created by the mantle movement and the heat of the earth[1]. This modelistic approach makes possible a reasonable guide line for analysis of a complicated phenomenon. We postulate the microstructural model inside the solid(Fig.2), which improves reproducibility of cold fusion related phenomena, i.e., heat evolution and nuclear products emission. Although the precise description about the model is not shown, an important aspect is cycling 4 sequential processes(some of them yet remain as speculation in this paper), which might be identified by the following measurements of the physical and mechanical properties of Pd[4].

In the recent experiments[5], significant changes of the α-β transition behavior of thin Pd film compared with that of bulk Pd suggests that the surface effect play a significant role in obtaining the bulk properties, i.e., resistance and dilation of Pd. Hence, we use rather thick Pd rods to achieve more sensitive measurements to the bulk properties, though much longer electrolysis is required to attain a steady state of diffused hydrogen in thick Pd rod.

Among many metal-hydrogen alloys Pd is particularly known as easily absorbing and desorbing material, which indicates that the formation of a surface layer does not play a significant role as a permeability barrier. However, the transfer of hydro-

gen is not determined only by the surface condition, but by the microstructural change of the bulk attributed to the electrochemical loading. Therefore, it is necessary to explain the physical and mechanical characteristics in connection with microstructure of Pd.

Potential, resistance and dilation of Pd under A mode electrolysis

After each increment of a cathodic discharge(Pd:2 mm$^{\phi}$ 50mm long, 0.2 and 2mA/cm^2, pulse duration 500s), the electrode potential changes with time and reaches at the steady state with an equilibrium between hydrogen atmosphere and hydrogen activity of Pd inside. Thus, 'equivalent hydrogen pressure' pH_2: the hydrogen pressure equilibrated with that in Pd metal(e.g., in a void), is expressed as, assuming Nernst equation under the limited condition

$$pH_2=\exp[-(E+E_{SCE})(2F/RT)]$$

where E_{SCE} is the potential of the reference electrode. Figure 3 shows the plot of electrode potential vs. hydrogen concentration of 1st absorption. Although the hydrogen concentration is calculated coulommetrically, the absorption efficiency is known to be 1 upto H/Pd ratio 0.6 and 0.8 over H/Pd ratio 0.6. At $x \leq 0.01$ the electrode potential obeys Nernst equation, while it exhibits constant value corresponding to the coexistence of the α and β phases($0.01<x<0.55$). The concentrations of the onset(α_{max}) and the end (β_{min}) of phase transition are well consistent with those predicted from Pd-H phase diagram. The equivalent hydrogen pressure of two phase region is 0.05 atm, which is agreed with that obtained from pressure and composition isotherms of Pd-H. The characteristic values presented in Fig.3, were consistent with those of Pd-H isotherm obtained by gas equilibrium method, which substantiates the correctness of the electrochemical loading method.

It must be keep in mind that electrochemically evolved hydrogen atoms are absorbed readily into Pd lattice because intense driving force, i.e., the gradient of hydrogen concentration under beneath the surface suffices complete infusion of hydrogen, due to the electrochemical overpotential applied. However, it is demonstrated that hydrogen atoms exist homogeneously over the whole electrode, where the attainment of stationary electrode potential is a least diagnosis (computer proceeds next charging step after checking the results of diagnosis).

The results of this equilibrium check can also be seen as evidence that the time dependence of resistance, as obtained by interrupting discharging is still for 30h within the uncertainty of the experiment. Figure 4 shows whole potential and resistance plot vs. H/Pd ratio, where intervening was indicated by an arrow.

On the other hand, hydrogen infusion causes lattice expansion, which resulted in the dilation ($\Delta l/lo$) of Pd. The plot of the dilation vs. H/Pd ratio in the α region is shown in Fig.5, which is measured simultaneously with the case of Fig.3. The dilation of Pd is almost in proportional to an increase in H/Pd ratio, whose slope, the molar volume of hydrogen is obtained as $V_H=1.64$ cm^3(mol H)$^{-1}$ with the $V_{Pd}=8.87$ cm^{3}mol^{-1}. The result coincides with the literature value $V_H=1.77-0.873$cm^3(mol H)$^{-1}$ [6].

The plot of the dilation in more than the α region is shown in Fig.6 with respect to $x>0.06$. The β phase has a larger lattice constant than the α phase, though the dilation is smaller in the α+β phase than in the α phase. Assuming that the lattice constant of Pd is a(0)=3.890Å, a(α_{max})=3.893Å and a(β_{min})=3.929Å can be obtained. The values coincide with the reported ones: a(α_{max})=3.894Å and a(β_{min})=4.025Å[7]. When the β phase is attained, large dilation can again be exhibited linearly to the H/Pd ratio upto 0.8.

Repeated absorption and desorption of hydrogen in Pd ($x<0.02$) under B mode electrolysis

Repeated absorption and desorption of hydrogen(Pd:0.8mm$^{\phi}$ 50mm long, 0.2mA/cm^2, 7000s) was performed using B mode($x<0.02$) electrolysis, where the H/Pd ratio of

absorption was controlled upto the on-set of the α-β transition: α_{max}. In this case hydrogen infusion does not heavily deteriorate the mechanical properties of desorption cycle, since the diffusion of hydrogen proceeds rapidly and without hysteresis to the α phase. The results of 1st to 5th cycle absorption and desorption show that the electrode potential obeys the Nernst equation while the potential shifts to less noble direction as the cycle number is increased. The plots of the potential vs. H/Pd ratio of 5 to 11th cycle show steep straight lines, thus the on-set of phase transition proceeds with much smaller H/Pd ratio. It is noted that the potential, that is, ultimate hydrogen pressure of the α-β coexistence is increased accompanying the evolution of the potential fluctuations. These features of a large number of cycle indicate that even the low level of discharging accumulate the mechanical effect(stress and/or stimulating hydrogen association) as evidenced by the increased, as well as, unstable hydrogen pressure.

The dilation vs. H/Pd ratio of absorption is shown in Fig.7, where the slopes of 2nd to 4th cycle increase progressively; most of the slopes after 5th cycle tend to converge into one line. For all the cycles except 1st cycle, the induction period of the dilation is appeared, whereupon the α single phase exists. Inspecting the dilation vs. H/Pd diagrams and taking into account of error of experiment, it is reasonable to assume that the dilation($\Delta l/lo$) is comprised of the linear term of lattice expansion and the complemental term as,

$$\Delta l/lo = a \cdot x + b \qquad a:\text{constant}$$

where the first term of the right hand corresponds to the change of dilation due to lattice expansion and the second term is attributable to sporadic dilation(discontinuous to H/Pd ratio and time): the plastic strain appears over work hardening region on a single crystal. Although it is questionable that the Pd rod under repeated absorption and desorption behaves like a heavily strained crystal, we often observe such sporadic and stepwise dilation under the electrochemical loading. It is highly possible to evaluate the progress of the critical condition in terms of the amplitude and /or frequency of the second term[4].

The results of the resistance ratio(R/Ro) vs. H/Pd ratio of absorption shows a monotonic increase with an increase of H/Pd ratio, where the effect of cycle number lies within the maximum experimental error. The resistance behavior suggests that hydrogen is readily mobile: irrespective of the dilation varied with the number of cycles and the appearance of the induction period.

Repeated absorption and desorption of hydrogen in Pd (x<0.8) under C mode electrolysis

The same repeated absorption and desorption of hydrogen was performed using C mode(x<0.8) electrolysis(Pd:0.8mmϕ 50mm long, 7000s) where the electric charge of absorption is more than that of hydrogen required to attain H/Pd ratio 1.0. It is known that the efficiency of absorption of hydrogen drops over H/Pd c.a. 0.6. We promote to examine the exact value of efficiency at various charging conditions.

Table 1 summarizes the comparison of repeated absorption and desorption cycle between B(x<0.02) and C(x<0.8) mode electrolysis. For example the resistance behavior for B mode electrolysis shows no distinct dependence on the cycle number, while the resistance ratio vs. H/Pd ratio under C mode electrolysis exhibits totally different dependence on the cycle number: the resistance ratio shows a steady increase and attains a flatten regime at R/Ro=1.7 with an increase of H/Pd ratio. During a few number of cycle the H/Pd ratio to reach the flatten regime shifts towards higher content.

One of the important characteristics of the repeated absorption experiments is seen in R/Ro vs. hydrogen pressure diagram, where one of typical data is shown in Fig.8. The comparison of these data shows that larger hysteresis of absorption and desorption cycle is attributable to deterioration of the mechanical property[4,8].

Material Science Studies

This work was supported by NHE fund of the Inst.App.Energy of NEDO.

REFERENCES

1)R.Takagi, H.Numata, I.Ohno, K.Kawamura, S.Haruyama, Fusion Tech.,**19**, 2135(1991)., H.Numata, R.Takagi, I.Ohno, K.Kawamura, S.Haruyama, "The science of Cold Fusion"(Conf.Proc.of SIF(Italy)) **33,** 71(1991).
2)R.Kirchheim, Acta Met.,**29,** 835(1981).
3)T.Ooi, I.Ohno, H.Numata, Denki Kagaku,**61,** 324(1993)., H.Numata, I.Ohno, 1995 Report of Basic Research Group in NHE Project IAE-C9513 p.302(1996) and Proc. 3rd Sympo. of Basic Research Group in NHE Project (July3-4, 1996, Tokyo, Japan), p.55-67.
4)H.Numata, I.Ohno, to be published.
5)M.Nicolas, L.Dumoulin, J.P.Burger, J.Appl.Phys., **60,** 3125(1986).
6)S.Kishimoto et al., J.Chem.Soc.Faraday Trans.,1,**82,** 2175(1986).
7)E.Wicke, H.Brodowsky,"Hydrogen in Metals"(Ed.G.Alfeld, J.Völkl), Vol.2 Springer p.73(1979).
8)F.A.Lewis, W.D.McFall, T.C.Witherspoon, Z.Physik.Chem. N.F.,**114,** 239(1979).

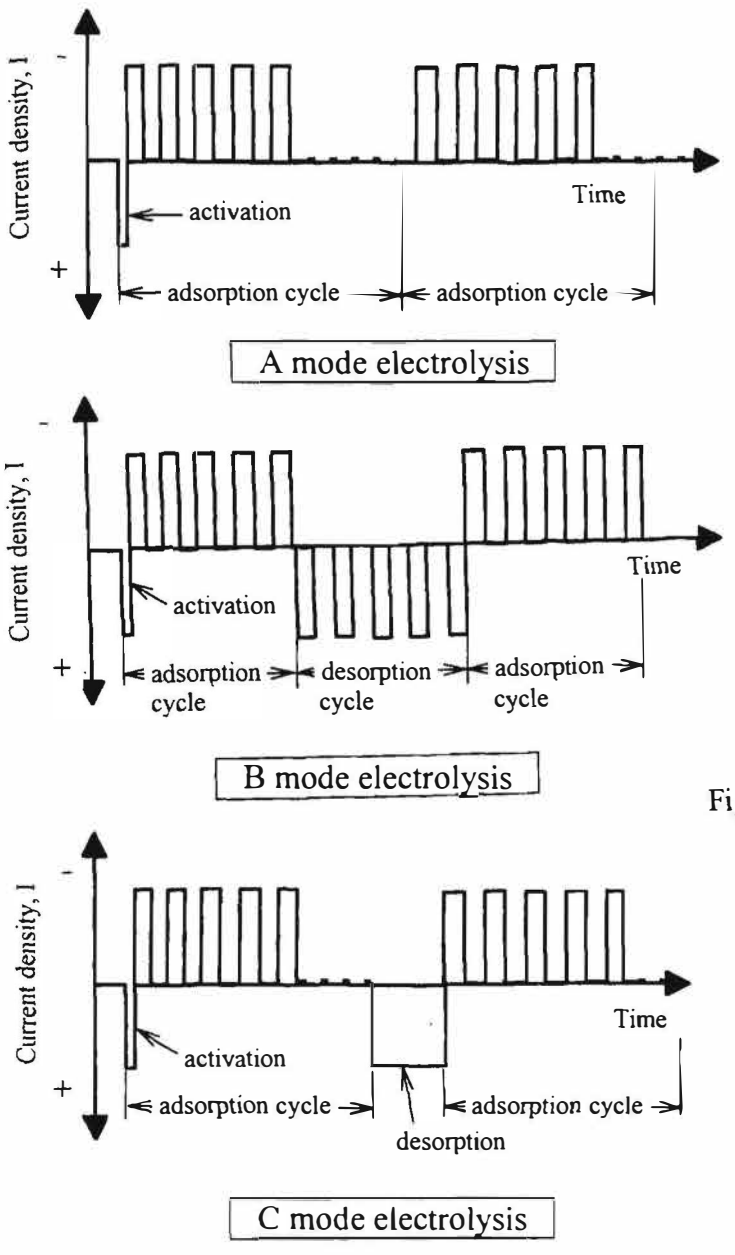

Fig 1 Patterns of current density-time

Material Science Studies

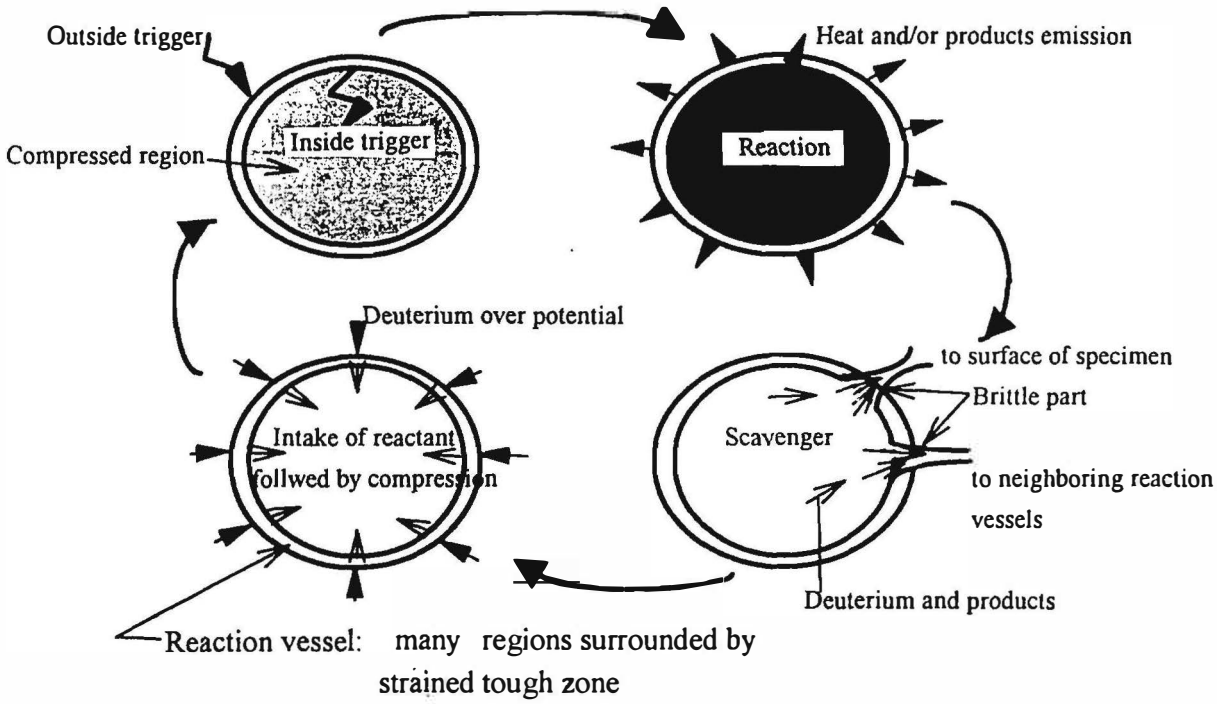

Fig.2 Cold fusion reaction in condensed matter(Pd-D)

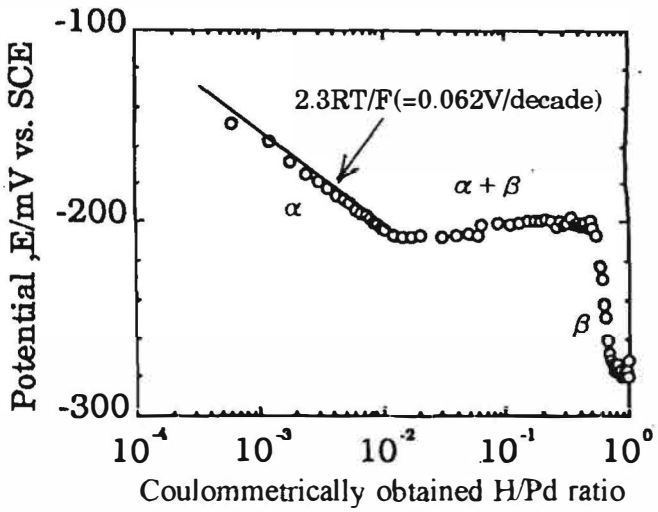

Fig.3 Potential vs. logarithm of H/Pd ratio at 40 ℃ .

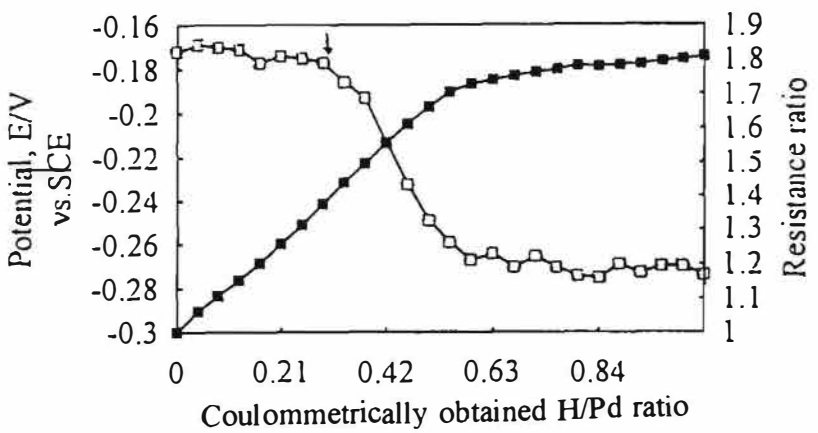

Fig.4 A mode potential, resistance ratio vs. H/Pd plots, 40 ℃
after 30h holding(at arrow) Pd was again electrolyzed.

Material Science Studies

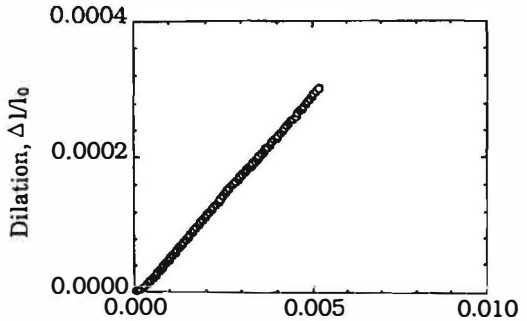

Fig.5 Dilation(Δ l/lo) vs. H/Pd ratio(x<0.005).
40 ℃ , 0.2mA, 500s

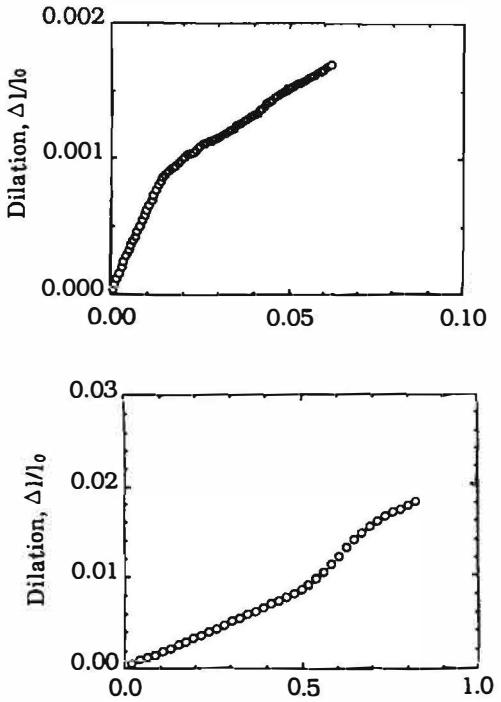

Fig.6 Dilation(Δ l/lo) vs. H/Pd (x<0.06 and <0.8)
top 40 ℃ , 0.5mA, 2000s,
bottom 40 ℃ , 5mA, 7000s

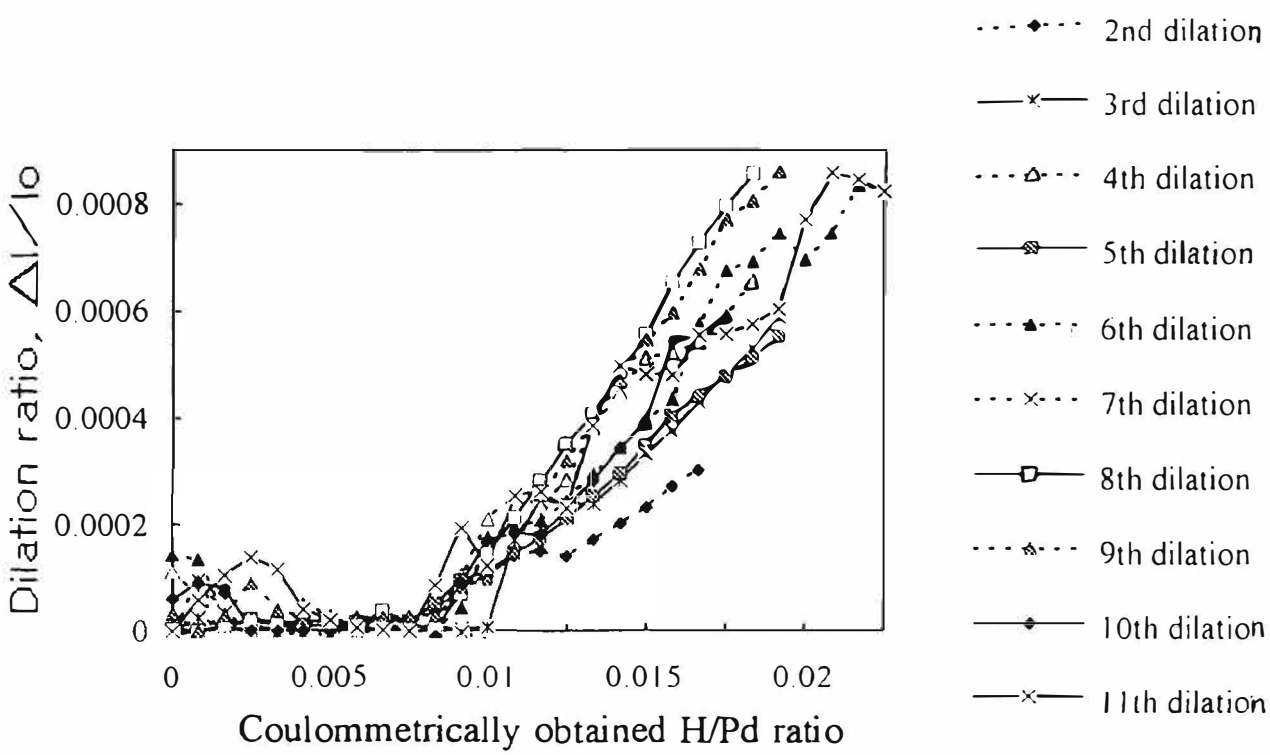

Fig.7 Effect of number of cycle on B mode dilation(Δ l/lo)
vs. H/Pd ratio(x<0.02) diagram.

Material Science Studies

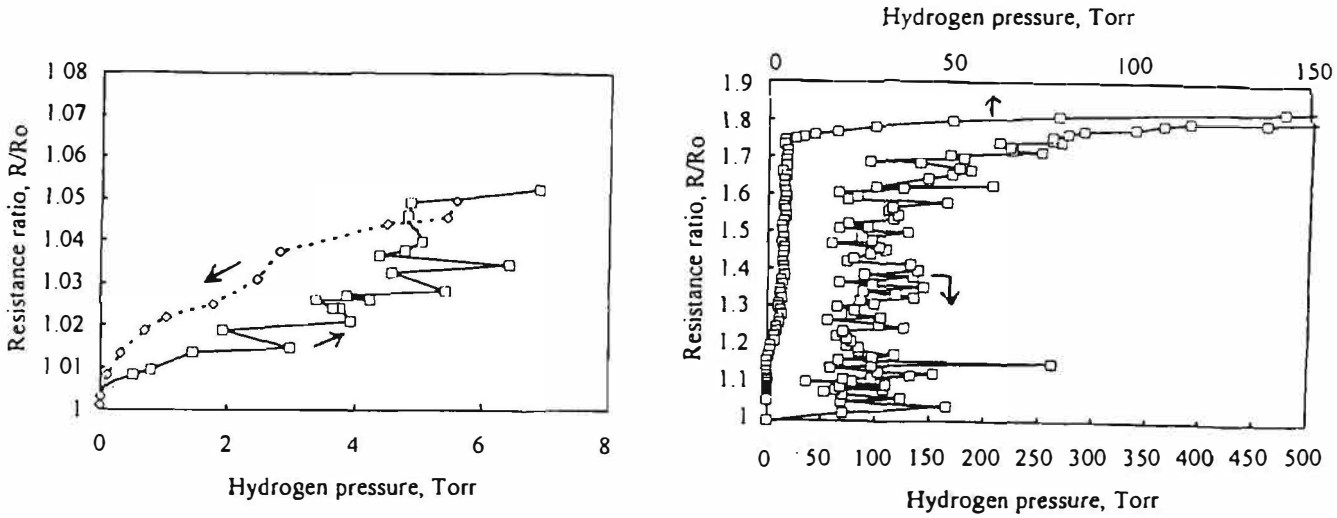

Fig.8 Comparison of R/Ro-hydrogen pressure diagrams,
left H/Pd ratio<0.02, right H/Pd ratio<0.8

Table1 Comparison of absorption cycle effect on E, R/Ro
and Δ l/lo-H/Pd ratio diagrams; B mode <0.02, C mode <0.8

Electrolysis cond.		Potential	Resistance ratio	Dilation, elongation	Hydrogen pressure
Mode	H/Pd ratio	E-log(H/Pd)	(R/Ro)-H/Pd	(Δ l/lo)-H/Pd	Tor-log(H/Pd)
B	<0.02 (c.d.0.2 mA/cm^2)	1st-5th Nernstian 6th-11th deviation from Nernstian	1st, 2nd: early jump, other cycle no hysteresis	1st to 3rd increased slope, 4th to 11th no cycle effect	small hysteresis
C	<0.8 (c.d.0.2& 2mA/cm^2)	Data scattered but much deviated from Nernstian	large hysteresis	Data not available	large hysteresis

note; Desorption cycle was mostly found to be orderly effective or less effective on these diagrams compared with adsorption ones. Mode C data of desorption cycle was not available because of its form of electrolysis mode.

Material Science Studies

QUANTUM MECHANICAL DESCRIPTION OF A LATTICE ION TRAP: Deuteron Approaching Mechanism in Condensed Matter

V. Violante, A. De Ninno

Associazione EURATOM-ENEA sulla Fusione, Centro Ricerche di Frascati,
C.P. 65 - 00044 Frascati, Rome, Italy

1. Introduction

The electrodynamic confinement of charged particles stored in a radio-frequency electric quadrupole trap has been widely investigated by several authors [1,2]. A remarkable similarity between the above mentioned quadrupole radio-frequency trap and the palladium lattice structure allowed a classical study of the dynamics of two deuterons moving within the Pd lattice around tetrahedral sites [3,4]. The theory of the harmonic oscillator with time dependent frequency has been reviewed by introducing an operator which is a constant of the motion [5]. In this paper a quantum description of a deuteron dynamics and its interaction with an other one inside the lattice ion trap is carried out taking advantage of an oscillating behaviour that can be traced back to a quantum harmonic oscillator. The calculations show, in both treatments, a reduction of the mean distance between the particles.

2. Quantum description of the oscillator with time-dependent frequency

The Hamiltonian for a particle of mass m, momentum $\bar{p}$ and position $\bar{x}$ moving as an harmonic oscillator with time-dependent frequency $\bar{\omega} = \bar{\omega}(t)$ can be written in terms of dimensionless position x and momentum p as in the following expression:

$$H = \frac{1}{2}p^2 + \frac{1}{2}\omega^2(t)x^2 \tag{1}$$

where:

$$\bar{x} = \sqrt{\frac{\hbar}{m\omega_0}}x;\ \bar{p} = \sqrt{\hbar m\omega_0}p\ ; \tag{2}$$

$$\omega(t) = \frac{\bar{\omega}(t)}{\omega_0} \tag{3}$$

The introduction of the dimensionless position and momentum operators $\hat{x}$ and $\hat{p}$ satisfying the commutation relation:

$$[\hat{x}, \hat{p}] = i \tag{4}$$

leads the transition to quantum mechanics. The quantum mechanical harmonic oscillator, with time-dependent frequency

$$\hat{H} = \frac{1}{2}\hat{p}^2 + \frac{1}{2}\omega^2(t)\hat{x}^2 \tag{5}$$

can be solved by defining the operator:

$$\hat{A}(t)=\frac{i}{\sqrt{2}}[\varepsilon(t)\hat{p}-\dot{\varepsilon}(t)\hat{x}] \tag{6}$$

which is a linear combination of the position and the momentum operators with time dependent coefficients. The time dependent function ε(t) satisfies the Newton equation of motion for the corresponding classical oscillator subjected to the appropriate initial conditions:

$$\ddot{\varepsilon}(t)+\omega^2(t)\varepsilon(t)=0 \tag{7}$$

It can be shown that the operator $\hat{A}(t)$ is a constant of motion:

$$\frac{d\hat{A}}{dt}=0 \tag{8}$$

With the following choice of the initial conditions:

$$\varepsilon(0)=1;\dot{\varepsilon}(0)=i \tag{9}$$

the operator $\hat{A}$ leads to:

$$\hat{A}(t=0)=\frac{1}{\sqrt{2}}(\hat{x}+i\hat{p}) \tag{10}$$

Then for t=0 the operator is identical to the annihilation operator $\hat{a}$ of the time-independent harmonic oscillator. It has been demonstrated [5] that:

$$[\hat{A}(t),\hat{A}^{+}(t)]=1 \tag{11}$$

In the following it will be shown that the ground state $|0;t\rangle$ and the excited states $|n;t\rangle$ of a deuteron behaving as a harmonic oscillator with time-dependent frequency can be obtained by using the constant of the motion $\hat{A}(t)$.

The time independence of the commutator (11) ensures that the Hamiltonian has a state $|0;t\rangle$ analogous to the ground state of the time-independent harmonic oscillator. The analogy allows us to define:

$$\hat{A}(t)|0;t\rangle=0\ , \tag{12}$$

leading, for the position representation $\psi_0(x,t)\equiv\langle x|0;t\rangle$ of the ground state, to the differential equation:

$$\langle x|\hat{A}(t)|0;t\rangle=\frac{i}{\sqrt{2}}\left[-i\varepsilon(t)\frac{d}{dx}-\dot{\varepsilon}(t)x\right]\psi_0(x,t)=0 \tag{13}$$

The resulting expression for the probability distribution in coordinate space is:

$$P_0(x,t)\equiv|\psi_0(x,t)|^2=\frac{1}{\sqrt{\pi}|\varepsilon(t)|}\exp\left(-\frac{x^2}{|\varepsilon(t)|^2}\right) \tag{14}$$

For the excited states the probability distribution in coordinate space is [5]:

$$P_n(x,t)\equiv|\psi_n(x,t)|^2=\frac{1}{\sqrt{\pi}|\varepsilon(t)|}\frac{1}{2^n n!}H_n^2\left(\frac{x}{|\varepsilon(t)|}\right)\exp\left(-\frac{x^2}{|\varepsilon(t)|^2}\right) \tag{15}$$

where H_n is the nth Hermite polynomial. Then, if we can obtain the value of the function ε(t) at a time t, the equations (14) and (15) allow us to estimate the probability that two particles are at a distance x after a time t for a system in the ground state or in an excited state respectively.

3. Lattice ion trap classical description

The model of the "lattice ion trap" has been carried out in ref. [3,4] to study the dynamics of two deuterons moving within the Palladium lattice space around the tedrahedral sites. The space around the tetrahedral sites can be seen as a quadrupole trap for the deuterons; then the effect of the electrodynamic containment on its dynamics can be studied by means of the equations of motion. The alternating signal of the lattice radiofrequency trap is assumed to be generated by the motion of electrons close to the Fermi energy: the electron motion can be traced back to an oscillating electronic cloud that produces an electric field because of the charge separation due to the oscillation. A coherent mechanism of the electron cloud is proposed for the model, since no phase is subject to random noise. Fig.1 shows the palladium lattice cell. The octhaedral sites are in the middle between the vertexes of the cubic structure. The tetrahedral sites, that could be available for deuterons above x=0.95, belong to the intersection between the (101) and the $(10\bar{1})$ planes. The similarity between a quadrupolar ion trap and the system shown in Fig.1 allows us to consider, for simplicity's sake, that the charges acting in the (101) plane are midway between Pd atoms 1 & 2, and 3 & 4, and the charges acting in the $(10\bar{1})$ plane are just atoms 5 and 6. The projection in the x-w plane gives a simplified two-dimensional view of the spatial oscillations of the electron clouds (see Fig.2). Their displacements in both (101) and $(10\bar{1})$ planes are oscillations of charge density producing an alternating potential difference that generates an electric field. Let z and r be the [101] and $[10\bar{1}]$ directions respectively, then E^z and E^r are the effective components of the electric field for the ion dynamics. The electric field in each plane achieves its maximum value when it is minimum in the other one, because of the orthogonality of the planes. Such a situation leads to sinusoidally time varying forces whose strengths are proportional to the distance from a central

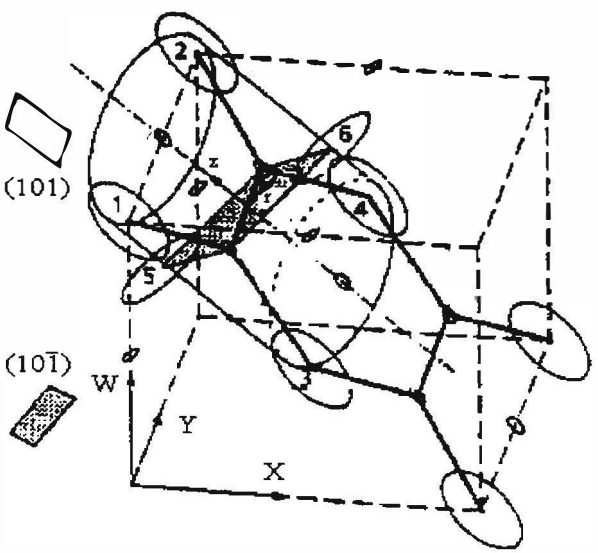

Fig.1. Lattice ion trap with cylindrical symmetry

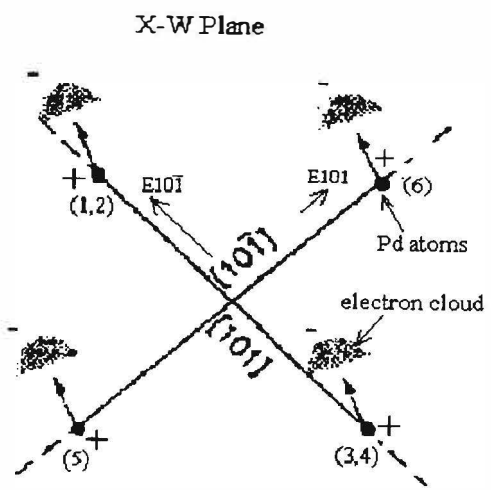

Fig.2. Representation of the alternating signal into the x-w plane

origin (in this case the intersection between the r and z axes) . The trap can be considered to have a cylindrical symmetry as shown in Fig.1. In order to link our system with the above mentioned quantum description of the Paul trap we will consider that one deuteron is located approximately in the midway between tetrahedral sites (i.e. the origin of the trap coordinate system) and the other one leaving the octahedral site (at the time t=0) and moving within the trap (i.e. $z(t=0)=l_o$).

Considering the cylindrical symmetry of the system, and introducing the following dimensionless variables:

$$\bar{r}=\frac{r}{l_0};\bar{z}=\frac{z}{l_0};\eta=\frac{t}{2\tau}, \tag{16}$$

the balance of the forces leads to the following equations of motion:

$$\begin{aligned}\frac{d^2\bar{r}}{d\eta^2}&=\frac{4\tau^2}{m}\bar{r}[e^2\frac{1}{(r^2+z^2)^{3/2}}\beta+\frac{(1-\alpha)eV_{acr}}{l_0^2}\cos(2\Omega\tau\eta+\frac{3}{2}\pi)]\\ \frac{d^2\bar{z}}{d\eta^2}&=\frac{4\tau^2}{m}\bar{z}[e^2\frac{1}{(r^2+z^2)^{3/2}}\beta-\frac{2\alpha eV_{acz}}{l_0^2}\cos(2\Omega\tau\eta)]\end{aligned} \tag{17}$$

where β is the Thomas Fermi screening term, V_{acr} and V_{acz} are the peak values of the alternating signal having angular frequency Ω, l_0 is the trap characteristic length (the radius or the distance from the symmetry point, which are equal in this case), r and z are the coordinates (in the trap coordinate system) of the deuteron moving in the trap, α is a random number, ranging between 0 and 1, taking into account the direction of oscillation (α can also change after a time interval of the order of the oscillation period), e is the electron charge, and m the particle mass.Time τ is the characteristic time of the moving deuteron: the ratio between l_0 and the initial velocity of the particles. This choice allows us to use always 1 as initial normalized velocity, whatever the initial velocity of the particle is. For instance if the initial energy of the moving deuteron is 0.1 eV its initial velocity is $\sim 3.1\times10^3$ m/s and $\tau \sim 4.5\times10^3$ s. Then if we change the initial deuteron velocitiy (energy) respect to which the normalization is carried out τ changes too: the information concerning the initial energy of the moving deuteron is given simply by using a proper value of τ in the equations (17). The terms on the right side of eq. (17) are due to the Coulomb interaction and the trap force respectively. The damping force that can be produced by the gradient of the energy barrier around the tetrahedral sites can be neglected in this approximation, since, as it can be easily seen, it is a low weight term in the equations of motion. The frequency of the alternating signal can be evaluated by means of the approximation to an ideal electron plasma [3,4]. The peak value of the alternating signal can be calculated on the basis of the electric field, in the classical approximation, associated with the plasma oscillation: $V_{acr,z}=4\pi ne\xi^2$, where ξ is the maximum distance between the positive and negative centres of charge during the oscillations: i.e. the distance between the Pd atoms.

4. Quantum description of two deuterons in the trap

Now we apply the previous described quantum theory of the harmonic oscillator with time dependent frequency to the moving deuteron which oscillates inside the lattice radio-frequency trap, as can be seen observing the evolution of its trajectory.

As we stated before, the function $\varepsilon(t)$ satisfies the Newton equation of motion for our corresponding classical problem:

$$\ddot{\varepsilon}(t) = \left[a_{r,z}(t) + q_{r,z}\cos\left(2\Omega\tau\eta + \phi_{r,z}\right)\right]\varepsilon(t) \tag{18}$$

where $a_{r,z}(t)$ represents the interaction term in the corresponding eq. (17), q_r and q_z are the coefficients of the cosine term in the eq. (17).

The equation (18) corresponds to the equation systems (17) and results to be formally identical to eq. (7), since also $a_{r,z}(t)$ is a function of the time; therefore the term inside the square brackets corresponds to $\omega^2(t)$. Then $\varepsilon(t)$ plays the role of the distance between the particles, whose components are r and z. It is important to underline that $a_{r,z}(t)$ contains the distance between the particles (i.e. $\varepsilon(t)$) and is a not linear term. If the distance between the particles is larger than the screening length (~0.4Å), $a_{r,z}(t)$ is negligible with respect to the cosine term, and the particle motion can be traced back to an harmonic oscillator. When the distance decreases below the screening length, the interaction term $a_{r,z}(t)$ becomes the dominant one and the oscillator becomes anharmonic. Therefore, for distances below the screening length we can roughly approximate the problem to a diffusion one. The interaction probability can be evaluated by means of the momentum value of the moving particle when its distance from the particle at rest is equal to the screening length. The scattering angle can be calculated on the basis of the r and z values after the interaction. We can apply the following relationship:

$$dw_{fi} = \left(\frac{z_1 z_2 e^2 m}{2p^2 \sin^2 \theta/2}\right)^2 \frac{p}{L^3 m} d\Omega \tag{19}$$

where Ω is the solid angle, w_{fi} the transition probability for unit time and θ the scattering angle.The interaction probability, for distances below the screening length, can be obtained by integrating w_{fi} over the time interval required by the particle, having momentum p, to move towards a distance of the order of the screening length (~0.1Å)

$$P_{\text{int}} = \int_0^{\Delta t} w_{fi} dt \tag{20}$$

Going back to the quantum description of the harmonic oscillator having a time dependent frequency, we can write the following positions:

$$z \equiv \text{Re}\,\varepsilon, \quad r \equiv \text{Im}\,\varepsilon \tag{21}$$

We have to satisfy the initial conditions (9) that can be simply imposed by taking advantage of the choice for the dimensionless time as explained above. Condition (3) is given by assuming $\omega_0 = 1/2\tau$. The initial conditions (9), with position (21), can be rewritten as follows:

$$\bar{z}(0) \equiv \text{Re}\,\varepsilon = 1;\ \bar{r}(0) \equiv \text{Im}\,\varepsilon = 0;\ \dot{\bar{z}}(0) \equiv \text{Re}\,\dot{\varepsilon} = 0;\ \dot{\bar{r}}(0) \equiv \text{Im}\,\dot{\varepsilon} = 1 \tag{22}$$

The solution of the classical motion equations with conditions (22) is obtained by numerical integration.

5. Results and conclusions

The study is mainly oriented to a comparison between the results of a classical description and the results arising from a quantum mechanical approach, even if the analysis of the trapped deuterons is limited to some particular cases. We considered two different initial conditions, in terms of the

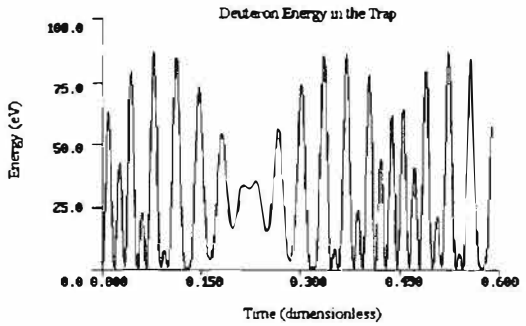

Fig. 3 Deuteron energy evolution in the trap

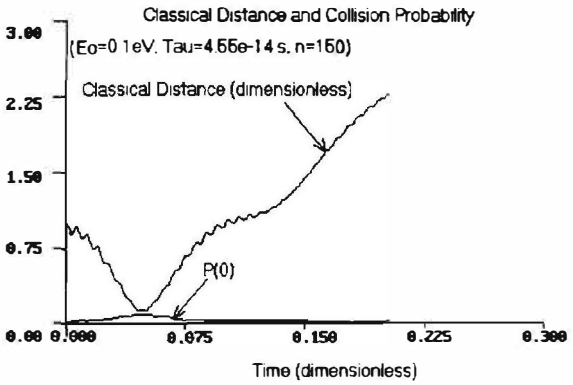

Fig.4 Evolution of the distance of the deuterons and collision probability (E_0=0.1 eV)

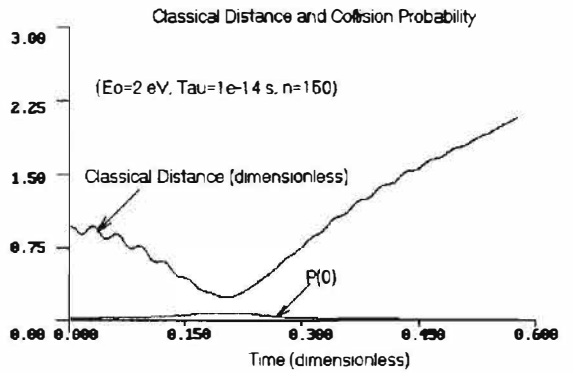

Fig 5 Evolution of the distance of the deuterons and collision probability (E_0=2 eV)

energy of the moving particles (i.e. of the τ value, such that the dimensionless initial velocity is always 1, as explained before). For the lattice cell parameters we consider in the model the β phase value.

Figure 3 shows the evolution of the moving deuteron energy classically evaluated. The average energy is some tenth of eV. The deuteron oscillation frequency is ranging between 10^{14} and 10^{15}. Therefore, from the oscillator energy calculation it follows:$(n+1/2)\hbar\omega=10^1$. Then a rough approximation gives n=150 to evaluate $P_n(x,t)$ with equation (15).

Figure 4 shows the calculation results for 0.1 eV as initial energy. The classical trajectory (the distance) and the probability to have the two particles at distance zero (collision) are plotted as a function of the dimensionless time. We can see that when the minimum distance between the particles, in the classical description, shows a minimum lower than 0.1 Å the quantum mechanical analysis produces a maximum collision probability. Figure 5 shows the results for an initial energy of 2 eV. In this case the initial conditions produce an approach, in the classical description, which is not effective for an interaction between the particles, but the quantum mechanical analysis gives a collision probability different from zero even if, in this case, the value is less than in the previous one. The oscillating behaviour of the deuteron moving inside the trap can be clearly observed in the classical trajectory evolution. The comparative analysis shows that the classical description of the particle dynamics in the lattice can be considered a satisfactory and conservative approximation, in accordance with the relatively high energy that the deuteron gains in the trap. However the results obtained should be considered indicative, since some approximations have been introduced as well as the hypothesis that a deuteron is at rest in the midway between the tetrahedral positions (not

exactly in the tetrahedral site as it should be), and since the problem is splitted in two separate regions.

In conclusion the approximation of the deuteron in the trap to an harmonic oscillator with time-dependent frequency and the approximation to a diffusion problem below the screening length gives a quantum mechanical description in reasonable accordance with the classical one. An interesting additional information is that the quantum mechanical description provides collision probabilities different from zero also when the classical description doesn't produce an effective approach to have an interaction between the particles.

The correlation existing between the classical and the quantum mechanical models allows us to extend to the quantum case all the considerations done in the classical description [3,4].

References

[1] R.F. Wuerker, H. Shelton, R.V. Langmuir, *Electrodynamic Containment of Charged Particles*, J. Appl. Phys. **30**, N.3 (1959) 342-349.

[2] R.G. Brewer, J. Hoffnalge, R.G. De Voe, L. Reyna, W. Henshaw, *Collision Induced Two Ion Chaos*, Nature **344** (1990) 305-309.

[3] V. Violante, A. De Ninno, *Lattice Ion Trap: A Possible Mechanism Inducing a Strong Approach between Two Deuterons in Condensed Matter*. Accepted for Pubblication by Fusion Technology.

[4] V. Violante, A. De Ninno, *Collision Between Two Deuterons in Condensed Matter: Ion Trap Mechanism*. Proceedings of V Int. Conference on Cold Fusion Montecarlo Apr. 1995.

[5] G. Schrade, V. I. Man' ko, W. P. Schleich, R.J. Glauber, *Wigner functions in the Paul trap*.Quantum Semiclass. Opt. **7** (1995) 307-325.

OBSERVATIONS OF STRONG RESISTIVITY REDUCTION IN A PALLADIUM THIN LONG WIRE USING ULTRA-HIGH FREQUENCY PULSED ELECTROLYSIS AT D/Pd > 1.

F.Celani, A.Spallone, P.Tripodi, D. Di Gioacchino, *
P.Marini, **
A.Mancini.***

(*) INFN Frascati National Laboratory, v. E.Fermi 40, 00044 Frascati (Italy)
(**) EURESYS, Rome (Italy)
(***) ORIM S.r.L, v. Concordia 65, 62100 Macerata (Italy)

Work supported by:
INFN, ORIM (Italy); NEDO-NHE (Japan)
Palladium wires fabricated by:
ORIM

ABSTRACT

We performed a ultra-short width high voltage pulse electrolysis using a thin Pd wire cathode; a diluted electrolytic solution of D_2O+LiOD was used in a peculiar wire-turned electrodes geometry.
The deuterated Pd loading was evaluated by the D/Pd normalised electric resistance curve (R/Ro). After a long time of electrolysis a very high D/Pd loading (1:1 or more) was reached.
Very low R/Ro (< 0.1) Pd wire was measured after switching off the electrolysis and this effect lasted for several minutes. The Deuterium deloading occurred in several typologies (fast and slow terms) showed as a resistance transition on the Pd wire.
This effect can be related to a peculiar surface structural condition.

APPARATUS SET-UP

In order to reach very high loading (D/Pd > 1) a new approch in respect to the typical loading techniques has been developed.
An electrodes cylindrical geometry has been adopted: a PTFE cylinder, as electrodes holder (5 cm diameter, 30 cm length), has been turned by 2 parallel wires (1 cm of distance). The Pd wire (100 μm diameter, 160 cm length) has been located as cathode and a Pt wire (1 mm diameter) as anode [fig. 1]. This geometry has been adopted to enclose in a symmetrical electric field along the cathode and moreover to produce "well" correlated electric fields: wire transversal (electrolytic type) and wire longitudinal (Ohm conductive type).
The electrolytic solution adopted was very diluted (LiOD-D_2O at 0.25 mN), having a high electric resistance (several KΩ) between the electrodes, in order to have a very low transverse current; in such a way is possible to apply a high voltage to the electrodes.
The Pd wire has been tested on 5 different points (4 sectors: ab, bc, cd, de, fig. 1) in order to measure the resistance (of the order of 10 Ω at D/Pd= 0.75) of each segment by mean of an a.c. resistance bridge realised by a proper home-made circuitry. We applyed a sinusoidal electrical current

$I(t) = I_o \sin \omega t$, with $\omega = 628\ 10^3$ rad/s, $I_o = 10$ mA (the total voltage drop along the wire was not producing self-electrolysis), we measured the AC voltage in 5 pick-up points (a,b,c,d,e) in respect to ground. The AC leakage current in the electrolyte is quite small because the impedance ratio between electrolyte and Pd wire was grather than 10^2.
The power supply applied to the electrodes has been realised by an other home-made pulse generator circuit [ref.1]. The pulse consists in a high frequency trapezoidal-like shape (rise time < 4 ns, about 20 ns width, amplitude between -40 and -80 V) having a repetition rate of about 27 MHz. This circuit is connected at the top edges of the electrodes. At the bottom edges of the Pd electrode is connected an other circuit (based on some high-power Zener diodes) in order to limit at a constant value the minimum drop voltage between anode and cathode. The motivation of this other circuit consists on to increase the current (or better to say: the voltage) along the wire without increasing the current along the electrolytic solution: in such a way the deuteron electromigration into the Pd wire can be increased producing a higher loading at the more cathodic point of the Pd (at the top edge).

MOTIVATION AND TEST PROCEDURE

The main goal of the pulse electrolysis consists on the reaching of a very high D/Pd loading which needs, to be sustained, a strong electric field onto the cathode surface. It is not convenient to apply a direct high voltage because in this case a high electrolytic current should be generated having the only effect to produce a lot of bubbles (D_2 electrolytic gas at the cathode); it is our opinion that very high current density at the cathode does not increase anymore the D/Pd value but moreover it is lowering of this value. Instead, the high voltage pulse generates the necessary strong electric field at the surface and because the short time being on, the mean current (and the relative gas production) is quite low. Obviously, the peak pulse must be repeated after a time much lower than the diffusion (deloading) time of the Deuterium coming out from the Pd surface (we estimate it of some ms) [ref. 2].
The procedure adopted to perform the measurement was the following:

a) first loading at low frequency (0.5 μs width, 200 V amplitude, 5 Khz pulse rate [ref. 1])
b) the sample underwent to ultra-high frequency pulse electrolysis for many hours
c) suddenly the electrolysis was switch off
d) the resistance of the 4 Pd-wire sectors were recorded
e) the measurement lasted until the resistance peak was reached and then decreasing
f) repetition of these statements (b->e) several times.

RESULTS

A direct measurement of D/Pd was not possible to perform with this apparatus set-up (the total Pd wire mass was just 160 mg). As a loading reference, we adopted the well known curve of R/Ro vs D/Pd [fig. 2] as reported in literature [ref. 3]. Because the peak value of the curve corresponding at R/Ro=2 is relative at D/Pd=0.75, to state if the D/Pd value is higher, it is necessary to record the resistance value occurring during the deloading: if this resistance increases during the deloading it means we are on the right side of the curve (otherwise we have the opposite condition). We adopted this criterion to realise if we had overcome the peak value after a long time electrolysis.
Several loading/deloading cycles have been performed using the same Pd wire running at the same nominal pulse supply conditions.
A very low resistance effect occurred several times (only at the a-b wire sector, as in fig. 1, while the other sectors appeared to be over-charged up to R/Ro down to 1.2) and this effect performed different typologies.

In one experiment [fig. 3] a low constant resistance value (roughly about zero) lasted for about 6 minutes and the transition time (R/Ro from 0 to 2, where D/Pd is equal at 0.75) was very short (less than 5 s, the minimum quantum computer acquisition time). The loading time, necessary to get this effect, was of about 2 hours.
In an other experiment (after about 15 hours of loading time) the R/Ro behaviour looks similar [fig. 4]; for about 16 minutes the wire resistance was very low and the transition lasted about 30 s. As reported above, the resistance stands very low and steady for several minutes and later it appears unstable for few minutes (but still at low values) before the "transition". We can suppose that this instability is related to the wire deloading: it occurs an interaction between the wire (still heavily loaded but not so high like the previous steady status) and the a.c. resistance bridge circuitry. Perhaps this unstable status, occurring at this over-loaded Pd wire (sector a-b), can be related to the wire surface degrading. In short, it looks as a reactive response of the impedance of the wire to whom it is applied a sinusoidal current of the a.c. bridge.
In a case [fig. 5 a,b,c] three sequential loading/deloading cycles (respectively of 10, 20, 30 minutes of loading time) have been performed. The low resistance standing time seems related to the loading time and the transition time is quite long (several minutes).

CONCLUSIONS

In conclusion we can stress these points coming out from the observations of the phenomenon:

- High conductivity occurs in D-Pd overloaded system;
- Pulse shape seems to be related to this effect;
- Calorimetric measurements were not performed in this set-up (because the cooling flow was set at high level in order to work at constant temperature of about 26 °C) but anyway no high level of heat generation was recorded;
- Reproducibility is not still defined (all data are correspondent just to 1 wire);
- Investigation is not yet available with H-Pd system (only D-Pd system);

Finally we can suggest that something of structure modification occurs onto the over-loaded Pd wire surface; it is not still clear if the Li plays an important role for this sort of modified surface layer.
It is only defined at this time that the high frequency and high voltage pulse and moreover a quite long time loading are necessary to obtain this effect.

REFERENCES

[1] F.Celani, A.Spallone, P.Tripodi et al.
Workshop "*On the loading of Hydrogen/Deuterium in metals: characterization of materials and related phenomema.*"
Asti, Italy - Oct. 11th-13th 1995.

[2] G. Mengoli, C.Manduchi et al.
"*Surface and bulk effects in the extraction of hydrogen from highly loaded Pd sheet electrodes.*"
Journal of Electroanal. Chem. 350 (1993) 57-72.

[3] B.Baranosky.
In "*Hydrogen in Metals II*"
ed. by G.Alefed, Topics Appl. Phys. Vol. 29 (Springer, Berlin, Heidelberg 1978) pg. 157.

Material Science Studies

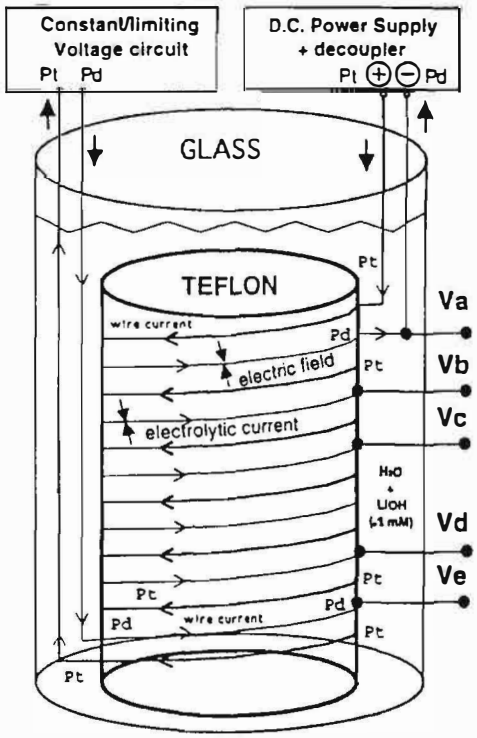

Fig. 1 - ELECTROLYTIC DEVICE:
Pd cathode and Pt anode wires are twisted around a PTFE cylinder. The electrolytic solution is very diluted. Along the Pd wire, some electric sensors are pointed.

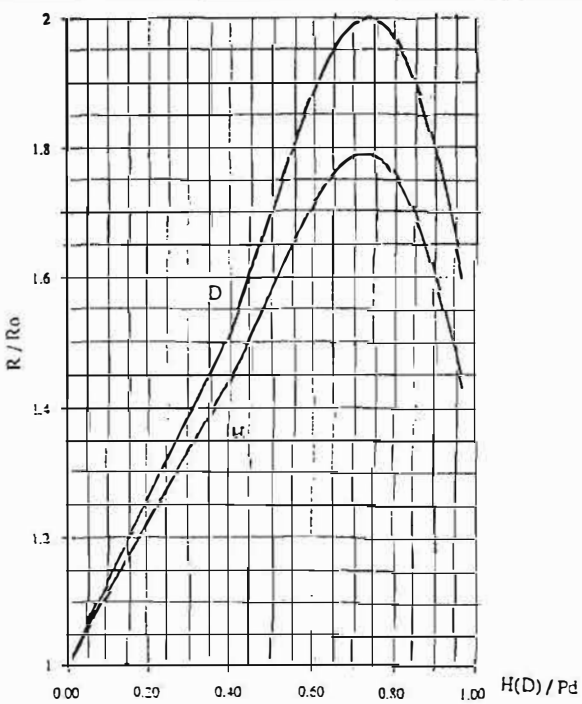

Fig. 2 - D/Pd RESISTANCE CURVE:
In this curve the resistance almost linearly increases with the loading. At the D/Pd= 0.75 the normalized resistance has the peak value of 2 (1.8 for H/Pd). The curve is known up to the point D/Pd=0.95 and R/Ro=1.6.

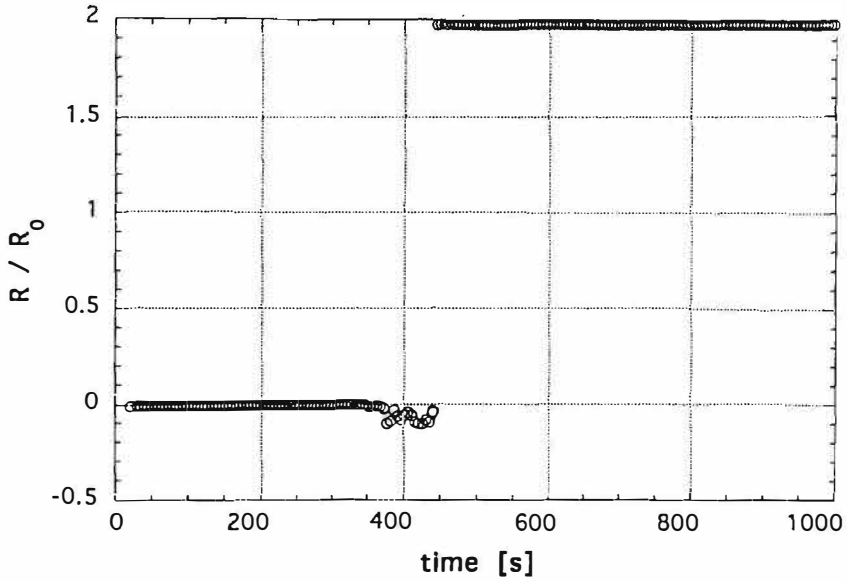

Fig. 3 - RESISTANCE vs TIME:
After switching off the electrolysis the Pd wire resistance is very low for about 7 minutes and the transition time is less than 5 s. The value R/Ro=2 is relative to the ratio D/Pd=0.75. Loading time was about 2 hours.

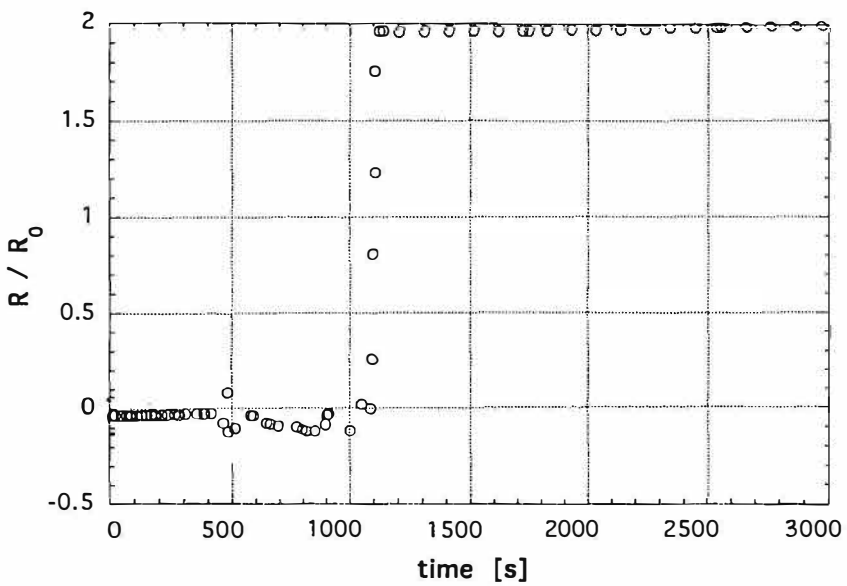

Fig. 4 - RESISTANCE vs TIME:
After switching off the electrolysis the Pd wire resistance is very low for about 15 minutes and the transition time is about 30 s. It is not shown, but after some hours the R/Ro value decreases much lower than 2. Loading time was about 15 hours.

Material Science Studies

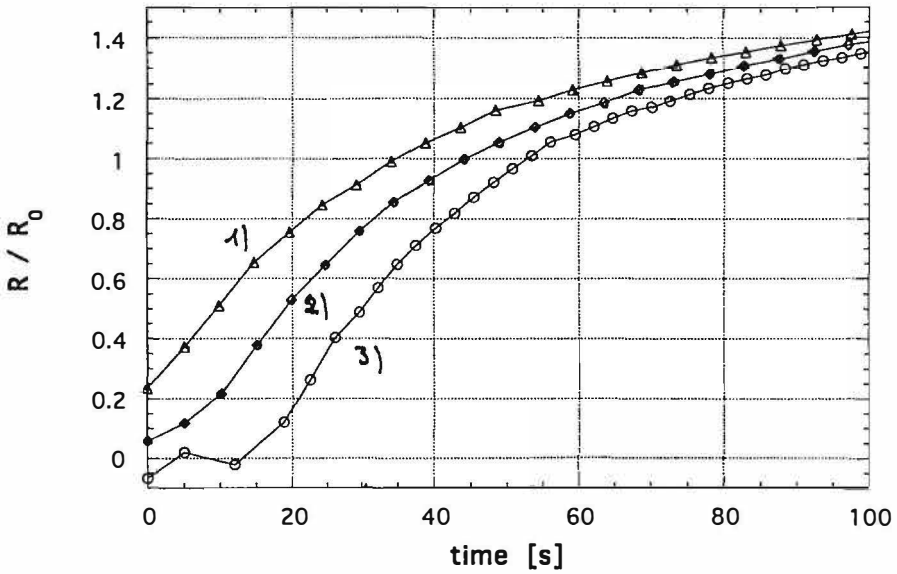

Fig. 5 - RESISTANCE vs TIME:
The Pd wire has operated for 3 load/deload progressive cycles: the resistance starts from very low values and needs many minutes to reach the value R/Ro=2 (not shown in the plot). The Pd surface structure probably plays an important role in this phenomenon. Loading times were respectively: 10, 20, 30 minutes.

Material Science Studies

In Situ Interferometric Microscopy of Pd Electrode Surface and Calorimetry during Electrolysis of D_2O Solution Containing Sulfur Ion

N. Oyama, M. Ozaki, S. Tsukiyama, O. Hatozaki and K. Kunimatsu*

Department of Applied Chemistry, Tokyo University of Agriculture and Technology, Japan
*IMRA JAPAN CO., LTD., Japan

Abstract

Highly sensitive calorimetry was carried out to assess excess heat production in the presence of sulfur ion (S^{2-}) in electrolyte solutions. Electrolysis of a D_2O solution containing 10mM S^{2-} produced "burst-like" excess heat up to 14% over 12 hours after 6 days' electrolysis. The production of excess heat was absent from a control experiment using $LiOH/H_2O$ in the place of $LiOD/D_2O$. It seemed that the magnitude and reproducibility of the excess heat production were improved by the addition of S^{2-} to the electrolyte solutions. In this study, in situ observations of topographic changes at electrode surfaces during the electrolysis were also conducted using phase measurement interferometric microscopy (PMIM). The absorption of hydrogen into a Pd cathode was clearly seen to bring about surface roughening even at a very low hydrogen content of less than H/Pd=0.005. Original surface topography was readily restored by desorbing hydrogen from the Pd electrode by using it as the anode. The absorption and desorption of deuterium similarly induced the reversible surface topography change. The extent of the surface roughening due to the hydrogen absorption varied with electrode materials and crystal facets of Pd single crystals.

1.Introduction

Excess heat production, which is a major impetus for researches on cold fusion phenomenon, has been reported from electrolysis of D_2O solutions under various experimental conditions. However, low reproducibility makes it difficult to gain a comprehensive understanding of the origin and mechanism of excess heat production. In seeking for an experimental factor which controls the reproducibility, we have conducted calorimetry with changing experimental parameters such as modes of electrolysis, magnitudes of electrolysis current and voltage, electrode pretreatments, etc[1,2]. In this study, calorimetry was carried out in the presence of sulfur ion (S^{2-}) to see if the addition of a substance which accelerated the hydrogen absorption into metals influences the production of excess heat.

We also carried out in situ measurements of topographic changes on cathode surfaces by phase measurement interferometric microscopy (PMIM)[3] during the electrolysis of H_2O and D_2O solutions. Topographic changes induced by the absorption and desorption of hydrogen (and deuterium) were measured at different current densities for Pd and Pd-Ag alloy electrodes. PMIM measurements were also carried out using Pd single crystals with different facets.

2. Experimental

2-1. Calorimetry

A detailed description of the system and principle of the calorimetric measurement were presented elsewhere[2]. We used a twin-type microcalorimeter (Model 5111, Tokyo Riko, Japan) and a closed electrolytic cell (25ml) equipped with a Pd black recombination catalyst deposited on a Pt wire. Operating temperature was set at 8°C. The error in the calorimeteric measurement is of the order of a few per cent. Electrolysis of solutions were carried out at a constant current density of 177mAcm^{-2} with a two-electrode system, the cathode being Pd (l=1cm, ϕ=0.1mm) or Pd-Ag alloy (l=1cm, ϕ=0.2mm) wires and the anode Pt gauze surrounding the cathode. The areas of the Pd and Pd-Ag alloy cathodes were 0.28cm^2 and 0.56cm^2, respectively. All the electrode materials were obtained from Tanaka Metals Company (Japan) and used without pretreatment. Electrolyte solutions were prepared from D_2O (Isotech Inc., USA) or H_2O purified through a laboratory water purification system. Li_2S was obtained from Aldrich and used as received. All other chemicals were reagent grade and used without further purification.

We evaluated excess heat in two ways as follows:

$$R_t = (W_{out}-W_{in})/W_{in} \times 100 \quad (1)$$

$$R_s = (W_{out}^*-W_{in}^*)/W_{in}^* \times 100 \quad (2)$$

R_t is the excess heat which is estimated based on the total output (W_{out}) and total input energy (W_{in}) integrated from the beginning of the electrolysis. R_s is the excess heat estimated by integrating the output (W_{out}^*) and input energy (W_{in}^*) over every one hour, being more sensitive to burst-like heat evolution than R_t.

2-2. PMIM measurement

PMIM measurements were carried out using a Zygo Maxim·3D Model 5700 laser interferometric microscope (Middlefield, CT) with 40x Mirau objective. The microscope is equipped with a low power He-Ne laser as a light source which emits a coherent and monochromatic (λ=632.8nm) light for optical phase measurement interferometry. PMIM detects the interference intensities on a 256x256 pixel charge injection device array camera over an area of ca.0.06mm^2. From the recorded spatially resolved intensities, the phase, ϕ, of light reflected from the Pd surface is calculated with respect to the light reflected from a reference surface. Differences in phase, $\Delta\phi$, between light reflected from two adjacent points on the surface is converted to an optical height, h.

$$\Delta\phi = 4\pi h/\lambda \quad (3)$$

Then the optical height can be straightforwardly converted to the physical height, d, yielding an physical image of the surface by

$$h = d \times n \quad (4)$$

where n is the refractive index of the surrounding medium. More detailed description and measurements theory of the PMIM is given elsewhere[4].

Constant-current electrolysis was carried out using a conventional three-electrode system. Pd, Pd-Ag alloy plates (A=0.9cm^2, thickness: 0.2mm, Tanaka Metals Company) or Pd single crystals disks (A=0.2cm^2, thickness: 2mm, Material-Technologie & Kristalle, Germany) were used as the working electrodes. A Ag/AgCl electrode and Pt spiral wire were used as the reference and counter electrodes, respectively. A potentiostat/galvanostat (Polarization Unit PS-07, Toho Technical Research, Japan) was used in all electrochemical experiments. A relatively small current density (3 to 20 mAcm^{-2}) was employed for the electrolysis to keep the working electrode surfaces free from bubbles which interfered with the in situ PMIM measurements.

PMIM experiments were conducted at an ambient temperature (20±2°C).

3. Results and Discussion

3-1. Calorimetry

Using our highly sensitive calorimeter, so far we have occasionally observed the production of excess heat which lasted a relatively short period intermittently after prolonged electrolysis of D_2O solutions: i.e.,"burst-like" excess heat production. In this study, sulfur ion (S^{2-}) was added to electrolyte solutions in order to promote the deuterium absorption into cathodes. Sulfur ion is capable of accelerating the hydrogen absorption into metals by retarding the competitive recombination reaction of the adsorbed hydrogen atoms into molecules and/or by lowering an energy barrier to the hydrogen permeation via strong chemisorption of sulfur ion at cathode surfaces[5].

Figure 1 shows typical calorimetric results obtained during the electrolysis of 0.1M LiOD/D_2O (Figure 1a) and 0.1M LiOH/H_2O (Figure 1b) containing 10mM Li_2S using the Pd cathode. As clearly seen in the R_s plot in Figure 1a, "burst-like" excess heat production up to 14% of the input energy (ca. 0.6W) was recorded several times over 12hr after 130 hours' electrolysis of the D_2O solution. On the contrary, the excess heat production was not observed in a control experiment using H_2O containing the same amount of S^{2-} as shown in Figure 1b. The magnitude of the excess heat generated in the presence of S^{2-} was about five times that recorded for a similar electrolytic system in the absence of S^{2-} (~5%). Furthermore, it seemed that the addition of S^{2-} to D_2O solutions slightly improved the reproducibility of the excess heat production. These results suggest that the augmentation in the rate of the deuterium entry through the solution/cathode interface is of advantage for the excess heat production.

It is considered that the negative heat balance recorded in the presence of S^{2-} is ascribable to a certain endothermic reaction occurring in the electrolytic cells. When a Pt cathode instead of Pd was used in the presence of S^{2-}, both R_t and R_s were observed to be 0% within experimental error.

We also observed "burst-like" excess heat production using a Pd-Ag alloy cathode the surface of which was modified with Ag_2S in the presence of S^{2-}. The observed maximum excess heat was ca. 6% on almost 0% heat balance.

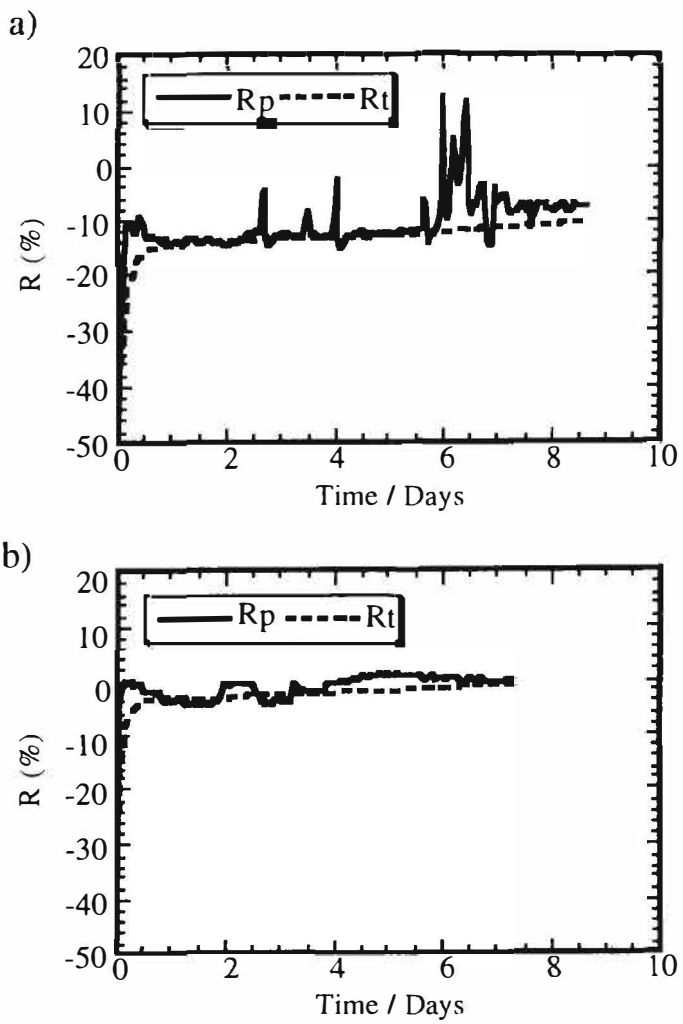

Figure 1 . Typical R_t and R_i for the electrolysis of D_2O(a) and H_2O (b) containing 10mM Li_2S using Pd cathode. Constant current density:-177mAcm^{-2}.

Material Science Studies

3-2. PMIM

It is well-known that the absorption of hydrogen into metals causes expansion and distortions of the crystal lattice of the metals, which bring about changes in physical and mechanical properties of the metals. Those property changes are considered to play an important role in cold fusion phenomena. In this study, surface topographic changes accompanying the hydrogen and deuterium absorption and desorption were measured in situ using PMIM.

Shown in Figure 2 are typical in situ PMIM optical images representing topographic changes at a Pd electrode surface observed during the electrolysis of 0.1M $LiOH/H_2O$ solution at $10mAcm^{-2}$. Figure 3 shows time-course change in PV (Peak-to-Valley) which is a measure of surface roughness: the distance between the highest and the lowest points in a certain surface profile plot. In the course of the electrolysis, the absorption of hydrogen into the Pd cathode caused significant surface roughening (Figure 2a-c). While there was retention time for the surface roughening, it began at a very low hydrogen content such as H/Pd=0.005. The retention period was dependent on the current density and almost independent on the charge passed (ca. $5mCcm^{-2}$), indicating a certain amount of hydrogen is required to be absorbed to cause the surface roughening. In the course of the electrolysis the Pd cathode surface became too rough for PMIM (the plateau region in Figure 3) and thus the optical image failed to represent the physical surface correctly (Figure 2c). Original surface topography was readily restored by desorbing hydrogen from the Pd electrode using it as the anode (Figure 2d) or, more slowly, leaving it in air for 24 hours. No qualitative differences were observed in topographic changes due to the absorption of hydrogen and deuterium .

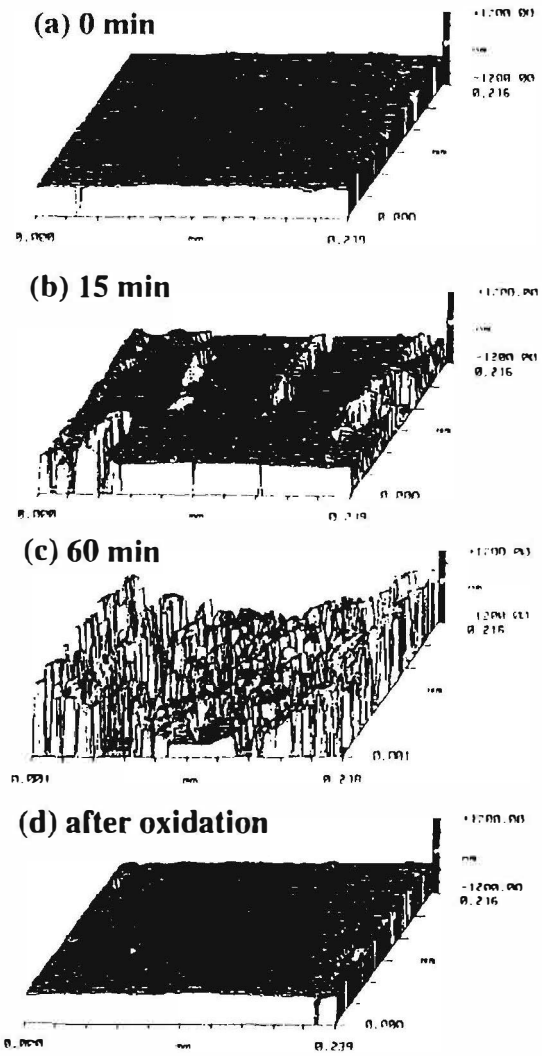

Figure 2. PMIM optical images and of Pd electrode profiles of surfaces obtained during the electrolysisof 0.1M $LiOH/H_2O$. Current density:$10mAcm^{-2}$.

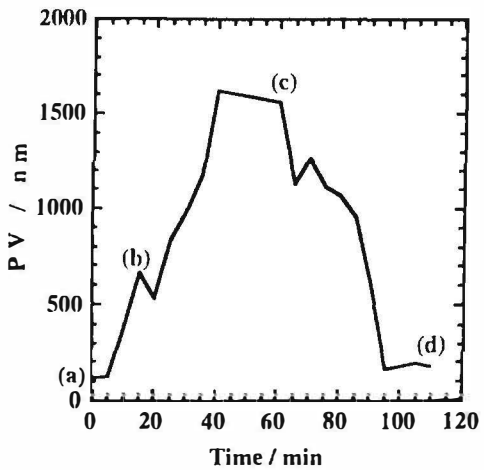

Figure 3. Peak-to-valley (PV) vs. time curves for Pd electrode surface during the electrolysis of 0.1M $LiOH/H_2O$. $A_{Pd}=0.12cm^2$. Currentdensity:$10mAcm^{-2}$. (a), (b), (c) and (d) correspond to the points where the images shown in Figure 2 were obtained.

Material Science Studies

The electrolysis was carried out using cathodes of Pd single crystals and topographic changes were measured. As shown in Figure 4, Pd (111) underwent significant topographic change as observed for the polycrystalline Pd, while surface topography of Pd (100) remained unchanged during the electrolysis. These results indicate that in Pd single crystals the distortions of the crystal lattice due to the hydrogen absorption occurs preferentially in a certain direction. When hydrogen atoms occupy the octahedral sites in Pd crystal, hydrogen atoms intercalates between Pd (111) planes, which could expand the distance between the (111) planes.

Topographic changes were measured also for Pd-Ag alloy electrode surfaces. Compared to the Pd, Pd-Ag alloys were found to be highly resistant to the topographic change as shown in Figure 5.

4. Conclusion

In this study we carried out calorimetry in the presence of sulfur ion (S^{2-}) and in situ measurements of topographic changes at electrode surfaces using PMIM. Results from the calorimetric experiments implies that the acceleration of the deuterium absorption into the cathode due to the addition of S^{2-} improves "burst-like" excess heat production. PMIM clearly showed that the hydrogen absorption-desorption caused the reversible topographical change. The extent of the surface roughening due to the hydrogen absorption was strongly dependent on not only the electrode materials but also crystal facets of the electrode surfaces.

References

1) N.Oyama et al., *Bull.Chem.Soc.Jpn*, 63, 2659 (1990).
2) N.Oyama et al., *Frontiers of Cold Fusion, Proceedings of the Third International Conference on Cold Fusion,* Ikegami H., Ed.; Universal Academy Press, Inc., pp67-70 (1993).
3) K.Takada, T.Haseba, T.Tatsuma, N.Oyama, Q.Li, H.S.White, *Anal.Chem.* 67, 4446(1995).
4) C.P.Smith, D.C.Fritz, M.Tirrell, H.S.White,*Thin Solid Films*, 198,369(1991).
5) *Corrosion of Metals and Hydrogen-Related Phenomena*; Flis, J., Ed.; Elsevier: Amsterdam, pp 254-263(1991)
6) Piesl, H. *Topics in Applied Physics Hydrogen in Metals I*; Alefeld G.; Volkl, J., Ed.; Springer-Verlag: Berlin, pp53-74(1978).

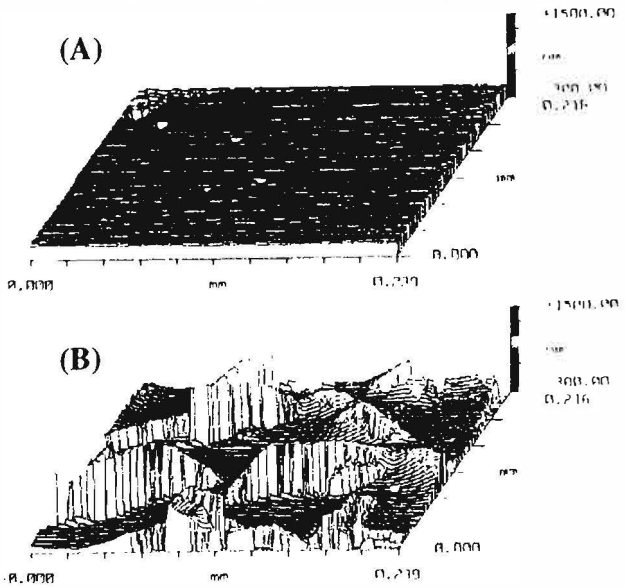

Figure 4. PMIM optical images for Pd single crystal cathodes during the electroreduction of 0.1M LiOH/H_2O. (A) (100) and (B) (111). Electrolysis time (A) 20min and (B) 50min.

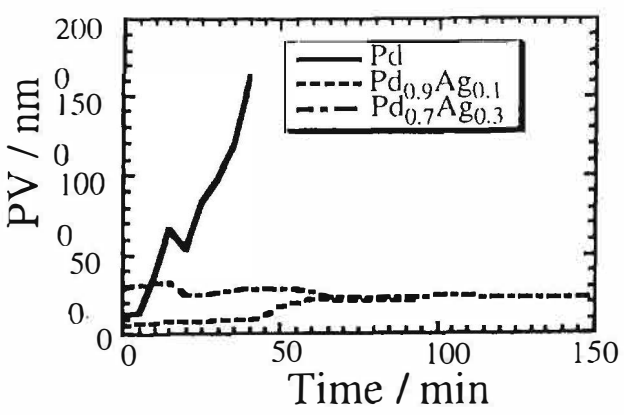

Figure 5. PV vs. time curves for Pd-Ag alloy surfaces during the electroreduction of 0.1M LiOH/H_2O. Current density: 10mAcm^{-2}.

Material Science Studies

Click here for a more readable copy of this paper.

The Effect of Microstructure on Deuterium Loading in Palladium Cathodes

Dawn D. Dominguez, Patrick L. Hagans and M. Ashraf Imam

Naval Research Laboratory, Washington, DC 20375, USA

Abstract

The effect of microstructure on deuterium loading in palladium cathodes was investigated. Cathode microstructure is determined by thermomechanical processing that includes electrode deformation (swaging) and the annealing conditions (time and temperature). Results will be presented on the extent of deuterium loading in rod-shaped (0.4 cm in diameter and 3.5 cm long) cathodes with controlled microstructure produced at The Naval Research Laboratory (NRL). Loading on NRL cathodes will be compared with that attained on commercially available electrodes routinely used at other laboratories.

Deuterium loading of the electrodes was accomplished electrochemically in 2.5 cm diameter by 15 cm length borosilicate-glass cells containing 0.1M LiOD in D_2O as the electrolyte and a cylindrical Pt anode. Loading was monitored in-situ by measuring the change in the axial resistance of the cathode and comparing the measured values with the known relationship between resistance and the D/Pd atomic ratio. Comparison of deuterium loading in well-controlled electrochemical experiments on Pd cathodes with different microstructure indicate that loading is facilitated in cathodes with large grains. In addition, it was found that commercially processed, high purity Pd (99.99% or better) produced limited grain growth compared to lower purity material under the typical annealing conditions (1100°C for 20 hours in vacuum) because of small residual stress.

Introduction

Anomalous effects, which include the production of excess power, helium-4, tritium and other forms of low energy radiation, have been reported in deuterated Pd systems. The experimental observations of anomalous effects are not generally reproducible, however. Many reasons for the lack of reproducibility have been postulated. These include variations in the composition and microstructure of the electrode materials, differences in the electrode geometry, and levels of deuterium loading attained. Results are presented in which the electrode material was thermomechanically processed to control the microstructure, characterized both chemically and metallurgically, and loaded electrochemically with either deuterium or hydrogen. The extent of loading is correlated with Pd microstructure. Loading on NRL Pd cathodes is compared to that attained on commercially available material used at other laboratories.

Experimental

Palladium Electrode Material Processing and Characterization. Thermomechanical processing was done to produce an electrode material with a homogeneous composition, controlled microstructure, and minimal defects. A single batch of high purity (nominally 99.999%) Pd sponge from Johnson Matthey was used as the starting material for cathode preparation. Both rod and plate cathode geometries were prepared. Processing for rod-shaped electrodes (0.4 cm diameter x 3.5 cm length; surface area = 4.5 cm^2) consisted of arc-melting, casting, swaging, machining, and annealing. For plate electrodes (0.07

cm x 0.7 cm x 3.5 cm; surface area = 4.9 cm^2), processing involved arc-melting, rolling, annealing, rolling again, machining, and re-annealing. For both rod and plate cathodes, arc melting was carried out in a water-cooled copper hearth, dry machining was used to avoid contaminating the cathode material with oil or water, and annealing was done in a vacuum of 10^{-5} torr or better. Annealed samples were cooled slowly in the furnace under an argon atmosphere to room temperature.

Cathode microstructure was determined by controlling the deformation and the annealing conditions. A separate metallurgical study was undertaken to examine grain growth behavior in Pd rod-shaped cathodes. The results of this study are shown in Figure 1 for Pd at a deformation level of 80% cold-rolled at 650°C and 950°C. In Figure 2 the grain size variation in a Pd rod annealed at 650°C for 1 hour is shown in an optical micrograph. The grain size variation was related to the deformation.

Plate electrodes were examined because the microstructure of plates is easier to control than that of rods since plates undergo less deformation in processing. As such, plate electrodes were expected to have a more uniform cross-section. Cross-section uniformity was expected to (1) remove diffusion barriers due to stresses present in the rods, (2) lead to more uniform loading and (3) lead to faster loading.

Grain size variations in rod and plate electrodes were obtained by varying the annealing conditions (time and temperature). Samples of rod and plate electrodes were given simultaneous annealing treatments for comparison. One pair of rod and plate electrodes was not annealed, a second pair of each was annealed at 650°C for 1 hour, and a third pair of each was annealed at 1100°C for 20 hours. The processing resulted in electrodes with elongated grains from cold working the material and those with equiaxed grains. A comparison of optical micrographs for the corresponding rod and plate cathodes showed little or no difference in microstructure. Electrodes annealed at 650°C and 1100°C had average grain sizes of 44 and 600 μm, respectively. Since the unannealed electrodes likely had more defects and strain than the annealed electrode, the effects of these on loading were also investigated.

Glow-Discharge Mass Spectroscopic (GDMS) Analysis (Shiva Technologies, Inc.) was used to determine the chemical composition of the Pd electrode materials. GDMS is a direct elemental analysis method for solids. The method analyzes for 76 elements in one cycle and has detection limits in the ppb concentration range. GDMS is considered to be a pseudo-"bulk" analysis technique since samples are analyzed end-on and several mm of sample are consumed in the analysis. The precision of GDMS analysis is generally ±10-15%, although light elements and halogens may have larger errors.

Two separate GDMS analyses were made on the as-received Pd sponge starting material. Selected elements from the analytical reports of these samples are shown in Table 1. As seen from the Table, the sponge had several metallic impurities present at the ppm concentration level: Na,, Ti, Cr, Fe, Ni, Rh, Ag, Ta, W, Pt, and Au. Differences noted in the analyses are attributed to inhomogeneities in the different samples of starting material. The purity of the starting material was found to be 99.99%, not 99.999% as specified.

GDMS analyses of NRL-processed Pd rod and plate cathodes (Table 1) showed an increased concentration of Cu, W and Pt over the starting material. Although care was taken to avoid contamination, these impurities were likely introduced into the samples during processing from the arc melter and the tools used to handle the material. In spite of the higher concentrations of these few impurities, the analyses showed that the purity of the processed materials remained essentially 99.99%.

Electrode Pretreatment and Cell Assembly. After machining the electrodes with four grooves for

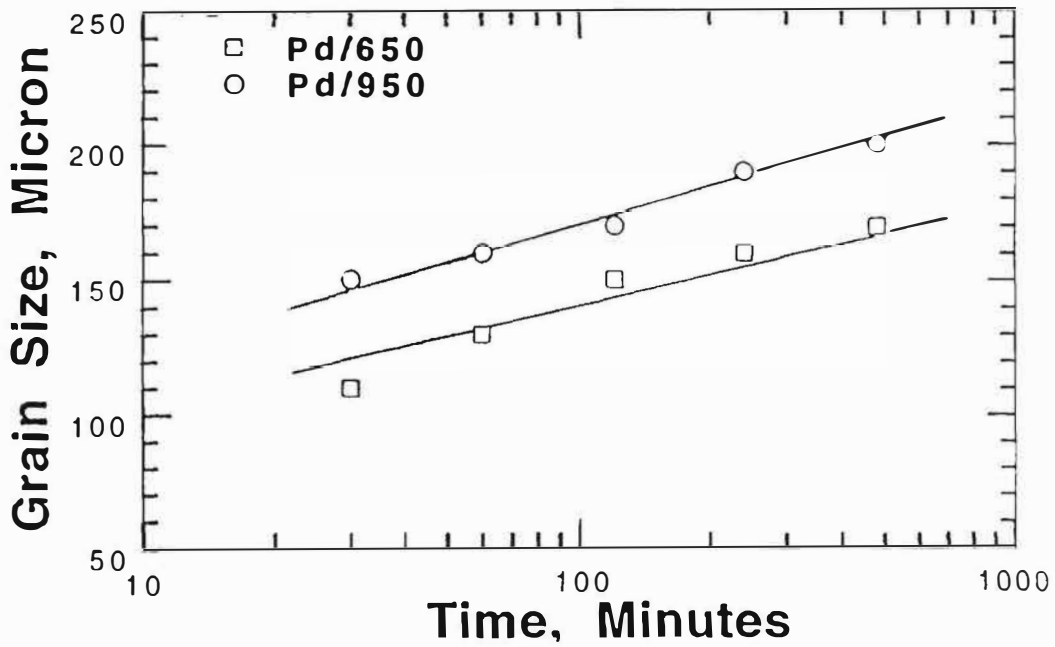

Figure 1. Grain growth vs. time plots for palladium cathodes (rods) processed at NRL. The starting materials were deformed to 80% by cold rolling and annealed at 650°C and at 950°C.

Figure 2. Optical micrograph of NRL palladium rod after annealing in vacuum (<10^{-5} torr) at 650°C for 1 hour. The micrographs show large grains close to the center and finer grains near the surface because of the gradient of residual stress before annealing.

Table 1 - Selected Elements from Glow-Discharge Mass Spectroscopic Analyses of NRL Palladium Cathodes (concentration in ppm by weight)

Element	Pd sponge 9/16/92	Pd sponge 3/31/94	Pd rod 3/31/94	Pd rod 11/28/94	Pd plate 3/31/94
B	0.1	0.007	<0.005	<0.001	<0.005
C	5	<10	<1	0.01	<0.1
N	1	<0.1	<0.1	0.03	<0.1
O	10	<20	<0.5	0.36	<1
Mg	0.1	<0.01	1.2	----	1.7
Al	0.5	0.06	0.3	0.52	0.3
Si	0.6	0.15	1	0.32	9.6
Ca	0.5	<0.05	0.8	0.67	1.1
Cr	2.5	2.8	1.1	1.2	1.8
Mn	0.9	1.3	0.75	----	1.1
Fe	45	31	30	33	50
Ni	1.3	1.1	0.84	0.96	1.3
Cu	0.8	0.44	31	24	12
Zn	0.9	0.3	1	1.1	2
Rh	8	6.3	9.3	10.5	11
Ag	1.5	1.6	1.1	1.1	1.7
W	1	0.01	0.5	3.4	3
Pt	12	6.3	31	29	26
Total	92	82	111	106	124

the Pt resistance wires, cathodes were either annealed or left as processed. Regardless of the treatment, Teflon-coated Pt lead wires were attached to the cathodes by spot welding. A 30 second etch in either "heavy" or "light" aqua regia followed the spot-welding to remove contaminates from the cathode surface. Other NRL work [1] showed that the etch also increases the initial reactive surface area of the Pd and aids in the development of surface structures that form with D_2O or H_2O electrolysis. The isotopically appropriate water was used to rinse the cathodes after an etch. Either Pt-clad Nb mesh, Pt mesh, or Pt helical anodes were used in the electrochemical loading experiments. Anodes were cleaned by immersion in a 50-50 mixture of concentrated nitric and sulfuric acids, rinsed with triply distilled water and oven dried in air.

Borosilicate-glass test tubes (2.5 cm O.D. x 15 cm length) were used as electrolysis cells in our experiments. The cells were fitted with Teflon stoppers and sealed with Viton o-rings. Cell tops held small diameter Teflon tubing for exit gases and electrolyte additions. Cathodes were centered within the circumference of the cell and cylindrical anodes were place symmetrically around the cathode. Cell assembly was done on the benchtop using clean, latex gloves to avoid excessive handling of the cell components. Serious attempts were made to avoid introducing impurities into the electrolytic cells in order to obtain reproducible electrochemical experiments. As such, only high purity reagents were used and precautions were taken to minimize the exposure of all reagents to the ambient atmosphere to avoid contamination with light water. Unopened bottles of deuterium oxide (Cambridge Isotope Laboratories, 99.9% or Ontario Hydro, 99.93%), cans of lithium foil (Johnson Matthey, 99.9%), aluminum shot (Johnson Matthey, 99.999%) and deuterated hydrochloric, nitric, and sulfuric acids were taken into a glove box with a boil-off nitrogen atmosphere for storage on receipt of the materials. Freshly prepared, 0.1 M LiOD electrolyte was made in the glove-box by dissolving Li metal in heavy water before each new electrochemical experiment. Reagents for light water experiments were stored outside the glovebox on the benchtop.

Results and Discussion

Electrochemical Loading Experiments on NRL Cathodes. Two nearly identical electrolytic cells were connected electrically in series in each electrochemical loading experiment. Usually, one cell contained heavy water while the second cell contained light water. Cells were run under galvanostatic control. Electrode loading was started as soon as possible after electrolyte addition (electrolyte volume was 30 mL). Initial charging was usually done with current densities of 20-25 mA cm^{-2} on the cathodes. For 0.4 cm diameter rod electrodes, initial charging took 2-3 days. Deuterium or hydrogen loading reached a D(H)/Pd atomic ratio of 0.70-0.75 during this time. The current density was then increased in 20-25 mA cm^{-2} steps every day or two to continue the loading.

Electrolyte was replenished with D_2O or H_2O before the total volume in the cell was 5 mL below the starting level. This procedure kept the cathode and anode completely submerged. The frequency of additions varied depending on the current density applied. For 0.4 cm diameter Pd cathodes at low current densities (25-50 mA cm^{-2}), additions were made every two or three days. At higher current densities (100-200 mA cm^{-2}), additions were made daily. Some electrolyte additions contained small amounts (typically 120-275 ppm) of dissolved aluminum metal. Aluminum was added to facilitate the attainment and maintenance of high D(H)/Pd loadings as described by McKubre et al. [2].

During all experiments cathode loading was monitored *in situ* by measuring the change in the axial resistance of the Pd with deuterium or hydrogen content as described by McKubre [14]. The resistance measurements were made with a standard 4-point probe technique. D/Pd and H/Pd loading atomic ratios were estimated from the resistance measurements and plots of the resistance ratio-loading

variations in the H/Pd and D/Pd systems at room temperature as shown in papers by McKubre et al. [3]. Loading atomic ratios, H/Pd and D/Pd, are often inferred from these plots, but care is taken in assuming a precise level of loading based on resistance measurements alone since other factors (temperature, electrode cracking, loading inhomogeneities, electrode impurities) can affect the Pd resistance [4].

Electrochemical loading experiments were carried out on six pairs of NRL Pd electrodes with different microstructures. Several observations regarding cathode loading were noted from these experiments. First, deuterium loading in both rod and plate cathodes did not exceed a D/Pd atomic ratio of 0.7-0.75, despite the extent of electrode processing. This level of loading corresponds to the α,β mixed-phase region; loading beyond this level would occur in the β-phase. Second, hydrogen loading into the pure β-phase, where the H/Pd atomic ratio was 0.8-0.85, occurred in the Pd rod with large grain morphology. Hydrogen loading did not exceed a H/Pd atomic ratio of 0.7-0.75 in rod cathodes with less processing. Third, hydrogen loading in Pd plates increased with electrode processing although all the plate cathodes loaded into the β-phase. Hydrogen loading reached a level where the H/Pd atomic ratio was 0.8-0.85 in an electrode with no processing, but it increased to where the H/Pd atomic ratio was approximately 0.95 with electrode processing. The comparison of hydrogen loading in rod and plate electrodes provided evidence that reducing the strain in the Pd led to higher loading.

Our experiments on Pd rod and plate electrodes with different microstructures showed that deuterium loaded more slowly in cathodes with a large grain morphology. Slower loading appeared to be advantageous for attaining higher levels of loading. In addition, thin plate electrodes were found to load more rapidly to D(H)/Pd~0.7 than 0.4 cm diameter rod electrodes with comparable grain sizes. Faster loading in plate electrodes can likely be attributed to the more uniform cross-section of the plates and to their higher surface area to volume (A/V) ratio. The influence of the A/V ratio on loading Pd with hydrogen to the β-phase had been observed by Hoare [5] who compared loading ratios in foils, wires and beads in acid solution.

Eventually, deuterium loading into the β-phase was routinely achieved in NRL rod and plate cathodes with large grain morphology. This was accomplished by improving the cathode surface preparation and better controlling the electrolyte purity. The changes decreased the thickness of surface films that deposited on the Pd and prevented high cathode loading. Resistance ratio-time variations for two pairs of these cathodes are shown in Figure 3 as a function of the applied current. Note that the resistance of the Pd shows a dynamic response to current.

Comparison With Commercial Cathodes. GDMS analyses of as-received, commercially available Pd rod and wire were done to confirm the purities of the materials acquired and to identify the impurities present. Selected elements from the analyses are shown in Table 2. As seen from the table, all the materials examined had essentially the purities specified. The Johnson Matthey 99.997% Pd wires (stock#10960) had the highest purity. Both lots (W12954 and W7403) had exceptionally low Fe and Pt concentrations. Lot W7403 had an elevated Si content, however. Pt, Rh, Fe and Si were the major impurities found in the majority of materials at the ppm concentration level. In addition, some 99.9% materials had relatively high concentrations of B, O, Al, Cu and Ag. Other impurities present at the ppm level included C, N, Ca, Cr, Mn, Ni, Zn and W.

The commercial Pd rods and wires were annealed at 1100°C for 20 hours to examine the grain morphology produced. The morphology of the grain depends not only on the annealing conditions, but also on how much residual stress was in the sample before annealing. Optical micrographs of the annealed materials showed that samples responded differently to the annealing conditions based on their

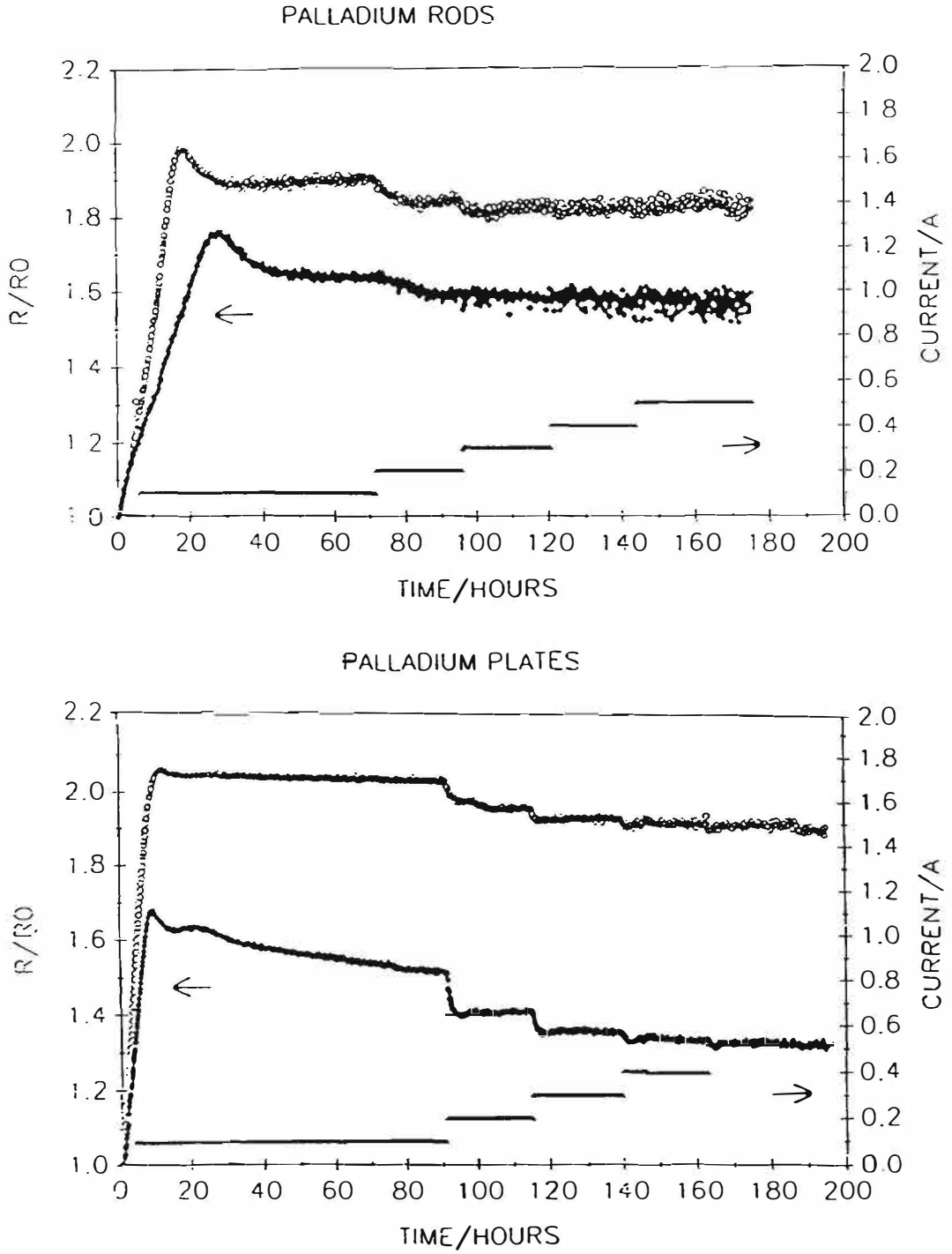

Figure 3. Resistance ratio (R/R_0) vs. time variations for two pairs of NRL palladium cathodes as a function of applied current. Open symbols - deuterium, closed symbols - hydrogen.

Table 2 - Selected Elements from Glow-Discharge Mass Spectroscopic Analyses of Commercial Palladium Cathodes (concentration in ppm by weight)

Element	J.Matthey 99.9% Wire K11C06	J.Matthey 99.997% Wire W7403	J. Matthey 99.997% Wire W12954	Goodfellow 99.95% Wire 005150/11	Engelhard #3 99.9% Rod	J. Matthey 99.99% Rod	J.Matthey 99.9% Rod F13E05
B	17	0.01	0.007	2.5	140	23	4.1
C	<5	<1	<1	<1	<1.8	<1	<0.1
N	<0.1	<5	<3	<0.1	<0.23	<0.1	<0.05
O	<10	<20	<10	<10	<290	<20	<6
Mg	0.29	0.008	0.009	0.04	0.59	0.09	0.09
Al	59	0.34	0.63	2.3	12	1.1	7.6
Si	67	43	3.5	6.6	280	1.8	16
Ca	7.3	0.11	0.29	<0.05	66	7.5	5.1
Cr	5.3	0.25	0.21	0.68	15	1.3	1.6
Mn	1.6	0.01	0.004	0.17	0.51	0.22	0.84
Fe	95	1.1	2.9	30	69	14	37
Ni	54	0.05	0.03	1.4	1.7	0.58	1.4
Cu	24	0.11	0.76	22	13	2.6	6.5
Zn	5.2	0.1	0.02	2.5	<0.021	0.55	3.6
Rh	110	0.56	4.2	6	<9.3	24	71
Ag	29	<0.1	0.45	13	<.76	1.6	0.7
W	1.4	0.15	0.1	0.2	1.1	0.06	0.91
Pt	1100	1.9	2.2	80	22	28	960
Total	1591	74	29	179	930	128	1123

processing history. For example, the annealing conditions we used produced a large grain morphology in all of the 99.9% materials and the 99.99% Johnson Matthey rod. However, the Johnson Matthey 99.997% wires (stock #10960) and a Goodfellow 99.99+% wire (stock #005155/11 - not analyzed by GDMS) had either fine, equiaxed grains or elongated grains after the anneal. In other words, the commercially processed, high purity (99.99% or better) wires produced limited grain growth compare to the lower purity (99.9%) materials under the annealing conditions because of residual stress in the materials. The grain morphologies observed reflected different thermomechanical treatments of the samples.

Based on this limited sample set, a possible correlation was found between sample purity and grain morphology. For example, in the high purity (99.99% or better) wires, hardly any grain growth occurred on annealing whereas all of the lower purity (99.9%) materials readily grew large grains. Very pure samples are generally expected to have very rapid rates of grain growth. Other factors such as the amount of deformation encountered during cold working and the grain size before cold working can have an adverse effect on grain growth.

Loading Experiments on Commercial Cathodes. Almost all of the commercial Pd cathode materials (except the Goodfellow 99.99+% wire #005155/11) were used in deuterium loading experiments. The materials were either annealed before being used in the experiments or left as processed. Metallurgical analysis of the annealed materials showed that the grains enlarged in these samples as result of the annealing treatment. Unannealed samples likely had elongated or small, equiaxed grain morphology although a metallurgical analysis was not done on all of these samples.

Electrochemical deuterium loading experiments on the commercial cathode materials were carried out as described in the section on NRL cathodes. In deuterium loading experiments on annealed cathodes with large grain morphology five out of six cathodes were loaded into the β-phase: 1 Johnson Matthey 99.99% rod, 1 Johnson Matthey 99.9% wire (#K11C06), 1 Goodfellow 99.9% wire (#005150/11), and 2 Engelhard #3 99.9% rods supplied by SRI. The annealed cathode that failed to load into the β-phase was a Johnson Matthey 99.99% rod.

Five deuterium loading experiments with unannealed, commercial cathodes were carried out. Only two of these loaded into the β-phase: a Johnson Matthey 99.9% wire (#K11C06) and a Johnson Matthey 99.9% rod (#F13E05). The three unannealed materials that did not load into the β-phase were 2 Johnson Matthey 99.997% wires (#W12954 and W7403) and 1 Goodfellow 99.9% Pd rod (#007940/5).

Based the these results, a possible correlation was found between sample morphology and deuterium loading. Specifically, most samples with a large grain morphology loaded into the β-phase of Pd while those with elongated or small grains were not as readily loaded.

Conclusions

1. Electrochemically loading Pd cathodes into the β-phase with deuterium or hydrogen is facilitated in a material with a large grain morphology.
2. Hardly any grain growth occurred on annealing high purity (99.997%) Pd wires at 1100°C for 20 hours whereas high purity rods and lower purity (99.9%) materials readily grew large grains.
3. Pd cathodes with elongated or small grains did not load into the β-phase while large grain materials loaded readily.

Acknowledgement

The authors greatfully acknowledge Drs. Fred Saalfeld and Robert Nowak of the Office of Naval Research for providing the financial support for this work.

References

1. D.R. Rolison and P.P. Trzaskoma, " Morphological Differences Between Hydrogen-Loaded and Deuterium-Loaded Palladium As Observed by Scanning Electron Microscopy," J. Electroanal. Chem., **261**, 1989, 301-308.

2. M.C.H. McKubre, S. Crouch-Baker, A.M. Riley, S.I. Smedley and F.L. Tanzella, "Excess Power Observations in Electrochemical Studies of the D/Pd System: The Influence of Loading," Proceedings of the Third International Conference on Cold Fusion, "*Frontiers of Cold Fusion*," H. Ikegami, Ed., Universal Academy Press, Inc., Tokyo, 1993, 5-19.

3. M.C.H. McKubre, S. Crouch-Baker, R.C Rocha-Filho, S.I. Smedley, F.L. Tanzella, T.O. Passell and J. Santucci, "Isothermal Flow Calorimetric Investigations of the D/Pd and H/Pd Systems," J. Electroanal. Chem., **368**, 1994, 55-56.

4. M.C.H. McKubre, R.C Rocha-Filho, S. Smedley, F. Tanzella, J. Chao, B. Chexal, T. Passell and J. Santucci, "Calorimetry and Electrochemistry in the D/Pd System," Proceedings of the First Annual Conference on Cold Fusion, The National Cold Fusion Institute, Salt Lake City, UT 1990, 20-31.

5. J.P. Hoare, "Surface to Volume Considerations in the Palladium-Hydrogen-Acid System," J. Electrochem. Soc., **106**, 1959, 640-643.

Material Science Studies

Click here for a more readable copy of this paper.

Surface Composition of Pd Cathodes

Patrick L. Hagans, Dawn D. Dominguez and M. Ashraf Imam,

Naval Research Laboratory, Washington, D.C. 20375. USA

Abstract

Results will be presented for the surface analyses of cathodes before and after electrolysis using X-ray Photoelectron Spectroscopy (XPS). Composition as a function of depth was obtained by employing argon ion sputtering to gradually erode away the surface. Although most of the emphasis will be on Naval Research Laboratory (NRL) Pd (i.e., Johnson Matthey high purity sponge processed into rod and plate at NRL), data will also be presented from other Pd sources and from reported excess heat-producing cathodes provided by SRI International and NAWC, Naval Air Warfare Center at China Lake, CA. XPS results will be compared with bulk sample cathode and anode analyses obtained by Glow Discharge Mass Spectroscopy (GDMS) and with electrolyte solution analyses obtained by Inductively Coupled Plasma (ICP) spectroscopy.

Introduction

Impurities on the cathode surface are expected to exert an influence on the ability of cathodes to attain D(H)/Pd ratios near unity and to retain this high loading for the time required to obtain excess heat. For example, Pd (and Pt) are the most efficient electrocatalysts for promoting reduction of D_2O and H_2O to form D_2 and H_2. The presence of other impurities would reduce the rate of this reaction (depending on the impurity, this could amount to many orders of magnitude). In addition, the ability to promote the dissociation of D_2 to form an adsorbed deuterium atom (D) and, subsequently absorbed D, could be reduced by the presence of surface and bulk impurities. The presence of Pt, a common contaminant found in Pd, could also be deleterious to obtaining high loadings since Pt is also an excellent recombination catalyst for the reaction: $D_{ads} + D_{ads} = D_2$. Since absorbed D is known to occupy interstitial positions within the Pd lattice, impurities, especially those of the lighter elements, can block these positions. For example, C atoms can penetrate into the Pd lattice if exposed to C-containing gases at moderate temperatures[1] (as might occur during processing). Interstitial solid solutions up to $PdC_{0.15}$ can form which can totally block the formation of ß-PdH which develops at H/Pd = 0.65 and is a precursor phase to the attainment of high loading. B, which also enters the Pd lattice interstitially, is known to totally block ß-Pd-H formation at a concentration of 16 atomic%[2]. Blockage of H atom ingress by the presence of high concentrations of C and B in the Pd lattice could also be caused by the formation of carbides and borides of Pd. B, at concentrations less than 10 at.% where borides do not form as indicated by the Pd-B binary phase diagram, will promote H absorption due to the expansion of the Pd lattice caused by the presence of B[3]. Thus, smaller amounts of interstitial impurities could actually exert a positive influence on the attainment of high loadings.

Experimental

The XPS spectra were recorded with a Surface Science Laboratories Model SSX-301 system utilizing a monochromatic Al Kα source. Survey scans from 0 to 1000 eV binding energy were recorded at a 100 eV pass energy. Sputtering was accomplished with a Perkin Elmer differentially pumped ion gun utilizing 3 kV argon ion beam at 20 mA emission current and a 3x3 raster. Base pressure of the main

chamber and fast entry chamber was $1x10^{-9}$ torr and $1x10^{-7}$ torr, respectively. In order to preserve the vacuum in the main chamber on occasion it was necessary to pump on the sample in the fast entry chamber overnight to remove the remaining absorbed D or H. A description of each sample examined can be found in the text and figure captions. A complete description of sample processing and electrochemical history can be obtained from the authors.

Results and Discussion

XPS of Unused Cathodes

A survey spectrum of a Johnson-Matthey 99.9% purity wire as received is shown in Figure 1A. Even though the Pd 3d doublet is clearly visible the surface is composed mostly of carbon and oxygen due to the large difference in peak area sensitivity factors ($Pd3d_{5/2}$=9.48, C1s=1.00, O1s=2.93). Si, Cl and Mg are also present but to a much lesser extent than C and O. This is a representative spectrum for all cathode materials examined which included NRL Pd and Pd-B rod, Engelhardt #3 and Johnson-Matthey 'special batch' rods from SRI, Goodfellow 99.95% and 99.99+% wire, and Johnson-Matthey 99.9% and 99.997% wire. In all cases the principal contaminants were always C and O and the Pd 3d doublet was always visible. The C1s peak was in all cases anywhere from approximately 1/2 to double the height of the Pd 3d doublet. This puts the contamination level of all surfaces easily in excess of 50 at.%. Other minor contaminants found included S and Na. On the surface most of the elements as determined from their binding energy were in the oxidized state except for C which appeared to be graphitic (B.E.=284.0eV). Sample preparation such as vacuum annealing and acid etching in aqua regia did not appear to significantly alter the surface composition. These data illustrate the ability of the Pd surface to become significantly contaminated upon exposure to air and water.

Most of the contamination observed in Fig. 1A is found to reside in approximately the top 10Å as illustrated in the survey shown in Fig. 1B obtained after a 10s argon ion sputter (sputter rate 1Å/s for SiO_2). Most of the original C and O have been removed and the Pd peaks now dominate the spectrum. An additional 20s sputter produces a further reduction in contaminant levels (see Figure 1C) although the effect is not as dramatic as that observed with the initial 10s sputter. Figures 1B and C also indicate the presence of Pt in this sample. This agrees with the GDMS results for this material which showed the presence of 1100 ppm Pt impurities. In the samples sputtered for longer than 30s, all the impurities were removed except for C (and Pt for 99.9% purity Pd). C would persist to the deepest levels indicating that it either was a bulk contaminant or that it diffused from the surface to the bulk during processing.

XPS of Used, Non-heat Producing Cathodes

The data for NRL-processed Pd cathodes is divided into two groups based on the XPS results. The first group comprises the thickest overlayers containing large concentrations of both Cu and Pt relative to Pd. The Cu and Pt can either be near the surface or buried under a silicate-containing overlayer. All of these samples were electrolyzed for approximately 1000 hrs. The second set of samples all contained thinner overlayers than the first with very little Cu. A high Pt concentration, however, was found on all of these samples. These samples were all electrolyzed for 500 hrs. or less and they received a large number (6) of cathodic-anodic current reversals.

Figure 2 is a series of survey spectra taken from the surface and various depths of an NRL Pd plate electrode. The following elements are found at the surface: Si, O, C, Cu, Nb, Pt, Zn, Na, Mg and Ca. The Zn, Mg, Ca and Na appear to be ubiquitous in small quantities to nearly all the samples examined by XPS. Several examples of much higher Ca concentrations also have been found. ICP analysis of the D_2O and the LiOD electrolyte before and after electrolysis show the presence of Na and Ca (before electrolysis: 0.00-0.07 ppm Ca, 0.01-0.30 ppm Na; after electrolysis: 0.00-0.18 ppm Ca, 0.16-2.53 ppm Na). No Zn or Mg above 0.01 ppm, however, was observed in any solution making their source

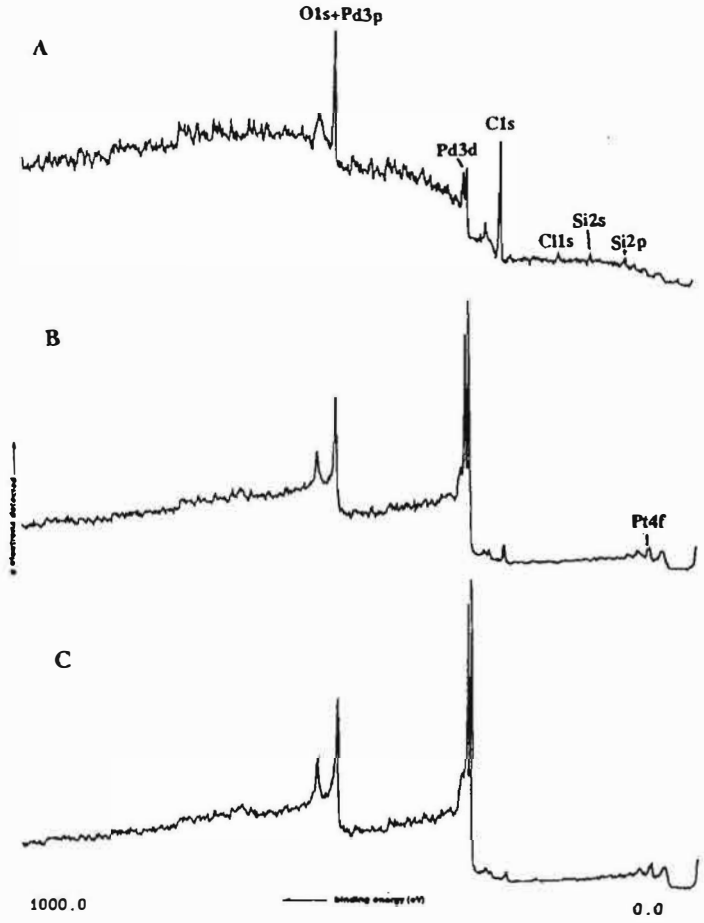

Figure 1. XPS survey spectra obtained from a 1-mm diameter Johnson Matthey 99.9% purity Pd wire (#010280, Lot K11C06). A: Surface, B: After 10-sec. sputter, C: After 30s sputter. Scans from 0 eV (right) to 1000 eV (left) binding energy.

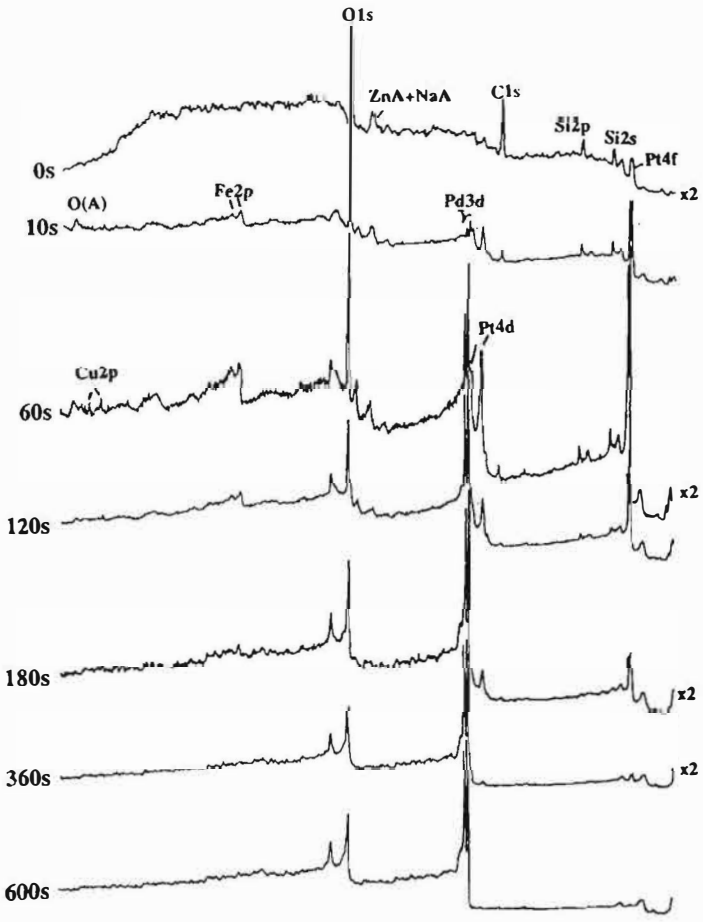

Figure 3. Series of XPS survey spectra obtained at various total sputter times from a large grain (600μm), 99.99% purity Pd rod cathode, 3.5 cm long by 0.4 cm in diameter, etched in aqua regia after Pt resistance wires attached by spot-welding with Pd/Pd-Ag electrodes, Pt mesh anode, pyrex cell, isoperibol calorimeter, 0.1M LiOD (Li from Johnson Matthey, D_2O from Ontario Hydro), 460 hrs. total electrolysis time, highest current density=455 mA/cm^2. Scans from 0 eV (right) to 1000 eV (left) binding energy.

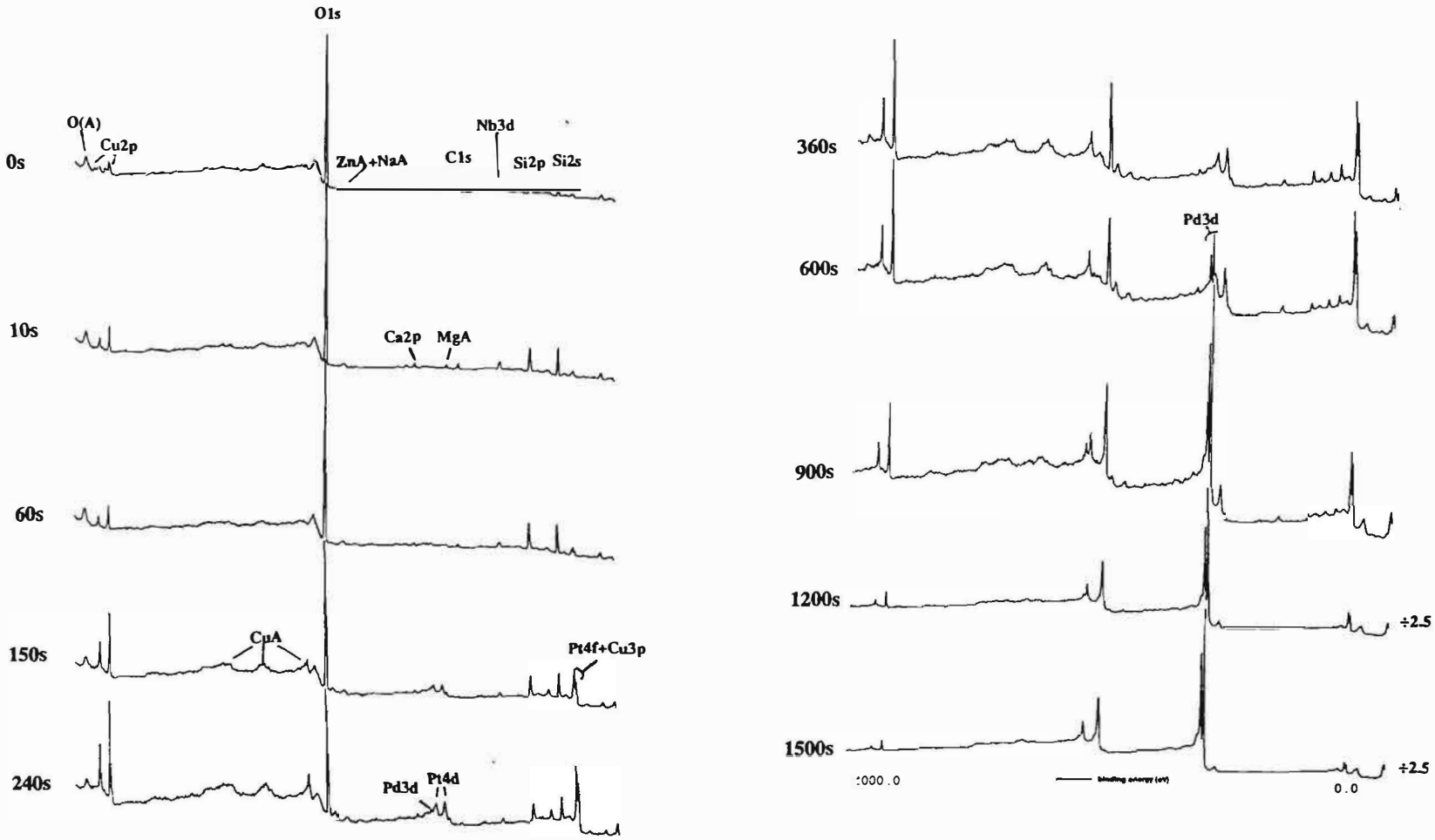

Figure 2. Series of XPS survey spectra obtained at various total sputter times from a large grain (600μm), 99.99% purity Pd plate cathode, 3.5x0.7x0.07cm thick, etched in aqua regia after spot-welding of Pt resistance wires using Pd/Pd-Ag welding tips, Pt-clad Nb mesh anode, pyrex cell, 0.1M LiOD (Li from Johnson Matthey, D_2O from Ontario Hydro), 980 hrs. total electrolysis time, highest current density=370 mA/cm^2. Scans from 0 eV (right) to 1000 eV (left) binding energy.

uncertain. Nb is found on all samples in which a Pt-clad Nb mesh was used as the anode. Nb is exposed to the electrolyte at all points where the material has been cut and at spot welds where damage to the Pt film can occur. The Cu (its potential source will be discussed later) is found to be in the +2 oxidation state as is indicated by the two sets of 3p doublets occurring between 930 and 970 eV. Due to their small area sensitivity factors, the major components of this surface are O, Si and C. Besides Cu (which has a sensitivity factor similar to that of Pd and Pt), the oxygen is also associated with both C, as evidenced by the small shoulder on the high binding energy side of the C1s peak, and Si. The binding energy of the Si peaks is indicative of the presence of a silicate-type species. The bulk of the C detected on the surface is merely the so-called 'adventitious' carbon contamination found on all air-exposed surfaces. No Pd is evident on the surface. In fact, Pd is not detected until after approximately 150s of sputtering and even then the Pd $3p_{3/2}$ peak is only a small shoulder on the Pt $3d_{3/2}$ peak. The Pd peak does not become easily discernible until somewhere between 360 and 600 seconds of sputter time. As sputtering proceeds both Cu and Pt, which were just observable on the surface, increase as the quantity of silicate species slowly decreases. The Cu and Pt reach a maximum after about 600s of sputter time and then decrease as the amount of Pd increases. After 1500s both Cu and Pt are still present which indicates that a relatively thick overlayer has grown on this electrode.

An example of a surface containing a thin overlayer after electrolysis is shown in Fig. 3. The surface contains silicate along with C and Pt. No Cu or Pd is observable in the first survey spectrum. After removal of much of the surface C contamination with a 10s sputter etch Pd is observed along with a significant increase in Si, O and Pt. Further sputtering removes the silicate with a concomitant increase in Pd. After 180s the Si has all been removed but Pt is still present. The Pt 4f signal decreases until after 600s where it is just barely discernible above the noise. Compared to the final spectrum shown in Figure 2 obtained at 2.5 times the total sputter time for this sample, it is easy to observe that the film on this electrode is much thinner. In addition, Cu never becomes a significant component of these types of films.

Film thickness appears to correlate with total electrolysis time. In addition, composition with respect to Cu is very different between the two different types of electrodes. Interestingly, there also appears to be a correlation with the maximum D/Pd obtainable. The thinner, non-Cu-containing overlayers reached loadings of D/Pd = 0.7 while the thicker, Cu-containing overlayers were found on samples with D/Pd = 0.9[4]. This indicates that the development of these Cu-rich layers at long electrolysis times may, in fact, have been beneficial to obtaining high loadings by acting as a blocking agent to D egress from the Pd lattice. The quest for low levels of excess heat with more sensitive calorimeters than used in our studies might have proven very interesting with these samples.

Alluded to in the above discussion are the sources of some of the impurities. Si most certainly comes from the etching of the pyrex or quartz container by the concentrated LiOD or LiOH. ICP analysis of the used solutions indicated that Si was present anywhere from approximately 30 to 80 ppm in the experiments where pyrex containers were used while around 10-20 ppm were found for experiments conducted in quartz holders. The source of Pt, found on every electrode examined with XPS, was likely from oxidation of the Pt anode at high current density. ICP analysis, however, showed less than 0.1 ppm Pt in all solutions. Another possible source was the Pd itself since most Pd used contained above 30 ppm Pt. Only one very high purity Pd sample containing a very small Pt level was examined: Johnson-Matthey 1mm diameter wire, 99.997% purity, where Pt by GDMS=1.9 ppm[5]. XPS indicated that very little Pt was present on this electrode.

A similar argument applies to the Cu except that, unlike Pt, there is no single solid source of Cu exposed in the cell. Sources of Cu include: D_2O, Li used to make LiOD from the D_2O, spot welds where Cu-containing tips are used, the Pt anode, the Pd cathode, Pyrex^R or quartz and the Teflon^R used

for the cell top and to shield the electrical connections. The Pyrex^R, quartz and Teflon^R seem unlikely candidates to supply such large amounts of a metallic impurity. The spot welds are unlikely as Cu was found on several cathodes where the welding tips were made of Pd and Pd-Ag alloy rather than Cu. Also, the cathodes were always acid etched after spot welding was completed. The Li was reported to have 20 ppm of Cu but so little is used to make up the 0.1M concentration that there is not enough present to supply such large amounts of Cu assuming the surface of the cathodes are uniformally covered. The Li was also reported to contain 90 ppm of Na and 78 ppm of Ca; these could have been the source of those impurities often found in small quantities on the cathode surface. The D_2O was not the source as believed in an earlier study[4]. Extremely pure D_2O was provided by Ontario Hydro in which the Cu concentration was less than 0.005 ppm; our ICP analysis indicated that there was less than 0.01 ppm in both the D_2O (Ontario Hydro and Cambridge Isotope) and the 0.1M LiOD. The Pt anode could be the source but GDMS analysis of one anode indicated that only 0.25 ppm Cu was present. A Pt anode was examined by XPS after an experiment and no Cu was observed on its surface. The final source is the Pd cathode itself. The NRL Pd material was found to contain 24 to 27 ppm Cu which was likely obtained from arc melting of the sponge which was conducted on a Cu hearth. Calculations indicate, assuming surface segregation of the bulk Cu, that this is enough Cu assuming uniform distribution in the bulk (verified by depth measurement made with GDMS) to provide concentrations found in the surface films observed on used cathodes. Two cathodes which produced high Cu were reground and polished on a lathe. High Cu was found again re-observed on both cathodes after electrolysis. In addition, a higher than usual Ca level found on one of the cathodes was repeated after repolishing and electrolysis. One of the 'high Cu' cathodes was examined by GDMS as a function of depth. Cu was found at a concentration of nearly 80 ppm throughout the entire sample suggesting that initially this NRL sample had a larger than average Cu content. Cu was also found on an NRL Pd rod electrode tested at SRI in a degree of loading experiment. Cu was found on a 99.9% purity 1mm Johnson-Matthey wire which contained 24 ppm Cu by GDMS. Little Cu was found on two NRL samples run at China Lake. A number of different chemicals, however, were added to the electrolyte in an attempt to increase D uptake. These may have had an influence on Cu mobility. One anomaly, however, does exist and this is the large Cu concentration found on a 99.997% purity Johnson-Matthey wire cathode. GDMS indicated that this material contained only 0.11 ppm Cu. Electrical connections to this cathode were made, however, with Cu spot welding tips. Even though these cathodes were acid etched after spot welding, perhaps some Cu remained behind.

Surface segregation of various elements during H or D absorption has been observed previously. Surface enrichment of ppm bulk contaminants Ag and Rh has been detected with Pd electrolysis in both H- and D-based acid electrolytes[7]. The room temperature segregation of La has been observed in the hydride battery material $LaNi_5$[8]. Running the electrode through charge-discharge cycles causes the La to diffuse to the surface where it is oxidized by the KOH electrolyte. The $La(OH)_3$ blocks H ingress and reduces the efficiency of the battery. Normally La mobility in the $LaNi_5$ lattice is practically zero at room temperature. The authors believe that the enhanced La mobility is caused by the severe distortion at the boundaries of the hydrogen-rich and hydrogen-poor regions which arise during charging and discharging. The severe lattice defects occurring over relatively large areas cause short circuit diffusion paths for the La atoms. The same type of mechanism could account for the enriched Cu and Pt surface layers found on used Pd cathodes.

XPS of Heat-Producing Cathodes

Two sources of heat-producing cathodes, NAWC at China Lake and SRI International, provided samples for XPS analysis. Only analysis of the SRI cathode will be described here. The SRI Pd cathode examined was sample number P15, a Pd rod made from Engelhard #1 material which was SRI's most successful heat-producing material. This sample was annealed and electrolyzed in 1991. Details of the P15 experiment have been published[9]. From ICPMS data provided by SRI, the

Material Science Studies

Engelhard #1 Pd is of 99.9% purity containing 140 ppm Pt and 13 ppm Cu plus significant levels of many other impurities. Heat-producing electrodes from China Lake[10] examined by XPS include: Johnson-Matthey high purity wires electrolyzed in two different calorimeters, NRL Pd rod and NRL Pd-B alloy rods.

Shown in Figure 4 are a series of survey spectra taken of the surface of the SRI P15 cathode and after various sputter times. The surface is a mixture composed of carbon- and oxygen-containing species of which silicate is the most prevalent. Small amounts of Pt, S, Zn, Na and N are also seen. No Pd is present on the surface. After a 10s-sputter some silicate is removed which results in a small increase in the C1s signal and a large increase in the Pt4f doublet. After 30s the Si is nearly all removed, the C begins to decrease, and the Pt and Pd continue to increase. Cu is also visible now. After 60s the metallic impurities, Cu and Pt, reach their maximum while C continues to decrease slowly and Pd increases. Further sputtering continues to uncover the Pd while the other impurities decrease. After 900s total sputter time, only Pt and C impurities are still visible. These are contaminants which are likely part of the bulk. As evidenced by the peak binding energies, the carbon always appeared to be mostly in the graphitic state while the Pt, even on the surface, was in the metallic state. The profile does not look all that different from that obtained for relatively thin overlayer samples tested at NRL and depicted in Figure 3. The P15 electrode was loaded to a maximum D/Pd of 0.99 and it produced anywhere from 5 to 10% excess power over the total input power. These amounts were just below the sensitivity of the NRL isoperibol calorimeters. This fact makes trying to draw conclusions based on the XPS results as to what impurities are necessary on the surface to obtain high loadings and excess power very difficult. Also, at the end of SRI 's experiments, they normally switch the potential on the cathode so that an anodic current is flowing in order to de-load the sample before removal from the cell. This could oxidatively remove certain species from the overlayer that normally would have been present.

Several observations can be made concerning excess heat-producing electrodes. All contain layers on part or all of the electrode which are relatively thin in the sense that Pd is either observed on the surface or very early in the sputter profile and the peaks due to Pd rise rapidly with continued sputtering. Pt is always visible on the surface of these electrodes. The electrodes, with the exception of the high purity Johnson-Matthey used at China Lake (2.2 ppm Pt by GDMS), generally have a large Pt impurity concentration in the bulk. Pt and Pd are in the metallic state when found on the surface. A silicate layer is observed on the surface but this can be sputtered away fairly rapidly. There is usually a graphitic component to the carbon which appears to extend, along with the Pt, into the bulk. Copper is a small impurity as are Zn, Na, Ca and Mg. Many of these observations can also be made for the cathode materials run at NRL. Since, however, the excess heat observed in the analyzed samples generally did not exceed 10% of the input power and the sensitivity of the NRL calorimeters was in the range of 10% and above, using the XPS data for NRL-run samples as representative of non-excess heat producing electrodes may not be correct. As a final note, many of the impurities found in the surface layers are also present in the bulk of the cathode at the ppm level. Certainly the source of all the impurities found on the surface is not the bulk: however, as discussed above there is data to suggest that loading and de-loading H-storage materials can greatly increase the room temperature diffusion rates of bulk elements.

Conclusions

1. Prolonged electrolysis at high current density in basic solution results in the formation of a relatively thick layer on the cathode (>1000Å) composed of a varied elemental composition with very little or no Pd identifiable on the surface. 20 different elements have been identified from XPS analysis of over 30 different electrode surfaces. Cationic, anionic and organic species in the electrolyte have

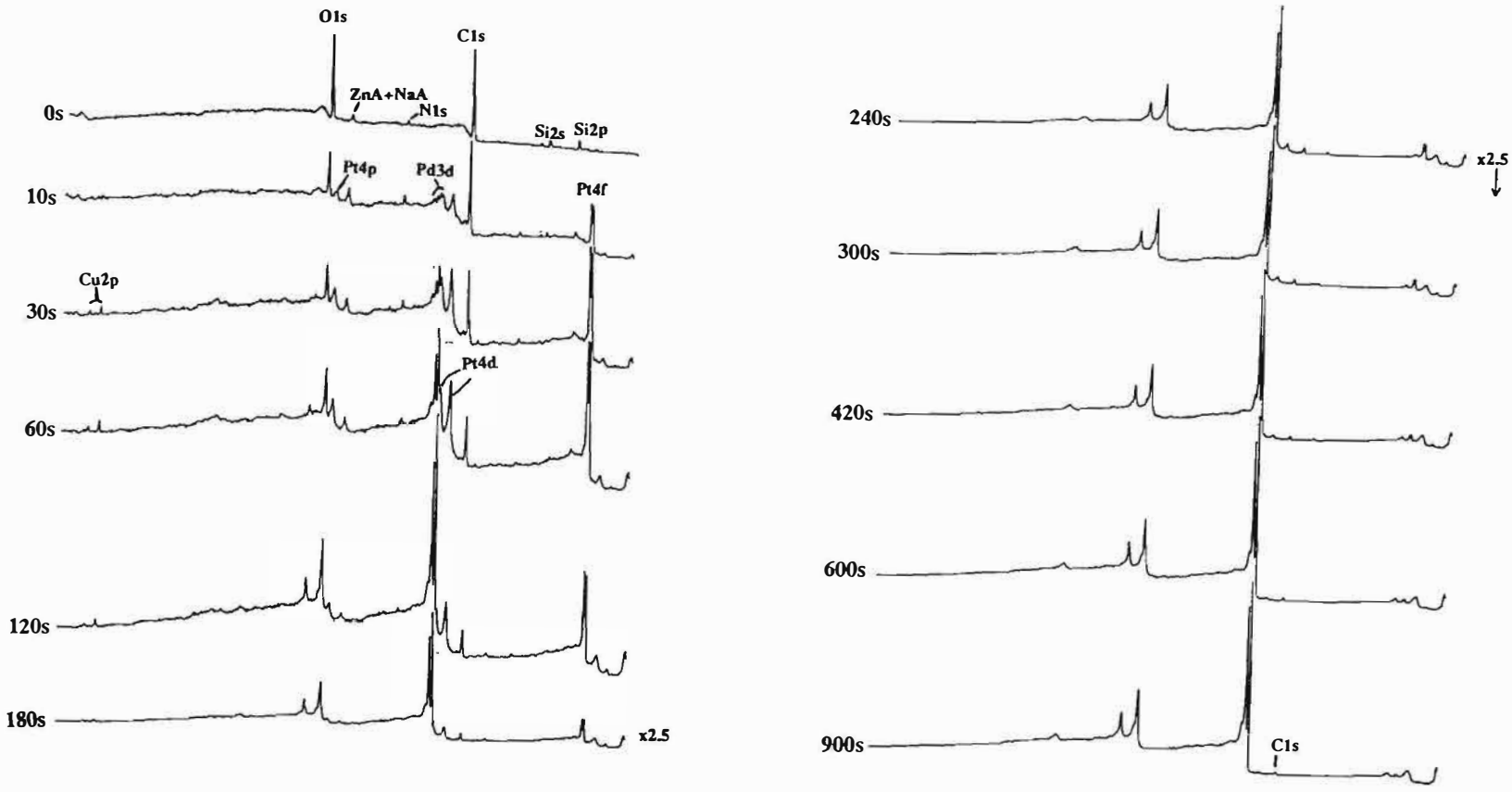

Figure 4. Series of XPS survey spectra obtained at various total sputter times from an SRI excess heat producing Pd rod cathode (#P15, Engelhardt #1 Pd). Scans from 0 eV (right) to 1000 eV (left) binding energy.

been detected as part of these surface overlayers. The anodes, however, remain relatively film-free.

2. The source of some of the elements found in the cathode overlayer may be bulk diffusion of impurities such as Pt and Cu caused by the severe lattice distortion produced by absorption of large quantities of D or H.

3. Longer electrolysis times (~1000 hrs.) produced thicker films on NRL Pd cathodes compared to shorter times (<500 hrs.). In addition, the thicker films contained larger quantities of both Cu and Pt relative to Pd and in general higher loadings were obtained with these films present. This suggests that thicker films may help block the egress of D from the Pd lattice.

4. Thinner films where Pd was present at or near the surface were found on excess heat producing electrodes obtained from SRI and NAWC (exceptions are where large quantities of certain species were added to the electrolyte to prolong or initiate excess heat formation). Very little copper was found in these films but appreciable amounts of Pt were present. Thin films with low Cu content may be necessary for excess heat measurement.

Acknowledgment

The authors wish to thank Dr. Fred Saalfeld, Deputy Chief of Naval Research, and Dr. Robert Nowak, Program Manager, both from the Office of Naval Research for providing funding for this research.

References

1. S. B. Ziemecki, G. A. Jones and D. G. Swartzfager, "Coexistence of Hydrogen and Carbon Solutes in the Palladium Lattice", J. Less-Common Metals, 131(1987)157-162.
2. R. Burch and F. A. Lewis, "Absoption of Hydrogen by Palladium + Boron and Palladium + Silver + Boron Alloys," Trans. Faraday Soc., 66(1970)727.
3. T. B. Flanagan and Y. Sakamoto, "Hydrogen in Disordered and Ordered Palladium Alloys," Platinum Metals Rev., 37(1993)26-37.
4. Average loading ratios were obtained by *in situ*, four-point probe resistivity measurements.
5. GDMS analyses were performed by Shiva Technologies, Inc., Cicero, NY.
6. C. T. Dillon and B. J. Kennedy, "The Electrochemically Formed Palladium-Deuterium System. I. Surface Composition and Morphology," Aust. J. Chem., 46(1993)663-679.
7. D. R. Rolison, W. E. O'Grady, R. J. Doyle, Jr., and P. P. Trzaskoma, "Anomalies in the Surface Analysis of Deuterated Palladium," Proceedings of the First Annual Conference on Cold Fusion, The National Cold Fusion Institute, Salt Lake City, UT, 272-280 (1990).
8. J. J. Willems and K. H. J. Buschow, "From Permanent Magnets to Rechargeable Hydride Electrodes," J. Less-Common Metals, 129(1987)13-30.
9. M. C. H. McKubre, S. Crouch-Baker, R. C. Rocha-Filho, S. I. Smedley, F. L. Tanzella, T. O. Passell and J. Santucci, "Isothermal Flow Calorimetric Investigations of the D/Pd and H/Pd Systems," J. Electroanal. Chem., 368(1994)55-66.
10. Cathodes provided by M. Miles and K. Johnson.

Nuclear Physics Approach

REACTION RATES OF THE D+D REACTION IN METAL AT VERY LOW ENERGIES

H.Yuki, T.Satoh, T.Ohtsuki, T.Yorita, Y.Aoki, H.Yamazaki, J.Kasagi
Laboratory of Nuclear Science, Tohoku University, Mikamine, Taihaku, Sendai 982, Japan

In order to study the electron screening effect on low-energy nuclear reactions in metals, the D+D reaction in metal was investigated. Measured were thick target yields of protons emitted in the D(d,p)T reaction from the bombardment of Ti and Yb metals with deuteron energies between 2.5 and 6.5 keV in Ti and between 3.3 and 7.2 keV in Yb, respectively. The obtained yields were compared with those predicted by using the parameterization of cross sections at higher energies. It was found that the reaction rates in Ti are slightly enhanced over those of the bare D+D reaction for E_d < 4.3 keV and those in Yb are also slightly enhanced for E_d < 6.0 keV. The enhancement can be interpreted as caused by the electron screening, and the electron screening potentials in Ti and Yb are deduced for the first time to be 19 ± 12 eV and 60± 15 eV, respectively.

I. INTRODUCTION

The effect of the electronic environment on nuclear phenomena has been investigated for many years [1]. For nuclear decay processes accompanied with a change of bound electrons, such as electron captures and internal conversions, it is shown that any change in the configuration of the outer electronic shells modifies the electron density near the nucleus, and, hence, causes a change in the transition rate, although the observed change is very small. The so-called cold fusion [2] has roused attention more generally on the influence of the environment where nuclear processes take place. Although most of the experiments reported at that time were known to have a difficulty in the reproducibility and, hence, to be under suspicion, the influence of the environment in various nuclear processes is one of the interesting subjects which need more study, because of its interdisciplinary nature involving nuclear physics, condensed matter physics, material science, and so on. In addition, one can develop its applications in various fields if the electron environment really affects the nuclear processes very strongly.

Nuclear reactions at very low energies are considered naturally to be affected by the environment, since surrounding electrons contribute to the effective Coulomb interaction between the projectile and target nuclei. Actually, recently reported experiments showed the non-negligible effect caused by the bound electrons in low energy reactions with solid or gas targets [3]. One might expect much stronger effects than caused by bound electrons when the nucleus is embedded in different materials [4]. Ichimaru *et al.* [5] suggested that hydrogen nuclei in metals are strongly screened, since the electrons both in metallic d-band and hydrogen-induced s-band can contribute to the screening effect. They calculated the effective static potential for hydrogens in Ti and Pd, and proposed that the screening distance between two hydrogens in metal is much shorter than that of atomic hydrogen.

The D+D reactions have been investigated with gas targets by many authors [6–11]. Krauss *et al.* [9] parametarized the S-factors for the D(d,p) and D(d,n) reactions by fitting their data with a quadratic polynomial for 5 < $E_{c.m.}$ < 120 keV. Bosch and Hale [10] parameterized the reaction cross sections by using the R-matrix parameters of the D+D reaction which were determined with all types of experimental data including integrated cross sections, differential cross sections and polarizations. Greife *et al.* [11] recently reported the measurement at center-of-mass energies down to 1.6 keV. The deduced astrophysical S-factors below 10 keV are clearly larger than predicted from the parameterization of Bosch and Hale [10]. They interpreted the observed enhancement as the screening effect of the bound electron, and obtained a screening potential of 25 eV. The D+D reaction in Ti was studied first by Roth *et al.* [12] They reported that no enhancement of the cross section of the D+D reaction is observed down to 3 keV within their statistical error of ±50%. Kasagi *et al.* [13] measured the reaction rate of the D+D reactions in Ti for bombarding energies between 4.8 and 18 keV. The obtained thick target yields are well explained with the S-factors deduced from the gas target experiment. Thus, for the D+D reactions in metal, experiments with much lower energies and with good statistics are highly desirable to observe the screening effects of metallic electrons.

Recently, a low-energy high-current ion beam generator was introduced to our laboratory to study the nuclear reactions with much lower energies. One of the present data is a natural extension of the previous measurement of the D+D reactions in Ti as in ref. [13], by using the newly installed machine. Lower energy data were obtained for the D+D reaction in Ti and Yb metals down to 2.5 keV and 3.3 keV respectively, in this experiment.

II. EXPERIMENTAL PROCEDURE

The low-energy high-current beam generator was designed to produce deuteron beams with several hundreds of μA from 1 keV to 100 keV. As shown in Fig.1, it consists of a duoplasmatron ion source, an ion beam extraction system, a 30-degree bending magnet, focusing

lenses, an acceleration/deceleration electrode and a neutral beam filter magnet. The duoplasmatron ion source can provide high current beam (~1 mA) with low energy spread ($\leq$ 25 eV). The beam is extracted from the ion source with ~25 KV. After passing through the magnet and focusing lenses, the beam is accelerated or decelerated by changing the connection of the main power supply providing stable voltage up to 80 KV (stability and voltage ripple is less than 0.01%). In the acceleration mode, the beam is transported straight to the target position. In the deceleration mode, however, the beam is bent by 45° with a dipole magnet placed in the scattering chamber, in order to remove neutral beams which cannot be decelerated. The beam energy is determined by the electrical potential between the ion source and the ground, which is measured by a register chain with a digital meter.

A thick plate of Ti (10 mm×30 mm×2 mm), in which deuterium gas was absorbed, was placed at the target position. The method of loading gas into the Ti plate is described in ref. [14]. In order to fix the beam spot on the target, a beam collimator was set between the filter magnet and the target. The beam spot on the target was about 4 mm in diameter. The target current, as well as the collimator current, was monitored during the run.

Since a spectrum measured with a single Si detector was found out to contain much electrical noise at low bombarding energies, a ΔE-E counter telescope consisting of 50-μm and 200-μm thick Si surface barrier detectors was employed. A requirement of a coincidence between two Si detectors almost completely reduced the electrical noise. The front face of the ΔE detector was covered with a 15-μm thick Al foil to prevent δ-rays and scattered deuterons from hitting the detector. The telescope was placed at 2 cm from the target and at 90° with respect to the beam direction. The target was tilted by 58° and the solid angle subtended with the telescope was about 3.5 % of 4π sr. Signals from the detectors were fed to preamplifiers which generate fast outputs for time information as well as slow outputs for pulse height information. The fast outputs were fed into timing filter amplifiers and time signals were picked up from constant fraction discriminators. CAMAC ADCs and TDCs were used, respectively, to measure pulse height spectra for each detector and time spectra between the two detectors.

As will be mentioned below, the present measurements only give relative values of the reaction rate. The total dose of the deuteron beam for each run was deduced from the electric current from the target, which might depend on the bombarding energy since an amount of secondary electron emission from the target may depend on the energy. Thus, the electric current was also measured with a Faraday cup and was compared to the target current. Ratios of the current from the target to that from the Faraday cup were found to be quite constant for $2.45 < E_d < 7.95$ keV; they fall between 1.02 and 1.06. Thus, no correction was made for the total dose deduced from the target current for each bombarding energy. The target current was about 500μA at E_d = 6.5 keV and 100μA at E_d = 2.5 keV.

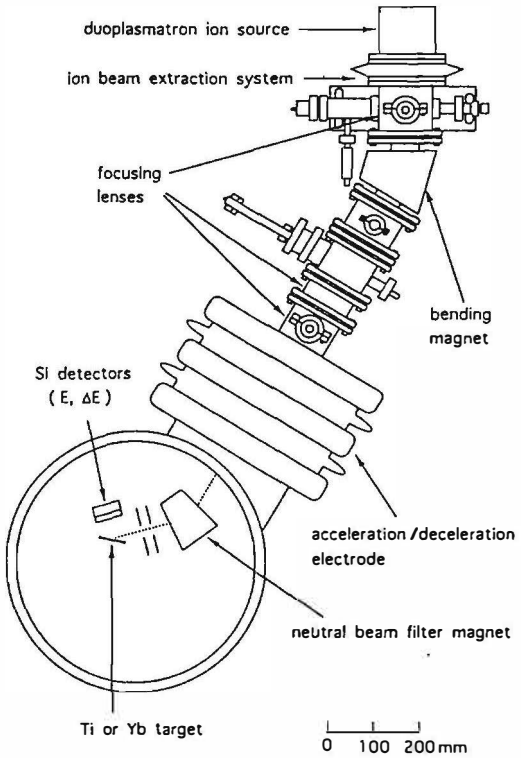

FIG. 1. Schematic diagram of low-energy beam generator and experimental setup.

As was described in ref. [13], the difficulty is to determine the number of target deuterons in the D+D reaction. Since the deuterons are accumulated in TiD_x during the deuteron bombardment, the number of the target deuterons changes. We applied the same method as described in ref. [13] in order to measure the relative values of the reaction rates. In the present work, the yields of protons at E_d = 6.45 keV were frequently measured during the run; for example, the yields at E_d = 6.45 keV were measured every 2 mC of the beam charge accumulation for 200 mC of the total bombardment at E_d = 2.55 keV. The reaction rate at E_d = 6.45 keV is much larger than those at lower bombarding energies so that it reflects the number of the target deuterons at that time. The measured thick target yields at lower incident energies were normalized to the yield at E_d = 6.45 keV.

The experimental procedure of the D+D reaction in a thick plate of Yb (10 mm×10 mm×1.1 mm) was almost same as the case of Ti metal. The bombardments were done with deuteron energies between 3.3 and 7.2 keV. The yields of protons at E_d = 7.2 keV were also frequently measured during the run. The measured thick target yields at lower incident energies were normalized to the yield at E_d = 7.2 keV.

III. EXPERIMENTAL RESULT

As mentioned, protons emitted in the D+D reaction

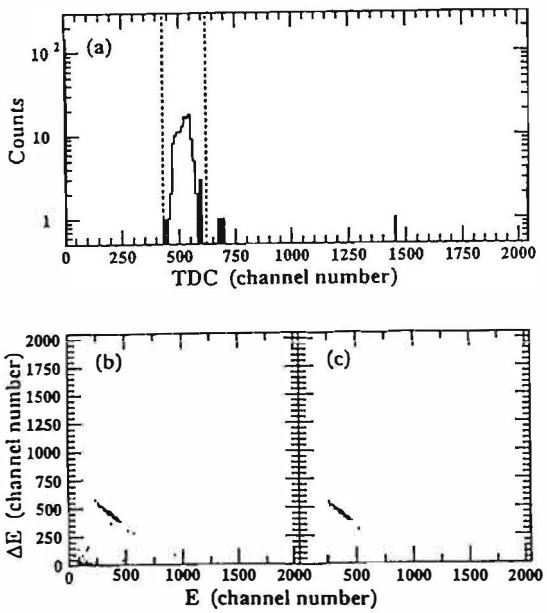

FIG. 2. Spectra measured with a δE-E Si counter telescope in the deuteron bombardment of TiD_x; (a) TDC spectrum with a gate position indicated by dotted lines, (b) two- dimensional spectrum of DE vs.E without any selection, and (c) same as in (b) but selected by setting the TDC gate.

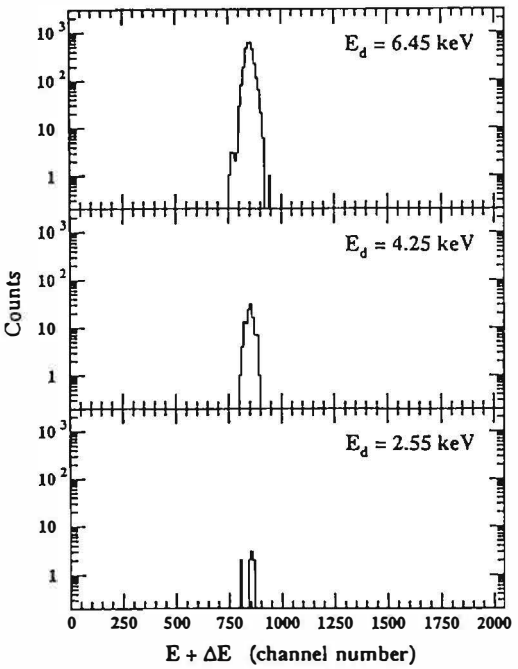

FIG. 3. Charged particle spectra measured in the D(d,p)T reaction in Ti plotted against δE+E.

were measured with a counter telescope in order to obtain good signal to noise ratio. Fig. 2, shows such spectra obtained at E_d = 4.5 keV; Fig. 2(a) is a TDC spectrum where a window employed to discriminate true events from those due to electrical noise is also shown, and two dimensional spectra of ΔE versus E are shown in Fig. 2(b) and 2(c); they are obtained, respectively, without and with setting a gate on the window. As expected, events due to electrical noise that are distributed mainly along both ΔE and E axes in Fig. 2(b) are completely eliminated in Fig. 2(c). A band seen as a line of a constant value of ΔE+E corresponds to the protons emitted in the D+D reaction, since heavier charged particles cannot punch through the ΔE detector. The solid angle and the area of both detectors are quite large and hence the energies deposited in the ΔE detector are rather widely spread.

In Fig. 3, yields of the true events are plotted against ΔE+E for various bombarding energies. As shown, the band observed in the two dimensional spectrum is seen as a sharp peak located at the same position, and no other events are observed than the peak. After the correction of the energy loss in Al absorber, the energy of the peak is deduced to be 3.0 MeV, corresponding to the proton emitted in the D+D → p+T reaction. The yield of the peak decreases steeply as the bombarding energy decreases.

In order to deduce the angle integrated yields, the correction only for the ratio of the detector solid angle $(\Delta\Omega)_{c.m.}/(\Delta\Omega)_{lab}$ was made, since the angular distributions are isotropic in the center of mass system at such low bombarding energies [9]. In Fig. 4, the deduced thick target yields of the D(d,p)T reaction in Ti are plotted against the bombarding energy. The data are normalized at 6.45 keV as mentioned in the previous section, and errors associated with the data in the figure include only statistical ones; i.e., statistics of the yield at each bombarding energy and those at 6.45 keV for the normalization runs. The same procedures were used to analyze the data of the D+D → p+T reaction in Yb metal. The deduced thick target yields in Yb are obtained and plotted in Fig.5 as a function of the bombarding energy, those are also normalized at 7.2 keV. As shown in the figure, these yield decrease very rapidly as the bombarding energy decreases.

IV. ELECTRON SCREENING EFFECT IN THE THICK TARGET

Since the bombarded deuterons are slowed down in the host metal and the reactions can occur until the deuteron stops, the thick target yield Y_t at the bombarding energy of E_b is given as follows.

$$Y_t(E_b) = A \cdot \int N_D(x) \cdot \sigma(E)\, dx = A \cdot \int N_D(x) \cdot \sigma(E) \cdot (dE/dx)^{-1}\, dE, \quad (1)$$

where $N_D(x)$, $\sigma(E)$ and dE/dx are the number of the target deuterons per unit area, the reaction cross section and the stopping power of the deuteron, respectively.

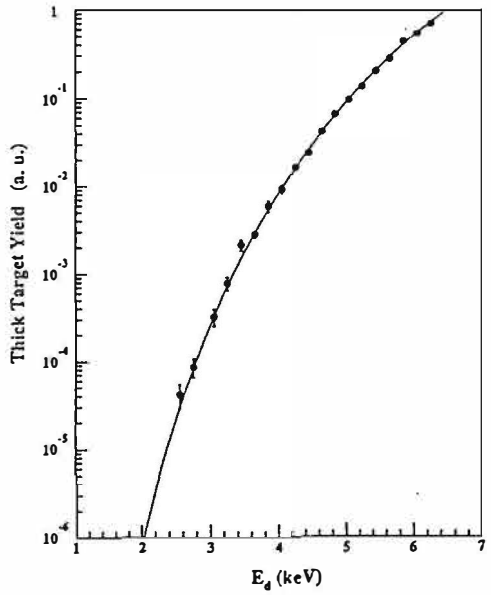

FIG. 4. Yield of the D(d,p)T reaction occurring in thick Ti metal target as a function of the deuteron bombarding energy. Data are normalized to the yield at 6.45 keV. A solid curve shows a thick target yield calculated with the bare cross section.

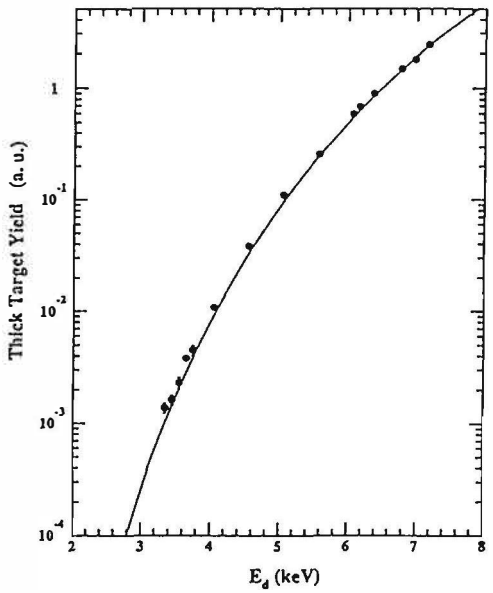

FIG. 5. Yield of the D(d,p)T reaction occurring in thick Yb metal target as a function of the deuteron bombarding energy. Data are normalized to the yield at 7.2 keV. A solid curve shows a thick target yield calculated with the bare cross section.

Thus, the obtained thick target yields should be compared with those calculated with the reaction cross section of the bare D+D reaction, in order to see whether the reaction rate in metal is larger than that of the reaction in vacuum or not.

The parameterization of Bosch and Hale [10] has been used for the cross section. The parameterization is based on the R-matrix theory which describes different reactions (T(p,p)T, D(d,p)T and D(d,n)^{3}He reactions) simultaneously with a single set of R-matrix parameters, and was made with the high-energy data (E_d > 15 keV), where no electron screening effects occur. Therefore, use of the parameterization is a better determination of the cross section of the D(d,p)T reaction, and the extrapolation of the reaction cross section to lower energies represents the case of the bare D+D reaction.

The stopping power of the deuteron is also necessary to calculate the thick target yield. Although an accurate value of the stopping power is important, no experimental information on the stopping power of the deuteron has been available in the region of the present bombarding energies. Thus we followed the recipe of Anderson and Ziegler [15] (we will call this the stopping cross section of AZ), in which the electronic stopping power is assumed to be proportional to the velocity of the projectile (normalized to the experimental data at higher energies) at very low energies in accordance with the Thomas-Fermi model of the atom and the LSS [16] nuclear stopping power is employed. The electronic stopping power is considered only for the host metal atom, whereas the nuclear stopping power of the D atom is included as well as the metal atom. The density distribution of the target deuterons

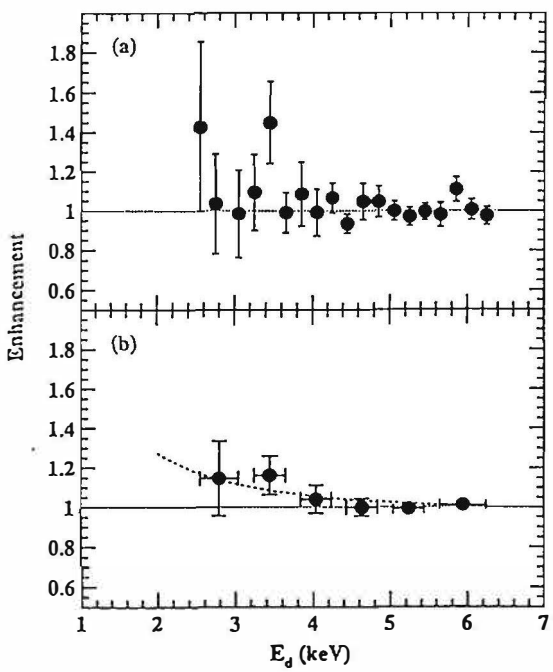

FIG. 6. Ratios of the thick target yield of the D(d,p)T reaction to the calculated one in Ti. The calculation was made with the bare cross section so that the ratio shows enhancement of the reaction rate. The ratios for each bombarding energy are shown in (a), and the weighted averages of the ratios of three points are shown in (b). A dashed curve in (b) shows the calculation with the electron screening potential of 19 eV.

Nuclear Physics Approach

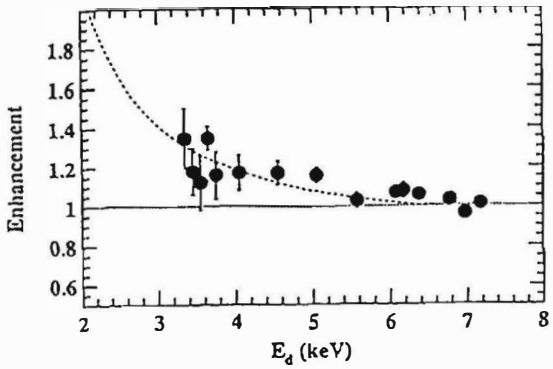

FIG. 7. Ratios of the thick target yield of the D(d,p)T reaction to the calculated one in Yb. A dashed curve shows the calculation with the electron screening potential of 60 eV.

along the incident deuteron path is also important for estimating the reaction rate. The projected range of the 6.5 keV deuteron is only about 40 nm in case of Ti, and the target deuterons are assumed to be uniformly distributed.

The thick target yields calculated with eq. (1) are normalized to that at 6.45 keV for Ti and 7.2 keV for Yb as the experimental ones and are plotted with the solid line in Fig.4 and Fig.5, respectively. Since it is difficult to compare the experimental data with the calculations quantitatively in a log-scale graph, the ratios of the experimental yields to the calculated ones are plotted in Fig.6 and Fig.7 as a function of the bombarding energy. To reduce the statistical errors, the averaging process is adopted in Ti. The ratios for all the experimental data are plotted in Fig. 6(a), in which the experimental reaction yields are slightly enhanced over the calculated ones at the lower bombarding energies, although large statistical errors and fluctuations obscure a definite conclusion. However, the enhancement can be seen more clearly for $E_d < 4$ keV in Fig. 6(b), where the weighted average values of the ratios of three points are plotted.

As seen in Figs. 6 and 7, the observed enhancement of the reaction rate seems to increase as the incident energy decreases. Thus it can be naively interpreted as the reduction of the effective Coulomb barrier due to the electron screening potential in metal. An enhancement factor of the reaction cross section is given as $f(E) \approx \exp(\pi\eta U_e/E\mathrm{p})$, where U_e is the electron screening potential and η is the Sommerfeld parameter. We calculated thick target yields for various values of U_e and compared them with the experimental ones. χ-squared values were calculated for $0 < U_e < 100$ eV and the result is plotted in Fig. 8 for Ti and Fig.9 for Yb, and these χ^2-plot have a minimum at 19 eV and 60eV, respectively. In case of Ti, a quadratic curvature around the minimum gives one standard deviation of 12 eV. Therefore, we can conclude that the electron screening potential affecting the D + D reaction is obtained for the first time in Ti metal as $U_e = 19 \pm 12$ eV. The dashed line in Fig. 6(b) is the calculated enhancement with $U_e = 19$ eV. The electron screening potential by the D+D reaction in Yb was

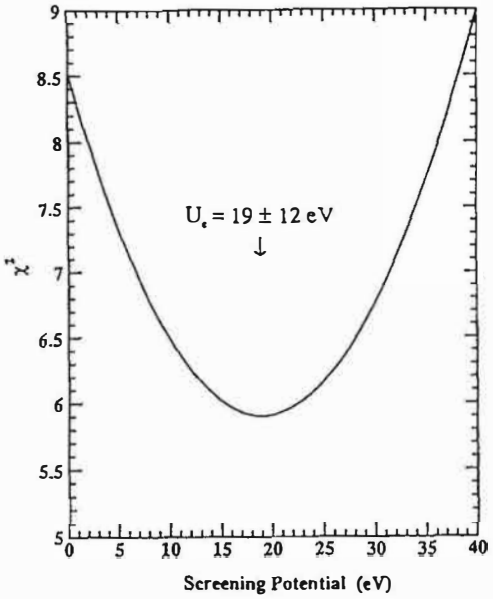

FIG. 8. Plot of the chi-squares against the value of the electron screening potential in Ti metal.

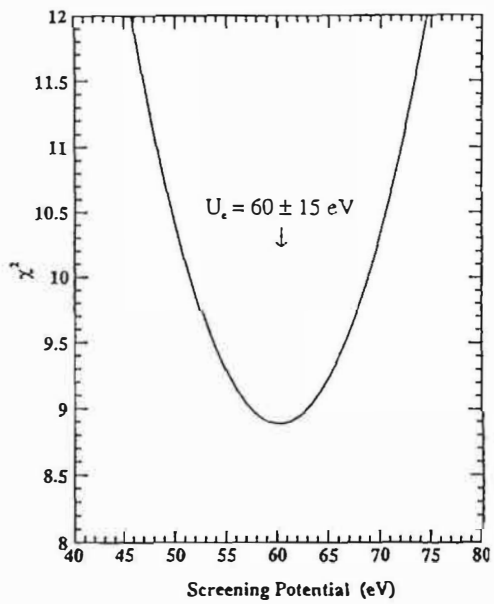

FIG. 9. Plot of the chi-squares against the value of the electron screening potential in Yb metal.

also deduced as $U_e = 60 \pm 15$ eV. The dashed line in Fig. 7 indicates the calculated enhancement with $U_e = 60$ eV. The electron screening potential in each case explain the data very well.

Morimoto *et al.* [17] measured the depth profile of the deuteron in the 1.6-μm foil of Ti at a bombarding en-

ergy of 5 keV. According to them, deuterons are accumulated rather uniformly inside the foil in the beginning of the implantation. However, the higher the deuteron fluency, the worse the uniformity of the deuteron density becomes. The final profile shows a broad peak at about 200 nm from the surface. The density of the deuteron almost linearly increases with the depth from the surface, and differs about 25 % between the surface and at 40 nm from the surface for the worst case. The reaction rate was calculated by using this distribution. The result gives $U_e = 23$ eV; the difference from the result with the uniform distribution is very small (+ 4 eV), since the reaction occurs effectively at surface region.

Although the present result clearly shows that the D+D reaction rate is enhanced in Ti for $E_d < 5$ keV, the deduced electron screening potential $U_e = 19 \pm 12$ eV is smaller than the one predicted by Ichimaru [5]. They calculated the effective D-D potential in TiD_2 and obtained the short-range screening distance to be 0.028 nm, which corresponds to $U_e = 51$ eV. However, the comparison of the present result with their prediction may not be pertinent, since only the thermal motion of the deuteron in the Ti lattice is considered in their calculation, whereas deuterons are impinging with several keV and diffuse in the Ti in the experiment. A theoretical treatment for the low energy nuclear reaction including the effect of the electronic environment is highly desirable. It should be noticed that the present result is in good agreement with the one ($U_e = 25 \pm 5$ eV) obtained in the gas target measurement by Greife *et al.* [11] They measured the reaction cross sections of the D(d,p)T reaction with a gas target down to $E_d = 3.2$ keV, and compared those with the same cross section as employed in the present analysis. Although their result is larger than the naive prediction ($U_e = 14$ eV) for the molecular D_2 gas case, the agreement of the two results indicates that electrons in the metallic d-band in Ti do not affect strongly the D+D reaction at a few keV.

V. SUMMARY

We measured the reaction rate of the D+D reaction in Ti and Yb metals at low bombarding energies down to $E_d = 2.55$ keV and 3.3 keV, respectively, by using a deuteron beam from the low-energy high-current beam generator, installed recently in our laboratory. Protons emitted in the D(d,p)T reaction were detected without any electrical noise by employing a δE-E counter telescope. The measured thick target yield at each bombarding energy was normalized to that at 6.45 keV in Ti and 7.2 keV in Yb. The thick target yields were compared with the bare D+D reaction cross section; the parameterization of Bosch and Hale [10] for the cross section and the stopping power of Anderson and Ziegler [15] were used for the comparison. The enhancement of the reaction rate is clearly seen below about $E_d < 5$ keV in the comparison, and can be interpreted as the reduction of the effective Coulomb barrier due to the electron screening in metal. The screening potentials affecting the D+D reaction in metal are obtained for the first time as $U_e = 19 \pm 12$ eV in Ti and $U_e = 60 \pm 15$ eV in Yb. The deduced value in Ti is smaller than the prediction of Ichimaru [5], but is in good agreement with the one obtained in the gas target measurement by Greife *et al.* [11] This indicates that the electrons in the metallic d-band in Ti do not affect strongly the D+D reaction at a few keV. A theoretical treatment for the low energy nuclear reaction including the effect of the electronic environment is highly desirable.

VI. ACKNOWLEDGMENTS

The author would like to thank to Dr. O. Konno and Mr. Y. Shibazaki for their help in preparing the experiment. This work is supported by the Basic Research Project of New Hydrogen Energy.

[1] G. T. Emery : Ann. Rev. Nucl. Sci. **22** (1972) 165.

[2] M. Fleischmann and S. Pons : J. Elec. Chem. **261** (1989) 301, S. E. Jones, E. P. Palmer, J. B. Czirr, P. L. Decker, G. L. Jensen, J. M. Thorne, S. F. Taylor and J. Rafelski : Nature **338** (1989) 737.

[3] S. Engstler, A. Krauss, K. Neldner, C. Rolfs, U. Schroder and K. Langanke : Phys. Lett. **B202** (1988) 179, S. Engstler, G. Raimann, C. Angulo, U. Greife, C. Rolfs, U. Schroder, E. Somorjai, B. Kirch and K. Langanke : Phys. Lett. **B279** (1992) 20.

[4] V. N. Kondratyev : Phys. Lett. **A190** (1994) 465.

[5] S. Ichimaru : Rev. Mod. Phys. **65** (1993) 255, and references therein.

[6] W. A. Wenzel and W. Whaling : Phys. Rev. **88** (1952) 1149.

[7] W. R. Arnold, J. A. Phillips, G. A. Sawyer, E. J. Stovall and J. L. Tuck : Phys. Rev. **93** (1954) 483.

[8] N. Jarmie and R. E. Brown : Nucl. Instr. Meth. **B10/11** (1985) 405.

[9] A. Krauss, H. W. Becker, H. P. Trautvetter, C. Rolfs and K. Brand : Nucl. Phys. **A465** (1987) 150.

[10] H. S. Bosch and G. M. Hale : Nuclear Fusion **32** (1994) 611.

[11] U. Greife, F. Gorris, M. Junker, C. Rolfs and D. Zahnow : Z. Phys. **A351** (1995) 107.

[12] J. Roth, R. Behrisch, W. Moller and W. Ottenberger : Nuclear Fusion **30** (1990) 441.

[13] J. Kasagi, T. Murakami, T. Yajima, S. Kobayashi and M. Ogawa : J. Phys. Soc. Jpn. **64** (1995) 3718.

[14] J. Kasagi, T. Ohtsuki, K. Ishii and M. Hiraga : J. Phys. Soc. Jpn. **64** (1995) 777.

[15] H. H. Anderson and J. F. Ziegler : *Hydrogen stopping powers and ranges in all elements* (Pergamon Press, New York, 1977)

[16] J. Lindhard, M. Scharff and H. E. Schiott : K. Dan. Vidensk. Selsk. Mat.-Fys. Medd. **33** (1963) No.14.

[17] S. Morimoto, S. Nagata, S. Yamaguchi and Y. Fujino : Nucl. Instr. Meth. **B48** (1990) 478.

Nuclear Physics Approach

Optical Theorem Formulation and Nuclear Physics Mechanisms for Gamow Factor Cancellation in Low-Energy Nuclear Reactions

Yeong E. Kim and Alexander L. Zubarev

Department of Physics, Purdue University
West Lafayette, Indiana 47907-1396, U.S.A.

Abstract

Based on the optical theorem formulation of low-energy nuclear reactions, we show that a Gamow factor cancellation can occur for nuclear fusion reactions if the imaginary part of the effective nuclear interaction in the elastic channel has a small component of a finite long-range interaction. It is recently shown that a near cancellation of the Gamow factor at low energies can occur if one of the final-state nuclei has a weakly bound ("halo") excited state. Another mechanism for the Gamow factor cancellation is a continuum-electron shielding of nuclear charge by a dense electron plasma. If the Gamow factor cancellation occurs, it can lead to a large enhancement of reaction rates and probabilities for low-energy nuclear fusion reaction and nuclear fission, and may provide nuclear physics mechanisms for explaining the anomalous effects observed in low-energy nuclear reactions. Several specific cases of the anomalous effects are discussed in terms of nuclear physics mechanisms, including cluster-impact nuclear reactions which may be relevant to the low-energy nuclear transmutation.

1. Introduction

Since the 1989 announcements of "cold fusion" phenomena [1,2] there have been persistent claims of observing the cold fusion phenomena, and hundreds of experimental papers have been published [3-5]. Most of the reported experimental results are not reproducible at a desirable level of 100%. However, there are a few experimental results which appear to be 100% reproducible.

There have been many theoretical models proposed to explain the cold fusion phenomena. Most of those theoretical models claiming to have explained the phenomena appear far from having accomplished their claims [6,7]. Recently, we developed a new alternative theoretical formulation of low-energy nuclear fusion reactions based on the optical theorem [8-10], which is much less model-dependent than previous theoretical approaches, and showed that some of the cold fusion phenomena may be justified theoretically, since a Gamow factor cancellation (GFC) can occur if the imaginary part of the effective nuclear interaction in the elastic channel (ENIEC) has a very weak component with a finite long range (FLR). However, we could not prove nor rule out theoretically the existence of such a FLR component in the imaginary part of ENIEC. In another recent paper [11], we demonstrated (without a rigorous derivation) a possibility of the existence of FLR components if the target nucleus has a weakly bound excited state ("halo" nuclear state). Recently, we have obtained a rigorous derivation [12] of a new type of FLR interaction in the imaginary part of ENIEC for the case in which one of the final-state nuclei has an excited halo nuclear state.

Nuclear Physics Approach

Another mechanism for GFC is a continuum-electron shielding of nuclear charge [13] by a dense electron plasma such as one observed in ultra-short-time discharge plasma experiments by Shoulders et al. [14,15].

If GFC occurs, theoretical opposition based on the Gamow factor to the cold fusion [3-5] and low-energy nuclear transmutation [16] phenomena may be premature, since it can enhance reaction rate and probabilities for nuclear fusion reaction and nuclear fission and it may provide theoretical explanations of the observed anomalous effects based on nuclear physics mechanisms. Several specific cases of the observed anomalous effects including recent observations of nuclear transmutation [16] are discussed in terms of nuclear physics mechanisms.

2. Uncertainties of Low-Energy Nuclear Reaction Rates

Nuclear reaction rates and cross-section at low energies ($\lesssim$ a few keV) are not well determined, since $\sigma(E)$ at low energies, relevant to the cold fusion phenomena and also relevant to the primordal and stellar nucleosynthesis, cannot be measured in the laboratory. They are extracted from the laboratory measurements of $\sigma(E)$ at higher energies by an extrapolation procedure based on nuclear theory [9,10]. Historically, both experimental and theoretical investigations of low-energy ($\lesssim$ 1keV) nuclear reactions were by-passed and have been neglected by nuclear physics community in favor of investigating nuclear physics phenomena at much higher energies. Therefore, it is important to turn our attention and efforts to investigating these neglected and unexplored new nuclear physics frontiers.

For non-resonance reactions, it is customary to extract the S-factor, S(E), from the experimentally measured $\sigma(E)$ using the following formula,

$$\sigma_G(E) = \frac{S(E)}{E} e^{-2\pi\eta(E)}, \tag{1}$$

where $\eta(E) = Z_i Z_j e^2/\hbar v, e^{-2\pi\eta(E)}$ is the Gamow factor representing the probability of bringing two charged nuclei to zero separation distance, and S(E) is expected to be a slowly varying function of E. The energy dependence of the nuclear reaction cross-section $\sigma(E)$ cannot be obtained rigorously from first principles. Therefore, one must relay on physically reasonable nuclear reaction models, such as Eq. (1), or phenomenological microscopic models, which may not be reliable nor accurate at low energies for some cases. It should be emphasized that Eq. (1) is obtained using a semi-classical approximation. In the following sections 3 and 4, a derivation of $\sigma(E)$ based on the quantum scattering theory is given.

3. Optical Theorem Formulation

The conventional optical theorem first introduced by Feenberg [17] is given by

$$\sigma_t = \frac{4\pi}{k} Im f(0) \tag{2}$$

where σ_t is the total cross-section and f(0) is the elastic scattering amplitude in forward direction ($\theta = 0$).

To avoid complications associated with the singularity of the forward Coulomb scattering amplitude when we use the conventional optical theorem, given by Eq. (2), for scattering of two charged nuclei, we describe a different formulation based on "partial-wave" optical theorem involving angle-integrated and/or angle-independent quantities in the following [8-10].

For the elastic scattering involving the Coulomb interaction and nuclear potential, the scattering amplitude can be written as a sum of two amplitudes:

$$f(\theta = f^c(\theta) + \tilde{f}(\theta), \tag{3}$$

where $f^c(\theta)$ is the Coulomb amplitude and $\tilde{f}(\theta)$ is the remainder. $\tilde{f}(\theta)$ can be expanded in partial waves [18] as

$$\tilde{f}(\theta) = \sum_{\ell}(2\ell+1)e^{2i\delta_\ell^c} f_\ell^{N(e\ell)} P_\ell(cos\phi), \tag{4}$$

where δ_ℓ^c is the Coulomb phase shift, $f_\ell^{N(el)} = (S_\ell^N - 1)/2ik$, and S_ℓ^N is the ℓ-th partial wave S-matrix for the nuclear part. Using Eq. (3) and Eq. (4), the integrated elastic cross section $\sigma^{e\ell}(e)$ can be written as

$$\sigma^{e\ell}(E) = \sigma^c + \sigma^{int} + \sigma^{N(el)}, \tag{5}$$

where σ^c is the pure Coulomb cross section (Rutherford scattering), σ^{int} is the interference term, and $\sigma^{N(e\ell)}$ is the nuclear elastic cross section. The partial wave expansion of $\sigma^{N(e\ell)}$ is given by $\sigma^{N(e\ell)} = \sum_\ell(2\ell+1)\sigma_\ell^{N(e\ell)}$ with $\sigma_\ell^{N(e\ell)} = \frac{\pi}{k^2}|S_\ell^N - 1|^2$.

For the reaction cross section $\sigma^{(r)}$, the partial wave expansion is given by $\sigma^{(r)} = \sum_\ell(2\ell+1)\sigma_\ell^{(r)}$ where $\sigma_\ell^{(r)} = \pi(1-|S_\ell^N|^2)/k^2$. Using the expressions of $\sigma_\ell^{(r)}$ and $\sigma_\ell^{N(e\ell)}$ derived above, we can write $\sigma_\ell^{(r)} + \sigma_\ell^{N(e\ell)} = 2\pi(1 - ReS_\ell^N)/k^2$. Combining this with $Imf_\ell^{N(e\ell)} = (1 - ReS_\ell^N)/2k$, we obtain the partial wave optical theorem for two-potential scattering case as

$$Imf_\ell^{N(e\ell)} = \frac{k}{4\pi}(\sigma_\ell^{(r)} + \sigma_\ell^{N(e\ell)}) \tag{6}$$

which is a rigorous result.

For low energies, $f_\ell^{N(e\ell)} \propto e^{-2\pi\eta}/k$ and hence $\sigma_\ell^{N(e\ell)} = 4\pi|f_\ell^{N(e\ell)}|^2 \propto e^{-4\pi\eta}/k^2$. Since $\sigma_\ell^{(r)} \propto e^{-2\pi\eta}/k^2$, we have $\sigma_\ell^{(r)} >> \sigma_\ell^{N(e\ell)}$ at low energies and hence we can write Eq. (6) as

$$Imf_\ell^{N(e\ell)} \approx \frac{4}{4\pi}\sigma_\ell^{(r)} \tag{7}$$

which is still a rigorous result at low-energies. We note that Eqs. (6) and (7) are non-radiative nuclear reactions and need to be modified for radiative nuclear reactions.

In terms of the partial wave T-matrix, T_ℓ, the elastic nuclear scattering amplitude, $f_\ell^{N(e\ell)} = (S_\ell^N - 1)/2ik$, can be written as

$$f_\ell^{Ne\ell)}(E) = -\frac{2\mu}{\hbar^2 k^2}\langle\psi_\ell^c|T|\psi_\ell^c\rangle \tag{8}$$

where ψ_ℓ^c is the ℓ-th partial wave regular Coulomb function nd μ is the reduced mass. Using the low-energy optical theorem Eq. (7) with Eq. (8), we obtain the ℓ-th partial-wave reaction cross section $\sigma_\ell(E)(=\sigma_\ell^{(r)}(E))$ as

$$\sigma_\ell(E) \approx \frac{4\pi}{kE}\int_0^\infty \psi_\ell^c(r)U_\ell(r,r')\psi_\ell^c(r)drdr' \tag{9}$$

where $E = \hbar^2k^2/2\mu$ and $U_\ell(r,r') = -Im\langle r|T_\ell|r'\rangle$ with T_ℓ representing the ℓ-th partial wave contribution of the T-mtrix operator. The total reaction cross-section $\sigma(E)$ is given by $\sigma_\ell(E) = \sum_\ell(2\ell+1)\sigma_\ell(E)$.

4. Reaction Cross Section Formula

It is recently shown [8,10] that $Im\langle r|T_\ell|r'\rangle(=-U_\ell(r,r'))$ is separable for the $\ell = 0$ two-channel case, and hence $U_0(r,r')$ in Eq. (9) is also separable for the case of two-channels (elastic and fusion). Therefore, to estimate the S-wave cross section $\sigma_0(E)$ for the two-channel

case, we can parameterize $U_0(r,r')$ in Eq. (9) by two parameters λ (strength/length) and β^{-1} (range) in a separable form as

$$U_0(r,r') = \lambda g(r) g(r') \tag{10}$$

where β^{-1} is a potential range parameter for g(r) and $\lambda = V_0\beta (V_0 > 0)$. λ is expected to be a slowly varying function of energy for the non-resonance case. (For the case of resonance reactions, the energy dependence of λ can be parameterized by the Breit-Wigner expression).

For $\ell = 0$ case, the Coulomb wave function $\psi_o^c(r)$ is given by

$$\psi_0^c(r) = C_0(\eta) M_{i\eta,\frac{1}{2}}(2ikr)/2i \tag{11}$$

where $C_0^2(\eta) = 2\pi\eta/(e^{2\pi\eta} - 1)$ and $M_{i\eta,\frac{1}{2}}(2ikr)$ is the Whittaker function. The reaction cross section given by Eq. (9), in the case of $g(r) = e^{-\beta r}/r$, can be written as

$$\sigma_0(E) = \frac{4\pi\lambda}{kE} \left| \int_0^\infty \psi_0^c(r) \frac{e^{-\beta r}}{r}\, dr \right|^2 = \frac{\pi\lambda}{kE} C_0^2(\eta) \left| \frac{1}{i} \int_0^\infty M_{i\eta,\frac{1}{2}}(2ikr) \frac{e^{-\beta r}}{r}\, dr \right|^2 \tag{12}$$

The integral in Eq. (12) can be evaluated exactly

$$\sigma_0(E) = \frac{4\pi\lambda}{kE} \left[\int_0^\infty dr \psi_0^c(r) e^{-\beta r}/r \right]^2 = \frac{4\lambda\pi^2}{E} R_B \frac{(e^{-2\phi\eta} - 1)^2}{(e^{2\pi\eta} - 1)} e^{4\phi\eta} \tag{13}$$

with

$$e^{4\phi\eta} = exp[4\alpha \frac{\mu c^2}{\hbar c} (\frac{Z_a Z_b}{k}) tan^{-1}(\frac{k}{\beta})] \tag{14}$$

where $\phi = tan^{-1}(k/\beta)$ and $R_B = \hbar^2/(2\mu Z_a Z_b e^2)$. The energy dependence of λ is expected to be weak.

The use of a more general form for $g(r) = (e^{-\beta r}/r) \sum_{i=0}^N c_i r^i$ instead of $e^{-\beta r}/r$ in Eq. (10) also leads to the same enhancement factor $e^{4\phi\eta}$. Therefore, the enhancement factor $e^{4\phi\eta}$ is independent of shape of the separable function $g(r)$ used in Eq. (10). For $g(r) = (e^{\beta r}/r) \sum_{i=0}^N c_i r^i$, we obtain for $\sigma_0(E)$ the following result,

$$\sigma_0(E) = \frac{\tilde{S}_0(E)}{E} e^{4\phi\eta} e^{-2\pi\eta} \tag{15}$$

where

$$\tilde{S}_0(E) = 4\pi^2 \lambda \sum_{ij} c_i c_j F_i^\beta(E) F_j^\beta(E) \tag{16}$$

with $F_0^\beta(E) = R_B(e^{-2\phi\eta} - 1)$, $F_1^\beta(E) = R_B^{-1}(\beta^2 + k^2)^{-2}$, $F_2^\beta(E) = R_B^{-3}(2R_B\beta + 1)/(\beta^2 + k^2)^4$, etc.

The enhancement factor $e^{4\phi\eta}$ is $e^{2/(R_\beta\beta)}$ at zero energy and decreases as E increases to $e^{\pi/kR_B} = 1$ for large E, and thus can account for the increase of experimentally extracted S(E) toward lower energies. The enhancement factor $e^{4\phi\eta}$ can be applied to both light nuclei reactions (small Z_a and Z_b) but also to heavy ion reactions (larger Z_a and Z_b) such as sub-barrier heavy ion fusion where $e^{4\phi\eta}$ can be very large. The enhancement factor $e^{4\phi\eta}$ is obtained together with the Gamow factor from our quantum mechanical derivation and can be regarded as a modification of the Gamow factor affecting it only at low energies, or as a part of the S-factor if we still wish to keep the semi-classical formula Eq. (1). The new exponential factor is a new quantum effect derived from the quantum scattering theory, and may provide new physical insights for the low-energy behavior of the reaction cross-section.

5. Effective Long-Range Interaction and Gamow Factor Cancellation

In the limit of $\beta \rightarrow 0$ (a long-range limit), we have $\phi = \tan^{-1}(k/\beta) = \pi/2$, and hence $e^{4\phi\eta}$ given by Eqs. (14) approaches to $e^{2\pi\eta}$ which can cancel the Gamow factor $e^{-2\pi\eta}$ in Eq. (15) for $\sigma_o(E)$. Therefore, a Gamow factor cancellation can occur if the interaction range β^{-1} is large (or β is small). If the imaginary part of the effective potential or $g(r)$ in Eq. (10) has a form

$$g(r) = e^{-\beta_1 r}/r + \Lambda e^{-\beta r}/r \tag{17}$$

with $\beta < \beta_1$, the second term could be dominant over the first term even if $\Lambda << 1$. In the limit of $\beta \rightarrow 0, \phi = tan^{-1}(k/\beta) = \pi/2$ and $e^{4\phi\eta} = e^{2\pi\eta}$ which can cancel the Gamow factor $e^{-2\pi\eta}$ in Eq. (15). Therefore, it is important to investigate both theoretically and experimentally the possibility of the existence of the finite long range interaction for the imaginary part of the effective potential.

Gamow factor cancellation (GFC) can occur for nuclear fusion reactions if the imaginary part of the effective nuclear interaction in the elastic channel (ENIEC) has a small component of a finite long-range (FLR) interaction. Recently, we have obtained a rigorous derivation of a new type of FLR interaction in the imaginary part of ENIEC for the case in which one of the final-state nuclei has an excited halo nuclear state [12]. The new FLR interaction behaves as $cos(k_0 r - \eta \ell n 2k_0 r + \delta)\psi_n(r)/r^4$ at large distances, where k_0, η, δ, and $\psi_n(r)$ are the final state wave number, the Sommerfeld parameter, the phase shift, and the wave function for the excited p-wave halo nuclear state, respectively. This demonstrates that we cannot rule out theoretically the GFC effect, and that theoretical opposition to the cold fusion [3-5] and low-energy nuclear transmutation [16] phenomena based on Eq. (1) may be premature.

The existence of the FLR interaction in the imaginary part of ENIEC, when one of the final-state nuclei has an halo excited state, leads to a selection rule for final nuclear products: nuclei with halo excited states are most likely observed in the final state, while production of nuclei without halo excited states is suppressed. This selection rule may be applicable to low-energy nuclear fusion reaction [3-5], nuclear fission, and nuclear transmutation [16], induced by a charged nuclei (proton, deuteron, oxygen, etc.). The selection rule should be tested by future experiments.

6. Gamow Factor Cancellation with Continuum-Electron Shielding

Recently, we have suggested a possibility of the GFC due to continuum-electron shielding [13]. For a three-body system (e+p+p) in continuum in which all three particles are mobile, there is a possibility that a solution of the three-body Schroedinger equation may lead to the GFC if the relative velocity v_{ep} between e and p is smaller than the relative velocity ν_{pp} between two protons, i.e. $v_{ep} < v_{pp}$. In general, this condition is $v_{ed} < v_{dA}$ for the case of the $[(e + d) + A]$ system where A is a nucleus such as d or Pd. These conditions may be realized in a localized packet of electrons with nuclei imbedded in the packet such as one produced by K. Shoulders [14, 15]. The continuum-electron shielding may be one possible mechanism for explaining the anomalous results observed by Kamada in his electron-impact experiments [19]. Our formulation of the continuum-electron shielding [13] may provide a theoretical justification of "swimming electron layer" model proposed earlier [20].

Since 1980, K. Shoulders has been investigating dense highly organized micro-size cluster of electrons produced in ultra-short-time discharge plasma experiments [14,15]. The experimental data indicate the existence of a plasma state representing a freely moving, localized packet of eletrons. A short Latin acronym EV (electrum validum or electromagnetic vortex) has been adopted to describe this collective plasma state of tightly bound groups of electrons with extremely high densities. The EV's have been reported to be roughly spherically symmetric with radii on the order of 1.0 μ m, to travel at speeds on the order of 0.1c (corresponding to the electron kinetic energy of $\sim$ 2.7 keV), to tend to move for distances of 1.0 to 10.0 mm in straight lines, to deflect and accelerate with electron characteristics

in experiments, and to have high electron densities on the order of 10^{22} to $10^{24} cm^{-3}$ with negligible ion content of $\sim$ one ion per 10^6 electrons.

Shoulders [14] reports the principle requirement for generating these EV structures to be a sudden creation of a very high, uncompensated set of electronic charges in a very small volume of space, i.e., a fast emission process coupled to a fast switching process. He notes the times of creation to be considerably less than 10^{-13} sec. The actual threshold initiation times for the particle packet are believed to be $\tau \sim 10^{-15}$ sec. The packet then travels approximately 10^5 before it catastrophically decays.

Ziolkowski and Tippett [21] interpret the EV theoretically as a stable packet of electrons moving collectively through space-time catalyzed by a localized electromagnetic wave, which can be attributed to localized wave (LW) solutions obtained from Klein-Gordon form of Maxwell equations for a joint system of plasma-fluid and electromagnetic field. Beckmann [22] offers a theoretical interpretation based on the oscillating Faraday field surrounding a moving electron.

It has been determined experimentally [15] that the size of EV structure is a function of the high specific energy delivered to the metal. This fact has been recently explained by G. Mesyats in his theoretical analysis [23]. Mechanical storage of energy is though to be the source for the small EVs produced.

The total number of electrons in a 1 μm diameter EV is $\sim 10^{11}$. This allows for inclusion of $\sim 10^5$ ions (or nuclei) which would not be detected in measurements of the charge-to-mass ratio of EV such as time-of-flight measurement, i.e. electrons and nuclei in the EV (NEV) would be collectively accelerated to the velocity of electrons. This would provide a simple nuclear accelerator for accelerating nuclei. Shoulders et al. [15] have proposed this nuclear acceleration mechanism (leading to cluster-impact reactions) as a possible explanation of the anomalous nuclear transmutation effect observed by several groups [16]. Cluster-impact fusion has been previously investigated both experimentally and theoretically with $(D_20)_n$ clusters, which is described in the next section 7. For the NEV velocity of $v = 0.1c$, deuterons entrained in the EV would attain kinetic energy of $M_d v^2/2 \approx 9.4$ MeV (or proton kinetic energy of ~ 4.7 MeV or oxygen kinetic energy of ~ 56.3 MeV). Although these higher energy deuterons (or protons) can have large reaction cross-sections, the total reaction rates with the NEV's containing $\sim 10^5$ nuclei per NEV are too small for explaining some of the observed reaction rates, unless a substantially large number of the NEV is produced per unit time and additional mechanisms such as shock-wave heating are invoked.

Acceleration process of positive ions to higher energies due to electron plasma was observed in 1960 [24] in experiments involving a rapid expansion of plasma in a vacuum spark discharge [25,26]. Plyutto et al. obtained protons with kinetic energies of 4-5 MeV and carbon ions with kinetic energies of 15-20 MeV, when pulsed voltages of only 200-300 kV were used for spark discharge. The average number of $10^{11} - 10^{12}$ per pulse was achieved for accelerated protons or deuterons [27].

If the number of nuclei (deuterons, protons, oxygens, or others) imbedded in the EV is of the same order as that of electrons (10^{11} electrons in μm diameter size) in the EV, kinetic energies of electrons and nuclei in the NEV become much smaller. However, a Gamow factor cancellation due to the continuum electron shielding can occur if the relative velocities between electrons and nuclei in the NEV are much smaller than the velocity of the NEV. If such a GFC condition and a high production rate of the NEV are achieved, most of the observed anomalous effects [3-5,16] can be explained by nuclear physics mechanism.

Once the GFC is achieved in the entrance channel, nuclear reactions can proceed either via the direct reaction mechanism (i.e. fusion) or via the compound nucleus mechanism (de-excitation by γ-ray or neutron emission, or by fission). The compound nucleus mechanism leading to fission may be consistent with some of observations of the anomalous nuclear transmutation [16].

Nuclear Physics Approach

For most of the electrolysis experiments, applied voltages were much smaller ($\sim 10V$) than the voltage $\sim$ 2.7 kV Shoulders used to generate the EV from his discharge experiments. However, some mechanisms such as the fractoemission may generate the EV at lower applied voltages $\sim$ 10 V. Generation of the EV has been observed with applied voltages as low as $\sim$ 50 V [14, 15]. If a sufficiently large number of smaller size ($< 1\mu m$) EV with lower velocities corresponding to the electron kinetic energy of $\gtrsim$ 10 eV can be produced at the surface of the cathode and/or inside microcavities and cracks of the cathode metal, the GFC due to the continuum electron shielding may offer a consistent explanation for most of the anomalous effects observed in electrolysis experiments, based on nuclear physics mechanisms (fusion, fission, etc.). Therefore it is important to verify the results of Shoulders independently by other experimentalists.

7. Cluster-Impact Nuclear Reaction (CINR)

Previous investigations of the cluster-impact nuclear reaction were carried out for heavy-water molecule-clusters $(D_2O)_n$. Unliked electrons in the NEV, electrons in $(D_2O)_n$ are bound electrons and not continuum electrons, and hence the GFC due to the continuum electron shielding is not applicable. The original claims [28-31] of the anomalous enhancement of $(D_2O)_n$ cluster-impact fusion cross-section were later found to be incorrect and attributed to contaminants. Nevertheless, most of theoretical formulations and models [32-39] developed to describe the cluster-impact fusion phenomena are still applicable to the cluster-impact nuclear reactions with the NEV (CINR/NEV). CINR/NEV is a way of coupling first the input energy into the electronic system and then into the target nuclei, as the laser induced fusion does. However, CINR/NEV may turn out to be more efficient than the laser induced fusion.

Shock-wave mechanisms for the cluster-impact fusion are theoretically investigated in references [34-39] such as pinch instability heating due to magnetic confinement [36-40] and shock wave heating [34-39].

8. Conclusions

It is shown that a near cancellation of the Gamow factor can occur under certain conditions. If one of the final-state nuclei has an excited halo nuclear state, it can lead to a GFC. Another mechanism for obtaining the GFC is due to the continuum electron shielding which can be achieved by creating high density cluster of mobile electrons and nuclei such as the NEV, in which the relative velocity between electron and incident nucleus in the NEV are much smaller than the NEV velocity between the NEV and the target nucleus. Therefore, theoretical opposition based on the Gamow factor to the anomalous low-energy nuclear reactions may be premature.

Once the GFC is achieved in the entrance channel, it can lead to the exit channel of nuclear fusion reaction (the direction reaction mechanism) or decay via emission of γ-rays or neutrons or via spontaneous fission (the compound nucleus mechanism). These nuclear physics mechanisms may offer a consistent explanation for many of the anomalous effects observed in low-energy nuclear reaction experiments including the nuclear transmutation.

The cluster-impact nuclear reaction with the NEV (CINR/NEV) may turn out to be a more efficient way of coupling first the input energy into the electronic system and then into the target nuclei, as compared with the laser induced fusion. Furthermore, CINR/NEV may offer other advantages such as possibilities of aneutronic reactions. Therefore, it is important to verify the EV phenomena by independent experiments.

Acknowledgement

One of the authors (Y.E.K.) wishes to thank Ken Shoulders for his helpful discussion on the EV.

References

1. M. Fleischmann, S. Pons and M. Hawkins: Electroanal. Chem, **261**, 301 (1989); for some corrections see J. Electroanal. Chem. **263**, 187 (1989).
2. S. E. Jones, E. P. Palmer, J. B. Czirr, D. L. Becker, G. L. Jensen, J. M. Thorne, S. F. Taylor, and J. Rafelski, Nature **338**, 737 (1989).
3. See references in *Transaction of Fusion Technology* **26**, (1994), Proceedings of the 4th International Conference on Cold Fusion, (ICCF-4), December 6-9, 1993, Lahaina, Mauii, Hawaii.
4. See references in Proceedings of the 5th International Conference on Cold Fusion (ICCF-5), April 9-13, 1995, Monte Carlo, Monaco.
5. Storms, Fusion Technology **20**, 433 (1991); ICCF-5, pp. 1-16.
6. M. Fleischman, S. Pons and G. Preparata, Nuovo Cimento **A107**, 143 (1994).
7. V. A. Chechin, V. A. Tsarev, M. Rabinowitz and Y. E. Kim, International J. Theor. Phys. **33**, 617 (1994).
8. Y. E. Kim and A. L. Zubarev, Nuovo Cimento **108A**, 1009 (1995).
9. Y. E. Kim and A. L. Zubarev, Few-Body Systems Suppl. **8**, 332 (1995).
10. Y. E. Kim, Y. J. Kim, A. L. Zubarev, and J. H. Yoon, "Optical Theorem Formulation of Low-Energy Nuclear Reactions", Purdue Nuclear Theory Group (PNTG)report PNTG-96-8 (August 1996).
11. Y. E. Kim and A. L. Zubarev, Genshikaku Vol. 40, No. 5 (1995), pp. 27-36.
12. Y. E. Kim and A. L. Zubarev, "Excited Halo Nuclear State and Long Range Interaction in Nuclear Reactions", Physical Review **C54**, 1805, (1996).
13. Y. E. Kim and A. L. Zubarev, "Three-Body Effects and Uncertainties for the $p(pe^-, \nu_e)d$ Reaction in Nuclear Astrophysics", Purdue Nuclear Theory Group (PNTG) Report PNTG-96-5 (May 1996).
14. K. R. Shoulders, EV - A *Tale of Discovery*, Austin, TX (1987). A historical sketch of early EV work having 246 pages, 153 photos and drawings, 13 references. Available from the author.
15. K. Shoulders and S. Shoulders, "Observations on Role of Charge Clusters in Nuclear Cluster Reactions", J. New Energy, vol. 1, no. 3 (1996).
16. See references in this proceedings and J. New Energy, vol. 1, No. 1, 2, and 3 (1996).
17. E. Feenberg, Phys. Rev. **40** (1932).
18. R. Newton, *Scattering Theory of Waves and Particles*, McGraw-Hill (New York, 1966).
19. K. Kamada, Jpn, J. Appl. Phys **31**, L 1287 (1992); Proc. 7th Int. Conf. on Emerging Nuclear Energy Systems (ICENES '93), World Scientific, Singapore (1994). pp. 165-175.
20. H. Hora, G.H. Miley, et al. Physics Letter A **175**, 138 (1993).
21. R. Ziolkowski and M. K. Tippet Phys. Rev. **A43**, 3066 (1991).
22. P. Beckmann, Galilean Electrodynamics **1**, 55 (1990).
23. G. A. Mesyats, "Ecton Processes at the Cathode in a Vacuum Discharge", Proc. XVII Int. Symp. Discharges and Elect. Insulation in Vacuum (21-26 July 1996) Berkeley, CA, pp. 721-731.
24. A. A. Plyutto, Soviet Physics JETP **12**, 1106 (1961).
25. A. A. Plyutto, V. N. Ryzhkov, and A. T. Kapin, Soviet Physics JETP **20**, 328 (1965).
26. P. E. Belensov, A. T. Kapin, A. A. Plyutto, and V. P. Ryzhkov, Soviet Physics-Technical Physics **9**, 1633 (1965).
27. A. A. Plyutto, P. E. Belensov, E. D. Korop, G. P. Mkheidze, V. N. Ryzhkov, K. V. Suladze, and S. M. Temchin, Soviet Physics JETP Letters **6**, 61 (1967).

28. R. J. Beuhler, G. Friedlander, and L. Friedman, Phys. Rev. Lett. **63**, 1292 (1989).
29. R. J. Beuhler, Y. Y. Chu, G. Friedlander, L. Friedman, and W. Kunnmann, J. Phys. Chem. **94**, 7665 (1990).
30. Y. K. Bae. D. C. Lorents, and S. E. Young, Phys. Rev. A **44**, 4091 (1991).
31. R. J. Beuhler, Y. Y. Chu, G. Friedlander. L. Friedman, A. G. Alessi, V. LoDestro, and J. P. Thomas, Phys. Rev. Lett. **67**, 473 (1991).
32. Y, E. Kim, M. Rabinowitz, G. S. Chulick, and R. A. Rice, Mod. Phys. Lett. **B5**, 427 (1991).
33. Y. E. Kim, R. A. Rice, G. S. Chulick, and M. Rabinowitz, Mod. Phys. Lett. **A6**, 2259 (1991).
34. Y. E. Kim, G. S. Chulick, R. A. Rice, M. Rabinowitz, and Y. K. Bae, Chem. Phys. Lett. **184**, 465 (1991).
35. Y. E. Kim, M. Rabinowitz, Y. K. Bae, G. S. Chulick, and R. A. Rice, Mod. Phys. Lett. **B5**, 941 (1991).
36. Y. E. Kim, M. Rabinowitz, Y. K. Bae, G. S. Chulick, and R. A. Rice, "Hot Plasma Shock-Wave Theory of Cluster-Impact Fusion," AIP Conference Proceedings **250**, 321 (1992).
37. Y. E. Kim, M. Rabinowitz, Y. K. Bae, G. S. Chulick, and R. A. Rice, "Cluster Impact Hot Fusion," in Proc. of ICENES '91, published in Fusion Technology.
38. Y. E. Kim, J.-H. Yoon, R. A. Rice, and M. Rabinowitz, Phys. Rev. Lett. **68**, 373 (1992).
39. Y. E. Kim, M. Rabinowitz, J.-H. Yoon, and R. A. Rice, "Hot Plasma Model for Cluster Impact Fusion", *Laser Interaction and Related Plasma Phenomena* (International Conference Series), Vol. 10, edited by H. Hora and G. H. Miley, Plenum, New York (1993), pp. 649-662.
40. A. Hasegawa et al., Phys. Rev. Lett. **56**, 139 (1986).

Click here for a more readable copy of this paper.

Correlation between Behavior of Deuterium in Palladium and Occurrence of Nuclear Reactions Observed by Simultaneous Measurement of Excess Heat and Nuclear Products

Yasuhiro Iwamura, Takehiko Itoh, Nobuaki Gotoh and Ichiro Toyoda

Advanced Technology Research Center, Mitsubishi Heavy Industries, Ltd.
1-8-1, Sachiura, Kanazawa-ku, Yokohama, 236, Japan

Abstract

We developed a new type of experimental apparatus for simultaneous measurement of excess heat and nuclear products with intent to induce continuous nuclear reactions in D_2-Pd system. It consists of two parts; an electrochemical cell for calorimetry and a vacuum chamber for nuclear measurement . There exits continuous flow of deuterium atoms from the electrochemical side to the vacuum side through a palladium plate and we might expect that nuclear reactions last for a long term in the system, since it is considered that diffusion process of deuterium atoms in palladium is important to induce nuclear reactions.

Our experimental results suggest that absorption and desorption behavior of deuterium was greatly influenced by unspecified factors (impurity or metallurgical conditions of palladium). X-ray emission lasting for long term and excess heat generation was observed, however, correlation between excess heat and x-ray is not clear under our experimental condition.

1. Introduction

We previously reported that diffusion process of deuterium, in addition to high D/Pd ratio, is important factor for causing nuclear reactions by the method of gas release experiments in vacuum[1,2]. Based on these experimental results, we developed a new experimental apparatus for simultaneous measurement of excess heat and nuclear products.

The basic idea of our apparatus is that we might make continuous nuclear reactions occur in D_2-Pd system by making continuous flow of deuterium under *certain appropriate conditions*. Although high D/Pd ratio is one of the *certain appropriate conditions*, the other necessary conditions still remain to be unclarified at present. Therefore it might be possible to clarify the other *appropriate conditions* by making continuous flow of deuterium in palladium under high D/Pd condition; For it is considered to be most probable way to induce nuclear reactions according to our experimental results[1-3].

In this paper, we describe our experimental apparatus and the results on simultaneous measurement of excess heat and nuclear products.

Nuclear Physics Approach

2. Experimental Method

Fig.1 shows a cross sectional view of the experimental apparatus. An electrolyte of 1M LiOD/D_2O and a vacuum chamber are separated by a palladium plate. Deuterium atoms are loaded by electrochemical potential into one side of the palladium sample and released from the other side.

Excess heat is estimated by the flow calorimetry method. Electrolyte side of the apparatus consists of a cathode of palladium plate(25x25x1mm; 99.9% Tanaka Kikinzoku Kogyo K.K.), a circular shape of anode of platinum mesh(ϕ1mm), a recombiner and a cooling pipe for measurement of excess heat generation. Two thermocouples each for measurement of inlet and outlet temperature of the water are provided. Solution, gas, recombiner and environmental temperatures are measured and consistency between these temperatures is always checked.

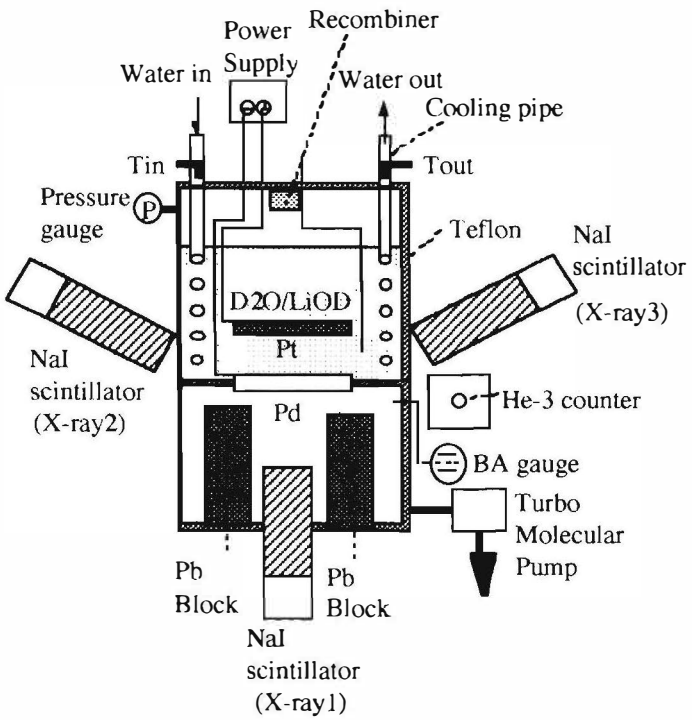

Fig.1 Experimental Apparatus

The apparatus is equipped with three NaI scintillation counters (Bicron:1.5XM1/2B) for x-ray spectroscopy and a He-3 neutron detector(Reuter-Stokes: RS-0806-207). The X-ray1 detector located in the vacuum chamber is surrounded by a lead cylinder (thickness; 2.5cm) to reduce background x-rays. X-ray spectroscopy and counting system consists of preamplifiers (EG&G Ortec : 276), amplifier and single channel analyzers (EG&G Ortec : 590A), counters (EG&G Ortec : 997) and multi-channel analyzers (SEIKO EG&G : MCA4100, 4200). As to neutron counting, we use a preamplifier (EG&G Ortec : 142PC), an amplifier and single channel analyzer (EG&G Ortec : 590A) and a counter (EG&G Ortec : 997).

Pressures of the upper part of electrolyte and vacuum chamber are monitored by a pressure gauge and a BA gauge, receptively. D/Pd is calculated by the obtained pressures as will be described. All the experimental data is acquired by personal computers.

Nuclear Physics Approach

The apparatus and measuring systems are located in a clean-room where temperature and humidity are always controlled at constant levels (23°C±1°C, 40%±5%). Furthermore, all these electric devices are supplied by an isolated power source to prevent electric noise from the outside of the clean room.

Procedure of sample preparation is as follows. Palladium plates were washed with acetone and annealed under vacuum condition (<10^{-7}torr) at 900°C for 10 hours. The samples were cooled down to room temperature in furnace and washed with aqua regia to remove impurity on the surface of the palladium samples. After that, some samples were covered with MgO or Al by ion beam sputtering, some samples were electroplated by copper or platinum, and the others had no films. The aim of the surface modification is to reduce the rate of deuterium gas release from the vacuum side of the palladium.

3. Data Analysis

D/Pd is estimated by the following procedure. Equation of state for the upper part of the electrolyte side is expressed as;

$$p_{O_2} V_{cell} = N_{O_2} \kappa T_{cell} \tag{1}$$

where *cell* denotes upper part of the electrolyte side and κ is the Boltzmann constant. The number of deuterium atoms absorbed into the palladium is given by

$$N_{D_{in}} = 2N_{D_2} = 4N_{O_2} = \frac{4V_{cell} p_{O_2}}{\kappa T_{cell}}. \tag{2}$$

As the vacuum chamber is evacuated by the pumping speed of S, an equation of mass balance is obtained as

$$\frac{d}{dt}(N_{vac} \kappa T_{vac}) = V_{vac} \dot{p}_{vac} + P_{vac} S \tag{3}$$

where denotation of *vac* means the vacuum side. Almost of the gas in the vacuum chamber is composed of D_2 gas, then time derivative of the number of deuterium atoms is given by

$$\dot{N}_{D_{out}} = 2\frac{V_{vac} \dot{p}_{vac} + p_{vac} S}{\kappa T_{vac}} \tag{4}$$

Combining equation (2) and (4), we obtain the following equation;

$$D/Pd = \frac{M_{Pd}}{\omega_{Pd} N_{AB}} \left[\frac{4V_{cell} p_{O_2}}{\kappa T_{cell}} - 2\int_{t_0}^{t} \frac{V_{vac} \dot{p}_{vac} + p_{vac} S}{\kappa T_{vac}} dt \right], \tag{5}$$

where N_{AB}, M_{pd}, ω_{pd} and t_0 denote Avogadro number, mass number of palladium, mass of the palladium sample and the time that D_2 gas begins to release out, respectively.

Next, we describe the excess heat analysis. Assumption of the analysis is that we consider only steady state and dissipated heat from the apparatus is estimated by Pd/H_2O system.

Heat balance equation of the apparatus is expressed as

$$P_{ex} + P_{in} - P_{out} - P_{diss} - \Delta \dot{H}_{gas} + \Delta \dot{H}_{abs} - \Delta \dot{H}_{des} = 0 \qquad (6)$$

where *ex, in, out, diss, gas, abs* and *des* mean excess, input, output, dissipation, gas release, absorption and desorption. The terms of gas release, absorption and desorption of deuterium are negligible if we use typical experimental parameters. Therefore excess heat is calculated by

$$P_{ex} = \dot{m}_w c_w (T_{out} - T_{in}) - IV + \int_A h(T_{sol} - T_{room})dA \qquad (7)$$

where IV is the input power, m_w and c_w are mass of the water and specific heat, h is the heat transfer coefficient and A means the whole surface of the apparatus.

4. Results and Discussion

Figure 2 shows an example of D/Pd analysis. In this case, the sample has no surface film. Since the deuterium atoms absorbed on the surface of the electrolyte side of the palladium do not reach the opposite surface, deuterium gas is not released at the early period of the experiment. D/Pd increases gradually and attains to 0.8 at the time of 1×10^5 sec. This results indicate that D/Pd reaches about 0.8 even for the palladium sample without surface barrier on the vacuum side of it.

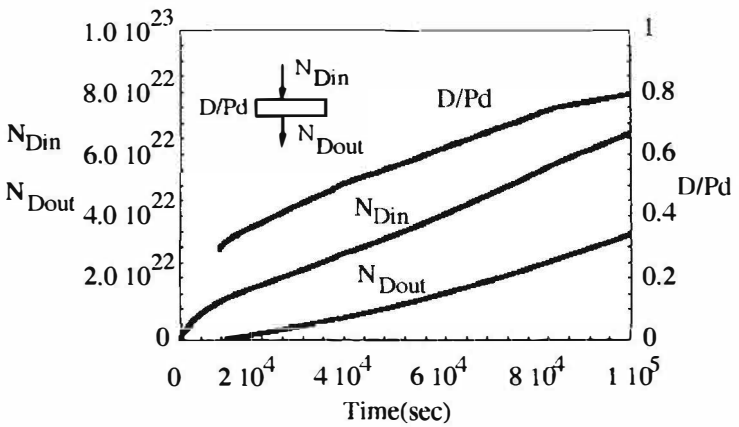

Fig.2 D/Pd Analysis

Variation of deuterium behavior depending on palladium samples is shown in Fig.3. Pressure(electrolyte) lines mean the pressures of the upper side of the electrolyte side which is correspond to the quantity of deuterium into palladium, and Pressure(vacuum) lines the vacuum side proportional to time derivatives of the number of released deuterium atoms.

These samples, EV29 and EV34, are prepared by the same procedure; they are derived from the same lot and the method of annealing and etching is all the same. However, it is easy to realize that absorption and desorption of deuterium is entirely different. It suggests that absorption and desorption behavior of deuterium is greatly influenced by unspecified factors; metallurgical conditions such as impurity and defects in palladium.

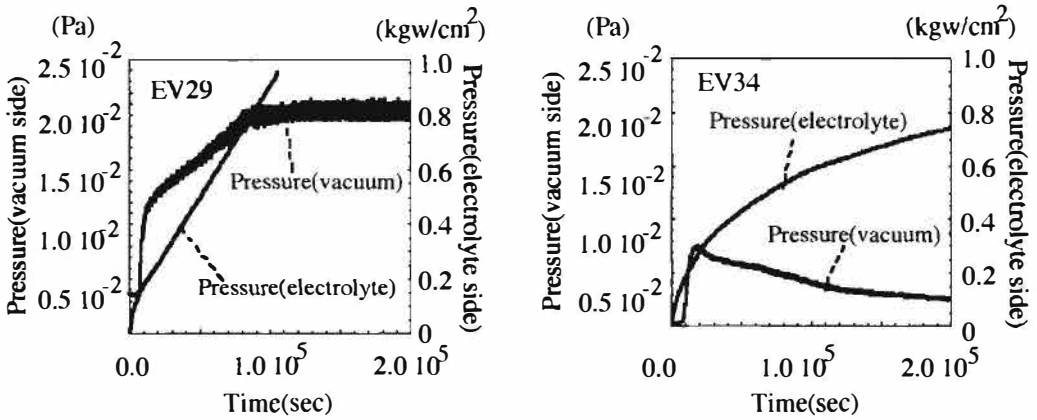

Fig.3 Variation of Absorption and Desorption of Deuterium

An example of long period x-ray emission and its energy spectrum is demonstrated in Fig.4. This samples has Al thin film(~400Å). Upper figure indicates time variation of x-ray1(see Fig.1) located in the vacuum chamber. X-ray count rate reaches over 10 times larger than that of background. We can see that x-ray emission lasts for a long period; more than 1day. It was a successful example in the meaning that we could make long-term continuos nuclear reactions occur in the Pd-D_2 system.

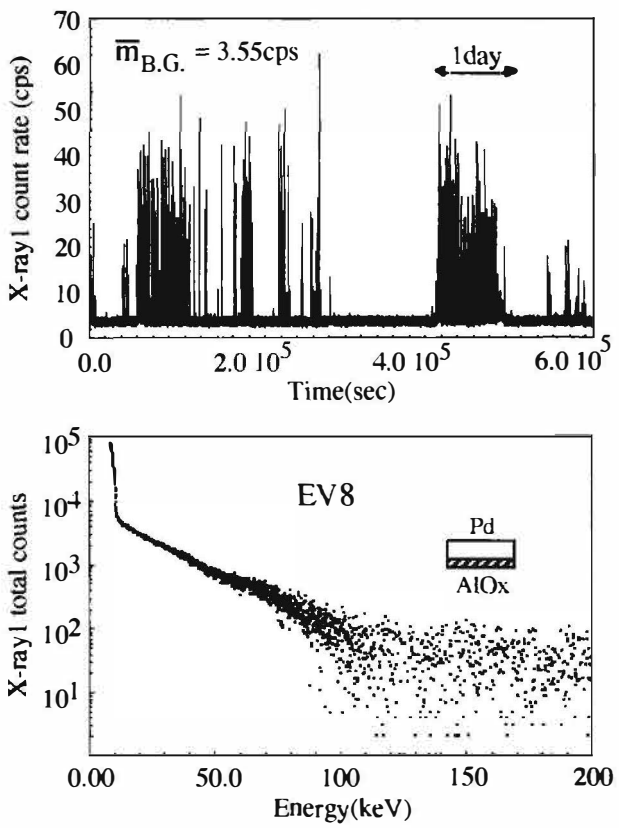

Fig.4 Long-term X-ray Emission and its energy spectrum

Nuclear Physics Approach

An energy spectrum of the x-ray emission for about a week is plotted in the lower figure. X-ray energy distributes continuously as shown in the figure. However, at present, the authors cannot explain consistently why such an energy spectrum was obtained. It is an important future work.

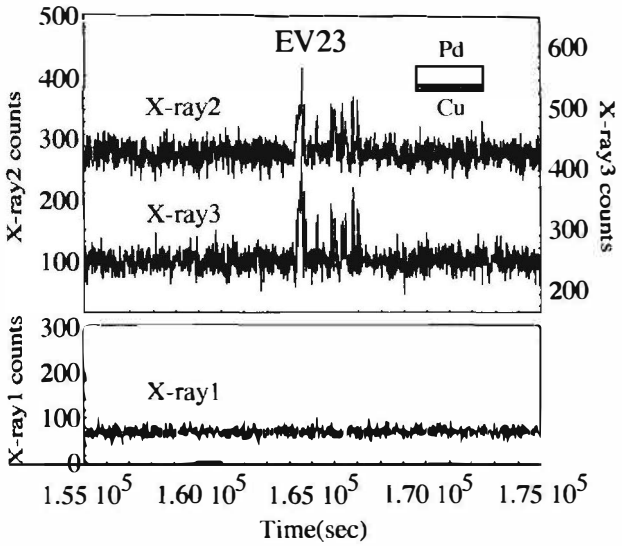

Fig.5 Simultaneous detection by upper side x-ray detectors

Next example shows simultaneous detection by the upper side of x-ray NaI counters(Fig.5). The sample EV23 is electroplated by copper. Coincidence of x-ray2 and x-ray3 is very good, on the other hand, counts of x-ray1 are almost equal to those of background. In the 14 out of 40 cases, we observed this kind of x-ray emissions. Judging from the experimental results, nuclear reactions must occur on the electrolyte side of the palladium. For the thickness of palladium is 1mm, reduction rate of x-rays through the palladium is larger than that through the D_2O(4cm).

Figure 6 illustrates the correlation between excess heat and the other parameters. In this case(EV39), we use a palladium sample covered with MgO thin film. At low current, any excess heat cannot be seen. However, after making the applied current up to 3A (current density : 1.5A/cm^2), we can observe a clear excess heat generation. Input power is about 40W when current of 3A is applied, therefore excess heat we obtain is a few percentages of the input power.

Comparison of heat distribution between EV39(excess heat generation) and EV40(no excess heat) is shown in Figure 7. In both cases, the other experimental conditions are the same except the palladium sample treatment. MgO thin film is formed on the vacuum side of EV39, and Fe thin film on the electrolyte side of EV40. It is clear that mean value and deviation of excess heat of EV39 are larger than those of EV40.

Up to now, several times we observed excess heat generation, however, we could not see any relations between excess heat generation and x-ray emission. In some cases, excess heat generation seems to be related with pressure in vacuum chamber; it corresponds to time derivatives of the number of deuterium atoms. As for neutron measurement, a clear emission has not been observed during the experiments using this apparatus. Nevertheless, the authors consider that we must investigate furthermore to conclude correlation between excess heat and nuclear products.

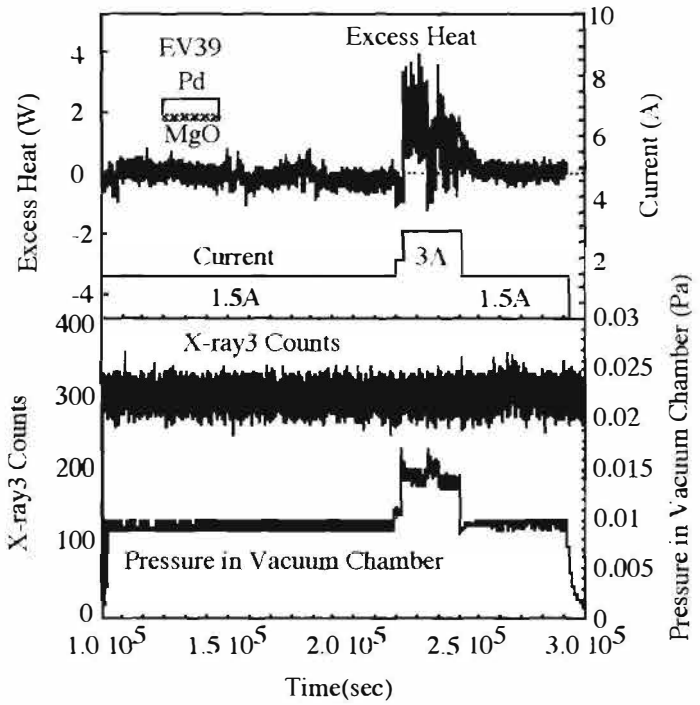

Fig.6 Correlation between Excess Heat and the other parameters

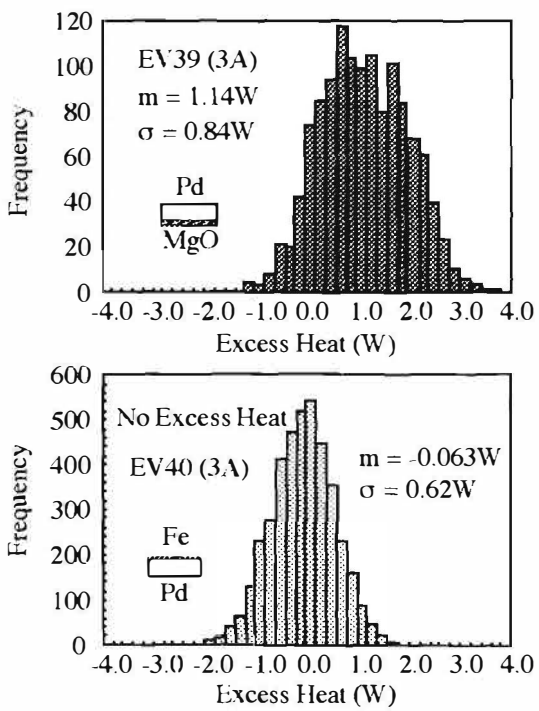

Fig.7 Excess Heat Distribution

Nuclear Physics Approach

If we assume a few MeV energy release by an event, obtained excess heat corresponds to the order of 10^{12} events/sec. On the other hand, observed x-ray emissions range from 10^2 to 10^4 events/sec (calibrated by an Am-241 source). Judging from these results, we might consider that excess heat and x-rays are generated by different nuclear reactions. In our previous paper[3], it was suggested that x-ray and neutron are generated by different reactions. Therefore it seems that we should not exclude the possibility that various nuclear reactions occur and produce various nuclear ashes.

5. Concluding Remarks

A new type of experimental apparatus for simultaneous measurement was developed. Absorption and desorption behavior of deuterium in palladium was greatly changed by the unspecified conditions of the palladium. X-ray emission lasting for long term and excess heat generation was observed. Up to now, correlation between excess heat and x-rays has not been clear under our experimental condition. Nevertheless, we must investigate furthermore to conclude correlation between excess heat and nuclear products.

References

1. Y.Iwamura, T.Itoh and I,Toyoda, "Observation of Anomalous Nuclear Effects in D2-Pd System", Proc. of ICCF-4, Maui, Hawaii, December 6-9, 1994, vol.2, p12
2. T.Itoh, Y.Iwamura, N.Gotoh and I.Toyoda, "Observation of Nuclear Products under Vacuum Condition from Deuterated Palladium with High Loading Ratio", Proc. of ICCF-5, Monte Carlo, Monaco, April 9-13, 1995, p189.
3. Y.Iwamura, N.Gotoh, T.Itoh and I.Toyoda, "Characteristic X-ray and Neutron Emission from Electrochemically Deuterated Palladium", Proc. of ICCF-5, Monte Carlo, Monaco, April 9-13, 1995, p197

Nuclear Physics Approach

SEARCH FOR NUCLEAR REACTION PRODUCTS IN HEAT-PRODUCING PALLADIUM

Thomas O. PASSELL

Nuclear Power Group
Electric Power Research Institute
P.O. Box 10412
Palo Alto, California 94303

ABSTRACT

Almost eight years have elapsed since the first announcement by Fleischmann, Pons and Hawkins (1) of the observation of excess heat from palladium heavily loaded with deuterium. The EPRI program began in April, 1989, and has successfully confirmed the presence of the claimed excess heat but has yet to determine its source. Measurable helium-4 has been observed in the cell vapor space in a few cases, but so far , not in a definitive manner. The major evidence that the heat may be from nuclear reactions is its magnitude - some 10 to 100 times larger than any known chemical reaction. The objective of the continuing effort is to identify the source of the excess heat. This paper focusses upon comparing measurements on cathodes that successfully produced excess heat with the same measurements on virgin material from the same batch of palladium. Initial measurements on one cathode that produced 0.56 megajoules of excess heat and its virgin counterpart are reported here. The analytical method chosen is a non destructive one known as prompt gamma activation analysis (PGAA) using thermal neutrons in beams from research reactors. Since almost every isotope captures neutrons with the emission of several gamma rays unique to that isotope, any isotopic ratio changes from the heat production process will be converted to a change in the relative ratios of gamma ray intensities. Such ratios can be measured to an accuracy in the range around 1% using high resolution germanium detection systems. Thus any changes due to the production or loss of any isotope present can be detected and related to the excess heat produced. One such measurement using PGAA appears to show an ~18% reduction in the ratio of boron-10 to palladium-105 in the active cathode relative to the ratio in virgin material. Conventional explanations of this result such as selective chemical leaching of boron by the electrolyte are currently being tested.

1. INTRODUCTION

The subject of cold fusion has aroused considerable controversy since its announcement almost than eight years ago. This atmosphere of controversy has slowed the resolution of the scientific issues. The EPRI program had two major objectives at the outset: 1) to obtain the largest possible amount of excess heat; and 2) to observe the neutrons and tritium everyone expected from the D + D fusion reaction. Since that time the focus has shifted to a search for helium-4 and possible isotopic abundance shifts among stable nuclei within cathodes that had produced the largest amounts of excess heat. This paper reports PGAA results from one cathode documented by SRI, International (2) to have produced, over its 356 hour lifetime in the electrochemical cell, about 0.56 megajoule of excess heat. The designation of the cathode is listed as C-2 in table 3-1 of reference 2. Briefly it consisted of three cathode foils of a thickness of 0.025 mm interleaved between four anodes of the same material.

The total cathode area was 60 cm2 (both sides of each foil were exposed to an anode) or 30 cm2 of total material (~0.90 grams Pd). The electrolyte was 1.0 M LiOD with the addition of 200 parts per million by weight of aluminum.

If the heat were uniformly produced within the cathode, this amounts to 66 megajoules per gram-molecular-weight of palladium. At this level of heat production per atom of cathode material, one would expect to observe measurable depletion of some isotope that is consumed in some nuclear reaction hypothesized to be producing the excess heat observed - only if the reaction is consuming some impurity in the cathode. One of the major impurities in normally pure palladium is boron, often observed at the 100 parts per million by weight (PPM) level. For the measurements reported here, the boron impurity level is close to 100 PPM.

This work is predicated on the hypothesis that some reaction OTHER than D+D is the likely heat (and helium-4) producing nuclear reaction. One of such hypothesized nuclear reactions addressed by this work is the Boron-10 + D => Helium-4 + Beryllium-8 followed by the breakup of beryllium-8 into two more nucleii of helium-4. The heat produced per reaction is 17.81 Mev (2.85 picojoules).

2. METHODS

Figure 1 gives the configuration of the PGAA apparatus. The sample is exposed to a neutron beam from a nuclear research reactor with an intensity of ~1E8 (100 million) neutrons/cm2-second. Each isotope present throughout the sample emits up to three or more gamma rays almost instantaneously after the neutron capture. These gamma rays are unique to that particular isotope and the intensity proportional to the abundance of that isotope in the sample. A high resolution (~2.0 kev at 1.1 Mev) detector resolves the gamma rays and the integral counts under the sharp photoelectric or pair production peaks serve to quantify the parent isotope. The detector used here is a high purity germanium semiconductor cooled to 77°K by liquid nitrogen. Relative ratios of each gamma ray give a sensitive measure of any changes in isotope abundance changes since the ratios of peak integrals are not affected by changes in sample preparation, position in the beam, variation in beam intensity, and many other experimental variables that are difficult to control precisely.

The main advantage of PGAA is its ability to observe the entire contents of a sample cathode nondestructively. Most other methods observe a small volume of material near the surface or are destructive in that they consume the sample. Thus one need not wonder whether the sampled part of the cathode is representative of the whole or a local artifact. Also, if it is suspected that the surface region is the only part of the cathode that is active, the surface can be mechanically separated from the sample and run as an independent sample. In many cases, only a few milligrams of material are needed for a reliable measurement.

One disadvantage of the PGAA method is the variability of neutron capture probabilities (cross sections) among the stable isotopes. For example the method is sensitive to boron-10 with its ~4000 barn cross section but almost blind to boron-11 with its 5 millibarn cross section. Isotopes in the 1 to 100 barn range are readily observed, which includes a large fraction of all stable isotopes of all elements. Another disadvantage is the Compton effect "continuum background " upon which the peaks are superimposed, making the integration of the peak intensity somewhat less certain without long run times of many hours. In the detector used here an anticoincidence Compton suppression annulus of sodium iodide surrounds the germanium - a method which reduces the continuum about a factor of ten. Also, a cadmium sheet shields the entire detection system from stray neutrons that

upon capture in the detector materials would give unwanted background peaks from the elements present. The main gamma ray emitted in cadmium neutron capture is less interfering than those from the formerly used boral alloy, since our main interest is in boron quantification.

Boron-10 gives only one prominent gamma ray upon capture of a neutron by boron for the (n,alpha) reaction to lithium-7, the reaction corresponding to the high 4000 barn cross section. Because the lifetime of the excited state in lithium -7 from which this gamma ray is emitted is sufficiently long, and because the lithium-7 nucleus is recoiling at high velocity from the reaction site due to the momentum of the almost equally massive helium-4 (alpha) particle, the gamma peak is doppler broadened into a "square" rather than the normal gaussian as shown in figure 2. This complicates the integration problem because other normal peaks from capture in other isotopes (mostly palladium) are sometimes superimposed on the "square" rather than being resolved. The smaller unresolved peaks constitute a dilution of the ratio changes because they are from palladium isotopes 105 and 108 showing no ratio changes between the virgin and active cathode material. Two minor gamma rays from capture in palladium isotopes lie in this region, giving the "square " a slightly peaked appearance.

3. RESULTS

A number of sample cathodes have been generously contributed for analysis by this method by Pons, Asami, Mizuno, and McKubre and their colleagues. Thus far only one sample (cathode from C-2 cell from McKubre's group) has been analyzed and that one only for the two isotopes boron-10 and palladium-105.

The gamma ray chosen to represent palladium is one of 615.9 keV energy emitted in the neutron capture by Pd-105 - shown for both the virgin and active cathodes in figure 3. The apparent difference in peak height arises from the fact that the cathode material was about 3 times the mass of the virgin material. This gamma was chosen for its prominence and clear separation from interferences. Many others could have been chosen, and when the analysis is complete, will provide redundancy in the measurement. The boron-10 "square peak" centered at 477.61 keV is our only option since no other gammas of significance are emitted in the high cross section B-10 neutron reaction.

Figure 4 gives three modified boron-10 peaks and their integrals for the background, virgin, and active cathode material, respectively. These integrals were for the same "live" times of the detector, about 12 hours.

Table 1. Integral Counts / Ratios for B-10 and Pd-105 Neutron Capture Gamma Rays

	Active Cathode	Virgin Material	Background	Cathode Net	Virgin Net
Boron-10	20,400	14,600	10,400	10,000	4200
Pd-105	12151	4173	nil	12151	4173
B-10/Pd-105				0.82	1.01
Estimated Uncertainty of Ratios				0.10	0.05

4. DISCUSSION

The boron impurity content of otherwise pure palladium is the remnant of materials added during the final pouring of the ingot to remove oxygen, calcium boride (CaB6) being the primary constituent. Since boron was so ubiquitous in normally pure palladium, as well as quite variable -from a few to several hundred PPM - it was the first trace impurity to be suspected of causing the widely observed batch effect. That is, favorable and unfavorable results of excess heat measurements tended to be roughly consistent within a given batch of palladium material supplied from a vendor. Also, the absence of tritium and neutrons made us consider the next few elements above hydrogen as candidates for heat-producing nuclear reactions, many of which result in helium-4.

These results showing an approximate 18% reduction in boron-10 in the active cathode relative to Pd-105 are still not definitive as a possible source of excess heat for one primary reason: other processes such as selective chemical leaching of boron by the 1.0 Molar LiOD electrolyte cannot yet be ruled out. It is encouraging to note that the 18% depletion in B-10 corresponds almost exactly to the number of reactions of B-10 via the d, alpha reaction to Be-8 needed to explain the 0.56 megajoules of excess heat observed. (2E17 B-10 atoms are missing from a total of 1.2E18 present in the virgin material)

However, if such changes as have been observed in the C-2 cathode are observed in other cathodes with a higher volume to surface ratio, the reason above can be ruled out. Furthermore, there are other light elements present in the system that might be reacting such as either of the lithium isotopes or beryllium. Lithium is likely since it has been observed to diffuse into the cathode surface to a depth of several microns from the electrolyte. Lithium is not easily measured by PGAA because of its very low neutron capture cross sections coupled with its low concentration in the surface. (The 941 barn neutron capture cross section of Li-6 to produce tritium and helium-4, produces no gamma rays).

If this system is distorting the normal D+D reaction to favor the pathway to He-4 and almost completely suppressing the normally observed reaction pathways to neutrons, tritium, helium-3, and protons, then the PGAA method will fail to observe any stable isotope ratio changes because the small fraction of deuterium depletion would not be detectable. Furthermore, deuterium is readily able to leave the host lattice under most storage or handling conditions.

5. CONCLUSIONS

Suggestive but not yet definitive evidence has been observed for the involvement of boron-10 in producing the excess heat previously observed in the C-2 cell cathode from the SRI, International, series of experiments (2). The 18% reduction in B-10 content in the active cathode material relative to its concentration in the virgin material, if confirmed by additional analyses, may indicate that the (d,alpha) reaction is a significant but perhaps not the only heat producing nuclear reaction in highly deuterated palladium.

The most troubling observation is the almost complete absence of radioactivity in palladium and nickel cathodes which have apparently produced excess heat. That is, "Why should nuclear reactions producing only stable isotopes be the heat producers?"

The search for the source of the excess heat will continue to dominate EPRI's interest because the power industry's major business is the conversion of heat to electricity. If it turns out that a

nuclear reaction is proved to be the source of the excess heat, then it would remain to find the laws for scale up to practical levels. However, that scaleup effort could occur with the assurance of a very large supply of fuel far beyond any existing ones in current use.

6. ACKNOWLEDGEMENTS

The support and encouragement of numerous EPRI colleagues have made the progress reported here possible. Particular thanks are due John Bateman, Bindi Chexal, Robin Jones, Albert Machiels, Bruce Rytkonen, Joe Santucci, John Taylor, Fritz Will, and Kurt Yeager. The PGAA analyses were performed at the Research Reactor at the University of Missouri, Columbia by Das Kutikkad and C.J. Lai. Thanks are due to Michael McKubre, Steven Crouch-Baker, and Frances Tanzella for generous help in selecting an appropriate cathode for the first PGAA analysis. I thank Stanley Pons, Naoto Asami, and Tadahiko Mizuno for sharing cathodes that will be analyzed in the future to extend the present results.

7. REFERENCES

1. Fleischmann, Pons, and Hawkins, "Electrochemically Induced Nuclear Fusion of Deuterium," J. Electroanalytical Chem., 261, 301 (1989).

2. McKubre, Crouch-Baker, Tanzella, Smedley, Williams, Wing, Maly-Schreiber, Rocha-Filho, Searson, Pronko, and Koehler, "Nuclear Processes in Deuterated Metals", EPRI Report TR-104195, (1994).

8. LIST OF FIGURES AND TABLES

Table 1. Integral Counts/Ratios for B-10 and Pd-105 Neutron Capture Gamma Rays

Fig 1. Experimental apparatus for PGAA

Fig. 2. Doppler-broadened "square" B-10 gamma peak centered at 477.61 keV with the commonly observed sodium capture gamma ray at 472.4 keV resolved.

Fig. 3 PGAA observation of the 615.9 keV gamma ray from neutron capture in Pd-105 for the C-2 cathode and its virgin material. The factor of 2.91 between these is due to the differing mass of the two samples.

Fig. 4. Three PGAA observations of the B-10 "square" gamma peak for the virgin material, cathode C-2, and the system background.

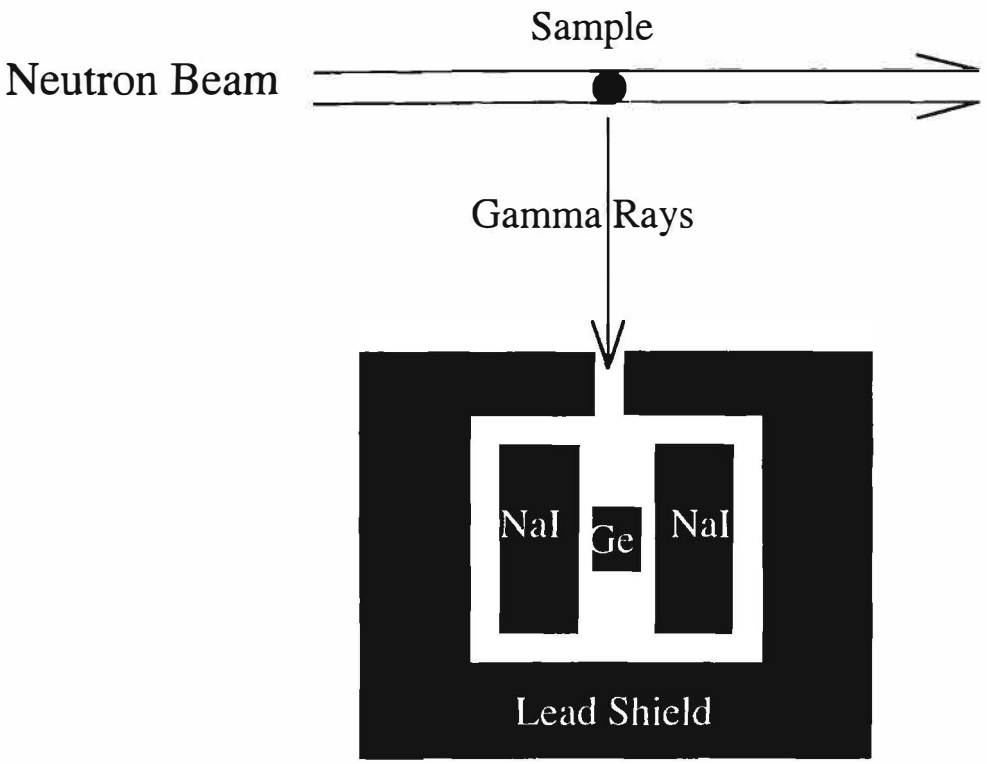

Figure 1. Experimental Apparatus for PGAA. The sample to detector distance is 100 cm, the germanium detector dimensions are 3.86 cm dia x 3.65 cm length, NaI Compton suppression annulus O.D. and I.D. are 20.3 cm and 7 cm, respectively, by 25.4 cm length, and the neutron beam diameter is 3.2 cm. A thin cadmium sheet encloses the outside of the shield.

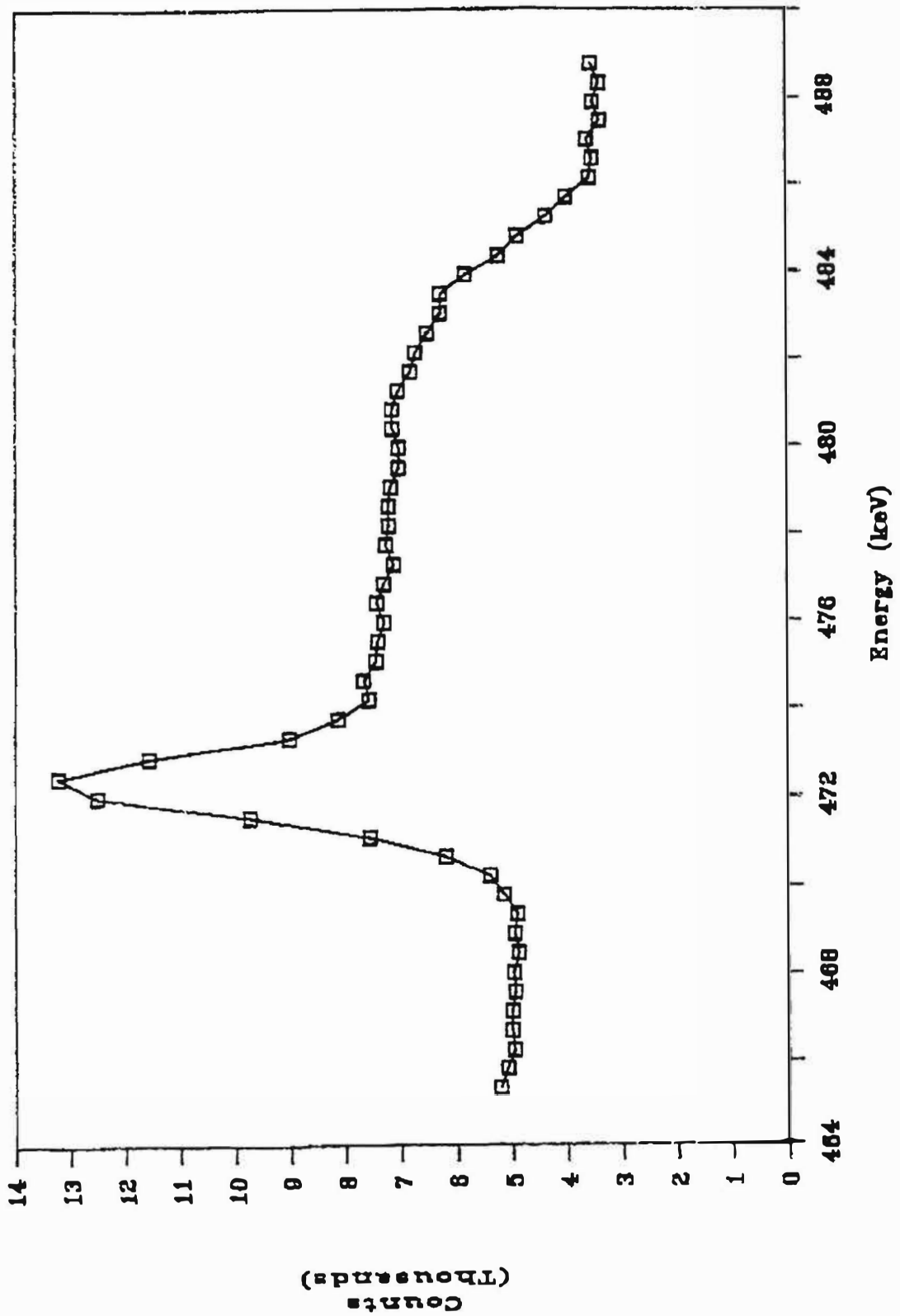

Fig. 2 Doppler Broadened "Square" B-10 Gamma Peak Centered at 477.61 keV with the commonly observed sodium capture gamma ray at 472.4 keV resolved.

Nuclear Physics Approach

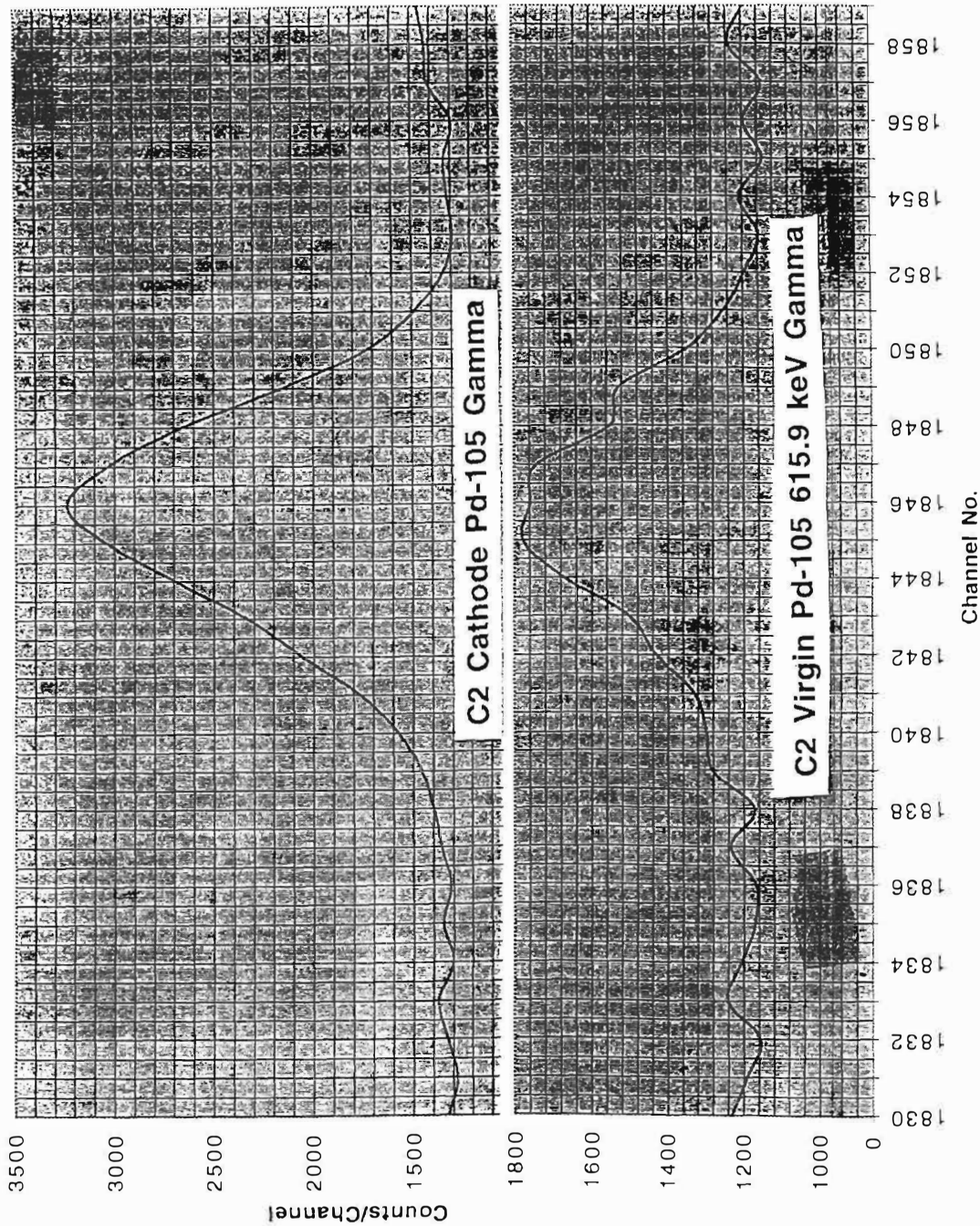

Fig. 3 PGAA Observation of the 615.9 keV Gamma Ray emitted upon thermal neutron capture in Pd-105 for the C-2 Cathode and Virgin Material. The factor of 2.91 between these Integrals stems from the Differing Masses of the Two Samples.

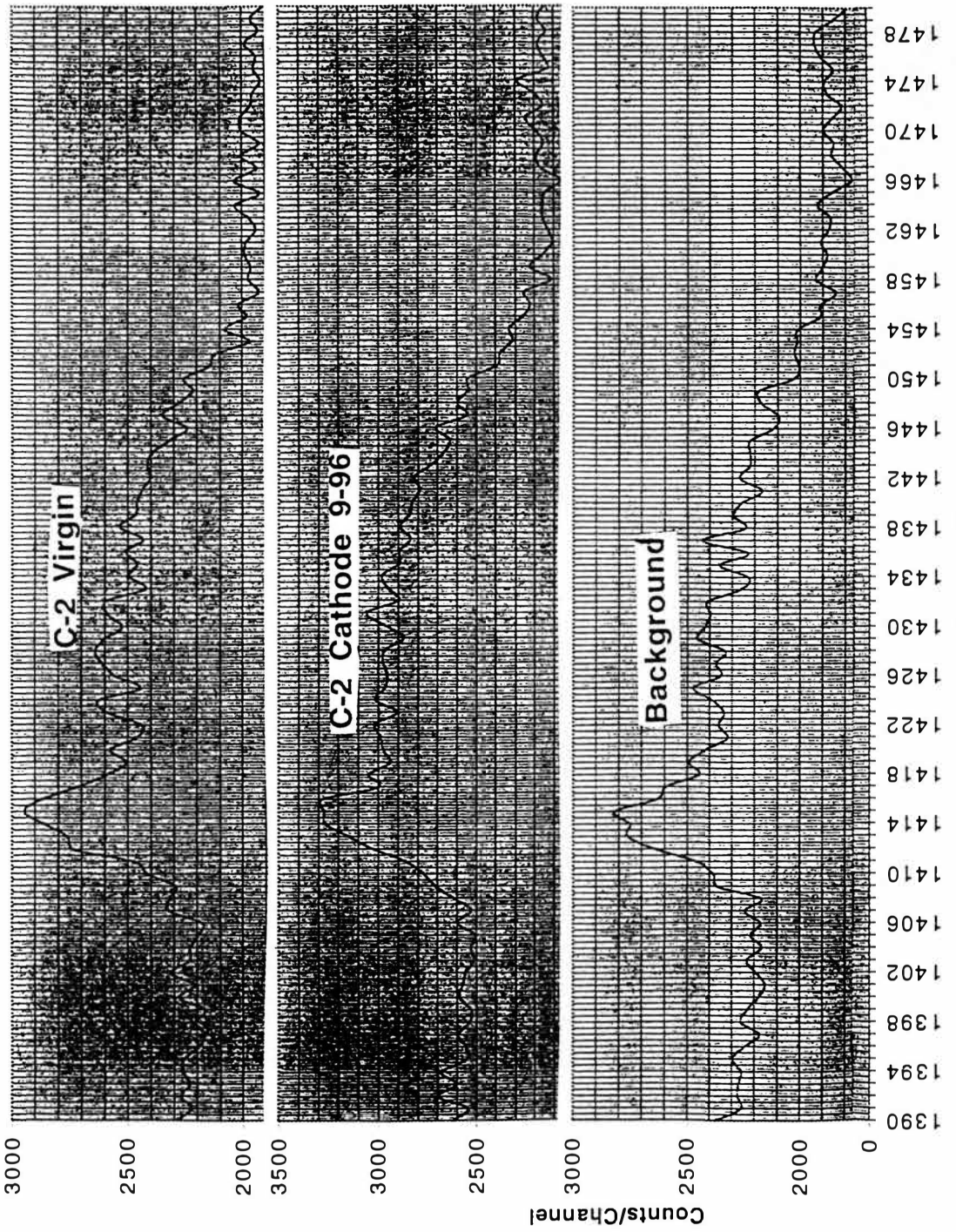

Fig.4 Three PGAA Observations of the Boron-10 Doppler Broadened "Peak" for the, C-2 Cathode, Virgin Material, and the System Background.

Nuclear Physics Approach

SEARCH FOR NEUTRONS EMITTED FROM SODIUM TUNGSTEN BRONZES

T. Aoki, Y. Kurata and H. Ebihara
Isotopecenter, University of Tsukuba
Tsukuba, Ibaraki 305, JAPAN

N. Yoshikawa
Institute for Nuclear Study, University of Tokyo
Tanashi-shi, Midori-machi, Tokyo 188, JAPAN

Abstract

An experiment on the neutron emission from the single crystals of the sodium tungsten bronze (Na_xWO_3, x=0.9) was started to check the reproducibility. After applying the cathodic treatment to the crystals in a heating chamber, the neutron emission had been expected in the instants of pressurizing and depressurizing the deuterium gas. However, the weighted mean values of the measured neutron counting rates at these moments were in agreement with those of the background rates. Therefore, a clear evidence of the neutron generation was not obtained yet.

Ⅰ. Introduction

Three years had been passed since a remarkable announcement that reproducible neutron generations were found from single crystal of sodium tungsten bronzes Na_xWO_3, in which many vacancies had been formed in cathodic treatments by applying negative voltage at high temperature in vacuum chamber[1]. The neutrons had been detected just at beginning of pressurization or depressurization of deuterium gas which interacted with the bronze. Since many experiments would be necessary to establish the phenomenon, we begun to follow the same experiment after growing the single crystals. Preliminary results were obtained.

Ⅱ. Experimental

A. Heating Chamber and Neutron Detection System

A vacuum chamber with a top flange and a flange cover was used for the cathodic treatment. Two heating plates and a stainless steel anode and a cathode were fixed in the center. Temperature of the anode was measured by a thermocouple. Cooling water was introduced into the chamber to cool down the whole system. The pressure was monitored by an ionization gauge and a solid state manometer.

Two standard Helium-3 filled proportional detectors (Model RS-P4-0810, Reuter-Stokes Inc.) were used to detect the neutron from the bronzes. Each detector was surrounding by a cylindrical plastic neutron moderators. The moderators were set on the flat flange cover of the chamber. Many plastic neutron shielding blocks were arranged over the moderators. Pulse signals from the two detectors were amplified and were fed to a multi-channel analyzer (MCA) and also fed to two single channel analyzers (SCA). The SCA's generated new logical discriminated signals for the input pulses between the two discrimination levels to reject the noise signals. The discriminated signals were finally fed to two scalers, A and B. The scalers and the manometer were controlled by a personal computer.

B. Sample Preparation

Fabrication methods of the single crystals of the sodium tungsten bronzes Na_xWO_3 were completely given in references [2-4]. The single crystals were prepared by electrolysis of molten mixtures of sodium tungstate and tungsten(Ⅵ) oxide. The bronze composition x was well controlled by changing the raw material composition[2]. Several cubic single crystals of Na_xWO_3 (x=0.9) with volumes up to 8.0 cm^3 were obtained.. One of the crystals (Crystal A) was sliced by a diamond saw to get some square pieces with thickness of 0.2 cm. The surfaces of the pieces were chemically cleaned.

C. Cathodic treatment

Two or three sliced pieces of the bronze were set on the anode in the heating chamber. A distance between the bronzes and the cathode was 2 mm. The bronzes were heated at the temperature between 700 ℃ and 970 ℃ under the pressure of 1×10^{-6} torr. Negative voltage was applied to the cathode to extract Na^+ ions from the surfaces of the bronzes. The voltage was set constant between −1.5 kV and −3.0 kV. The cathodic treatments were applied several times for the groups of the bronzes, A-1 group and A-2 group. The run number and the used values of the bias voltage, the current, the integrated charge and the temperature for these groups are summarized in Table 1.

Table 1. Group and run numbers and conditions of cathodic treatments

			CATHODIC TREATMENT			
GROUP NO.	CRYSTAL DIMENSION	RUN NO.	TEMP. (°C)	VOLT (V)	CURRENT (μA)	INT.CHARGE (C)
A - 1	(2 crystals)	1	970	- 2000	35 ~ 60	1.3
	22×16×2t	2	970	- 2000	20 ~ 54	2.4
	15×16×2t	3	980	- 3000	50 ~ 80	4.8
A - 2	(3 crystals)	1	735	- 3000	~ 5	0.1
	15×19×2t	2	740	- 3000	~ 4	0.7
	14×20×2t	3	760	- 3000	~ 4	1.0
	20×22×2t	4	780	- 1500	~ 23	4.0

D. Neutron Measurement

It had been expected that the increase of the neutron counting rate would be observed just at short time intervals when the deuterium gas was introduced into the chamber and also when the gas was evacuated since the interacting D^+ ions could move back and forth in the string of vacancies in the bronzes, which were formed by the extraction of Na^+ ions by the cathodic treatment.

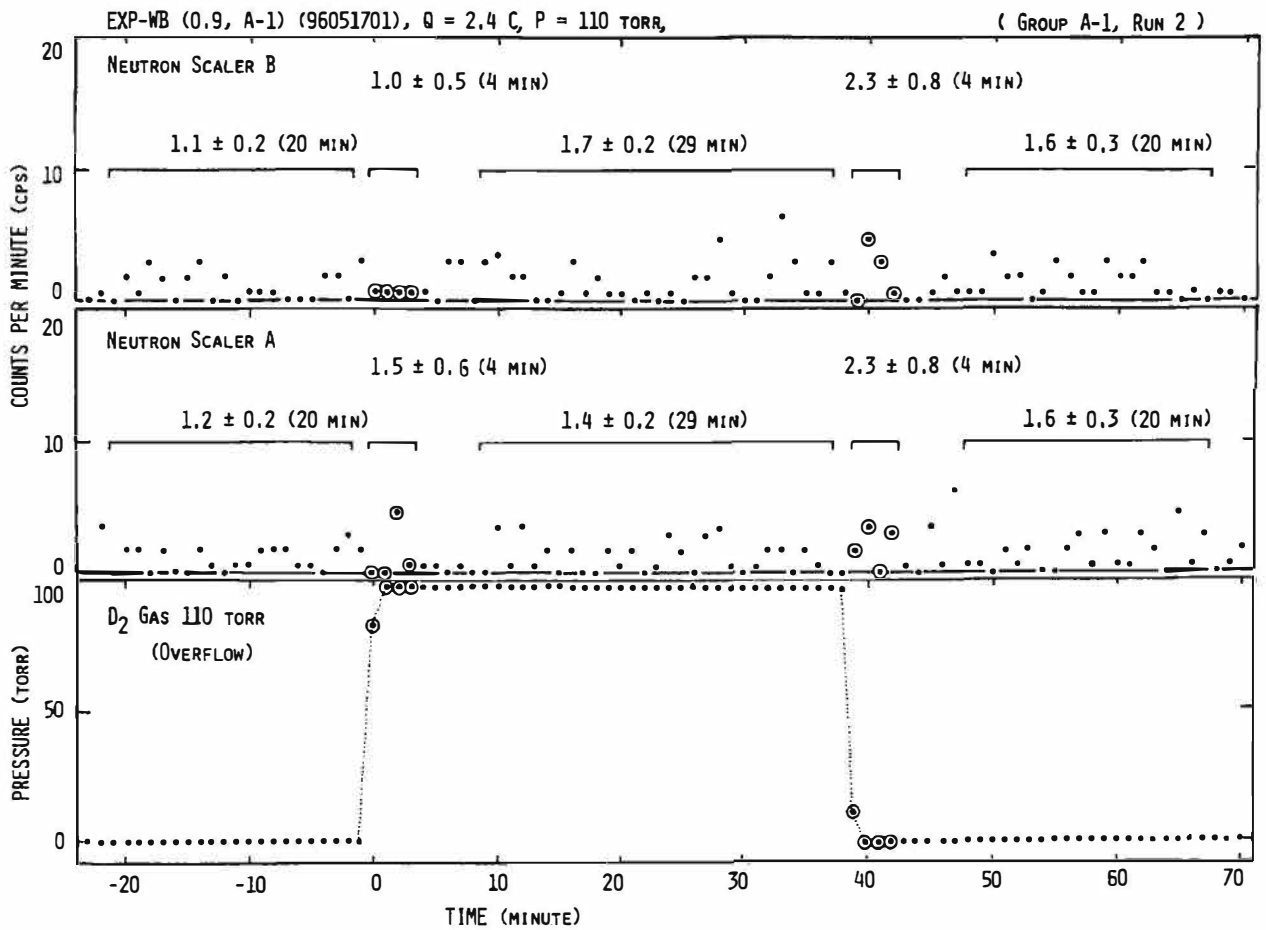

Fig. 1. The neutron counting rates and the deuterium gas pressure as a function of the time for Run No.2 in A-1 Group.

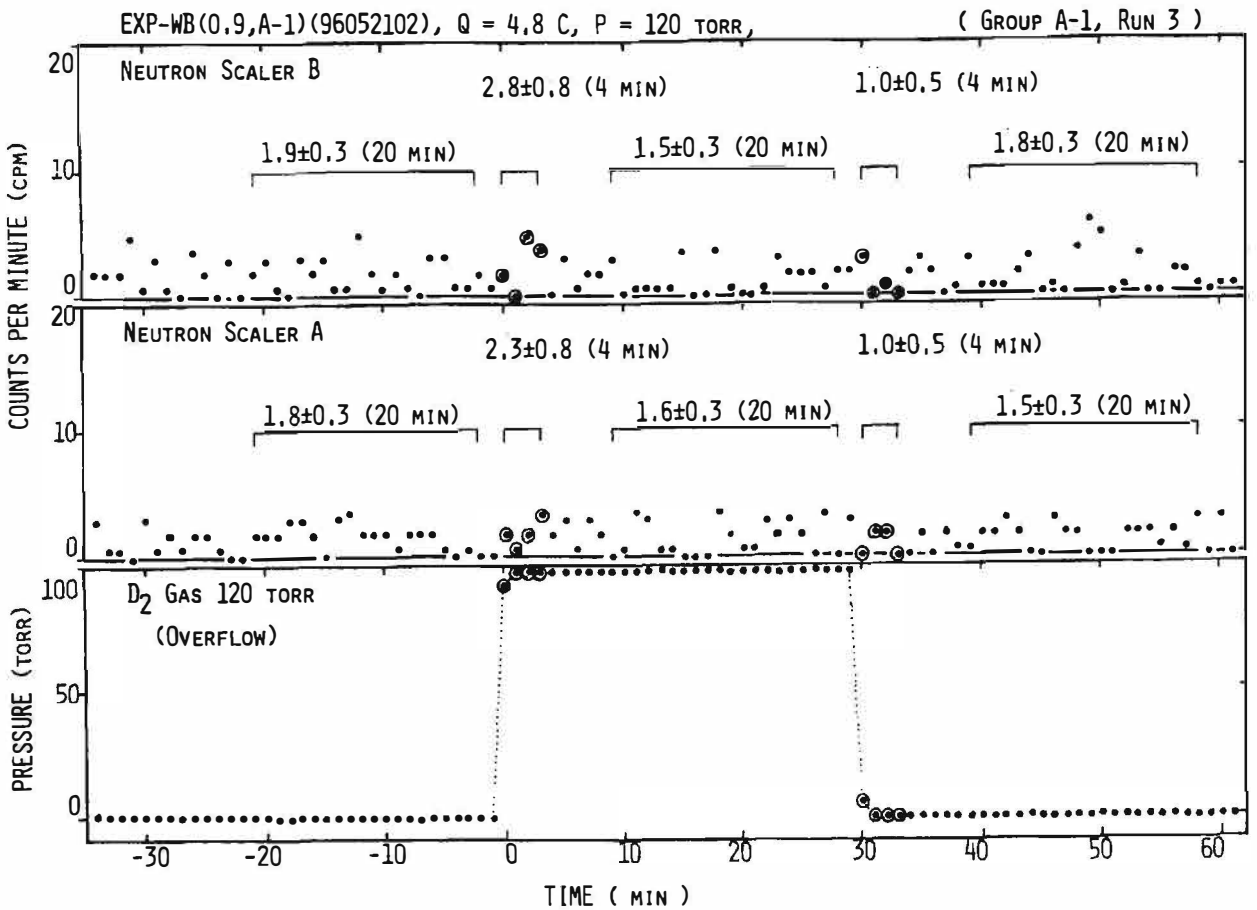

Fig. 2. The neutron counting rates and the deuterium pressure as a function of the time for Run No.3 in A-1 Group.

After finishing the cathodic treatment, the bronzes were cooled down. The application of the negative bias was stopped and the integrated charge was recorded. The pumping system and the vacuum valve were stopped. The measurements of the neutron counting rates and the deuterium gas pressure were started 30 minutes before the pressurizing the deuterium gas into the chamber, and were kept continued. It took 30 seconds to pressurize the gas up to 120 torr. After 30 minutes had passed ,the gas was evacuated to the pressure of 1×10^{-3} torr within 30 seconds. The measurements were ended at 30 minutes after the evacuation. The data collection was made every one minute. The total about 90 minutes elapsed time for the one measurement were divided into five time regions of interest (ROI). ROI 1 was 20 minutes elapsed time region just before the pressurization. ROI 2 was the 4 minutes time interval just after starting the pressurization. ROI 3 was 20 minutes time region before starting the evacuation. ROI 4 was the 4 minutes region after starting the evacuation. And ROI 5 was the 20 minutes region just before ending the measurement. The back ground neutron counting rates would be obtained in the ROI 1,3 and 5, while the expected increases of the rates might be found in the ROI 2 and 4. After finishing the first neutron measurement, the cathodic treatment was reapplied and was followed by the measurement again. Three or four cycles were made for the different heating temperatures and the integrated charges.

Ⅲ. Result and Discussion

The observed neutron counting rates and the deuterium pressure are shown in Fig.1 and Fig.2 as a function of the time for the A-1 bronze group with the different integrated charge Q = 2.4 C and 4.8 C, respectively. The weighted mean values of the counting rates as a function of the ROI number are shown in Fig.3 (A) and (B) for the A-1 group and the A-2 group with different Q values, respectively. The dotted lines represent the values for the three or four data points, which are given numerically. It is seen in the these Fig.'s that the expected values in the ROI 2 and 4 did not exceed the back ground values obtained in the ROI 1, 3 and 5. They agreed within one standard deviation. Therefore, the increases of the counting rates at the pressurization and the

depressurization were not observed in these runs. However, further investigations will be necessary varying the bronze composition x and the heating temperatures.

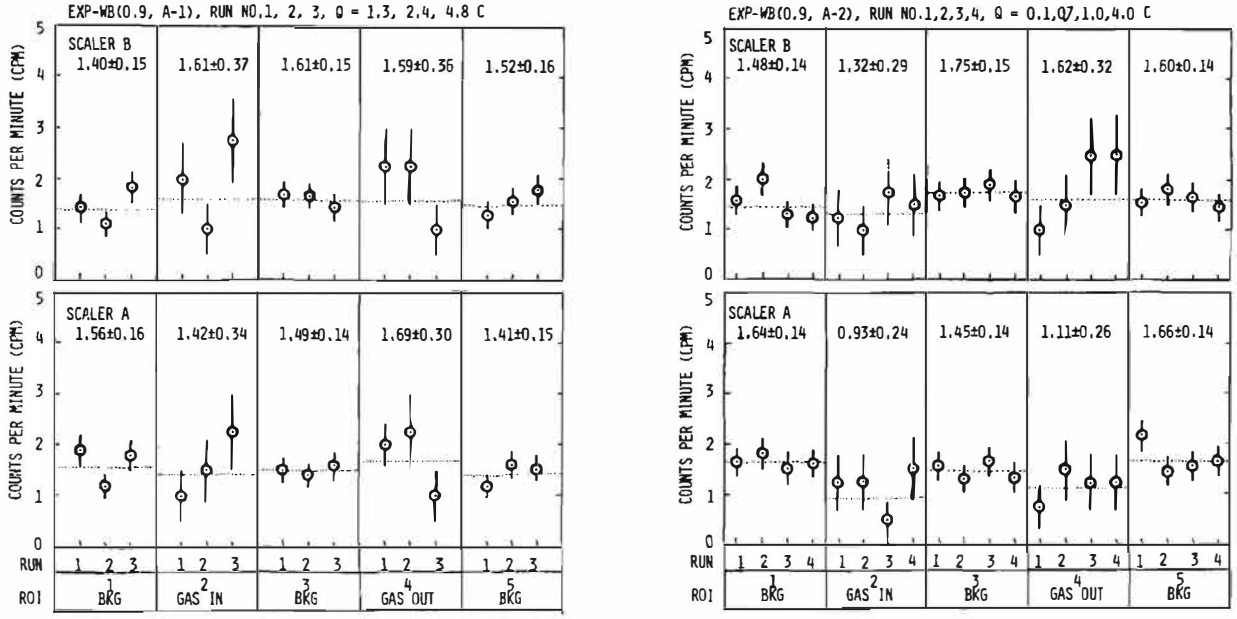

(A) **(B)**

Fig. 3. The weighted mean values of the counting rates as a function of ROI numbers. (A) for A-1 Group and (B) for A-2 Group with different Q values.

Ⅳ. Acknowledgments

We are gratefully acknowledge Drs. J. Kawamoto and K. Yamamoto (Toyota Central Res. & Develop.Labs. Inc.) to show us the fabrication method of the bronzes.

Ⅴ. References

(1) K. Kaliev et al, Proceedings of the Third International Conference on Cold Fusion, October 21-25. 1992, Nagoya, P241.
(2) R. A. Fredlein and Damjanovic, J. Solid State Chem. 4, (1972) 94-102
(3) "Comprehensive Inorganic Chemistry", ed. by J.C. Bailar et al., Permagon Press, 1975.
(4) private communication with Dr. J. Kawamoto.

Nuclear Physics Approach

Temperature dependency on counting efficiency of NE213 liquid scintillator for low level neutron measurements

Tadashi Akimoto, Tadahiko Mizuno, Takashi Saito,
Ikuo Murai and Toshiaki Kumada

Nuclear Engineering, Faculty of Engineering, Hokkaido University
Sapporo 060, Japan

Abstract

Examination of the temperature dependency on counting efficiency of a NE213 liquid scintillator showed that the efficiency decreased with the detector temperature. This was explained as a decrease in fluorescence emission of the scintillator with the temperature increase. Therefore, correction is needed for background data in electrolysis experiments.

1. Introduction

The measurement of neutron energy spectra is important to elucidate the mechanism of cold fusion phenomena. Many reports have shown that the neutron counting rate in the foreground measurement was as low as the background in studies of cold fusion[1]. We have measured neutron energy spectra in an electrolysis experiment over a long time by a liquid scintillator NE213 with a gamma-neutron pulse shape discrimination to detect 2.45 MeV neutrons. We found the counting rate of the detector decreases as the temperature rises in the detector. The temperature dependence for measurements of very weak level neutrons under the temperature difference between foreground and background measurements needs to be clarified. This is a report of the temperature dependence on the counting efficiency for the NE213 system.

2. Experimental

Detections of neutrons and pulse height analysis were performed in a laboratory where the temperature is very stable, under ground at the linear accelerator facility of Hokkaido University. The neutron detectors were set on both sides of the electrolysis cell filled with 0.5 mol LiOD of heavy water: the cell and the detector were shielded with boron mixed polyethylene. The detector temperature was continuously measured by an IC thermometer probe taped to the detector surface.

Another IC thermometer measured ambient temperature.

The measurement system for the neutron energy spectrum of the NE213 liquid scintillator (5" ϕ ×5"t) is shown in Fig.1. The NE213 is very efficient for fast neutrons and has good pulse-shape discrimination properties. The measurement system is composed of high (3 MeV for the neutron energy) and low gain (7 MeV) detection systems. The pulse shape discrimination was performed by a pulse rise time analysis system to eliminate background gamma rays.

The background measurements were first performed by changing the detector temperature to obtain the temperature dependence, and next the measurements were made by a ^{252}Cf spontaneous fission source. The detector temperature was changed by an electric heater surrounding the electrolysis cell and the neutron source was placed on the cell. Ambient temperature did not change. Neutron spectra of the source showed the Maxwell distribution with an average energy of 2.13 ± 0.027 MeV[2].

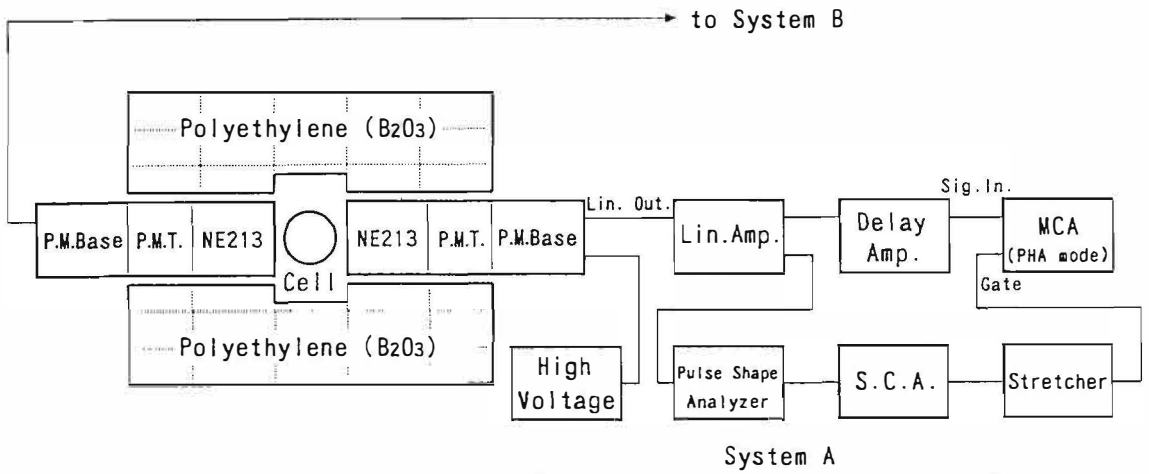

Fig.1 Measurement system for neutron energy spectrum

3. Results

3-1 Background measurement

Figure 2 shows the relation between the counting rates for background measurements integrated over the whole region of interest of pulse height data and the temperature of the detector by the high gain system. The data was stored every 8-16 hours and measurements continued for about two weeks at each temperature level. The regression analysis showed a tendency for the counting rate of NE213 to decrease with temperature rises. A similar tendency was observed in the low gain system. The relations between the counting rate and the temperature of the detector are obtained by the least squares method as follows:

High gain system: y=-0.00081x+0.056, Low gain system: y=-0.00105x+0.059

The correlation coefficients were 0.65 and 0.71 respectively. It is difficult to say if the value of the correlation coefficient is statistically significant, because of the large statistical error due to low counting rates.

Nuclear Physics Approach

3-2 Measurement by ^{252}Cf neutron source

The neutron pulse height distribution measurement was performed using a ^{252}Cf neutron source to obtain high counting rate data. Measurements were continued for 10,000 seconds at each temperature. Figure 3 shows the relation between the counting rate for the high gain system and the temperature. The relations between the counting rate and the temperature of the detector were obtained by the least squares method as follows:

High gain system: y=-0.092x+6.676, Low gain system: y=-0.096x+6.883

The correlation coefficients are 0.97 for both of them being 95% significant. Similarly, for the background measurements there was a decrease in the counting rate with the increase in temperature of the detector.

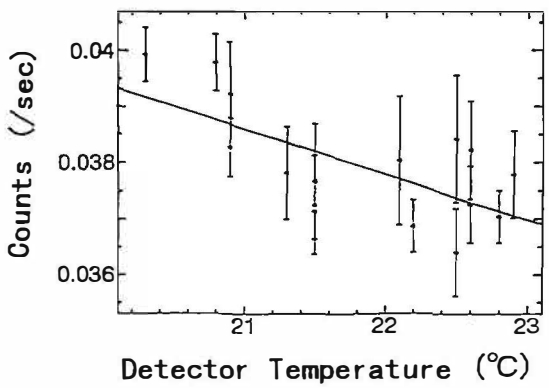

Fig.2 The relation between the counting rate for background measurements and the detector temperature (high gain system)

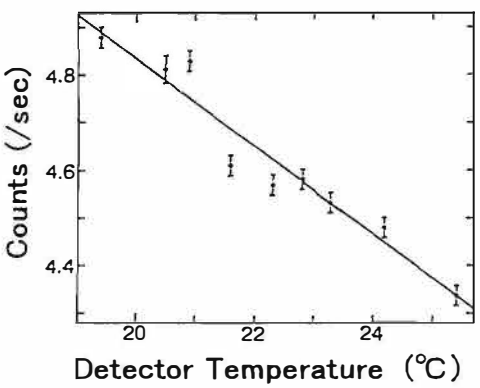

Fig.3 The relation between the counting rate for measurements by ^{252}Cf neutron source and the detector temperature (high gain system)

3-3 Discussion

All other instrumentation, except the detector, was kept a constant temperature during the measurements. Therefore, we are confident that we have isolated the effects of the changing temperature to the detector alone in this study. In previous studies we determined that when the temperature of photomultiplier rises, thermal noise increases, resulting in increased counts. One of the few other studies on the effects of temperature on the NE213 was performed by F.Ul-haq et al.[3] Their results support our findings.

The reason that the NE213 shows the temperature dependency is not certain. The two following causes for the temperature dependency of NE213 may be postulated: (1) If the temperature rises, the fluorescence efficiency (light output per unit energy) of the scintillator becomes small. (2) The rise time of output pulse from the scintillator shortens when the temperature rises.

(1) Change in fluorescence efficiency of the scintillator

The pulse height from the recoil proton becomes small if the temperature of the scintillator rises. The proton is of lower energy than that at the low detector temperature as shown in Fig.4(a). Therefore,

the spectrum shifts to the low energy side and the total counts in the region of interest decreases as shown in Fig.4(b).

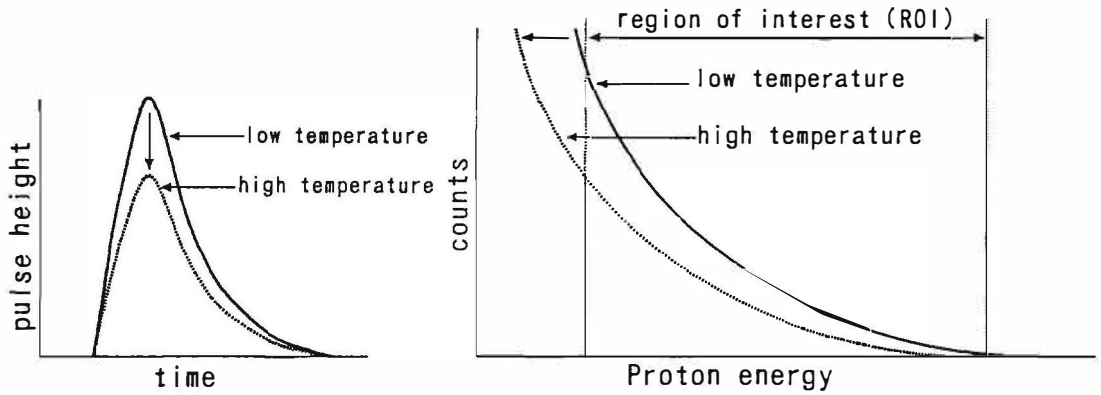

(a) pulse shape (b) pulse height spectra

Fig.4 Pulse shape and pulase height spectra of proton

The pulse height data from Fig.2 was divided into five pulse height regions. The relation of counting rate at each pulse height region and the detector temperature is shown in Fig.5. The decrease in the counting rate of the low pulse height region is larger than that of high pulse height region. The pulse height shift on the low pulse height region is remarkable, and the entire spectrum shifts to the lower pulse height side as the temperature rises. The fluorescence efficiency of the scintillator becomes smaller as the temperature rises.

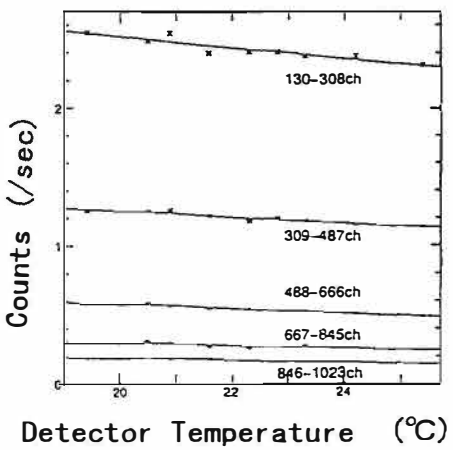

Fig.5 Change of counting rate of five pulse height regions as a function of detector temperature

(2) Changing of rise time

The rise time spectrum of the detector output pulse is shown as Fig.6, at low detector temperature, and the rejection level of the γ -ray is set at level c. The rise time spectrum shifts to b when the rise time shortens due to increased temperature. First, a signal with a rise time in the shifting part (shown in the area with slashes) is recognized as a neutron signal. This is recognized as a gamma ray signal at the high temperature, and is not counted. Therefore, the counting rate decreases.

The rise time spectrum of the gamma ray and the neutron signal were measured as the temperature of the detector was changed. The detector temperature was changed by an electric heater surrounding the electrolysis cell as well as the pulse-height distribution measurements. Shifts in peak and dip channels were observed with the temperature change.

Figure 7 shows the relation between the detector temperature and the channel number of rise time

of neutron and gamma ray peak and γ -n dip channel. The straight line was obtained by the least squares method. The peak channels of the gamma ray and neutron, and the γ -n dip channel are almost constant. This shows that the rise time does not depend on the detector temperature.

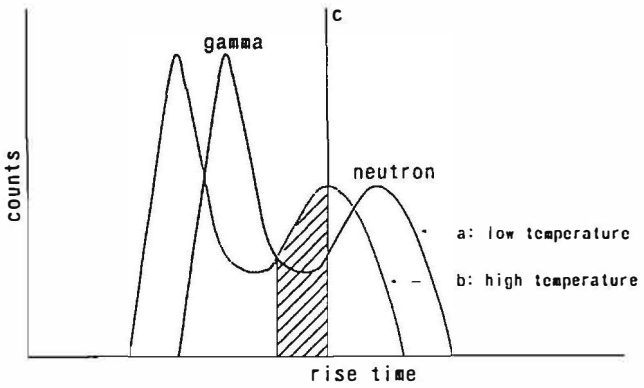

Fig.6 Neutron-gamma rise time spectra

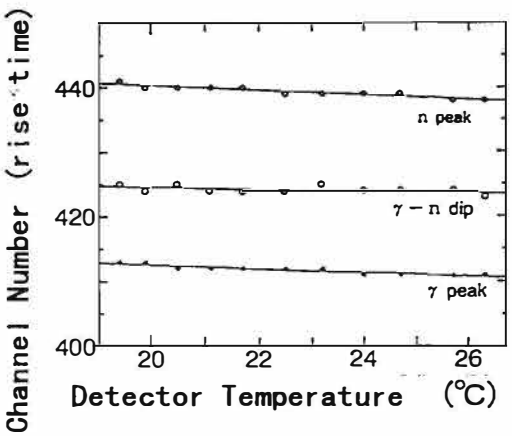

Fig.7 Temperature dependency of NE213 on rise time of output pulse

4. Conclusion

In this study the temperature dependency of a NE213 on the counting efficiency in low level neutron measurements was examined experimentally. Conclusions and a problem for the future are as follows:

(1) It was confirmed that the counting efficiency of the NE213 detector decreases as the detector temperature rises.

(2) In neutron spectra measurements by the NE213 under conditions where the temperature of foreground measurements is different from background measurements, such as occur in electrolysis experiments, the influence of the temperature dependency of the detector on the counting rate is large. It is necessary to examine the temperature dependence of the detector in detail and to determine correction factors for the background data.

(3) It is thought that the fluorescence efficiency of the scintillator will decrease with higher temperature and the changes in fluorescence intensity is due to changes in the absolute scintillation efficiency. A precise analysis of the temperature dependency of the energy transfer between molecules, the specific energy loss, and the velocity constant of photon emission is necessary. Experiments by a monoenergy neutron source are also necessary.

References

1) S.E. Jones et al.: Nature, 338, p.737 (1989)

2)L. Green et al.: Nucl. Sci. Eng., 50, p.257 (1973)

3)F.Ul-haq, M.Z. Butt, W. Ali, S. Jamil and S.A. Durrani: Radiation Effects and Defects in Solids, 115, p.135-137 (1990)

Nuclear Physics Approach

Nonlinear Barrier Penetration and Cold Fusion

Chang Yi-Fang
Department of Physics, Yunnan University,
Kunming, 650091, CHINA
Liu Zheng-Rong
Department of Mathematics, Yunnan University,
Kunming, 650091, CHINA

Abstract
The great difficulty of cold fusion as the nuclear reaction is the barrier penetration. The quantilativite calculation of the multistage chain reaction theory can explain some experimental facts of cold fusion. Further, we propose a new mechanism, the nonlinear barrier penetration. Its quantilativite results show some new characters even in a simplied model, for example, the penetration factor has a periodicity with the barrier thinckness. This is a new method which may be developed and applied further.

1. Introduction

At the present it shows by more and more experiments that cold fusion should be the nuclear reaction, including nuclear fusion and fission, because some new elements which do not exist in the beginning of experiments appear. For instance, a large number of triton appears [1], helium produces in Yamaguchi's and Takahashi's experiments, rhodium appears in deuterium of Karabut's glow discharge [2], the abundance ratio of Sr-88 to Sr-86 shifts [3], etc. The most puzzling problem on the theory of cold fusion is the barrier penetration, which is too small in comparison with the experimental facts. In order to explain this contradiction, based on the standart quantum theory, we have derived the multistage chain reaction theory [4]. In this paper we propose a new penetration mechanism based on the nonlinear quantum mechanics.

2. Multistage chain reaction theory of cold fusion

From various internal conversion mechanism on cold fusion, or from collisions

and interactions among various particles and nuclei [4], we have derived the multistage chain reaction theory of cold fusion : the first chain reactions are

$$e^- + D \rightarrow 2n + \nu_e, \tag{1}$$

$$2n + D \rightarrow {}^4H^* \rightarrow {}^4He + e^- + \bar{\nu}_e, \tag{2}$$

$$e^- + D \rightarrow 2n + \nu_e \cdots \tag{1}$$

The second reactions are

$$e^- + p \rightarrow n + \nu_e, \tag{3}$$

$$n + p \rightarrow D, \tag{4}$$

$$e^- + D \rightarrow 2n + \nu_e \cdots \tag{1}$$

According to the barrier penetration of quantum mechanics, the penetration factor is

$$D_p = \exp\left\{-\frac{2}{\hbar}\int_a^b [2m(U-E)]^{1/2} \mathrm{d}r\right\}. \tag{5}$$

If U is the Coulomb potential ke^2/r, $a = R$ is the distance of interaction between incident particle and target, $b = r_0 = ke^2/E$,

$$D_p = \exp\left\{-\frac{2}{\hbar}\sqrt{2m}\left[-\frac{ke^2}{\sqrt{E}}\mathrm{arctg}\left(\frac{ke^2}{RE}-1\right)^{1/2} - \left(\frac{ke^2}{R}-E\right)^{1/2}R\right]\right\}. \tag{6}$$

For $D + Pd^{106}$, because $m = 1876.0289\mathrm{MeV}/c^2$, $R = 1.25A^{1/3} = 5.9158\mathrm{fm}$, $k = Z = 46$, even if $E = 240\mathrm{KeV}$, $D_p = 9.64827 \times 10^{-52}$. It is too small. According to the multistage chain reaction theory, for the reaction (1), $m_e = 0.511\mathrm{MeV}$, $E = 220\mathrm{eV}$ is the energy of electron, $k = Z = 1$, $R = 1.5749\mathrm{fm}$, so the penetration factor of electron–deuteron is $D_p = 1.7767 \times 10^{-13}$. Since the section ratio between deuteron and D–atom is about 3.814×10^{-11}, the penetration probability of nuclear reaction between an electron, whose energy is $E = 220\mathrm{eV}$, and a D–atom is 6.777×10^{-24}, and the number of D–atom is 1.6×10^{15} per cm^2. It is consistent with Jones' experiment [5] and with Manduchi's result [6]. The current density is $\rho = 400\mathrm{mA}/\mathrm{cm}^2 = 2.5 \times 10^{18}$ electron $/ \mathrm{scm}^2$, the size of a rod cathode is $0.4 \times 1.25 = 0.5\mathrm{cm}^2$, and $t = 6\mathrm{day} = 5.184 \times 10^5\mathrm{s}$ in Fig.1 of Ref. [7], so the total rate is $2.712 \times 10^{10}/\mathrm{scm}^2$. From the total reaction

$$D + D \rightarrow {}^4He + \nu_e + \bar{\nu}_e({}^4He + 23.9\mathrm{MeV}), \tag{7}$$

the total released energy is $2.69 \times 10^4\mathrm{J}$. It agrees completely with this result 26KJ

in the Fig.1. In a word, the nuclear reactions and the nuclear phenomena are complex process, in particular, when time accumulate continuously.

3. Nonlinear Barrier Penetration

So far, all theories of the barrier penetration are based on the linear quantum mechanics, for example, the Schrödinger equation. Combining the nonlinear quantum theory, which was developed at present, assume that a separate incident particle likes a solitary wave, and obeys a nonlinear Schrödinger equation

$$\psi_{xx} + i\psi_t - 2a^2\psi^3 = 0. \tag{8}$$

For the stable state and a square potential barrier,

$$U = \begin{cases} 0 & (x < 0,\ x > d) \\ V_0 & (0 < x < d) \end{cases}$$

the equation (8) bacomes,

$$\frac{d^2\psi}{dx^2} + k_1^2\psi - 2a^2\psi^3 = 0 \quad \text{for} \quad x < 0, \text{ or } x > d. \tag{9}$$

$$\frac{d^2\psi}{dx^2} + k_2^2\psi - 2a^2\psi^3 = 0 \quad \text{for} \quad 0 < x < d. \tag{10}$$

where

$$k_1^2 = \frac{2m}{\hbar^2}E, \qquad k_2^2 = \frac{2m}{\hbar^2}(E - V_0),$$

Let the integral constants $c_0 = 0$, $c_1 = k_1^4 / 4a^2$, when $|\psi| < k_1 / \sqrt{2}a$, a particular solution is

$$\psi_1 = \frac{k_1}{\sqrt{2}a} \cdot \frac{A^2 e^{\sqrt{2}k_1 x} - 1}{A^2 e^{\sqrt{2}k_1 x} + 1} \qquad (\text{for } x < 0), \tag{11}$$

or

$$\psi_3 = \frac{k_1}{\sqrt{2}a} \cdot \frac{C^2 e^{\sqrt{2}k_1 x} - 1}{C^2 e^{\sqrt{2}k_1 x} + 1} \qquad (\text{for } x > d). \tag{11}'$$

It shows that this particle corresponds a soliton. When $V_0 > E$, $k_2^2 < 0$, let $k_2'^2 = -k_2^2 = 2m(V_0 - E)/\hbar^2 > 0$, $c_0 = 0$, $c_1 = k_2'^4 / 4a^2$,

$$\psi_2 = k_2' \mathrm{tg}(k_2' x / \sqrt{2} + B) / \sqrt{2}a \tag{12}$$

According to the continuity conditions at points $x = 0$ and $x = d$,

$$\mathrm{tg}B = \frac{1}{k}\frac{A^2 - 1}{A^2 + 1}, \qquad \mathrm{tg}\left(\frac{k_2'}{\sqrt{2}}d + B\right) = \frac{1}{k}\frac{C^2 e^{\sqrt{2}k_1 d} - 1}{C^2 e^{\sqrt{2}k_1 d} + 1}, \tag{13}$$

Nuclear Physics Approach

where $$k = \frac{k_2'}{k_1} = \sqrt{\frac{V_0}{E} - 1}\ . \tag{14}$$

From above we obtain

$$A^2 = \frac{\mathrm{tg}\left(\frac{k_2'}{\sqrt{2}}d\right)[C^2 e^{\sqrt{2}k_1 d}(1-k^2) - (1+k^2)] + 2kC^2 e^{\sqrt{2}k_1 d}}{\mathrm{tg}\left(\frac{k_2'}{\sqrt{2}}d\right)[C^2 e^{\sqrt{2}k_1 d}(1+k^2) - (1-k^2)] + 2k}. \tag{15}$$

One-order approximation is $C^2 / A^2 = e^{-\sqrt{2}k_1 d}$. In the linear theory, the penetration factor is $D_p = |C^2 / A^2|$.

In the nonlinear theory, a probability current density is still

$$J = \frac{i\hbar}{2m}(\psi \nabla \psi^* - \psi^* \nabla \psi), \tag{16}$$

In this case,

$$\psi^* = \frac{k_1}{\sqrt{2}\,a}\mathrm{tg}\left(\frac{k_1}{\sqrt{2}}x + A'\right), \tag{17}$$

Therefore, the penetration factor is

$$D_p = \frac{(A^2 e^{\sqrt{2}k_1 d} + 1)^2 \cos^2\left(\frac{k_1}{\sqrt{2}}d + A'\right)}{(C^2 e^{\sqrt{2}k_1 d} + 1)^2 \cos^2\left(\frac{k_1}{\sqrt{2}}d + C'\right)} \times \frac{[(C^2 e^{\sqrt{2}k_1 d})^2 - 1 - 2\sin(\sqrt{2}k_1 d + 2C')]}{[(A^2 e^{\sqrt{2}k_1 d})^2 - 1 - 2\sin(\sqrt{2}k_1 d + 2A')]}. \tag{18}$$

where $$\mathrm{tg}A' = \frac{1-A^2}{1+A^2}, \qquad \mathrm{tg}C' = \frac{1-C^2}{1+C^2}.$$

The one-order approximation is $D_p \sim 1$. It is just a character of the soliton, which has an invariant shape for the collision. But, the calculating results show that D_p has a periodicity with d (barrier thickness), when those other quantities are difinited (Fig. 1). Although it is irrational that D_p tends toward infinite because of the tangert function, Fig. 1 possesses some similar rules with the shape of Fig. 4 in Ref.[7], where d becomes the four-dimensional time-space, and D_p is directly proportional to the number of reaction particle, the released energy and temperature. Therefore, it may be a new basis of the various resonance-penetration theories of cold fusion.

4. Discussion

Based on the known theory, some experimental results may be explained quantilativitely by the multistage chain reaction theory. But a fundamental outlet is possibly the barrier penetration of nonlinear quantum mechanics. It shows some new characters even in a simplied model. Further, the different nonlinear equations and their various solutions (kink, chaos, instanton, string, etc.) may be obtained, this new method can be discussed by the details, and may be applied to explain other experiments.

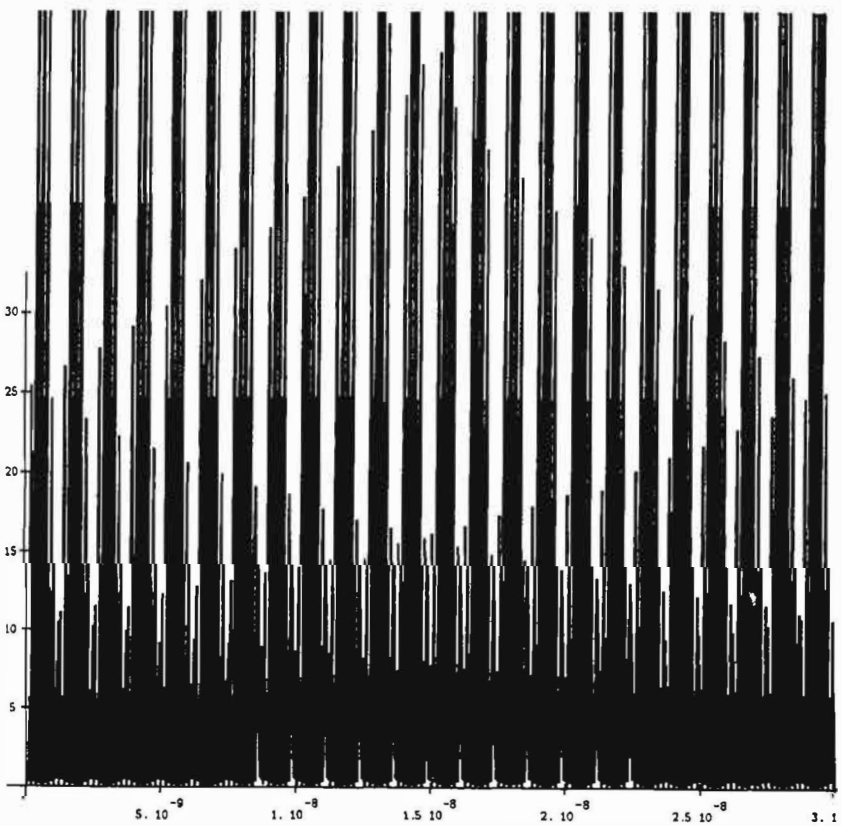

Fig. 1. Segment of D_p–d

[1] M.Fleischmann, S.Pons and G.Preparata: Nuovo Cimento A.107, 143(1994).
[2] A.B.Karabut, et al.: Phys. Lett A.170, 265(1992).
[3] H.Fox, ed. Cold Fusion Source Book. Minsk, Belarus. May 24-26(1994).
[4] Yi-Fang Chang and Chuan-Zan Yu: Fusion Facts (ICCF 5). 6, 11, 15(1995).
[5] J.E.Jones, E.P.Palmer, et al.: Nature. 338, 737(1989).
[6] C.Manduchi, G.Zannoni, et al.: Nuovo Cimento A.107, 171(1994).
[7] M.Fleischmann and S.Pons: Phys. Lett A.176, 118(1993).

Nuclear Physics Approach

About Nuclear Coulomb Barrier and The Electron Over-Concentration

Dan Chicea
Physics Dept., University "Lucian Blaga", Str. Dr. Ion Ratiu 5-7,
Sibiu, 2400, Romania; email: chicea@sibiu.ro

Abstract

When a conductor is the subject of a negative electric potential an electron concentration increase, located very near the surface occurs. A simple model for computing the increase of electron concentration on a grainy metal surface caused by an applied negative potential is presented and used in calculating the excess electron concentration and the size of the electric charge layer. The screening effect caused by the high negative electric charge density is considered for assessing the transparency of the nuclear Coulomb barrier at low incident energies. The results are discussed in connection with the processes grouped in the Cold Fusion class [1].

Introduction

When a conductor is the subject of an applied electric potential, it receives an excess electric charge proportional to the potential value. It is stated in the literature [2] that the charge in excess is located on the conductor surface. If the electric potential is negative, an excess of electrons will be located on the conductor and if the potential is positive, uncompensated positive ions will exist. The electrons in excess can not be outside the conductor in case of a negative potential because once expelled, they will be repelled by the Coulomb force and they will not contribute to the negative potential, therefore they must be located in a layer right under the surface.

The size of the shell and the excess electron concentration are calculated hereafter.

The Electron Excess Concentration

When a fluctuation of the electron concentration, consisting of a layer of electrons escaping from a layer of positive ions occurs in a plasma, the size of the displacement can be calculated from the condition that the electric interaction energy equals the thermal kinetic energy. The size of the displacement, called the Debye length [3], is given by:

$$l_D = \sqrt{\frac{\varepsilon_0 \cdot k \cdot T}{n_0 \cdot e^2}} \qquad (1)$$

where ε_0 is the free space constant, k is Boltzman's constant, T the temperature (K), e is the electron electric charge and n_0 the ion concentration in a plasma.

The hypothesis of the model is that the gradient of the electron concentration near the metal surface is equal to n_0/l_D [4], which leads to a linear increase of the electron excess concentration towards the surface. Defining the electron excess concentration n_e as the difference between the actual electron concentration, n, and the free electron concentration in the

absence of the applied electric potential, n_0, and forcing the border condition that the electron excess concentration must be zero at a radius r=R-D, n_e is given by:

$$n_e(r) = \frac{n_0}{l_D} \cdot (r - R + D) \quad \text{for } r \in [R - D, R]$$
$$n_e(r) = 0 \quad \text{for } r \in [0, R - D] \tag{2}$$

If we consider a grain on the metal surface with a negative electric potential U, having a spherical shape of radius R (figure 1), then the total electric charge on the grain, Q, located under the surface in a layer with the thickness D, is connected to the value U through (3) where ε is the permittivity of the substance the conductor is located in.

$$U = \frac{Q}{4 \cdot \pi \cdot \varepsilon \cdot R} \tag{3}$$

Considering an average value of the excess electron concentration to be half of the maximum value with respect to the linear variation with the radius, and with the observation that D is comparable with the Debye length which is much smaller than the radius of the grain, the condition that Q should be located in the layer can be written:

$$\frac{1}{2} \cdot \frac{n_0 \cdot D \cdot e}{l_D} \cdot 4 \cdot \pi \cdot R^2 \cdot D = 4 \cdot \pi \cdot \varepsilon \cdot R \cdot U \tag{4}$$

therefore D can be expressed as:

$$D = \sqrt{\frac{2 \cdot \varepsilon \cdot U \cdot l_D}{e \cdot R \cdot n_0}} \tag{5}$$

and the average electron excess concentration as (6):

$$n_m = \sqrt{\frac{\varepsilon \cdot n_0 \cdot U}{2 \cdot l_D \cdot e \cdot R}} \tag{6}$$

The computed values of the electron excess concentration, for three values of the radius, 0.01 μm (upper curve), 0.1 μm (middle curve) and 1 μm (lower curve) respectively, (values consistent with the grain sizes mentioned in [5]), are plotted versus the negative electric potential in figure 1, the conductor being placed in free space.

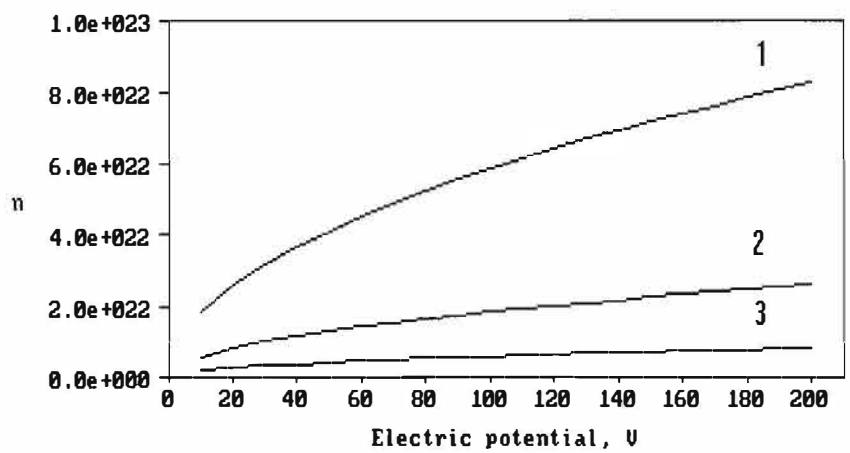

Figure 1: Electron excess concentration (cm^{-3}), for three values of the radius, 0.01μm (1), 0.1μm (2) and 1 μm (3).

A value of a few hundred volts for a small grain on the surface will make the excess electron concentration to be of the magnitude 10^{23} cm^{-3} which is relatively high compared to the concentration of free electrons in palladium, $6.25*10^{22}$ cm^{-3}. If the conductor is placed in a substance with the relative electric permittivity ε_r over-unity, or if the surface is covered with oxide, as mentioned in [6], the electron excess concentration increases as many times as the square root of ε_r, accordingly to (6).

The Screened Coulomb Barrier

In order to describe the screening of the Coulomb barrier a Thomas-Fermi-like effective interaction potential V(r) between two ions has been used [7]; the screening length has been considered to be l_D, the Debye length.

$$V(r) = \frac{e^2}{4 \cdot \pi \cdot \varepsilon \cdot r^2} \cdot \exp\left(-\frac{r}{l_D}\right) \qquad (7)$$

The barrier penetration probability P has been numerically integrated for the values of the Debye length corresponding to several electron concentration, using the WKB approximation. The (decimal) logarithm of the probability is plotted versus the (decimal) logarithm of the electron concentration (m^{-3}), for three values of the incident deuterium ion energy, in figure 2 (5 eV lower curve, 50 eV the middle and 500 eV the upper curve).

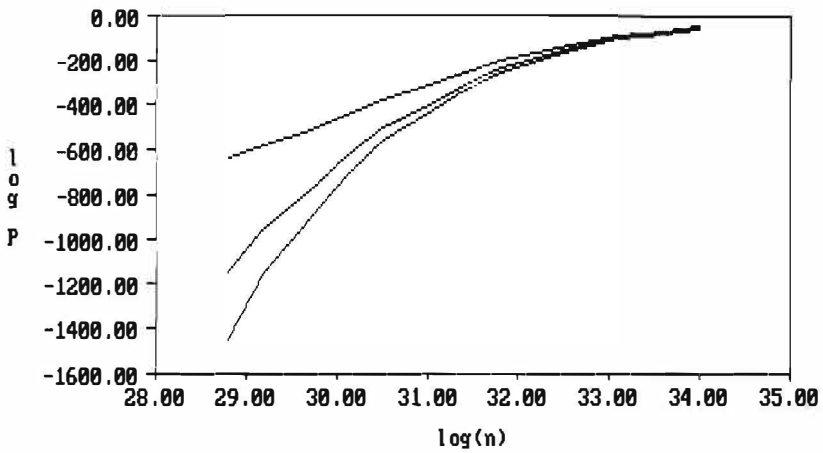

Figure 1: The Coulomb barrier penetration probability versus the electron concentration (m^{-3}), for three values of the deuteron energy, 5 eV lower curve, 50 eV the middle and 500 eV the upper curve.

If we consider the volume rate of the fusion reaction W [8] of two deuterons to be (8):

$$W = \frac{1}{2} n_D^2 < \sigma v > \qquad (8)$$

were σ is the nuclear reaction cross-section, n_D is the concentration of the deuterons trapped in a metal's lattice, like in palladium, of the magnitude of 10^{22} cm^{-3} for a high loading ratio and $W_{min}=10^{-3}$ $cm^{-3}s^{-1}$ the minimum detectable reaction rate [8], and if we write the cross section of the reaction as $\sigma=\sigma_0 P$ with $\sigma_0 = 10^{-24}$ cm^2 [8], assuming an average velocity of 10^8 $cm \cdot s^{-1}$ [8], if the deuterons are considered to be flowing resonantly through the palladium lattice [9], we find a minimum detectable value of 10^{-30} - 10^{-32} for P, which is far too high to be achieved by means of electron screening in the absence of an acceleration mechanism [10].

Conclusion

The simple model described in this paper was used to calculate the increase of the electron concentration near the grainy metal surface. The values of the "free" electron concentration can double themselves for a negative electric voltage of the magnitude of a hundred volts and can increase further more if the surface is covered by oxide. The increase of the deuterium nuclear fusion reaction cross section produced by the electron screening, can not represent the only possible explanation for the processes involved in the heat excess described in many experimental works.

Acknowledgments

I fully acknowledge Dr. Gheorghe Vasaru and Dr. Peter Glück for their help, encouragement and fruitful discussions.

References

[1] M. Fleischman, S. Pons, Phys. Lett. A 176, (1993), 118.
[2] Hudson A., Nelson R., University Physics, 2nd ed. (Sounders College Publishing, 1990)
[3] Linhart J.G., Plasma Physics, (EURATOM, 1969).
[4] Chicea D., Vasaru Gh., Submitted to Surface Science Letters.
[5] Reifenschweiler O., Phys. Lett. A 184 (1994), 149.
[6] Chatterje L. & all, Ind. J. of Pure and Appl. Phys., 65, No. 2, (1993), 265.
[7] Ichimaru S., Rev. Mod. Phys., 65, No.2 , (1993), 265.
[8] Goldanskii V.I., Dalidchik F.I., Phys. Lett. B 234, no. 4, (1990), 465.
[9] Bush R., Fusion Technology 19 (1991), 313.
[10] Chicea D., "Cold Fusion" No. 14, (1995), 2.

Nuclear Physics Approach

ON THE COLD FUSION MIRACLES

Swe-Kai Chen, the Materials Science Center, National Tsing Hua University, Kuang-Fu Road Sec. II, Hsinchu 30043, TAIWAN

Abstract

This paper consists of two parts. One part describes a new analytical method for the conventional electrolytic cold fusion experiment. The other part contains a discussion and explanation on the cold fusion effect. Heat bursts are observed in this experiment for both Ni(-)/Pt(+)/H_2O/K_2CO_3 and Pd(-)/Pt(+)/D_2O/LiOD cells. Careful detection of neutron and tritium has not been available, although very preliminary neutron detection of heavy water cell shows roughly two times of the background level during electrolysis. The vast experimental data worldwide show a low neutron-tritium ratio of 10^{-8} to 10^{-4}, far below the equal branching ratio, having been explained in this paper by a secondary nuclear process by the author. According to this secondary nuclear process, the generated neutrons and protons inside the solid has the chance to recombine into deuterium atoms for heavy water systems. In this sense the Huizenga's second and third miracles, the branching ratio miracle and the no nuclear products miracle, are therefore equivalent. This paper also proposes a "pycnon field" to try to treat the correlation of the high d/Pd ratio and pycno-reactions. Although the detail has not been worked out yet.

Introduction

An accurate calibration curve for heat is difficult to obtain even for a close-type electrolysis cell. However, a comparison among temperatures in cell, T_{cell}, temperatures in circulating water bath, T_{bath}, and input powers, W, in the same time period, shows an easier alternative for this matter. This method can also apply to an open cell system. Therefore it uses an open cell system in this experiment to illustrate the method.

In the paper entitled "Opposition and support for cold fusion" by Rabinowitz et al. [1], they mentioned the challenge of cold fusion with Huizenga's three miracles [2], (a) the fusion rate miracle, (b) the branching ratio miracle, and (c) the no nuclear products miracle. The review of experimental observations by Storms [3] has listed all the up-to-date reported data before 1991, showing the fact of Huizenga's challenge. Of the support most came from experimenters, while those of the opposition came from theorists. The miracles result from the fact that experimental data and observations cannot fit the conventional theory. It is no wonder that the effect is hard to consider as a fusion.

In a "Letter to the Editor," to Fusion Technology [4], Chen proposed a "fast neutron model" or "secondary nuclear fusion model" to explain the Huizenga's miracles. It is the second purpose of this paper to further discuss this model. Because the condition of the high d/Pd ratio for a high loading cathode is similar to that in stars where high pressure exists and pycno-reactions occur [5]. The high d/Pd ratio is one of the essential factors for generation of the cold fusion effect. Treating the field where the primary and secondary fusion reactions can occur, like that of the meson field, herein a "pycnon field" is proposed.

Experimental

Nuclear Physics Approach

The cell is a double-layered quartz tube with inner and outer diameters of 63.7 mm and 97.5 mm, respectively. The cell height is approximately 120.6 mm and the cell volume is about 400 ml. When the electrodes and detectors are in the cell the net volume of the solution is about 350 ml. Cooling water circulates inside the double layer of the cell and a temperature-controlled bath. The bath is with a totally 5,000 ml of water and with a pumping capacity of 15,000 ml/min. To start the experiment the bath is initially set at 55 ℃. A power supply can operate with controlled-current or voltage mode, and is with a maximal output of 300 watts. The accuracy of the power supply is plus or minus 0.1 ampere or volt. The cathode is a Ni or a Pd rod with 4.7 mm in diameter and 120 mm in length and the anode is a Pt wire with 0.1 mm in diameter. The shape of the Pt anode winding is a cylinder using a quartz sketch for support of the wire winding. The cathode is placed in the center of the Pt winding. The electrolyte of the Ni-Pt cells is light water solution of K_2CO_3, while that of the Pd-Pt cells is heavy water solution of LiOD. The cell current, I, and voltage, V, are measured once per minute with sensors. They transform into signals that can be read in a computer system to an accuracy of plus or minus 0.01 ampere or volt. Temperature readings are through Pt electric resistors and the computer minute by minute, with a measuring accuracy of plus or minus 0.01 ℃. Each resistor inserts in a quartz tube. The Ni rod melts in a VAR, homogenizes, forges, anneals and swages in laboratory. The Pd rod is from an outside supplier. A Dewar buffer helps the circulating water to keep temperature stability of the system during electrolysis. Current keeps below 10 amperes to avoid the leading head of the Pt wire to melt. Total cell resistance, R, which is the quotient of the cell voltage to the cell current, is always kept from 2 to 9 ohms.

There are two kinds of electrolytic operations, one for manual-controlled change and the other for change controlled by the cell itself. The measured cell-controlled voltages vary by a range of 2 volts during electrolysis, although there is a constant manual-controlled voltage. For a controlled-voltage mode, the V-I and W-I (W=VI, see Fig.1) relations are almost linear functions with a negative slope and a positive slope, respectively. The R-I curve is almost inversely linear dependence during electrolysis. This is due to the small value, i.e., 0.4-1 ohm, of the connecting resistance in the electric circuit. However, one can see the "average" of the manual-controlled values of currents and voltages roughly obey the Ohm's law (Fig.2). There are similar curves in a V-I, W-I, or R-I plot, each corresponding to a specific composition of cell parameters. These parameters contain the following factors: the degree of the cell temperature, the extent and concentration of the solution, the loading degree of the H or D atoms in cathode rods, conditions of the cathode rods, and the action of addition of H_2O or D_2O into the cell (For keeping a constant

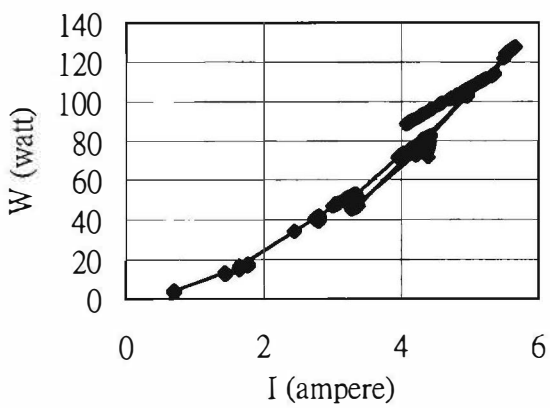

Fig. 1. The plot of W-I for a Pd/Pt/D_2O/LiOD cell

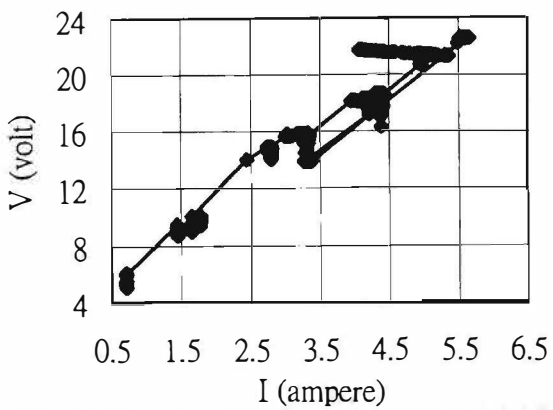

Fig. 2. The plot of V-I for a Pd/Pt/D_2O/LiOD cell

solution extent in the electrolysis cell). One can have two kinds of filling of water, i.e., by manual or by an automatic device with a level sensor. The manual-charge of light or heavy water changes

the cell electrolytic condition violently, as compared with the automatic charge of water. A black film deposits to the surface of the electrodes and precipitates in solution. Chemical analysis of the black film and precipitation with the ionized coupled plasma method (ICP) show a composition of mainly Pt (78.7 %, see below). A magnetic stirrer uses in the cell in order to keep a homogeneous distribution of cell temperature. To make sure that the bath temperature is supplied from the cooling of the cell, the circulating power of the bath is checked every minute in experiment. All curves in this experiment have lines, each connecting two time-consecutive points.

Results and Discussion

The $Ni/Pt/H_2O/K_2CO_3$ electrolysis cell

The chronicle record of T_{bath} shows two heat bursts during electrolysis (Fig. 3). One can see from the record of measured power (Fig. 4) that for heat burst at $35{,}200^{th}$ minute there is a five-watt increase, induced by manual filling of H_2O in the cell. For heat burst of $35{,}400^{th}$ minute there is a big increase in power, 70 watts, also induced by filling of H_2O in the cell. In electrolysis process total amount of K_2CO_3 keeps nearly constant. No K_2CO_3 is added in the cell. Not every time of H_2O filling can rise the measured power. It depends on the cathode condition. If one is checking the hysteresis loop of T_{bath} to T_{cell} for an experiment during $45{,}362^{nd}$ to $48{,}602^{nd}$ minute (Fig. 5), one can verify this point. The point density in the curves stands for the time length of stay for states of sets of T_{bath}-T_{cell}. The longer stay, the heavy density of points. The lower part of the hysteresis loop is generally the heating condition, while the upper portion is the cooling condition (e.g., the H_2O charge). In the T_{bath}-T_{cell} plot the cooling curve of the cell (addition of H_2O into the cell) extends to the left of the hysteresis loop, and the cooling curve of the bath (addition of cooling water into the bath) extends downwards. There are also minor and major loops in the T_{bath}-T_{cell} plot. The T_{bath}-W plot show different states of T_{bath} at two specific values of measured power (Fig. 6). The key to the heat burst in this experiment is to understand the following questions. Why does the H_2O addition to the cell change the cell resistance so much and irregularly? Does this mean the resistance of the cathode also change in a similar way the resistance does?

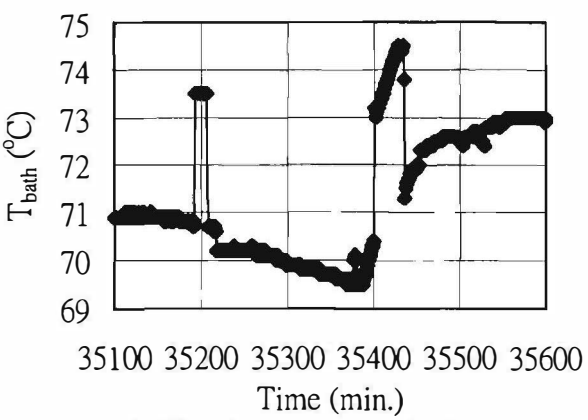

Fig. 3. The chronicle record of T_{bath} for a $Ni/Pt/H_2O/K_2CO_3$ cell

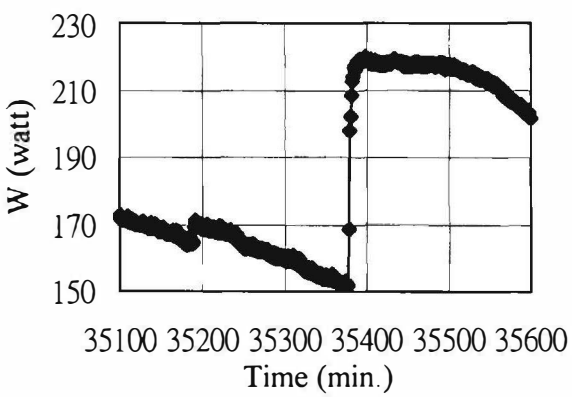

Fig. 4. The chronicle record of W for a $Ni/Pt/H_2O/K_2CO_3$ cell

The $Pd/Pt/D_2O/LiOD$ electrolysis cell

A big heat burst occurs at 3550^{th} minute during an experiment (Fig. 7). For this heat peak T_{bath} and T_{cell} increase at the expense of decreasing power (Fig. 8). The plot of T_{bath}-W shows increase of 85 to 100 °C for decrease of 109 to 88 watts (Fig. 9), while the plot of T_{cell} -W shows increase of 94 to 100 °C for the same decrease of watts (Fig. 10). The resistance of the cell at this peak is a maximum because of the water boiling during the occurrence of the heat burst.

Nuclear Physics Approach

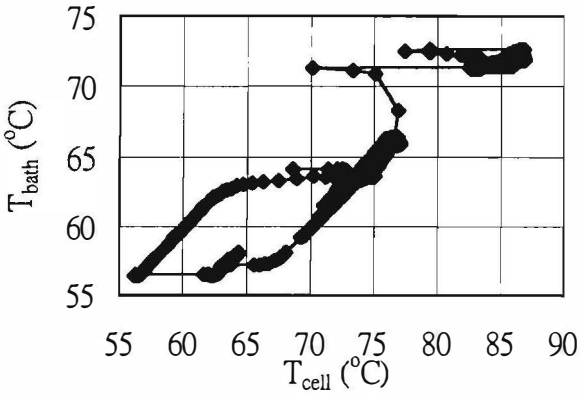

Fig. 5. The plot of T_{bath}-T_{cell} for a Ni/Pt/H_2O/K_2CO_3 cell

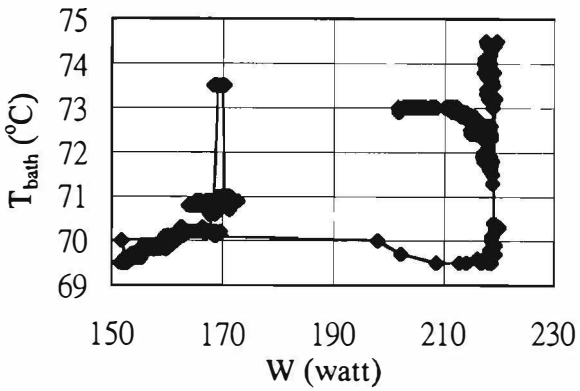

Fig. 6. The plot of T_{bath}-W for a Ni/Pt/H_2O/K_2CO_3 cell

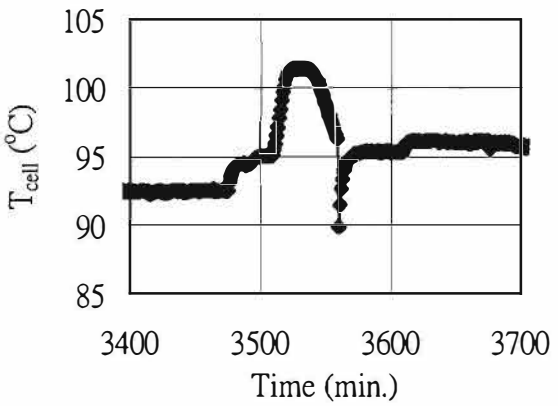

Fig. 7. The chronicle record of T_{cell} for a Pd/Pt/D_2O/LiOD cell

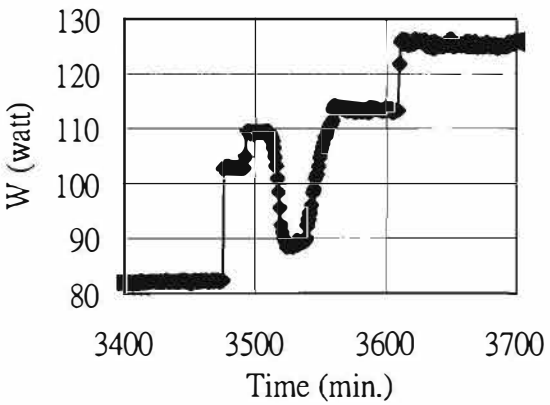

Fig. 8. The chronicle record of W for a Pd/Pt/D_2O/LiOD cell

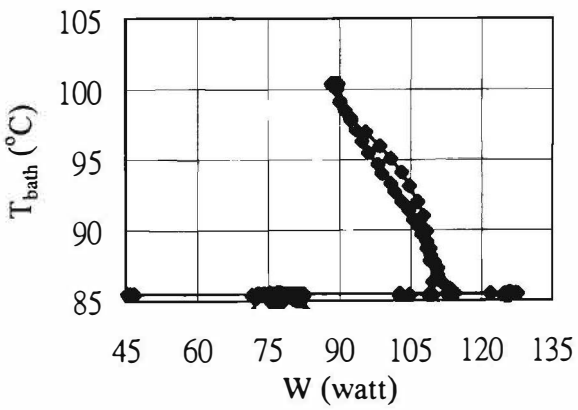

Fig. 9. The plot of T_{bath}-W for a Pd/Pt/D_2O/LiOD cell

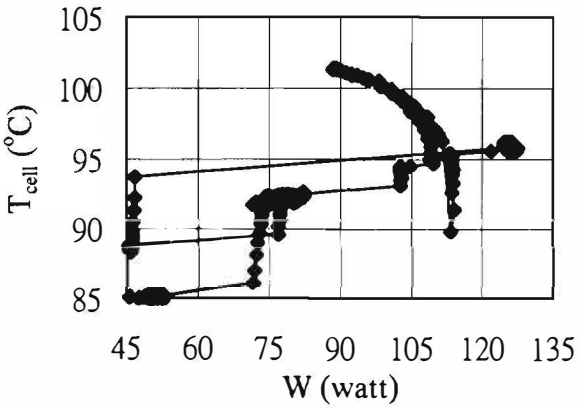

Fig. 10. The plot of T_{cell}-W for a Pd/Pt/D_2O/LiOD cell

The analysis of black precipitation in Ni/Pt/H_2O/K_2CO_3 cells

During the electrolysis there is accumulation of black precipitation in the electrolytic cell. The precipitation sticks on the surface of both electrodes as a thin film until the thickness of the film is large enough. Then the thick film breaks from the surface, and precipitates in solution. Although the establishment of the film rises the resistance of the cell, it shows that the resistance only ranges

of a small value, i.e., from 2 to 9 ohms, most of the time during electrolysis. It is observed that V-I curves are always straight lines with negative slope and with different set values of controlled-voltage of the power supply as parameters in curves. The slope of the Ni-H_2O cells is about 0.375 ohm, while that of the Pd-D_2O cells is about 0.35 ohm in this experiment. The W-I curves are also straight lines with different set values of controlled-voltage of the power supply as parameters in curves, but with positive slopes. Although the separation of the thick film from the electrode surface prevails frequently during electrolysis, there are occasionally large changes in current for a specific controlled voltage. However, the filling of water in cell changes the current to a large extent. It is believed that the loading condition of the cathode is key to the current change.
The collection of black precipitation during two-month electrolysis can reach an amount up to 1-gram order. This amount is helpful for doing chemical analysis. The original K_2CO_3 contains Na lower than 0.05 wt. %, silicate lower than 0.003 wt. %, Ca lower than 0.002 wt. %, Al and Mg lower than 0.001 wt. %, Fe, Cu, and Pb lower than 0.0005 wt. %, and As lower than 0.0001 wt. %. The electrodes, Ni and Pt, are 99.99 wt. % in purity. Chemical analyses of the black precipitation by a precision ICP-AES show a composition of 78.73 Pt-6.33 K-1.81 Ca-1.15 Mg-0.755 Fe-0.6 Ni-0.358 Si-0.184 Cr-0.137 B-0.13 Na-0.123 Pb-0.030 Zr-0.025 Nd-0.024 Mn-0.019 Zn-0.018 Cu-0.016 Ti-0.011 Sr-0.008 Li-9.52 others (including O) in weight percentage. Only contents of Pt, K, Ni, and Si indicate that they come obviously from the materials of the system. The high contents of Ca, Mg, Fe, Cr, B, Na, Pb, Zr, Nd, Mn, Zn, Cu, Ti, Sr, and Li are not present in the system at the start of the electrolysis. From the total amount estimation of the individual element, except Pt, K, Ni and Si, the concentration seems to be higher in 1 to 2 orders. It is hard to say that some of them come from the product of the nuclear reaction. But it is worth to take a thorough analysis of the precipitate.

The explanation of the cold fusion effect using a secondary reaction and a pycnon field
According to the conventional fusion theory in d-d reactions, there are two nearly equal branches,

(1) $d + d = t(1.008\ MeV) + p(3.052\ MeV)$

(2) $d + d = {}^3He(0.817\ MeV) + n(2.452\ MeV)$.

If in the solid state these two primary reactions can occur, neutrons with 2.452 MeV are "fast", and a "free" neutron is with a half-life of 12.8 minutes [6], then neutrons coming from Reaction (2) can recombine with protons coming from Reaction (1) to form a deuterium,

(3) $n(2.452\ MeV) + p(3.025MeV) = d(6.41\ keV) + \gamma(7.696\ MeV)$

One can easily see that the equal branching ratio (or n/t ratio ~ 1) showing in Reactions (1) and (2) is equivalent to n/t ratio ~ 10^{-8} to 10^{-4} [3], if a secondary reaction, Reaction (3), fully involves in reactions. In this case the total enthalpy generation in one event will be

(4) $Q = (4.033 \times 0.5 + 3.269 \times 0.5 + 2.226)\ MeV = 5.877\ MeV$.

The densities of the sun and white dwarf are 1.76×10^2 and 4×10^8 kg/cm^3, respectively. Although most of solid materials have relatively small densities, at the order of 10, the density of nucleus in an atom is 2.3×10^{17} kg/cm^3. One can see from the phase diagram of d-Pd that high d/Pd ratio means a high fugacity (pressure) of deuterium. The high d/Pd ratio is one of the essential factors for generation of the cold fusion effect. If the secondary reaction, Reaction (3), is possible, there should be a field correlated to the high fugacity and the pycno-reactions in stars [5]. Treating the

solid state field where the primary and secondary fusion reactions can occur like the meson field in the nucleus of an atom, a pycnon field is proposed here. If one assumes that the reaction under a condition of a very high nucleus density and a high deuterium fugacity in Pd lattice is governed by an exchange of a virtual pycnon, like the meson change in nucleus, one may deduce reaction details. The mass of the pycnon, m_{pycnon}, may be calculated by

(5) $m_{pycnon} = \Delta E/c \sim h/(\Delta t \cdot c^2)$,

where
Δt is the life time of p and n produced in Reactions (1) and (2).
If one assumes that $\Delta t \sim \Delta x/c$ and $\Delta x \sim 10^{-10}$ m in solid state, then $\Delta t \sim (10^{-10}\ m)/(3 \cdot 10^8\ m/sec) = 0.3 \cdot 10^{-18}$ sec. Therefore,

(6) $m_{pycnon} \sim (6.626 \cdot 10^{-34}\ J \cdot sec) / [0.3 \cdot 10^{-18}\ sec \cdot (3 \cdot 10^8\ m/sec)^2]$
$\sim 2.21 \cdot 10^{-32}\ kg / (9.11 \cdot 10^{-31}\ kg/electron\ mass)$
$\sim 0.0243\ m_e$.

It is assumed that the secondary reaction can occur under the pycnon field during the time of Δt after the primary reactions.

Conclusions

1. The hysteresis loop of T_{bath} to T_{cell}, and T_{bath}-W and T_{cell}-W curves show discrete enthalpy states in hydrogen-loaded nickel or deuterium-loaded palladium cells. When there are extra temperature-affected factors from surroundings and the system, the hysteresis curves are distorted or changed. From analysis of the curves, one can properly indicate that if there is excess heat generation at a specific moment in the cell.
2. Heat bursts are observed for both Ni-H_2O and Pd-D_2O cells in this experiment.
3. A secondary fusion reaction for the recombination of neutrons and protons is proposed to explain the equivalent of Huizenga's second and third miracles on Pd-D_2O cold fusion effect. A pycnon field is also discussed in this paper.

Acknowledgments

The author wants to thank the Materials Science Center of the National Tsing Hua University and the National Science Council of the Republic of China for financial support under contract Nos. NSC 81-0405-E007-548, 83-0405-E007-012 and 84-2216-E007-035. Thanks are also due to Messrs Chi-Yung Liang and Chih-Lung Chang, and Profs. Chi-Meen Wan, Chi-Chiao Wan and Liq-Ji Yuan for their help in experiment.

References

1. M. Rabinowitz, Y.E. Kim, V.A. Chechin and V.A. Tsarev, "Opposition and Support for Cold Fusion," Transactions of Fusion Technology, 26, 3(1994).
2. J.R. Huizenga, "Cold Fusion: The Scientific Fiasco of the Century," University of Rochester Press, (Rochester, NY, 1992), p.110.
3. E. Storms, "Review of Experimental Observations about the Cold Fusion Effect," Fusion Technology, 20, 433(1991).
4. S.K. Chen, "A Letter to the Editor," Fusion Technology (Sep. 1995), submitted and unpublished.
5. A.G.W. Cameron, J. of Astrophys., 129, 676(1959).
6. J.M. Rabson, Phys. Rev., 77, 747(1950).

Nuclear Physics Approach

Hidden Results of the Ion Band State Theory

Scott R. Chubb and Talbot A. Chubb

Oakton International Corporation
5023 N. 38th Street
Arlington, VA 22207, U.S.A.

Abstract
Using the Ion Band State (IBS) theory[1,2], we predicted a number of important effects that were subsequently observed[3] in Cold Fusion anomalous heat experiments. Despite this fact, the theory has inspired controversy[4] and confusion[5]. By addressing[5,6] the skeptics[4], we have learned that both the success of the theory and the controversy it seems to provoke have a common origin: our application of conventional, mainstream, solid state, many-body physics ideas that are known[7] to describe the physics of hydrogen inside[7] and on the surface[7] of transition metals, to the PdD Cold Fusion problem. Our application of these mainstream ideas is inconsistent with the predominant paradigm[3,8] that is commonly applied to Cold Fusion because it uses important ideas that relate periodic order to coherence that are known to apply at low temperature (LT) in solids and to hydrogen-in-metal systems that are not consistent with the conventional high temperature (HT) models that have formed the basis of conventional thinking. Implicit in this alternative (LT) picture is the important result that symmetry provides a means of "hiding" the potential location of a particular nuclear reaction. As a consequence: 1. it becomes impossible to distinguish the locations of the associated (periodically distributed) nuclear interactions, and 2. the associated energy release is initiated through a coherent release of energy and charge at the crystal boundaries.

Introduction:

This paper describes fundamental ideas behind the Ion Band State (IBS) theory[1,2] and the associated Lattice Induced Nuclear Chemistry (LINC) model[2] for solid state nuclear reactions that explain Fleischmann-Pons (FP) Cold Fusion experiments. Both IBS theory and LINC follow from mainstream quantum mechanics as it applies to ordered, hydrogen-in-transition metal systems. This is made possible by the first, and most important of the "hidden results" of IBS theory: it is possible for hydrogen and deuterium nuclei to become so mobile within a periodically ordered transition metal lattice that they behave in a "wave-like", delocalized manner that resembles the way conduction electrons behave in metals. The reason this "hidden result" seems to be relevant to FP-Cold Fusion (as suggested by loading measurements) is because of a second "hidden result": fully-loaded PdD (defined by PdD_x, $x \rightarrow 1$) crystals that are sufficiently large not only provide a natural environment for D and H to occupy these "electron-like", ion band states, it is also plausible that once this occurs (through energy minimization), order-preserving, coherent D^+-D^+ overlap can occur with unanticipated results, including coherent forms of non-local energy release and charge transfer from the bulk to an unexpected location: outside the bulk region where the main nuclear overlap occurs.

Nuclear Physics Approach

IBS theory predicts that this scenario occurs only in a very specific situation, in which periodic order is present and energy is minimized by the occupation of these "electron-like" ion band states. Neither the theory or model has been widely accepted, possibly, because both seem to contradict the "conventional wisdom" that FP-Cold Fusion simply is impossible. It is also possible that this failure reflects a more serious difference: IBS theory and LINC apply rigorously in a limit (temperature T=0) that differs significantly from the higher temperature (HT) limit where the conventional picture applies. This has resulted in a serious clash between the intuitive pictures provided by IBS/LINC theory with conventional thinking because at T=0, rigorous quantum mechanics must be used, resulting in a number of IBS/LINC predictions of "Black-Box" like effects associated with our (and nature's) inability to identify how and where specific phenomena take place, which have no counter-part at high temperatures, where nuclear overlap and reactions may be described using a semi-classical limit, involving distinctly identifiable events that occur at specific loactions.

Although it is not clear that it would ever be possible to perform Cold Fusion experiments with $T \to 0$, pedagogically, there is value in examining this limit because it provides a distinct picture that illustrates the very different paradigms that follow from conventional wisdom and IBS/LINC theory. Also, in the low T limits of both IBS's and LINC, simplifications become possible that quantify rules and effects that are not immediately obvious, such as the requirements that periodic order be preserved in bulk regions during nuclear reactions, and in effects associated with ion-ion correlation. In an accompanying paper[1], we have provided an overview of a number of important results associated with the IBS theory[1,2] and the LINC model[2]. In particular, we discuss some experimental evidence for IBS occupation and the underlying behavior of IBS's. We also discuss the potential implications for Coulomb barrier penetration, and provide an overview of the assumptions of LINC. The focus of the present paper is the underlying microscopic theory of LINC, its relationship to the LT paradigm, and the relationship of this paradigm to the conventional HT paradigm.

Cold Fusion at Absolute Zero:

In the T=0 limit, no energy or momentum can be transferred into or away from a solid, and the solid really must be viewed as a "Black Box." Somewhat remarkably, when a solid also possesses perfect periodic order, it still is possible to maintain temperature T=0 conditions inside (or within a large portion of the interior of) a solid but to extract momentum and energy from the solid through resonant processes that couple to the bulk but do not alter the interior of the solid. In this context, the bulk still must be "viewed as a black box;" while the important interactions "appear" to be taking place in the surface regions. These processes, which are referred to as "UmKlapp"- or "U"-processes[6], play a fundamental role in heat conductivity in electron-band systems. For this reason, it is not entirely surprising that they would become important in the transport of heat in systems in which heat is initiated from H^+ and/or D^+ ions that occupy "electron-like" IBS's. Previously[6], we have discussed the governing equations, based on a statistical treatment, of transport phenomena and reaction possibilities that are associated with the manner in which these processes can affect IBS $^4He^{++}$- and D^+- occupations, at finite T. There[6], we suggested that these processes probably are dominant at room temperature. When T=0 within the bulk, in fact, these are the only processes that enter since they are the only processes that couple to the outside world. Then, the statistical Boltzmann equation treatment[6], can be replaced by a rigorous microscopic limit in which the only allowed changes in energy occur through a shift in the zero of kinetic energy of each ion band state relative to the zero of kinetic energy. This is because this mode of energy transfer merely shifts the energies of all IBS's relative to all of the remaining charged particles in the system and is equivalent to a constant uniform shift of the IBS chemical potential. Although such a change does alter the occupation of IBS's in the surface regions that surround the solid, in bulk regions, it does this through a coherent redistribution of charge, either by eliminating it from or adding it to each

unit cell by altering the occupation of the highest occupied band state.

The Fermi Golden rule calculations[2,6] that we have used to describe "coalescence fluctuations" are based on coupling of the IBS center-of-mass wave functions to these shifts in chemical potential. Previously, we have not fully described how these fluctuations physically couple to the outside world. This is because at finite T, a number of different energy dissipation paths (phonons, and other lattice excitations, etc) are available besides surface-dipole mediated processes. At T=0, the only available path preserves order. This occurs from coherent U- processes that transfer charge to the surface dipole by a constant change in the bulk potential.

In the T=0 limit, for sufficiently large crystals, the Coulombic barrier interaction that prevents normal D-D overlap is suppressed by a decrease in the amplitude of wave function cusps[1,6]. As a result potentially reactive nuclei have near-complete overlap. Then, nuclear and Electromagnetic (E.M.) interactions are constrained to be separable[2] provided IBS concentration is sufficiently low ($<\sim 10^{-4}$). A sufficient condition that maintains this limit in the bulk during potential nuclear reactions is that the possible nuclear reactions involve ground-state to ground-state transitions and occur in a manner that preserves both E.M./nuclear separability and periodic order. Then, the ion band state and nuclear wave functions possess "Born-Oppenheimer Separability" (BOS), and the nuclear portions of the wave function interact only through the strong force. This separability is required in the bulk region because it holds there initially and is needed to preserve an absolutely ordered, T=0, state.

Because all portions of the E.M. interaction (including the ion-ion corelation[1]) in the bulk are described using band states, the center of mass locations of potentially reactive nuclei become indistinguishable and delocalized. This is clearly very different than in the HT case, where a nuclear reaction always occurs at a single point. As a consequence, in the T=0 limit, effectively, four "hidden results" become possible that have no HT counterpart: 1. It is possible to "hide" the locations of the nuclear reactants and by-products as a result of periodic order and the "Black Box"- type of behavior that occurs at T=0. 2. It is possible for energy to be released through coherent processes in regions distinctly different from the locations where nuclear overlap occurs. 3. To maintain separability between nuclear and electromagnetic interactions, complete isospin conservation is required between initial and final states within the bulk. 4. As a consequence of the first three results, a "bosons in and bosons out" selection rule[2], in which each "boson" consists of an integer number of proton-neutron pairs, becomes rigorously valid.

Implicitly, we have applied the "Black Box-like" conditions of the T=0 limit in previous Fermi Golden Rule reaction rate calculations. Here, the transition rate is estimated from the following assumptions: 1. reversible fluctuations in mass occur at each bulk interior point. 2. Average energy of these fluctuations V ($\equiv 2.38 \times 10^7/N_{cell}$; N_{cell}= number of bulk unit cells) couples to band states through a perturbing barrier height, inhibiting D^+_{IBS} ($\equiv$ IBS D^+) overlap with locations where energy is released (equivalent to lowering constant zero of kinetic energy K_o of each bulk D^+_{IBS} relative to the comparable K_o of the $^4He^{++}_{IBS}$ product). In the present work, we illustrate that these changes in K_o can be coupled at T=0 with the outside world through discontinuous changes in the wave-function at the boundaries of the solid (similar to those outlined[6] during ICCF5) that are consistent with an Umklapp-process that coherently alters the boundary, through a sudden, discontinuous change in K_o in regions where periodic order is lost, accompanied by a redistribution of positive and negative band state charge in the surface region.

These changes induce a breakdown of BOS, illustrating how energy transfer can couple to the outside world through surface region variations δK_o in the zero of kinetic energy K_o. δK_o equals the nuclear energy change resulting from $D_{nuc}+D_{nuc} \rightarrow {}^4He$. This change alters each nucleon wave

Nuclear Physics Approach

function by an amount $\delta\psi_{nuc} = -\partial\psi_{nuc}/\partial E \times N_{cell} V$. By construction, this energy is treated as a perturbation to the band state potential in the bulk, but in the surface region it is treated as a shift in the kinetic energy of each band state wave function. BOS breaks down through the implicit relationship, $\delta\psi_{nuc}(\mathbf{r}) = \partial\psi_{nuc}/\partial E \times \delta K_o$, where $\delta K_o (= -N_{cell} V)$ is implicitly treated as a functional of the continuation of $\psi_{IBS}(\mathbf{r}')$ at points $\mathbf{r}'$ extending into the surface region. The implicit relationship between K_o and ψ_{IBS} is defined by an UmKlapp process involving a transfer $\Delta\mathbf{p}$ of momentum from the solid to the surface through a "resonant matching condition" requirement: Debroglie wavelength $\equiv h/\Delta\mathbf{p} = n^{-1}$ bulk lattice spacing, n=integer. This introduces discontinuous behavior in $\nabla\psi(\mathbf{r})$ in the surface region. Minimal transfer of kinetic energy to the outside world occurs when these discontinuities alter K_o only at the classical turning points of each band state wave function. From the definition of kinetic energy $K \equiv \hbar^2/(2m) \int d\mathbf{r}\, |\nabla\psi(\mathbf{r})|^2 / \int d\mathbf{r}'\, |\psi(\mathbf{r}')|^2$, it follows from the calculus of variations that

$$\delta K \equiv \frac{\hbar^2}{(2m)} \Big(\int_{\text{boundary}} d\mathbf{r}\, \Big[\delta\psi^* \frac{\partial\psi}{\partial \mathbf{n}} + \frac{\partial\psi^*}{\partial \mathbf{n}} \delta\psi \Big] - \int d\mathbf{r}\, \big[\delta\psi^* \nabla^2\psi + \nabla^2\psi^* \delta\psi \big] \Big)$$

$$- K \int d\mathbf{r}\, \big[\delta\psi^* \psi + \psi^* \delta\psi \big] \quad . \qquad (1)$$

Here, the first term is evaluated at all boundaries surrounding locations where possible discontinuities occur. The UmKlapp process occurs when $\delta\psi$ vanishes except in the surface region at classical turning points $\mathbf{r}_{tp}$ (defined by $\mathbf{r}$ such that $\nabla^2\psi(\mathbf{r}) = 0$), and is minimized absolutely when K_o is minimized absolutely. Denoting this minimal value by K_o, and, for simplicity, requiring that two-dimensional order be preserved in the x-y plane, we find

$$\frac{\delta K_o}{\delta\psi(\mathbf{r})} \equiv \frac{\hbar^2}{(2m)} \Big(\sum_{z_b \in \text{boundary}} \delta(z - z_b) \frac{\partial\psi^*(\mathbf{r})}{\partial \mathbf{n}} - K_o \psi^*(\mathbf{r}) \Big) \quad \delta(\mathbf{r} - \mathbf{r}_{tp}) \, . \qquad (2)$$

By using Eq. 2, and the previous result $\delta\psi_{nuc}(\mathbf{r})/\delta\psi_{IBS}(\mathbf{r}') = \delta\psi_{nuc}/\delta E \times \delta K_o/\delta\psi_{IBS}(\mathbf{r}')$, we obtain the desired result, illustrating the breakdown of BOS that results from changes in IBS's through UmKlapp process induced changes in K_o in the surface region.

1. T. A. Chubb and S. R. Chubb, this proceedings.
2. S. R. and T. A. Chubb, Fus Tech, 24, 403, (1993). T. A. and S. R. Chubb, ibid, 20, 93, (1991). S. R. and T. A. Chubb, in AIP Conf. Proc. 228, 691, (eds. S. E. Jones et al, AIP (New York), 1991).
3. M. H. Miles et al., in Conf. Proc. Vol 33, 363, (eds. Bressani et al, Ital. Phys. Soc. (Bologna, 1991). M.C.H. McKubre et al., in Frontiers of Cold Fusion, 5, (ed. H. Ikegami, Univ. Acad Press (Tokyo, 1993)). K. Kunimatsu et al., ibid, 31.
4. D. Lindley, NATURE, 344, 376 (1989). Bressani et al, "Editorial Note to the Paper 'An Explanation of Cold Fusion...' by S.R. Chubb and T.A. Chubb", in Conf. Proc. Vol 33, 204, (eds. Bressani et al, Ital Phys Soc (Bologna, 1991)). V. A. Chechin et al., Int. J. Theor. Phys., 33, 636 (1994). M. Rabinowitz et al., Trans. Fusion Tech., 26, 3 (1994).
5. S.R. Chubb and T.A. Chubb, ICCF5 Book of Abstracts, p 409 (1995).
6. T.A. Chubb and S.R. Chubb, Proc. ICCF5, pp 315-326 (1995). S.R. Chubb and T.A. Chubb, Bull. Amer. Phys Soc, 41, 341 (1996).
7. R.C. Casella, Phys. Rev. B, 27, 5943 (1983). R. Niemenen, NATURE, 356, 289 (1992). M.J. Puska et al., Phys. Rev. Lett., 51, 1081 (1983).
8. A.J. Leggett and G. Baym, Phys. Rev. Lett, 63, 191 (1989).

Nuclear Physics Approach

A Model for Neutron Emission from Condensed Matter

Toyu Tani[1] and Yukio Kobayashi[2]

1 Rika Gakkou, 1194-13 Nagase, Moroyama-cho, Iruma-gun, Saitama 351-04, JAPAN
2 Department of Information Systems Science, Faculty of Engineering, Soka University, 1-236 Tangi-cho, Hachioji-shi, Tokyo 192, JAPAN, E-mail: koba@t.soka.ac.jp

Abstract

We propose a quantum-mechanical model for the neutron emission from condensed matter. This model is based on two new phenomena: the tunnel disintegration of an ionized deuterium molecule and the subsequent dipole disintegration of a deuteron. We calculated the probabilities of the neutron emission from condensed matter by considering the mechanisms of the dipole disintegration, especially the transition from the ground state to the decaying state. The results of the numerical calculation can successfully explain the important features of the neutron energy spectrum : the 2.45-MeV peak, the high-energy component at $3 \sim 7$ MeV, and the large T/n ratio. This indicates that the 2.45-MeV neutrons can be predicted by the dipole disintegration of the deuteron instead of the d-d nuclear fusion.

1. Introduction

Since 1989, the nuclear events in condensed matter has attracted attention. Many researchers have expended much effort to elucidate the mechanisms of these phenomena in metal such as palladium and titanium. Most of the researchers believing the nuclear events in condensed matter expect that the phenomenon arises from the d-d nuclear fusion and consequently this phenomenon is termed the cold nuclear fusion. According to new experiments, these nuclear events present three important features: (i) The neutron-energy spectrum shows the peaks at about 2.45 MeV and at $3 \sim 7$ MeV (Takahashi *et al.*, 1990; Nakada *et al.*, 1993). (ii) T/n ratio is extremely large ($10^4 \sim 10^9$) (Iyenger and Srinivasan, 1990). (iii) The correlation between excess heat and nuclear products is little. These experimental results, however, are not consistent with the d-d nuclear fusion from the following reasons. The neutron emission due to the d-d nuclear fusion presents the 2.5-MeV peak in the neutron-energy spectrum. Additionally the neutron-emission rate is almost equivalent to the tritium-emission rate. Therefore we can not ascribe the above three features to the cold nuclear fusion.

In this paper, we propose a quantum-mechanical model against the cold nuclear fusion to explain the neutron emission from condensed matter by predicting two new phenomena: the tunnel disintegration of an ionized deuterium molecule on metal surface and the subsequent dipole disintegration of a deuteron. On the basis of the quantum theory Tani proved that the fusion probability of the two nuclei in a composite system such as a free diatomic molecule is exactly zero (unpublished; For example, see Tani and Kobayashi, 1993). From this standpoint, a qunatum-mechanical composite system (nuclei and electrons in molecular state) should turn

into another system (nuclei and electrons in continuous spectrum state), if the two nuclei in the composite system penetrate into the region which would be insurmountable on the classical theory. Therefore the two nuclei can not approach each other to zero separation but on the contrary the composite system disintegrates, which we termed the tunnel disintegration. Therefore when an ionized diatomic molecule interacts so strongly with such metal as palladium and titanium in its surface region, the two nuclei pass through the barrier and consequently the molecule disintegrates with the electron transition to the continuous-spectrum states. The intensive excitation of collective modes will occur in the surface region simultaneously with the tunnel disintegration. As a result instantaneous strong localized electric field will be induced at the position of D_2^+. The electric field will excite the dipole oscillations between proton and neutron in the deuteron, and consequently the dipole disintegration of the deuteron will occur.

We calculated numerically the probabilities of the neutron emission from condensed matter on the basis of this model. In contrast to our previous paper (Tani and Kobayashi, 1993), we considered the mechanisms of the dipole disintegration in detail. Our numerical results are consistent with the experiments. Therefore we believe that our model is valid for explaining the mechanisms of the nutron emission from condensed matter.

2. Mechanisms of the Dipole Disintegration of a Deuteron

2.1. Tunnel Disintegration of D_2^+

The tunnel disintegration of D_2^+ (molecular explosion) will be accompanied by the release of energy of $\sim$ 30 eV. Simultaneously the released energy will induce the intensive excitation of collective modes, which yields instantaneous strong localized electric fields at the position of D_2^+. If, however, the electric field varies quickly, any nuclear events cannot occur. On the other hand, if the electric field varies slowly as compared with the characteristic period ($\sim 10^{-21}$ s) of the nuclear motion, the deuterons emitted from the collapsed D_2^+ can absorb energy from the localized electric field and consequently any nuclear events will occur.

We considered the ^{3}P-state in the theoretical calculation, although the ^{3}P-state of the deuteron is not detected experimentally. Hence the dipole oscillation will be excited between proton and neutron in the deuteron. The amplitude of the dipole oscillation increases as the deuteron absorbs the energy from the localized electric field. The deuteron will disintegrate when the electric field reaches a threshold.

2.2. Process of Dipole Disintegration

We derived the formula for the probability of the dipole disintegration of a deuteron in the following procedure, where we assumed that the electric field starts to act on the deuteron at time $t = 0$ and the amplitude of the dipole oscillation attains to the maximum at $t = T$.

1. $t < 0$: *Deuteron in the Ground State*

Let the deuteron be in $^3S_1$-state before the energy absorption, since the primary purpose of this paper is to investigate the validity of the model. The state of the unperturbed deuteron can

be represented by the Hamiltonian operator H_0 as follows: $H_0\psi_0^{(0)}(\mathbf{r}) = E_0\psi_0^{(0)}(\mathbf{r})$ for $^3S_1$-state and $H_0\psi_k^{(0)}(\mathbf{r}) = E_k^{(0)}\psi_k^{(0)}(\mathbf{r})$ for ^3P-state.

2. $t = 0$: *Dipole Oscillation of Deuteron*

We represented the localized electric field as the pulselike form

$$f(t) = \epsilon_0 \lambda t(2 - \lambda t)\exp(-\lambda t), \tag{1}$$

where $\lambda \ll 10^{21}s^{-1}$. We determined the $^3S_1$-state and the ^3P-state of the deuteron in the electric field $f(t)$ directed along the z -axis. The Schrödinger equation is

$$i\hbar\frac{\partial\Psi}{\partial t} = H_r\Psi, \tag{2}$$

where $H_r \equiv H_0 - \frac{eM_n}{M}f(t)z$, z being the z-component of the relative vector $\mathbf{r}$ of the proton to the neutron, M the total mass, M_n the neutron mass, and e the elementary charge.

In the first approximation, the solution of Eq. (2) can be written as

$$\Psi(\mathbf{r},t) = \psi_0^{(0)}(\mathbf{r})\exp(-iE_0t/\hbar) + \sum_k a_k^{(0)}(t)\psi_k^{(0)}(\mathbf{r})\exp(-iE_k^{(0)}t/\hbar), \tag{3}$$

where $a_k^{(0)}(t) = \frac{ieM_n}{\hbar M}\int_0^t f(t)z_{k0}^{(0)}\exp[i(E_k^{(0)} - E_0)t/\hbar]dt$ with $z_{k0}^{(0)} = \int \psi_k^{(0)\dagger}(\mathbf{r})r\cos\theta\psi_0^{(0)}(\mathbf{r})d\mathbf{r}$.

3. $0 < t < T$: *Deuteron in the Decaying State*

The direct transition from the ground state can not occur because of the low-energy nature of the phenomenon. Therefore we assumed a decaying state as an intermediate step prior to the dipole disintegration. The transition from the ground state to the decaying state will take place gradually by steps, since the deuteron can absorb only a little energy at a time. For $\lambda \ll 10^{21}s^{-1}$ the deuteron can form a quasi-stationary state at every step, which will be repeated until the deuteron attains to a final decaying-state. The $^3S_1$-state parameters will change little by little during the self-regularization process, while the ^3P-state will not be affected.

We represented the quasi-stationary state at time t as

$$\psi_0^{(1)}(\mathbf{r}) = N[\psi_0^{(0)\prime}(\mathbf{r}) + \sum_k a_k^{(0)\prime}(t)\psi_k^{(0)}(\mathbf{r})\exp(-i(E_k^{(0)} - E^{(1)})t/\hbar)], \tag{4}$$

where $\psi_0^{(0)\prime}$ is the $^3S_1$-state with energy E_0' at time t just before the energy absorption and N is a normalization factor. We assumed $\tilde{H}_0\psi_0^{(1)}(\mathbf{r}) = E^{(1)}\psi_0^{(1)}(\mathbf{r})$ where $\tilde{H}_0$ is an effective Hamiltonian.

We determined the $^3S_1$-state parameters by an iterative method:

(i) Choose $\psi_0^{(0)\prime} = \psi_0^{(0)}$ with $E_0' = E_0$ as a trial function and put $a_k^{(0)\prime}(t) = a_k^{(0)}(t)$.

(ii) Calculate $E^{(1)} = (\psi_0^{(1)}, \tilde{H}_0\psi_0^{(1)})$ with $\tilde{H}_0 = H_0$ by assuming a square-well potential.

(iii) Replace E_0 by $E^{(1)}$.

(iv) Find the $^3S_1$-state parameters (the well depth V_s and the radius r_s) with the ^3P-state

parameters (V_p and r_p) unchanged.

(v) Recalculate $a_k^{(0)}(t)$ by using $\psi_0^{(0)}$ with the new $^3S_1$-state parameters.

(vi) Replace $\psi_0^{(0)\prime}$ and $a_k^{(0)\prime}(t)$ by $\psi_\bullet^{(0)}$ with the new $^3S_1$-state parameters and the recalculated $a_k^{(0)}(t)$ in Eq. (3) with $E_0' = E^{(1)}$, respectively.

We repeated this procedure until $E^{(1)}$ exceeds a criterion energy (-0.02 MeV).

4. $t = T$: *Maximum Amplitude of Dipole Oscillation*

The dipole disintegration of the deuteron will occur when the amplitude of the dipole oscillation attains to the maximum.

5. $t > T$: *Dipole Disintegration of Deuteron*

We expressed the Hamiltonian operator of the deuteron in the decaying process as

$$H_r = \tilde{H}_0 + V_{res}(r) - \frac{eM_n}{M} f(t) z, \tag{5}$$

where V_{res} denotes a residual interaction. For $t > T$ the solution of Eq. (2) with Eq. (5) can be written as

$$\Psi(\mathbf{r}, t) = \psi_0^{(1)}(\mathbf{r}) \exp[-iE^{(1)}(t - T)/\hbar] + \sum_{\ell,m} \int a_{E\ell m}(t) \psi_{E\ell m}^{(0)}(\mathbf{r}) \exp[-iE(t - T)/\hbar] dE, \tag{6}$$

where $\tilde{H}_0 \psi_{E\ell m}^{(0)}(\mathbf{r}) = E\psi_{E\ell m}^{(0)}(\mathbf{r})(E > 0)$. The probability that the neutron of the energy between E and $E + dE$ is emitted due to the nuclear dipole oscillation is

$$\sum_{\ell,m} |a_{E\ell m}(\infty)|^2 dE. \tag{7}$$

We assumed that the residual interaction can be written as a delta-function type: $V_{res}(r) = -\gamma V \delta(r - a)$, where γ is a length to make $\gamma\delta(r - a)$ a dimensionless quantity and a and V are adjustable parameters. The effective Hamiltonian can be approximately represented as

$$\tilde{H}_0 = -\frac{\hbar^2}{2\mu} \triangle_r + V_0(r). \tag{8}$$

We simplified the calculation by assuming a square-well potential: $V_0(r) = V_s^{(1)}$ for $r \leq r_s^{(1)}$ and $V_0(r) = 0$ for $r > r_s^{(1)}$, where $V_s^{(1)}$ and $r_s^{(1)}$ are the parameters of the $^3S_1$-state at the decaying state.

3. Results

We calculated numerically the probabilities of the neutron emission by assuming the pulse-like electric field represented by Eq.(1) with $\epsilon_0 = 5.0 \times 10^{18}$ V/m and $\lambda = 1.0 \times 10^{17}$ s^{-1}. We chose $E_0 = -2.226$ MeV, $V_s = -21.3$ MeV, and $r_s = 2.80$ fm as the $^3S_1$-state parameters and determined the ^3P-state parameters to make the mixing ratio of ^3P-state to $^3S_1$-state, $M(t) = \sum_k |a_k^{(0)}|^2$, as small as possible. Figure 1 illustrates the theoretical spectrum for the

case of $E_k^{(0)} = E_p = -0.01$ MeV, $V_p = -18.7$ MeV, and $r_p = 4.68$ fm. The calculated spectra present the 2.45-MeV peak and the high-energy component at $3 \sim 7$ MeV. The ratio of the probability of the neutron emission at 0 MeV and that at 2.5 MeV is $\sim 10^4$. The details will be published elsewhwere.

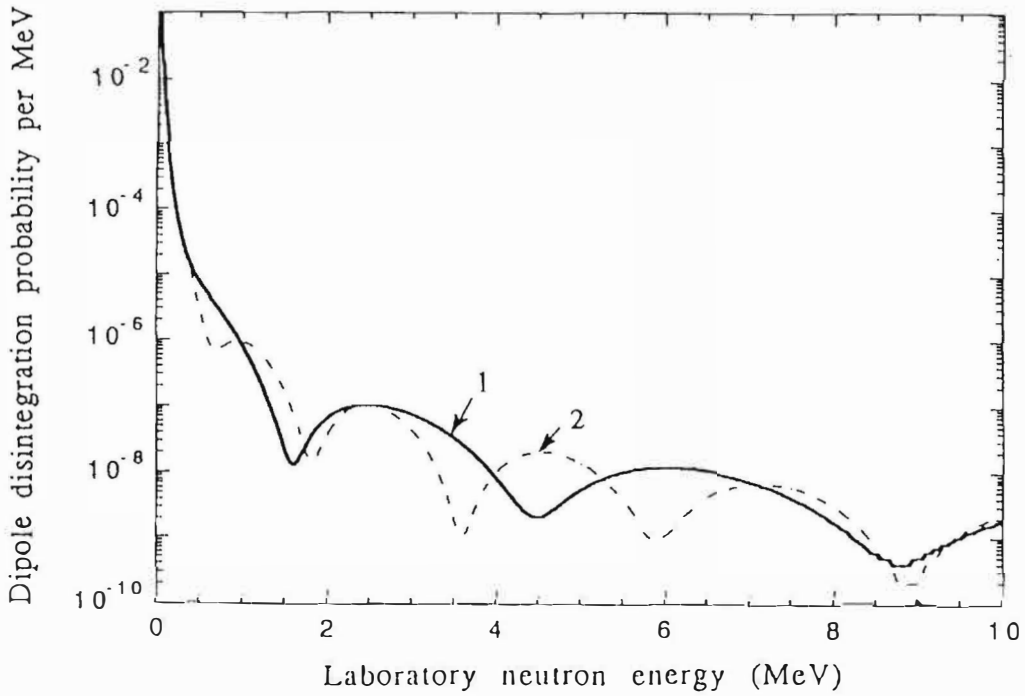

Figure 1. Dipole disintegration probability for: 1, $\epsilon_0 = 5 \times 10^{18}$ V/m, $\lambda = 2 \times 10^{17}$ s^{-1}, $V = 8.5 \times 10^{-2}$ MeV, and $a = 18.3$ fm; 2, $\epsilon_0 = 5 \times 10^{18}$ V/m, $\lambda = 1 \times 10^{17}$ s^{-1}, $V = 1.0 \times 10^{-1}$ MeV, and $a = 27.8$ fm. The energy of stationary neutron is twice the energy of laboratory neutron.

4. Conclusion

We summarized the three features of the experimental spectrum in Sect. 1. Our numerical calculation can successfully explain these features: the peak at 2.45 MeV, the high-energy component at $3 \sim 7$ MeV, and the large T/n ratio. Therefore this model can predict the experimental neutron-energy spectrum. These results indicate that the 2.45-MeV neutrons can be predicted by the dipole disintegration of a deuteron instead of the d-d nuclear fusion. We should reconsider also the tunnel effect in such composite systems as muon.

Refernces

Iyengan, P. K. and Srinivasan, M. (1990) *Proc. ICCF1.* Salt Lake City, Utah, 62.

Nakada, M., Kusunoki, T. and Okamoto, M. (1993) In Ikegami, H. (ed.), *Frontiers of Cold Fusion*. Universal Academy Press, Tokyo, p.173.

Takahashi, A., Takeuchi, T. and Iida, T. (1990) *J. Nucl. Sci. Technol.*, 27, 66.

Tani, T. and Kobayashi, Y. (1993) In Ikegami, H. (ed.), *Frontiers of Cold Fusion*.Universal Academy Press, Tokyo, p.589.

Click here for a more readable copy of this paper.

COMMENT ON EXACT UPPER BOUND ON BARRIER PENETRATION PROBABILITIES IN MANY–BODY SYSTEMS

Yeong E. Kim and Alexander L. Zubarev
Department of Physics
Purdue University
West Lafayette, Indiana 47907-1396, U.S.A.

Abstract

We investigate conditions under which it is not possible to establish an exact upper bound for the barrier penetration probability of nuclei tunneling to classically forbidden small relative separation, by a value calculable in terms of the Born–Oppenheimer potential between nuclei.

1. Introduction

Leggett and Baym (LB) [1] investigated an upper bound on barrier penetration probabilities in many–body systems and claimed to obtain the result that the rate of tunneling of nuclei to classically forbidden small relative separation, in a fully interacting quantum–mechanical many–body system in equilibrium, is rigorously bounded above by a value calculable in terms of the Born–Oppenheimer potential between the nuclei. As LB cautioned in their paper, this potential can differ from conventional Born-Oppenheimer potential. In this report, we describe the conditions under which it is not possible to obtain such an exact upper bound.

2. Outline of the Derivation by LB

LB [1] start from a stationary–state wave function $\psi(\vec{r},\vec{\xi})$ of the many–body system,

$$\left[-\frac{\hbar^2}{2\mu}\nabla^2+\widehat{H}(r)\right]\psi(\vec{r},\vec{\xi})=E\psi(\vec{r},\vec{\xi})\ , \tag{1}$$

and obtain

$$\int d\xi\psi^*(\vec{r},\vec{\xi})\widehat{H}(r)\psi(\vec{r},\vec{\xi})\geq U(\vec{r})\rho(\vec{r})\ , \tag{2}$$

where

$$\rho(\vec{r})=\int d\xi|\psi(\vec{r},\vec{\xi})|^2\ , \tag{3}$$

$\vec{r}$ is the relative deuteron pair coordinate and $\vec{\xi}$ are all other coordinates. Using eqs. (1) and (2), and the Schwartz inequality, they obtain

$$\frac{\hbar^2}{2\mu}\frac{\Delta\chi(\vec{r})}{\chi(\vec{r})} \geq U(\vec{r}) - E \ , \tag{4}$$

where

$$\chi(\vec{r}) \equiv \rho(\vec{r})^{1/2} \ . \tag{5}$$

They introduce a potential $V_1(\vec{r})$, defined as

$$V_1(\vec{r}) \equiv \frac{\hbar^2}{2\mu}[\Delta\chi(\vec{r})]/\chi(\vec{r}) + E \ , \tag{6}$$

and, using eqs. (4) and (6), write the following bounds

$$V_1(\vec{r}) \geq U(\vec{r}) \geq V_2(\vec{r}) \ , \tag{7}$$

where $U(\vec{r})$ is the effective potential in the Born–Oppenheimer approximation, and $V_2(r)$ is a direction–independent lower bound on $U(\vec{r})$. From eq. (7), they find that the Born–Oppenheimer approximation leads to an upper bound on the barrier penetration probability.

3. Validity of the Exact Upper Bound by LB

We first note that Eq.(2) is valid for the wave function, which is normalizable over $\vec{\xi}$. For the initial state of $d+$ metal, for which d is free in the continuum, we do not expect $\int d\vec{\xi}|\psi(\vec{r},\vec{\xi})|^2 < \infty$, because the $d+$ metal system is multichannel system. Therefore, Eq.(7) is valid only for the case in which all particles form a bound state.

Introducing $\phi(r)$ as the regular s-wave solution of the Schroedinger equation

$$-\frac{\hbar^2}{2\mu}\Delta\phi + V_2\phi = E\phi, \tag{8}$$

it is straightforward to obtain, for any $r \leq r_0(E)$, ($r_0(E)$ is the largest distance for which $V_2(r) - E \geq 0$), a general inequality given by Eq.(1) of LB [1]:

$$\ell n\left[\frac{\rho(r)}{\rho(0)}\right] \geq \ell n\left[\frac{\phi^2(r)}{\phi^2(0)}\right] . \tag{9}$$

Noting that $\phi^2(r) \geq \phi^2(0)$ for $r \leq r_o(E)$, we can obtain from Eq.(9) the following inequality,

$$\rho(0) \leq \int_0^{r_0(E)} \rho(r)r^2dr \cdot \phi^2(0)[\int_0^{r_0(E)} \phi^2(r)r^2dr]^{-1}. \tag{10}$$

If we assume as in ref. [1] that $\int_0^{r_o(E)} \rho(r)r^2dr = \frac{1}{4\pi}$, and $\phi(r) = F_0(r)/r$, where $F_0(r)$ is the regular Coulomb wave function with screening energy for $(d+d)$, then we obtain the inequalaity given in Eq.(10) of ref. [1].

Nuclear Physics Approach

We note that LB [1] use the following definition of reaction rate R

$$R = A\rho(0) \tag{11}$$

where A is the nuclear constant. Eq.(11) is not valid since the nuclear interaction range is not equal to zero. In general, the reaction rate from the ℓ-partial wave contribution, R_ℓ, can be written as [2]

$$R_\ell \propto \int_0^\infty \rho_\ell^{1/2}(r) U_\ell(r,r') \rho_\ell^{1/2}(r') r^2 dr r'^2 dr', \tag{12}$$

where $U_\ell(r,r') = Im < r|T_\ell|r' >$ with T representing the ℓ-th partial wave contribution of the elastic T-matrix operator. It is shown [2] that, if $U_\ell(r,r')$ has a weak component with a finite long-range interaction, the upper bound given by LB [1] is not valid.

4. Conclusions

The exact upper bound given by LB [1] is not valid,
(i) if many-body system (electrons, nuclei) does not form a stationary bound state, and also
(ii) if the imaginary part of the effective nuclear interaction in the elastic channel has a very weak component with a finite long interaction-range.

References

[1] A.J. Leggett and G. Baym, Phys. Rev. Lett. **63**, 191 (1989).
[2] Y.E. Kim and A.L. Zubarev, Nuov. Cim. **108A**, 1009 (1995).

Nuclear Physics Approach

Analysis of the Electrolytic Cold Fusion Experiments on TNCF Model

KOZIMA Hideo, HIROE Katsuhiko, NOMURA Masahiro and OHTA Masayuki

Department of Physics, Faculty of Science, Shizuoka University
836 Oya, Shizuoka 422, JAPAN

ABSTRACT

A model based on the stable existence of thermal neutrons in crystals was used to analyze experimental data obtained in electrolytic systems. The density of the trapped thermal neutron n_n in samples was determined using experimental results on the excess heat, helium 4 (^{4}He), tritium and neutron. The values of the density n_n determined by the experimental data were $10^2 \sim 10^{12}$ cm^{-3}. Other quantities which we could determine from experimental data were the ratio of events generating tritium and neutron N_t/N_n and the ratio of events generating the excess heat and tritium N_Q/N_t, which had been a point of controversy in today's physics. The values determined on our model have been $N_t/N_n \sim 10^5$ and $N_Q/N_t \sim 10$, almost consistent with experimental data of a few orders of magnitude.

1. Introduction

In the cold fusion phenomenon, discovered in 1989 and developed in the last seven years, there has been a lot of experimental data which has piled up. Various phases of the results obtained hitherto are lacking a consistent explanation.

The experimental results of the cold fusion phenomenon have been obtained in a variety of materials generating various products including excess heat, ^{4}He, tritium, neutron, γ and the nuclear transmutation. These results were difficult to understand in the framework of conventional physics. Therefore, it became necessary to have a common basis possible to explain all of the data. A model proposed by one of the authors (K.H.) is now being investigated[1~3]. It seems to be able to explain the various events consistently.

2. The TNCF Model

The TNCF (Trapped Neutron Catalyzed Fusion) model assumes the existence of the trapped thermal neutron and its stability. The fusion probability may be calculated

by the same formula as the usual collision process between a thermal neutron and a nucleus:

$$P_f = 0.35\, n_n v_n n_N V \sigma_{nN} \quad (1)$$

where $0.35 n_n v_n$ is the flow density of the neutron per unit area and time, n_N is the density of the nucleus, V is the volume of the region where the nucleus fuses with the thermal neutron, and σ_{nN} is the fusion cross section for the reaction.

Typical reactions related with the TNCF model are written down as follows. The trapped thermal neutron can fuse with the ^{6}Li nucleus with a large cross section $\sim 1 \times 10^3$ barns in the surface layer formed on the cathode by electrolysis of D_2O+LiOD:

$$n + {}^6\mathrm{Li} = {}^4\mathrm{He}\ (2.1\ \mathrm{MeV}) + t\ (2.7\ \mathrm{MeV}). \quad (2)$$

The triton with 2.7 MeV generated in this reaction can pass through the crystal along the channeling axis on which is an array of occluded deuterons or can proceed along a path of finite length ($\simeq 1 \sim 10\ \mu$m) determined by interaction with charged particles in the crystal. In these processes, the triton can fuse with a deuteron with a cross section $\sim 1.4 \times 10^{-1}$ barns:

$$t\ (2.7\ \mathrm{MeV}) + d = {}^4\mathrm{He}\ (3.5\ \mathrm{MeV}) + n\ (14.1\ \mathrm{MeV}). \quad (3)$$

The neutron with 14.1 MeV generated in this reaction can interact with particles, especially with deuterons in the crystal, giving a large amount of energy to the deuteron by elastic collision and dissociating it by inelastic collision. The generated energetic particles sustain breeding chain reactions which produce a lot of the excess heat and nuclear products. Some of the increased thermal neutrons will be captured by nuclei, and cause the nuclear transmutation reactions.

3. Analysis of Typical Quantitative Experimental Data

In measurements of several cold fusion events, it was possible to obtain several quantities simultaneously. Lack of general understanding of relations between physical quantities, however, have made descriptions of the results vague or sometimes, even chaotic. Generally speaking, there were too much data observed without a definite relation between them.

Therefore, it is usually impossible to explain all of the data obtained in an experiment including the interrelated physical variables. For the time being, we will select data from a point of view which neglects others, leaving them for a future program to explain in relation with known factors. We will examine only five events regarding quantitative relations between observed quantities taken from reliable experimental results obtained.

1) M. Fleischmann, S. Pons and M. Hawkins.[4)]

From the abundant data in the first cold fusion paper, we examined[5)] the case of a thin rod Pd cathode with dimensions 0.4 cmϕ × 10 cm. When the electrolyzing current density was 64 mA/cm^2, the system consisting of a Pd cathode, Pt anode and LiOD+D_2O gave the excess power of 1.75 W (= 1.1×10^{13} MeV/s), tritium atoms

4×10^{11}/s , and neutrons 4×10^{4}/s (perhaps in the same sample but not described explicitly).

To analyze this data, we assumed the thickness of the Li atom surface layer (area S) of the cathode as $l_0 = 1\ \mu$m, the natural abundance of ^{6}Li in LiOD at 7.5 %, and the average velocity of the trapped neutron at $v_n = 2.7 \times 10^5$ cm/s (T = 300 K). Then, we could determine the density of the trapped neutron n_n using the relation between n_n and the number of tritium atoms N_t generated in time τ by the reaction (2):

$$N_t = 0.35\ n_n v_n n_{^6Li} l_0 S \sigma_{nLi} \tau, \tag{4}$$

where S = 12.8 cm^2, $\sigma_{nLi} = 10^3$ barns and $n_{^6Li} = 3.5 \times 10^{21}$ cm^{-3}. The observed value of N_t per unit time 4×10^{11}/s gave us

$$n_n = 9.4 \times 10^9 \mathrm{cm}^{-3}. \tag{5}$$

The triton generated in the reaction (2) induces the reaction (3), and which produces a neutron with energy 14.1 MeV. Taking the path length of the triton in the cathode PdD_x as $\sim 1\mu$m and using the cross section of reaction (3) for 2.7 MeV triton as σ_{t-d} $\sim 1.4 \times 10^{-1}$ barns, and the density of deuterium near the surface layer as 6.8×10^{22} cm^{-3}(D/Pd = 1), we calculated the probability of reaction (3) induced by a triton, as 9.5×10^{-7} which gives a ratio of events generating tritium and neutron,

$$N_t/N_n \sim 1.1 \times 10^6. \tag{6}$$

This value is compared with the experimental value 10^7. Another quantity we can use as an index of the cold fusion phenomenon is the ratio of events producing the excess heat and tritium atoms N_Q/N_t. Assuming that nuclear reactions liberate energy of about 5 MeV per reaction on average, we obtained a value,

$$N_Q/N_t = (1.1 \times 10^{13} \div 5)/(4 \times 10^{11}) = 5.5. \tag{7}$$

This value suggests that the origins of the excess heat are the n + ^{6}Li reaction and several other reactions which follow.

2) A. Takahashi, T. Iida, T. Takeuchi, A. Mega, S. Yoshida and M. Watanabe.[6)]

Next, we will take up an experiment which observed the excess heat, tritium and neutron in Pd/D_2O+LiOD system with L-H mode electrolysis. The dimensions of the Pd cathode were 20 mmϕ $\times$ 30 mm and a surface area S = 25 cm^2. The total number of observed neutrons was 6.8×10^6, and that of tritium measured in the solution was 4.2×10^{11}. Then,

$$N_t/N_n = 8.7 \times 10^4. \tag{8}$$

This value has only one order of magnitude difference with the value of Eq.(6) which is also applicable in this case.

Besides, we obtained[7)] the density of the neutron in the sample as $n_n \sim 10^2$ cm^{-3} by using Eq.(4). In this calculation, we assumed the time duration τ of tritium generation as a month by looking at the experimental data. This value of n_n is a little too small,

but not too troubling. It's natural that there are differences in capability of neutrons because of the condition or the history of samples.

3) M.H. Miles, R.A. Hollins, B.F. Bush and J.J. Lagowski.[8]

Third, we will give a result of the analysis[5] of an experiment which observed excess heat and helium in Pd/D_2O+LiOD system using a massive cylindrical Pd cathode with a surface area of 2.6 cm^2. They measured $10^{11} \sim 10^{12}$ ^{4}He atoms/s per watt of excess power in the ambient gas. Similar analysis, as given above, resulted as follows:

$$n_n = 10^9 \sim 10^{10} \mathrm{cm}^{-3}, \quad N_Q/N_{He} \sim 10. \tag{9}$$

4) C.C. Chien, D. Hodko, Z.Minevski and J. O'M. Bockris.[9]

Fourth, we will give a result of the analysis of an experiment which observed the concentrations of tritium and ^{4}He in Pd/D_2O+LiOD system. In their paper, the total number of tritium atoms was evaluated as $\sim 10^{11}$ in the cathode, and as $\sim 10^{15}$ in the whole system (including the electrolyte and gas). The number of ^{4}He atoms was evaluated only in the cathode sample as $0.4 \sim 166.8 \times 10^9$. In the surface layer, the n + ^{6}Li reaction generated tritium and ^{4}He, while the n + d reaction generated tritium in the volume. Therefore a direct comparison of the numbers of tritium and ^{4}He is difficult, though the observed numbers are not inconsistent with our model.

The neutron density was evaluated using the maximum value of tritium production rate in the total system, 3.8×10^7 atoms/s cm^2, as follows:

$$n_n = 1.1 \times 10^6 \mathrm{cm}^{-3}. \tag{10}$$

5) Y. Arata and Y.C. Zhang.[10]

Finally, we will give a result of the analysis of an experiment which observed a huge excess heat (several hundred MJ/cm^{-3}) for over several months and a tremendous number of helium atoms as high as $10^{20} \sim 10^{21}$ cm^{-3} in Pd-black contained in a Pd cylinder cathode as follows:[11]

$$n_n \sim 10^{12} \mathrm{cm}^{-3}, \quad N_Q/N_{He} \sim 4. \tag{11}$$

Because of the ambiguity in the description of the results in their papers, we had to assume concrete numerical values for the amount of excess energy at 3×10^9 J, and a time duration τ of 1×10^7 s. These results are also consistent with others.

4. Conclusion

The analyses of experimental data on the TNCF model gave us a unified view of the physics of cold fusion. Though the analyses given above have been confined to the experiments with electrolysis, the results were remarkable. The reliable data showed clearly, facets of the truth. Only assuming the existence of the stable thermal neutrons in cold fusion materials, can we have a consistent understanding of events in the phenomenon with quantitative relationships in them. (It is unavoidable that these results have errors in a range of a few figures, because of the numerical ambiguities included in data and our assumptions.) The success of these analyses suggests the reality of the concept of the trapped neutron.

Nuclear Physics Approach

The other three papers[12~14] given in this conference will help the reader to understand the physics of cold fusion.

References

1) H. Kozima, "Trapped Neutron Catalyzed Fusion of Deuterons and Protons in Inhomogeneous Solids", *Trans. Fusion Technol.* (Proc.ICCF4) **26**, 508 (1994).
2) H. Kozima and S. Watanabe, "Nuclear Processes in Trapped Neutron Catalyzed Model for Cold Fusion", *Cold Fusion* **10**, 2 (1994) and *Proc. ICCF5* 347 (1995).
3) H. Kozima, "Cold Fusion Phenomenon on the TNCF Model", *Proc. 4th Russian Conference on Cold Fusion and Nuclear Transmutation* (May 23-27, 1996, Sochi, RUSSIA) (to be published).
4) M. Fleischmann, S. Pons and M. Hawkins, "Electrochemically Induced Nuclear Fusion of Deuterium", *J. Electroanal. Chem.* **261**, 301 (1989).
5) H. Kozima, S. Watanabe, K. Hiroe, M. Nomura and M. Ohta, "Analysis of Cold Fusion Experiments Generating Excess Heat,Tritium and Helium", *J. Electroanal. Chem.* (to be published).
6) A. Takahashi, T. Iida, T. Takeuchi, A. Mega, S. Yoshida and M. Watanabe, "Neutron Spectra and Controllability by PdD/Electrolysis Cell with Low-High Current Pulse Operation", "The Science of Cold Fusion" (Conference Proceedings of SIF(Italy) **33**, 93 (1991)
7) H. Kozima, M. Nomura, K. Hiroe and M. Ohta, "Analysis of Tritium and Neutron Generation in Pd+LiOD/D_2O System", *Cold Fusion* **19** (1996) (to be published).
8) M.H. Miles, R.A. Hollins, B.F. Bush and J.J. Lagowski, "Correlation of Excess Power and Helium Production During D_2O and H_2O Electrolysis Using Palladium Cathodes", *J. Electroanal. Chem.* **346**, 99 (1993).
9) C.C. Chien, D. Hodko, Z.Minevski and J. O'M. Bockris, "On an electrode producing massive quantities of tritium and helium", *J. Electroanal. Chem.* **338**, *189 (1994)*
10) Y. Arata and Y.C. Zhang, "Achievement of Solid-State Plazma Fusion ("Cold Fusion")", Proc.Jpn Acad. **71B**, *304 (1995); and "A New Energy caused by 'Spillover-Deuterium'", Proc.Jpn Acad.* **70B**, *106 (1994)*
11) H. Kozima, S. Watanabe, K. Hiroe, M. Nomura and M. Ohta, "Analysis of Excess Heat and ^4He Generation in Pd-black Cathode by D_2O+LiOH Electrolysis", Cold Fusion (to be published)
12) H. Kozima, "On the Existence of the Trapped Thermal Neutron in Cold Fusion Materials", Proc. ICCF6 (in this issue)
13) H. Kozima, M. Nomura, K. Hiroe, and M. Ohta, "Nuclear Transmutation in Cold Fusion Experiments", Proc. ICCF6 (in this issue)
14) H. Kozima, M. Ohta, M. Nomura and K. Hiroe, "Analysis of Nickel-Hydrogen Isotope System on TNCF Model", Proc. ICCF6 (in this issue)

Nuclear Physics Approach

On the Existence of the Trapped Thermal Neutron in Cold Fusion Materials

KOZIMA Hideo

Department of Physics, Faculty of Science, Shizuoka University
836 Oya, Shizuoka 422, JAPAN
Tel. +81-54-238-4738, Fax. +81-54-238-0993, E-mail. sphkoji@sci.shizuoka.ac.jp

Abstract

The stable existence of the thermal neutron assumed in the TNCF model has been discussed in this paper on the basis of the interaction of the neutron and the nuclei on the lattice points in the crystal. If an optimum shape of a boundary is formed stochastically, neutrons could be trapped in a crystal region surrounded by the boundary. The trapped neutron can form the neutron Cooper pair lowering its energy interacting each other through the phonon. The stabilized neutron, then, will not decay spontaneously and also not be captured by one of the lattice nuclei. To specify the stability of a neutron in a crystal, a new concept "neutron affinity of a nucleus" was introduced. Trapped neutron destabilized by a large perturbation can induce a trigger and succeeding breeding reactions resulting in the cold fusion phenomenon.

1. Introduction

In 1989, Fleischmann et al.[1] published a paper showing the discovery of the so-called Cold Fusion. After the discovery of the cold fusion, it has been recognized that the cold fusion phenomenon includes not only the generation of the excess heat, small nuclei, neutron and the photon but also the nuclear transmutation including the heavy nuclei in metals occluding hydrogen isotopes (D and H) and compounds including them. The cold fusion is used as such in this paper.

To explain the cold fusion phenomenon, the first proposal[2] of a phenomenological model was made in the November 1993 on an assumption of the trapped thermal neutron catalyzing fusion reactions in crystals (TNCF model).

The model has been developed [3~7] in this three years to fit the various phases of the phenomenon. The electrolytic experiments including the first one by Fleischmann et al.[1] were analyzed[7] with success: The questions solved by the model included the poor reproducibility of the events, large N_t/N_n ($\equiv t/n$) ratio, large N_Q/N_n ratio and also the large value of N_{He} comparable to N_Q where N_t, N_n, N_Q and N_{He} are the number of events generating tritium, neutron, the excess heat and ^{4}He, respectively. $N_{trigger}$ is also used as a number of trigger reaction.

In the next section, we will give the basic postulates of the model and the result of the analyses of the experimental data by the model. In the section 3, we will discuss the existence

Nuclear Physics Approach

Table 1: Neutron Density n_n and Relations between the Numbers N_x of Event x Obtained by Theoretical Analysis of Experimental Data on TNCF Model ($(N_Q)_{exp} \equiv Q(\mathrm{MeV})/5\ (\mathrm{MeV})$, $(N_Q)_{theo} \equiv N_{trig}$)

Authors	System	Measured Quantities	n_n (cm^{-3})	Other Theoretical Results (Remarks)
M.Fleischmann et al.[1]	Pd/D/Li	Q, t, n $N_t/N_n \sim 10^7$ $N_Q/N_t \sim 5.5$	$\sim 10^{10}$	 $N_t/N_n = 1.1 \times 10^6$ $N_Q/N_t = 1$
A.Takahashi et al.[8]	Pd/D/Li	t, n $N_t/N_n \sim 8.7 \times 10^4$	10^3	 $N_t/N_n \sim 1.1 \times 10^6$
M.H.Miles et al.[10]	Pd/D/Li	Q, ^{4}He (N_Q/N_{He}=1~ 10)	$10^9 \sim 10^{10}$	 $N_Q/N_{He} = 1$
R.Bush et al.[11]	Ni/H/Rb	NT (^{85}Rb→ ^{86}Sr) $N_Q/N_{NT} \sim 3$	1.6×10^7	 $N_Q/N_{NT} = 1$
M.Okamoto et al.[13]	Pd/D/Li	Q, NT(^{27}Al → ^{28}Si)	$\sim 10^{10}$	$N_Q/N_{NT} \sim 1.4$
Y.Arata et al.[15]	Pd/D/Li	Q ^{4}He($10^{20} \sim 10^{21}$ cm^{-3}) $N_Q/N_{He} \sim 6$	$\sim 10^{12}$	(Assume t channeling in cathode wall) $N_Q/N_{He} = 1$
M.C.H.McKubre[17]	Pd/D/Li	Q (Formula)	$10^9 \sim 10^{10}$	Qualit. explanation
D.Cravens (P.P.C.)[19]	Pd/H/Li	Q (Q_{out}/Q_{in}=3.8)	8.5×10^9	(If PdD exists)
J.O'M.Bockris et al.[22]	Pd/D/Li	t ($\sim 3.8 \times 10^7/\mathrm{cm}^2\mathrm{s}$)	1.1×10^6	$N_t/N_{He} \sim 1$
A.G.Lipson et al.[26]	Pd/PdO/D,Na	γ (E_γ=6.25 MeV)	4×10^5	(If efficiency = 1 %)
V.Romodanov et al.[24]	Mo/D_2	t ($\sim 10^7$ /s)	1.8×10^7	(If sample is MoD)
I.Savvatimova[23]	Pd/D_2	NT (^{106}Pd→ ^{107}Ag)	9×10^{10}	
O.Reifenschweiler[27]	$TiT_{0.0035}$	Reduction of β decay	1.1×10^9	(T = 0 ~ 450 °C)
J.Dufour[29] (SS is for Stainless Steel)	Pd,SS/D_2 Pd,SS/H_2	Q, t, n	9.2×10^{11} 4.0×10^9	(D(H)/Pd ~ 1 is assumed)
T.N.Claytor et al.[30]	Pd/D_2	t (0.15 nCi/h)	1.4×10^7	(If D/Pd ~ 1.)
F.G.Will et al.[31]	Pd/D_2SO_4	t ($\sim 1.8 \times 10^5/\mathrm{cm}^2\mathrm{s}$)	3.5×10^7	(If $\ell_0 \sim 10$ μm)
M.Srinivasan et al.[32]	Ti/D_2	t ($t/d \sim 10^{-5}$)	1.9×10^8	
A.DeNinno et al.[33]	Ti/D_2	t (5.4 Bq/g D_2)	1.2×10^6	(D/Ti=1,τ =1 week)
S.Focardi et al.[34]	Ni/H_2	Q	3.0×10^{12}	($N_p = 10^{21}$ was used)

of the stable trapped neutrons in the cold fusion materials in terms of the verification of the postulates.

2. Result of the Analyses of Typical Quantitative Experimental Data by the TNCF Model

The TNCF model stands on the four basic postulates:

1) Trapping of thermal neutrons in a specific region of a crystal,

2) Stabilization of the trapped neutron in a crystal made of nulei having positive "neutron affinities" against β decay and also against a fusion reaction with a nucleus in the crystal,

3) Destabilization of the trapped neutron by a perturbation due to foreign atoms at boundaries and in crystal to induce the trigger reactions generating energetic particles.

4) Breeding reactions induced by the energetic particles born in the trigger reaction generate cold fusion products (the excess heat, nuclear products and transmuted nuclei).

Using these postulates, typical experimental data in the cold fusion phenomenon have been analyzed[8~36] and the result is recited here in Table 1 with some modification.

Nuclear reactions used in the calculation were usual ones between the trapped neutron and

nuclei in the material and some examples were written down as follows:

$$n + {}^{6}\mathrm{Li} = {}^{4}\mathrm{He}\ (2.1\ \mathrm{MeV}) + t\ (2.7\ \mathrm{MeV}), \quad (1)$$

$$t\ (2.7\ \mathrm{MeV}) + d = {}^{4}\mathrm{He}\ (3.5\ \mathrm{MeV}) + n\ (14.1\ \mathrm{MeV}) + 2.7\ \mathrm{MeV}, \quad (2)$$

$$n\ (14.1\ \mathrm{MeV}) + d = n'\ (\varepsilon) + d'\ (\varepsilon'), \quad (3)$$

$$n\ (14.1\ \mathrm{MeV}) + d = n'\ (\varepsilon) + p\ (\varepsilon') + d'\ (\varepsilon''), \quad (4)$$

$$n + d = t + \gamma + 6.25\ \mathrm{MeV}, \quad (5)$$

$$n + p = d + \gamma + 2.2\ \mathrm{MeV}, \quad (6)$$

$$n + {}^{7}\mathrm{Li} = {}^{8}\mathrm{Be} = 2\,{}^{4}\mathrm{He} + e^{-} + \bar{\nu}_e + 16.2\ \mathrm{MeV}, \quad (7)$$

$$d\ (\varepsilon) + d = t\ (1.01\ \mathrm{MeV}) + p\ (3.02\ \mathrm{MeV}) + \varepsilon, \quad (8)$$

$$= {}^{3}\mathrm{He}\ (0.82\ \mathrm{MeV}) + n\ (2.45\ \mathrm{MeV}) + \varepsilon, \quad (9)$$

$$n + {}^{A}\mathrm{M} = {}^{A+1}\mathrm{M}' + e^{-} + \bar{\nu}_e. \quad (10)$$

In the last equation, M and M' are symbols of nuclei with mass number A and $A+1$, respectively, relevant with the nuclear transmutation.

3. Existence of the Trapped Thermal Neutrons in the Cold Fusion Materials

The success of the explanation of the cold fusion phenomenon by the TNCF model illustrated in the preceding section has shown the reality of the basic postulates of the TNCF model in which is the stable existence of the trapped thermal neutrons in the cold fusion materials.

Therefore, the supposed existence of the trapped thermal neutron should be investigated on the knowledge of solid state and nuclear physics. A preliminary treatment of this problem was given in the previous paper[4] and the essential points are explained as follows:

1) Trapping.

There are several causes to reflect a thermal neutron to trap it in a crystal; the difference of the neutron band structure (band effect), the Bragg reflection and the total reflection at a boundary. The difference of the neutron band structure seems effective in massive samples with a thick surface layer and the total reflection in the case of special samples with such an appropriate geometry as the Patterson's beads and Arata's Pd-black.

2) Stabilization.

The trapped thermal neutron behaves as a Bloch wave in the crystal and it is possible to become stable through the interactions with the lattice nuclei having a positive neutron affinity against the beta decay and also against a fusion with one of lattice nuclei[4]. Formation of the neutron Cooper pair enforces the stability of the trapped neutrons in an optimum situation.

3) Destabilization and Trigger Reaction.

The trapped thermal neutron, though, can fuse with a nucleus as a trigger reaction in the surface layer or in the volume of the crystal if a perturbation is strong enough to destroy the stability of the neutron. From the results of the analyses, we can say that it occurs usually near the surface of the sample where the neutron is reflected, i.e. where it stays long in the classical sense. Otherwise, when the temperature of the sample is fairly high, it occurs even in the volume of the sample.

4) Breeding Reaction.

The fusion reaction between the neutron and nuclei becomes as a trigger reaction inducing successive reactions breeding the excess heat and nuclear products. The particles generated by a trigger reaction such as the reaction (1), (2) and (6) react with particles and nuclei in the sample. The triton reacts with a deuteron to generate ^{4}He and a neutron; the neutron with an energy 14.1 MeV can accelerate several deuterons (protons) to energies enough to fuse with another deuteron (and nucleus) with a large probability. These breeding reactions can occur

successively and then generate gigantic amount of heat and particles in optimum situations. These processes would be the causes of some experimental data showing such an extraordinary result as explosion and neutron bursts. This phase of the cold fusion phenomenon was not fully analyzed yet though some possibilities were shown with model calculations[43,44].

The variety of numerical values n_n of the trapped thermal neutron n_n from 10^3 to 10^{12} cm^{-3} determined from experimental data shows variety of the trapping ability of materials used hitherto in the cold fusion experiments. Also, the variety of events from the excess heat and several nuclear products, such as from tritium t , helium 4 ^4He, neutron n and gamma γ , to the transmuted nuclei shows how the TNCF model is universally applicable in nuclear processes occurring in cold solids.

There were many experiences showing the effect of the aging of samples to realize the cold fusion phenomenon like that shown in the experiment analyzed before[32]. The present author had a similar experience in which Pd plate bought many years ago gave a positive result[45] while a newly bought one did not (which was not written in the paper). Such experiences are explained by the TNCF model if the aged Pd samples had the surface layer by oxidation in the air to trap the thermal neutron and kept much neutrons in them.

The conditions to facilitate the existence of the trapped thermal neutron explain the poor reproducibility of the phenomenon; The trapping conditions can be formed by stochastic processes such as the atomic diffusion in crystals or crystal growth on the solid surface and are not reproducible quantitatively by its nature. The cold fusion phenomenon induced by the trapped thermal neutron, therefore, has qualitative reproducibility but not quantitative.

4. Conclusion

The phenomenological analysis of typical experimental data obtained hitherto in the cold fusion experiments with electrolysis or discharge gave us a unified consistent concept of physics of the cold fusion. The reliable data showed clearly several facets of truth in the solid state - nuclear physics. The facets united by a paste have formed a whole figure of the physics of particles in a crystal with the trapped thermal neutron.

The postualtes of the existence of the stable thermal neutron in crystal itself has a theoretical verification[4,5] based on the neutron - lattice nuclei interaction with a new concept "neutron affinity of lattice nuclei".

The success in the analysis of the cold fusion phenomenon on the TNCF model shows in reverse the reality of the trapped thermal neutron. This feature of the analysis will open a new science of the low energy neutron in solid interacting with lattice nuclei through the nuclear force. The existence of the trapped neutron in appropriate systems as Pd-black and the Patterson bead will be checked by the neutron magnetic resonance (nMR) like NMR or ESR used in the solid state physics and in the physical chemistry.

Other systems than the electrolytic and discharge ones have also shown the characteristic cold fusion phenomenon not even more exciting than the latter. It will be fascinating program to analyze various experimental data in various systems on the TNCF model as done above. If we have a hint to get rid of obstacles disturbing our route to a goal, it is easy then to find out paths to reach the goal. Exploration of the cold fusion phenomenon as answering to the energy crisis will be accelerated by the new idea to unify the abundant separate facts obtained hitherto in experiments.

The other three reports[46~48] to be presented in this Conference by us will supplement the description given in this report.

The author would like to express his thanks to Dr. M. Okamoto of Tokyo Institute of Technology, Dr. A. Takahashi of Osaka University and Dr. M. McKubre of SRI International

(USA) for their valuable discussions through the work. He is also much indebted to Dr. I.B. Savvatimova and Dr. V.A. Romodanov of the Research Institute LUTCH and Dr. A.G. Lipson of Inst. of Physical Chemistry, Russian Acad. Science for their help in the analyses of their data.

References

(1) M. Fleischmann, S. Pons and M. Hawkins, *J. Electroanal. Chem.* **261**, 301 (1989). (2) H. Kozima, K. Kaki, T. Yoneyama, S. Watanabe and M. Koike, *Fusion Technol.* (submitted in November 1993). (3) H. Kozima, *Trans. Fusion Technol. (Proc. ICCF4)* **26**, 508 (1994). (4) H. Kozima, *Cold Fusion*, **16**, 4 (1996); *Proc. 3rd Russian Conference on Cold Fusion and Nuclear Transmutation (RCCFNT3)* (Oct. 2 - 6, 1995, Sochi, Russia), 224 (1996). (5) H. Kozima, *Cold Fusion* **18**, 17 (1996). (6) H. Kozima, *Proc. Fourth Russian Conference on Cold Fusion and Nuclear Transmutation* (May 23 - 27, 1996, Sochi, RUSSIA) (to be published). (7) H. Kozima, S. Watanabe, K. Hiroe, M. Nomura and M. Ohta, *J. Electroanal. Chem.* (to be published). (8) A. Takahashi, T. Iida, T. Takeuchi, A. Mega, S. Yoshida and M. Watanabe, *"The Science of Cold Fusion" (Conference Proceedings of SIF (Italy))* **33**, 93 (1991). (9) H. Kozima, M. Nomura K. Hiroe and M. Ohta, *Cold Fusion* **19** (1996) (to be published); (10) M.H. Miles, R.A. Hollins, B.F. Bush and J.J. Lagowski, *J. Electroanal. Chem.* **346**, 99 (1993). (11) R. Bush and R. Eagleton, *Trans. Fusion Technol. (Proc. ICCF4)* **26**, 344 (1994). (12) H. Kozima, K. Hiroe, M. Nomura and M. Ohta, *Cold Fusion* **16**, 30 (1996). (13) M. Okamoto, H. Ogawa, Y. Yoshinaga, T. Kusunoki and O. Odawara, *Proc. ICCF4*, **3**, 14-1 (1994). (14) H. Kozima, M. Ohta, M. Nomura and K. Hiroe, *Cold Fusion* **18**, 12 (1996). (15) Y. Arata and Y.C. Zhang, *Proc. Jpn Acad.* **71B**, 304 (1995) and *Proc. Jpn Acad.* **70B**, 106 (1994). (16) H. Kozima, S. Watanabe, K. Hiroe, M. Nomura and M. Ohta, *Cold Fusion* (to be published). (17) M. C. H. McKubre, S. Crouch-Baker and F. L. Tanzella, *Proc. ICCF5* (April 9 - 13, Monte-Carlo, Monaco), 17 (1995) and also in *Proc. 3rd Russian Conference on Cold Fusion and Nuclear Transmutation (RCCFNT3)* (Oct. 2 - 6, 1995, Sochi, Russia), 123 (1996). (18) H. Kozima, *Cold Fusion* **17**, 12 (1996). (19) D. Cravens, *Cold Fusion* **11**, 15 (1995) and also *Proc. ICCF-5*, 79 (1995). (20) Report by V. Lapuszynski, *Cold Fusion* **7**, 1 (1995); U.S. Pat. No. 5,318,675, U.S. Pat. No. 5,372,688. (21) H. Kozima, *Cold Fusion* **17**, 8 (1996). (22) J. O'M. Bockris, C-C. Chien, D. Hodko and Z. Minevski, *Frontiers of Cold Fusion (Proc. ICCF3)* p.231, ed. H.Ikegami, Universal Academy Press (Tokyo), 1993.. (23) I.B. Savvatimova, A. B. Karabut, *Proc. RCCFNT3* (Oct. 2 - 7, 1995, Sochi, RUSSIA), 20 (1996) and private communication. (24) V.A. Romodanov, V.I. Savin and Ya.B. Skuratnik, *Proc. RCCFNT2* (Sept. 1994, Sochi, RUSSIA), 99 (1995). (25) V.A. Alekseev, V.I. Vasil'ev, V.A. Romodanov, Yu.F. Ryshkov, S.V.Rylov, V.I. Savin, Ya.B. Skuratnik and V.M. Strunnikov, *Tech. Phys. Lett.* **21**, 231 (1995) and private communication. (26) A. G. Lipson, D. M. Sakov and E. I. Saunin, *JETP Lett.* **62**, 828 (1995) and private communication. (27) O. Reifenschweiler, *Phys. Lett.* **A184**, 149 (1994). (28) H. Kozima, *Physics Letters* (submitted). (29) J. Dufour, *Fusion Technol.* **24**, 205 (1993). (30) T.N. Claytor, D.D. Jackson and D.G. Tuggle, *Presentation at ICCF5*, **No.306** and also *Trans. Fusion Technol. (Proc. ICCF4)* **26**, 221 (1994). (31) T.G. Will, K. Cedzynska and D.C. Linton, *Trans. Fusion Technol. (Proc. ICCF4)* **26**, 207 (1994). (32) M. Srinivasan, R.K. Rout, S.C. Misra, M. Lai, A. Shyam, P.S. Rao and P.K. Iyengar, *Fusion Technol.* **18**, 88 (1990). (33) A. De Ninno, F. Scaramuzzi, A. Frattolillo, S. Migliori, F. Lanza, S. Scaglione, P. Zeppa and C. Pontorieri, *The Science of Cold Fusion (Proc. ICCF2)*, Conference Proceedings **33**, 129 (1991), SIF, Bologna. (34) S. Focardi, R. Habel and F. Piontelli, *Nuovo Cimento* **107A**, 163 (1994). (35) H. Kozima, *Cold Fusion* **8**, 5 (1995); M. Ohta, M. Nomura, K. Hiroe and H. Kozima, *Cold Fusion* (to be published). (36) H. Kozima, *Proc. 3rd Symposium of Basic Research Group in NHE Project* (July 3 - 4, 1996, Tokyo, Japan), 17 (1996) and also *Cold Fusion* **18**, 30 (1996). (37) G. F. Cerofolini, G. Boara, S. Agosteo and A. Para, *Fusion Technol.* **23**, 465 (1993). (38) G. Shani, C. Cohen, A. Grayevsky and S. Brokman, *Solid State Comm.* **72**, 53 (1989). (39) A.A. Yuhimchuk, V.I. Tichonov, S.K. Grishechkin, N.S. Ganchuk, B.Ya. Gujofskii, Yu.I. Platnikov, Yu.A. Soloviev, Yu.A. Habarov, A.B. Levkin, *Kholodnyi Yadernyi Sintez*, p. 57, ed. R. N. Kuz'min, Sbornik Nauchnykh Trudov (Karinngrad) 1992. (in Russian). (40) F. Celani, A. Spallone, L. Libaratori, F. Groce, A. Storelli, S. Fortunati, M. Tului and N. Sparviari, *Fusion Technol.* **22**, 181 (1992). (41) B. Stella, M. Corradi, F. Ferrarotto, V. Milone, F. Celani and A. Spallone, *Frontiers of Cold Fusion (Proc. ICCF3)* p.437, ed. H.Ikegami, Universal Academy Press (Tokyo), 1993. (42) A. G. Lipson and D. M. Sakov, *Proc. ICCF 5* (April 9 - 13, 1995, Monte Carlo, Monaco), 571 (1995). (43) H. Kozima and S. Watanabe, *Proc. Intern. Sympos. Cold Fusion and Advanced Energy Sources* (May 24 = 26, 1994, Minsk, Beralus) p. 299 (in Russian). (44) H. Kozima and S. Watanabe, *Proc. ICCF5* (April 9 - 13, 1995, Monte Carlo, Monaco), 347 (1995); *Cold Fusion* **10**, 2 (1995). (45) H. Kozima, S. Oe, K. Hasegawa, H. Suganuma, M. Fujii, T. Onojima, K. Sekido and M. Yasuda, *Rep. Fac. Science, Shizuoka Univ.* **24**, 29 (1990). (46) H. Kozima, K. Hiroe, M. Nomura and M. Ohta, *Proc. ICCF6* (in this issue). (47) H. Kozima, M. Nomura, K. Hiroe and M. Ohta, *Proc. ICCF6* (in this issue). (48) H. Kozima, M. Ohta, M. Nomura and K. Hiroe, *Proc. ICCF6* (in this issue).

Nuclear Physics Approach

The Theory of Bose-Einstein Condensation in Finite System for Explanation of Cold Fusion

Peng Kuangding and Chen Shanna

Yunnan University, Kunming 650091
People's Republic of China

Abstract
The effect of contraction of potential well and Bose-Einstein condensation has been discussed. Due to the two processes of concentrating energy, cold fusion is possible at special conditions.

1. The effect of contraction of potential well

When deuterium ions (D^+) enter from electrolyte of heavy water into the gaps of palladium (Pd) lattice, the potential well containing D^+ changes from a big space to a small one. The process can be regarded appoximately as a contracted process of a potential well. In a cuboid well a × b × c, under Dirichlet boundary conditions, the energy level is[1]

$$E_{l_1,l_2,l_3}=\frac{h^2}{8m}\left[\frac{l_1^2}{a^2}+\frac{l_2^2}{b^2}+\frac{l_3^2}{c^2}\right],l_1,l_2,l_3=1,2,\cdots. \tag{1}$$

Under periodic boundary conditions, the energy level is

$$E_{l_1,l_2,l_3}=\frac{h^2}{2m}\left[\frac{l_1^2}{a^2}+\frac{l_2^2}{b^2}+\frac{l_3^2}{c^2}\right],l_1,l_2,l_3=0,\pm1,\pm2,\cdots. \tag{2}$$

If the well has contracted α^{-1} of the original well, from (1), we have

$$E_{n_1,n_2,n_3}=\frac{h^2}{8m\alpha^2}\left[\frac{n_1^2}{a^2}+\frac{n_2^2}{b^2}+\frac{n_3^2}{c^2}\right],n_1,n_2,n_3=1,2,3,\cdots. \tag{3}$$

The wave functions corresponding (1) and (3) are recpcetively

$$\psi_{l_1,l_2,l_3}(\vec{r})=\sqrt{\frac{8}{abc}}\sin\left(\frac{l_1\pi}{a}x\right)\sin\left(\frac{l_2\pi}{b}y\right)\sin\left(\frac{l_3\pi}{c}z\right). \tag{1a}$$

$$\psi_{n_1,n_2,n_3}(\vec{r})=\sqrt{\frac{8}{\alpha^3abc}}\sin\left(\frac{n_1\pi}{\alpha a}x\right)\sin\left(\frac{n_2\pi}{\alpha b}y\right)\sin\left(\frac{n_3\pi}{\alpha c}z\right). \tag{3a}$$

If a particle is in an eigenstate (l_1,l_2,l_3) before contraction, the particle will no longer be in a definite energy eigenstate after contraction[2]. Let wave function after contraction be

$$\Phi(\vec{r},t)=\sum_{n_1,n_2,n_3}c_{n_1,n_2,n_3}\psi_{n_1,n_2,n_3}(\vec{r})e^{-iE_{n_1,n_2,n_3}t/\hbar}. \tag{4}$$

From (1), (3a) and (4), we have computed and obtained

$$C_{n_1,n_2,n_3}=\frac{8l_1l_2l_3\alpha^{3/2}}{\pi^3}(-1)^{l_1+l_2+l_3}\sin\left(\frac{n_1\pi}{\alpha}\right)\frac{1}{n_1^2-(l_1\alpha)^2}\sin\left(\frac{n_2\pi}{\alpha}\right)\cdot \frac{1}{n_2^2-(l_2\alpha)^2}\sin\left(\frac{n_3\pi}{\alpha}\right)\frac{1}{n_3^2-(l_3\alpha)^2},n_1\neq\alpha l_1,n_2\neq\alpha l_2,n_3\neq\alpha l_3, \tag{5}$$

$$C_{\alpha l_1,\alpha l_2,\alpha l_3}=\frac{1}{\alpha^{3/2}}\delta_{n_1,\alpha l_1}\delta_{n_2,\alpha l_2}\delta_{n_3,\alpha l_3}.$$

From (5), we have proved the mean energy of particle at new states

$$\overline{E}=\sum_{n_1,n_2,n_3}\left|C_{n_1,n_2,n_3}\right|^2E_{n_1,n_2,n_3}=E_{l_1,l_2,l_3}. \tag{6}$$

(6) shows that the conservation law of energy is obeyed before and after contraction, but energy can be redistributed. We have also obtain that the mean square error of particle energy at new states

$$\overline{(E-\overline{E})^2}=\sum_{n_1,n_2,n_3}\left|C_{n_1,n_2,n_3}\right|^2E^2_{n_1,n_2,n_3}=\infty. \tag{7}$$

For periodic boundary conditions, the same proof can be completed. Equations (3), (5) and (7) show that after contraction, Maxwell-Boltzamann distribution (MBD) is not satisfied. From (7), we know that the possibility of distinct deviation of particle energy from mean energy increases greatly. If $\alpha >>1$, from (3), we know that the energies of near ground state decrease clearly. Before contraction, the distribution of particle energy satisfies MBD. Mean energy of a particle is $\overline{E}=\frac{3}{2}k_BT$. Let T=273K, one obtains $\overline{E}=3.5\times10^{-2}$ ev. Let a=b=c, a' =b'=c'= α a=1 nm, from (3), we have obtained $E_{111}=3.1\times10^{-4}$ ev, $E_{121}=6.2\times10^{-4}$ ev. Under periodic boundary conditions, $E_{000}=0$, $E_{100}=4.1\times10^{-4}$ ev. Clearly, $\overline{E}>>E_{111}$, E_{121}, E_{100}. After contraction, when a particle is at states near ground state, its energy was transfered to a particle at state with high energy. This is a process of concentrating energy.

2. The effect of Bose-Einstein condensation (BEC)

Deuterium nucleus ${}_1D^2$ is a boson. If the system of ${}_1D^2$ is regarded as a system of ideal bosons, its teperature of BEC is

$$T_c(\infty)=\frac{h^2}{2\pi mk_B}\left(\frac{n}{2.612}\right)^{2/3}. \tag{8}$$

Let n_D equal the density of Pd, $n_D=0.67\times10^{23}/cm^3$. Substituting this in (8), one obtains $T_c(\infty)\approx 13.15K$. Considering the effects of finiteness of system[1], under Dirichlet and Periodic boundary conditions, we have respectively

Nuclear Physics Approach

$$t_c = \frac{T_c - T_c(\infty)}{T_c(\infty)} = \frac{4\pi^2}{75\zeta\left(\frac{5}{2}\right)}\left(\frac{\pi}{15}\right)^{\frac{1}{4}} N^{\frac{1}{4}}, \tag{9}$$

$$t_c = \frac{8}{15}\frac{\zeta\left(\frac{3}{2}\right)}{\zeta\left(\frac{5}{2}\right)} N^{-1}. \tag{10}$$

From the two equations, finiteness can increase T_c, but T_c is still less that room temperature 273k.

Diameter of Pd is 0.275 nm and one of atom D is 0.092 nm. When a lattice point of Pd is displaced by atoms D, the number of atoms D, which can be contained, is

$$\left(\frac{0.275}{0.092}\right)^3 \approx 26.71.$$

If four neighboring lattice points of Pd are displaced by atoms D, the number of D is 106.84. This equivalent to a increase in N_D by 106.84 times. From (8) and (9), we obtain $T_{c'}$ (∞)=296.1K and $T_{c'}$=320.1K. Then, the system can produce BEC. The N_0 of particles at ground state is

$$N_0 = N\left[1 - \left(\frac{T}{T_c}\right)^{3/2}\right]. \tag{11}$$

We obtain N_0=0.212N. These particles transfers their energy to the particles at excited states. The contribution of energy which is supplied by one particle of ground state equals about 10^{-2} ev. But the process of concentraing energy has only a less probability to supply at energy several ev to particles at excited states. Thus, cold fusion connot take place.

If the space of size 27.5 nm in Pd lattice is occupied by D atoms, n_D increases to 26.7×10^6 times over the original value. We obtain $T_c = 1.17 \times 10^6$K. From (11), we obtain that the number of particles at exited states is $N' = 3.5 \times 10^{-6}\ N_0$. Each particle at ground state contributes energy 10^{-2} ev. A particle at excited states can obtain energy $10^{-2} \times (N_0/N') = 2.8 \times 10^3$ ev averagely. Deuterium nucleus ${}_1D^2$ having 10 ev can lead cold fusion at considerable probability through quantum tunnel effect.

Therefore, when atoms D concentrate in large quantities or a large cluster of atoms D are poured into Pd lattice, BEC can lead cold fusion. This work was supported by Chinese National Science Foundation Grant and by Yunnan Science Foundation Grant.

Reference

1. Peng, Kuangding, Phys. Rev. B, 48(1993), 9636.
2. J.G. Cordes et al., Am. J. Phys., 52(1986), 155.

THE NUCLEAR REACTIONS IN CONDENSED MEDIA FOR INTERACTION OF CHARGED PARTICLES IN ENERGY REGION IS FORMING BY MAXIMUM ELASTIC LOSSES

V. A. ROMODANOV, V. I. SAVIN, * Ya. B. SKURATNIK, ** V. N. MAJOROV

StateSRI SPA "LUTCH", Zheleznodorozhnaya 24, Podolsk, Moscow reg. 142100. RUSSIA.
T. :095-137-9258. F. :095-137-9384. E-m.: luch@adis.msk.su
* StateSC RF "Karpov SRPCI", Vorontsov pole 10, Moscow, 103064. RUSSIA.
** RSC "Kurchatov Institute", sq. Kurchatov 1, Moscow, 123292. RUSSIA

Abstract

The main requirements to reproduce the generation of nuclear reactions in condensed media (NRCM), have been identified which appear to influence the interaction of fast hydrogen ions with a solid target in a powerful plasma glow discharge. Phenomenon of three branches of physics have contributed to this work: nuclear physics, solid state physics and low energy plasma physics, and have in turn opened a new direction of fundamental research. The essence of this new direction is the ability of a low-energy plasma to interact with a solid target, creating nuclear reactions at a rate several orders of magnitude than predicted by calculations for the some conditions.
The experimental results are presented which validation the formation of a new direction for nuclear research.

1. Introduction

Earlier work [1-3] as shown, that by using particular conditions to stimulate NRCM at low energies of interacting particles, excess energy can be created. These reactions arise at bombardment of a solid specimens by accelerated of a hydrogen isotopes, besides the quantity of generated energy can be registered on such products of the nuclear reactions, as for example, tritium. The set of experimental results is already sufficient as for formation of scientific problems, as main directions of use NRCM.

The present work is devoted to formulating this new field of nuclear phenomena and assessing the prospects of their practical use power systems.

2. Equipment and Methodology

Experiments to study excess heat, production of transportation elements and generation of neutrons and tritium, helium-3 and helium-4, charged particles, and gamma and x-ray radiation were carried out primarily by using DC glow discharge in the upgraded installation UVN-84R-1 [4].

The 250-1 vacuum chamber included a heater for outgassing the chamber. The discharge unit consisted of a sample-cathode, anode, ceramic insulators and thermocouples. The vacuum system consisted of two turbo-molecular pumps TMN-200 and TMN-500, trap by nitrogen, a mechanical pump and control valves. The plasma-forming gas was filled into the chamber through a system of filtering and control valves. The pressure was controlled by thermo-coupling, ionization, mechanical and oil pressure gauges in a range from 10^{-6} Pa up to 10^{5} Pa.

The essence of our experiments [4-7] consisted that ions of hydrogen isotopes were bombarded the sample-cathode of plasma glow discharge at submission of negative potential on the sample. For sample use plates, tubes with thickness of walls of 0.2-5 mm and rods by a diameter of 2-20 mm. Samples were made from diverse metals, predominantly from hydride-formation and refractory. The basis of a plasma-formation gas was deuterium with the contents protean in atomic fractions up to 5% and tritium up to $(6\text{-}8)*10^{-10}$% pressure which supported in limits $(1\text{-}1.5*10^{5})$ Pa.

The energy of ions, depending on pressure, was evaluated within the limits of 0.7-0.01 from voltage of the glow discharge, which changed from 200 V up to 10,000 V. The current density made 5.10^2 – 10^5 A/m^2. The sample temperature during researchers set of 700 K for 3600 K.

Registration of slow neutrons executed by a system RTM from 60 gauges SNM-12 on the basis helium-3. The registration of fast neutrons was executed in addition by a shield the device RUP-one with scintillator on the basis of a zinc sulfide activated by silver. The sensitivity of measurement a flow of neutrons reached 1 neutrons/S, and the air was limits within of the order from measured magnitude.

Analysis of the deuterium on tritium, assembled before and after ions bombardment, conducted on beta-activity by a liquid scintillation method on the equipment Beta-2. The error of measurement of the contents tritium in tests made 10-50%.

3. Main results

Researches on measurement of flow neutrons, conducted at bombardment of various elements by accelerated deuterium ions from a plasma of glow discharge with energy up to 10 keV have shown, that the excess of background level on fast neutrons reaches not more double excess even for a tritium-titanium target [4].

The most significant results are received by us at registration NRCM on a tritium generation. The initial level tritium in deuterium, measured on beta activity, is exceeded on four-five orders, and the tritium generation rate reached 10^9 Atom/s four glow discharge and 1015 Atom/s for a device on the basis Z-pinch. Thus the coefficient of nuclear interaction has about 10-10 Atom/ion.

Measurements of tritium in a gas confirmed by duplication of measurements on flowing beta-recorder from a surface sample, at simultaneous registration of a spectrum energy, radiography of a surface at the x-ray films as well as control of the tritium contents in the material sample.

It is fixed tritium transmutation in zirconium on high-energy beta-activity of radiated samples, with zirconium-to-tritium flux ratio at the level 10^{-7} – 10^{-6}. The main experimental results, which permit to declare formation of a new direction of nuclear researchers, can be grouped in the following order:

1. The rate NRCM in the energy range of ions 10 - 10,000 eV, determined on the tritium generation rate, exceeded of the calculation for thermonuclear channel on a some orders.

2. The neutron-to-tritium branch ratio on generation rate measured by us reached 10^{-9} - 10^{-7}, which while it is impossible to consider final of in comparison, small flows of neutrons [4]. These results will be well agreed other researchers, for example, with [8]. Usually, at high-energy interaction, this ratio is close unit.

3. The speed of nuclear reactions depends on the nuclear number of a target material and concentration of a hydrogen in the material. According to experimental results, the rate NRCM was increased with increasing concentration of the hydrogen and increasing nuclear number of the target material and maximum results, up to the present time, are received on zirconium, niobium and tungsten [2, 4]. However, for heavy materials, located higher in the middle Mendeleev table, unequivocal results to receive has not managed. While it is not known, whether it is connected with insufficient optimization regimes of ion bombardment or with new law.

4. Dependence of efficiency NRCM from energy of ions is present by self threshold dependence (about 100 eV) and is weak varying at energy higher threshold.

5. Four processes NRCM the dependence of a tritium generation efficiency from current density is close to linear [1]. It give a opportunity to select parameters of ion bombardment for maintenance of necessary speed of nuclear reactions.

6. The dependence of efficiency tritium generation from pressure of the plasma-forming gas has maximum in the range 100000-300000 Pa and has no analogues in usual processes [5].

The submitted dependences are received in a plenty of experiments, the general number of which exceeds thousand, that makes results statistically determined and conclusion-safety.

4. Discussion

At use bombardment by accelerated ions for targets of containing hydrogen , for stimulation of nuclear reactions in condensed media, maximal specific excitation for loading hydrogen is reached at maximal relation for elastic and unelastic losses of energy by ions, driving in given media. This energy depends on the masses of interacting particles and for hydrogen is on level of several tens eV [4]. This energy already enough for creation radiations, structural damage of materials [9]. Thus, intensive ion bombardment can render the influence as on characteristic of interaction protons of solid in surface layer (the nonactivation interaction on length of free run and for reason of diffusion parameters change in process radiation), as in volume of solid at increased temperatures (for reason change of static and dynamic parameters on structure of material, affecting diffusion and solubility). At temperatures above 0,3 $T_{пл}$ the moving of dot defects and defects of dislocation type from surface layer of metal deep into, on distances, considerably the exceeding zones of free run of ions (some of orders) [9] is observed as diffusion. The study of this question has shown, that the intensity of change of structure is possible to be evaluated on "effective coefficient of dislocation diffusion". We made assumed, that effective coeffitient diffusion dislocation it is present the multiplication of self-diffusion coefficient under condition thermo-activation and self-diffusion coefficient under condition ion bombardment : $D_{эфф} = D_{терм} \cdot D_{рад}$. We used dependence $f(x) = kx/ a + x$ for approximation of the experimental datas and for getting the self-diffusion coefficient under condition of ion bombardment $D_{рад}$ on known $D_{терм}$ and $D_{эфф}$. The coefficients a and k was got out experimental datas by the method of lesser squares:

$$D_{efd}=0.280^{\left(\frac{386020}{RT}\right)}\cdot 0^{\frac{[E_t\cdot 0.25\sqrt{\rho(\varepsilon)}\cdot\sqrt{M_1/M_2}]/(0.2+\sqrt{\rho(\varepsilon)})\cdot(0.2+\sqrt{M_1/M_2})}{KT}}$$

Were: R-gase constant; k-constant of Bolzman; T-temperature; E_t-threshold energy for displacement of atomtarget; r(e)-specific projection run of ion in target material; M_1-ion masse; M_2-atom masse of target.

The calculation accurasy by this formula for energy (10 - 10000 eV) and temperature (0.3 - 0.7) $T_{пл}$ it is estimate in one order of value (Fig. 1). From drawing it is visible, that the change of structure happens much slower of hydrogen diffusion. So for molybdenum, at temperature 1900 K effective coefficient diffusion for protium has made about $4\cdot10^{-7}$ $m^2\cdot s^{-1}$, and coefficient diffusion for dislocations made about 10^{-10} - 10^{-11} $m^2\cdot s^{-1}$ at energy of ions, order 500 eV and density of current 300 A/m^2. It is thus possible to conclude, that the stimulating action of ion bombardment on efficiency NRCM flowing can consist in increase for quantity of protons collisions and deuterons in surface layer and in increase of hydrogen concentration in volume as for reason of surface barriers, as for reason structures radiation damage and formations new one.

5. Use Direction Of NRCM

- Power engineering.

The new class offered to use of reactions will allow to expand scientific base of a nuclear power and to create the new areas for its application. On the basis of use for offered reactions it is probably to develop technological pro-

Nuclear Physics Approach

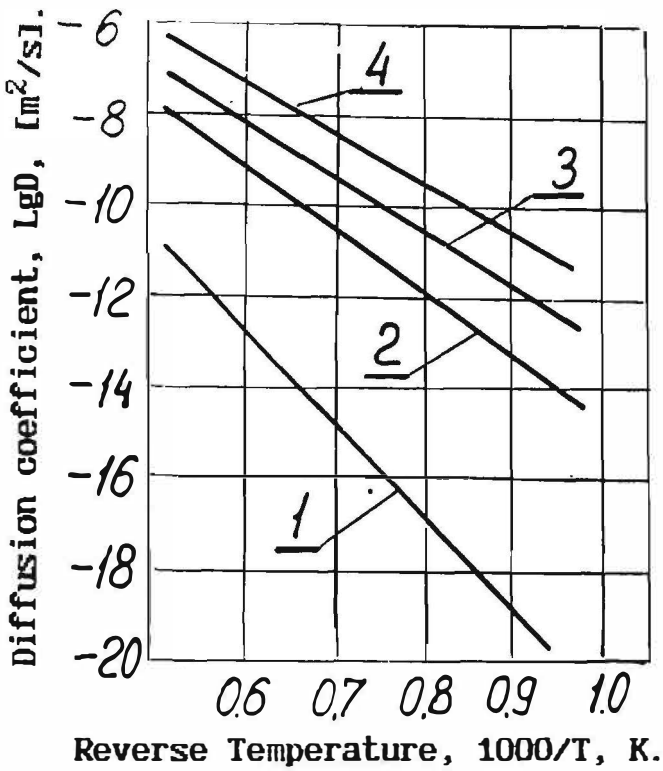

Fig. 1. The dependence of coefficient diffusion for dislocation versus reverse temperature. 1-Energy ions- 0 eV; 2- 40 eV; 3- 4000 eV; 4- 40000 eV.

cesses of manufacturing stationary, mobile and transport power installations with increased ecological.

Storage and processing wastes.

The increase of ecological safety to bury of a fulfilled nuclear fuel is possible at revealing of a acceptable way to transfer of long time living nucleuses a radio-active elements, for example, Pu in a few time living isotops. Offered use of directed reactions in condensed media for processing a wastes is based on experimental results and theoretical reasons, that the speed of specified reactions for heavy elements can be whole on two and four order less in comparison with speed for easy.

- Rare isotops generation.

As the most perspective direction transmutation at the expense of nuclear reactions in condensed media at low energy of interacting particles it is possible to consider a operating time of astable easy elements for a science, manufacture and medicine, for example, to the tritium generation for termonuclear reactors.

-Isotops sources of a light and energy.

The low cost of generation for low energy isotops in offered nuclear reactions makes it is possible development of diverse technologies for use isotops in independent sources of the light and energy.

6. Conclusion

6.1. The submitted complex of experimental results testifies that a new direction of nuclear researches as on a range used energy, as on features flowing of reactions and structure of products which generated.

6.2. It is shown, that safety of received results is reasonably high, as far as they are received in a plenty of experiments by poweful glow discharge for high temperature and structure modification, statistically are determined .

Nuclear Physics Approach

6.3. It is marked, that the main directions of use NRCM in a power engineering, rare isotops generation and processing waste are expand a sphere of application to conventional sources of nuclear energy and improve its the economic and ecological characteristics.

References

1. V.A.Romodanov, V.I.Savin, Ya.B.Skuratnik.
" The Demands to System Plasma - Target for Obtaining a Balance Energy from Nuclear Reactions in Condensed Media ".- **Cold Nuclear Fusion** (Materials of the 2-d Russian conference on cold fusion and nuclei transmutation. Sochi, Russian, 19-23.09.94 y.) M.: SRC PTP "ERZION", (1995), p. 99-106. (In Russian).

2. V.A.Romodanov, V.I.Savin, V.A.Alekseev, Ya.B.Skuratnik at al.
" The Tritium Generation in Dependence from Material of Target for Interaction of Plasma Flux Dense with Metal Surface ".- Ibidem., p.91-98.

3. V.A.Alekseev, I.I.Borisov, V.A.Vasil´ev, V.A.Romodanov at al.
" The Tritium Generation for Interaction of Plasma Flux Dense with Metal Surface".- **Letters in JTP**, (1995), v.21, n.6, p.64-68. (In Russian).

4. V.A. Romodanov, V. Savin, Ya. Skuratnik and Yu. Timofeev.
" Nuclear Fusion in Condensed Matter ".- **Frontiers of Cold Fusion**. Proceedings of the Third International Conference on Cold Fusion. October 21-25, 1992, Nagoya, Japan. Ed. By H.Ikegami. Universal Academy Press Inc., Tokyo, Japan, (1993), p.307-319.

5. V. Romodanov, V. Savin, Ya. Skuratnik, V. Elksnin.
" Reproducibility of Tritium Generation from Nuclear Reactions in Condensed Media " .-Proceedings; Fourth International Conference on Cold Fusion. December 6-9, 1993, Lahaina, Maui, Hawaii. TR-104188-V3, EPRI, (1994), p. 15 (1-15).

6. V. Romodanov, V. Savin, Ya. Skuratnik, S. Korneev.
" Concept of Target Material Choice for Nuclear Reactions in Condensed Media ".- // Ibidem, TR-104188-V3, EPRI, (1994), p.22 (1-13).

7. V.Romodanov, V.Savin, Ya.Skuratnik, S.Korneev, A.Glagolev.
" Ecological Aspects of Thermal Systems Using Hydrogen Isotopes ".- // Ibidem, TR-104188-V4, EPRI, (1994), p.40 (1-15).

8. S.F.Taylor, T.N.Claytor, D.G.Tuggle, S.E.Jones.
" Search for Neutrons from Deuterided Palladium Subject to High Electrical Currents ".- **Transactions of Fusion Technology**, (1994), v.26, n.4 T, part 2, fuste 8 (4) 1-540, p.180-185.

9. A.A.Babad-Zakhrjapin, V.A.Romodanov.
" Hydrogen Permebility for Single-Cristal Molybdenum ".- Questions Of Nuclear Sciences And Engineering. Ser.: Physics of radiation damages and radiation material science. 1991, n. 2 (56), p. 69-72. (in Russian).

Nuclear Physics Approach

INVESTIGATION OF NUCLEAR EMISSIONS IN THE PROCESS OF D(H) ESCAPING FROM DEUTERIZED (HYDROGENIZED) PdO-Pd-PdO AND PdO-Pd-Ag SAMPLES.

A.S. ROUSSETSKI
P.N. Lebedev Physical Institute,
Russian Academy of Sciences,
Leninsky Prospect 53, 117924, GSP,
Moscow, RUSSIA

ABSTRACT
Emission of proton-like and neutron-like events was observed in the process of escaping deuterium from deuterized PdO-Pd-Ag and PdO-Pd-PdO samples. The ratio of the proton-like and neutron-like event fluxes was estimated as $N_p/N_n \cong 1$.The charged particle emission was also observed in the process of escaping hydrogen from hydrogenized PdO-Pd-Ag and PdO-Pd-PdO samples. The emitted charged particles may be identified asprotons and α-particles. Investigation of charged-particle emission was carried out by 3 methods: (1) plastic scintillation counter; (2) Si-SSD; (3) CR-39 plastic track detector. The results obtained by these independent methods are in good agreement with each other.An effect of the weak thermal neutron flux on the processesof cold fusion in the samples loaded with D(H) was also investigated. It was observed that the flux of neutrons emitted from deuterized PdO-Pd-Ag samples exposed by thermal neutrons was approximately 300 times as large as in the case of unexposed samples.

1.INTRODUCTION

As was shown in /1/, heat bursts and neutron emission takeplace as a result of escape of deuterium from electrolytically deuterized PdO-Pd-Au samples. This effect was reproduced inmany series of experiments performed by dr. A. Lipson's group from the Institute of Physical Chemistry, Russian Academy of Sciences.The PdO-Pd-Ag and PdO-Pd-PdO samples demonstrate the same properties as PdO-Pd-Au ones. These are the samples that were used by us for investigating nuclear emission.The experimental task was to study channels of nuclear reactions that take place in Pd samples electrolytically loaded with D(H).

The PdO-Pd-Ag and PdO-Pd-PdO samples were prepared by vacuum annealing of the Pd foil 30 μm thick in the Institute of Physical Chemistry of the RAS. The PdO-layer 200 A thick was produced by annealing in the oxygen while the Ag-layer was created by deposition in the electrolyte. The sample area was 21 x 16 mm^2. The technology of the sample preparation was described in /1/.

2.METHODS

The neutron detector consists of 8 scintillation counters. Each counter contains of a plastic scintillator 5x5x30 cm^3 covered with the 0.5 mm-thick Cd foil and is supplied by 2 end-view FEU-85 photomultiplier tubes (PMT) connected to the coincidence circuit (Fig.1). The detector was surrounded by CH moderator blocks (5 x 5 x 30) cm^3 covered with the Cd foil. A fast neutron emitted as a result of the nuclear reaction in the sample can interact in 1 of

Nuclear Physics Approach

8 scintillation counters.Then it spends its energy in collisions with atoms of C and H of the scintillator and moderator and is slowing down to thermal energy E = 0.026 eV. At the final stage, the thermal neutron is captured by Cd with emission of gamma-quanta that also can be detected by the same counters.The efficiency of the neutron detector measured with the neutron (Po-Be) source placed in the central detector cell was n ≅ 1%. The measured background rate was N_b = (0.050 ± 0.005) 1/s.The charged-particle emission was investigated by 3 methods:(1) Plastic scintillation detector; (2) Si-SSD; (3) CR-39 plastic track detector.

The plastic scintillation detector is 1 mm thick and 30 mm in diameter and has a photomultiplier (PMT). A sample was placed at a distance of 1.5 cm from the scintillator (Fig. 2). There was Al foil 12 μm thick between the sample and the scintillator to prevent the effect of light on the PMT. The detector was calibrated by α-particles from Pu-239 source and by secondary protons from interactions of neutrons of (Po-Be) source with scintillator nuclei.Si-SSD with the active area of 1.25 cm and the active thickness of 100 μm was screened by the 12 μm Al-foil. The distance between the sample and the detector was 3 mm. The detector was calibrated by α-particles of the Pu-239 source.

The track detector was the 600 μm-thick plastic film. Charged particles stopping in outer detector layer produce tracks that became visible after etching. The 6N NaOH solution at a temperature t = 70°C was used for etching for 7 hours. The track shape presents information on the type of the particleand its energy. For calibration, the CR-39 film was exposed to α - particles and protons of known energies.

In the process of electrolysis of the 1M solution of NaOD in D_2O or KOH in H_2O, the PdO-Pd-Ag and PdO-Pd-PdO samples were used as cathodes. The Pt was taken as an anode. The current density was 15 ÷ 20 mA/cm^2. The duration of the electrolysis was 5 ÷ 15 min. The sample loaded with D(H) was washed in pure $D_2O(H_2O)$ and dryed by the filter paper. Then, it was placed near one of the detectors mentioned above. The measurement time was about 1 hour. Furthermore, the sample was loaded with D(H) again. Each sample was used for 15-20 cycles of electrolysis and then was changed.

3. RESULTS

3.1. Measurements using neutron detector and plastic scintillation detectors.

The experimental task was to estimate the yields of two possible channels of (dd) fusion reactions:

$$d + d \Rightarrow n(2.45\ MeV) + He^3\ (0.82\ MeV) \quad (1)$$

$$d + d \Rightarrow p(3.02\ MeV) + T(1.01\ MeV) \quad (2)$$

The PdO-Pd-PdO sample was loaded with D(H) according to the procedure mentioned above and then was placed at the distance 1.5 cm from the scintillator, that was screened by the 12 μm Al foil. (Fig. 2). To stimulate the escaping gas from the sample, it was heated up to 40°C by the hot air during the first 300 s of the experiment. The controlling experiment was carried out with an unloaded sample during the same time and under the same conditions.As a result of the experiments, it was found that the spectra of emission from the deuterized, hydrogenized and unloaded samples which were measured by the scintillation detectors

differed from each other. (See Figs. 3a, 3b). The detector lower energy threshold corresponded to proton energy $E_p \cong 0.5$ MeV.

To estimate the yield of reaction (2), the number of events withthe energy 0.5-2.5 MeV for the hydrogenized sample was substracted from that for the deuterized sample. Thus, the proton flux from reaction (2) was estimated as $N_p = (0.75 \pm 0.08)$ 1/s into 4π steradian. The neutron emission was also studied. However, it did not differ from the background level $N_b = (0.050 \pm 0.005)$ 1/s. If we take into account the neutron detector efficiency n = 1%, the minimum neutron flux accessible to registration was on the level 5 n/c into 4π steradian. Therefore, another method was used to estimate the neutron flux from reaction (1).It was assumed that a neutron from reaction (1) can, at first, interact in the thin plastic scintillator. Then the second inter- action takes place in the scintillators of the neutron detector. The neutron flux can be estimated as a number of such double coincidences. The detection efficiency was estimated as $\cong 4\ 10^{-4}$. The difference between spectra of deuterized and hydrogenized samples in the case of signal coincidence from 2 detectors is presented in Fig. 3c. The neutron flux was estimated by number of events in the energy range 0.5÷2.45 MeV as $N_n = (0.6 \pm 0.2)$ 1/s into 4π steradian. Thus, we may conclude that the ratio of neutron and proton fluxes from reactions (1) and (2) is $N_n/N_p \cong 1$.

3.2. Measurements with Si-SSD.
To verify the results obtained, the measurements with Si-SSD were carried out. A PdO-Pd-Ag or PdO-Pd-PdO sample was loaded with D(H) according to the procedure mentioned above. Then, the loaded sample was placed near the Si-SSD. The charged-particle spectra obtained with different samples are presented in Figs. 4a, b. In this case, the measurement with the same sample in 1 hour after the first experiment (when the main part of D(H) excaped the sample) was used for control .The spectrum of the charged particles detected by Si-SSD is in good agreement with the spectrum for the same samples obtained with plastic scintillation detector.The disadvantage of both methods was impossibility to determine the type of charged particles. Therefore, measurements using CR-39 plastic track detector were performed, which allowed us to obtain information on the type of the emitted particles.
3.3. Measurements with CR-39 plastic track detector.
A sample was electrolytically loaded with D(H). Then the PdO side of the sample was kept in contact with the 1 half of the track detector. The unloaded sample was kept in contact with the other one-half of the track detector. In both cases the time of contacting was 0.5-1 hour. In total, the detector was exposed for 15 hours (15÷30 cycles of sample loading). Then it was etched in 6N solution of NaOH at 70° C during 7 hours. The results of measurements with using a microscope are presented bystograms (Figs. 5a,b). They show the number of tracks per cm^2 in a certain range of track diameters. The background was estimated as a number of tracks per second from the unloaded sample. The effect-to-background ratio was found to be 2-4 depending on the type of a particle. Particles were identified by calibration measurements, showing that track diameters less than 8 μm corresponded to

protons, while track diameters of 8÷15 μm corresponded to α-particles. Track diameters exceeding 15 μm correspond to heavier charged particles (Li, Be-nuclei). Thus, it is possible to conclude that the samples were emitting protons. α -particle emission is also possible. According to /3/, α-particles may result from fusion reaction of 3 and more particles (p or d).The events with track diameters more than 15 μm were investigated separately. The density of such events for deuterized PdO-Pd-Ag sample was (66 ± 11) $1/cm^2$ against the background of (8 ± 3) $1/cm^2$. It seems probably that this effect was caused by emission of heavier particles (Li or Be nuclei).

3.4. Effect of thermal neutrons on particle emission from deuterized PdO-Pd-Ag samples.

As was shown in /2/, neutron emission caused by (dd) fusion reaction in the KD_2PO_4-crystals is enhanced by an influence of weak thermal neutron flux. We made an attempt to check a possibility of increasing the fusion reaction yield for PdO-Pd-Ag samples electrolytically loaded with D(H) by exposing them with thermal neutron flux. Cf-252 was used as a neutron source $E_n \leq 2.3$ MeV. Its intensity was $A \cong 180$ n/s into 4π steradian. The source placed in the Pb container was installed into the central cell of the neutron detector. There was a (CH) moderator between the neutron source and the sample as well as behind the sample. The PdO-Pd-Ag sample was electrolytically loaded with D(H). The PdO side of the loaded sample was in contact with the CR-39 track detector. The control CR-39 detector was in contact with the unloaded sample. Then the assembly was placed at a variable distance r from the Cf-252 source.The efficiency of the neutron detector with the central cell filled with CH was $n \cong 2 \cdot 10^{-4}$. The intensity of background in the presence of the Cf-252 source was N_b = (0.085±0.005) 1/s. The dependence of the fast neutron flux emitted by deuterized PdO-Pd-Ag sample as a function of the distance r between the sample and the source is presented in Fig 6. In contrast to the neutron flux from the unexposed sample which was estimated as N_n = (0.6 ± 0.2) n/s into 4π steradian (3.1), the neutron flux from the exposed sample attained N_n = (200 ± 20) n/s into 4π steradian. Thus, the fast neutron flux from the deuterized sample increases by a factor of $3 \cdot 10^2$ in the presence of the external thermal-neutron irradiation.The track density for protons in CR-39 was estimated as $4 \cdot 10^5$ $1/cm^2$. It is ~10^2 times more than the case of unexposed sample.The estimated proton flux was N_p = (160 ± 20) 1/s into 4π sr.So the ratio of proton and neutron fluxes in the case of thermal neutron exposed sample was $N_p/N_n \cong 1$.

4. CONCLUSION

As the result of the experiments, we may make the following conclusions.

(1) Emission of proton-like and neutron-like events was observed in the process of escaping D from deuterized PdO-Pd-Pd and PdO-Pd-Ag samples. The ratio of the fluxes of the proton-like and neutron-like events is $N_n/N_p \cong 1$. It is possible to conclude that the fusion reactions (1) and (2) take place in these samples.

(2) Charged-particle emission was observed in the process of escaping H from hydrogenized PdO-Pd-Ag and PdO-Pd-PdO samples. These particles may be identified as protons and α-particles. We failed to determine the nature of this emission. The emission of neutron-like events was not observed in the case of hydrogenized samples.
(3) We observed an effect of the weak thermal neutron flux on the emission from the deuterized PdO-Pd-Ag samples. The gain factor for the fast neutron emission $3 \cdot 10^2$ as compared to the unexposed samples. Possible explanations for the mechanism of this effect was proposed by Kozima /4/ and Hagelstein /5/.

ACKNOWLEDGMENTS
In conclusion, the author would like to thank Prof. G.I. Merzon and Prof. V.A.Tsarev for their support and stimulating discussions. I am also grateful to Dr. A.G. Lipson and B.F. Lyakhov for their help in preparation of the samples and fruitful discussions. I would like also to thank Dr. A.M. Marenny and N.A. Nefedov for their help during the work with CR-39 track detectors.

REFERENCES

1. A.G. Lipson, B.F. Lyakhov, B.V. Deryagin, and D.M. Sakov, Letters to JTP, 1992, v. 18, 20, p. 58 (in Russian); B.F. Lyakhov, A.G. Lipson and D.M. Sakov, Proc. of the 1-st Russian Conf. on CF (Sept.28 - Oct.2,1993, Abrau-Durso, Novorossiisk) p.154 (in Russian).
2. A.G. Lipson and D.M. Sakov, Proc. of 5-th ICCF (April 9-13, 1995,Monte-Carlo, Monaco) p. 571.
3. A. Takahashi et al., Proc. of the 1-st Russian Conf. on CF (Sept.28 - Oct.2, 1993, Abrau-Durso, Novorossiisk) p. 76
4.H. Kozima and S. Watanabe , Proc. of 5-th ICCF (April 9-13, 1995,Monte-Carlo, Monaco) p. 347.
5. P.L. Hagelstein, Trans. Fusion Tech., 1994, v. 26, No 4T, 461

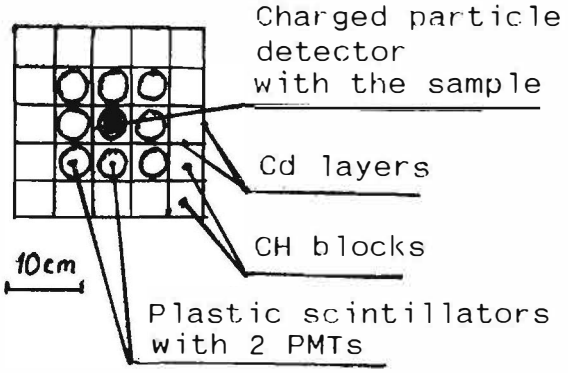

Fig.1. Diagram of the experimental set-up.

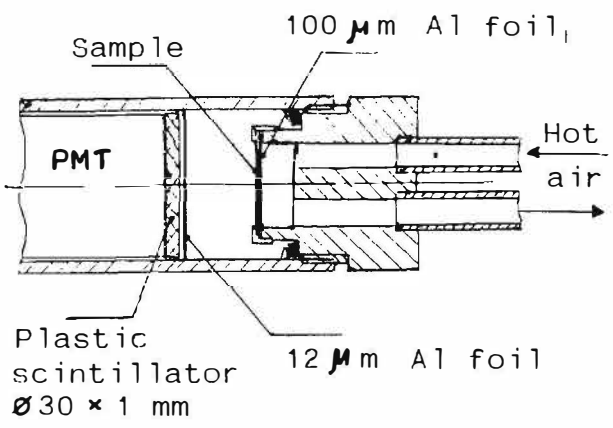

Fig.2. Plastic scintillation detector.

Nuclear Physics Approach

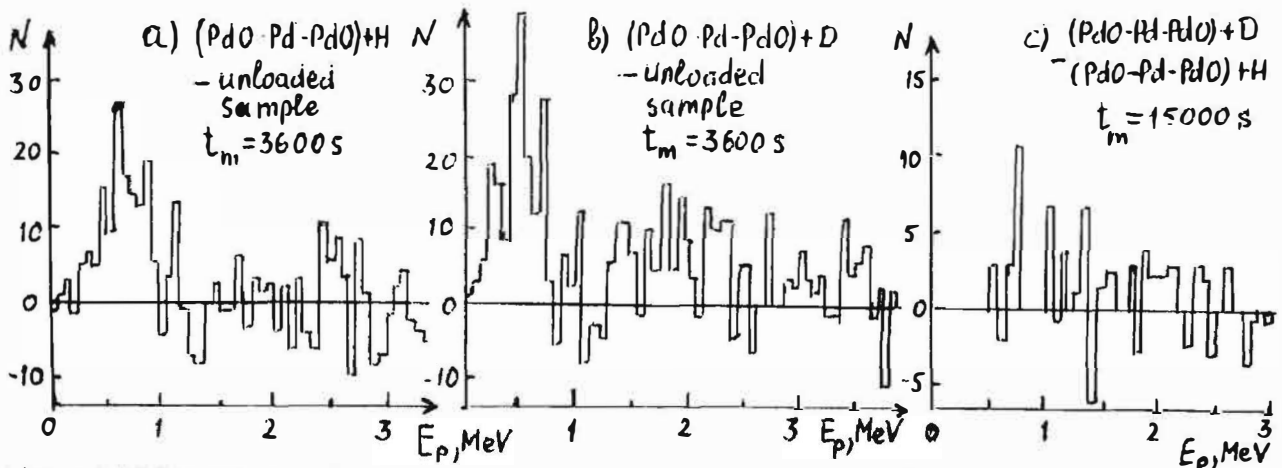

Fig.3 Difference of energy spectra measured by plastic scintillation detector for (a) hydrogenized and unloaded PdO-Pd-PdO samples; (b) deuterized and unloaded PdO-Pd-PdO samples; (c) deuterized and hydrogenized samples in the case of coincidence with the neutron detector.

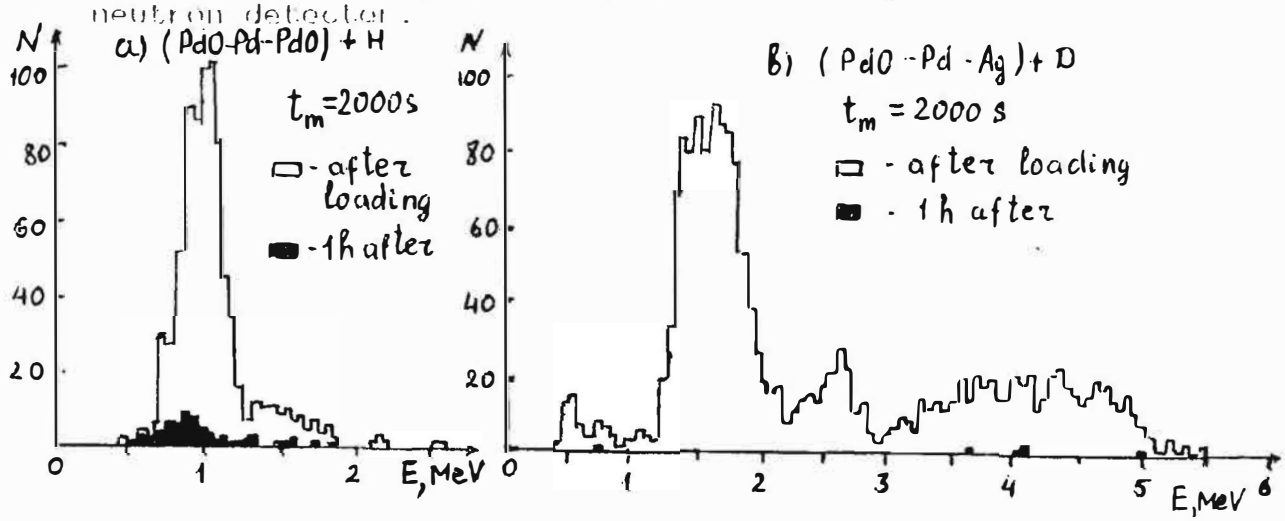

Fig.4 Energy spectra measured by Si-SSD for (a) hydrogenized PdO-Pd-PdO sample; (b) deuterized PdO-Pd-Ag sample (measurement time is tm = 2000s).

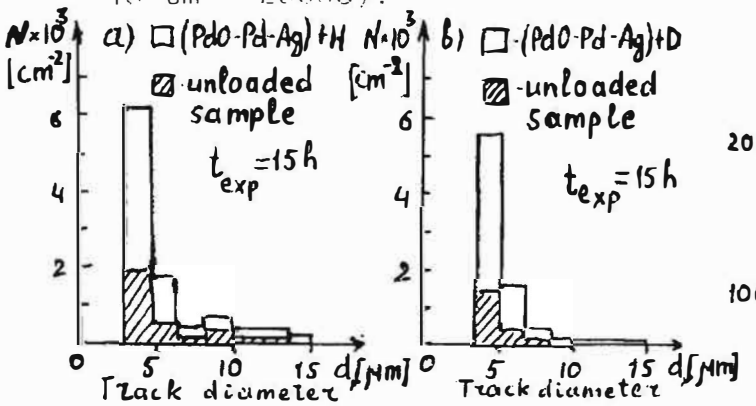

Fig.5.
Diagrams for track density in CR-39. (a) deuterized PdO-Pd-Ag sample; b) hydrogenized PdO-Pd-Ag sample (exposition time is texp = 15h).

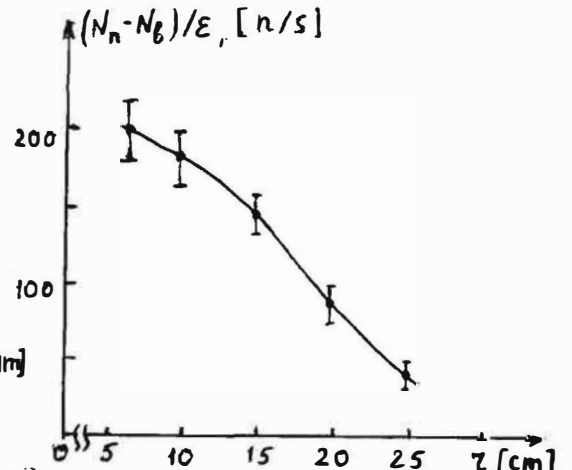

Fig.6.
Neutron flux emitted from PdO-Pd-Ag sample vs thickness r of the moderator between the sample and the neutron source.

Nuclear Physics Approach

Detection for Nuclear Products in Transport Experiments of Deuterium through Palladium Metals

Hiroyuki Shinojima, Takashi Nishioka, Koji Shikano
and Hiroshi Kanbe

NTT Basic Research Laboratories
3-1 Morinosato-Wakamiya,
Atsugi-shi, Kanagawa 243-01 Japan

Abstract

To investigate the possibility of deuterium-deuterium nuclear fusion in a palladium metal, we carried out two kinds of experiments: low-energy deuterium ion bombardments with deuterated palladium, and deuterium transport through palladium. In the bombardment experiments, the cross sections for d(d,p)t reactions were measured to be less than 1.5×10^{-11} b at an ion energy of 2 keV. Measured branching ratios between d(d,p)t and d(d,n)^{3}He were unity in the ion energy range between 2 and 40 keV, even though the deuterium-deuterium nuclear fusion occurred in palladium. We also estimated the minimum detectable values for the charged-particle detection system, NE213 nuclear detector system, ^{3}He counter, and a quadrupole mass-spectroscope system used in both the experiments. In the deuterium transport experiments, we tried to detect nuclear fusion products by using these detector systems placed in a vacuum chamber which extracted deuterium from the sample palladium. Any extraordinary nuclear products, however, could not be observed in the experiments carried out under various temperature variations and for various modifications of palladium surfaces.

Introduction

Since Yamaguchi and Nishioka have reported that the nuclear product ^{4}He, which is direct evidence of nuclear fusion in deuterated palladium metals, was detected by using the "vacuuo method",[1] we have studied the dynamics of deuterium in palladium metals in order to reproduce and confirm the phenomenon. Because the processes by which a palladium metal is loaded with deuterium and the processes by which it is released from the deuterated palladium metals are important for understanding the deuterium dynamics in palladium metals, we measured the loading ratio, the electrical resistance, the surface temperature, and the deuterium pressure in a vacuum chamber.[2]

From the point of view of nuclear physics, on the other hand, as the d+d reactions in the palladium metals by the deuterons with the energy of a few keV are very important for understanding the generation and detection of ^{4}He in the vacuuo method, we have also studied the low-energy nuclear reactions of d+d in the palladium metals by colliding deuterium ions in a palladium metal. We found that above the deuterium ion energy of 5 keV, there was no enhancement of the cross sections of d(d, p)t and d(d, n)^{3}He and that the branching ratios between d(d, p)t and d(d, n)^{3}He were unity independent of the deuteron energy[3].

In this paper we report the two kinds of the experiments - the deuterium ion bombardments with ion energies less than 2 keV and the deuterium transports through the palladium disks - in order to clarify the reaction mechanisms and deuterium dynamics in a palladium metal. The cross sections of d(d, p)t reaction were evaluated in the bombardment experiments. From the results of the bombardment experiments, we also estimated the minimum detectable count-rates of the products due to nuclear fusion reactions. The deuterium transport is a release process of a constant amount of deuterium from palladium surface. In the transport experiments, we tried to detect nuclear products such as protons, toritons, ^{3}He, neutrons, and ^{4}He, in order to confirm the occurrence of

nuclear fusion in a palladium metal using the detection systems.

Experiment

1) Evaluations of the detection limits

In the ion-bombardment and transport experiments, we tried to detect protons, toritons, and ^{3}He by the charged-particle system, neutrons by the NE213 system and the ^{3}He counter, and ^{4}He by the quadrupole mass-spectroscope (Q-mass) system, respectively.

The active areas of silicon surface detectors (SSD) were 450 mm^2. The sensitive depths of two detectors were 100 and 300 μm. A detector was covered with aluminum foil with a thickness of 7 μm or carbon foil with the density of 50 μg/cm^2 held by Ni meshes having 99% open area. Carbon foil was used when trying to detect ^{3}He.

The NE213 system and ^{3}He counter (Aloka Ltd:TPS-451S) were used to detect neutrons. The diameter of the active area of the NE213 detector was 20 inches. Comparing the counts-per-seconds (cps) of the systems for detecting charged particles and neutrons with the natural background cps, we evaluated the detection limits, the minimum detectable values of the systems. The detection limits of the charged-particle detection system were $2x10^{-4}$, $4x10^{-4}$, and $1x10^{-3}$ cps for protons, toritons, and ^{3}He, respectively. The limits of the NE213 system and ^{3}He counter (Aloka Ltd:TPS-451S) for neutron detection were 2 cps.

^{4}He was tried to detect by Q-mass with a cold trap system (Extrel:C50 Mass Spectrometer System). The temperature of the cold trap was 4.2 K to condense hydrogen and deuterium gas. The detection limit of ^{4}He was improved to be better than 1000 times of the limit without the trap. The ^{4}He detection limit of the Q-mass with the cold trap system was estimated to be $3x10^{11}$ cps using ^{4}He standard-leak of $1.3x10^{-7}$ atmcm^3.

2) Deuterium ion bombardment

We have already reported that we measured the cross sections and branching ratio between d(d, p)t and d(d, n)^{3}He as a function of deuterium ion energies (E_d) from 5 to 40 keV[3]. Figure 1 shows the results of the detection of charged particles at E_d=5 keV. The natural background is excluded in Fig. 1.

We tried to detect nuclear products in the deuterium ion bombardments with ion energies less than 2 keV by using the charged-particle, the NE213, the ^{3}He counter, and the Q-mass with a cold trap system. To obtain an ion current density as high as 10 mA/cm^2, an electron-cycrotron-resonance (ECR) ion source with an ion accelerating plate was used to generate the 2-keV deuterium ions. A 30x30x1-mm palladium plate with the loading ratio (D/Pd) of 0.65 was used as a target.

The count rate due to protons generated from d(d, p)t at 2 keV deuterium ion energy was less than that of the natural background. The cross section was estimated from the detection limit to be less than $1.5x10^{-11}$ b. The cross sections and branching ratios of d(d, p)t are shown in Fig. 2 as a function of the deuterium ion energy and good agreement with the theoretical results.[3) 4)] We could not detect ^{4}He in the bombardments of deuterium ion having the energies from 5 to 40 keV.

3) Deuterium Transport

To investigate the deuterium dynamics in the palladium metals and obtain evidence of nuclear fusion within the metals and/or at the metal surfaces, we tried to detect the nuclear products by the same detection systems as we used in the ion bombardment experiments.

The sample was a palladium disk of 21 mm in diameter and 0.5 mm thick. This size is the same as that of the gasket for ICF32-flange. The surface of the sample disks were cleaned chemically by acetone and aqua regia. Some samples were annealed or etched by ECR plasma sputtering. After cleaning the surface of a palladium disk, one side of the disk was coated with a thin film of MnO_x, SiO_2, LiF, Au, or Ag. The Experimental setup was shown in Fig. 3. The vacuum chamber was separated into two parts by the palladium disk. One side was filled with the deuterium at 200 kPa. The other side was evacuated. The deuterium was transported by diffusion through the palladium disk when the sample temperature was raised by a heater. We measured the temperature of the sample surface and the pressures of the deuterium-filled chamber and the vacuum chamber, and tried to detect the nuclear products by using the detection systems described above. All the detectors for nuclear products were placed at the side of the evacuated chamber.

We carried out the transport experiments under various conditions of temperature and deuterium pressure. The results of typical experiments with the deuterium transport through the palladium

disk are shown in Fig. 4, where T is the temperature of the sample surface, and where P_1, P_2 and P_3 are respectively the pressures of the deuterium-filled chamber, the vacuum chamber, and the Q-mass. After 5-hour heating under a constant voltage to keep the temperature at 170℃, the deuterium was filled with the chamber. From 5 to 20 hours, P_1 was constant at 200 kPa. During the following 20 hours, we periodically changed the temperature of the palladium disk from 70℃ to 185℃ by adjusting the heater voltage. After 40 hours, the heater voltage was kept constant. The number of the deuterium molecules transported through the sample was estimated to be from 1.5×10^{17} to 3×10^{17} cps. The outputs of the neutron and ^{4}He detections are shown in Figs. 5 and 6. We could not any signals of the nuclear products during the deuterium transport experiments.

Conclusions

We tried to detect nuclear products in low-energy-ion bombardment experiments and in deuterium transport experiments by using the charged-particle detection system, the NE213 system, the ^{3}He counter, and the Q-mass system. In the ion bombardment experiments, the cross section of d(d, p)t was measured to be less than 1.5×10^{-11} b at the deuterium ion energy of 2 keV. It was found that we could not observe the distinguished enhancement of the cross section at the ion energy above 2 keV as the values of the measured cross section was good agreement with the calculated values from the theoretical results.[5)]

In deuterium transport experiments, we did not detect any fusion products within the detection limits and the accuracy of the systems. We thus obtained no evidence to confirm the extraordinary fusion phenomena in a palladium metal within our detection limits.

References

1) E. Yamaguchi and T. Nishioka, Frontiers of Cold Fusion (University Academy Press), (1993) 179.
3) K. Shikano, H. Shinojima and H. Kanbe, Proceedings of the 5th International Conference on Cold Fusion, (1995) 251.
4) H. Shinojima, T. Nishioka, K. Shikano and H. Kanbe, Proceedings of the 5th International Conference on Cold Fusion, (1995) 255.
5) A. Krauss, H. W. Becker, H. P. Trautvetter, C. Rolfs and K. Brand, Nucl. Phys., A465 (1987) 150.

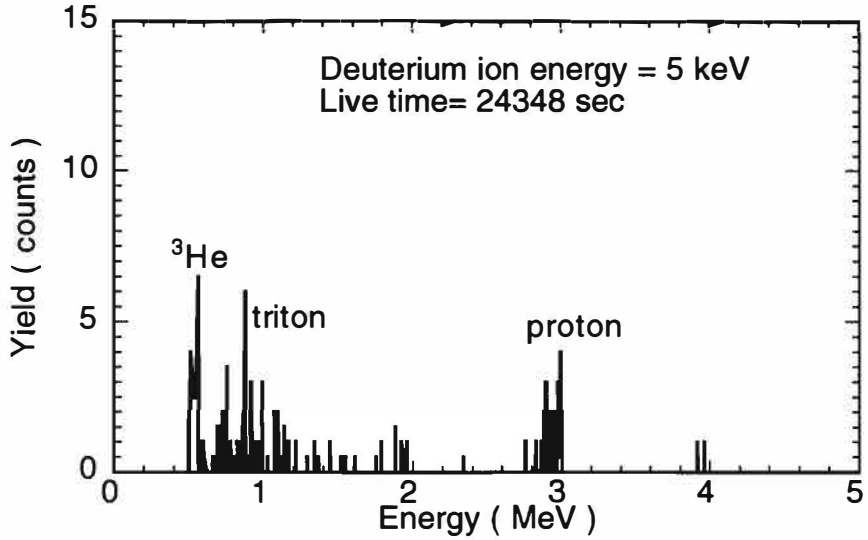

Figure 1. Energy spectrum of charged particles at E_d=5 keV.

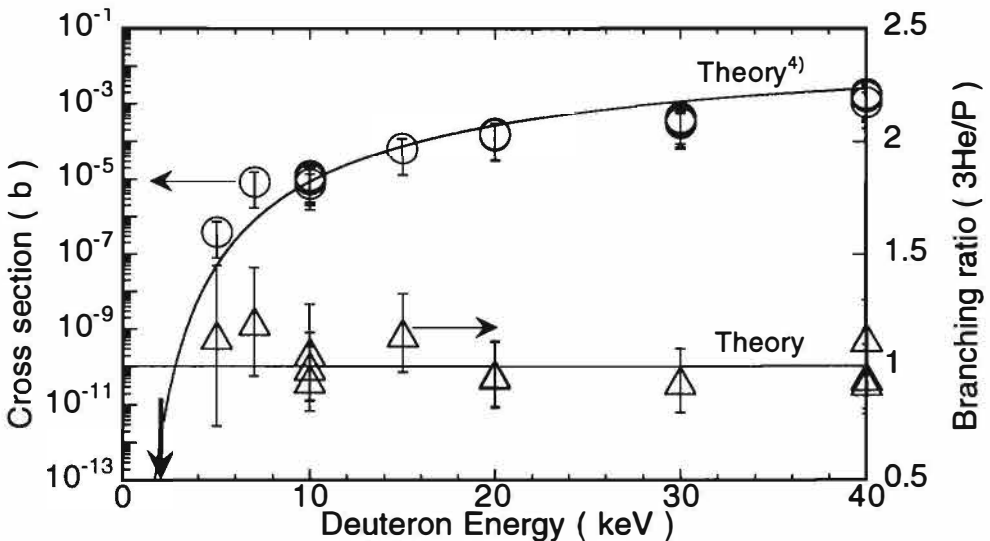

Figure 2. Cross sections of d(d,p)t as a function of deuterium ion energy[3)], adding the new result at E_d=2keV.

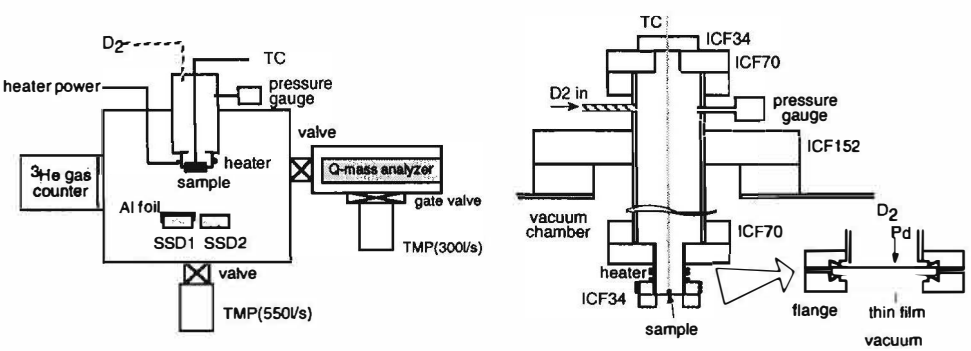

Figure 3. Experimental setup for deuterium transport.

Nuclear Physics Approach

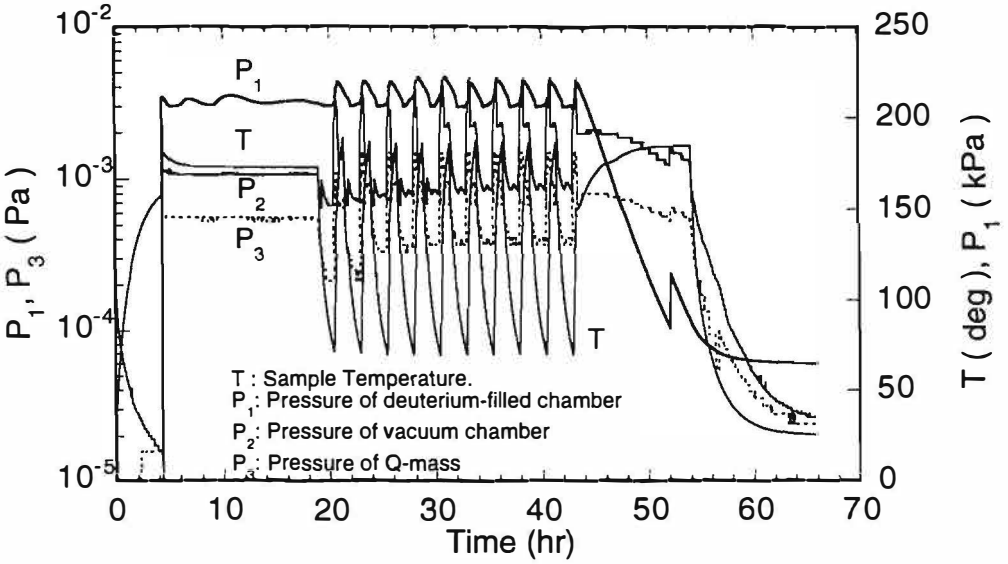

Figure 4. Temperature and pressure measurements.

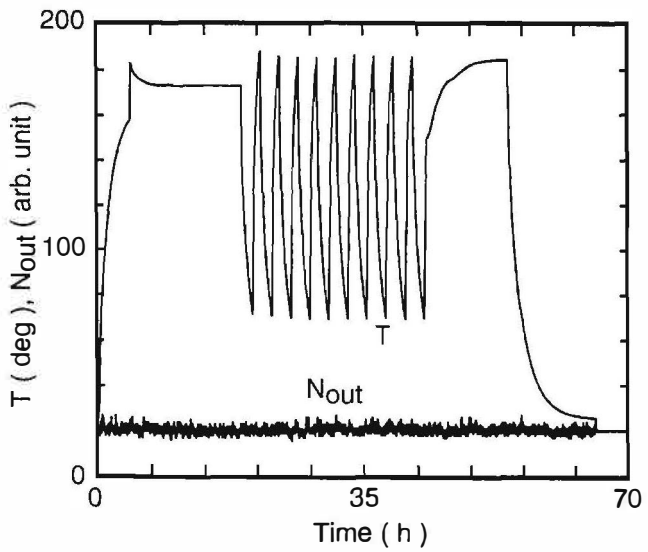

Figure5. Neutron detection by ^{3}He counter.
N_{out} is the output signal of the ^{3}He counter

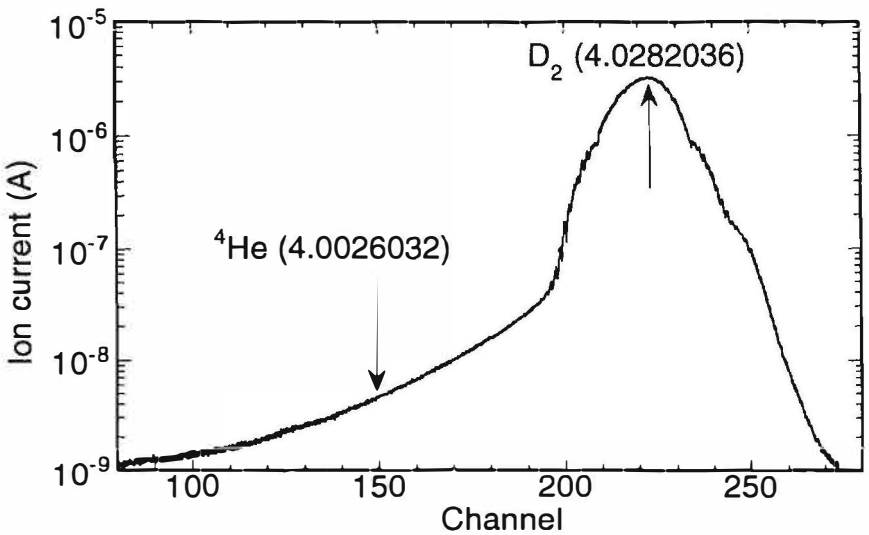

Figure 6. ^{4}He detection using Q-mass system.

Nuclear Physics Approach

Search for Anomalous Nuclear Reactions in PdDx by Detection of Nuclear Products in Vacuum/Gas System

M.Taniguchi, N.Kaji*, A.Takahashi
Department of Nuclear Engineering, Osaka University
2-1 Yamadaoka, Suita, Osaka, Japan.
*Present address, PNC, Tokai, Japan.

Abstract

To detect charged particles from deuterated palladium for the direct evidence of anomalous nuclear reactions in solids, the heat-and-gas-release experiments have been performed. No very clear data for charged particle emission, neutron emission and helium-4 production have been obtained until now. The cause of mass-5 peak increase was discussed.

Introduction

It has past seven and a half years from the announcement of the cold fusion phenomena by Fleischmann and Pons.[1] In past years, anomalous results of helium-4 detection and mass-5 breeding with high resolution mass spectrometers have been reported by some researchers[2-5], but the phenomena show very poor reproducibility and we have had only few distinct data. Therefore, our group has started the research to obtain very clear data showing the existence of nuclear products that are supposed to be directly correlated to excess heat phenomena.

To detect the charged particles from deuterated palladium samples for the direct evidence of anomalous nuclear reactions in solids, an experimental system of vacuum chamber was designed and made. We can measure charged particles and neutrons and make mass spectrum analysis of released gas from the deuterated palladium in the vacuum chamber. The chamber is equipped with a silicon surface barrier detector for charged particle spectroscopy, an NE213 scintillation counter for fast neutron spectroscopy and a high-resolution quadrupole mass spectrometer for gas analysis. Mass-5 breeding has been reported by Itoh et al.[5] Mass-5 is supposed to be either DT^+ or DDH^+ molecule and has been reported that mass-5 breeding would be thought as the tritium increase in released gas with heating deuterated palladium metals. In this work we have performed the mass-1 analysis in addition to the mass-5 analysis to make sure whether the "mass-5 breeding" is due to the DDH^+ increase by the increase of hydrogen partial pressure, or not. Two-type experiments have been performed to try to induce anomalous nuclear effects. The first one is the heating experiment of the deuterated palladium

plates that were deuterated by electrolysis. In correlation with the deuterium gas release from a palladium plate with relatively high D/Pd ratio, some anomalous effects would be expected. The second experiment is the thermal cycle experiment. Palladium plates or powder samples in a vacuum chamber that was filled with deuterium gas were loaded with deuterium by thermal cycle condition, so that palladium samples absorbed and discharged deuterium repeatedly. This repeating condition was advantageous for the mass spectrum analysis of released gas.

Experimental

Figure 1 shows experimental apparatus. Deuterated palladium plate(12.5x25x1 or 25x25x1mm) were prepared as follows, for the heating experiment. Palladium plate was washed with acetone for removing organic impurities that sticked on the palladium plate surface, and some of the samples were set up in vacuum chamber and annealed with pressure less than 0.13 Pa at 900 ℃ for several hours. The palladium plate was set in the F.P. type open cell which was filled with 0.2M, LiOD/D_2O and then electrolyzed with current 1～3A over 6 hours. We determined the loading ratio of sample from the change of weight, the ratio reached around the range of D/Pd=0.74 ～0.91. We used Pd-Rh(10%) and Pd-B(0.2%) alloys as well as pure palladium plates, because Pd-Rh alloy is reported to be advantageous for attaining high loading ratio. The average of loading ratio was 0.89. Palladium plate that contains boron may be effective to produce excess heat[6] and then excess heat may be associated with nuclear reactions. Some of palladium samples were plated with copper layer of about 1 μ m thickness by electrolysis with $CuSO_4/H_2O$ solution, because copper film is expected to work as blocking layer for deuterium diffusion. Deuterated palladium sample was then set up in the vacuum chamber and the chamber was evacuated to be less than 0.13 Pa. Deuterium gas was released from the deuterated palladium sample by heating and stored in the vacuum chamber for gas analysis. The chamber was equipped with a silicon surface barrier detector(Si-SSD) which was surrounded by a copper cylinder which equipped coolant water passage for the heat protection of the Si-SSD during charged particle spectroscopy. The Si-SSD and NE213 detectors were operated to collect data while a palladium sample was releasing deuterium gas.

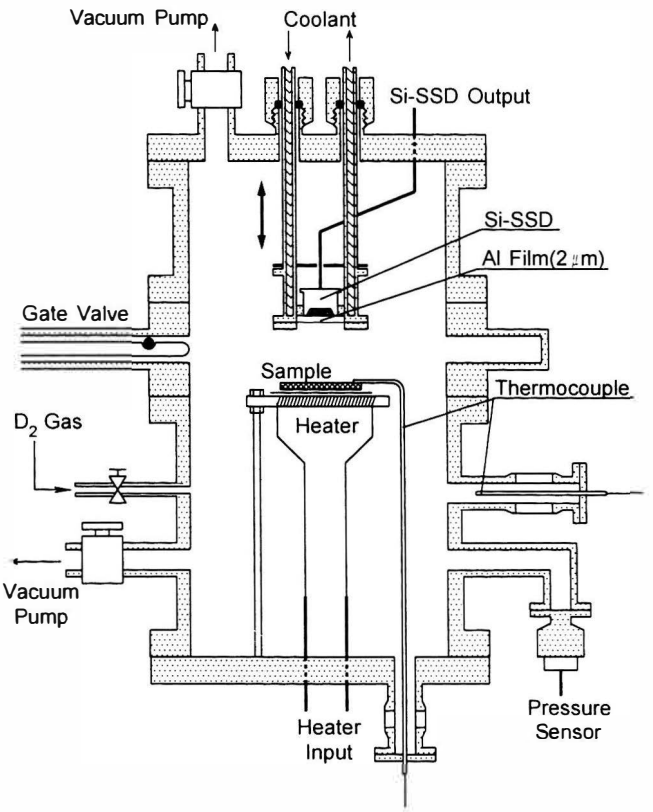

Figure 1 Experimental Apparatus

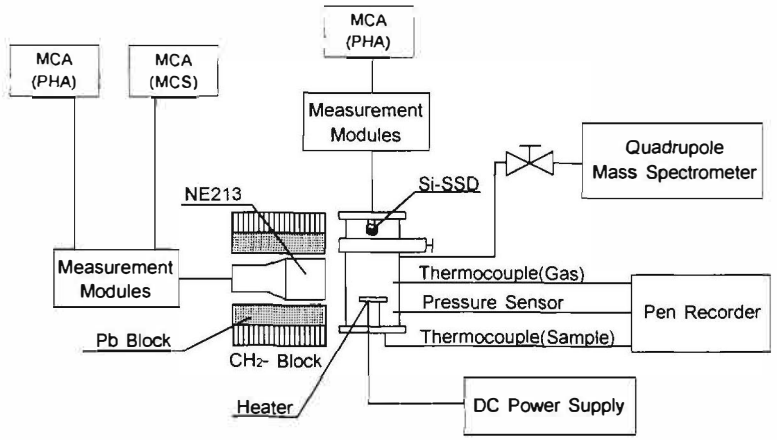

Figure 2 Experimental System

Figure 2 shows the experimental system. The output signal of the NE213 detector was led to the n-γ pulse shape discrimination circuit to reject γ-ray signals from neutron signals. The temperature of palladium sample was monitored by a CA-type thermocouple.

Palladium samples for the thermal cycle experiment were prepared as follows. In the present experiments, we used palladium plates and powder samples. Palladium powder has wide surface area, compared to its weight, and it is advantageous for gas loading. Palladium plate was washed with acetone to remove organic impurities that sticked on the palladium plate surface. Palladium plate or powder sample was set up in the vacuum chamber, which was then evacuated to 0.13 Pa and annealed at about 500 ℃ for several hours. Deuterium gas was introduced into the chamber until the pressure became about 2 atm, and applied the cyclic heating with 24 hours period for several times after keeping the sample under deuterium gas for a couple of days, and the gas was analyzed by a quadrupole mass spectrometer. During the thermal cycles, the NE213 detector was operated for neutron measurement, and then the chamber was evacuated and the sample was heated for gas release with monitoring charged particle emission.

Results and Discussion

Figure 3 shows an experimental result of mass-5 breeding ratios by the heating experiment, comparing with that by the gas loading experiment, where mass-5 breeding ratio is defined as the ratio of mass-5 peak amplitude for the sample and that of original deuterium gas. Mass-5 obviously increased and the average was 7 for the heating

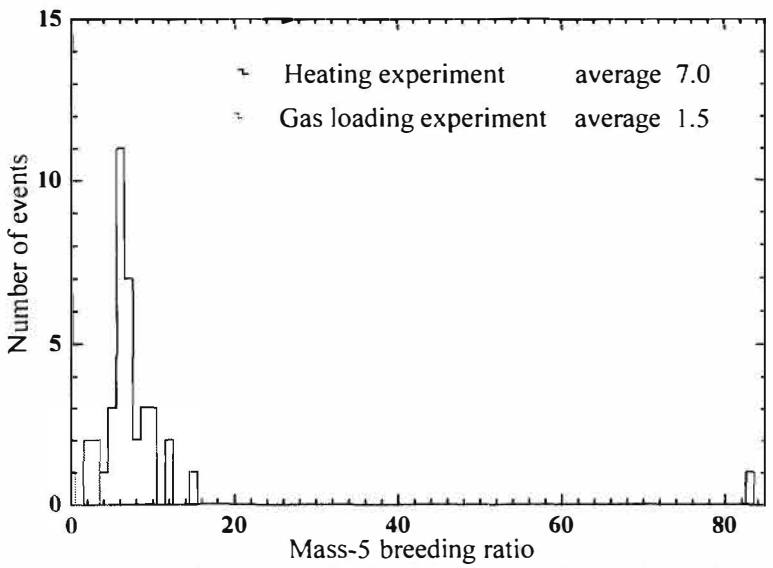

Figure 3 Events distribution for mass-5 breeding ratios

	mass-5 increse	mass-1 increse
Exp. 1-41	6.8	7.5
Exp. 1-42	5.4	12.3
Exp. 1-43	14.1	7.6

Table 1 Mass-5 and mass-1 increse

experiment and 1.5 for the gas loading experiment. Only one event by the heating experiment showed extremely high breeding ratio(82.5). Mass-5 ion is supposed to be either DT^+ or DDH^+ molecule, so that increase of mass-5 peak can be attributed to the increase of either tritium or hydrogen partial pressure in the released gas of which content is predominantly deuterium gas. The present quadrupole mass spectrometer does not have enough resolution for distinguishing the DT(5.030amu) peak from the DDH(5.036amu) peak. With the present experimental system, it was difficult to confirm the increase of tritium. Instead, we analysed the amplitude change of mass-1 peak by the quadrupole mass spectrometer to monitor the hydrogen partial pressure. Table 1 shows the ratios of mass-5 and mass-1 ion current peaks for the sample relative to the peak amplitude for the case of original deuterium gas. Not only mass-5 peaks but also mass-1 peaks increased, but amounts of these increases show no obvious correlation between mass-5 and mass-1. We analyzed only for 3 cases for the mass-1 peaks together with mass-5 peaks, so that quantitative estimation is not properly made, except pointing out that the mass-1 increase is one of the causes for the mass-5 increase. The reason of the hydrogen partial pressure increase is probably due to H impurity in D_2O(99.9 at%) or D_2 gas(99.9 at%). However, one event showed extremely high mass-5 increase (82.5 times) and the reason is not yet clarified.

There was no such data that exceeded the lowest detection limit of the quadrupole mass spectrometer for the helium-4 production possibility throughout these experiments.

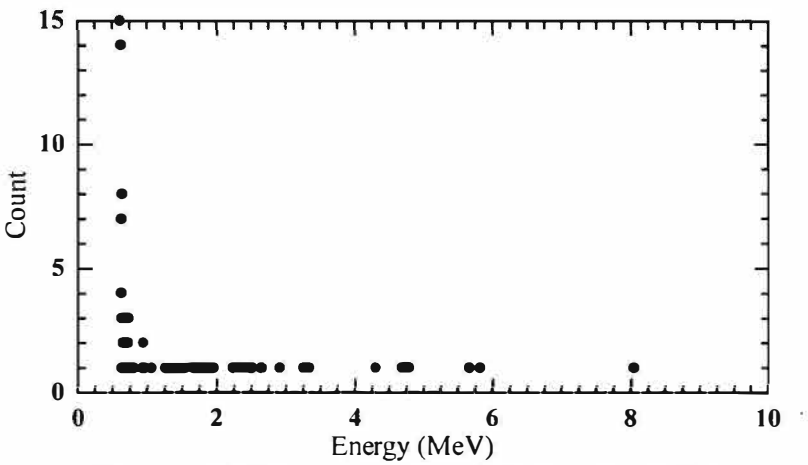

Figure 4 Si-SSD spectrum (Exp.1-33, Live time 3,580sec)

In the present experiments, charged particles which we would regard emitted from deuterated palladium samples have never been detected clearly, but some experiments showed several counts up to ~10 MeV. Because of poor statistics of counts, we can not identify whether these high energy counts were from noise signals or true signals originated from charged particles. (See Figure 4, for example)

Figure 5 shows an example of experimental results on neutron measurement for the gas loading experiment. Several other-experiments showed few neutron events slightly over 3 σ levels. In Figure 5, there are data points that exceed 3 times (broken line in Figure 5, where

solid line shows average level) the standard deviation σ of the background fluctuation. However, we cannot find meaningful structure change of recoil proton spectrum of the NE213 detector since the statistics was not enough. Background neutron level was comparatively high throughout the experiments and fluctuations were so big that the increase of neutron events might be attributed to the change of background level.

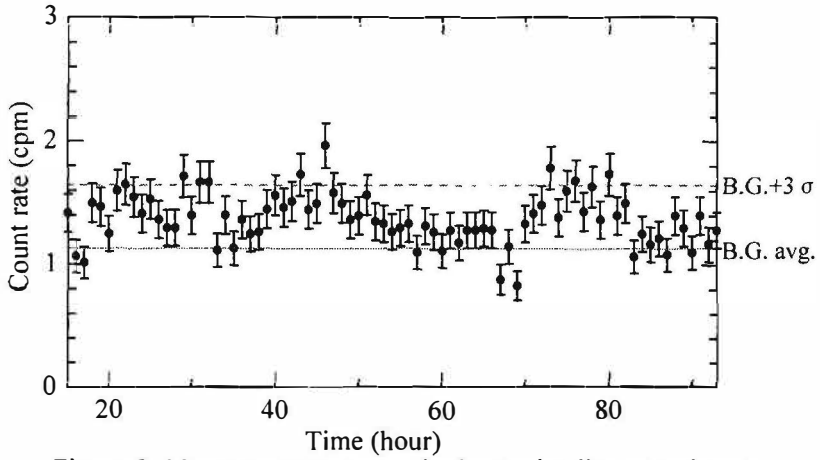

Figure 5 Neutron measurement in the gas loading experiment with Pd plate sample (Exp. 2-02)

Conclusions

We have performed the heating experiments of deuterated palladium metal samples in vacuum chamber. The deuterations of palladium were prepared by the electrolysis or the gas loading method. In the heating experiments with electrolyzed palladium samples, we observed increase of mass-5 breeding ratios, but the increase of hydrogen partial pressures was suspected to be one cause for this event. We also observed several counts of unusual energies in 3～10 MeV region of charged particle spectrum, but we could not conclude that these signals originated from charged particles, due to poor statistics. In the gas loading experiments, we observed neutron increase events but with so marginal levels that we could not confirm that these events indicated true neutrons from deuterated palladium samples. We shall run more experiments and seek for the causes of these "anomalous" events in the future efforts.

Reference

1. M.Fleishmann, S.Pons : J.Electroanal.Chem.,261(1989) P.301
2. E.Yamaguchi and T. Nishioka : Proc. ICCF-3, Nagoya, (1993) P.179
3. T.N.Claytor, et al. : Proc. ICCF-3 , Nagoya, (1993) P.217
4. D.G.Tuggle, et al. : Proc. ICCF-4 , Lahaina, EPRI TR-104188-V1, 7 (1994)
5. T.Itoh, et al. : Proc. ICCF-5, Monte Carlo, (1995) P.189
6. M.Mckubre, et al. : Proc. ICCF-5, Monte Carlo, (1995) P.17

Nuclear Physics Approach

DIAGNOSIS OF NEUTRONS FROM THE GAS DISCHARGE FACILITY

Wang Dalun Chen Suhe Li Yijiu Liu Rong Wang Mei Fu Yibei
(Institute of Nuclear Physics and Chemistry,
China Academy of Engineering Physics, Chengdu 610003)
Zhang Xinwei Zhang Wushou
(Institute of Applied Physics and Computational Mathematics , Beijing 100088)

ABSTRACT

The phenomena of nuclear fusion at normal temperature have been studied using a gas discharge facility and about 10^4 neutrons per second have been detected. The neutron yield is controllable and reproduceable. The BF_3 neutron detectors, the ^6Li thermoluminescence films, the NE-213 organic liquid scintillation neutron spectrometer and the n-γ discrimination technique were used to diagnose the neutrons. It was confirmed that neutrons were emitted from the gas discharge facility.

There were some non beam-target neutrons among these neutrons, especially when the discharge voltages was low(<7kV).

KEY WORDS Neutrons, Gas discharge, ^{10}B (n, α)$^7Li^{\#}$ reaction, n-γ discrimination spectra, Neutron energy spectra, Thermal neutrons

On the base in principle that same activated transitional-metals or hard-melted metals have the strong capability of adsorption to active gas in certain range of temperature, the research that loading metals with deuterium by way of gas discharge and studying the anomalous phenomena of metals loaded with deuterium have been developed.[1-2] Neutrons were detected in our experiments. There were neutrons detected by way of gas discharge in experiments of former Soviet Union and Japan as well.[3-4] In order to confirm further the existence of neutrons emitted from the gas discharge facility (abbr. GD neutrons), the following methods were used to diagonosing the said neutrons.

1. Diagonosis of GD neutrons

1.1 The characteristic spectra of the pulse height distribution (abbr. CSPHDs) for ^{10}B (n, α)$^7Li^{\#}$ reaction

First we slowed part of the GD neutrons down to thermal neutrons. Thermal neutrons reacted with ^{10}B in two channels as follows:

$^{10}B + n \rightarrow \alpha + {}^{7}Li^{\#} + 2.31$ MeV (93.9%)

$^{10}B + n \rightarrow \alpha + {}^{7}Li + 2.79$ MeV (6.1%)

So thermal neutrons would produce two kinds of CSPHD which expressed characteristic of the two said reaction channels. The CSPHDs of the GD neutrons and of the Am-Be source neutrons had been measured respectively with BF_3 neutron detectors, as shownin figure 1.

1.2 The filtering of thermal neutrons

The thermal neutrons slowed down from GD neutrons were measured by the ^{6}Li thermoluminescence films. In order to differentiate this kind thermal neutrons, Cd films (0.5 mm thickness) were used as thermal neutron filters and the ^{6}Li thermoluminescence films were irradiated both in the covering cadmium and in non-the covering cadmium. For estimating influence of γ rays, those thermoluminescence films of ^{6}Li and ^{7}Li were irradiated simultaneously. The sensitivities of the ^{6}Li and ^{7}Li thermoluminescence films to γ rays were calibrated with γ source in advance. The difference coefficient of the said two sensitivities, i.e. Nr(^{6}Li) / Nr(^{7}Li), was 1.13.

The thermoluminescence films were irradiated by the GD neutrons . Pb plate (5 mm thickness) was used to eliminating X rays background from gas discharge process and to increasing thermalization effect of polythene to GD neutrons.

The background counts of ^{6}Li thermoluminescence films originated from the following two aspects. one was natural background counts, which could be cut with the background counts of a set of thermoluminescence films that were not irradiated. The other was γ background counts, which could be estimated with the counts of ^{7}Li thermoluminescence films that were irraditated simultaneously.

The results of GD neutrons measurement were listed in table 1. The experimental results showed: (1) the counts of ^{6}Li thermoluminescence films in non-the covering cadmium were higher than those of ^{7}Li thermoluminescence films; (2) the counts of ^{6}Li thermoluminescence films in the covering cadmium were equal to that of ^{7}Li thermoluminescence films within the range of experiment error.

1.3 n-γ discrimination spectra

Neutrons were differentiated from γ rays by an n-γ discrimination technique with NE-213 organic liquid scintillation neutron pectrometer. This device was also used to measuring the n-γ discrimination spectra from an Am-Be neutron source, an ^{22}Na γ source and the gas discharge facility (here were the background γ rays). The results of measurement were shown in figure 2.

1.4 Neutron energy spectra

The neutron energy spectra of GD neutrons have been measured with NE-213 organic liquid scintillation neutron spectrometer by a n-γ discrimination technique . A 0.5 mm thick Cu film was placed in front of the spectrometer, for eliminating the influence of strong X rays (27 keV) from the gas discharge facility. The recoil proton

Neutron energies were calibrated with ^{22}Na source. The measurements of recoil proton spectra were shown in figure 3.

The neutron energy spectra, which were solved from the recoil proton spectra and those relevant respond functions, were shown in figure 4.

The GD neutron energy measured in experiments and the D-D neutron (90 ° direction) energy were both 2.38 ± 0.15 MeV, which agreed with the average energy 2.45 MeV of normal D-D reaction neutrons within the range of experiment error.

1.5 The comparative experiments of hydrogen discharge

There were not neutrons detected in hydrogen discharge under otherwise equal conditions.

2. The measurement of GD neutron yield

The GD neutron yield was measured by using BF_3 counting devices. The counting mode of the BF_3 counting devices was anticoincidence mode in order to eliminating influence of electromagnetic disturbance and high voltage sparking. For this purpose, a "simulating BF_3 neutron detectors" system was designed to cooperate with the "signal BF_3 neutron detectors" system. The two system formed an anticoincidence counting system.

The efficiency of the BF_3 neutron counting devices, which was calibrated with Am-Be neutron source, was 8.33×10^{-3}. The time dependence of GD neutron yield was shown in table 2.

Reference

1. Wang Dalun, Chen Suhe, Fu Yibei, et al. Chinese Joural of Atomic and Molecular Physics, 1993;10(3):2789.
2. Wang Dalun, Chen Suhe, Fu Yibei,et al.High Power Laser and Particle Beams,1993;5(3):333.
3. Karabut A B,Kucherov Ya R,Sawatimova I B,Phys Lett,1992;A170:265.
4. Nobuhiko Wada,Kunihide Nishizawa,Jap J Appl Phys,1989;28(11):2017.

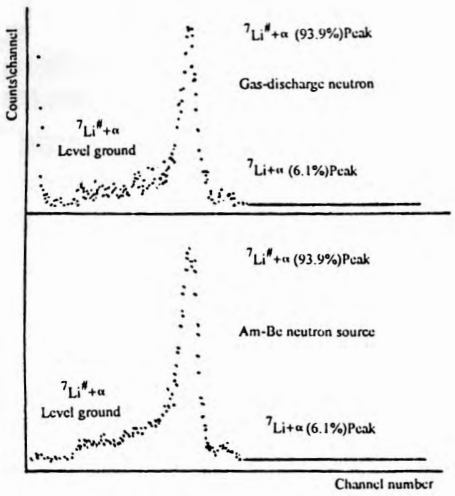

Fig 1. Characteristic spectra of the pulse height distribution for ^{10}B $(n,\alpha)^7Li^{\#}$ reaction

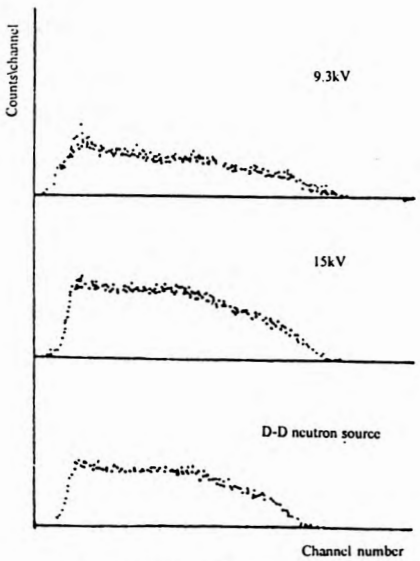

Fig 3. The recoil proton spectra produced by gas-discharge

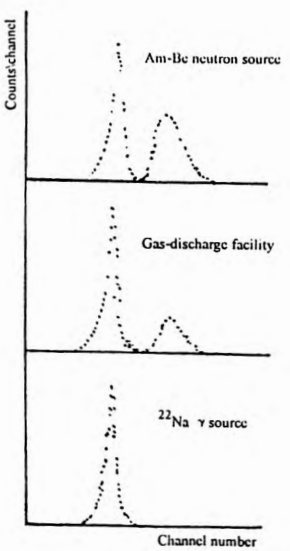

Fig 2. n-γ discriminating spectra of gas-discharge neutron

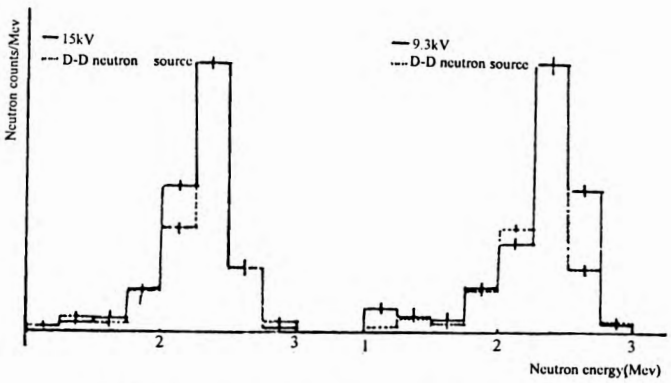

Fig 4. The neutrons spectrum produced by gas-discharge

Table 2. Time dependence of gas-discharge neutrons

order	time	counts of BF_3 detector(n/100s)	the yiedl of neutrons (n/s)
1	10:30	8276	0.993×10^4
2	11:00	8690	1.043×10^4
3	11:20	7444	0.893×10^4
4	11:40	8454	1.014×10^4
5	12:00	8305	0.996×10^4
6	12:20	8141	0.997×10^4
7	13:00	8567	1.028×10^4
8	13:30	8373	1.005×10^4
9	14:00	8615	1.034×10^4
10	14:30	8289	0.995×10^4

Table 1. The measurable result of neutron detector for ^6Li thermolaminescence

counts of ^6Li thermolaminescence			counts of ^7Li thermolaminescence		
not the covering cadmium	the covering cadmium	nature background	not the covering cadmium	the covering cadmium	nature background
0.235 ± 0.04	0.064 ± 0.02	0.045 ± 0.007	0.158 ± 0.022	0.06 ± 0.022	0.041 ± 0.005

Nuclear Physics Approach

Search for tritium in Pd + D systems by a gas proportional chamber

Nobuharu Yoshikawa

Institute for Nuclear Study, University of Tokyo, Tokyo,188,Japan

Takayohi Aoki, Yoshitugu Kurata and Hiroshi Ebihara

Isotope Center, University of Tsukuba, Tsukuba,Ibaragi,305,Japan

Kenya. Mori

Technical Center, Tanaka Kikinzoku Kogyo K.K., Hiratsuka,kanagawa,254,Japan

Abstract
Tritium concentration in deuterium gas from Pd + D systems was measured by a gas proportional chamber. This type of detector was able to observe directly a beta ray spectrum of tritium and give a genuine number of tritium in studying gas phase system. For this purpose, the gas proportional chamber was made and was operated in low background. The detection limit was 20 Bq in one liter of deuterium gas. Tritium searches in deuterium gas phase of several different systems were done by this detector. The clear spectrum of beta ray originated from tritium decay could not be observed due to low concentration of tritium in the examined deuterium gas phase.

1.Introduction

There were several reports[1,2,3] to claim the generation of tritium in the gas phase of Pd + D systems. In the reports, the methods used for tritium detection were the ion chamber or the mass analyzer system. But in those measurements, some possibilities to measure other kinds of events could not be excluded, so that the different type measurements to confirm the generation of tritium caused by nuclear reaction were essential. If the measurement of beta ray spectrum from tritium disintegration could be possible, it would give the direct evidence of existence of tritium. The gas proportional chamber was made for this purpose and could measure the energy spectrum of beta ray of tritium. Tritium concentrations in deuterium gas released from Pd and Titanium alloy powder were studied to search for the evidence of cold fusion. The detector of this type was used in our laboratory for the tritium searches in the gas phase of the electrolysis cells, in which the generations of excess heat were observed[4]. In this work, the detection limit was confirmed by the calibrated tritium gas. During operation of the systems, neutron measurements were done by ^{3}He counters.

2.Detection method of tritium

(a) Detector and measuring method

The chamber was formed by two cathode planes of 100 μm mesh and an anode plane with five 20 μm sense wires and six 100 μm potential wires. The spacing between sense and potential wires was 5 mm. The gap between cathode and anode was 5 mm. The sensitive area was 50 mm × 140 mm and the thickness was 10 mm. The chamber was shielded by aluminum and copper plates and lead blocks. Cosmic rays were suppressed by plastic scintillation counters which were placed just above

the chamber to cover the whole surface.
Pulse signals from the sense wires summed to one output were amplified and fed to a pulse height analyzer. Digitized signals were stored in a personal computer and analyzed by the KODAQ code[5]. The signals due to cosmic rays were rejected by anti-coincidence technique. Sampled gas was put into the chamber by a syringe. It was confirmed that the hydrogen gas didn't disturb the energy resolution of chamber but higher voltage was needed. The counter gas was Ar + 10%CH_4.

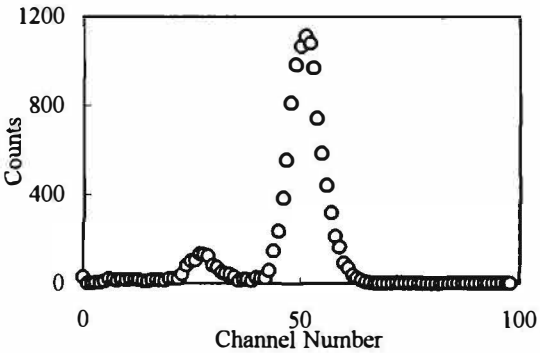

Fig.1 X-Ray spectrum of ^{55}Fe

(b) Energy and efficiency calibration
The energy calibration was done using 5.9 keV X ray from ^{55}Fe source. As the window of the chamber was a thin plastic film, X-ray could penetrate it. The X-ray spectrum was shown in Fig.1. There were the 5.9 keV full energy and 3.0 keV escaped peaks and both peaks were used for the energy calibration.
The calibration of detection efficiency was done by several different volumes of deuterium gas which contained a little tritium gas.
The deuterium gas used for the calibration was obtained by the electrolysis of heavy water in which a very small amount of tritium water was added.

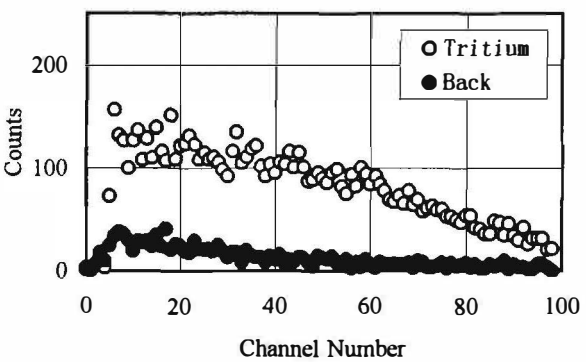

Fig.2 Tritium and Background Spectra

The tritium spectrum was shown in Fig.2, together with background spectrum. Counts of detector as a function of input gas volume were shown in Fig.3. The linearity of counts to input gas volume was fairy good. The tritium concentration in deuterium gas was estimated in the following way; the deuterium gas was once more reduced to the heavy water using a Pt black and measured by a liquid scintillation counter. Using this value, the efficiency was estimated to be 42 ± 8 %.

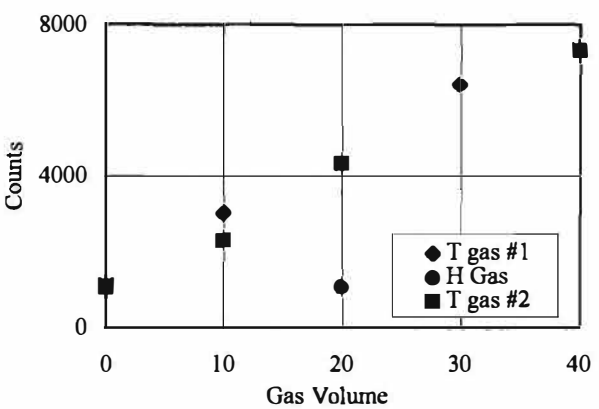

Fig.3 Tritium counts per input gas volume

3.Detection method of neutron
The neutron monitors were set near the Pd + D systems. Two ^3He counters(Model Rs-P4-0810, Reuter-Stokes Inc) were used. Each counter was surrounded with a cylindrical plastic moderators. Output signals of counters were digitized and recorded in the personal computer.

4.Tritium search
(a) Deuterium gas from palladium wires in gas phase
Palladium wires of 2 mm diameter and 10 cm length were used. The wires were annealed at 800 °C

in a vacuum for 12 hours, and the surfaces of wires were modified by a method of sand blast. Those were set in a vacuum duct(3.5 cm diameter and 21 cm length) which was connected with a standard volume of 2 liter. After evacuation of the duct, deuterium gas was supplied from the standard volume. The maximum pressure was 3 atm. Normally, after one week, D/Pd loading ratio; n = 0.65 was achieved. Then wires were heated up to 230 °C by a heater which was wound on the outside of the duct. Within 10 minutes, the temperature rose and gas released. After holding the high temperature for several tens of minute, the system was cooled down to the room temperature. The relation of temperature and pressure was shown in Fig.4. Hereafter this type experiment was referred to as external heating. The gas samples were taken by a syringe through a gas sampling port at the high temperature and the room temperature. After injection of the sample gas into the chamber, a measurement was done for 10 minutes. The gain of the chamber was checked by the X-ray source before and after the measurement. This measurement was repeated 4 times.

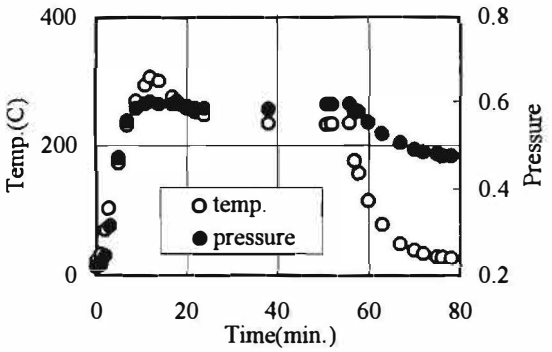

Fig.4 Temperature and Pressure

In the Pd + D system, a cyclic absorption and desorption was tried but the complete cycle was not achieved. Titanium alloys were also used for hydride material in the same setup of the palladium wire. Several absorption and desorption cyclic processes were succeeded. Titanium alloys were mechanically powdered to dimensions less than 100 μm and heated up to 300 °C in a vacuum for 12 hours. After cooled down to the room temperature, deuterium gas was filled up to 3 atm. It was heated up to 230 °C for desorption and cooled down to 0 °C for absorption. This cycle was repeated several times. The D/Pd ratio; n was 0.3 - 0.4. Compared with the palladium wires, this value was not high.

(b) Deuterium gas from Pd wires loaded by the electrolysis

In the gas phase experiment(external heating), there were two disadvantages, one was that the loading ratio was not so high, another was that long time was needed for heating, because the heater was wound on the outside of the chamber to avoid the existence of any materials in the gas phase. To improve these two points, deuterium gas was loaded in Pd wire(28 cm length,2 mm diameter)by a electrolysis. The wires were coated with thin Au layers by electroplating, before

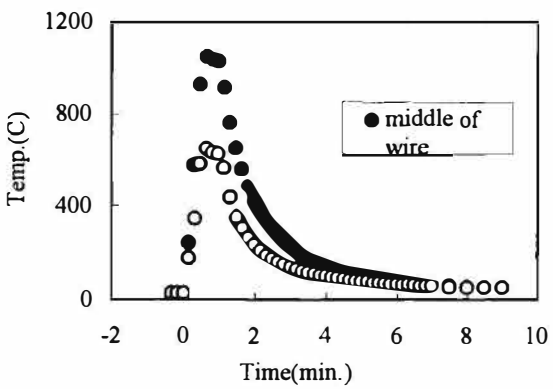

Fig.5 Temperature of Pd wire

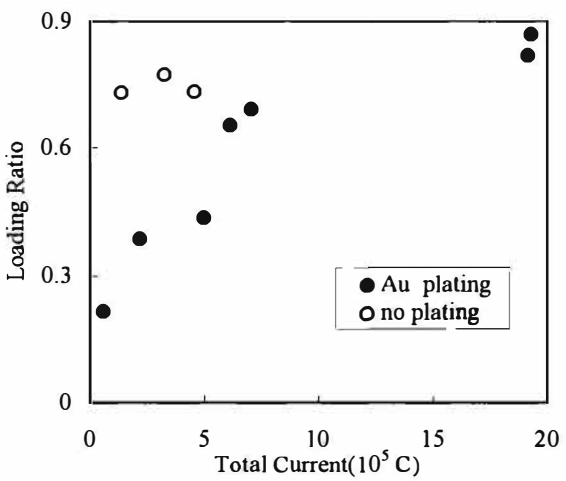

Fig.6 Loading ratio by electrolysis

and after the electrolysis. Those wires were set in a vacuum duct and high currents (first 1 min.,80 A and next 1 min., 60 A) were supplied to the wires. The temperatures at center of wire(closed circles) and near the electric contact(open circles) were shown in Fig.6. Hereafter this type experiment was referred to as internal heating. The wire was heated up to 1000 °C, then deuterium gas was abruptly released within 35 seconds. The released deuterium gas from the wire was stored in a balloon which was immersed in a water vessel. By the water level, the exact gas volume was known. Deuterium gas was sampled from the balloon and measured by the chamber in the same way of the external heating experiment. In Fig.6, loading ratios were plotted as a function of total current which was used in the electrolysis. Closed circles were those of gold plating and open circles were no plating . Thickness of gold was from 0.026 μm to 1.16 μm. After electrolysis, further gold was plated in the 5 wires of total 7 wires with thickness of about 1 μm.

5.Summary of measurement

(a) Tritium

Many gas samples were collected from the external and internal heating experiments. Those were measured by the chamber in the same manner . Before and after measurements of the sampled gas,

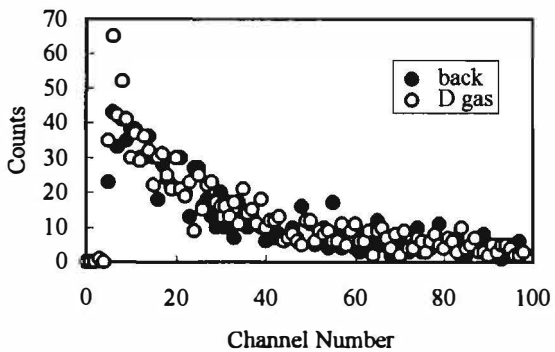

Fig.7 Spectra of sampled gas and background

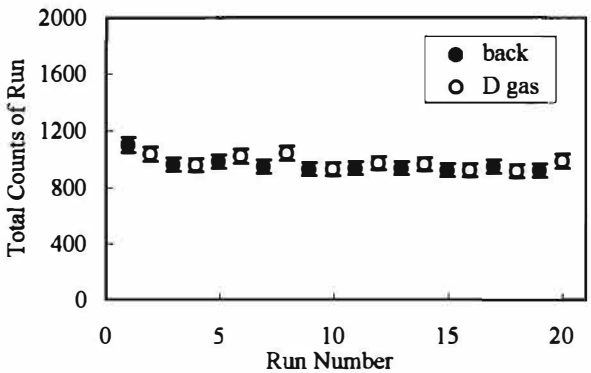

Fig.8 Summary of internal heating

background spectra were also measured. When sampled gas was input into the chamber by the syringe, the counter gas was stopped and the gain of the chamber was adjusted to the same as the background measurement by increasing the counter voltage. The measurement time for one run was 10 minutes. Before and after measurement of spectrum, the gain was checked by X-ray spectrum. This run was repeated 4 times, after measurement, the sampled gas was purged by the counter gas. Several background runs were taken after the

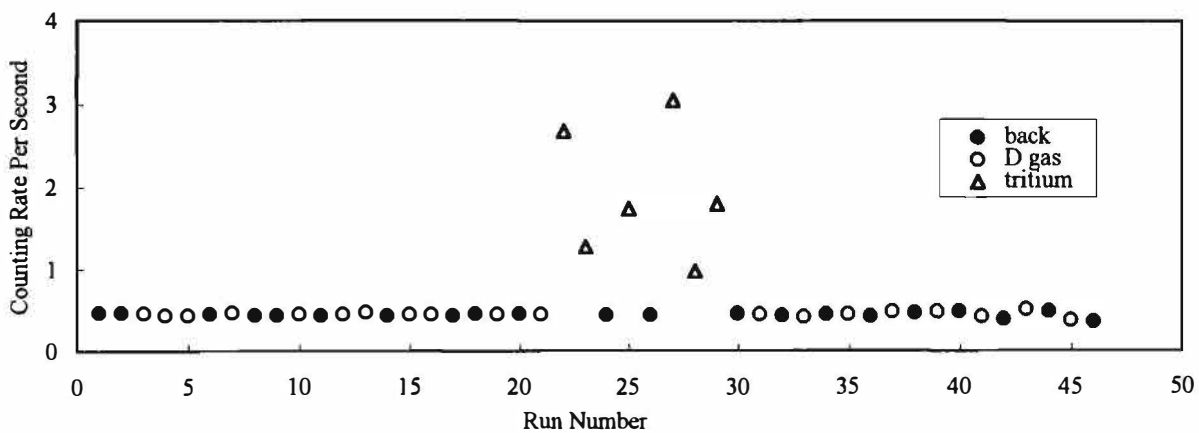

Fig.9 Summary of measurements

sampled gas was fully purged. The spectrum of sampled gas in the internal heating experiment was shown in Fig.7, together with background spectrum, where both spectra were the sum of 4 runs. As shown in the spectra, statistics were not enough. To compare with sampled gas and background runs, spectra were integrated to obtain better statistics. In Fig.8, obtained values of internal heating experiment were shown. The differences between background and sampled gas runs were very little. If sampled gas contained 1 Bq tritium, these values should increase to 50 % more. The other results obtained until now were shown in Fig.9. The data from run 1 to run 20 were the experiments of electrolysis cells, in which excess heats were observed. The data from run 21 to run 30 were those of the calibration gas. The total tritium number in the calibration gas was from 1 to 7 Bq. The runs more than 30 were the results of the external heating experiments.

b)Neutron

In the external and internal heating experiments, the two ^{3}He counters were set near the systems. The output signals of counters were recorded in every one minute, it started before heating and ended when the systems were completely cooled down. Clear increases of neutron were not observed. Results of the internal heating system in the highly loaded cases were shown in Table 1.

Table 1

Run number	Loading ratio	Coulomb[a)]	thickness of gold(μm)[b)]	neutron (1) counts /min.	neutron (2) counts/min.	neutron (3) counts/min.
				2.03 ±1.42	1.00 ±1.00	2.33 ±1.52
1	0.65	6.18×10^5	0.638(0)	2.70 ± 1.64	0.5 ± 0.707	2.63 ±1.62
				2.26 ±1.50	3.00 ±1.73	2.36 ±1.53
2	0.69	7.08×10^5	0.0408(1.05)	2.23 ±1.49	2.00 ±1.41	2.03 ±1.42
				2.10 ± 1.44	4.52 ± 2.12	2.26 ± 1.50
3	0.87	1.93×10^6	0.026(1.0)	2.00 ± 1.41	1.00 ± 1.00	2.13 ± 1.46
				2.06 ± 1.43	2.50 ± 1.58	2.30 ± 1.51
4	0.82	1.92×10^6	0.055(1.0)	2.46 ± 1.57	5.00 ± 2.23	2.20 ± 1.48

a) total current used for electrolysis

b) thickness of gold plated by electroplating, after loading, gold was once more plated, which was given in parentheses

1) average count of 30 minutes measurement before heating, upper column was detector A, lower was detector B

2) average count of 2 minutes measurement under heating 3) average count of 30 minutes measurement after heating

6.Conclusion

The gas proportional chamber was proved as the suitable detector for tritium hunting, especially in gas phase systems. The detection efficiency and detection limit were confirmed by calibration gas which contained tritium of 1 to 7 Bq. The detection limit was 0.5 Bq per 20 ml gas volume. External and internal heating methods were applied to the Pd + D systems. Deuterium gas from these systems were measured by the chamber. Clear differences between the deuterium gas and the background spectra were found until now . Further investigation for various systems should be needed in our laboratory, although it is important to do joint-works with other laboratories where anyone have samples for studies of this type .

References

1) T.N. Claytor et al., Proceedings of the 3rd International Conference on Cold Fusion p217
2) Y.Iwamura et al., Proceedings of the 4th International Conference on Cold Fusion p160
3) D.G.Tuggle et al., ibid., p221
4) T.Aoki et al., ibid., p214
5) K.Omata et al., INS-T-496

Nuclear Physics Approach

HYDROGEN ISOTOPE EFFECT INDUCED BY NEUTRON IRRADIATION IN PD-LIOD(H) ELECTROLYSIS

Y.Oya, H.Ogawa, T.Ono, M.Aida and M.Okamoto
Res. Lab. Nucl. Reactors, Tokyo Institute of Technology
Ookayama, Meguro-City, Tokyo 152 Japan
Tel: 81-3-5734-3065, Fax: 81-3-5734-2959

Abstract

The effects of the incident of the neutrons to the hydrogen condenced matter systems ,have been investigated by the irradiation of neutrons from ^{252}Cf into the Pd-LiOD(H) electrolysis cells. The thermal neutron irradiation test and the epithermal neutron irradiation test have been carried out for the background runs with light water electrolysis and the foreground runs with heavy water electrolysis. The anomalous hydrogen isotope effects in the neutron ratios were found slightly in the thermal neutron irradiation and evidently in the epithermal neutron irradiation runs.

Introduction

The anomalous accumulation of deuterium and its dynamic movement have been discussed as the key factors of the occurrence of the anomalous nuclear effects in deuterium-condensed matter systems, like d-Pd and d-Ti etc[1][2]. However, these half-classic dynamics of deuterium may not have enough potential to initiate the deuteron based nuclear reactions in solid states. To search the trigger to initiate the deuteron based nuclear reaction in d-Pd systems, the incident of the external neutron was discussed theoretically by K.Shiraishi[3]. The concept seems to be consistent with the specific characteristics of the evidences obtained in the deuteron based solid state nuclear reactions, such as very weak neutron emission, very weak radiations and very low reproducibility and so on.

In the present concept, the higher energy neutrons might give some influences to the movement of deuterons in the lattice, by which the possibility of the collisions of the deuterons may be enhanced, while there are many studies including papers of the present authors which reported the detections of the excess neutrons from the reaction cells enclosed tightly by the neutron shield. In these cases, only thermal neutrons can invade into the reaction cells.

In the present work, the neutron irradiation effects has been investigated especially for the neutron ratios between Pd-LiOD electrolysis and Pd-LiOH electrolysis with the thermal neutron irradiation or the epithermal neutron irradiation.

Experimental

1, Neutron irradiation

Nuclear Physics Approach

The experimental system including the electrolysis cell has been modified to perform the neutron irradiation experiments. ^{252}Cf was used as the neutron source. The neutron irradiation was repeated in every other day to the electrolysis cell through a collimator for 26～30days. In the thermal neutron irradiation experiments, light water in the collimator was used as a moderator and placed between the electrodes and the neutron source in Fig.1.

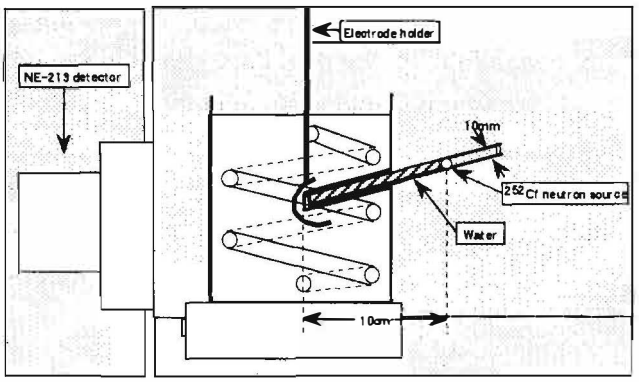

Thermal neutron irradiation experiment

Fig.1 Location of the ^{252}Cf neutron source and electrode

2, Neutron detection and the neutron energy spectra

Neutron measurements were conducted using a NE-213 liquid scintillation counter (5 × 5 inches) which measured recoil-proton energy spectrum for the fast neutron events with multichannel analyzer, and nine ^{3}He proportional counters. The ^{3}He neutron counters were divided into two groups: channels A and B in Fig.2. The channel A consisted of six ^{3}He counters and The channel B consisted of three ^{3}He counters. The counters of channel A were embedded in polyethylene blocks surrounding the electrolysis cell. Channel B was located in the end of the collimator and surrounded by polyethylene blocks. The background neutrons from outside of the system were slowed down and captured in the solution of boric acid and in the polyethylene blocks.

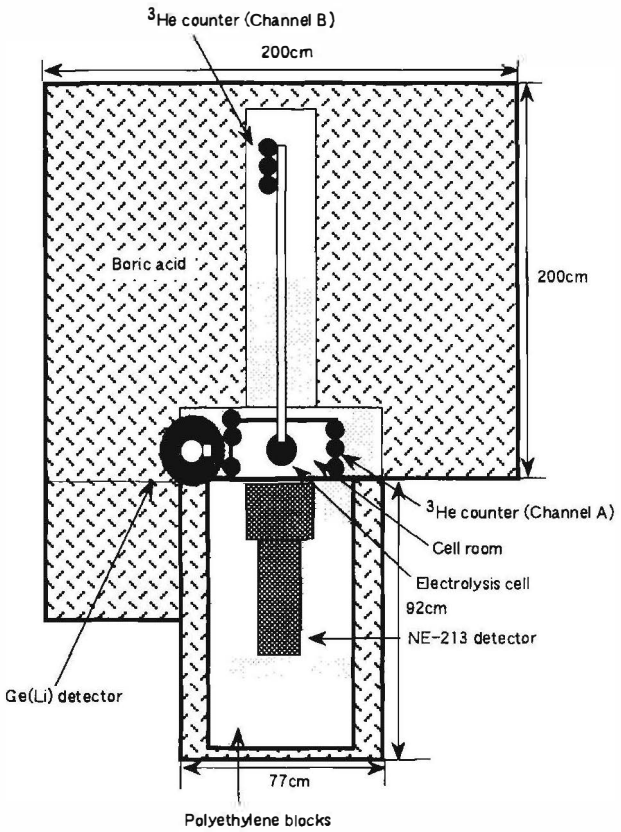

Fig.2 Schematic drawing of the experimental system

The neutron energy spectra were obtained by the same method reported previously[4][5]. The neutron signals obtained by the NE-213 detector were so weak to evaluate the neutron energy directly from the spectrum. The neutron counting raw data were divided into 10 or 27 bins. The foreground/background neutron ratios were calculated in each 10 or 27 bins for 1024 channels of the PHA by using Eq.1 in day by day. When the neutron ratio is over unity, it is concluded that

$$Neutron\ ratio = \frac{Foreground\ neutron\ counts\ of\ the\ n\ th\ day\ after\ electrolysis\ was\ started.}{Background\ neutron\ counts\ of\ the\ n\ th\ day\ after\ electrolysis\ was\ started.} \quad \text{(Eq.1)}$$

excess neutrons were detected by the NE-213 detector. The neutron energy calibration of the NE-

213 detector was done according to the method reported by A.A.Naqvi et al[6].

In the epithermal neutron irradiation experiments, the ^{252}Cf neutron source was used without any moderators. The 2-D pulse-shape vs. pulse-height analysis was employed for the neutron measurements.

The NE-213 detector also detects gamma-rays. Using the pulse shape discrimanation (PSD) technique, gamma-ray counting raw data were obtained. The stability of the NE-213 detector was checked by the natural gamma-ray spectra from ^{40}K and ^{208}Tl.

3, Gamma-ray detection and the energy spectra.

The gamma-ray energy spectroscopy was performed on a Ge(Li) semiconductor detection system. The gamma-rays which was emitted by pd(5.49MeV), np(2.22MeV) and nd(6.25MeV) reactions were monitored. Using ^{60}Co, ^{22}Na and ^{152}Eu standard source, the energy range of the gamma-ray spectrometer was ascertained to be smaller than 10MeV.

The detector head of the Ge(Li) detector was covered with lead sheet to shield the background gamma-rays from outside of the system.

4, Electrolysis cell and experimental conditions

The schematic view of the experimental system is shown in Fig.2. The cell room in which electrolysis was operated, was located in the center of the system. The cell room and nuclear instruments were enclosed very thick neutron absorber with the aqueous solution of boric acid and polyethylene blocks. A sandgrass typed electrolysis cell was designed as illustrated in Fig.3. The volume of the cell was about 400 mℓ. Coolant pipe was installed in the cell and the flow rate of coolant was 3.6 ℓ /min. The three resistance thermometers were located in the electrolyte for measuring the electrolyte temperature and two resistance thermometers were placed in the outlet and inlet part of the cooling water. A magnetic stirrer had been employed to diminish the temperature gradient

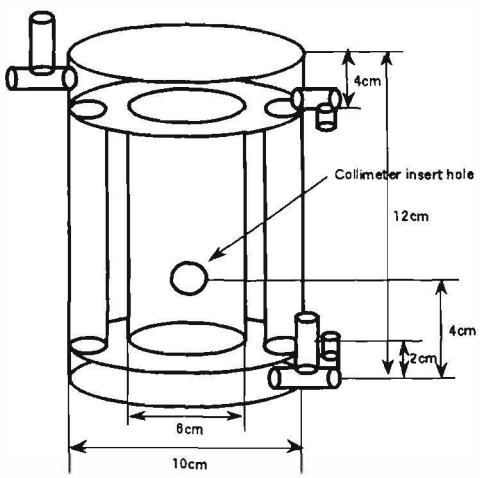

Fig.3 Schematic drawing of the sandglass typed cell

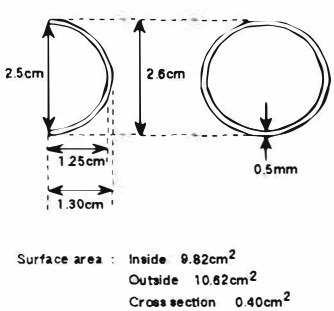

Fig.4 Schematic drawing of the bowl typed palladium cathode

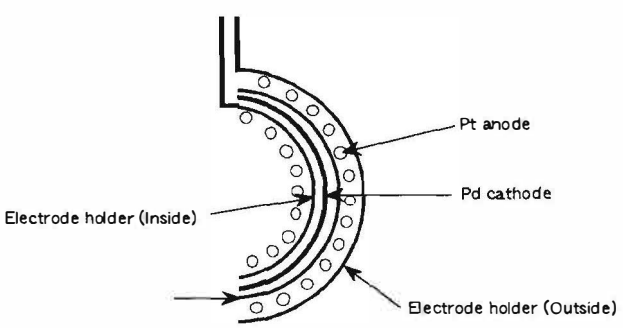

Fig.5 Schematic drawing of the electrode

in the electrolyte. In Run2, 3 and 5, a bowl typed palladium cathode was used to be able to irradiate neutron from ^{252}Cf neutron source efficiently as shown in Fig.4. The configuration of the anode and cathode was illustrated in Fig.5. The aqua resia etching (10 minutes) and vacuum annealing (2 hours) was applied to all the palladium cathodes.

Table1 Experimental Conditions

	Electrolysis cell	Period	Cathode	Pretreatment	^{252}Cf Irradiation conditions	Neutron irradiation
Run1 (Pre.)	Usual type	17days×2	Flat type (Palladium)	Mechanical polish	Long distance pulse irradiation	Thermal neutron
Run2	Unified type	32days×2	Bowl type (Palladium)	Etching Anneal	Short distance pulse irradiation	Thermal neutron
Run3 & 3a	Sandglass type	26days×3	Bowl type (Pd or Pt)	Etching Anneal	Short distance pulse irradiation	Thermal neutron
Run5 & 5a	Sandglass type	26days×3	Bowl type (Pd or Pt)	Etching Anneal	Short distance pulse irradiation	Epithermal neutron

Electrolysis method : Pulse mode➡ High mode 3hours, Low mode 3hours
Current density : Run1～3 High mode⇨200mA/cm² Low mode➡5mA/cm²
Run5 High mode⇨400mA/cm² Low mode➡10mA/cm²
Neutron irradiation method : Pulse mode (Every one day)
Data Acquisition : Every 23hours and 30minutes (Maintenance 30minutes)

The experimental conditions were summarized in Table1. In Run3a and 5a, only a reference run (Pt-LiOD) was carried out. The electrolysis mode was a pulse mode with 3 hours repetition in square pulse, and current density was 200mA/cm² in the high mode and 5mA/cm² in the low mode. The neutron irradiation mode was also a pulse mode with 1 day repetition. The data were acquisitioned for 23 hours and 30 minutes, and resting 30 minutes were used for maintenance. In each electrolysis experiment, the electrolyte (D_2O(LiOD) or H_2O(LiOH)) was added by the automatic supply system to keep the constant level of the electrolyte.

Results and Discussion

Neutron measurement

◎ Thermal neutron irradiation experiments

Neutron Measurement

The neutron energy spectra without the thermal neutron irradiation obtained in Run2 were illustrated in Fig.6. All the neutron ratios are over unity or nearly equal to unity within an error of 2 σ . The neutron ratios in the range of 2.4MeV～4MeV was clearly larger than unity. The neutron ratios without the neutron irradiation fluctuate over unity and the tendency is coincident with those

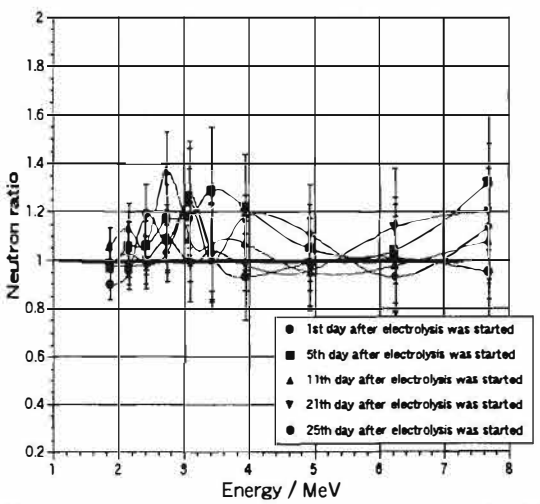

Fig.6 Neutron energy spectrum without the thermal neutron irradiation obtained in Run2

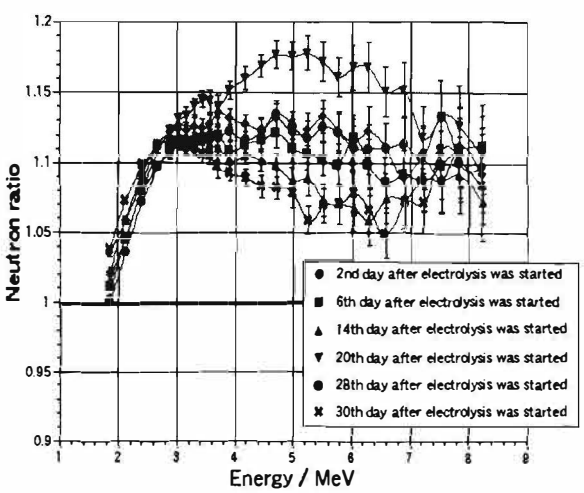

Fig.7 Neutron energy spectrum with the thermal neutron irradiation obtained in Run2

reported in the previous study. The neutron spectra with the thermal neutron irradiation obtained in Run2 were plotted in Fig.7. It can be said that the neutron ratios varied so widely from 4MeV to 7MeV. All the neutron ratios are over unity. The difference between the foregorund run and the background run is only the difference of the light water and the heavy water. The neutron capture cross sections of all the materials in the experimental system should be same in the both runs, except the difference between the protons and deuterons. Moreover, the neutron capture cross section of the deuteron is much larger than that of proton. The neutron ratios over unity found in the thermal neutron irradiation should be recognized as to be an anomalous hydrogen isotope effect.

Gamma-ray measurement

The gamma spectra over the energy range 140-2700keV with the neutron irradiation obtained in Run2 were shown in Fig.8. All these peaks are assigned to the natural radiation or the gamma-rays emitted from Pb radiation shielding. The gamma-ray spectrum over the energy range 140-2500keV and 5000-7500keV with the neutron irradiation obtained in Run2 was displayed in Fig.9. The FWHMs of the peaks obtained under the neutron irradiation are wider than these of the natural gamma-ray peaks. Those peaks were indicated to be the neutron-induced pulses. All the positions and the intensities of the peaks obtained in the foreground run were same as those obtained in the background run. It can be said that no characteristic γ -rays were detected in the present γ -ray spectroscopy.

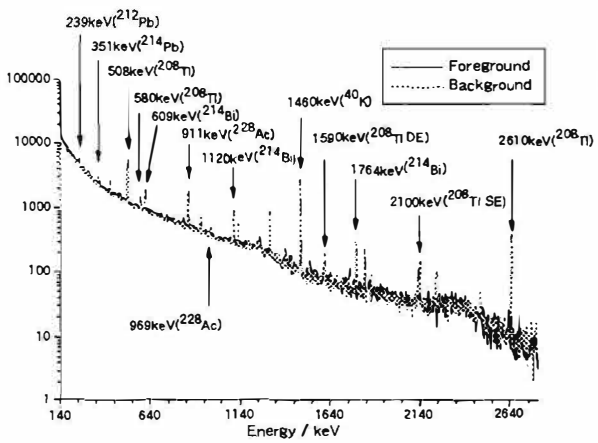

Fig.8 Gamma Spectrum over the energy range 140–2700keV without ^{252}Cf irradiation

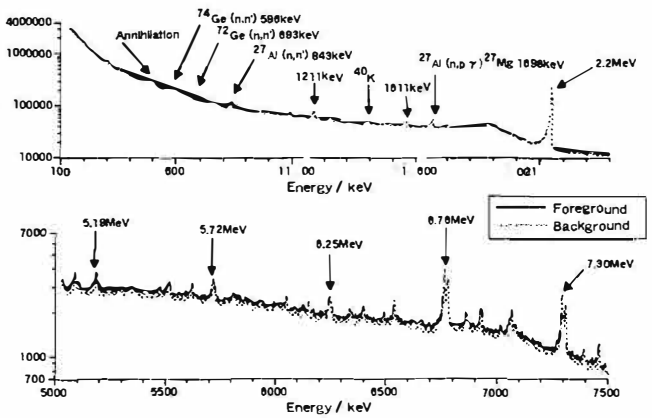

Fig.9 Gamma spectrum over the energy range 140–2500keV and 5000–7500keV with ^{252}Cf irradiation

◎ Epithermal neutron irradiation experiment

The 2-D pulse-shape vs. pulse-height analysis was employed in this experiment. The multiparameter MCA spectrum of NE-213 without the neutron irradiation obtained in Run5 was displayed in Fig.10. Neutron events were discriminated from gamma-ray or noise events with two dimensions. The gamma-ray contamination was checked throughout the electrolysis. The neutron ratios with the epithermal neutron irradiation obtained in Run5 were displayed in Fig.11. The neutron ratios are much larger than unity. The neutron capture cross section of the deuteron is much larger than that of proton, as mentioned in the thermal neutron irradiaiton experiment.

Nuclear Physics Approach

Reflection on some of these will make clear that anomalous hydrogen isotope effect are found much clearly in the epithermal neutron irradiation experiment.

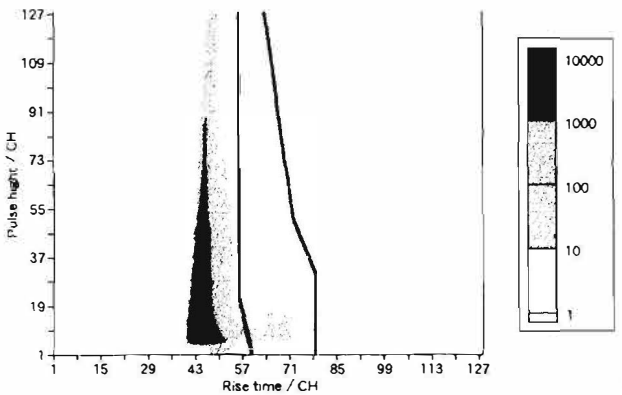

Fig.10 Multiparameter MCA spectrum of NE-213 in Run5
(28th day after electrolysis was started.)

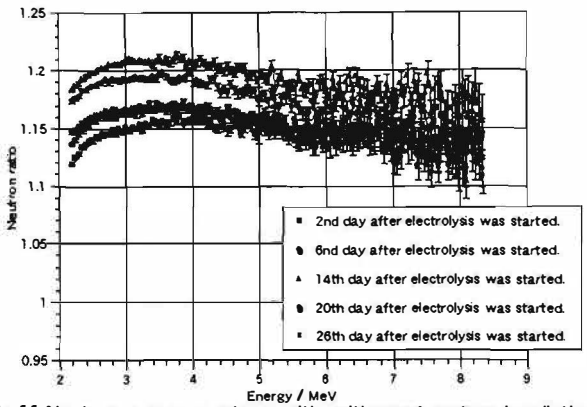

Fig.11 Neutron energy spectrum with epithermal neutron irradiation obtained in Run5

Conclusion

To elucidate the neutron irradiation effects, the heavy water and light water electrolysis have been operated. Anomalous distribution of the neutron ratios was found with the neutron irradiation experiments. It seems reasonable to suppose that the neutron capture cross section of the deuterium is much larger than that of proton. On these grounds, we have come to the conclusion that only the diffrence between light water and heavy water give the anomalous distribution of the neutron ratios. Anomalous hydorgen isotope effect with epithermal neutron irradiation was much clearer than that with the thermal neutron irradiation. Further studies have to carry out to elucidate the isotopes effects.

Excess heat (up to 2.5W (10% of input power)) was observed in the thermal neutron irradiation experiments.

Acknowledgments

The present study has been carried out as a part of the Basic Research Project of New Hydrogen Energy financially supported 20 industries of Japan.

Reference

[1] M.Okamoto, H.Ogawa, Y.Yoshinaga, T.Kusunoki and O.Odawara, "Behavior of Key Elements in Pd for the Solid State Nuclear Phenomena occurred in Heavy Water Electrolysis", Proceedings of Fourth International Conference on Cold Fusion, EPRI, 3, 14-1～14-8 (1994)

[2] A.Takahashi, A.Mega, T.Takeuchi, H.Miyamaru and T.Iida, "Anomalous Excess Heat by D_2O/Pd Cell under L-H Mode Electrolysis", Frontiers of Cold Fusion, Tokyo:Universal Academy Press Inc., 79～91 (1992)[Book]

[3] K.Shiraishi, "Neutron-Induced Nuclear Fusion Reaction in Solid", Journal of the Materials Science Society of Japan, **32**, 75～81 (1995)[Japanese]

[4] H.Ogawa, S.Yoshinaga, Y.Yoshida, M.Aida and M.Okamoto, "Correlation of Excess Heat and

Neutron Emission in Pd-Li-D Electrolysis", Proceedings of The Fifth International Conference on Cold Fusion, 116～119 (1995)

[5] M.Nakada, T.kusunoki and M.Okamoto, "Energy of the Neutrons Emitted in Heavy Water Electrolysis", Frontiers of Cold Fusion, Tokyo:Universal Academy Press Inc., 173～178 (1992)[Book]

[6] A.A.naqvi et al., "Light yield measurement of NE-213 detector for 2.8-14.8MeV neutrons", Nucl. Inst. and Meth. In Phys. Res. A, **325**, 574 (1993)

Nuclear Physics Approach

Deuteron Fusion Experiments in Metal Foils Implanted with Deuteron Beams

K.Ochiai, T.Iida, N.Beppu, K.Maruta, H.Miyamaru, A.Takahashi

Department of Nuclear Engineering ,Osaka University
2-1 Yamadaoka,Suita,Osaka565,Japan.

Abstract

Deuteron beam implantation experiments have been carried out for the examination of the hypothesized new class of fusion reactions to explain the Fleischmann-Pons effect. Some additional techniques were introduced in the implantation experiments by considering the effects of temperature change, pulsed-current stimulation and molecular ion beam. Energetic charged particles from the Ti and Pd foils implanted with 100~250keV deuteron beams were measured with Si-SSDs. In some of the experiments, unusual counts were observed in the energy region higher than the proton peak of the well-known D-D reaction, and they might be related to the new class of fusion reactions with large Q-values. However statistics of the counts were too poor to identify the types of their original reactions. More detailed and long-term measurements are necessary for the explanation of the unusual counts in the high energy region.

Introduction

New class of fusion reactions[1-3] with large Q-values has been proposed and discussed for the explanation of the Fleischmann-Pons(F-P) effect or the large excess heat production in D_2O/Pd electrolysis experiments[4]. Deuteron beam implantation experiments with Ti and Pd foils have been performed to find out energetic charged particles which would be emitted by the new class of fusion reactions in metal-deuterium system. Vacuum environment in the beam implantation experiments is suited for the identification of nuclear reactions in a foil sample, i.e. for the exact measurement of the type and energy of the charged particles emitted from the foil.

In the present experiment, some additional techniques were introduced to consider the following effects; (1) temperature change, (2) pulsed-current stimulation and (3) injection of clustered particles molecular deuteron ions. The dynamic conditions like transient temperature change and pulsed-current stimulation could induce temperature change and pulsed-current stimulation could induce non-equilibrium movement of lattice atoms and could more selectively excite deuteron motion in the lattice due to their lighter mass, which might lead to the opening of the new class of fusion reactions like the multibody fusion reactions[1-2]. The use of the molecular ion beams might be effective in enhancing the local deuterium density and consequently reducing inter-atomic distances of neighboring deuterons in the foil from a microscopic point of view, in other words the proximity probability between deuterons in solid. This paper describes the experimental method and some results obtained for Ti and Pd foil samples, after our previous experiments[5-6].

Nuclear Physics Approach

Experimental

Figure 1 shows a schematic drawing of the experimental apparatus installed in a beam line of a 300kV deuteron accelerator. The central portion of a foil sample was implanted with 2~10μA deuteron beams collimated with a 5mmϕ aperture. Inside a sample foil, deuteron beams slow down and many deuterons can come to exist between lattice metal atoms which are thermally excited by the energy of the beams. Moreover, some additional techniques concerning the temperature change, pulsed-current stimulation and molecular ion effects. were introduced in expectation of the

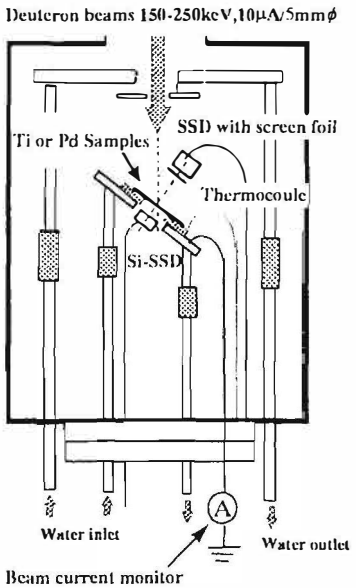

Fig.1 Configuration of experimental apparatus

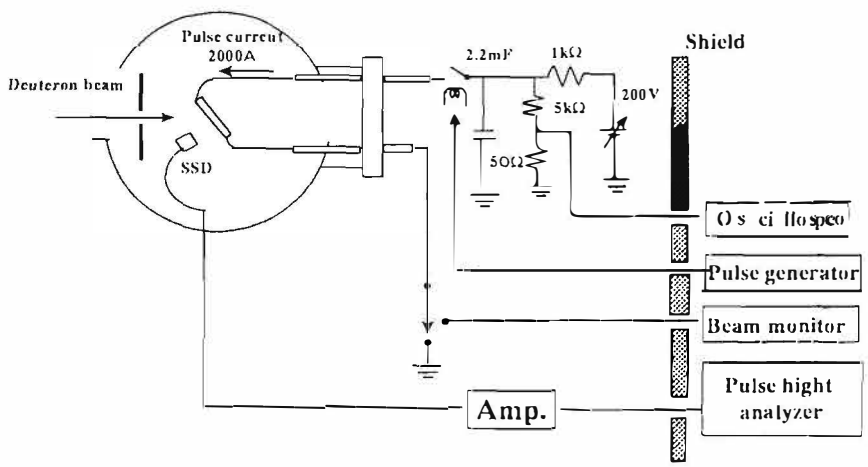

Fig2. Schematic drawing of experimental apparatus for examination of pulsed current stimulation effect

enhancement of the deuteron fusion reaction rate in the sample. The temperature of the sample foil, monitored with a thermocouple, was controlled by using a ceramic heater.

Nuclear Physics Approach

Figure 2 shows a schematic drawing of an apparatus for the pulsed-current stimulation experiment. Pulsed-currents were generated by dischange from a capacitor and were periodically supplied to the sample during deuteron beam implantation. The characteristics of the current pulses were about 2500A in peak, 300μs in pulse with and 0.2Hz in repetition rate. Occasionally molecular ions(D_3^+) were also used as implantation beams. They were easily provided by adjusting the current for the ion analyzing magnet of the accelerator. A pair of Si-SSDs with screen foils analyzed the energy, and type of the correlated particles emitted in opposite directions. The Si-SSDs were placed at the position 15~30mm away from the sample foil and had the effective window area of about 35mm^2 . One of the Si-SSDs had the depletion layer thickness of about 2mm and could analyze high energy proton up to about 18MeV.

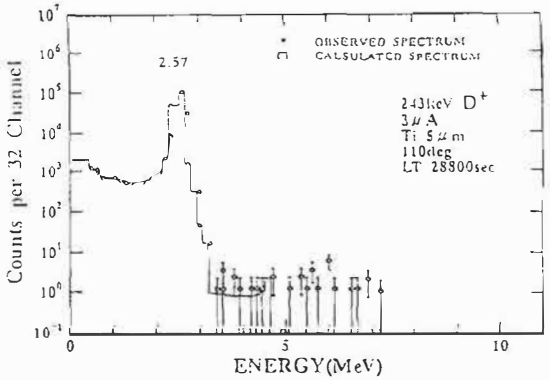

Results and Discussions

Figure 3 shows typical energy spectra of charged particles emitted from a 5μm Ti foil bombarded with 243keV deuteron beams. Besides the normal proton peak from the well-known D-D reaction, unusual counts were measured in the higher energy region, though statistics of the counts were very poor. In order to discuss the counts in the higher energy region, the amount of the counts due to the pile up of the D-D proton and other signals should naturally be estimated and thus we have developed a computer simulation program for the estimation of the pile-up effect in detected signals[7]. The spectra shown in solid line in the figures were calculated by using this program, and they indicate that the counts in the energy region over 5~6MeV are not due to the pile-up effect. However, statistics of the counts are too poor to identify the types of their original reactions.

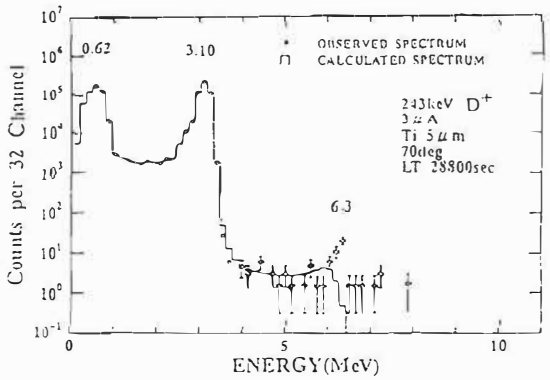

Fig3. Typical energy spectra of charged particles emitted from, a 5μm Ti foil bombarded with 243keV deuteron beams; detected at 110deg (upper) and at 70deg (lower).

Nuclear Physics Approach

Figures 4 and 5 show results for 50μm Ti foils implanted with D_3^+ and D^+ beams. There was no significant difference in the energy spectra between the D_3^+ and D^+ beam experiments. Moreover, the counts measured in the higher energy region agreed well with the high energy component estimated from the calculation of the pile up simulation. These spectra also do not show any counts in the energy region over 5MeV, which are different from the spectra shown in Fig.3. The reason is not clear.

As for the temperature effect, the temperature of the sample was controlled from 100 to 573K and was kept constant during the deuteron beam implantation. The counting rate of D-D protons went down at higher temperature due to the enhancement of deuteron diffusion in metal. The energy spectra of the charged particles, as shown in Fig.6, seem to be similar as a whole to those shown in Fig.3, though sufficient statistics of the counts are not obtained in the higher energy region. We have not done such transient experiments as that the temperature of the sample is changed quickly during the deuteron beam implantation.

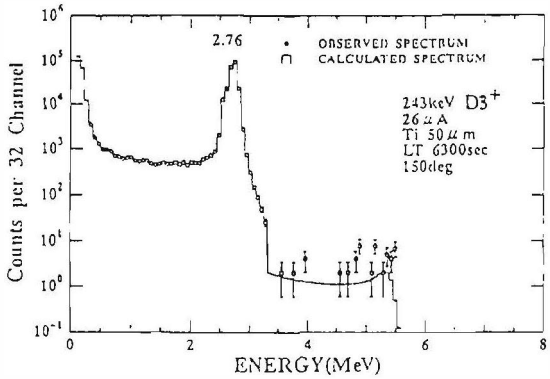

Fig4. Energy spectrum of charged particles measured for a 50μm Ti foil implanted with 243keV D_3^+ beams

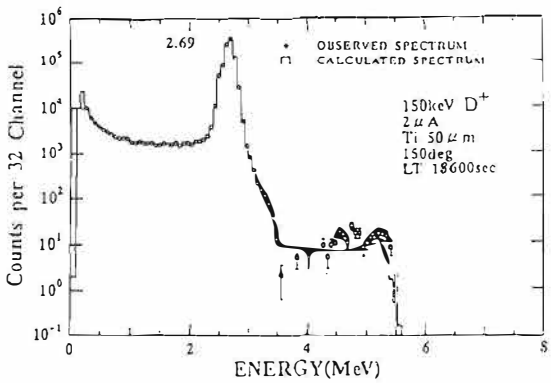

Fig5. Energy spectrum of charged particles measured for a 50μm Ti foil implanted with 150keV D^+ beams

Figure 7 shows results for the pulsed-current stimulation experiments. Measured energy spectrum of the charged particles resembles the spectra shown in Fig.3. Though some counts were measured in the higher energy region than 5MeV, their statistic were too poor to definitely say the effectiveness of the pulsed-current stimulation. Here, it should be noted that many efforts were made for rejecting possible noise signals in this experiment.

Nuclear Physics Approach

Summary

Deuteron beam implantation experiments have been done for the examination of the new class of fusion reactions for the explanation of the F-P effect. The energetic charged particles from the Ti and Pd foils were measured with Si-SSDs. In principle, the types of the particles can successfully be identified from the energy loss in the screen foil set up in front of the Si-SSDs. Considering the low counting rate in the higher energy region, we have developed the computer simulation program for the estimation of the pile up component in the energy spectrum. This program should be useful for the detailed discussion on measured energy spectra and for the subtraction of the pile-up component from the spectrum. In addition to the deuteron beam implantation, some modified experiments in consideration of temperature change, pulsed current stimulation and molecular ion effects were done. Unusual high energy counts were measured in the spectra of some of the experiments. These counts might be related to do with the new class of fusion reactions hypothesized by several authors, but statistics of the counts were too poor to identify the type of their original reactions. More detailed and long term measurements are needed to clarify the origin of usual high energy counts.

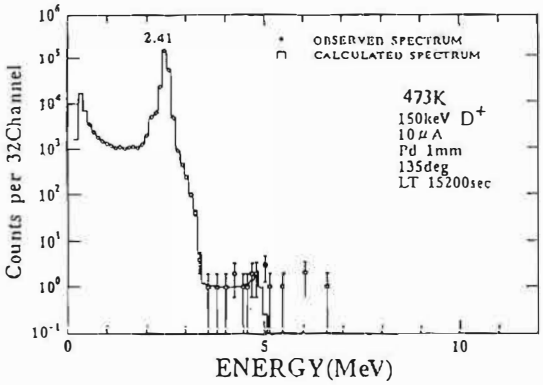

Fig6. Energy spectrum of charged particles measured for a 1mm Pd plate implanted with 150keV deuteron beams. The plate was heated with a ceramic heater.

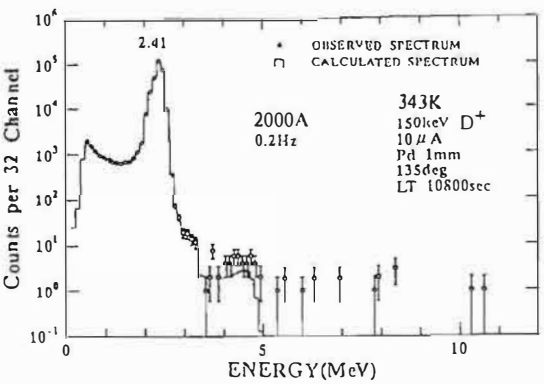

Fig7. Energy spectrum of charged particles measured for 50μm Ti foil implanted with 243keV deuteron beams. Pulsed current were periodically supplied to the plate.

References

[1] A. Takahashi, et al., Fusion Technology, 19, 380 (1991).
[2] A. Takahashi, et al., Fusion Technology, 27, 71 (1995).
[3] J. Kasagi, et al., J. Phys. Soc. Jpn.64 (1995) 777
[4] M. Fleischmann and S. Pos, J. Electroanal. Chem., 261, 301 (1989).
[5] T.Iida, et al; Proceedings: Fourth International Conference on Cold Fusion, Vol.3, 13-1
[6] T. Iida, et al; genshikaku Kenkyu, Vol. 40, No.5, pp. 77-83 (1995).
[7]N. Beppu, Master Thesis, Dept. Nucl. Eng., Osaka Univ., (1996) in Japanese.

Nuclear Physics Approach

Anomalous Energy Transfer between Nuclei and the Lattice

Peter L. Hagelstein

Massachusetts Institute of Technology
Research Laboratory of Electronics
Cambridge, MA 02139

1. Introduction

We have continued our theoretical efforts to develop models that are relevant to the experimental claims of the observation of anomalies in metal hydrides. Of these anomalies, we have been particularly interested in heat generation both in heavy water and in light water systems, electrochemically induced radioactivity, tritium production and neutron emission. There have been a rather significant modification in our direction over the course of the past year, resulting in new models that appear to be more closely related to the experimental claims.[1]

2. Failure of the Neutron Hopping Model

We proposed that inelastic neutron hopping might account for the claimed heat and tritium production in experiments involving metal hydrides and deuterides.[2] The potential advantage of neutron hopping as a mechanism was that neutrons experience no Coulomb barrier, thus removing the Coulomb barrier problem. Neutron hopping with the exchange of low momentum virtual neutron states appeared to be the only possible mechanism for tritium production, which must be produced with nearly zero kinetic energy to be consistent with the observed lack of secondary *dt*-fusion neutrons that would accompany energetic tritium nuclei.

Potential problems associated with this proposal were recognized early on by this author and by other theorists. The basic problem is that it is not obvious that neutrons can hop from one nucleus to a distant (on the Fermi scale) nucleus. While it was clear that significant energy exchange with the lattice would be required for heat and tritium production, the initial attempts at developing a model for this process suggested that neutron delocalization might occur without MeV-level energy input from the lattice.

Subsequently, the neutron hopping model was analyzed in great detail. A basic quantitative understanding of both elastic and inelastic neutron hopping is now believed to be in hand, and the results indicate that no neutron hopping is possible without MeV-level energy transfer from the lattice. While a very large sub-threshold virtual neutron hopping effect is predicted, the effect would require more than 5 MeV input energy from the lattice,

which was not appreciated in our previous work. There are two important consequences of this observation: (1) neutron hopping driven by such large lattice energy transfer would be accompanied by real neutron emission (not in agreement with experiment); and (2) that many other observable effects are predicted to be observable at much lower energy transfer. We have therefore turned our attention back to lattice-induced reactions at lower energy transfer.

3. The basic energy transfer model

Atomic and nuclear reactions that occur within a lattice (and that involve energy transfer with the lattice) can be be described in general through Fermi's Golden Rule using coupled lattice and nuclear states

$$\Gamma = \frac{2\pi}{\hbar} |\langle \Psi_f | \hat{V} | \Psi_i \rangle|^2 \rho(E_f) \tag{1}$$

where the interaction operator depends on both nuclear and lattice coordinates. The prototypical interaction operator includes recoil and lattice rearrangement; these effects can be modeled using site-dependent interaction operators of the form

$$\hat{V}_j \sim e^{i\mathbf{k}\cdot\hat{\mathbf{R}}_j} e^{-i\hat{S}_D} \tag{2}$$

The first term on the RHS describes momentum exchange through recoil; the second term describes lattice mode rearrangement ($e^{-i\hat{S}_D}$ is a Duschinsky operator).[3]

Modeling anomalous energy transfer requires operators that are capable of transferring large amounts of energy when a reaction occurs. The recoil operator is well known in condensed matter, and in our view cannot support anomalous energy transfer. Mode rearrangement fundamentally involves operations on all excitation present; consequently, the Duschinsky operator is potentially capable of mediating anomalous energy exchange, given a large initial excitation of an initial state mode that projects into final state modes with a finite energy spread.

For anomalous energy transfer through this mechanism, we require an initial strong excitation of a phonon mode, either through the presence of a phonon laser or through strong coherent excitation. We have conjectured that exothermic desorption may drive a phonon laser. For this mode to project into final state modes with a large energy spread, it probably needs to be in the band gap away from other modes (we are considering nonlinear frequency shifting of a mode near the band gap). Mode rearrangement would be driven by a change in the vacancy distribution, and hence involve vacancy modes. The resulting energy transfer would then occur as fluctuations, with an energy transfer on the order of

$$\Delta E \sim \sqrt{N_{ph}}\, \hbar\delta\omega \tag{3}$$

We suggested previously[4] that a larger energy exchange (proportional to N_{ph}) might be possible; but this can be shown to be inconsistent with moment theorems that apply to phonon mode rearrangement.

The resulting theory leads to reaction rate predictions of the form

$$\Gamma = \int P(\epsilon)\, \gamma_0(\epsilon)\, d\epsilon \tag{4}$$

where $\gamma_0(\epsilon)$ is the reaction rate assuming that an energy ϵ is transferred, and $P(\epsilon)$ is the associated probability. For energy transfer by fluctuations, the probability would be described locally by a Gaussian distribution

$$P(\epsilon) = f_0 \exp\left\{-\left(\frac{\epsilon}{\delta\epsilon}\right)^2\right\} \quad (5)$$

4. Understanding experimental claims with the model

Within the framework of the model, different effects would be induced depending on the amount of energy transfer, the number of vacancies present, and on the type and abundance of impurities. For energy transfer on the order of 10s to 100s of eV, atomic recoil would be predicted; a possible observable might be atomic hydrogen or deuterium ejection from the surface. At the keV-level of energy transfer, deuteron recoil would lead to low level *dd*-fusion neutron production and electron recoil from light isotopes. Above about 100-200 keV of energy transfer, beta decay and electron capture reactions would be induced; these would be sensitive to the presence of vacancies since the recoil energy imparted to moderately heavy nuclei is low. Above about 1.5 MeV of energy transfer, alpha decay reactions would become dominant. Significantly larger energy transfer (more than about 5 MeV) does not presently appear to be likely, but would induce other more energetic effects.

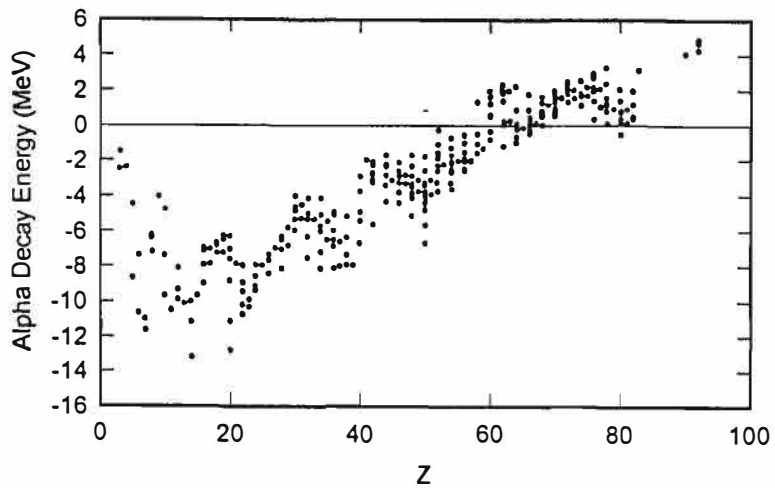

Figure 1: Alpha decay energy as a function of Z.

Heat production in this model would come about from lattice-induced exothermic alpha decays of heavy nuclei that are present (see Figure 1). The optimum naturally occurring "fuel" isotope in this picture is ^{147}Sm; others are listed in Table I. For example, Pt is present in many heat-producing experiments at low levels; in this model, some of the Pt are candidate fuels for heat production (see Figure 2 for a comparison of the lattice-induced decay rate for Pt compared with that of other elements). If this basic mechanism is correct, then significant prompt gamma emission should be observable as lattice-induced alpha decay would give a finite yield of excited state daughters.

Tritium production would come about from lattice-induced alpha decay of ^{7}Li (at 2.47 MeV of energy transfer). The reaction rate is computed to approach its maximum for lattice

transfer energies only a few keV above threshold; such a mechanism has the potential to account for slow tritium formation at low levels. The related lattice-induced decay of ^{6}Li (at 1.47 MeV of energy transfer) would similarly produce deuterons with keV-level energy, that could result in low-level *dd*-fusion neutrons. Lattice-induced alpha decay of light nuclei, if it occurs, could be studied through lattice-induced ^{9}Be decay which would lead to fast neutron production as a primary observable.

Parent Nucleus	Abundance %	Daughter Nucleus	Abundance %	Q_α (MeV)	$\Delta\epsilon^{(1)}$ (MeV)	Daughter half-life
^{147}Sm	15	^{143}Nd	12.2	2.31	2.40	
^{144}Nd	23.8	^{140}Ce	88.48	1.91	2.59	
^{152}Gd	0.20	^{148}Sm	11.3	2.20	2.71	
^{148}Sm	11.3	^{144}Nd	23.8	1.99	2.72	
^{149}Sm	13.8	^{145}Nd	8.3	1.87	2.83	
^{151}Eu	47.8	^{147}Pm		1.97	2.84	2.62 y
^{234}U	0.005	^{230}Th		4.86	2.91	8×10^4 y
^{145}Nd	8.3	^{141}Ce		1.58	2.91	32.5 d
^{142}Ce	11.08	^{138}Ba	71.7	1.31	2.97	
^{235}U	0.72	^{231}Th		4.68	3.08	25.5 h
^{190}Pt	0.01	^{186}Os	1.58	3.25	3.10	

Table I: Lattice-induced alpha decays of alpha unstable naturally occurring isotopes. Q_α is the alpha decay energy. The isotopes in this table are ordered by the characteristic lattice energy $\Delta\epsilon^{(1)}$ required for a 1 sec^{-1} decay rate.

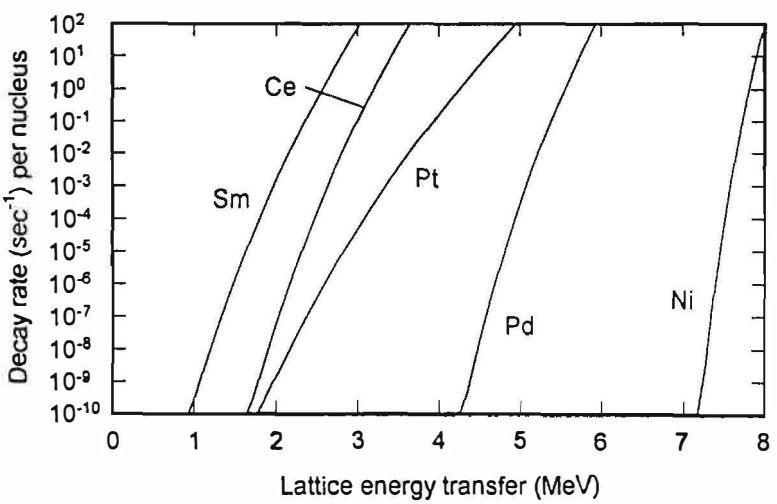

Figure 2: Element-averaged lattice-induced alpha decay rates per nucleus.

5. Modeling cathode activation

Cathode activation in this model could come about in the absence of heat through lattice-induced beta decay. Calculations for some of the attractive candidates for lattice-induced beta decay are shown in Figure 3.

Such a mechanism is proposed to account for the cathode activation described by Passell at ICCF5.[5] We attempted to use the model to fit some of the experimental data from this experiment, assuming that the observed radioactivity is due to lattice-induced beta decay of Pd and ppm levels of Ru, Rh, Ag, and Cd impurities. While the comparison is imperfect, the data appears perhaps to be most consistent with a Gaussian energy transfer model described by $f_0 \sim 0.05$ and $\delta\epsilon \sim 350$ keV. This level of energy transfer is too low to produce detectable heat production. The relatively large value of f_0 within the model would have the interpretation that energy transfer was allowed on essentially a CW basis throughout the activated region, presuming the presence of host lattice vacancies at the per cent level.

The results of this comparison are inconsistent with the presence of an optical phonon laser, as we had proposed earlier. It is more consistent with an acoustic phonon laser, combined with nonlinear coupling between acoustic modes and vacancy modes within the band gap as we proposed at ICCF5.

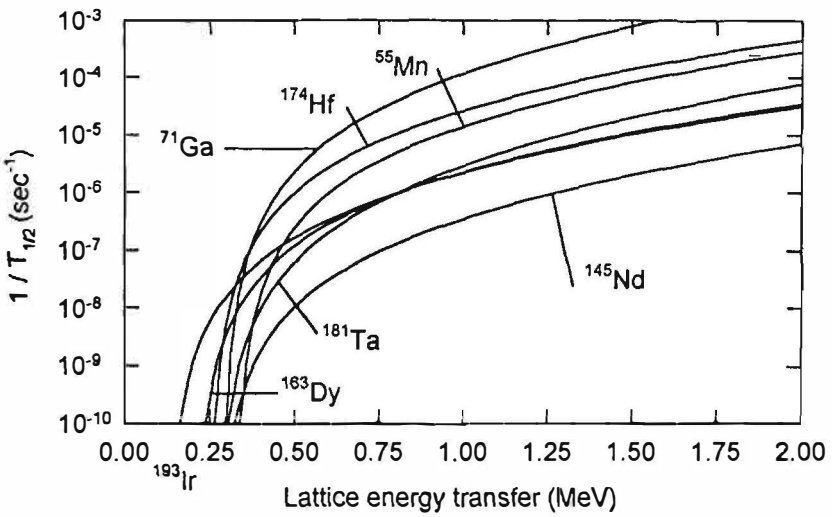

Figure 3: Lattice-induced beta decay rates for isotopes with low thresholds for allowed transitions.

References

1. P. L. Hagelstein, EPRI final report (1996).
2. P. L. Hagelstein, ICCF5 Proceedings (1995).
3. P. L. Hagelstein, *Hyperfine Interactions* **92** 1059 (1994).
4. P. L. Hagelstein, *Trans. Fusion Tech.* **26** 461 (1994).
5. T. Passell, ICCF5 Proceedings (1995).

Nuclear Physics Approach

TRITIUM, NEUTRON, AND RADICARBON REGISTRATION WITH THE YUSMAR HYDROFACILITY RUNNING

Yu.N.Bazhutov[1], V.P.Kor etsky[1], A.B.Kuznetsov[1], Yu.S.Potapov[2], V.P.Nikitsky[3], N.Ya.Nevezhin[3], E.I.Saunin[4], V.O.Kordukevich[5], A.F.Titenkov[5]

[1]Erzion center, P.O.Box 169, 105007 Moscow, Russia
[2]Vizor Scientific Firm, Kishinev, Moldova
[3]Energiya Rocket Space Corporation, Kaliningrad, Moscow Region, Russia
[4]Institute of Physical Chemistry, Russian Academy of Sciences, Moscow, Russia
5Institute of Nuclear Physics, Moscow State University, Moscow, Russia

Abstract
High statistical (>3σ) and systematic confidence levels have been reached in recording the nuclear products (tritium, neutron emission, and radiocarbon) that occurred in the Yusmar hydrofacility working fluid as predicted by the Erzion model for catalyzed transmutation of nuclei. The pending extension of the Erzion model research is expected to improve the Yusmar properties relevant to energy.

1. Introduction

Cold fusion is well-known to proceed under nonequlibrium conditions, namely, under electrolysis, electric discharge, mechanical impact, sonoluminescence, ultrasonic effects, etc. J.Griggs [1] and Yu.Potapov [2] have reported a feasibility of generating additional power in the hydrodynamic facilities where the nonequilibrium cavitation process is induced in pure water. The increased energy output in the like facilities was accounted for earlier in terms of the Erzion model of cold fusion [3-5]. In the present work, the Erzion model representations are verified using the Yusmar hydrofacility designed by Dr. Yu.Potapov.

The Erzion model assumes that intensive cavitation of a hydrofacility working fluid may prove to be a trigger of nuclear reactions involving enion, $Э_N$, and erzions, $Э^o$ and $Э^-$, should some requirements be met as regards the working fluid composition. Namely, the presence of donor nuclei ($Э_N$, carriers of reaction catalysts) and of fuel nuclei (used in the nuclear reactions involving $Э_N$ together with sporadic $Э^o$ and $Э^-$). The Erzion model predicts that some experiments can give rise to yields of neutrons or gamma-rays that accompany the nuclear transmutation reactions and production of radioactive isotopes. According to the model, ^{16}O, ^{12}C, and ^{64}Ni can be donors. In case cavitation triggers the mechanism of enion emission from a donor nucleus, the following erzion-induced catalytic reactions may proceed if the working fluid comprises such elements as tritium, lithium, and carbon:

$$D + Э_N = Э_O + T + 011\ MeV, \quad (1)$$

$$D + Э^- = Э_N + n + 558\ MeV, \quad (2)$$

$$T + Э_N = Э^- + {}^4He + 12.0\ MeV, \quad (3)$$

$${}^6Li + Э^- = Э_N + {}^4He + n + 4.2\ MeV \quad (4)$$

$${}^6Li + Э_N = Э^- + {}^8Be(2\times{}^4He) + 9.6\ MeV, \quad (5)$$

$${}^{13}C + Э_N = Э^o + {}^{14}C + 2.03\ MeV, \quad (6)$$

$$^{13}C + Э^{0} = Э_{N} + ^{12}C + 1.20\ MeV. \quad (7)$$

In other words, a heavy water admixture to the Yusmar working fluid (light water) may result in production of tritium (reaction (1)), a tritium-contaminated heavy water admixture or lithium admixture in neutron production (reactions (2),(3) or (4), (5)), and carbon-containing admixtures in radiocarbon production (reactions (6), (7)). The main aim of the present work was to verify the Erzion model predictions by detecting eventual products of reactions (1)-(7). The fact the reactions proceed actually may be confirmed by operating the hydrofacility (detection of neutrons) or by analyzing the working fluid samples after the facility is turned off. The hydrofacility was in operation for 16 working days from April to September, 1995. The facility was turned on 142 times (the operation modes are described in Section 2 below). The working fluid was a mixture of tap water, various combinations of LiJ, LiBr, Li_2SO_4, LiCl, LiOH, and $NiSO_4$ solutions, and D_2O; totalling to about 40 different solutions. A fraction of the experimental results thus obtained are reported here.

2. Yusmar hydrofacility

The hydrofacility (see Fig.1) is a closed system of tubes of different cross sections (the largest diameter is 5 cm) connected to an electric pump and an electric motor. The pump capacity is 12 m^3/hour, the motor power is 7.5 kW, the working fluid volume is 10 l. Fluid flow control devices placed inside the tubes in the upper part of the facility make the fluid rotate. A cavitation-inducing insert is also mounted inside the tubing. The maximum admissible pressure is 10 amt. The hydrofacility is equipped with heat sensors (1-4, Fig.1), a pressure gauge that supplies its data to recorders, and valves at the facility top and bottom for varying the working fluid composition and for sampling water and solutions.

Single and multiple operation modes were used. In the single mode, the continuous operation time was up to T = 1 hour). In the multiple mode, the facility was turned on up to 15 times for T = 15 min). The turn-off moment was indicated by occurrence of the maximum admissible pressure of 10 atm and the maximum temperature of casing (100°C, normally at point 4, Fig.1). The fluid pressure variation rate (see Fig.2) was defined to a great extent by the volume of an air bubble that remained in the tube system after filling. With an air bubble volume below 10 cm^3, the domain of gradual pressure variations (1 in Fig.2) decreased and could actually disappear and turn into the domain of avalanche-like pressure rise (2 in Fig.2) up to 10 atm within a very short time (below 1 min.). In this case temperature inside the facility increased gradually during a single operation run, so any pronounced bend was absent in the P(T) curve. The avalanche-like pressure rise was probably accounted for by initiation of violent cavitation.

3. Tritium measurements

Tritium production was recorded by measuring beta-activity in the working fluid samples taken when the Yusmar facility was not in operation and after it was turned on. The working fluid was a mixture of light (10 l) and heavy (10 ml) water. The tritium beta-activity (the highest beta-spectrum energy is 18.6 keV, the half-life is 12.3 years) was measured by a liquid scintillate.

The initial samples were 50-ml portions of tap water and a mixture of heavy and light water. The activity of two initial tap water samples did not exceed the 0.5 Bq/ml background. The specific activity of the initial mixture sample was 28±0.5 Bq/ml. After the first and second 12-min long operation runs the sample specific activity was 33±0.5 Bq/ml and 34±0.5 Bq/ml, respectively.

Thus, a 20% specific activity excess (5±0.7 Bq/ml) over the background occurred in the Yusmar working fluid with a 0.7% heavy water admixture after a 12-min long facility operation. The second 12-min long operation run failed actually to raise the specific activity of the solution.

Nuclear Physics Approach

The test study of the tritium measurement method is described in [7]. Reliability of the results obtained was confirmed in the repeated measurement run of the same fluid samples with Beta-2 radiometer a month later. After the first and second operation runs the specific activity was 6±0.8 and 5±0.8 Bq/ml in excess of the background.

4. Neutron measurements

Neutrons were detected in two channels of unit 5 (Fig.1) that included 6 ^{3}He counters encased in Plexiglas (fast and thermal neutrons, channel 1) and six counters of the same type without a moderator (thermal neutrons, channel 2). The effectiveness of either channels (some 0.5% and 0.25%) was experimentally tested with a ^{252}Cr source. Each run of neutron flux measurements lasted for 2 min in either of the channels and, besides, the results of the channels were summed up. Background radiation was measured before each of the runs. The total background measurement time was 24.8 hours. The measurement time of the effect was 29.2 hours. Presented below are the results obtained in three neutron measurement runs using the following working fluid compositions:

(1) 10 l H_2O + 300 ml D_2O, a 3.5 Bq/ml specific activity for tritium;
(2) 10 l H_2O + 200 g LiBr;
(3) 10 l H_2O +150 g D_2O (3.5 kBq/ml) + 400 g LiBr + 250 g $NiSO_4$.

Composition (3) was prepared with a view to increasing the contents of neutron converter (D+T and Li) and donor (Ni), thereby intensifying the neutron flux in conformity with the Erzion model.

None of neutrons (an excess of -10.2±25.5 neutrons) were detected for 17 min in the two channels by operating the Yusmar facility without any admixtures to the working fluid. In the composition (1) tests, 38.5±12.3 neutrons were detected for 9 min after two Yusmar operation runs. In the composition (2) tests, 113.3±36.5 neutrons were detected for 34 min after two operation runs. In the composition (3) tests, 304±21 neutrons were detected for 2.5 hours after 13 operation runs (from 1.5 min to 6 min each). In the last case neutrons occurred only after the 8th operation run and were recorded with two interruptions for 80 min after the facility was turned off (Fig.3).

So, admixture of definite elements (D+T or Li) to the Yusmar working fluid results in occurrence of neutron emission. The process is sporadic id gets initiated only at the moment of pressure rise (cavitation) and may proceed after the hydrofacility is turned off (so called life after death).

5. Radiocarbon measurements

The feasibility of beta-active carbon-14 production (E = 156 keV, a 5.7x103 half-life) was tested using Tosol A40M antifreeze (manufactured in October, 1992) as the carbon-containing fluid. The sample activity was measured by the same techniques as in tritium measurements, the only exclusion was that the beta-energy detection threshold was raised).

Specific activity measured in the initial sample proved to be 1.6±0.02 Bq/ml. A 4.6±0.2 Bq/ml specific activity was recorded in the sample for 1.5 hours after 7 operation runs of the facility (from 1.5 min to 10 min each).

So, after repeated operation runs of Tosol-operated Yusmar facility the specific beta-activity of the working fluid due to radiocarbon emission increased by 3.0±0.03 Bq/ml.

6. Discussion of results

Analysis of the tentative experimental results has demonstrated that the predictions of the Ersion model for nuclear transmutation realized with the Yusmar hydrofacility are correct. Namely, as predicted by the model, nuclear products (tritium, neutrons, and carbon-14) were detected quite

safely (the effect magnitude exceeds three standard deviations, and even a hundred standard deviations for radiocarbon). The nuclear products were recorded only in the presence of quite definite elements in the composition of the facility working fluid.

On the other hand, the transmutation product occurrence probability is far from unity and may be 0.2-0.3 (as estimated in the neutron detection experiment). Besides, having been once initiated (by cavitation in the fluid, for instance), the process may last for a sufficiently long time of dozens of minutes (see Fig.3). Therefore, the process has still to be optimized by, first of all, varying the contents of reagents (donor nuclei and fuel nuclei) and modifying the materials and design of the hydrofacility. The pending extension of works in these research lines is expected to improve the Yusmar properties relevant to energy and ecology.

References

1. J.Griggs. Proc. Intern. Symp. on VCold Fusion and New Power Sources, Minsk, May, 1994, p.252.
2. Yu.S.Potapov. Patent of Russian Federation No.2045715, Priority of April 26, 1993. Filed October 10, 1995.
3. Yu.N.Bazhutov and G.M.Vereshkov. Preprint TsNIImash No.1, 1990.
4. Yu.N.Bazhutov and G.M.Vereshkov. Proc. 1st Russian Conf. on Cold Fusion, Abrau-Durso. September-October, 1993, p.23
5. Yu.N.Bazhutov and A.B.Kuznetsov. Proc 2nd Russian Conf. on Cold Fusion. Sochi, September, 1995, p.25.
6. Yu.N.Bazhutov, A.B.Kuznetsov aand E.B.Pletnikov. Preprint NITs FTP ERZION No.1, TsNIImash, 1993.
7. Yu.N.Bazhutov, A.B.Kuznetsov, YU.P.Chertov et al. In: Cold Fusion, TsNIImash, Kaliningrad, 1992, p.76.

FIGURE CAPTIONS

Fig.1. A schematic of Yusmar hydrofacility
1-4 - heat sensors
5 - fast and slow neutron detection unit

Fig.2. Variations of fluid pressure P within a Yusmar operation run (domains 1 and 2) and after the facility is turned off (domain 3).

Fig.3. Neutron detection (the $\pm\sigma$ range is indicated) during repeated Yusmar operation runs (the black intervals along t-axis) using T+D and Li admixtures.

Fig.1. "Yusmar" hydrofacility

EE - electric engine
P - pump
C - cavitators
1-4 - thermometers, manometers
5 - neutron registration block

Fig.2. Working liquid pressure during switch-on (1-2) and switch-off (3) periods of the "Yusmar" hydrofacility

Fig.3. Neutron emissions ($\pm\sigma$) during switch-on (dark regions on time axis) and switch-off periods of the "Yusmar" hydrofacility

Nuclear Physics Approach

Possibility of Radioactive Waste Utilization in Terms of the Erzion Model

Yu.N.Bazhutov, V.P.Koretsky

Erzion Center, P.O.Box 169, 105077 Moscow, Russia

Abstract

The possibility of transmutation of twenty six elements which form the main part of radioactive wastes is analysed in terms of the Erzion Model. The final products of the transmutation reactions are examined. It is concluded that practically all of the radio nuclides may be utilized.

The Erzion Model of catalytic nuclear transmutation can predict the possibility of radioactive waste utilization. Transmutation of some isotopes, which form a part of nuclear reactor wastes, was analysed earlier [1, 2]. It was shown that transmutation can be initiated with a lot of radioactive isotopes on the following two conditions:

1. A definite ratio of donor-nuclei (transmutation catalyst carriers) to fuel-nuclei has to exist.
2. Initiation mechanism of the reactions must be effective. Natural radiation of wastes can be used for this purpose.

Possible procedure of waste treatment was discussed earlier [2]. The detailed method of burning away of one long-lived isotope - Cesium-137 - was proposed as well. The aim of present paper is the analysis of other radio nuclides burning away possibility.

It is known that the main sources of environment radioactive pollutants are: the natural radioactivity; the nuclear weapon treatment; the natural uranium mining; the nuclear station operation; the nuclear fuel processing; the nuclear emergencies. The radioactive composition of these pollutants was analysed [3]. The final products of exothermic reactions with catalyst particles - enion $Э_N$ and erzions $Э^•$ and $Э^-$ were defined for each radio nuclide [4]. The examples of such reactions for isotopes ^{137}Cs and ^{99}Tc are as follows:

$^{137}Cs(Э_N,Э^-)^{138}Ba$ + 1,20 MeV;
$^{137}Cs(Э^-,Э_N)^{136}Xe$ + 0,38 MeV;
$^{99}Tc(Э_N,Э^-)^{100}Ru$ + 1,38 MeV;
$^{99}Tc(Э^-,Э_N)^{98}Mo$ + 1,30 MeV;
$^{99}Tc(Э_N,Э^0)^{100}Tc$ + 0,61 MeV; 16s.: β^-; γ;
$^{99}Tc(Э^-,Э^0)^{99}Mo$ + 1,08 MeV; 66hr: β^-; γ;

These reactions can proceed validly as a catalytic particle ($Э_N$, $Э^0$ or $Э^-$) appears in each channel.

Nuclear Physics Approach

The results are presented in Tables 1 and 2 for fusion and transuranium products correspondingly. Some first isotopes in each Table bounded by double line are in decreasing order of their radiation danger [5]. The other isotopes are in decreasing order of half-life period.

Table 1.

Transmutation reactions for fusion products

Initial isotope	Half-life period	Final isotope	Half-life period
^{137}Cs	30y.	^{136}Xe	stable
		^{138}Ba	stable
^{99}Tc	2,1·10^{5}y.	^{98}Mo	stable
		^{99}Mo	66hr
		^{100}Tc	16s.
		^{100}Ru	stable
^{107}Pd	6,5·10^{6}y.	^{107}Ru	22min.
		^{108}Pd	stable
^{129}I	1,6·10^{7}y.	^{128}Te	stable
		^{129}Te	70min.
		^{130}I	12.4hr
		^{130}Xe	stable
^{147}Pm	2,6y.	^{146}Nd	stable
		^{147}Nd	11d.
^{154}Eu	8,8y.	^{153}Sm	47hr
		^{154}Sm	stable
		^{155}Eu	5y.
^{40}K	1,3·10^{6}y.	^{39}Ar	2.7y.
		^{40}Ar	stable
		^{41}K	stable
		^{41}Ca	1.4·10^{5}y.
^{126}Sn	1·10^{5}y.	^{127}Sb	3.85d.
^{79}Se	6,5·10^{4}y.	^{79}As	9min.
		^{80}Se	stable
^{210}Pb	22,3y.	^{210}Pb	3.25hr
^{60}Co	5,27y.	^{60}Fe	3·10^{5}y.
		^{60}Ni	stable
		^{61}Ni	stable
		^{61}Co	1.7hr
^{106}Ru	372d.	^{107}Rh	21.7min.
^{54}Mn	312d.	^{53}Cr	stable
		^{54}Cr	stable
		^{55}Fe	2.7y.
		^{55}Mn	stable
^{57}Co	271d.	^{56}Fe	stable
		^{57}Fe	stable
		^{58}Co	71d.
		^{58}Ni	stable
^{103}Ru	39d.	^{104}Ru	stable

Nuclear Physics Approach

Table 2.

Transmutation reactions for transuranium elements

Initial isotope	Half-life period	Final isotope	Half-life period
^{239}Pu	2,4·10^{4}y.	^{238}Np	2.12d.
		^{239}Np	2.35d.
		^{238}Pu	88y.
		^{240}Pu	6.5·10^{3}y.
^{240}Pu	6537y.	^{239}Np	2.35d.
		^{240}Np	65min.
^{241}Pu	1.44y.	^{240}Np	65min
		^{241}Np	16min.
		^{240}Pu	6.5·10^{3}y.
		^{242}Pu	3.8·10^{5}y.
^{241}Am	432y.	^{240}Pu	6.5·10^{3}y.
		^{241}Pu	14.4y.
^{232}Th	1,4·10^{10}y.	^{231}Ac	7.5min.
^{238}U	4,5·10^{9}y.	^{237}Pa	8.7min.
^{237}Np	2,1·10^{6}y.	^{236}U	2.3·10^{7}y.
		^{237}U	6.8d.
^{243}Am	7380y.	^{242}Pu	3.8·10^{5}y.
		^{243}Pu	5hr
^{226}Ra	1600y.	^{225}F	3.9min.
^{244}Cm	18.1y.	^{243}Am	7380y.
		^{244}Am	10.1hr

As Table 1 illustrates, stable ore short-lived isotopes appear as a result of most reactions with radio nuclides. More long-lived isotopes can appear for three isotopes only (^{60}Co, ^{106}Rh and ^{54}Mn). But each such long-lived isotope can enter to transmutation reaction with enions and erzions and create new isotopes [5] - ^{61}Co (with 1,6 hr life time); ^{107}Rh (22 min.) and ^{108}Pd (stable); ^{55}Mn (stable) and ^{56}Fe (stable) correspondingly. One of the main fusion products ^{90}Sr is absent in the Table 1 because all six possible erzion transmutation reactions are endothermic if some model parameters are true. But some of this reactions can be exothermic if such parameters will be changed during the future investigations. In this case the generation of some other isotopes is possible [5] - rubidium, strontium or yttrium with maximum life time 59d. (^{91}Y). This suggests the possibility of ^{90}Sr transmutation in terms of the Erzion Model.

The more long-lived isotopes (^{240,242}Pu, ^{236}U and ^{243}Am) may appear for some transuranium radio nuclides also. But as seen from Table 2, two of them (^{240}Pu and ^{243}Am) may be transmuted into more short-lived ones on the next steps of transmutation. The Erzion Model also predicts transmutation of remaining two isotopes into short-lived isotopes [5] - ^{241}Np (16 min.) and ^{235}Pa (24 min.).

So if the Erzion Model is true, it predicts the transmutation possibility for, actually, all radio nuclides that occur in the composition of all kinds of radioactive wastes.

Nuclear Physics Approach

References

1. Bazhutov Yu. N., Koretsky V. P., and A. B. Kuznetsov, "Burning Away of Radioactive and Production of Some Stable Isotopes within the Framework of the Erzion Model", Proc. 4-th International Conference on Cold Fusion, Hawaii, 1993, 4, 27
2. Bazhutov Yu. N., Koretsky V. P., Kordukevich V. O., and E. M. Sakharov, "Setting up of Experiment on Burning Away of Radioactive Isotopes within the Framework of the Erzion Model", Proc. 2-nd Rissian Conference on Cold Fusion and Nuclear Transmutation, Sochi, 1994, 169-174
3. Kuznetsov B. B., "Levels of Environment Radioactive Pollution and some Aspects of Modern Radio Ecology", Atomnaya Tekhnika za Rubezhom, 1992, 11, 20
4. Bazhutov Yu. N., Kuznetsov A. B., and E. V. Pletnikov, "Spectroscopy of Erzion-Catalytic Transmutation of Nuclei ", Preprint N1, "Erzion" Center,, Kaliningrad, Moscow Region, 1993, 172
5. Korenkov A. P., "Several Studies on the Classification of Hardened Radioactive Wastes", Atomnaya Energiya, 1992, v.73, 2, 12

Nuclear Physics Approach

Erzion Model of Catalytic Nuclear Transmutation and Its Interpretation of Ball-Lightning and Other Anomalous Geophysical Phenomena

Yu.N.Bazhutov

Erzion Center, P.O.Box 169, 105077 Moscow, Russia

Abstract

The principles that underlie the Erzion Model of catalytic nuclear transmutation are described. The Erzion Model permits the main anomalous features of Cold Fusion to be readily interpreted. Ball-Lightning and some other anomalous geophysical phenomena are interpreted in terms of this model. The fundamental and applied problems resolved with Erzion Model are indicated.

1. Introduction

Long before Cold Fusion discovery [1] I and my co-authors had proposed the hypothesis [2] of new massive stable hadrons existence in Universe for interpretation of large series of anomalous Cosmic Ray experiments. To put this hypothesis in accordance with Salam-Weinberg-Glashow Standard Elementary Particle Model G. Vereshkov could find the decision of this problem in terms of Gauge Mirror Model -Vereshkov Model (VM) by means of introduction of new massive mirror fermions (leptons and quarks) into Standard Model (SM) [3]. The lightest mirror untiquark ($\overline{U}$) can provide the existence of hypothetical stable massive meson doublet - erzions ($Э^- \equiv \{\overline{U}d\}$; $Э^0 \equiv \{\overline{U}u\}$). Moreover the existence of only one stable erzion nucleus singlet - enion ($Э_N \equiv \{\overline{U}uudd\}$) which can be considered as compound state of erzion and nucleon ($Э^- p$, $Э^0 n$) is possible in terms of VM. All the rest erzion nuclei are not stable and decay by nuclei lifetime (~10^{-20}s) into erzions (enions) and usual nuclei. VM can create only one quark version of the hypothetical particles which does not contradict SM, Cosmology and Cosmogony and so all high energy physics and nuclear physics experimental results and results of new particle search at accelerators and in matter. Moreover it can explain large totality of anomalous experimental results not only in Cosmic Rays but in Astrophysics too: low solar neutrino flux: Jupiter radiation excess; catastrophic reducing of Li, Be, B contents in the abundance curve of Solar and Earth matter chemical elements; big flux of neutral high energy particles from local space sources [4]. And all these 15 years we are working constantly in the field of direct erzions search to decide is this hypothesis true or not [5].

Nuclear Physics Approach

2. Erzion model of catalytic nuclear transmutation

From the beginning Cold Fusion (CF) has caused strong objections of orthodox scientists due to obvious contradictions of CF experimental results to the traditional theoretical notions. And it was very pleasant and surprise opportunity for us to give natural and straight scientific interpretation of CF experiments due to erzion (enion) nuclei interaction features [3,6].

During first year of CF investigation it was found out the following main CF features [7]:

1) running process unstationarity;
2) great (~10^5) yield fluctuation;
3) attenuation and following unreproducibility;
4) yield suppression of neutron to tritium (10^3 - 10^{11}) and of tritium to energy (~10^3);
5) new elements and isotopes production.

The Erzion Model (EM) of catalytic nuclear transmutation could give interpretation for all these CF features [8]. EM based on the assumption of enion-nucleus bounded state existence in matter with few concentration (C~10^{-21} - 10^{-16} nucl.$^{-1}$). Enions may be captured (E_c~1 - 100eV) by small kind of some isotopes (donors) and are stored in this state rather long (~10^6 - 10^9 years) until their release by nuclear interactions. Enions can be either relict enions or they can come to Earth in Cosmic Ray component. Erzion nuclei can not exist that's why enions and erzions take part only in exchange reactions, that is enion ($Э_N$) turns into erzion ($Э^-$ or $Э^0$), and erzion either changes its sign ($Э^0 \rightarrow Э^-$ or $Э^- \rightarrow Э^0$) or turns into enion ($Э_N$). Thus in principle it is possible to exist 6 different erzion-nucleus exchange reactions on every nucleus ($Э_N \rightarrow Э^0$; $Э_N \rightarrow Э^-$; $Э^0 \rightarrow Э_N$; $Э^0 \rightarrow Э^-$; $Э^- \rightarrow Э_N$; $Э^- \rightarrow Э^0$). In this case nucleus either loses nucleon (proton or neutron) or acquires nucleon or changes its sign (±1) preserving nucleon number. In EM only 2 free parameters exist: enion coupling constants from ($Э^-, p$) fusion and ($Э^0, n$) fusion. If we know them we can compute all output energy for all 6 erzion-nucleus exchange reactions for all known isotopes. These enion coupling constants were chosen to provide running of deuterium fusion reactions with only tritium (T) generation and helium-3 generation prohibition. Moreover the tritium energy must be rather small (<0,1 MeV) for fast neutrons (~14 MeV) would not be generated by fusion reaction with deuterium. Good agreement of EM predictions with Rolison and O'Gredy results of palladium transmutation experiment showed possible truth of EM [9]. Further testing of EM was in good agreement with another nuclear transmutation results of CF experiments too [10].

Thus all output energies for all erzion nucleus exchange reactions for all stable [11] and unstable [12] isotopes had been calculated. It permits us to test the EM with all experiment results not only in CF but in Geophysics and Astrophysics too and to predict most optimum experiments.

3. Interpretation of ball-lightning and some other anomalous geophysical phenomena

Ball-lightning (BL) is the local (~10cm) stable (~100s) powerful (~1kW) cold plazmoid [13]. Although about 100 ball-lightning theoretic models exist there is not generally accepted among them (the same is in CF) because it is very difficult to give correct and obvious interpretation to such exotic phenomenon. We shall try to give simple principal interpretation of the main BL peculiarities in terms of EM.

Let us suppose that lightning discharge crushes tree and sets in fire and evaporates some decigrams of wood. On some conditions about billion (~10^9) enions may become free (T~2000°C) and to turn on the following catalytic nuclear reactions among chemical elements (H, C, N, O) of evaporated wood:

$^1H(Э^-,Э^0)n$	+ 1.65 MeV	(100)	(1)
$^2H(Э_N,Э^0)^3H$	+ 0.11 MeV	(0.02)	(2)

$^{2}H(Э^{0},Э_{N})^{1}H$	+ 3,9 MeV	(0,02)	(3)
$^{13}C(Э_{N},Э^{0})^{14}C$	+ 2,0 MeV	(1,1)	(4)
$^{13}C(Э^{0},Э_{N})^{12}C$	+ 1,2 MeV	(1,1)	(5)
$^{14}N(Э_{N},Э^{0})^{15}N$	+ 4,7 MeV	(100)	(6)
$^{14}N(Э^{-},Э_{N})^{13}C$	+ 0,25 MeV	(100)	(7)
$^{14}N(Э^{-},Э^{0})^{14}C$	+ 2,3 MeV	(100)	(8)
$^{15}N(Э_{N},Э^{-})^{16}O$	+ 4,3 MeV	(0,3)	(9)
$^{17}O(Э_{N},Э^{0})^{18}O$	+ 1,9 MeV	(0,04)	(10)
$^{17}O(Э^{0},Э_{N})^{16}O$	+ 2,0 MeV	(0,04)	(11)
$^{18}O(Э_{N},Э^{-})^{19}F$	+ 0,2 MeV	(0,2)	(12)

The isotope composition (%) is indicated in brackets assuming that composition of different chemical elements is the same.

Now let us suppose that average density of plazmoid matter will be a few more than air density. Then let us find out what reactions will be main in the erzion-nuclear transmutation cycle.

For neutral cycle ($Э_{N} \rightarrow Э^{0} \rightarrow Э_{N}$) it will be (5) and (6) reactions:

$^{14}N(Э_{N},Э^{0})^{15}N$	+ 4,7 MeV	(100)	(13)
$^{13}C(Э^{0},Э_{N})^{12}C$	+ 1,2 MeV	(1)	

For charged cycle ($Э_{N} \rightarrow Э^{-} \rightarrow Э_{N}$) it will be (12), (9), (7) reactions:

$^{18}O(Э_{N},Э^{-})^{19}F$	+ 0,2 MeV	(0,2)	
$^{15}N(Э_{N},Э^{-})^{16}O$	+ 4,3 MeV	(0,3)	(14)
$^{14}N(Э^{-},Э_{N})^{13}C$	+ 0,25 MeV	(100)	

The mixed cycle ($Э_{N} \rightarrow Э^{-} \rightarrow Э^{0} \rightarrow Э_{N}$) is possible too:

$^{15}N(Э_{N},Э^{-})^{16}O$	+ 4,3 MeV	(0,3)	
$^{18}O(Э_{N},Э^{-})^{19}F$	+ 0,2 MeV	(0,2)	
$^{1}H(Э^{-},Э^{0})n$	+ 1,65 MeV	(100)	(15)
$^{14}N(Э^{-},Э^{0})^{14}C$	+ 2,3 MeV	(100)	
$^{13}C(Э^{0},Э_{N})^{12}C$	+ 1,2 MeV	(1)	

It is evident from the isotope composition that the main cycle must be neutral cycle (13) if the cross-sections of reactions (1 - 12) don't differ each from other strongly.

To define cycle (13) power let us remember that such cycle frequency in condensed matter (PdD or TiD_2) is equal to ~ $10^{11}s^{-1}$ and in such a way the equivalent power must be equal to ~ 0,1W. Moreover let us remember that plazmoid matter density is 10^{3} times less than condensed matter density and ^{13}C isotope concentration is equal to ~ 0,01. As a result we have the erzion cycle frequency of BL is equal to ~ $10^{6}s^{-1}$, and the equivalent cycle power is equal to ~ 10^{-6}W.

The whole BL (10^{9} enions) power is ~ 1kW. If we suppose that erzion velocity in (5), (6) reactions will be ~ $10^{4}cm \cdot s^{-1}$ we can find erzion middle interaction range to be equal to ~ 0,1mm. It is much less than BL radius. But in such a way the middle BL life time must be only ~ 1s due to erzion diffusing. If BL kernel density was as condensed matter density, BL power would increase in proportion up to ~ 1MW, BL life-time - up to ~10^{3}s, and BL radius - up to ~ 10cm. If BL radius was ~ 1cm, BL life-time would be ~ 10s. This fact was noticed for artificial BL [13] at high voltage discharges in polymethylmethacrylat. At high voltage discharge in water it is possible to have free enion which can provide erzion nuclear cycle reactions on the H and O isotopes. The ^{17}O and ^{2}H densities are 10^{3} times less than PdD system ones. That is why the cycle frequency will be ~$10^{8}s^{-1}$ and cycle power will be ~ 10^{-4}W. Middle interaction range of neutral erzion ($Э^{0}$) in water

will be ~ 1μm. If BL life-time is ~ 0,1s and about 100 erzions participate in this cycle than plazmoid radius is ~ 1mm and its power is ~ 10^{-2}W. It corresponds to results of paper [14]. Unknown radiation with wave lengths 795 nm and 743 nm (ε ~ 1.6 eV) may be interpreted as characteristic radiation of enions captured by ^{16}O nuclei in hot plasmoid matter. Wave length doublet is due to thin splitting of L-S interaction.

As it was shown earlier EM can give principal interpretation for BL phenomenon (just as natural so artificial) and can indicate BL main parameters (radius, life time, power) rather well. This BL interpretation with help of EM is not single. Earlier such interpretation was made in two different works [15] by means of different mechanisms of CF but these models introduced new elementary particles. It must be very symptomatic.

Except BL there are another geophysical anomalous phenomena, which can be interpreted in terms of EM. One of them is indication on abundance of tritium and ^{3}He concentration in the volcano eruption products [16]. It may be interpreted as the result of reaction (2) running in the Earth entrails. Another interest anomalous phenomenon is ^{13}C isotope impoverishment inside of diamonds of North Yakutia (-14‰) and Australia (-11‰), although carbon isotope discrepancy is not more than 3 - 5‰ in Earth entrails. This fact may be interpreted by reaction cycles (4), (5) initiated by enions released from ^{12}C donor after cracking of diamond crystal.

4. Conclusion

Interpretation of BL and other anomalous geophysical phenomena described in terms of EM of catalytic nuclear transmutation extends more the list of anomalous nature phenomena interpreted by EM and published earlier.

If resume all publications on this subject we can give the list of possibilities provided by EM:

1) Interpretation of anomalous experimental results in Cosmic Rays, Astrophysics and Geophysics;
2) Interpretation of anomalous CF peculiarities;
3) Creation and optimisation of energy sources;
4) Radioactive waste utilization;
5) Some stable chemical elements and isotopes production (He, Ne, Au).

All this demonstrates great opportunities of EM.

In conclusion I want to thank A.M.Drobyshevsky, P.I.Golubnichiy and A.I.Klimov for useful discussions on this problem and express gratitude to all my colleagues for their faithfulness loyalty to Erzion idea.

References

1. Fleischmann M., and S. Pons, J. Electroan. Chemistry, 1989, 261, 301
   Jones S. et al., Nature, 338,1989, 737
2. Bazhutov Yu. N., Khrenov B. A., and G. B. Khristiansen, "About One Opportunity of Second Shower Spectrum Interpretation Observed at Small Depth Underground", Isvestiya AN USSR, ser. phys., v.46, 9, 1982, 2425-2427
3. Bazhutov Yu. N., and G. M. Vereshkov, "New Stable Hadrons in Cosmic Rays, Their Theoretical Interpretation and Possible Role in Cold Fusion", Preprint N1, CSRImash Kaliningrad, Moscow Region, 1990
   Bazhutov Yu. N., and G. M. Vereshkov, "Model of Cold Nuclear Transmutation by Erzion Catalysis Erzion Model of Cold Fusion", Proc. 4-th International Conference on Cold Fusion, Hawaii, 1993, 4, 8
4. Bazhutov Yu. N., "Possible Exhibition of the Erzion-Nuclear Transmutation in Astrophysics", Proc. 4-th International Conference on Cold Fusion, Hawaii, 1993, 4, 25

5. Bazhutov Yu. N., "Search for the Decays of Hypothetical Heavy Hadrons in Cosmic Rays", Proc. 18-th International Cosmic Ray Conference, Bangalore, 1983, v.11, 24-26
6. Bazhutov Yu. N., Vereshkov G. M., Kuzmin R. N., and A. M. Frolov, "Interpretation of Cold Fusion by Erzion Catalysis", Proc. "Plasma Physics and Some Questions of General Physics", CSRImash Kaliningrad, Moscow Region, 1990, 67-70
7. Bockris I. O'M. et al., Fusion Technology, 1990, 18, 1, 31
8. Bazhutov Yu. N., and G. M. Vereshkov, "Erzion Catalysis of Cold Fusion Reactions", Proc. 1-st Russian Conference on Cold Fusion, Abrau-Durso, 1993, 22-39
9. Bazhutov Yu. N., and A. B. Kuznetsov, "Isotopic and Chemical Composition Changes of Palladium in Cold Fusion Experiments in the Erzion Model", Proc. 4-th International Conference on Cold Fusion, Hawaii, 1993, 4, 26
10. Bazhutov Yu. N., and A. B. Kuznetsov, "Interpretation of Cold Fusion Experiments in the Erzion Model Framework", Proc. 1-st Russian Conference on Cold Fusion, Abrau-Durso, 1993, 40-43
    Bazhutov Yu. N., and A. B. Kuznetsov, "Interpretation of New Set of Experiments on Cold Fusion in the Erzion Model Framework", Proc. 2-nd Russian Conference on Cold Fusion and Nuclear Transmutation", Sochi, 1994, 25-29
11. Bazhutov Yu. N., and A. B. Kuznetsov, "Erzion-Nuclear Spectroscopy of Stable Isotopes", Preprint N4, CSRImash, Kaliningrad, Moscow Region, 1992
12. Bazhutov Yu. N., Kuznetsov A. B., and E. V. Pletnikov, "Spectroscopy of Erzion-Catalytic Transmutation of Nuclei ", Preprint N1, "Erzion" Center, CSRImash, Kaliningrad, Moscow Region, 1993, 172
13. "Ball-Lightning in Laboratory, Moscow, "Khimiya", 1994
14. Golubnichy P. I. et al., Proc. of International Symposium "Cold Fusion and New Energy Sources", Minsk, 1994, 41-48
15. Lewis E., Fusion Technology, Submitted in December (1992)
    Matsumoto T., Bulletin of the Faculty of Engineering Hokkaido University, 175(1995), 72-86
16. Jones S. E. et al., Preprint BYUPHYS, 1989, 339-389
17. Galimov E. M., and S. Apstain, "Hypotheses. Prognoses", Moscow, "Znaniye", 1990, 93-105

Nuclear Physics Approach

Anomalous Phenomena in E<18 KeV Hydrogen Ion Beam Implantation Experiments on Pd and Ti

WANG Tieshan* PIAO Yubo HAO Jifang* WANG Xuezhi****
JIN Genming* and NIU Zhanqi**

***Institute of Modern Physics, Chinese Academy of Sciences**
Lanzhou 730000, P. R. China
****Department of Modern Physics of Lanzhou University**
Lanzhou 730000, P. R. China

Abstract

Implantation experiments of very low energy (1KeV<E<18KeV) hydrogen ions on hydrogen loaded metals have been performed with high beam density ($J_{max.}$~1.2 mA/cm^2) and weak beam density ($J_{min.}$~ 0.02 mA/cm^2). Palladium and titanium foils (plates) have been bombarded with proton and deuteron beams in order to compare the atomic and nuclear interactions between different ion beams. X ray and charged particles have been measured, and neutron and gamma doses were also monitored during implanting experiments. An anomalous peak in X-spectra, which energy is about four times of beam energy, has been observed during high beam density experiment. The peak moved from about 40 KeV to 62 KeV and FWHM reduced rapidly, while the beam energy and intensity increased. Another wide peak with over twice of the beam energy has been measured in experiment with low beam density. This peak located between 16 and 30 KeV, and its peak position grew with the growth of integrated implantation dose (implantation time). Some anomalous intensities of neutrons correlated with a charged particle peak (3-4 MeV) have been also observed in deuteron-palladium experiment. The highest neutron intensity reached about 8×10^4n/s, while the beam energy and intensity was about 15 KeV and 1.0 mA, respectively.

1. Introduction

Since 1989, much pioneering works about 'cold fusion' have been reported, and various anomalous phenomena have been observed[1-5]. The existence of 'excess power' has been represented by more and more experiments and different laboratories. However, the nature of 'excess power' is still unidentified. Especially, most of the phenomena could not be reproduced, and not enough reaction products beside 'heat' have been measured[2-5]. So that, the research about occurrence mechanism of 'excess power' is very important.

Beam implantation with low energy and high current density is used to approach the reaction mechanism and phenomena of the metal-hydrogen system described in this work.

The deuterium-palladium ratio (D/Pd) can be increased rapidly to over 0.85, because of the short implantation deeps of low energy beams. The target temperature can be easily controlled under room temperature in order to avoid the escape of deuterium atoms from metal, during experiments. At the same time, ion beam type, energy, intensity and target matter and other conditions can be easily changed and chosen in experiment, so that, the conditions corresponded to anomalous phenomena can be directly determined. Otherwise, neutron, charged particles, γ and X rays etc. parameters may be measured similarly during experiments. Thus the correspondence between reaction products and excess power can be directly set up.

In this work, some anomalous X-ray spectra have been measured, and the enhancement of neutron intensity correlated with some charged particles was also observed.

2. Experimental description and results

In our experiments, both of proton and deuteron beams, which energy and beam intensity could be adjusted from 1 to 18 KeV and 0.05 to 5.0 mA, were employed to bombard palladium and titanium targets. Palladium targets with thickness of 0.005 mm and 1 mm and titanium target with thickness of 0.3 mm have been used. An effective cooling system with a thermal temperature monitor was employed to keep targets under room temperature. A Si(Li) X-ray detector and a Si(Au) detector have been applied to measured X-rays and charged particles. At the same time, a gamma-dosimeter and a neutron-dosimeter were used to monitor the change of gamma and neutron doses.

Some reproducible anomalous X spectra (Fig. 1-a) have been measured during high density (J~1.0 mA/cm^2) implantation experiments. Other spectra (Fig, 1-b) with a wide anomalous peak have been also observed during the experiment with low beam density (J~0.02 mA/cm^2).

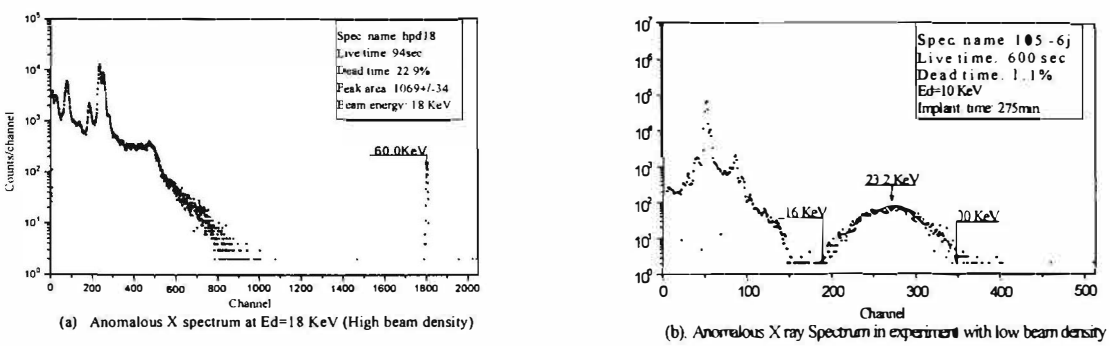

(a) Anomalous X spectrum at Ed=18 KeV (High beam density)

(b). Anomalous X ray Spectrum in experiment with low beam density

Fig. 1 Anomalous experimental X ray Spectra

In the experiment with high beam density, the position of anomalous peak with about 10^8-10^{10}/s intensity moves from about 40 KeV to 60 KeV, while increasing the beam energy and intensity, in both of P+Pd and D+Pd experiments (Fig. 2). At the same time, the FWHM reduced rapidly (Fig. 3).Anomalous phenomena occurred only when the energies of proton and deuteron were higher than 7.5 KeV and 10 KeV, respectively. It

needed to identify, whether these threshold energies were induced by absorption of the carbon foil deposited on target surface or physical nature. When a titanium target was used to instead of palladium to do the same experiment, similar phenomena have been observed, but the energy of the anomalous peak was a little lower than using palladium target at same reaction conditions. It is not sure, if the energy difference was same type interaction but between different atoms.

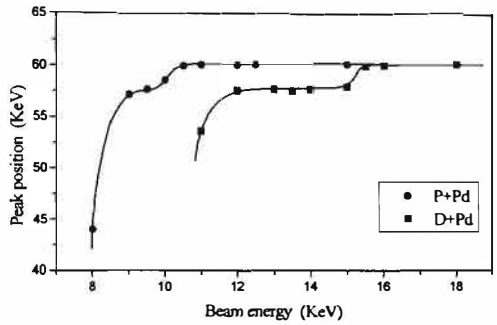

Fig.2 Curves of anmalous peak positions vs. beam energy (High beam density)

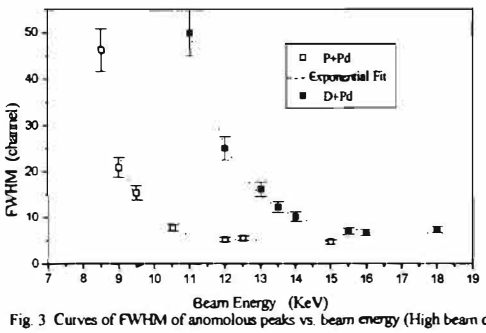

Fig. 3 Curves of FWHM of anomolous peaks vs. beam energy (High beam density)

In the experiment with low beam density, the position and intensity of the anomalous peak increased with the implantation dose or time. The total peak is located between 12 KeV to 30 KeV region. The maximal position of peak moved from 17 KeV to 23.2 KeV during about 300 minutes implanting. At the beginning, a part of the peak located on the tail of the normal spectrum, and then separated slowly. After about 275 min. implanting, the anomalous peak was total separated with the normal spectrum (Fig. 1-b).

A quasi-atom multi-body theoretical model[6] has been proposed to interpret these phenomena. However, both the anomalous phenomena and the theoretical model are needed to investigate further.

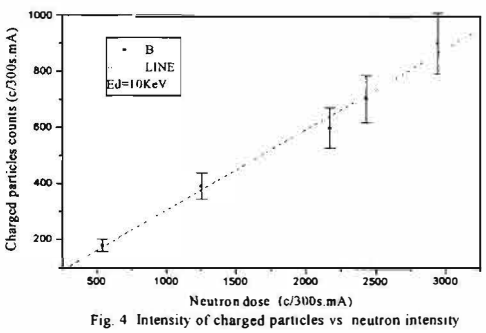

Fig. 4 Intensity of charged particles vs neutron intensity

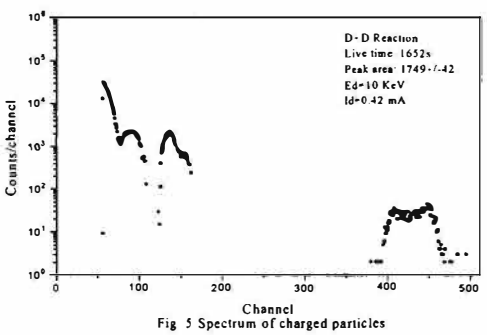

Fig 5 Spectrum of charged particles

In D+Pd experiments, some anomalous intensities of neutrons correlated with a wide charged particle peak has been observed. The neutron intensity grew linearly with the growth of beam intensity, but rapidly with the growth of beam energy. The highest neutron intensity was about $8x10^4$n/s, while about 1 mA, 15 KeV deuteron beam was applied. That was much higher than the prediction for D-D neutron with a self built-up target at such beam conditions. The ratio of neutron and charged particle intensities changed not evidently (Fig. 4), while beam intensity and energy were changed.

Otherwise, the energy of charged particles was located among 3-4 MeV region, thus, the charged particles should be protons from D(d,p)T reaction (Fig. 5), and then the neutrons should be neutrons from D(d,n)^{3}He reaction.

3. Discussion and Conclusion

The identifying experiments have shown, that the anomalous phenomena were beam-target effects. However, what was the anomalous peak in experimental spectra could not be determined. If the peak was only some pile up of electronic signals, why did it change regularly with the change of beam energy and intensity? and why were there no double pile up peak in the spectra? If the peak was really from X ray, it was unable to be interpreted with basic physical theory, why the energy of the anomalous peak in the X spectra moved continuously among 4-5 times of implanting beam energy with the change of beam parameters. If further investigation could identify above experimental results as X ray or other emission of energy, that could be correlated with 'excess power' observed in other pioneering works. Maybe, a new physical interaction can be discovered.

To interpret the phenomena, a quasi-atom multi-body model is proposed[6]. In such a quasi-atom, two deuterons rotate around a negative center, which can be a complex effect of one or more electrons. Electrons could rotate around the axis connecting two deuterons in some orbits. In the process to form a quasi-atom, some energy may be released in emission of X rays. Because two deuterons have been bound in about 10~150 fermi scale in such a 'Quasi-atom,' so that, the cross section of general D-D reaction could be much larger than they were in separated state. Thus, there were some enhancements of neutron intensity. Otherwise, the state of such quasi-atom might depend on reaction conditions, so, the peak moved with change of beam and there were seems to be two energy states in the curves of Fig. 2. That should be investigated, whether these two energy states were corresponded with electron orbits or other inner structures of the quasi-atom.

4. Acknowledgments

This work is supported by Institute of Modern Physics of Chinese Academy of Sciences. T. Wang gratefully acknowledges Prof. A. Takahashi, Osaka University, Japan, for his support to finish this paper in his laboratory.

REFERENCE

1. M. Fleischmann and S. Pons, J. Electroanaly. Chem., 261, 301 (1989).

2. A. B. Karabut, Ya. R. Kucherov and I. B. Savvatimove, Physics Letters A, 170 (1992) 265-72

3. E. Y. Yamaguchi and T. Nishioka, Japanese J. of Appl. Physics, Vol. 29, No.4, (1990) L660-9.

4. A. Takahashi, T. Inokuchi, Y. Chimi et al. Proc. of ICCF5, 1995, France.

5. B. F. Bush, J. J. Lagowski, J. Electroanal. Chem. 304 (1991)271-8

6. T. Wang , Y. Piao, G. Jin et al., Interpretation of Excess Energy in Terms of Quasi-Atom Multi-body Model. Proc. of ICCF6, 1996, Hokkaido, Japan. P-061

Nuclear Physics Approach

Interpretation of Excess Energy in Terms of Quasi-Atom Multi-body Model

WANG Tieshan* PIAO Yubo** JIN Genming* NIU Zhanqi**
HAO Jifang* WANG Xuezhi**

*Institute of Modern Physics of Chinese Academy of Sciences
Lanzhou 730000 P. R. China
**Department of Modern Physics, Lanzhou University
Lanzhou 730000 P. R. China

Abstract

A quasi-atom multi-body model is proposed for interpreting excess energy in some "cold fusion" experiments, based on analyzing experimental results. In such a quasi-atom, two nuclei rotate around a negative image center, which can be a complex effect of one or more electrons. Electrons could rotate around the axis connecting two nuclei in some orbits. In the process to form a quasi-atom, some energy may be emitted. There may be double hydrogen nuclei and metal-hydrogen double nuclei, two types of quasi-atoms in metal-hydrogen systems. Some theoretical estimation and approaches about structure and energy states have been presented for discussion purposes.

1. Introduction

The nature of excess energy observed in different 'cold fusion' experiments[1] is unclear, although many theoretical models have been proposed since 1989. In order to interpret the origin of excess energy, a quasi-atom multi-body theoretical model is proposed, based on understanding and analyzing pioneering theoretical and experimental results.

In such a quasi-atom, two nuclei rotate around a negative image center, which can be a complex effect of one or more electrons. Electrons rotate around the axis connecting two nuclei in different orbits. The energy of such a multi-body cluster is lower than two separated atoms. So that, some energy may be relaxed in the process to form such a quasi-atom under some extreme conditions. The metal (e.g. palladium metal) with high hydrogen loading ratio (D/Pd>0.85) might be one of the essential conditions.

2. Description of theoretical model

Quasi-atom may be a bound state under some extreme condition. In such a quasi-atom, two nuclei rotate around a negative image center, which can be a complex effect of one or more electrons (Fig.1). Electrons rotate around the axis connecting two nuclei in some orbits. Double hydrogen nuclei and metal-hydrogen double nuclei, two types of quasi-atoms in metal-hydrogen system are proposed in this work.

2.1. Double hydrogen nucleus quasi-atom

In some micro spots among metal, hydrogen atoms may be concentrated to a very high density. Distances between different hydrogen nuclei in such spots are smaller than the radius of

the hydrogen atom. When electrons go into such a spot, a quasi-atom, consisted of two hydrogen nuclei and one or two electrons might be formed .

2.2. Metal-hydrogen double nucleus quasi-atom

Hydrogen ions (e.g., deuterons) in metals (e. g., Pd) getting some energy can go through the electron cloud of palladium without the occurrence of nuclear reaction and might stay inside the palladium atom, because of the electron screening effect of palladium and other interactions (e.g., spin coupling) from the palladium nucleus and other atoms. They could be either between the nucleus and electron cloud or between different electron shells, and form a double nucleus quasi-atom even like a cluster. The total energy of this quasi-atom might be lower than separate deuterium and palladium. Thus, some excess energy should be released in the process. Otherwise, the deuteron may catch an orbital electron and become a quasi-deuterium among the palladium, then a new electron jump from another orbit to fill the empty inner shell with emission of anomalous X-ray.

3. Theoretical Approaches

3.1. Theoretical estimation

The schematic of a quasi-atom is shown in Fig.1.

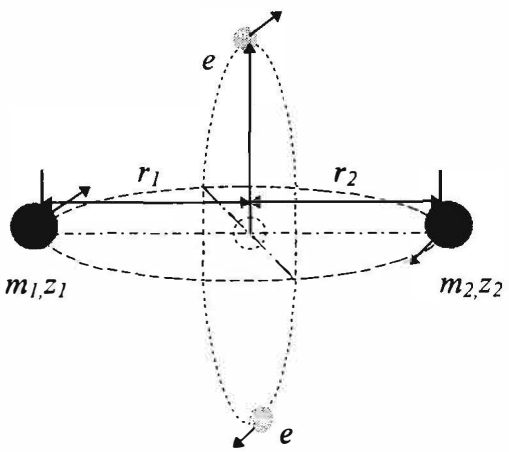

Fig.1. Schematic of Quasi-atom Multi-body Model (right)

The schördinger equation of such a quasi-atom is:

$$[-\frac{\hbar^2}{2m_1}\nabla_1^2 - \frac{\hbar^2}{2m_2}\nabla_2^2 + U(r)]\psi(r) = E\psi(r) \quad \text{.....(1)}$$

Here, z_1, z_2, m_1, m_2 are charge and mass of two nuclei, respectively. ψ (r) is the distribution function, and potential energy U(r) is described by following equation:

$$U(r) = -e^2(-\frac{z_1 z_2}{r_1+r_2} + \frac{z_1 z}{r_1} + \frac{z_2 z}{r_2}) \quad \text{.....(2)}$$

Here z is the charge of the negative image center between two nuclei, and mass of the center can be neglected. Rotation radii of two nuclei has the following relationship

$$r_2 = \sqrt{\frac{z_2}{z_1}}\, r_1 \quad \text{.....(3)}$$

When eq. (2) is brought into eq. (3), the potential energy equation is changed into:

$$U(r) = -\frac{z_1 e^2}{r_1}[(1+\sqrt{\frac{z_2}{z_1}})z - \frac{z_2}{1+\sqrt{\frac{z_2}{z_1}}}] \quad \text{.....(4)}$$

Now if we define $z' = (1 + \sqrt{\frac{z_2}{z_1}})\, z - \frac{z_2}{1+\sqrt{\frac{z_2}{z_1}}}$ and put it into eq. (4), then

$$U(r) = -\frac{z_1 z' e^2}{r_1} \quad \text{.....(5)}$$

If $\mu = \frac{z_2 m_1 m_2}{z_1 m_1 + z_2 m_2}$ is defined and eq. (5) is brought into eq. (1), then the eq. (1)is changed into

$$[-\frac{\hbar^2}{2\mu}\nabla^2 - \frac{z_1 z' e^2}{r}]\psi(r) = E\psi(r) \quad \text{.....(6)}$$

Now, eq.(6) is converted into the global coordinate system, eq. (7) can be gotten.

$$\frac{d^2\psi}{dr^2} + \frac{2}{r}\frac{d\psi}{dr} + \frac{2\mu}{\hbar^2}(E + \frac{z_1 z' e^2}{r})\psi(r) = 0 \quad \text{.....(7)}$$

If this equation is calculated with $\psi(r) = Ce^{-\alpha r}$, the following results can be obtained.

$$\alpha = \frac{\mu z_1 z' e^2}{\hbar^2} = \frac{z'}{a_0}$$

$$E = -\frac{\alpha^2 \hbar^2}{2\mu} = -\frac{\mu z_1^2 z'^2 e^4}{2\hbar^2} = -z'^2 R$$

Here $a_0 = \frac{\hbar^2}{\mu z_1 e^2}$, and $R = \frac{\mu z_1^2 e^4}{2\hbar^2}$ is energy factor. According to the following essential condition equation,

$$\int_0^\infty 4\pi r^2 \psi(r) dr = 1 \quad \text{.....(8)}$$

$C = \frac{z'^3}{8\pi a_0^3}$ and $\psi(r) = \frac{z'^3}{8\pi a_0^3} e^{-\frac{z'}{a_0} r}$ can be gotten.

By use of the distributed probability equation:

$$D = 4\pi r^2 \psi(r) \quad \text{.....(9)}$$

the maximum of distributed probability is gotten at the position of $r = \frac{2a_0}{z'}$ within condition of $\frac{dD}{dr} = 0$.

3.2. Results

A. Results for the hydrogen double nucleus quasi-atom

Deuteron-two electron-deuteron (d-2e-d) four body system, proton-electron-proton (p-e-p) and deuteron-electron-deuteron (d-e-d) three body systems have been studied in this work.

For deuteron-two electron-deuteron (d-2e-d) four body system, $z_1=z_2=1$ and $m_1=m_2= 2$, then $\mu=1$ and $z' = 2z - \frac{1}{2}$

$$a_0 = 2.88 \times 10^{-14} m$$

$$r_1 = r_2 = r = \frac{1}{4z-1} \times 1.15 \times 10^{-13} m$$

E=-24.7KeV,
r=28 fermi.

For the p-e-p and d-e-d three body systems, only the rotation of nuclei and vibration of electron between two nuclei are calculated. The stable energy states and orbit radii for p-e-p and d-e-d system may be 28.1, 56.2 KeV and 140, 35 fermi, respectively.

The ratio of reaction cross section of forming a quasi-atom and occurring a D-D fusion is:

$$\sigma_q / \sigma_n \sim 10^4$$

and ratio of integrated energy from these two interactions is:

$$\Sigma E_x / \Sigma E_n \sim 200$$

here, σ_q is the reaction cross section of forming a hydrogen double nucleus quasi-atom, σ_n is cross section of a D-D fusion reaction event, ΣE_x is total energy relaxed from forming quasi-atom processes and ΣE_n is the total energy relaxed from occurring D-D reactions at the same time.

B. Metal-hydrogen double nucleus quasi-atom

In this system, many bodies might be involved. For instance, in the palladium-deuterium quasi-atom, 49 bodies might be included. Detail parameters for a palladium-deuterium quasi-atom are following: z_1=1, m_1=2, z_2=46, m_2=106, then μ=2 and

$$a_0 \approx 5.76 \times 10^{-14} m$$

$$z' = 7.8z - 5.9$$

$$r_1 = \frac{1}{7.8z - 5.9} \times 1.15 \times 10^{-13} m$$

$$r_2 = 6.8 r_1 \approx \frac{1}{1.1z - 0.87} \times 1.15 \times 10^{-13} m$$

The exact calculation about such an involved system of 49 bodies is impossible. Thus, there are no exact energy states and orbits can be obtained.

4. Discussion and conclusion

X rays may be easily absorbed in a very short distance and turned into heat in the surrounding media, thus, only excess heat has been measured in most experiments without enough corresponding reaction products. So that, X rays may be one of the possible of origin of excess energy. Some experimental phenomena with emission of anomalous X rays have been reported[2,3]. That can be correlated with this theoretical model.

If there really is such a quasi-atom state, it might be some stable bound states under very extreme conditions (e.g., D/Pd>0.85). So that, experimental phenomena could be reproduced only very occasionally. Otherwise, the reaction cross section of D-D fusion in such a bound state may also be increased by some orders[2,3]. This conclusion can be also associated with observation of anomalous neutron intensity. However, the reaction cross section of the quasi-atom is about four orders higher than D-D fusion cross section, and the total exoergic quantity from quasi-atoms is over two orders higher than that from D-D reaction at the same time. Thus, the energy from the quasi-atom reaction might be the main origin of excess energy, if there are such processes. Otherwise, some multi-body nuclear reaction (e.g. 3D or 4D reactions) proposed by another paper[4] can also be easily induced in such a quasi-atom.

Some results about transmutation have been reported[5] recently. It is thought, that the metal-hydrogen double nuclei is associated as a intermediate process to induce transmutation phenomena.

Comparing with halo neutron atom (e.g.^{11}Li), halo proton atom under extreme condition

has been also proposed. So that it is also thought, that if the quasi-atom is only some means of halo proton (deuteron) atom. However, the distance (more than 20 fermi) between two nuclei is difficulty to image for a halo proton atom. Perhaps, electron screening effect and spin coupling forces should be considered to interpret the phenomena.

This model is proposed to interpret some anomalous phenomena which were observed in some experiments[2,3]. Some correlation between experimental phenomena and this model can be set up. However, both of experimental phenomena and the theoretical model need to be identified. Further experimental and theoretical approaches are very necessary.

5. Acknowledgments

This work was supported by Institute of Modern Physics of Chinese Academy of Sciences. T. Wang gratefully acknowledges Prof. A. Takahashi, Osaka University, Japan, for his support to finish this paper in his laboratory.

References

1. M. Fleischmann and S. Pons, J. Electroanaly. Chem., 261.301 (1989).

2. T. Wang, Y. Piao, J. Hao, et al., Anomalous Phenomena in E<18KeVHydrogen Beam Implantation Experiments on Pd and Ti, Proc. of ICCF6, Oct. 1996, Japan. P-060

3. S. Chen, D. Wang, G. Cui, X-ray Diagnostic in Gas Discharge, Proc. of ICCF6, Oct. 1996, Japan. P-065.

4. A.Takahashi, et al., Fusion Tech., 27(Jan), 71-85, (1995)

5. G. H. Miley, H. Hora, E. G. Batyrbekov, et al. Fusion Tech., 26, T, Part 2,313-320 (1994)

Nuclear Physics Approach

Observation of Nuclear Products in Gas Release Experiments with Electrochemically Deuterated Palladium

Takehiko Itoh, Yasuhiro Iwamura, Nobuaki Gotoh and Ichiro Toyoda

Advanced Technology Research Center, Mitsubishi Heavy Industries, Ltd.
1-8-1, Sachiura, kanazawa-ku, Yokohama, 236, Japan

Abstract

Gas release experiments have been performed using electrochemically deuterated palladium. We developed a gas storage system to store gas released from a deuterated palladium. Using the system, we analyzed the released gas and investigated effects of hydrogen concentration on mass number 5 gas. As a result, mass number 5 gas cannot be explained by hydrogen concentration and we conclude that DT gas is produced in the gas release experiments.

1. Introduction

Since Fleichmann and Pons reported on "cold fusion" phenomena in 1989, much research has been carried out and many reports indicated that nuclear reactions occurred in deuterated palladium. From those reports and our research[1,2,3], it is necessary for inducing anomalous nuclear effects to make deuterium atoms diffuse in palladium metals under high D/Pd condition. In order to clarify this point, we have performed gas release experiments to release absorbed gas by heating electrochemically deuterated palladium metals in a vacuum chamber and reported on anomalous nuclear effects(neutron emission, X-ray emission, DT gas breeding)[1,2].

We demonstrated that mass number 5 gas increased during heating in previous paper[1,2]. Mass number 5 gas measured by Q-Mass is composed of DT and DDH^+. DDH^+ ions are formed of deuterium and hydrogen. Deuterium derives from samples and hydrogen is contained in samples and a vacuum chamber. In previous paper, we estimated mass number 5 gas without taking account of effects of hydrogen contained in samples. In this paper, therefore, in order to confirm that DT gas is released in our experiments, we analyze the sample gas and investigate effects of hydrogen concentration on mass number 5 gas using two kinds of method as follows.

(1)monitoring mass number 5 gas and hydrogen simultaneously during experiments with two quadrupole mass spectrometers.

(2)estimating of hydrogen concentration of the released gas from the sample using a gas storage system described in this paper.

Nuclear Physics Approach

2. Method

An experimental procedure is as follows. Palladium metals(ϕ3 × 25mm : Tanaka Kikinzoku Kogyo K.K.) are annealed at 900°C in a vacuum chamber(<10^{-7} torr) for 10 hours and are washed with heavy aqua regia. The palladium samples are loaded with deuterium in D_2O-LiOD electrochemical cell and are electroplated with Cu in a $CuSO_4$-D_2O electrochemical cell to maintain high deuterium loading ratio. After that, the sample is heated up to 180°C to release absorbed gas in a vacuum chamber. As described in ICCF-5 proceedings[2], the vacuum chamber is equipped with nuclear measurement apparatus(He-3, SSB, CdTe, NaI, Q-Mass) in order to observe anomalous nuclear effects. As for Q-Mass, we use two quadrupole mass spectrometers (one is high resolution and the other is normal resolution). All these devices are located in a clean-room where temperature and humidity are always controlled at constant levels(23°C±1°C, 40%±5%) in order to prevent contamination and false counts induced by humidity in the air.

We, furthermore, developed a gas storage system connected with the vacuum chamber to store and to analyze the released gas from the sample. Figure 1 shows a scheme of the system. This system is composed of a gas storage chamber and a dry pump to hold backing vacuum of a turbo-molecular pump and to compress the sample gas into a gas storage chamber. Using this system, we store released gas from the sample during experiments. After experiments, the gas is analyzed by a mass spectrometer.

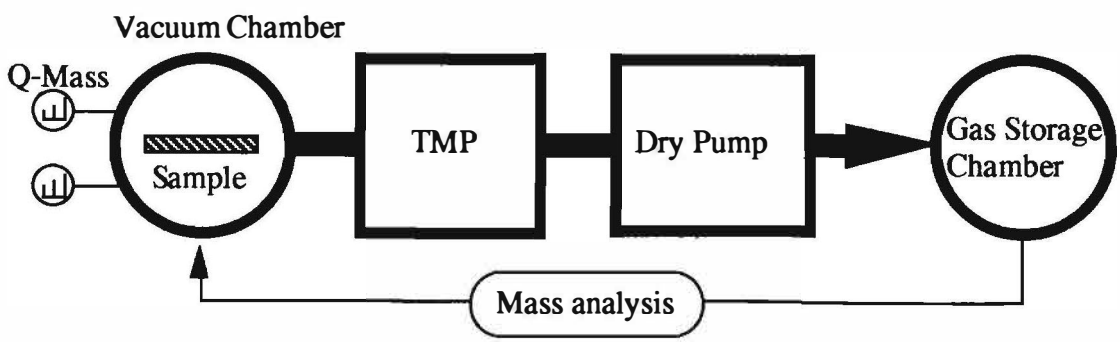

Figure 1. A scheme of gas storage system

3. Results and Discussion

We simultaneously monitored mass number 5 gas and mass number 1 gas(H^+) using two quadrupole mass spectrometers during experiments. Figure 2 shows the result of time evolution of mass number 1 signals and mass number 5 signals during heating. Mass number 1 signal is proportional to hydrogen concentration. The figure indicates that mass number 5 gas increases while hydrogen decrease. Therefore, time variation of mass number 5 gas does not correspond with DDH^+ time evolution. It is considered that mass number 5 gas is not composed of DDH^+ alone.

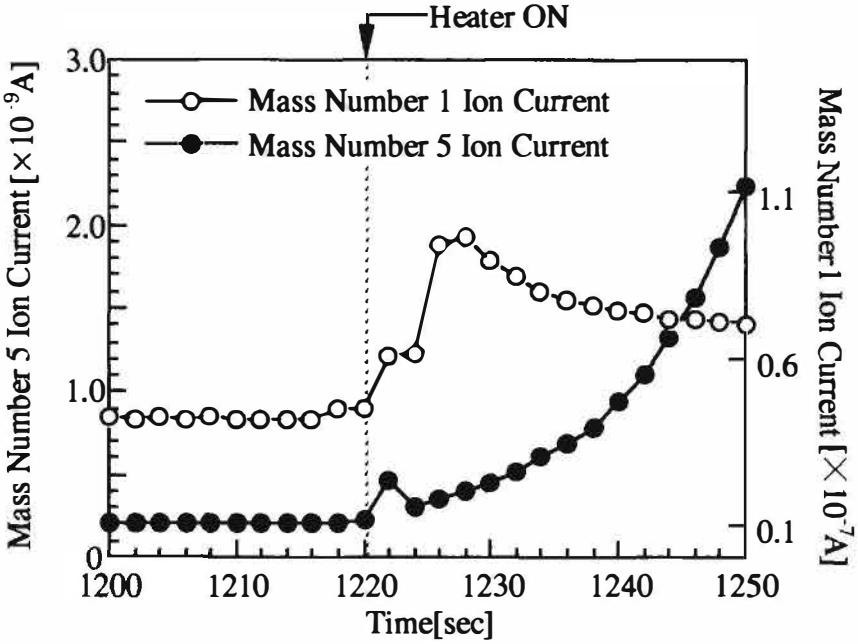

Figure 2. Time evolution of mass number 1 ion current and mass number 5 ion current

We stored released gas from the sample in order to analyze hydrogen concentration with a mass spectrometer. Figure 3 shows mass spectrum of the released gas. Comparing mass number 3(HD) ion current intensity with mass number 4(D_2) ion current intensity, hydrogen concentration is estimated 3.4% (deuterium is 96.6%). Since the released gas contains hydrogen, it is important for analyzing mass number 5 gas to take account of DDH^+ formation depending on hydrogen concentration.

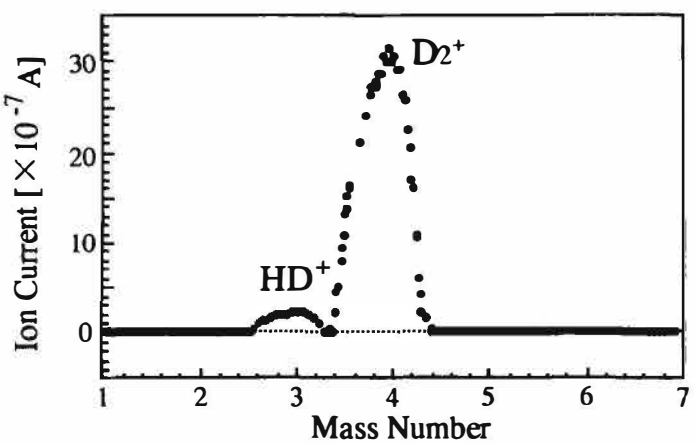

Figure 3. Hydrogen concentration in released gas

Figure 4 shows effects of hydrogen on DDH^+ formation. DDH^+ ion current is measured by introducing mixing gas of deuterium and hydrogen into the chamber. The figure indicates that DDH^+ ion current intensity increase with increasing hydrogen concentration. Threfore, DDH^+ formation depends on hydrogen concentration. In a previous report[2], however, we evaluated DT gas breeding ratio without considering effects of hydrogen and defined DT gas breeding ratio as

equation(1) using DDH^+ ion intensity of standard gas of D_2 cylinder (D: 99.6%, H: 0.4%).

$$\text{DT Gas Breeding Ratio} = \frac{\text{Mass 5 Ion Current}}{DDH^+ \text{ Ion Current}} \qquad (1)$$

In this paper, we estimate hydrogen concentration of samples and determine DDH^+ background intensity using figure 4. Introducing the DDH^+ background intensity into equation(1), we evaluate DT gas breeding ratio. If DT gas breeding ratio is larger than 1.0, DT gas is released from deuterated palladium.

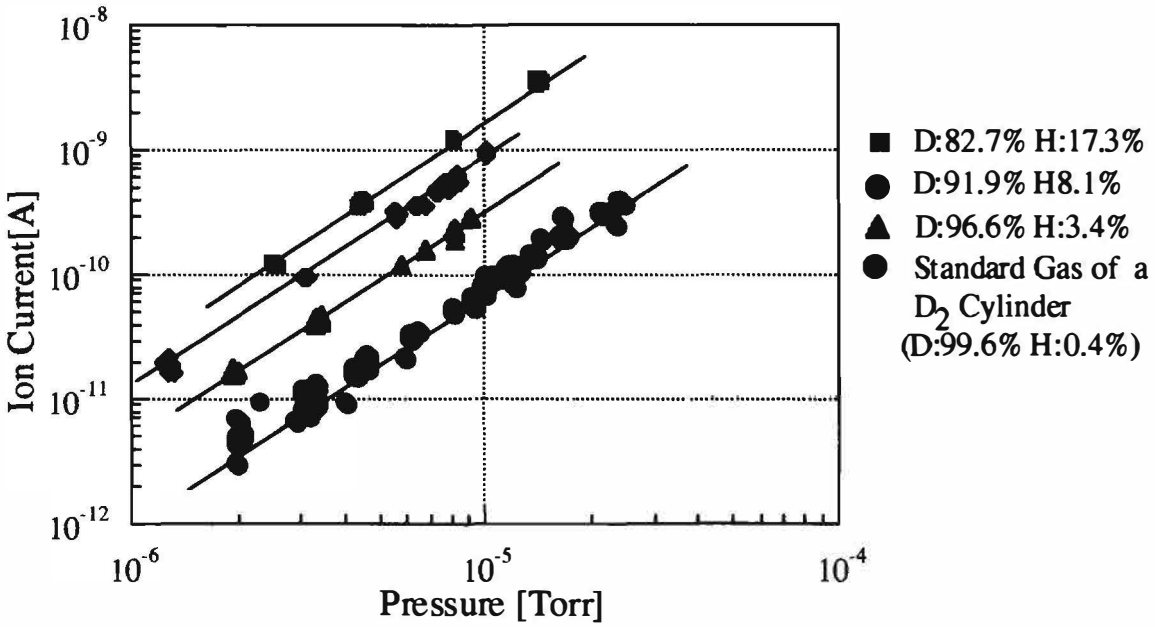

Figure 4. DDH^+ formation depending on hydrogen concentration

Figure 5-(a), 5-(b) shows time evolution of mass number 1 ion current, total pressure and DT gas Breeding ratio analyzed using this procedure. Mass number 1 signals correspond with hydrogen concentration and total pressure is proportional to deuterium density. Hydrogen concentration is 5.7% in this experiment. In figure 5, DT gas breeding ratio is larger than 1.0 during heating. It is considered that DT gas is released from the sample. Furthermore, in figure 5-(b), DT gas breeding ratio changes rapidly, though mass number 1 signals(hydrogen concentration) and total pressure(deuterium density) do not change. This indicates that time variation of DT gas breeding ratio does not correspond with time evolution of DDH^+. Therefore, DT gas breeding ratio cannot be explained by DDH^+ formation.

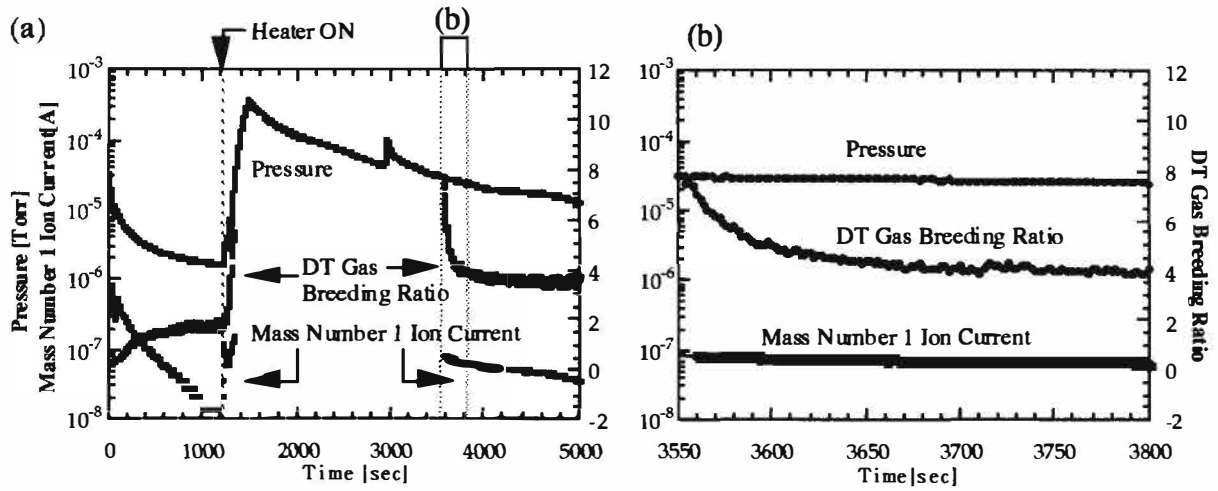

Figure 5. DT gas breeding ratio time evolution

4. Conclusion

DT gas breeding ratio analysis with taking account of DDH^+ formation depending on hydrogen concentration has been performed. As a result, DT gas breeding ratio is higher than 1.0 and time evolution of DT gas breeding ratio does not correspond with hydrogen time evolution. Therefore, mass number 5 gas cannot be explained by the formation of DDH^+ and we conclude that DT gas is contained in mass number 5 gas in gas release experiments.

Reference

1. Y.Iwamura, T.Itoh and I,Toyoda, "Observation of Anomalous Nuclear Effects in D_2-Pd System", Proc. of ICCF-4, Maui, Hawaii, December 6-9, 1994, vol.2, p12
2. T.Itoh, Y.Iwamura, N.Gotoh and I.Toyoda, "Observation of Nuclear Products under Vacuum Condition from Deuterated Palladium with High Loading Ratio", Proc. of ICCF-5, Monte Carlo, Monaco, April 9-13, 1995, p189.
3. Y.Iwamura, N.Gotoh, T.Itoh and I.Toyoda, "Characteristic X-ray and Neutron Emission from Electrochemically Deuterated Palladium", Proc. of ICCF-5, Monte Carlo, Monaco, April 9-13, 1995, p197

Appendix

Authors' Index

Authors' Index

Authors' Index

First printing :	December, 11, 1996
Name of the proceedings :	Progress in New Hydrogen Energy Vol. 1
Published by :	New Energy and Industrial Technology Development Organization (NEDO) The Institute of Applied Energy (IAE)
Supported by :	The Agency of Natural Resources and Energy of the Ministry of International Trade and Industry
Edited by :	Makoto Okamoto (Tokyo Institute of Technlogy)